Atlas of Multiplane Transesophageal Echocardiography

Volume 1

Martin G St John Sutton MB BS FRCP
John Bryfogle Professor of Cardiovascular Diseases and
Director, Cardiac Imaging Program
Cardiovascular Division
University of Pennsylvania Medical Center
Philadelphia PA
USA

Alan R Maniet DO FAAIM
St Louis University Medical Center
Cardiology Division
St Louis MO
USA

Atlas of Multiplane Transesophageal Echocardiography

Volume 1

Dedication

Clare, Eleanor Isabelle, Eugenie Alice
Christina Marie, Jennifer Ann, Jacqueline Michelle, Alycia Yvonne, Dan, Laura Nicole,
Alan III, Maria

Atlas of Multiplane Transesophageal Echocardiography

Volume 1

Martin G St John Sutton MB BS FRCP
*John Bryfogle Professor of Cardiovascular Diseases and
Director, Cardiac Imaging Program
Cardiovascular Division
University of Pennsylvania Medical Center
Philadelphia PA
USA*

Alan R Maniet DO FAAIM
*St Louis University Medical Center
Cardiology Division
St Louis MO
USA*

MD Martin Dunitz
Taylor & Francis Group

LONDON AND NEW YORK

Contents

Preface

Over the past few years transesophageal echocardiography has become one of the most exciting imaging modalities available today in modern clinical cardiology. Transesophageal echocardiography through its portability, relatively inexpensive equipment and semi-noninvasive nature is currently available and readily accessible to almost every cardiac patient in comparison to other radiographic techniques. Multiplane transesophageal echocardiography is the result of the technologic evolution of echocardiography from single plane and biplane transducers over the past decade. Multiplane transesophageal echocardiography provides high resolution cardiac images in an infinite number of planes which, combined with conventional color Doppler modalities, offers a superlative diagnostic tool for evaluating cardiac structure and function. In addition to enhanced diagnostic capabilities, multiplane technology allows for greater patient safety with less discomfort because transducer manipulation is minimized. The advantages of multiplane transesophageal echocardiography are that it provides an array of multiplane images in real time which offers a three-dimensional perspective of cardiac anatomy that cannot be appreciated even by the cardiac pathologist.

The aim of this atlas is to provide medical students, anesthesiologists, cardiac surgeons and cardiologists with a concise but in-depth analysis of cardiac imaging from an experience of over 10,000 transesophageal echocardiograms performed by the authors. This atlas may also serve as a reference for diagnostic examples of cardiac pathology physicians who practice transesophageal echocardiography. The format of each chapter is consistent throughout, starting with normal cardiac structure and function, followed by abnormalities of structure and function. Chapters include evaluation of prostheses, interventional cardiology techniques and intraoperative transesophageal echocardiography. A concise explanation of measurements of cardiac chamber sizes and function and Doppler are provided only for transesophageal echocardiographic applications. Transesophageal echocardiographic images are juxtaposed with correlative anatomic specimens to provide a clear understanding of normal and abnormal cardiac anatomy.

Martin G St John Sutton
Alan R Maniet

Acknowledgements

1
Normal transesophageal echocardiographic examination

"A picture is worth a thousand words"

Historical perspective

In an effort to overcome the shortcomings of the transducers available for routine transthoracic echocardiographic imaging, the possibility of imaging the heart posteriorly, from within the esophagus, was explored, thus avoiding ultrasound attenuation by the lung. Transesophageal echocardiography grew from the development and the concurrent advancements of the fiber-optic gastroscope, as shown in the historical time line in figure 1.1. Most notably, the development of a flexible scope meant that the transducer could be positioned within the esophagus, aiming the ultrasound beam towards the heart and permitting airfree contact with the esophageal wall.

The evolution of transesophageal echocardiography began essentially with the introduction of an M-mode transducer mounted on an endoscope by Frazin[1] in 1976. Left ventricular function was assessed and monitored by measuring the change in left ventricular dimensions between systole and diastole. Initially, M-mode transesophageal echocardiography was restricted to the surgical arena, with the patient fully anesthetized.

Figure 1.1 Historical timeline illustrating the significant developments of transesophageal technologies. Biplane transesophageal

echocardiography (TEE) was introduced in the early 1980s with multiplane TEE probes introduced almost 10 years later. Multiplane transesophageal technology represents a significant advance in imaging capability over biplane imaging, thus caution should be exercised when evaluating the transesophageal literature so as not to confuse the improved diagnostic capability for multiplane transesophageal echocardiography.
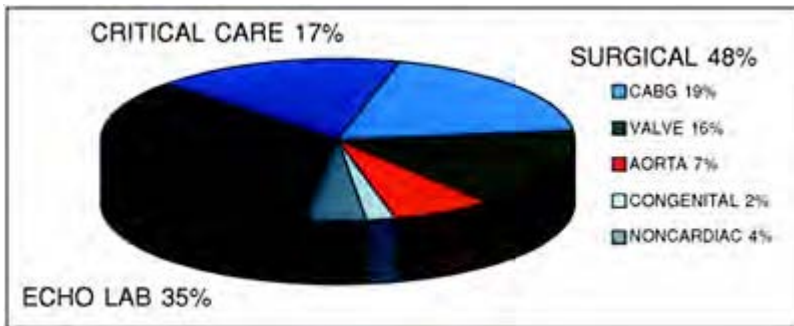
Figure 1.2 Indications for TEE can be grouped according to the venue where TEE is performed. TEE performed in the echocardiography laboratory, largely consist of outpatient studies and comprise 35% of the total number performed. TEEs in this setting are performed to evaluate cardiac source of systemic thromboembolism and for endocarditis. TEEs in the critical care setting include evaluation of patients in the critical care units for deteriorating hemodynamics and in the emergency department to evaluate the aorta for dissection. TEEs performed during

cardiac surgery (48%), constitute the largest number of procedures performed in our institution. transducer in Germany, which changed the focus of transesophageal echocardiography from cardiac monitoring to clinical cardiac diagnosis.

The development of electronic scanners, by Souquet and colleagues[2] in 1982, introduced the first phased-array two-dimensional transesophageal echocardiographic transducer in Germany, which changed the focus of transesophageal echocardiography from cardiac monitoring to clinical cardiac diagnosis.

Single plane transesophageal echocardiography transducers were soon developed for clinical use, with 64 elements using a carrier frequency of 5.6 MHz. These transducers provided excellent resolution and spatial two-dimensional echocardiographic images of the left transverse plane of the left ventricular short axis. Color flow Doppler mapping was added in the mid 1980s, and continuous wave Doppler technology was subsequently incorporated in transesophageal echocardiographic transducers by the late 1980s, setting the standards for the single plane (90° sector) transesophageal echocardiographic transducer.

Biplane transesophageal echocardiographic transducers were developed, which paralleled the introduction of smaller and more flexible endoscopes. Two small 32-element 5.0 MHz transducers in opposite planes were mounted in a linear fashion at the tip of the probe, allowing transverse and longitudinal axis imaging. Despite slight degradation in image quality because of fewer elements, clinical diagnostic utility was established by Hanrath and colleagues[3] in Germany, Seward and colleagues[4] at the Mayo Clinic, and Omoto and colleagues[5] in Japan.

Further advances in endoscope technology led to smaller and more flexible scopes, and to the development of pediatric transesophageal echocardiographic transducers, which utilized fewer elements and higher frequencies (7.5 MHz).

The panoramic transducer introduced in the early 1990s stemmed from the development of the annular array transducer. This technology allows for a wider field of view (approximately 270°), which provides a full transaxial plane of the heart, and paracardiac structures. Development of matrix-array transducers allowed horizontal and longitudinal biplane images to be visualized simultaneously on the viewing screen; however, matrix-array images compromised image resolution and quality.

Multiplane transesophageal echocardiographic transducers were introduced in the late 1980s, which derived from the ability to mechanically steer the transducer array from 0° to 180°. A single transducer using phased-array technology allowed improved imaging capabilities in an infinite number of planes with minimal probe manipulation. Current developments in multiplane technology image acquisition and processing by computer in real time has spurred the dynamic reconstruction of true three-dimensional cardiac imaging in the conscious patient.

Indications

The primary indications for transesophageal echocardiography are when adequate information is not obtained from the transthoracic approach. The excellent cardiac images that are obtained from the transesophageal echocardiogram may entice the echocardiographer or the referring physician to request the transesophageal procedure, resulting in overuse of transesophageal echocardiography. It is important to bear in mind that transesophageal imaging is an invasive procedure, and that the small risk of complication that exists must be outweighed by the information that can be obtained from the transesophageal echocardiogram.
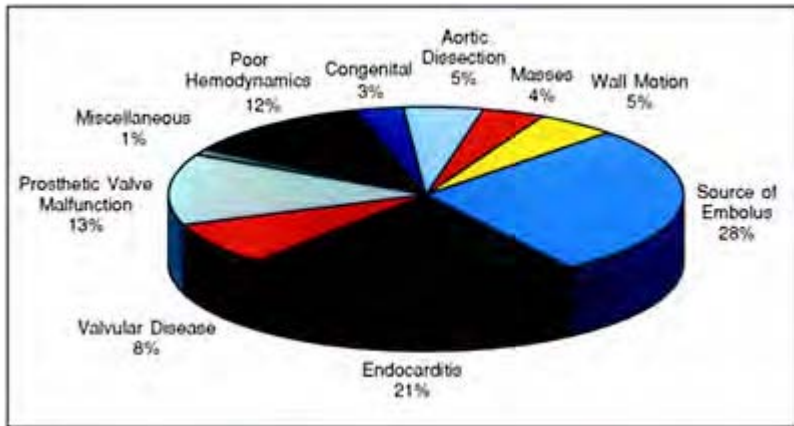
Figure 1.3 The primary indication for transesophageal echocardiography is when adequate information is not obtained from the transthoracic approach. The indications for TEE have evolved over the past decade due to improvements in technology, and the increasing awareness by other subspecialists regarding the information that may be obtained regarding specific cardiac abnormalities. Current indications for TEE vary according to the institution and the availability of the procedure. The pie chart illustrates the indications for performing TEE over the past 10 years.

The primary indications for transesophageal echocardiography are for evaluating the posterior structures of the heart that cannot be adequately visualized due to poor acoustic penetration with standard transthoracic transducers. In our institutions, transesophageal echocardiography is performed only after the transthoracic echocardiogram is performed and reviewed by the echocardiography staff physicians. Cardiac abnormalities are better visualized with multiplane transducers than with monoplane or biplane transducers.[6–10]

The indications for transesophageal echocardiography have evolved over the past decade due to improvements in technology, better understanding of certain disease processes, and realization by other subspecialists of the information that can be obtained about cardiac structure and function (figure 1.2). In the cardiac surgical arena,[11–19] transesophageal echocardiography has expanded its role as cardiac surgeons and anesthesiologists have gained a better appreciation and recognition of the diagnostic opportunities available with cardiac ultrasound. In many academic institutions, transesophageal echocardiography is performed routinely during open-heart surgery. In our institutions, 48% of all transesophageal echocardiograms are done in the operating room. Transesophageal echocardiograms are done routinely during all valve replacement cases (16%) to assess the valve pre-operatively for potential repair or replacement, and postoperatively for mechanical performance, left ventricular function, and to assess the seating of the valve ring and the presence of paraprosthetic leaks. Transesophageal echocardiography plays a pivotal part during the repair of congenital cardiac abnormalities in the pediatric and adolescent population (2%), and has largely replaced cardiac catheterization as the diagnostic procedure of choice.[20–22] Transesophageal echocardiography also has an increasingly important role in routine coronary artery bypass surgery (19%). Transesophageal echocardiography allows the early recognition of complications that may occur during the coronary artery bypass grafting, assists in the weaning from cardiopulmonary bypass, and enables assessment of the results of wall motion abnormalities after bypass graft placement. Although the role of monitoring cardiac function with transesophageal echocardiography initially met with much enthusiasm, it has yet to be fully evaluated prospectively in non-cardiac surgical patients.[23–27] Transesophageal echocardiography may play an extremely important part in non-cardiac surgical cases (4%) when conflicting information is obtained from right heart catheter monitoring, when the patients do not respond appropriately to standard therapy, or when a patient is believed to have sustained a new cardiac event during the perioperative period.

Transesophageal echocardiograms done in the echocardiography laboratory, which comprised 35% of the total number of studies, were largely performed on outpatients for diagnostic purposes; ie, to assess cardiac source of systemic thromboembolism, to rule out endocarditis, to evaluate prosthetic valve function, and to assess cardiac structural abnormalities, etc. (figure 1.2). Transesophageal echocardiograms done in the emergency department or critical care units, which consisted of 17% of the total, have special importance for the patient with hemodynamic collapse, to assess new cardiac and aortic events, and to guide management of intravenous fluid and inotropic therapy.

Current applications and indications

In a review of 10,000 cases done over the past decade by the authors, figure 1.3 illustrates the specific indications for transesophageal echocardiograms. The major indications for transesophageal echocardiography in our laboratories were to rule out a cardiac source of embolus (28%) in patients with cerebrovascular events, to rule out vegetation in suspected endocarditis (21%), and to evaluate valvular disease in native valves (8%) and malfunction in prosthetic valves (13%).

Cardiac source of embolism

Transesophageal echocardiography has opened a whole new arena for identifying intracardiac thrombi and other cardiac sources of thromboembolism.[28–30] Transesophageal echocardiography is ideally suited for identifying thrombi, vegetation, intracardiac masses, and tumors, pannus around prosthetic valves in the left heart chambers, and atheromatous plaques and thrombus in the ascending, transverse, and descending aorta.[31–33] Structural abnormalities that predispose to formation or allow the transit of thrombi from the venous system to the arterial system are easily visualized. These abnormalities, which include atrial septal aneurysm, patent foramen ovale, right to left shunts, and spontaneous echocardiographic contrast (signifying stasis of blood flow), are all readily recognized with transesophageal echocardiography. In patients with suspected pulmonary embolism, clots may be seen in the right heart chambers, and, during the acute event, may even be seen in the proximal pulmonary arteries.[34–36]

Transesophageal echocardiography is used as a screening tool to detect left atrial thrombus prior to cardioversion and also before mitral balloon valvuloplasty.[37,38] Many large-scale studies are currently underway to determine the efficacy and use of transesophageal echocardiography in these clinical situations.

Endocarditis

Multiplane transesophageal echocardiography is a sensitive tool for detecting vegetations in patients with bacteremia and suspected endocarditis.[39–41] Vegetations can be identified on valves or shunt regions down to approximately 2 mm in diameter. Transesophageal echocardiography plays a major role in assessing the valvular and paravalvular complications that lead to hemodynamic compromise in patients with documented endocarditis. The results of transesophageal echocardiography have been so encouraging that transesophageal echocardiography is commonly requested in patients with bacteremia irrespective of clinical signs or symptoms. However, when endocarditis is suspected, there should be a low threshold for recommending transesophageal echocardiography.

Valvular and prosthetic valvular disease

Transesophageal echocardiography plays a major part in the assessment of valvular disease when adequate image quality or image resolution is not achieved from transthoracic echocardiography imaging. Patients are frequently taken directly to surgery on the basis of echocardiographic results, without preoperative cardiac catheterization.[42–45] Transesophageal echocardiography is extremely useful for visualizing the aortic valve orifice and the number of cusps present in aortic stenosis, for evaluating the mitral and tricuspid valvular apparatus before surgical valve repair, and to assess postoperative results. Transesophageal echocardiography is of great value in determining the suitability for transcatheter mitral balloon valvuloplasty and for excluding atrial thrombi that are a contraindication for mitral valvuloplasty. Abnormalities of the pulmonary valve can only be reliably and fully appreciated with transesophageal echocardiography.[46] A comprehensive evaluation of prosthetic valves can be done more easily with multiplane transesophageal echocardiography because the transducer can be maneuvered around the acoustic shadowing and ghosting produced by the mechanical components of the prosthesis.

Poor hemodynamics

In critically ill patients,[47] transesophageal echocardiography can provide invaluable information, and is commonly useful in identifying the cause of hemodynamic collapse. Transthoracic echocardiography is frequently inadequate because of suboptimal image quality, in part because positioning of the patient does not usually give optimum echocardiographic windows, and it therefore is not possible to obtain the necessary echocardiographic views. Transesophageal echocardiography is important for detecting or excluding the presence of new global or regional wall motion abnormalities, for assessing left and right heart systolic function, and detecting diastolic dysfunction, and restrictive and tamponade physiology.

Cardiac mass and tumor

Transesophageal echocardiography is the diagnostic method of choice for detecting cardiac masses and tumors,[48–50] especially when the diagnosis by transthoracic echocardiography is equivocal. There is debate over the sensitivity of transesophageal echocardiography compared with magnetic resonance imaging (MRI); however, transesophageal echocardiography is easier to obtain because it can be brought to the bedside and also because MRI is not available in every medical institution.

Thoracic aorta

Transesophageal echocardiography is excellent for the evaluation of aortic aneurysm, aortic rupture, and dissection.[51,52] Transesophageal echocardiography is the procedure of

choice for diagnosing acute aortic dissection allowing early classification of the type of dissection, and identification of the entry and re-entry site or sites of the initial tear and planning management. Transesophageal echocardiography enables measurements of the aorta in regions of aneurysmal dilation, and determination of the size of the aortic annulus for selecting appropriate graft sizes. Transesophageal echocardiography is also helpful in identifying sites of aortic atheromatous plaques and thrombus in the ascending aorta, arch, and, in the descending aorta.

Contraindications

Contraindications to multiplane transesophageal echocardiography are the same as those for monoplane and biplane transesophageal echocardiography. Contraindications may be considered relative or absolute as in table 1.1. The risk of transesophageal echocardiography must be considered according to the clinical circumstances, so that the benefit of establishing the diagnosis outweighs the risk of complication.

Transesophageal echocardiographic transducers are passed in a "blind" fashion. Transesophageal echocardiography should not be done in patients with esophageal neoplasm, severe stricture, laceration, and perforations, or esophageal diverticulum. The gastroenterology specialist is usually extremely helpful in determining which patients

Table 1.1 Contraindications for transesophageal echocardiography

Relative
Recent meal
Recent GI or abdominal surgery
Therapeutic endoscopy
Gastrointestinal hemorrhage bleed
Unevaluated dysphagia
Esophageal varicies
Large hiatal hernia
Absolute
Severe stricture
Esophageal neoplasm
Esophageal trauma/laceration
Esophageal perforation
Esophageal diverticular disease

should not undergo a transesophageal echocardiographic examination.

Transesophageal echocardiography should not be done when there is instability of the cervical spine. This is very important to consider in trauma patients when the trauma team is requesting a transesophageal echocardiogram to evaluate a cause for a widened mediastinum. The authors have done many transesophageal echocardiography examinations in patients with neck braces and Philadelphia collars without consequence.

The procedure is technically more difficult, because the patient is usually supine even when conscious. It is easier to pass the probe when the patient is heavily sedated if the sedation is tolerated hemodynamically; however, it is safer to pass the transesophageal probe when these patients are intubated.

The most important relative contraindication, in our experience, is performing a transesophageal echocardiogram when the patient is not in the fasting state. It is advantageous to wait for at least a minimum of 4–6 hours after eating before intubating the esophagus, to prevent aspiration of the stomach contents. In critically ill patients this may not be possible, and good judgment must be used to assess the risk/benefit ratio. In selected patients with severe trauma with suspected aortic dissection, we have performed gastric lavage via a nasogastric tube to empty gastric contents prior to transesophageal echocardiography.
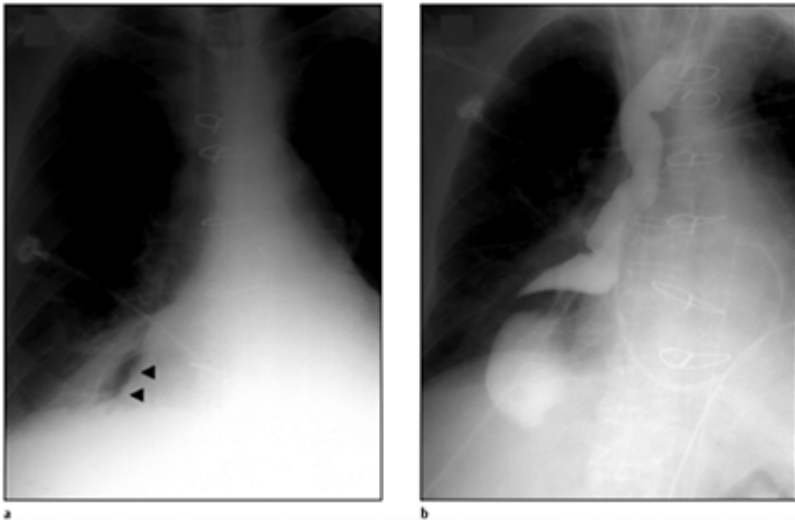

Figure 1.4 (a) Standard P–A chest X-ray demonstrating the radiographical appearance of a large hiatal hernia with the abnormal displacement of the gastric air bubble. (b) Barium swallow demonstrating an abnormal esophagus associated with a large hiatal hernia. A history of dysphagia or hiatal hernia may warrant further investigation before attempting TEE to eliminate complications during the procedure.

Other relative contraindications include recent gastrointestinal surgery, recent abdominal surgery, therapeutic endoscopy, upper gastrointestinal bleeding, unevaluated

symptoms of dysphagia, esophageal varicies, and large hiatal hernias. When considering recent gastrointestinal surgeries, recent major abdominal surgeries must be included, because positioning the patient with a large incision may be difficult and retching may deleteriously affect the surgical incision. For these reasons, transesophageal echocardiography is generally postponed for 6–8 weeks in non-life-threatening cases. Gastrointestinal consultation must be done before deciding to perform the procedure. In a few patients, esophageal varicies have been discovered during transesophageal echocardiography, and we have been surprised that we have had no complications in these cases. We have frequently done transesophageal echocardiography in our institutions during liver transplantation and have not experienced problems, since portal hypertension is usually relieved once the patient is anesthetized and the liver is removed. In patients with large hiatal hernias it is helpful to observe the gastric air bubble on the chest X-ray (figure 1.4), looking for deviation of the bubble to the right or left chest to help determine if the patient might present a problem when entering the stomach with the probe, thereby limiting the examination to the lower and mid esophagus in these patients.

Complications

Although transesophageal echocardiography is a safe procedure, there is always the potential risk of minor or major complications. Our complication rate is comparable to the experiences reported by the European Multicenter Trial[53] and by the Mayo Clinic.[54] In the authors' experience, there were 226 major and minor complications (2.3%) noted during the first 10,000 transesophageal echocardiograms done (figure 1.5). There is a learning curve for performing transesophageal echocardiography, after which the likelihood of complications drops, which usually occurs after the first 200 cases. Complications are either mechanical problems in passing the probe that are directly related to the transducer and are similar to those for all upper endoscopic procedures, or those related to topical oral anesthesia, intravenous sedation, emotional instability related to the patient's anxiety level, or physiological problems related to the underlying medical condition. Mechanical problems consist of esophageal perforation or laceration, contusions and lacerations to the oropharynx, mouth, and tongue edema, and extrinsic pressure to paraesophageal structures consequent on probe buckling. Esophageal perforation occurs in 0.02% of cases during diagnostic gastrointestinal endoscopy and in 1–8% of cases during therapeutic gastrointestinal endoscopy.[55–57] Since transesophageal echocardiography is a blind procedure, the prevalence of perforation is probably between 0.05 and 0.10% because the probe is larger that those currently used by most gastroenterologists, and sometimes a history of gastrointestinal pathology is not available. There are only sporadic reports of esophageal perforation related to transesophageal echocardiography, indicating that it is a rare complication. However, the transesophageal echocardiographer should be aware that the reported mortality for endoscopy-related esophageal perforation approaches 50%. Mortality of an esophageal perforation is highest when diagnosis and treatment are delayed, and depends on the location of the tear (upper versus lower esophagus). Cervical or upper perforations usually result from esophageal intubation, especially when there is initial difficulty in passing the scope. Perforation of

the esophagus in the cervical region is usually better tolerated and carries a lower mortality.
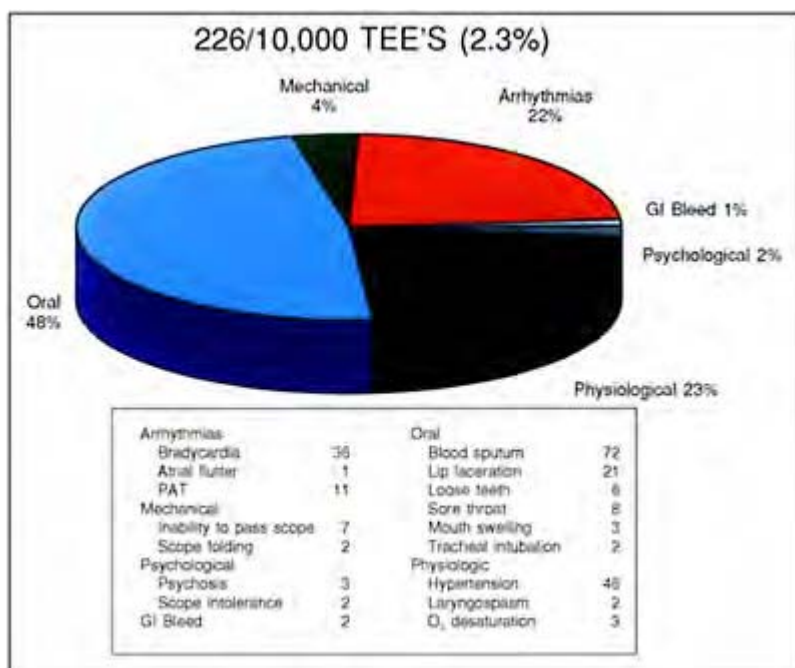

226/10,000 TEE'S (2.3%)

Mechanical 4%

Arrhythmias 22%

GI Bleed 1%

Psychological 2%

Physiological 23%

Oral 48%

Arrhythmias		Oral	
Bradycardia	36	Blood sputum	72
Atrial flutter	1	Lip laceration	21
PAT	11	Loose teeth	6
Mechanical		Sore throat	8
Inability to pass scope	7	Mouth swelling	3
Scope folding	2	Tracheal intubation	2
Psychological		Physiologic	
Psychosis	3	Hypertension	48
Scope intolerance	2	Laryngospasm	2
GI Bleed	2	O₂ desaturation	3

Figure 1.5 It is important to consider that transesophageal imaging is an invasive procedure and that there is a small risk for minor or major complications. There is a learning curve for performing TEE, after which the prevalence for complications decreases. The pie chart illustrates the complications experienced over the past decade.

Perforation of the lower esophagus usually occurs with manipulation of the probe at a site of esophageal disease. Perforation of the lower thoracic esophagus carries a higher mortality due to mediastinitis and pleural infections, which usually require immediate repair and drainage. The most frequent symptom of esophageal perforation is exquisite chest pain. The hallmark of cervical perforation is crepitus and tenderness in the neck, development of nasal speech, and radiographic evidence of air in the cervical prevertebral space (figure 1.6a). Lower thoracic esophageal perforations usually present with a new pleural effusion, pneumothorax, or pneumomediastinum on chest X-ray. Radiographic

contrast studies are very helpful in locating the site of perforation (figure 1.6b). In the cases of esophageal perforation known to the authors, patients developed hemodynamic collapse during the procedure. If perforation is suspected, appropriate attention should be given to the patient.
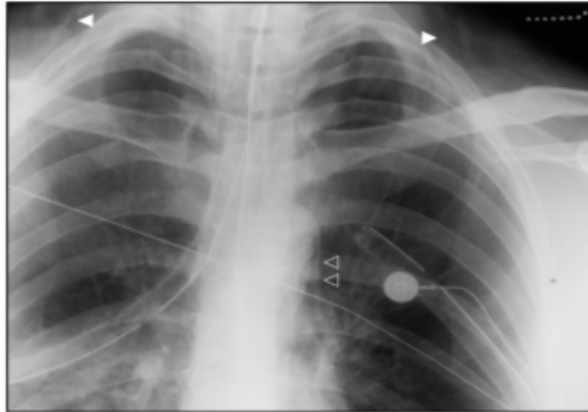
a
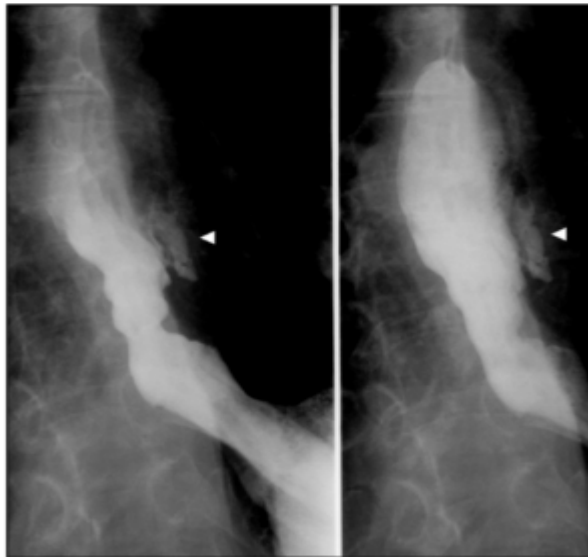
b

Figure 1.6 The most devastating complication of transesophageal echocardiography is esophageal perforation. Esophageal perforation can occur in the cervical esophagus or

in the lower esophagus during esophageal endoscopy. Recognition of esophageal perforation is paramount to patient survival. (a) Plain film P–A chest X-ray demonstrating signs of upper esophageal perforation. Subcutaneous emphysema denoted by the solid arrows and mediastinal air, open arrows. (b) Radiographic contrast study obtained in a patient with suspected lower esophageal perforation. Abnormal lower esophageal contour with extravasation of contrast agent (solid arrow) outside the esophageal lumen above the gastroesophageal junction.

Small minor lacerations of the oral mucosa, gums, and lips may be treated supportively. Occasionally, in patients with poor and loose dentition, passage of the transesophageal probe may dislodge a tooth, therefore care must be taken to insure that loose teeth are recognized before the procedure and that aspiration is avoided. Mouth and tongue edema have been reported, possibly related to prolonged examination times usually during prolonged intraoperative monitoring.

There are various reports of damage to paraesophageal structures transmitted by pressure exerted by manipulation of the larger probes.[55–57] One report describes laryngospasm induced by pressure applied to the trachea causing airway obstruction. These types of complications are more prevalent in the younger pediatric population in whom the size of the probe is more important. Transient vocal-cord paralysis has been reported after a prolonged neurosurgical procedure. Vocal-cord damage may also occur after mistaken tracheal intubation with the probe.

Buckling of the probe[58] may occur during difficult intubations, especially when the patient is uncooperative. When buckling of the tip of the probe occurs (ie, the tip folds up on itself), the probe is difficult to maneuver and causes crushing pain when manipulation of the probe is attempted. This complication has occurred in our laboratories when smaller probes have been used in large adult patients. When buckling of the probe occurs, the patient is given more sedation and/or analgesia, and the probe is slowly passed into the stomach, which allows it to unfold. In our patients, following this maneuver, a full study was completed.

There have been several reports of contact pressure damage from the probe during prolonged examinations[59,60] but this is transitory and no significant residual damage has been reported. There has been no damage to the lungs reported from the effects of continuous ultrasound during open heart procedures, nor is there any conclusive evidence of thermal injury from the probe, as was initially suspected.

Most complications that occur are related to the procedure itself and to the patient's underlying clinical condition. In our experience, hypertension and cardiac arrhythmias, which are usually self limiting and without hemodynamic consequence, are the most common minor complications. They are probably caused by exaggerated sympathetic response in anticipation of and during performance of the procedure. Although patients are kept fasting before the procedure, we permit medications with small sips of water. Occasionally the patient voluntarily withholds medications, or is instructed to do so by the referring physician, which may predispose them to these types of complications.

Laryngospasm can occur after application of topical oral anesthesia or by inhalation of the anesthetic agents. In our experience this is generally short lived, lasting approximately 15 minutes, and is relieved by securing an open airway and administration of oxygen by nasal cannula. Lidocaine toxicity has been reported on rare occasions during transesophageal echocardiography from topical oral anesthesia. Care should be exercised when using these agents in critically ill patients who may have a high lidocaine level (patients receiving lidocaine intravenously for arrhythmia control)[61] or in patients with congestive heart failure or liver dysfunction that can not clear these agents. This complication is manifested by mental confusion.

Inability to pass the probe during intubation is rare, but occurs most notably after trainees make multiple attempts, thereby losing the patient's cooperation. This complication diminishes with operator experience and with adequate conscious intravenous sedation. Some patients will refuse to continue with the examination once the probe is passed, on account of extreme anxiety at the sensation of the probe in the pharynx and esophagus.

We have also experienced anxiety and emotional problems in patients with a history of drug or alcohol abuse. Two patients with a history of substance abuse not revealed during preparation had psychotic episodes with the administration of sedation, and the procedure had to be terminated prematurely.

Aspiration pneumonia is probably more common than currently reported, and can occur with or without the administration of sedation. Aspiration can be anticipated in patients who are not fasting, or who have significant retching, vomiting, and coughing, or who are uncooperative during the procedure. Additionally, in patients that are difficult to position properly during the procedure, difficulty may arise in protecting their airway, making these patients more prone to aspiration. Generally this complication is unrecognized, but occasionally treatment is required, especially in cases where the diagnosis is delayed. Aspiration should be suspected when the study is prolonged, if the patient has a previous history of aspiration and desaturation, or if respiratory difficulty is recognized during monitoring. In the authors' experience, aspiration is more common in the subset of patients with recent cerebrovascular events, and accounts for most patients (95%) who aspirated in our series (illustrated in figure 1.5). It is not unusual that these patients present with new, underestimated swallowing difficulties and gastrointestinal dysfunction due to their recent cerebrovascular event—the tendency is to probably undersedate these patients, which may result in more difficulty when passing the transesophageal probe. In addition, oversedation may easily occur, rendering the patient incompetent to handle secretions during and after the procedure.

Most procedure-related complications are due to the administration of intravenous sedation to conscious patients. Multiple agents may be used, but in hospital the selection

of narcotics it generally dictated by the anesthesia department or by conscious sedation policies set forth by the hospital. In our institution, we use midazolam in doses up to 10mg intravenously. At doses higher than 5 mg, the patient must be carefully observed for signs of respiratory depression, and may require reversal with flumazenil. Despite all the precautions taken outlined above, in occasional patients conscious sedation needs to be reversed and may require temporary respiratory support with a mask and ambu bag or, rarely, tracheal intubation and ventilation.

Bradycardias may occur during conscious sedation, especially with the propensity for patients to perform uninstructed Valsalva type maneuvers during esophageal intubation. Bradycardia usually occurs during the initial intubation and resolves promptly during the exam. When bradycardia persists for more than 5 minutes into the examination, it invariably responds to 0.5 mg intravenous atropine sulfate. The operator must be aware that bradycardias may reflect respiratory difficulty or hypoxia.

Hypotension may occur during the procedure and may be attributed to multiple factors: intravenous sedation, narcotics, analgesics, and hypovolemia accentuated in cardiac patients by prolonged fasting prior to the procedure. Hypotension usually responds quickly to administration of intravenous fluids.

Antibiotic prophylaxis

The routine use of antibiotics for endocarditis prophylaxis is not warranted during transesophageal echocardiography. The risk of bacteremia during transesophageal echocardiography is extremely low[62–68] and there have been only sporadic reports that implicate transesophageal echocardiography as a cause of endocarditis. It is probably not reasonable to associate the risk for bacteremia from transesophageal echocardiography with that of general gastroenterology endoscopy, since there is a greater chance of developing bacteremia when the mucosal barrier of the esophagus is broken with biopsy or therapeutic measures. Therefore, the use of antibiotics during transesophageal echocardiography is left to the discretion of the operator.

In our institutions, routine antibiotic prophylaxis is not used. Recommendations by the American Heart Association (AHA) for the prevention of bacterial endocarditis were revised recently in 1997.[69] Endocarditis prophylaxis is not recommended for transesophageal echocardiography, but prophylaxis is optional for high-risk patients. The antibiotic recommendations for high-risk patients pertaining to transesophageal echocardiography are listed in table 1.2. The AHA high-risk category for conditions associated with endocarditis include: prosthetic cardiac valves, including bioprosthetic and homograft valves, previous bacterial endocarditis, complex cyanotic congenital heart disease (single ventricle states, transposition of the great arteries, tetralogy of Fallot), and surgically constructed systemic pulmonary shunts or conduits.

Table 1.2 Prophylactic regimens for
dental,oral,respiratory tract,or esophageal
procedures

Situation	Agent	Regimen
Standard general prophylaxis	Amoxicillin	Adults 2.0 g; children 50 mg/kg orally 1 h before procedure
Unable to take oral medications	Ampicillin	Adults 2.0 g IM or IV; children 50 mg/kg IM or IV within 30 min before procedure
Allergic to penicillin	Clindamycin or	Adults 600 mg; children 20 mg/kg orally 1 h before procedure
	Cephalexin+ or cefadroxil+ or	Adults 2.0 g; children 50 mg/kg orally 1 h before procedure
	Azithromycin or clarithromycin	Adults 500 mg; children 15 mg/kg orally 1 h before procedure
Allergic to penicillin and unable to take oral medications	Clindamycin or	Adults 600 mg; children 20 mg/kg IV within 30 min before procedure
	Cefazolin+	Adults 1.0 g; children 25 mg/kg IM or IV within 30 min before procedure

IM = intramuscularly; IV = intravenously.
*Total children's dose should not exceed adult dose.
+Cephalosporins should not be used in individuals with immediate-type hypersensitivity reaction (urticaria, angioedema, or anaphylaxis) to penicillins.
Ref: Dajani AS, Taubert KA, Wilson W, et al. Prevention of bacterial endocarditis: recommendations by the American Heart Association. *JAMA* 1997;227:1794–801.

Esophageal intubation

Successful intubation of the esophagus with the transesophageal echocardiography transducer is dependent upon the patient's willingness to have the procedure performed. Most patients that present for transesophageal echocardiography have misconceptions and apprehension before the procedure. Good patient preparation and satisfaction after the procedure requires a thorough explanation of the procedure ahead of time, including how the results will be handled, and reassurance before and during the procedure. Due to the general perception of echocardiography being a non-invasive procedure, we have observed that the invasive nature of transesophageal echocardiography is commonly overlooked by physicians in training as well as by referring physicians. Since transesophageal echocardiograms may be done on an emergency basis the contraindications, especially noting when the patient ate last, are frequently ignored. Due to the relative ease and portability of transesophageal echocardiography and the potential for obtaining a rapid diagnosis, the appropriate indications for performing the procedure may be overlooked. Although the risk of a transesophageal echocardiogram is low, complications can and will occur if adherence to a systematic protocol is omitted.

Techniques of esophageal intubation

Conscious patient

In the awake patient, topical oral anesthesia is required. Before any sedation or anesthesia is given, the procedure of transesophageal echocardiography and the likelihood of obtaining a diagnosis are explained to the patient by the physician performing the study, and written informed consent is obtained. In our laboratory, patients are placed on a stretcher and sit upright initially to avoid aspiration during the administration of oral anesthesia. All dental appliances are removed. Patients are presented with a lidocaine popsicle, which is a 4 × 4 inch gauze pad, applied to a tongue blade which is saturated with 5% lidocaine paste. The patient sucks on the popsicle for 5 to 10 minutes. The nurse or sonographer applies the EKG electrodes, automated blood pressure cuff, and O_2 saturation device. The patient is instructed to expect slight discomfort, which usually
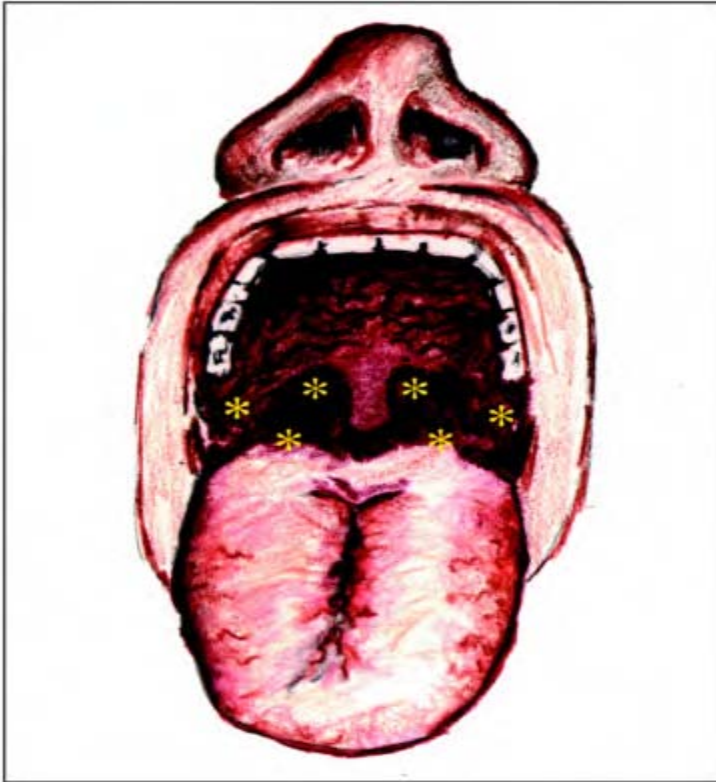
Figure 1.7 Adequate pharyngeal anesthesia is important for patient comfort during the TEE procedure, especially during prolonged

examinations. The diagram illustrates key areas (stars) for administering topical anesthesia to provide adequate anesthesia.

resolves after passage of the transducer. The pharynx is then anesthetized with 10% lidocaine spray (figure 1.7). The patient is instructed to fully exhale and then hold his breath as the tongue is maneuvered to adequately anesthetize the whole pharynx.

Patients are instructed that they experience a choking sensation, dryness of the throat, and numbness of the mouth. Adequate pharyngeal anesthesia cannot be overemphasized since it is usually the deciding factor in patient comfort that determines the success in passing the transducer. Drying agents are generally not necessary and do not prevent drooling in our experience, but are left to the discretion of the individual physician performing the procedure. Nasal oxygen is used in all patients that receive intravenous conscious sedation, and the patient is instructed to breath through their nose during the procedure. The patient is also instructed to pant to overcome the sensation of gagging during the procedure, and this is rehearsed before transducer insertion. We have found that in many patients good oral anesthesia is all that the patient requires, but if apprehension or anxiety persist at this point intravenous sedation may be administered if necessary. Patients are also given the option of intravenous sedation during the procedure. We have observed that mild sedation generally stabilizes labile hypertension and reduces the incidence of cardiac arrhythmias.
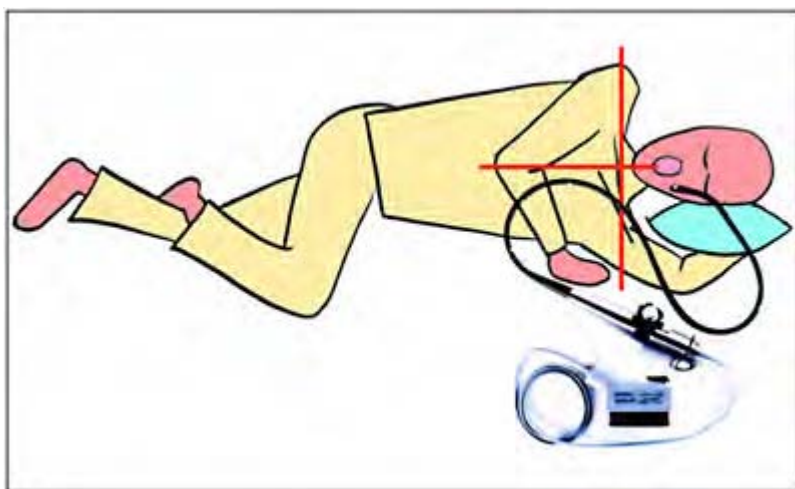
Figure 1.8 Diagram illustrating proper patient positioning in a TEE examination in a conscious patient. To aid in esophageal intubation it is important to maintain proper

anatomical alignment of the head to ensure a straight path for probe insertion. The two major reasons for difficult esophageal intubation is improper head and neck alignment and an uncomfortable patient.

The patient reclines on the stretcher with the head of the bed placed upright at 10 to 15° in the left lateral position (figure 1.8). The right leg is bent and locked behind the left knee. The left arm is folded and rested behind the patient's head. The blood pressure cuff and an intravenous line are placed in the right arm to allow easy access during the procedure. Intravenous lines are routinely placed in all patients who may require intravenous sedation, rhythm control, or who need a contrast echo study. The patient's head is propped up in anatomical alignment so that the neck is not laterally flexed, twisted, or extended (figure 1.8). The neck is flexed so that the chin touches the chest, which opens the pharynx and prevents the transducer from entering the airway. The two major reasons for difficulties in transducer intubation are: first not ensuring the proper alignment of the head and neck; and second, not ensuring the patient's comfort. The overhead lights are dimmed, and the transducer is not shown to the patient unless requested, to avoid any anxiety about the size of the transducer. The transesophageal echocardiographic transducer is not connected to the machine before intubation to allow easier manipulation and less resistance during intubation. This is especially important with mechanical transducers that vibrate, which can cause excessive gagging during transducer insertion. When the transducer is placed on the back of the tongue the patient is instructed to swallow. Careful attention to the transducer is necessary at all times during the procedure, and slight traction is constantly applied to the transducer to prevent buckling in the oral cavity that promotes gagging. In patients with excessive secretions, tonsillar suction should be immediately available, and the patient is instructed that drooling may occur during the procedure.

All instrument controls should be in the free (unlocked) neutral position (figure 1.9). Bite blocks are used unless the patient is edentulous, to prevent damage to the transducer's protective covering if the patient inadvertently bites down during intubation. There are two methods to use the bite block during intubation. Many operators prefer to position the bite block in the mouth, in the midline prior to intubation, and the transducer is introduced in this fashion. This technique has the advantage that it is easier for some patients to swallow as they bite on the guard, but the operator has less control of the tip of the transducer unless the index finger is used to guide the probe. Alternatively, the bite block may be mounted on the probe and passed up to the control handle. Care must be observed not to mount the bite block backwards, which is done occasionally by trainees.

The tip of the transducer is lightly coated with 2% lidocaine jelly for lubrication. The operator faces the patient's mouth as the nurse or sonographer assistant supports the back of the patient's head. The transducer is slightly anteflexed and placed into the mouth in the midline. The face of the transducer should be resting square on the tongue so that when it is advanced it is facing anterior with respect to the patient. The probe is gently passed over the tongue into the pharynx (figure 1.10). In small patients, full flexion of the transducer may be too large for the oropharynx and soft palate, so the tip of the probe
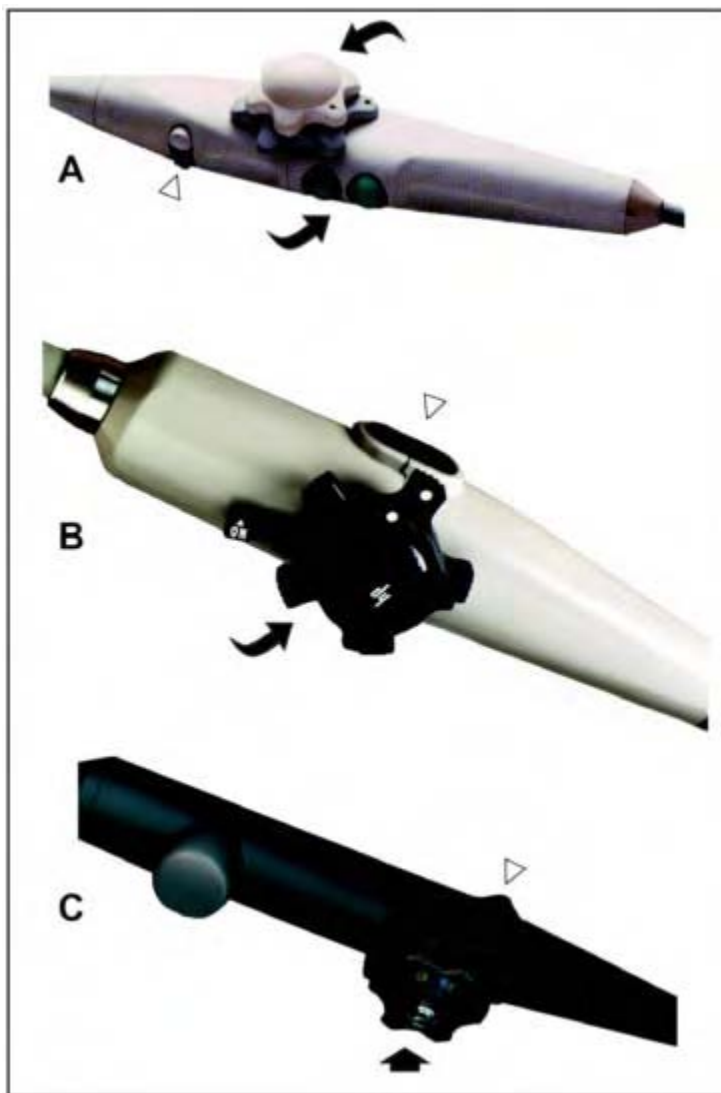
Figure 1.9 Photographs of currently available TEE probe handles, demonstrating the placement of knobs for probe tip flexion and transducer rotation.

must be manually anteflexed and guided with the index finger into the pharynx. The probe is advanced approximately 10–15 cm into the midline of the pharynx and held there for a few seconds, so that the patient gets used to the feel of the probe in the mouth. Slight traction is placed on the probe to pull it forward against the tongue, preventing the

probe from buckling in the back of the oropharynx and stimulating the gag reflex. The patient is instructed to take a deep breath, which reinforces the patient's confidence. The probe is then advanced in the midline to the esophageal orifice and the patient is instructed to swallow, which helps open the upper esophageal sphincter. When the sphincter relaxes, it produces a popping sensation as the operator advances the probe with slow steady pressure to approximately 45–55 cm. The tip of the transducer should then be in the stomach. If the probe is not in the midline, or if the patient manipulates the probe
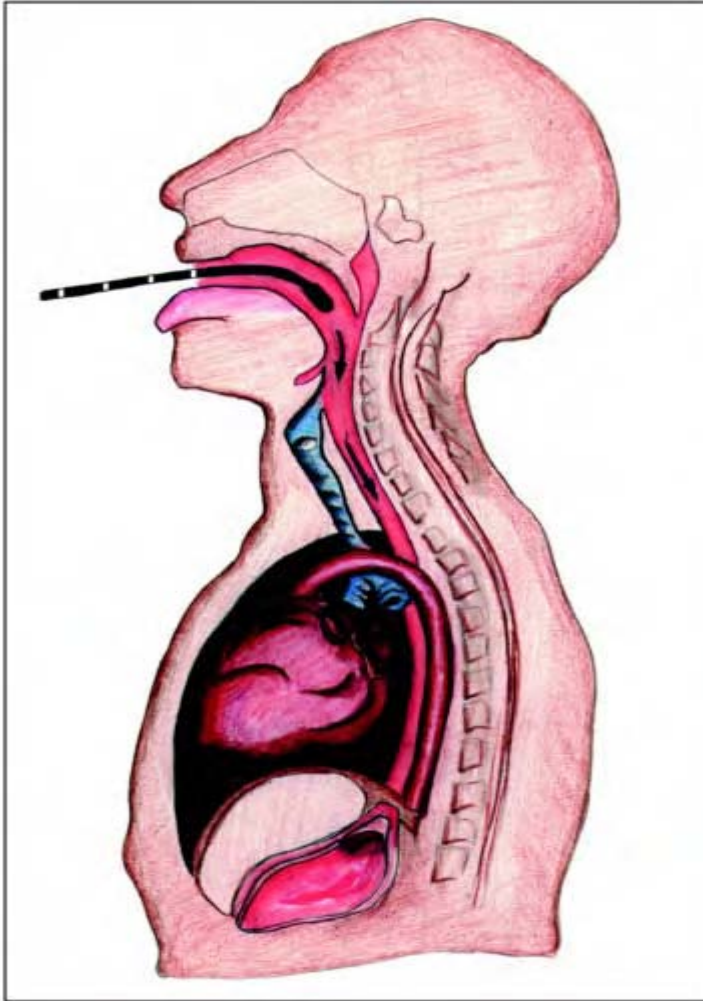
Figure 1.10 Anatomic drawing displaying the course of the TEE probe from the oral pharynx to the esophagus. The esophagus is posterior to the trachea and esophageal intubation may be performed with more ease with mild forward flexion of the neck (ie chin to chest position). The first

obstacle encountered in passing the TEE probe in some patients is getting the transducer head past the soft palate. Different TEE probes may be easier to pass in these regards.

with their tongue, the tip of the transducer usually enters one of the piriform fossae, which lie lateral to the upper esophageal sphincter. If the operator can not pass the probe beyond 15–20 cm before resistance is encountered, and the patient complains of pressure or pain in the neck region, the probe should be withdrawn immediately and redirected toward the midline. Failure to do so can result in rupture of the upper esophagus, which is the most common site of endoscopic perforation. Occasionally, smaller transducers can pass into the trachea, when resistance is encountered and the patient develops intractable coughing. The transducer must immediately be withdrawn, with a slow steady traction to avoid injury to the vocal cords. The patient should be allowed to stop coughing and relax before further attempts are made to pass the transducer. Vital signs should be checked for hypoxia and bradycardia. The operator or assistant should auscultate the lung fields and upper airway for laryngospasm, and the patient should be instructed to talk. If an abnormality is found or suspected the procedure should be abandoned and appropriate action taken.

When the transducer can not be easily passed in patients with thick, short necks or with excessive gag reflexes, the scope may be passed successfully in the sitting position with the head flexed forward to keep the airway patent. It is helpful to have the back of the patient's head supported by the assistant to avoid the patient pulling away and extending the neck and sustaining injury. Some operators allow the patient to hold on to the probe as it is being passed. This technique should be avoided as it reduces the operator's control, and may result in injury if the patient pulls the probe out rapidly. During esophageal intubation, intravenous sedation can be given at any time as required to aid in patient compliance when the transducer is being passed. The re-administration of oral and topical anesthesia should not be repeated with the patient lying down or following sedation, since this increases the likelihood of aspiration.

Once the transducer is in the stomach, the bite guard should be secured in the mouth firmly between the teeth. The operator should apply steady traction of the probe in order to avoid excessive manipulation.

Sporadically, resistance is met between 35 and 45 cm in patients with hiatal hernias. If the patient is repositioned toward the prone position, the transducer tip may find the lower esophageal sphincter and be advanced into the stomach. Care must be taken never to advance the probe forcefully because excessive manipulation may cause retching and vomiting of gastrointestinal secretions, or rupture of the distal esophagus.

Unconscious patient

In the unconscious or anesthetized patient a different approach is required, since the patient is usually in the supine or semi-supine position and intubated. These patients are usually the easiest to perform esophageal echocardiograms upon, but the operator must pay careful attention to the endotracheal tube to avoid extubating the patient. The object of esophageal intubation is to adequately open the oropharynx to allow passage of the probe. If a nasogastric tube is in place, it may be necessary to remove it in order to pass

the transducer after initially aspirating the gastric contents. The operator should be positioned at the head of the table. The mouth should be inspected for previous injury and loose teeth. The transducer should be held with the left hand, with all
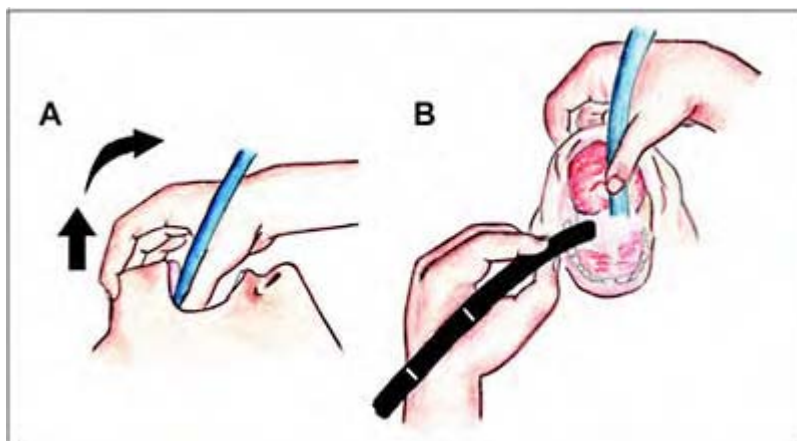

Figure 1.11 TEE esophageal intubation may be most difficult in the unconscious patient, especially when there are multiple tubes present in the pharynx. This drawing demonstrates the proper technique for TEE probes insertion in the unconscious, endotracheal intubated patient in the supine position. (a) The endotracheal tube is supported with the thumb and gentle traction is applied to the mandible, pulling up and cephalad. This maneuver opens the posterior pharynx allowing entry to the upper esophagus. (b) Frontal view demonstrating the same maneuver.

of the controls free and unlocked (figure 1.11a,b). The handle can dangle free towards the floor, or the probe can be draped over the operator's left shoulder. If the sonographer assistant supports the probe, care must be taken to follow the motion of the operator, so as not to twist the transducer or inadvertently move or lock the controls. The right hand is used to support the endotracheal tube and open the oropharynx. The operator should open the thumb and forefinger to form a letter "C". The thumb is inserted along the endotracheal tube with the tongue sandwiched between the tube and the floor of the

mouth. The index and second fingers are wrapped around the mandible, with the tips of the fingers in the submandibular fossa. With this position, the jaw can be moved upwards and outwards with slightly cephalic traction, to open the oropharynx. The transducer is then easily passed with the left hand without resistance in the midline. If resistance is felt or if the scope can not be passed further than 15 to 20 cm, the esophagus is probably compressed by the inflated endotracheal cuff (balloon). In this case a few cubic centimeters of air can be removed from the endotracheal cuff until the probe is passed and then the cuff should be reinflated. Extreme caution should be exercised with this maneuver since it will be easy to inadvertently remove the endotracheal tube and extubate the patient. In rare cases, a laryngoscope may be necessary to help support the endotracheal tube and directly visualize the esophagus in order to pass the probe, to avoid esophageal perforation. In our experience, all cases of upper esophageal perforations from transesophageal echocardiography have occurred in unconscious patients. The transducer is then passed into the stomach.

Throughout the procedure, continuous monitoring of blood pressure, heart rate, oxygen saturation, and electrocardiography is mandatory in both conscious and unconscious patients, and permanent records of all three should be obtained in each patient. Following completion of transesophageal echocardiography the patient's oropharynx will remain partially numb and the protective gag reflex will not completely return for 4 hours, and therefore patients should not eat or drink for 4 hours after the procedure. Furthermore, when conscious sedation is used, blood pressure O_2 saturation and ECG should be monitored for 1 hour after the procedure, and the patient should not be permitted to drink for 4–6 hours.

Multiplane transesophageal echocardiography examination

The main advantage of multiplane imaging is that the transducer may be electronically or mechanically steered from 0° to 180° (figure 1.12). One transducer allows imaging with more elements for visualization, and permits multiple frequencies in the same size or smaller transducer shafts than previously available (figure 1.13). This allows multiple planes between 0° and 90°, with less rotation and/or lateral and medial flexion than would be necessary with a biplane probe. Thus, patients tolerate a multiplane examination much better than a biplane examination, even though multiplane transducers are generally larger.

The multiplane transducer is oriented perpendicular to the shaft of the probe in a horizontal or transverse plane. The sector or ultrasound beam at this point is at 0°. When the transducer array is rotated to 90° with the switch on the control handle, the ultrasound beam orientation and sector is parallel to the shaft of the probe and gives a longitudinal or sagittal plane of the heart. All of the available echocardiographic instruments have a specific icon on the display, which orients the operator to the degree of rotation of the transducer position

The operator must be extremely familiar with the viewing screen of the particular echocardiographic instrument used, in order to recognize readily the proper image orientation. The operator should also be familiar with the recommendations of the American Society of Echocardiography[70] on conventional image orientation. In our

laboratory, in the long axis planes, the right heart is on the left and the left heart is on the viewer's right, with the transducer artifact and the base of the heart at the top of the viewing screen, and the apex of the heart at the bottom of the screen. In the short axis planes, the cardiac apex will be oriented to the viewer's right and the cardiac apex will be oriented to the viewer's left. When visualizing the cardiac anatomy, the depth of field is set to 16 cm and the field is set to 6 cm for viewing the aorta. Consistent use of the same sector orientation and depth of field allows rapid recognition of cardiac anatomy and abnormalities of cardiac dimension, once expertise is gained in transesophageal echocardiography.

When the transducer is passed to approximately 50–55 cm from the incisor teeth, the probe is in the stomach and imaging may begin. Starting the examination in the stomach gives the operator the knowledge and assurance that there is no gross esophageal or gastric pathology, if the probe passes without significant complication. An entire examination can be performed with one or two passes of the probe. The transducer can be withdrawn to each level (figure 1.14a,b) and the entire heart and aorta interrogated with one pass, by rotating the probe by 360°. Alternatively, the probe can be withdrawn to each level and the heart visualized, and then the probe can be passed again into the stomach and rotated by 180° to visualize the whole aorta by withdrawing a second time. Although this second method uses two passes of the probe there is actually less manipulation of the probe, which is especially important in the conscious patient.
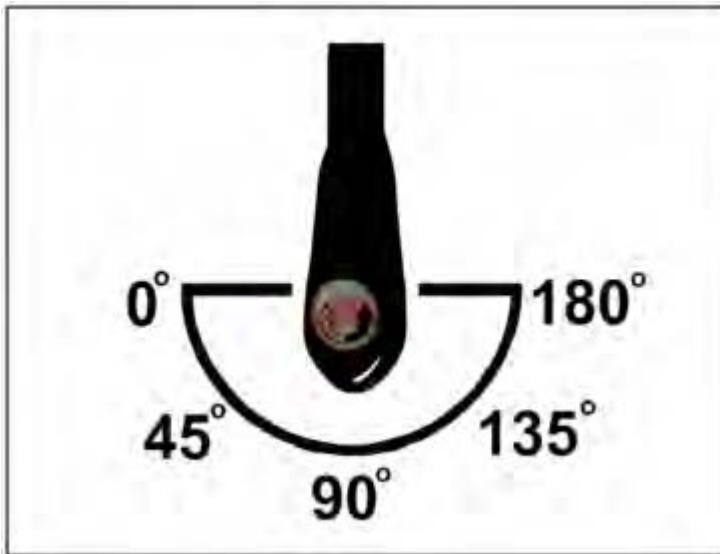
Figure 1.12 Diagram of the transducer tip of a multiplane TEE probe illustrating the rotating transducer

array. Most multiplane probes can be
rotated through a 180° arc.

Figure 1.13 Photograph of a currently
available multiplane TEE probe.

Some operators begin the examination as soon as the probe reaches 25–30 cm from the incisor teeth, imaging the base of the heart instead of the transgastric approach, which first images the cardiac apex. There are three potential disadvantages to this approach. First, the operator advances the transducer as he/she is imaging, and esophageal problems may not be readily recognized because attention is directed towards imaging. Secondly, imaging at 20–25 cm to evaluate the base of the heart and great vessels is probably the most uncomfortable part of the procedure for the conscious patient, especially if significant anteflexion is required. Occasionally a patient will not tolerate further examination at this point, which precludes a full study. Thirdly, the authors have observed that the less experienced operator occasionally fixates on the pathology initially discovered, and runs the risk of not obtaining a full study if the patient becomes uncooperative, since the probe has to be inserted further instead of withdrawn. No matter which method is used, the aim of every transesophageal echocardiography examination is to obtain a full study including all scan planes with as little probe manipulation as
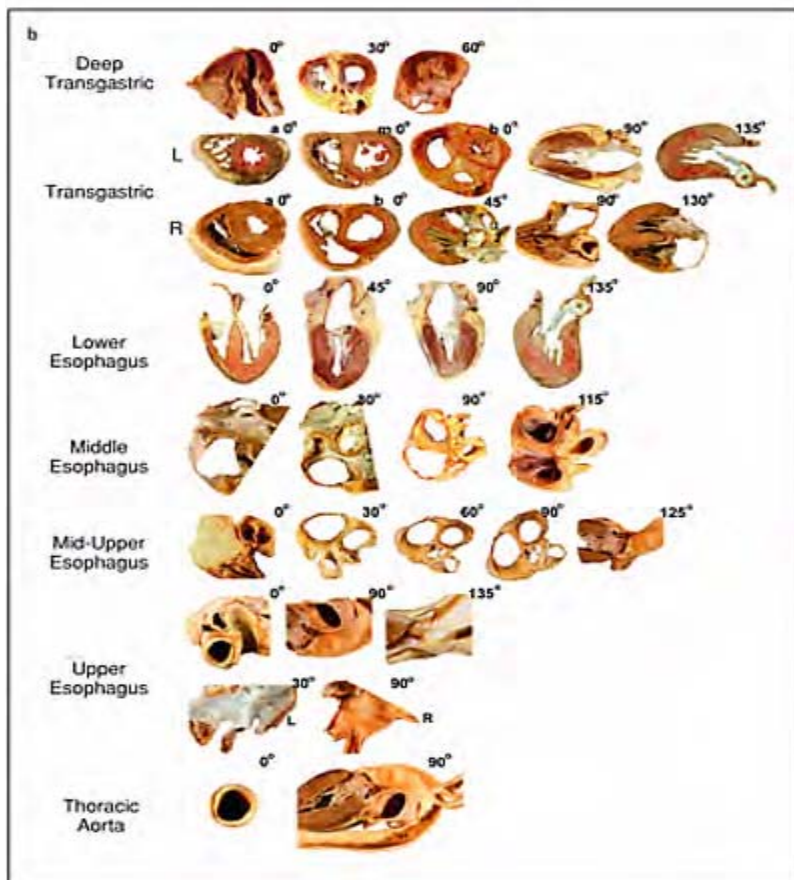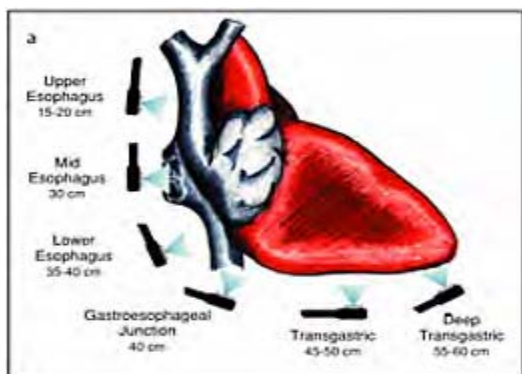
Figure 1.14 Multiplane TEE provides a large number of planes, which are obtained from various esophageal windows. (a) Typical esophageal probe

positions for obtaining standard echocardiographic views with multiplane TEE. (b) Corresponding anatomic preparations illustrating the anatomy visualized from different esophageal windows and transducer array angles that may be obtained with multiplane TEE. a, apex; m, mid ventricular; b, base; L, left; R, right.

possible, and to maintain optimal patient comfort and safety. Performing the transesophageal echocardiography examination the same way in a regimented fashion limits the duration of the overall procedure and minimizes complications. In our experience, transesophageal echocardiogram should take about 15 to 20 minutes for diagnostic studies, and really should never take longer than 30 minutes in the conscious patient.

Visualization of the heart

The transducer should initially face anterior to the patient, maximally anteflexed, and the probe should be withdrawn slightly to catch the probe at the gastroesophageal junction so that the heart is visualized in the horizontal short axis plane. In hearts vertically oriented in the chest, true short axis planes are obtained easily at 0°. In patients with more horizontally oriented hearts, the transducer may need to be steered between 0° and 20° to obtain a true horizontal scan. The operator should note the best transducer angle at this point, and if it deviates from 0°, use the difference as a correction factor during the rest of the examination for the appropriate orientation of the heart in the standard views.

Deep transgastric view

The probe is advanced slightly with a little more anteflexion to obtain the deep gastric view (figure 1.15). This is an ideal view for evaluating the mitral subvalvular apparatus, because the left ventricle is foreshortened and displays the papillary muscles and chordae tendineae in the middle of the viewing sector. In patients with prosthetic mitral or aortic valves, shadowing from the prosthesis occurs in the opposite direction from the upper esophageal views. In this plane, the ventricular outflow tract is parallel to the ultrasound beam in the middle of the sector, and permits good Doppler interrogation of the outflow tract and proximal aorta without the need for any angle correction. With transducers that image at lower frequencies, occasionally the whole ascending aorta and aortic arch, with the proximal takeoff of the great vessels and the superior vena cava, may be visualized at depths of field of 20–24 cm. With slight clockwise rotation, the right ventricular outflow tract can be visualized.

Transgastric views

The scope is withdrawn to approximately 45–50 cm from the incisors, and serial "breadloaf" horizontal short axis planes of the left ventricle may be obtained from the apex to the base of the left heart (figure 1.16). Slight clockwise rotation of the ultrasound beam enables interrogation of the right ventricle (figure 1.17). At least three planes are interrogated: distal, apex, mid ventricular cavity, and base at or below the level of the atrioventricular valves. After obtaining the standard horizontal scans, the transducer is steered from at least 45° from center to 90° (figures 1.18 and 1.19). At 45° the left ventricle is obliquely cut and at 90° the left ventricle is cut longitudinally from the apex to the mitral valve level (figure 1.18). This is probably the optimal view to visualize the true left ventricular apex without foreshortening. Further steering of the transducer to 100° post center with slight counter clockwise rotation enables visualization of the left ventricular outflow tract. With clockwise rotation past neutral, the right ventricular inflow and outflow tract can be visualized in the same plane. In all these longitudinal views, slight lateral or medial flexion may be required to obtain the highest image quality. After completing these views, the transducer is steered back to center and the scope is withdrawn to the gastroesophageal junction with less anteflexion.

Lower esophageal views

When the probe is being withdrawn from the stomach and the lower esophagus it should be rotated slightly to visualize the right ventricular inflow and the coronary sinus (figures 1.20–1.23). We prefer this view for performing color flow Doppler of the right ventricular inflow tract. Further withdrawal of the probe to 35–40 cm, with mild retroflexion that maintains contact with the esophageal wall, yields a four chamber view of the heart with the apex of the left ventricle foreshortened. The transducer should be rotated slightly counterclockwise to direct the ultrasound beam to the left heart. The transducer is steered from 0° to 135° to visualize incrementally all the walls of the left ventricle. The left ventricular outflow tract is usually initially visualized at 0° but is best interrogated at about 120°. Typically, a color flow examination can be done of the left ventricular outflow and inflow tracts as the transducer is steered back to zero, by rotation of the probe clockwise from the neutral position. The right heart can be interrogated in a similar fashion. Returning the probe to neutral and withdrawing the probe with slightly more retroflexion directs the ultrasound beam towards the atria and inter-atrial septum. With counterclockwise rotation, the left atrial appendage is well seen and the transducer may be steered to about 90° to obtain full horizontal and longitudinal planes of the left atrial appendage and pulmonary veins.
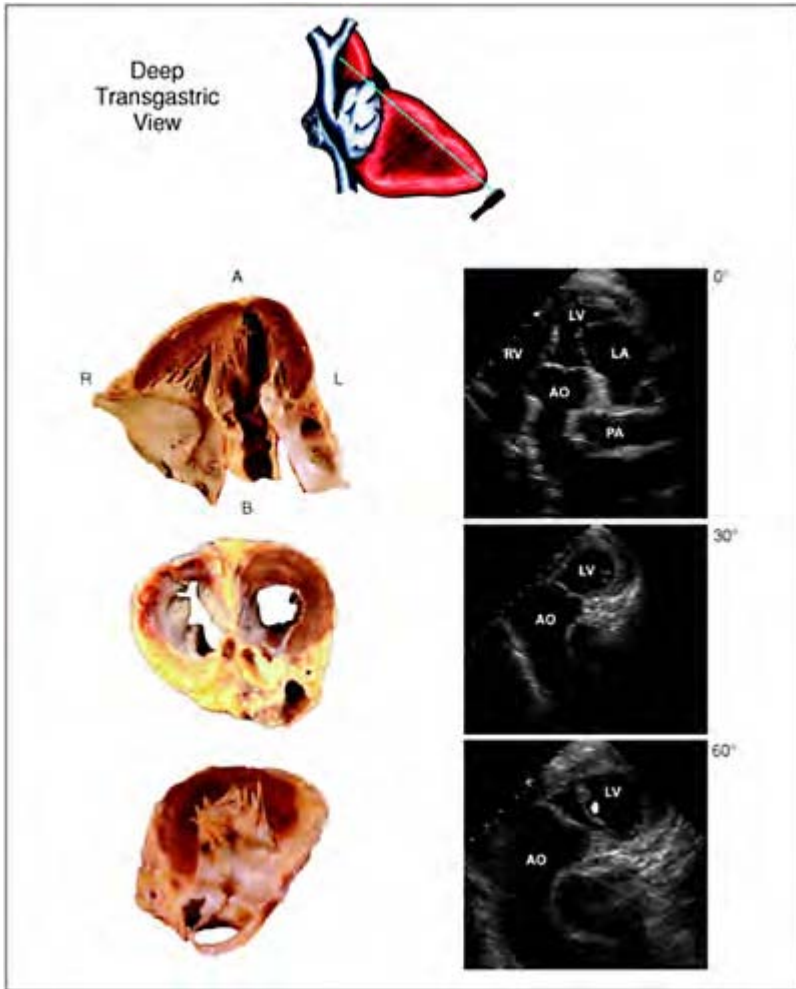
Figure 1.15 Deep transgastric view. Anatomic specimens and corresponding multiplane echocardiographic images obtained from the deep transgastric window. A, apex; B, base; R, right; L, left; LV, left ventricle; RV, right ventricle; Ao, aorta; PA, pulmonary artery; arrow indicates anterior mitral leaflet.
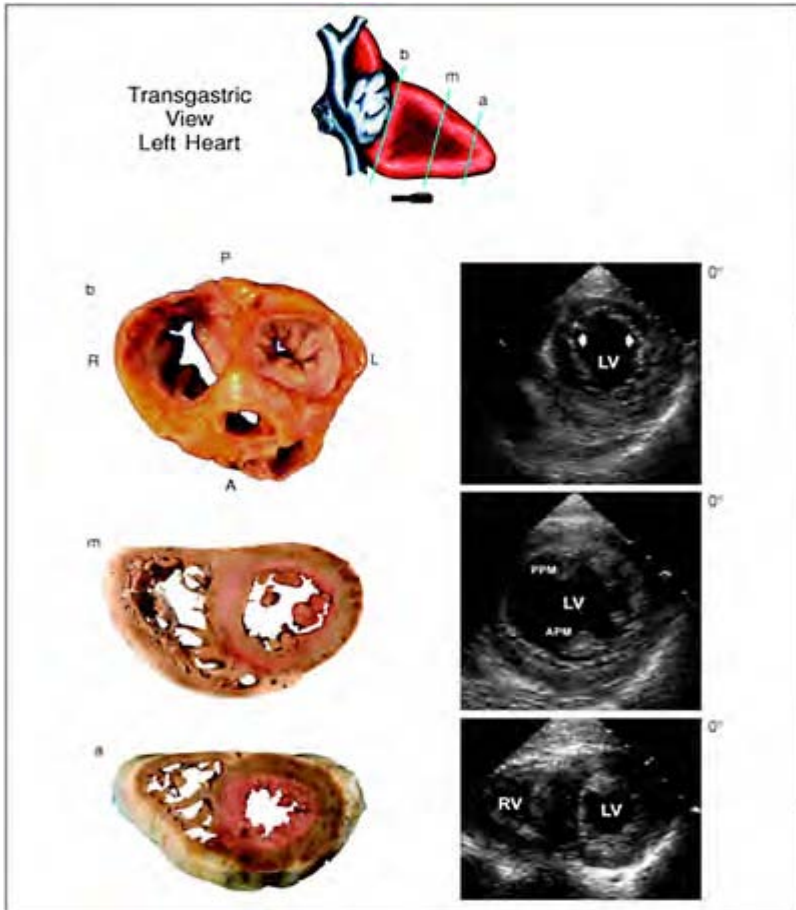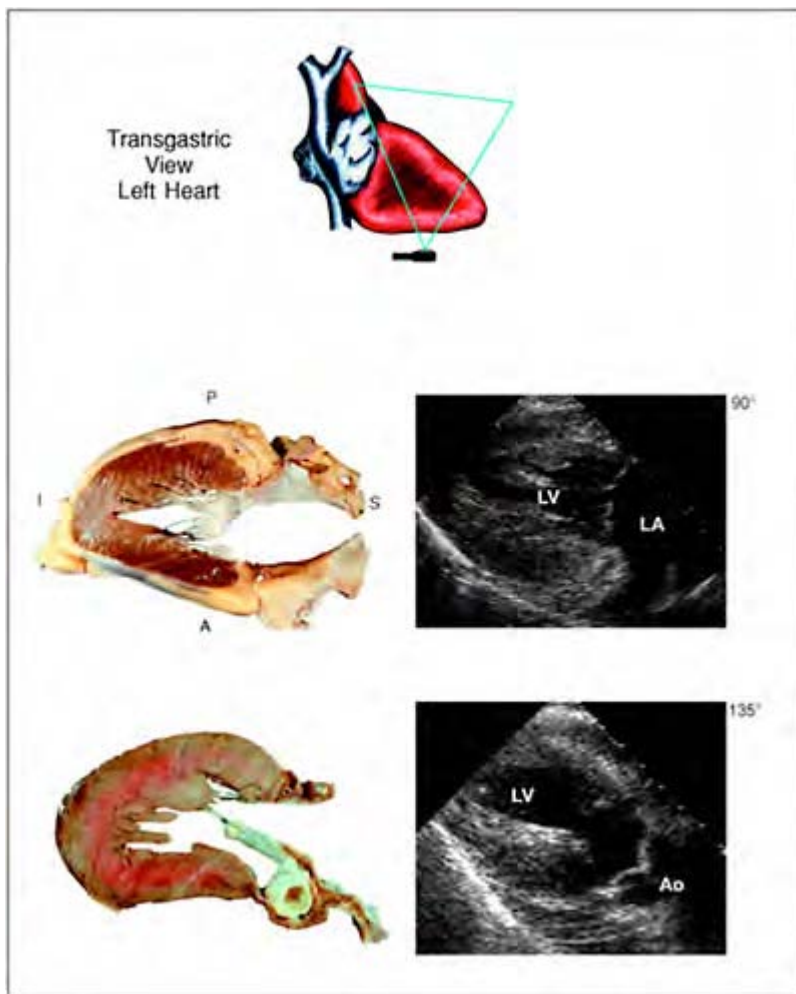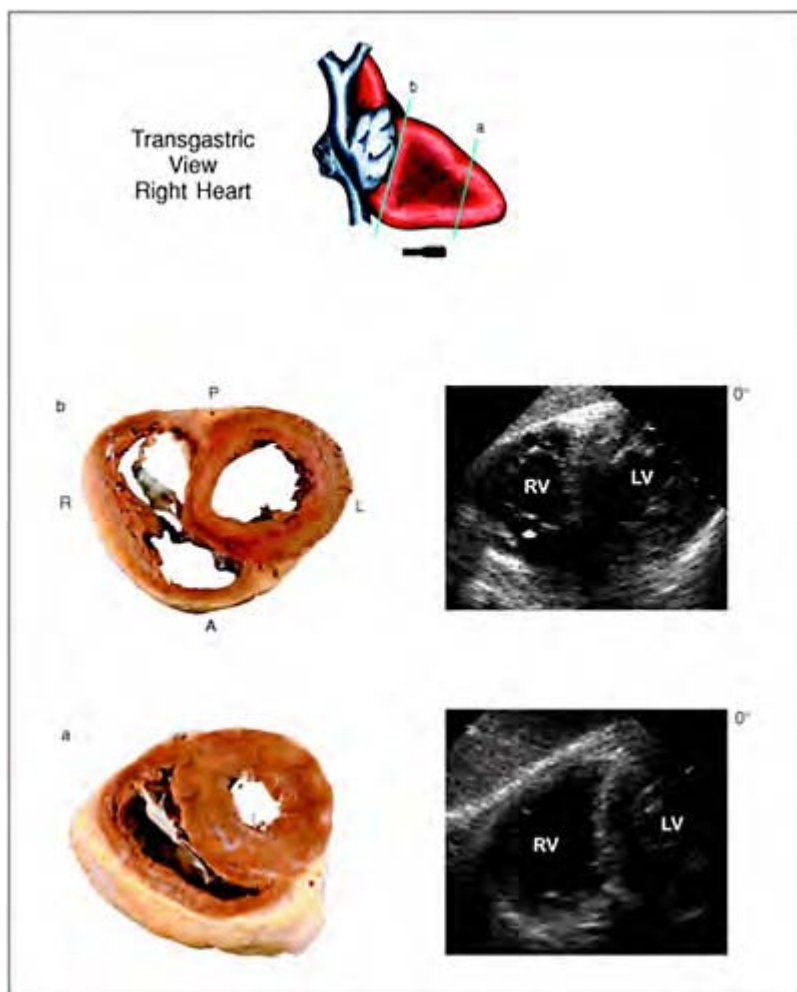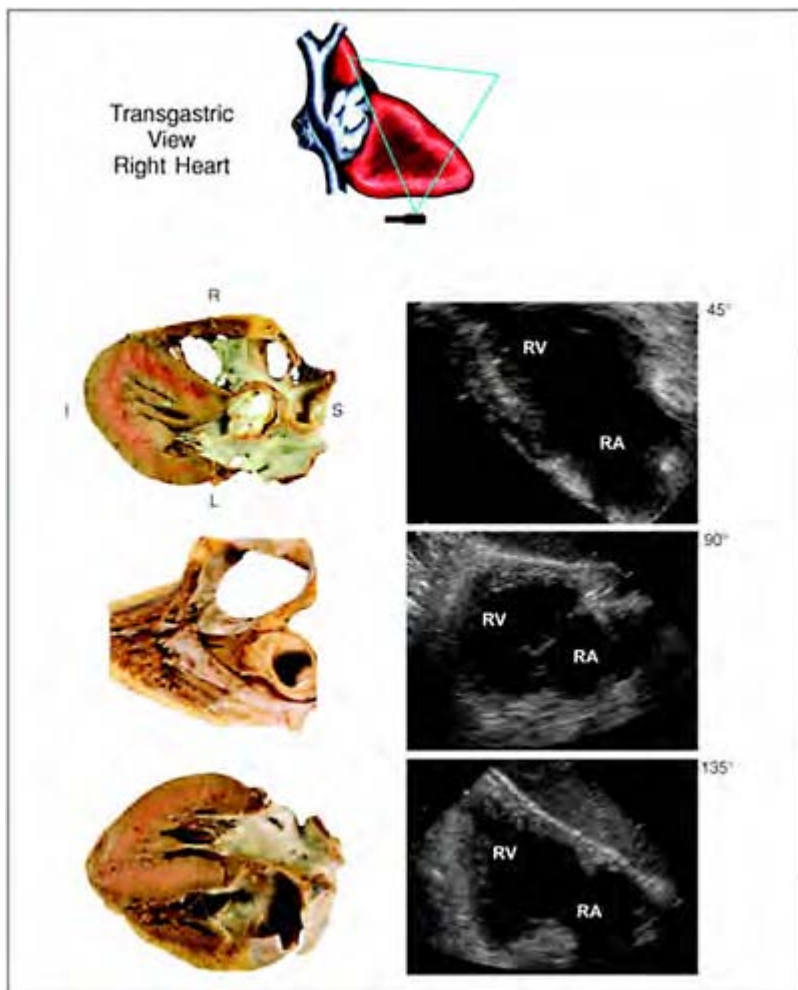
Figure 1.16 Transgastric view of left heart obtained at 0°. Anatomical specimens and corresponding multiplane echocardiographic horizontal images obtained from this window. P, posterior; A, anterior; L, left; R, right; b, base; m, mid; a, apical; LV, left ventricle; PPM, posterior papillary muscle; APM, anterior papillary muscle; RV, right ventricle; arrows mitral valve leaflets. Transgastric

Figure 1.17 Transgastric view of the left heart obtained at 90°. Anatomical specimens and corresponding multiplane echocardiographic longitudinal images obtained from this window. P, posterior; A, anterior; S, superior; I, inferior; LV, left ventricle; LA, left atrium; Ao, aorta.

Figure 1.18 Transgastric view of the right heart obtained at 0°. Anatomical specimens and corresponding multiplane echocardiographic horizontal images obtained from this window. P, posterior; A, anterior; L, left; R, right; b, base; a, apical; LV, left ventricle; RV, right ventricle.

Figure 1.19 Transgastric view of the right heart obtained at 90°. Anatomical specimens and corresponding multiplane echocardiographic longitudinal images obtained from this window. R, right; L, left; S, superior; I, inferior; RV, right ventricle; LV, left ventricle; RA, right atrium.
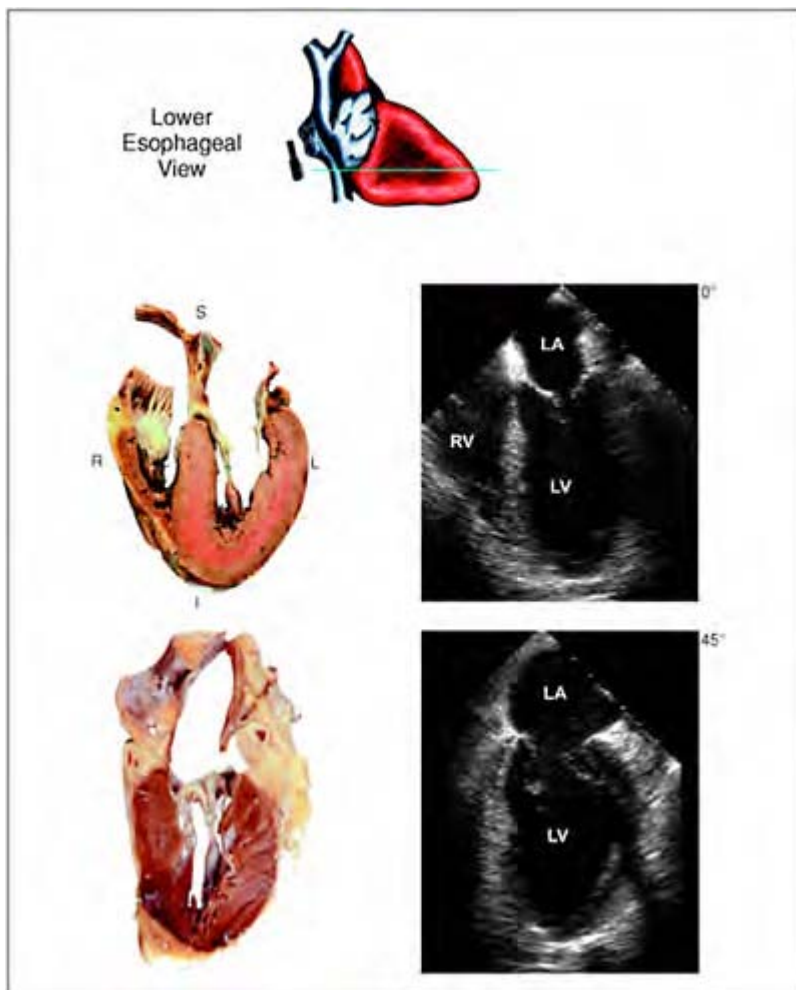
Figure 1.20 Lower esophageal view obtained at 0° and 45°. Anatomical specimens and corresponding multiplane echocardiographic images obtained from this window. R, right; L, left; S, superior; I, inferior; RV, right ventricle; LV, left ventricle; LA, left atrium.
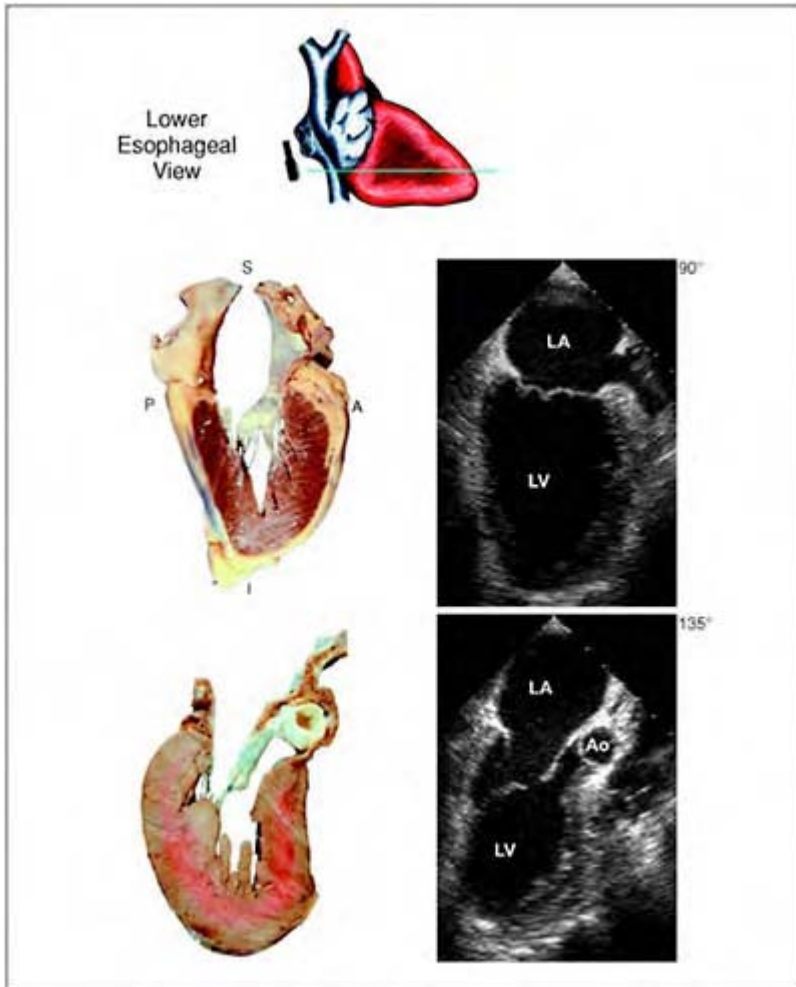
Figure 1.21 Lower esophageal view obtained at 90° and 135°. Anatomical specimens and corresponding multiplane echocardiographic images obtained from window. A, anterior; P posterior; S, superior; I, inferior; LV, left ventricle; LA, left atrium; Ao, aorta.
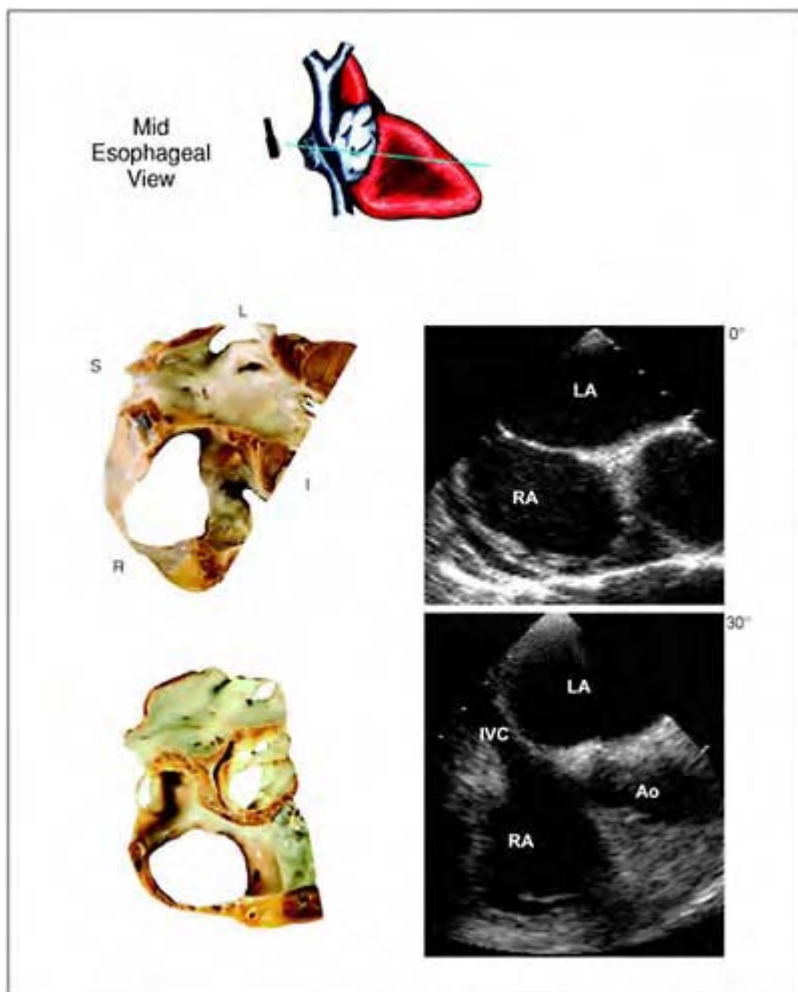
Figure 1.22 Mid esophageal view obtained at 0° and 30°. Anatomical specimens and corresponding multiplane echocardiographic images obtained from this window. R, right; L, left; S, superior; I, inferior; RA, right atrium; LV, left ventricle; LA, left atrium; IVC, inferior vena cava; Ao, aorta.
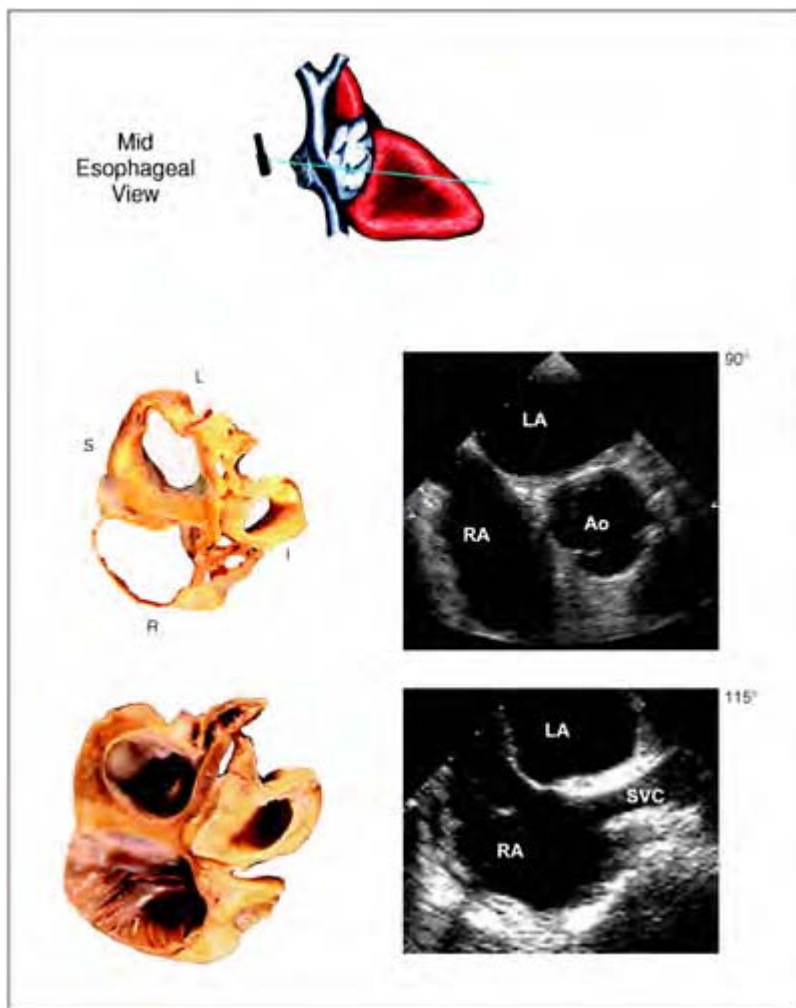
Figure 1.23 Mid esophageal view obtained at 90° and 115°. Anatomical specimens and corresponding multiplane echocardiographic images obtained from window. R, right; L, left; S, superior; I, inferior; RA, right atrium; LA, left atrium; SVC, superior vena cava; Ao, aorta.

Upper esophageal views

The probe is withdrawn to about 25 cm in the neutral position without flexion in order to interrogate the base of the heart with the aortic valve in the center of the image (figures 1.24–1.27). The aortic valve is imaged en face at approximately 15° from center. Steering the transducer to 100° gives images of the ascending aorta in long axis. With clockwise rotation, the right atrium is visualized, with the atrial septum and superior vena cava and inferior vena cava cut in longitudinal section. Returning the probe to neutral and anteflexing the transducer tip, the main and right pulmonary arteries are imaged longitudinally with short axis views of the aorta and superior vena cava.

Thoracic aortic views

With the controls in the unlocked position, the scope is again advanced to the stomach with the transducer face rotated a full 180° to visualize the thoracic aorta (figure 1.28). The scope is withdrawn slowly, with images obtained at 0° short axis planes and 90° long axis cuts. While withdrawing, the probe must be rotated in a clockwise fashion because the aorta is posterior and medial to the esophagus at the level of the diaphragm and twists around the esophagus to assume an anterior and lateral position at the level of the aortic arch. Further clockwise rotation at the aortic arch enables the distal portion of the ascending aorta to be visualized. This is sometimes referred to as the blindspot area of the aorta, since it is the area where the right bronchus courses between the esophagus and the aorta, limiting the field of view especially with monoplane and biplane transducers. This blindspot of the aorta is virtually eliminated by multiplane technology with experienced operators.

Normal Doppler examination

Color Doppler can be recorded in all the standard views. Care must be exercised in performing conventional continuous and pulsed wave Doppler, since it is difficult to obtain parallel imaging planes of specific flows. This issue is addressed individually in subsequent chapters.

Post transesophageal echocardiographic care

Following the removal of the transducer, patients are encouraged to cough and expectorate excessive secretions. When only oral and topical anesthesia are used, the patient may be sat up and given a basin to expectorate excessive secretions. In patients receiving intravenous sedation, the mouth and pharynx are suctioned. Nasal oxygen is left in place and the patient is monitored for 30 minutes after oral and topical anesthesia and for 2 hours after intravenous sedation. The anesthetic effect of topical anesthesia usually
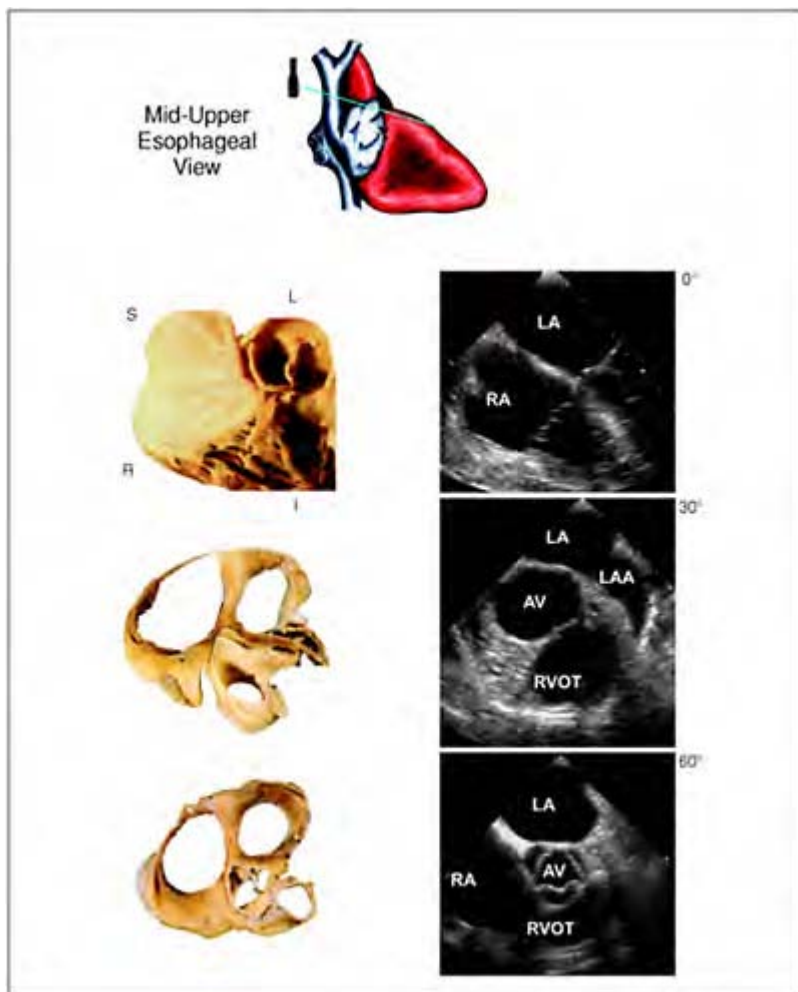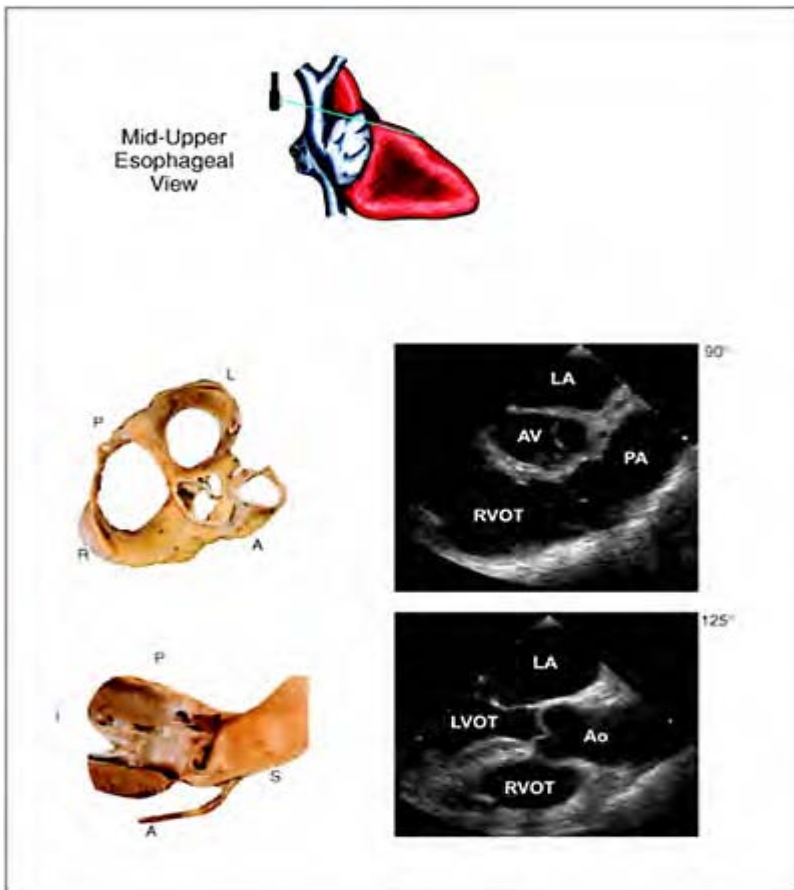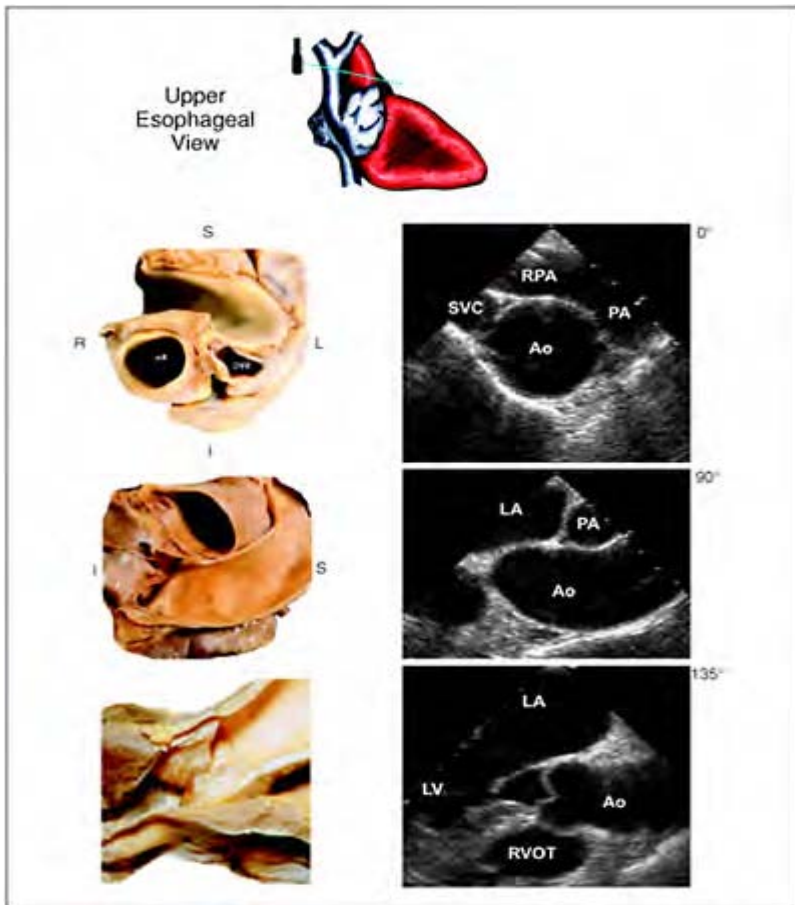
Figure 1.24 Mid to upper esophageal view obtained at 0°, 30° and 60°. Anatomical specimens and corresponding multiplane echocardiographic images obtained from this window. R, right; L, left; S, superior; I, inferior; RA, right atrium; LA, left atrium; LAA, left atrial appendage; RVOT, right ventricular outflow tract; AV, aortic valve.

lasts about 30 minutes to 2 hours, and the patient is kept fasting during this time. In our experience, patients tolerate solids better than liquids initially, with less gagging. If patients inadvertently have not taken their medications before transesophageal echocardiography, these are taken under observation 30 minutes after transesophageal echocardiography. When intravenous sedation is used, patients are watched carefully, regardless of the dosage of medication received. We have experienced respiratory depression due to the intravenous sedation for up to 1 hour after the procedure. Vital signs, including oxygen saturation, are checked and recorded every 15 minutes for 2 hours, then every 30 minutes until stable. Outpatients who receive intravenous sedation are instructed that they must be accompanied from the laboratory with another adult before being discharged. The patient is specifically instructed not to drive, operate heavy machinery, or make important decisions for 12 hours after the procedure. The patients are strongly encouraged not to work for the rest of the day.

Figure 1.25 Mid to upper esophageal view obtained at 90° and 125°.

Anatomical specimens and corresponding multiplane echocardiographic images obtained from this window. L, left; P, posterior; R, right; A, anterior; S, superior; I, inferior; LA, left atrium; AV, aortic valve; RVOT, right ventricular outflow tract; PA, pulmonary artery; LVOT, left ventricular outflow tract; Ao, aorta.

Figure 1.26 Upper esophageal view obtained at 0°, 90° and 135°. Anatomical specimens and

corresponding multiplane echocardiographic images obtained from this window. R, right; L, left; S, superior; I, inferior; RPA, right pulmonary artery; PA, pulmonary artery; SVC, superior vena cava; Ao, aorta; LA, left atrium; LV, left ventricle; RVOT, right ventricular outflow tract.
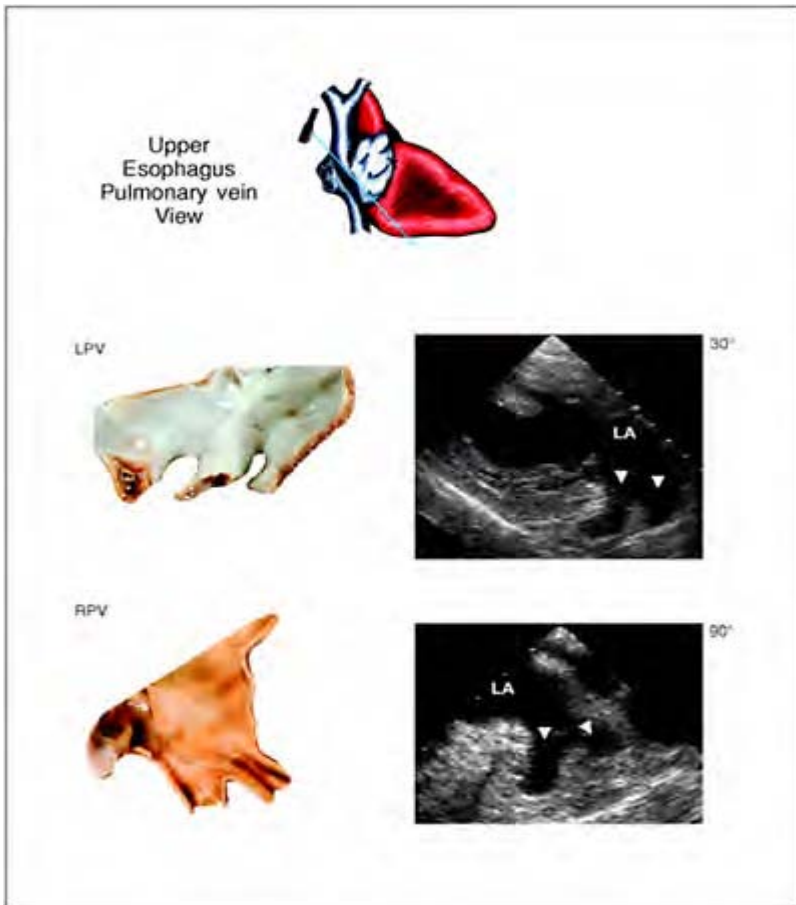
Figure 1.27 Upper esophageal view of the pulmonary veins. Anatomical specimens and corresponding

multiplane echocardiographic images obtained from this window. LPV, left pulmonary vein; RPV, right pulmonary vein; LA, left atrium, arrows indicate the orifice of the pulmonary veins.
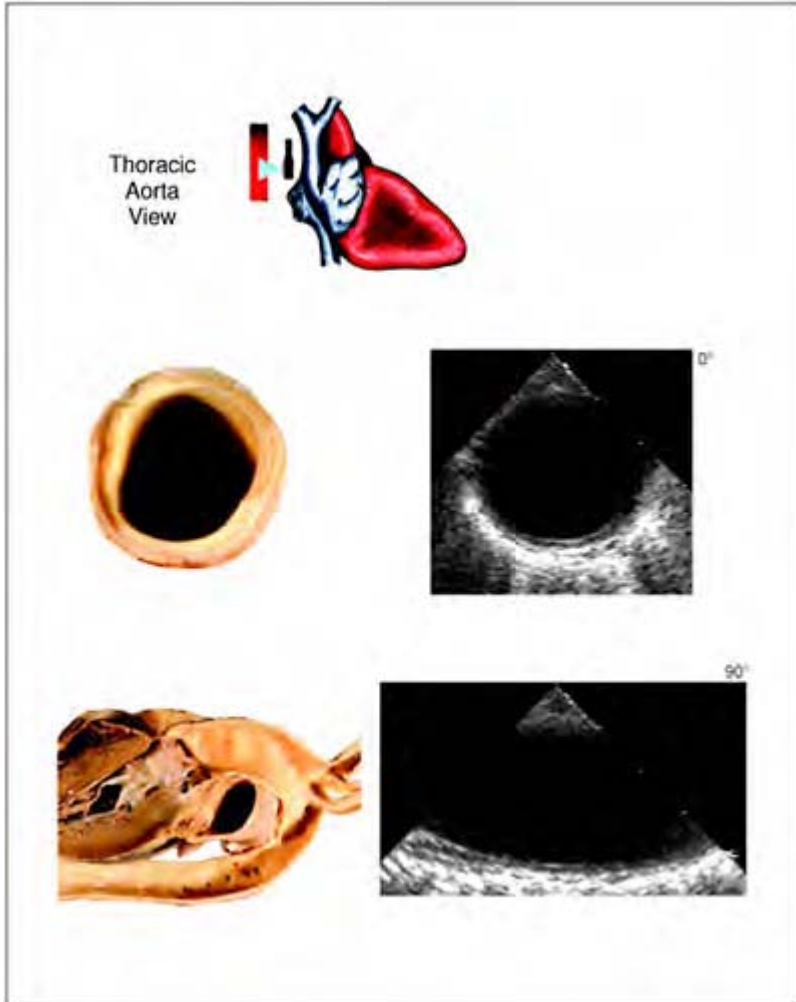
Figure 1.28 Descending thoracic aorta view obtained at 0° and 90°. Anatomical specimens and corresponding multiplane horizontal

and longitudinal echocardiographic
images obtained from this window.

1. I hereby authorize Dr. _____ to perform
upon _____ (Patient Name) , a transesophageal
echocardiogram (insert a echocardiographic transducer or microphone
in the esophagus or food tube to visualize the heart and record images
for diagnostic purposes).

2. I understand that the procedure will be performed at Thomas Jeffer-
son University Hospital, by or under the supervision of
Dr._____, who is authorized to utilize the services of other
physicians, or member of the house staff as he or she deems necessary
or advisable.

3. I consent to the performance of procedure(s) different from those
listed above, which my physician considers necessary or advisable in the
course of the procedure(s).

4. I understand the nature and purpose of the transesophageal echocar-
diogram, possible alternative methods of diagnosis, the risks involved,
the possibility of complications, and the consequences of the trans-
esophageal echocardiogram. I acknowledge that no guarantee or assur-
ance has been made as to the results that may be obtained.

5. I consent to the administration of local or regional anesthesia to be
applied by or under the direction of my physician.

6. I hereby allow authorized representatives from TJUH to examine,
photograph, use or authorize the use for research or development
purpose(s) the images obtained from the transesophageal echocardio-
gram.

7. I certify that I have read and fully understand the above consent
statement. In addition, I have been afforded an opportunity to ask
whatever questions I might have regarding the transesophageal echocar-
diogram to be performed and they have been answered to my satisfac-
tion.

_____ (Witness)

_____ (Patient or Authorized Representative)

_____ (Physician Obtaining Signature)

Date: Time: AM/PM

Figure 1.29

Transesophageal Echocardiography Consent
Form. Typicalpatient form designed for our

laboratory utilized to obtainnformed consent
prior to performing TEE.

The written informed consent form (figure 1.29) is attached to the vital sign record sheet that is completed for each patient (figure 1.30). Outpatients are discharged with written instructions (figure 1.31) to notify the laboratory directly if any problems are encountered or if questions arise after the transesophageal echocardiogram.

Transesophageal echocardiography scope care

Following the procedure the transesophageal echocardiography transducer also requires special attention. The probe should be carefully inspected for damage (bite marks, breaks in the integrity of the protective insulating cover, normal probe tip movement). Periodically the transducer should be checked for electrical leakage, to ensure electrical safety according to manufacturer's recommendations. In our laboratories, the probe is initially scrubbed with a soft brush and a non-harsh disinfectant soap (without iodine) to remove any mucous material especially near the bends of the probe, before placing in a 2% glutaraldehyde (cidex) solution for 12–15 minutes. Disinfectant solution and cleaning tubes are commercially available. These tubes allow the probe to hang straight. The probes are then removed from the disinfectant solution, rinsed off with soap and allowed to air dry for another 20 minutes.

Recommendations for transesophageal echocardiography training

Transesophageal echocardiography trainees must have full knowledge and understanding of cardiac anatomy and echocardiography. Transesophageal echocardiography should be done only by specially trained physicians. Transesophageal echocardiography requires the physician operator to be expert in the field of echocardiography and Doppler, cardiac pathophysiology, and cardiac anatomy, to be able to masterfully manipulate the transducer to obtain all necessary views, and to be sufficiently adept to interpret all of the above in the context of cardiovascular disease. In the authors' experience, erroneous interpretations of transesophageal echocardiograms revolve around artifacts of ultrasound and unconventional scan orientations that are not readily recognizable. It is extremely helpful to comprehend the specifics of both medical and surgical treatment options, to provide the necessary information needed for optimal patient management.

Transesophageal echocardiography training is usually provided as an additional fourth year of cardiac fellowship training. Our laboratories closely adhere to the recommendations set forth by the American Society of Echocardiography outlined in tables 1.3 and 1.4.[71]

In our institutions, trainees are required to concentrate on the technical and mechanical aspects of esophageal intubation, including pre and post procedure patient care, recognition and management of complications, and full understanding of the contraindications of the procedure.

Transesophageal Echocardiography
Nursing Note

Name
Room
Medical Record Number
Sex
Age
Doctor

MEDICATIONS   ALLERGIES
1 _____   6 _____   1 _____
2 _____   7 _____   2 _____
3 _____   8 _____   3 _____
4 _____   9 _____   4 _____
5 _____   10 _____   5 _____

AIRWAY
limited neck mobility   ☐ NO   ☐ YES   dentures   ☐ NO   ☐ YES
limited jaw mobility   ☐ NO   ☐ YES   snoring   ☐ NO   ☐ YES
facial/neck mobility   ☐ NO   ☐ YES

PATIENT STATUS
• CONSCIOUSNESS   preprocedure: _____   post procedure: _____   post recovery: _____
    (1) awake and oriented   (3) lethargic but responsive
    (2) drowsy but oriented   (4) comatose
• NEUROLOGIC   preprocedure: _____   post procedure: _____   post recovery: _____
    (1) normal motor and sensory function, all extremities
    (2) normal motor function, reduced or abnormal sensation, single extremity
    (3) reduced motor function, with or without sensory changes, single extremity
    (4) reduced motor function, abnormal sensation, more than one extremity
    (5) complete loss of motor or sensory function, one or more extremities
• CARDIAC   preprocedure: _____   post procedure: _____   post recovery: _____
    (1) B.P. within 20% of baseline, normal rhythm   (2) B.P. within 20% of baseline, abnormal rhythm
    (3) B.P. 20–50% of baseline (4) B.P. less than 50% of baseline
• RESPIRATORY   preprocedure: _____   post procedure: _____   post recovery: _____
    (1) normal respirations   (2) shortness of breath when supine
    (3) labored respirations, !!!! required   (3) ventilator dependent

PROCEDURE MEDICATIONS SUMMARY
Versed (midazolam)   _____ (total dose)   other: _____   _____ (total dose)
Valium (diazepam)   _____ (total dose)   other: _____   _____ (total dose)
Fentanyl   _____ (total dose)   other: _____   _____ (total dose)
Inapsine (droperidal) _____ (total dose)   other: _____   _____ (total dose)

FLUIDS   begin: end: total: OUTPUT   begin: end: total:

time	B.P.	HR	rr	SaO2	temp	medication	comments
							– baseline –

Figure 1.30 vital sign Record utilized
during the performance of TEE
procedures in our laboratory.

Trainees in the echocardiography laboratory start with understanding the indications and contraindications for performing transesophageal echocardiograms, followed by

understanding the clinical utility of the information. Trainees are instructed to do a full study and to concentrate on specific issues pertaining to the diagnosis obtained. Each cardiac fellow must have obtained at least Level II training as specified by the American Society of Echocardiography guidelines, and generally performs 250 transesophageal echocardiography studies during their fourth-year fellowship training period.

Patient name: _____   Date: _____

1.   You have received medication that may cause drowsiness.

     For the next 24 hours, you may not:
     •   Drive an automobile or operate any machinery
     •   Drink alcoholic beverages
     •   Conduct important business or sign legal documents

2.   You may resume your regular activity level tomorrow.

3.   For the next ___ hours, you may not have anything to eat or drink.

     You may then resume your regular diet.

4.   You may continue to take your normal prescription medications.

5.   If you develop a sore throat, gargle with warm salt water or use throat lozenges of your choice. If you have a sore throat, which persists for longer than 2–3 days, please contact your physician.

6.   Contact your physician to schedule a follow-up appointment.

Additional instructions:

_____

_____

Discharge in care of: _____

Discharge instructions reviewed with patient and escort by: _____

I understand the above instructions: _____   (Patient signature)

_____   (Escort signature)

If you have any questions, please call the Division of Ultrasound Echo Lab at (215) 955-7100. After 5pm, please call the TJUH page operator at (215) 955-6060 and request to speak to the Cardiology Fellow.

Figure 1.31 Patients that have TEE procedures in our laboratory are given writen instructions following the administration of conscious sedation medications before being discharged from the echocardiography laboratory.

Table 1.3 Recommended training components for developing and maintaining skills in transesophageal echocardiography (TEE)

Component	Objective	Duration	No. of cases (approx.)
General echocardiography, Level II	Background needed for performance and interpretation	6 months or equivalent	300
Esophageal intubation	TEE probe introduction	Variable	25
TEE examination	Skills in TEE performance and interpretation	Variable	50
Ongoing education	Maintenance of competence	Annual	50 to 75

Ref: Pearlman AS, Gardin JM, Martin RP, et al. Guidelines for physician training in transesophageal echocardiography: recommendations of the American Society of Echocardiography Committee for Physician Training in Echocardiography. *J Am Soc Echocardiogr* 1992;5:187–94.

Our laboratories provide transesophageal echocardiography training for cardiologists and anesthesiologists after routine fellowship training. The requirements are a little less stringent, but 100 cases must be done in total before independent status is granted. Formal training in transesophageal echocardiography requires first-hand experience, which can not be obtained by watching videotapes or attending postgraduate courses, although these unquestionably supplement training and are required to maintain a state-of-the-art approach to transesophageal echocardiography in this rapidly changing field. The practicing transesophageal echocardiography physician should continue to do a minimum of 50–75 cases per year to maintain their competence in the procedure. Quality assurance should also be undertaken periodically in institutions where transesophageal echocardiography is done, to maintain competence, high quality, and optimal patient safety. This should include comparing transesophageal echocardiography results with cardiac catheterization, other radiographic techniques, and surgical and autopsy data whenever available.

Table 1.4 Skills needed to perform transesophageal echocardiography (TEE)

Cognitive skills	Technical skills
Knowledge of appropriate indications, contraindications, and risks of TEE	Proficiency in performing a complete standard echocardiographic examination, using all echocardiographic methods relevant to the case
Understanding of differential diagnostic considerations in each clinical case	
Knowledge of physical principles of echocardiography image formation and blood flow velocity measurement	Proficiency in safely passing the TEE transducer in to the esophagus and stomach and in adjusting probe position to obtain the necessary tomographic images and doppler data

Familiarity with the operation of the ultrasonographic instrument, including the function of all controls affecting the quality of the data displayed	
Knowledge of normal cardiovascular anatomy, as visualized tomographically	Proficiency in correctly operating the ultrasonographic instrument, including all controls affecting the quality of the data displayed
Knowledge of alterations in cardiovascular anatomy resulting from acquired and congenital heart diseases	
Knowledge of normal cardiovascular hemodynamics and fluid dynamics	Proficiency in recognizing abnormalities of cardiac structure and function as detected from the transesophageal and transgastric windows, in distinguishing normal from abnormal finding, and in recognizing artifacts
Knowledge of alterations in cardiovascular hemodynamics and blood flow resulting from acquired and congenital heart diseases	
Understanding of component techniques for general echocardiography and TEE, including when to use these methods to investigate specific clinical questions	Proficiency in performing qualitative and quantitative analysis of the echocardiographic data
Ability to distinguish adequate from inadequate echocardiographic data and to distinguish an adequate from an inadequate TEE examination	
Knowledge of other cardiovascular diagnostic methods for correlation with TEE findings	Proficiency in producing a cogent written report of the echocardiographic findings and their clinical implications
Ability to communicate examination results to patient, other health care professionals, and medical record	
Ref: Pearlman AS, Gardin JM, Martin RP, et al. Guidelines for physician training in transesophageal echocardiography: recommendations of the American Society of Echocardiography Committee for Physician Training in Echocardiography. *J Am Soc Echocardiogr* 1992;5:187–94.	

References

1. Frazin L, Talano JV, Stephanides L, et al. Esophageal echocardiography. *Circulation* 1976;54:102–8.
2. Souquet J, Hanrath P, Zittelli L, et al. Transesophageal phased-array for imaging the heart. *IEEE Trans Biomed Eng* 1982;29:707–12.
3. Hanrath P, Schüter M, Langestein BA, et al. Transesophageal horizontal and sagittal imaging of the heart with a phased-array system: initial clinical results. In: Hanrath P, Bleifeld W, Souquet J (eds). *Cardiovascular Diagnosis by Ultrasound.* Martinus Nijhoff: Publishing: London, 1982:280.

4. Seward JB, Tajik AJ, DiMagno EP. Esophageal phased-array sector echocardiography: an anatomic study. In: Hanrath P, Bleifeld W, Souquet J (eds). *Cardiovascular Diagnosis by Ultrasound.* Martinus Nijhoff: Publishing: London, 1982:270–9.
5. Omoto R, Kyo S, Matsumura M, et al. New directions of biplane transesophageal echocardiography with special emphasis on real-time biplane imaging and matrix phased-array biplane transducer. *Echocardiography* 1990;7:691–8.
6. Roelandt JRTC, Thomson IR, Vletter WB, et al. Multiplane transesophageal echocardiography: latest evolution in an imaging revolution. *J Am Soc Echocardio* 1992;5:361–7.
7. Flachskampf FA, Hoffmann R, Hanrath P. Experience with a transesophageal echotransducer allowing full rotation of the viewing plane: the Omniplane probe (abstract). *J Am Coll Cardiol* 1991;17 (suppl A):34A.
8. Roelandt JRTC, Pandian NG. Rationale and advantages. In: Roelandt JRTC, Pandian NG (eds). Multiplane transesophageal echocardiography. Churchill Livingston: New York, 1996:11–14.
9. Seward JB, Khandheria BK, Freeman WK, et al. Multiplane transesophageal echocardiography: image orientation, examination techniques, anatomic correlations and clinical applications. *Mayo Clinic Proc* 1993;68:523–51.
10. Chandrasekaran K, Walsh DV, Ross JJ, et al. Multiplane transesophageal echocardiography increases diagnostic capability beyond biplane transesophageal echocardiography (abstract). *J Am Coll Cardiol* 1993;21:487A.
11. Pandian NG, Hsu Tl, Schwartz SL, et al. Multiplane transesophageal echocardiography: imaging planes, echocardiographic anatomy and clinical experience with a prototype phased-array Omniplane probe. *Echocardiography* 1992;9:649–66.
12. Topol EJ, Weiss JL, Guyman PA, et al. Immediate improvement of dysfunctional myocardial segments after coronary revascularization: detection by intraoperative transesophageal echocardiography. *J Am Coll Cardiol* 1984;4:1123–34.
13. Curan SE, Kimball TR, Meyer RA, et al. Efficacy of intraoperative transesophageal echocardiography in children with congenital heart disease. *Am J Cardiol* 1989;63:594–8.
14. Currie PJ. Transesophageal echocardiography: intraoperative applications. *Echocardiography* 1989;6:403–14.
15. Oka Y, Inoue T, Hong Y, et al. Retained intracardiac air: transesophageal echocardiography for definition of incidence and monitoring removal by improved techniques. *J Thorac Cardiovascular Surg* 1989;91:329–37.
16. Fraser AG. Disease of the mitral and tricuspid valves. In: Suther-land GR, Roelandt JRTC, Fraser AG, Anderson RH (eds). Transesophageal echocardiography in clinical practice. Gower Medical Publisher: London, 1991.
17. Mendelson LS, Steers JC, Pieniek MS, et al. Is there utility for transesophageal echocardiography during routine coronary artery surgery (abstract)? *Circulation* 1996;94(suppl 1):455.
18. Freeman WK, Schaff HV, Khandheria BK, et al. Intraoperative evaluation of mitral valve regurgitation and repair by transesophageal echocardiography: incidence and significance of systolic anterior motion. *J Am Coll Cardiol* 1992;20:599–609.
19. Carpentier A, Chauvaud S, Fabiani JN, et al. Reconstructive surgery of mitral valve incompetence; ten year appraisal. *J Thorac Cardiovasc Surg* 1980;79:338–48.
20. Hsu Y-H, Santulli T Jr, Wong A-L, et al. Impact of intraoperative echocardiography or surgical management of congenital heart disease. *Am J Cardiol* 1991;67:1279–83.
21. Weintraub R, Shiota T, Elkadi T, et al. Transesophageal echocardiography in infants and children with congenital heart disease. *Circulation* 1992;86:711–22.
22. Ritter SB, Thys D. Pediatric transesophageal color flow imaging: smaller probes for smaller hearts. *Echocardiography* 1989;6:431–40.
23. Sutton DC, Cahalan MK. Intraoperative assessment of left ventricular function with transesophageal echocardiography. *Cardiol Clin* 1993;II:389–98.

24. Muhiudeen IA, Kuecherer HF, Lee E, et al. Intraoperative estimation of cardiac output by transesophageal pulse Doppler echocardiography. *Anesthesiology* 1991;74:9–14.
25. Smith JS, Cahalan MK, Benefiel DJ, et al. Intraoperative detection of myocardial ischemia in high-risk patients: electrocardiography versus two-dimension transesophageal echocardiography. *Circulation* 1985;72:1015–21.
26. London MJ, Tubau JF, Wong MG, et al. The "natural history" of segmental wall motion abnormalities in patients undergoing noncardiac surgery. *Anesthesiology* 1990;73:644–55.
27. Eisenberg MT, London MJ, Leung JM, et al. Monitoring for myocardial ischemia during noncardiac surgery. A technologic assessment of transesophageal echocardiography and 12–lead electrocardiography. the study of Perioperative Ischemia Research Group. *JAMA* 1992;268:210–16.
28. Daniel WG, Angermann C, Engberding R, et al. Transesophageal echocardiography in patients with cerebral ischemic events and arterial embolism. A European Multicenter Study (abstr). *Circulation* 1989;80 (suppl 2):473.
29. Lee RJ, Bartzokis TC, Grogin HR, et al. Superiority of transesophageal echocardiography in detection intracardiac sources of emboli (abstract). *Circulation* 1989; 80(suppl 2):II-403.
30. Pearson AC, Labovitz AJ, Tatineni S, Gomez CR. Superiority of transesophageal echocardiography in detecting cardiac source of emboli in patients with cerebral ischemia of uncertain etiology. *J Am Coll Cardiol* 1991;17:66–72.
31. Leung DY, Walsh WF, Cramny GB. Assessment of aortic valve and ascending aorta by transesophageal echocardiography: incremental information of multiplane over biplane imaging (abstract). *J Am Coll Cardiol* 1994;24:328A.
32. Karalis DG, Chandrasekaran K, Victor MF, et al. Recognition and embolic potential of intraaortic atherosclerotic debris. *J Am Coll Cardiol* 1991;17:73–8.
33. Yvorchuk KJ, Sockowski RA, Chan KL. Distribution of mobile aortic masses and their relationship to aortic atherosclerosis: a transesophageal echocardiographic study of the thoracic aorta. *J Am Coll Cardiol* 1994;1A:442.
34. Erbel R, Wittlich N, Shuster S, et al. Assessment of pulmonary embolism. *Int J Cardiac Imaging* 1993;9(suppl 2):39–49.
35. Patel JJ, Chandrasekaran K, Maniet AR, et al. Impact of the inadvertent diagnosis of clinically unsuspected central pulmonary artery thrombo-embolism in treatment of critically ill patients. *Chest* 1994;105:986–90.
36. Klein Al, Stewart WC, Cosgrove DM III, et al. Visualization of acute pulmonary emboli by transesophageal echocardiography. *J Am Soc Echocardopgr* 1990;3:414–15.
37. Manning WT, Reis GJ, Douglas PS. Use of transesophageal echocardiography to detect left atrial thrombi before percutaneous balloon dilatation of the mitral valve: a prospective study. *Br Heart J* 1992;67:170–3.
38. Kronzon I, Tunick PA, Schwinger ME, et al. Transesophageal echocardiography during percutaneous mitral valvuloplasty. *J Am Soc Echocardiogr* 1989;2:380–5.
39. Erbel R, Rohmann S, Drexler M, et al. Improved diagnostic value of echocardiography in patients with infective endocarditis by transesophageal approach. A prospective study. *Eur Heart J* 1988;9:43–53.
40. Mugge A, Daniel WG, Frank G, Lichtlen PR. Echocardiography in infective endocarditis: reassessment of prognostic implications of vegetation size determined by the transthoracic and the transesophageal approach. *J Am Coll Cardiol* 1989;14:631–8.
41. Shively BK, Gurule FT, Roldan CA, et al. Diagnostic value of transesophageal compared with transthoracic echocardiography in infective endocarditis. *J Am Coll Cardiol* 1991;18:391–7.
42. Castello R, Lenzen P, Aquirre F, Labovitz AJ. Quantitation of mitral regurgitation by transesophageal echocardiography with Doppler color-flow mapping: correlation with cardiac catheterization. *J Am Coll Cardiol* 1992;19:1516–21.

43. Klein Al, Obarski TP, Stewart WJ, et al. Transesophageal Doppler echocardiography of pulmonary venous flow: a new marker of mitral regurgitation severity. *J Am Coll Cardiol* 1991;18:518–26.
44. Dittrich HC, McCann HA, Walsh TP, et al. Transesophageal echocardiography in the evaluation of prosthetic and native aortic valves. *Am J Cardiol* 1990;66:758–61.
45. Hofmann T, Kasper W, Meinertz T, et al. Determination of aortic valve orifice area in aortic valve stenosis by two-dimensional transesophageal echocardiography. *Am J Cardiol* 1987;59:330–5.
46. Shapiro SM, Young E, Ginzton LE, Bayer AS. Pulmonic valve endocarditis as an underdiagnosed disease: role of transesophageal echocardiography. *J Am Soc Echocardiogr* 1992;5:48–51.
47. Oh JK, Seward JB, Khandheria BK, et al. Transesophageal echocardiography in critically ill patients. *Am J Cardiol* 1990;66:1492–5.
48. Vargas-Barron J, Romero-Cardenas A, Villegus M, et al. Transthoracic and transesophageal echocardiographic diagnosis of myxomas in the four cardiac cavities. *Am Heart J* 1991;121:931–3.
49. Reeder GS, Khandheria BK, Seward JB, Tajik AJ. Transesophageal echocardiography and cardiac masses. *Mayo Clin Proc* 1991;66:1101–9.
50. Hsu T-L, Hsiung M-C, Lim S-L, et al. The value of transesophageal echocardiography in the diagnosis of cardiac metastasis. *Echocardiography* 1992;9:1–7.
51. Nienaber CA, von Kodolitsch Y, Nicolas V, et al. The diagnosis of thoracic aortic dissection by non invasive imaging procedures. *N Engl J Med* 1993;328:1–9.
52. Nienaber CA, Spielmann RP, von Kodolitsch Y, et al. Diagnosis of thoracic aortic dissection: magnetic resonance imaging versus transesophageal echocardiography. *Circulation* 1992;85:434–47.
53. Daniel WG, Erbel R, Kasper W, et al. Safety of transesophageal echocardiography: a multicenter survey of 10,419 examinations. *Circulation* 1991;83:817–21.
54. Khandheria BK, Seward JB, Bailey K, et al. Safety of transesophageal echocardiography: experience with 2070 consecutive procedures (abstract). *J Am Coll Cardiol* 1991;17(suppl A):20A.
55. Dawson J, Cockel R. Oesophageal perforation at fiberoptic gastroscopy. *BMJ* 1981;283:583.
56. Silvas SE, Nevel O, Rozas G, et al. Endoscopic complications: results of the 1974 American Society of Gastrointestinal Endoscopy Survey. *JAMA* 1976;235:928–30.
57. Bladergroen M, Lowe J, Postlethwait R. Diagnosis and recommended management of esophageal perforation and rupture. *Ann Thorac Surg* 1986;42:235–9.
58. Kronzon I, Cziner DG, Katz ES, et al. Buckling of the tip of the transesophageal echocardiographic probe: a potentially dangerous technical malfunction. *J Am Soc Echocardiogr* 1992;5:176–7.
59. O'Shea JP, Southern JF, D'Ambra MN, et al. Effects of prolonged transesophageal echocardiography imaging and probe manipulation on the esophagus: an echocardiographic-pathologic study. *J Am Coll Cardiol* 1991;17:1426–9.
60. Meltzer RS, Adsumelli R, Risher WH, et al. Lack of lung hemorrhage in humans at intraoperative transesophageal echocardiography, with ultrasound exposure conditions similar to those causing lung hemorrhage in laboratory animals (abstr). *Circulation* 1996;94(suppl I):I455.
61. Grauer SE, Giraud GD. Toxic methemoglobinemia after topical anesthesia for transesophageal echocardiography. *J Am Soc Echocardopgr* 1996;9:874–6.
62. Shorvan PJ, Eykyn SJ, Cotton PB. Gastrointestinal instrumentation, bacteremia, and endocarditis. *Gut* 1983;24:1078–93.
63. Steckelberg JM, Khandheria BK, Anhalt JP, et al. Prospective evaluation of the risk of bacteremia associated with transesophageal echocardiography. *Circulation* 1991;84:177–80.

64. Melendez LJ, Chan K-l, Cheung PK, et al. Incidence of bacteremia in transesophageal echocardiography: a prospective study of 140 consecutive patients. *J Am Coll Cardiol* 1991;18:1650–4.
65. Voller H, Schorder KM, Gast D, et al. Does the incidence of positive blood cultures during transesophageal echocardiography necessitate antibiotic prophylaxis (abstr). *Circulation* 1990;82(suppl 3):III–244.
66. Nikutta P, Mantey-Stiers F, Becht I, et al. Risk of bacteremia induced by transesophageal echocardiography: analysis of 100 consecutive procedures. *J Am Soc Echocardiogr* 1992;5:168–72.
67. Gorge G, Erbel R, Henricks KJ, et al. Positive blood cultures during transesophageal echocardiography. *Am J Cardiol* 1990;65:1404–5.
68. Foster E, Kusumoto FM, Sobol SM, Schiller NB. Streptococcal endocarditis temporally related to transesophageal echocardiography. *J Am Soc Echocardiogr* 1990;3:424–7.
69. Dajani AS, Taubert KA, Wilson W, et al. Prevention of bacterial endocarditis: recommendations by the American Heart Association. *JAMA* 1997;227:1794–801.
70. Henry Wl, DeMaria A, Gramiak R, et al. Report of the American Society of Echocardiography Committee on Nomenclature and Standards in Two-Dimensional Echocardiography. *Circulation* 1980;62:212–17.
71. Pearlman AS, Gardin JM, Martin RP, et al. Guidelines for Physician Training in transesophageal echocardiography: Recommendation of the American Society of Echocardiography Committee for Physician Training in Echocardiography. *J Am Soc Echocardiogr* 1992;5:787–94.

2
Mitral valvular disease

Over the years, echocardiography has played an enormous part in the understanding of mitral valvular disease. In the early days of M-mode echocardiography, the mitral valve was frequently the only discernible cardiac structure identified,[1] thus the diagnosis of mitral stenosis could be made reliably by non-invasive means. With the development of two-dimensional echocardiography, a spatial evaluation of the mitral valve was possible, and the importance of the mitral subvalvular apparatus in conjunction with the valve leaflets and their motion was recognized for the first time, eliminating many of the misconceptions about the mitral valve.[2–7] The notorious mitral valve prolapse syndrome was recognized and perpetuated by echocardiography. Doppler echocardiography together with two-dimensional imaging has provided the physiological assessment of mitral valvular disease for quantifying the degree of stenosis and regurgitation. With the advent of reparative surgical techniques in the intervention of mitral valvular disease,[8] transesophageal echocardiography provides the complimentary image method necessary for the precise assessment of mitral valvular structural abnormalities to direct appropriate treatment.

In the past, the decision to intervene in mitral valvular disease was based on the development of severe physiology (stenosis or regurgitation), followed by replacing the valve with a prosthesis. Unfortunately, this frequently resulted in an imperfect functional result (substituting one disease process for another) with rather disconcerting morbidity and mortality.[9] In the mid-1990s, largely due to improved imaging techniques, a better appreciation of mitral valvular disease has evolved. With the ability to precisely define specific structural abnormalities for the valve leaflets and subvalvular apparatus, reparative surgical techniques were developed that overcame the short-comings associated with prosthetic valves. Due to the successful results obtained with these reparative techniques in valvular function, and in improved morbidity and mortality, interventions in the disease process are being contemplated before the valve disease becomes severe in an effort to improve further the longevity of patients with mitral disease.[10–13]

It is paramount that the physician performing transesophageal echocardiography has a complete and thorough understanding of normal mitral valvular anatomy to recognize abnormalities. Next in importance, the physician must be able to assess the motion of the valve leaflets in concordance with the subvalvular apparatus to describe anatomical abnormalities produced by the disease process.[14–16] The physician must be well versed in

the principles and practice of Doppler methodology to implement them properly and identify abnormalities in physiology. The echocardiographer must have the technical ability to obtain all the views necessary to evaluate the whole structure and function of the mitral valve, which are uniquely acquired with multiplane transesophageal echocardiography in order to provide a complete assessment.

Normal mitral valve anatomy

Leaflets

The normal mitral valve sits in the fibrous skeleton of the heart separating the left atrium from the left ventricle (figure 2.1). The normal valve has two leaflets that act in conjunction with the subvalvular apparatus as one functional unit.[17–22] The mitral leaflets are attached at their bases to the fibro-muscular ring or annulus fibrosis, and by their free edges to the subvalvular apparatus consisting of chordae tendineae and papillary muscles.
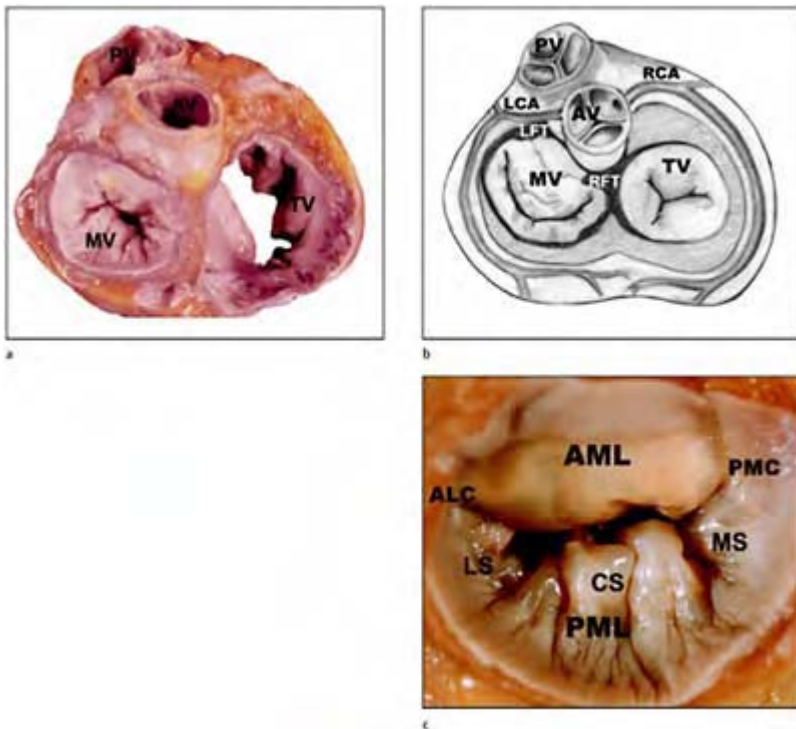
Figure 2.1 Normal mitral valve anatomy. (a) Anatomical section at the

base of the heart illustrating the position of the four cardiac valves. The mitral valve (MV) is seated posterior to the semilunar valves and is lateral and to the left of the tricuspid valve (TV). The anterior leaflet of the mitral valve is contiguous and opposite the left and non-coronary cusps of the aortic valve. The posterior medial commissure of the mitral valve lies opposite the septal leaflet of the tricuspid valve. The posterior position of the mitral valve allows optimal examination by multiplane transesophageal echocardiography. (b) Corresponding drawing of the fibrous skeleton of the heart. The anterior mitral leaflet is firmly attached to the aortic annulus by dense fibrous connective tissue forming the mitral curtain or mitral-aortic fibrous continuity. Two fibrous trigones situated near each commissure represent fixation points for the fibrous skeleton providing stability for cardiac contraction and the valve annulus. The right fibrous trigone (RFT) is centrally located between the aortic valve (AV), mitral and tricuspid valves. The left fibrous trigone (LFT) extends superiorly and blends into the aortic root. Both trigones project connective tissue fibers laterally and posteriorly to encircle the mitral annulus. In the most posterior portion of the annulus the fibers progressively diminish leaving the central posterior annulus devoid of dense collagen fibers and only composed of loose connective tissue.

This composition of the mitral annulus allows for annular dilatation to occur largely in the posterior aspect of the valve. The left coronary artery (LCA) courses superiorly and laterally around the mitral annulus and the circumflex artery wraps around the posterior aspect of the valve to the crux of the heart. (c) Gross specimen of the mitral valve leaflets. The posterior mitral leaflet (PML) is divided into three scallops; lateral scallop (LS), central scallop (CS) usually the largest, and the medial scallop (MS) by prominent indentations in the leaflet margin. Note the anterior mitral leaflet (AML) is free of these indentations or scallops. The anterior leaflet is rather triangular in shape. The posterior leaflet is more rectangular in shape and wraps around the free margin of the anterior leaflet. Although the leaflet width of the anterior leaflet is larger than the posterior leaflet, both leaflets are approximately equal in surface area. In addition, both leaflets are really continuous as demonstrated at the commissures, which do not extend entirely to the annulus. ALC, anterolateral commissure; PMC, posteromedial commissure; PV, pulmonary valve; RCA, right coronary artery.
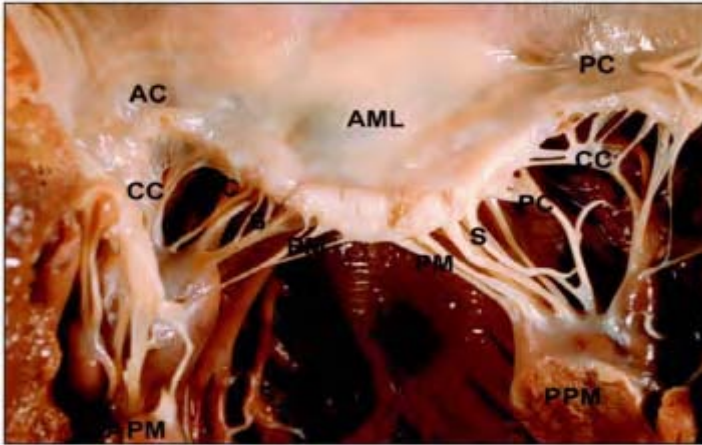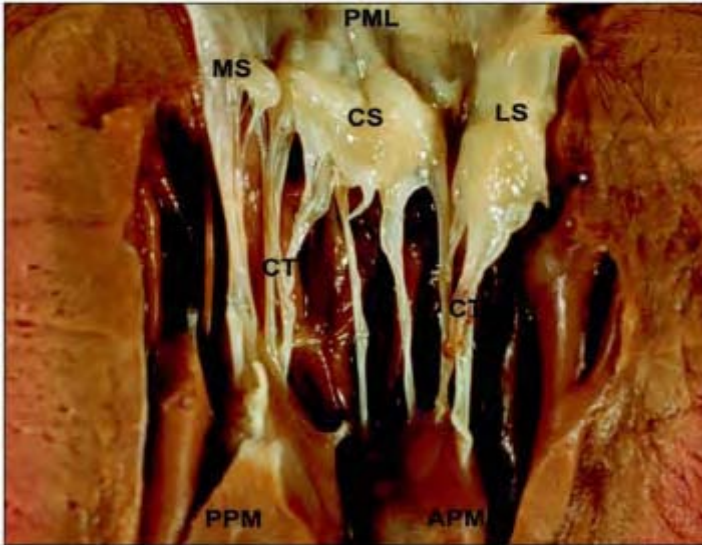
Figure 2.2 Normal anterior and posterior leaflet anatomy. (a) The anterior mitral leaflet is triangular in shape with a broad base of attachment and a rounded apical contour. The body of the leaflet is thin and translucent in comparison to the leaflet margin. Chordal insertion to the ventricular surface of the free margin

thickens the leaflet and produces the rough zone, which aids in providing for maximum leaflet coaptation. Both papillary muscles supply chordae tendineae in an oblique, symmetrical fashion to the anterior leaflet. The oblique orientation of the chordae allow for maximum and unrestricted movement of the anterior leaflet. Anterior leaflet chordae tendineae are labeled according to their point of attachment to the leaflet and by some degree to their shape. PM, paramedial; S, strut, PC, paracommissural chordae; APM, anterior papillary muscle; PPM posterior papillary muscle. (b) The posterior mitral leaflet (PML) is rectangular in shape and comprises a larger circumference and therefore portion of the annulus in comparison to the anterior leaflet. Both papillary muscles (PPM) supply chordae tendineae (CT) to the posterior leaflet in a symmetrical and parallel fashion. This parallel arrangement is attributed to the shorter distance between the papillary muscles posteriorly in the ventricle and lends to the pressure support theory for the function of the posterior leaflet. Also the arrangement of the papillary muscles project chordae tendineae which when relaxed are evenly spaced at a distance free from each other with normal motion. The three scallops of the posterior leaflet are readily identifiable with the central scallop (CS) being the largest scallop. MS, medial scallop; LS, lateral scallop.
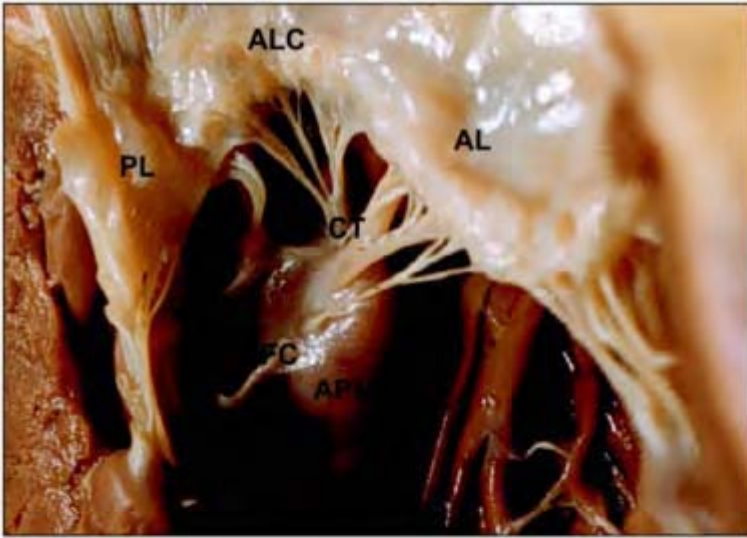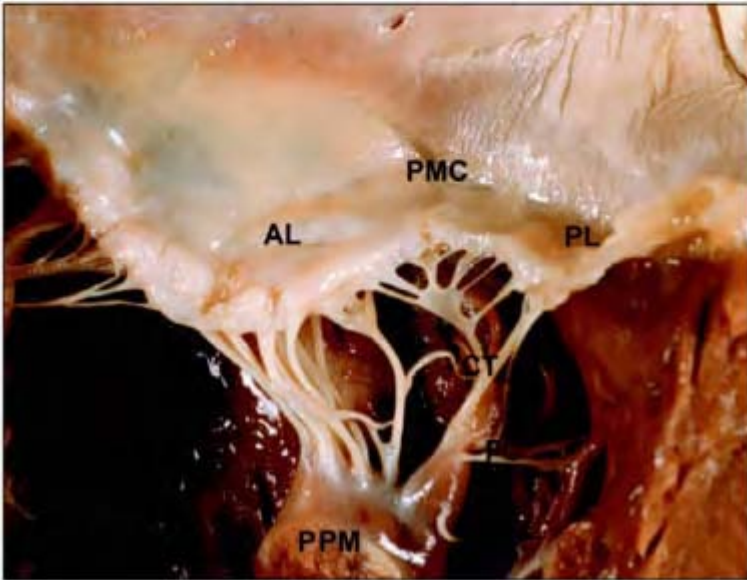
Figure 2.3 Normal anterior and posterior commissures. Each commissure receives one chordae tendineae from its respective papillary muscle. Commissural chordae are

broad at their origin, project perpendicularly to fan out intersect the commissural portion of each leaflet. In this manner, adequate support is provided to the whole commissure serving as a hinge point for leaflet motion. (a) Anterolateral commissure. (b) Posteromedial commissure. Due to the oblique orientation of the mitral valve in the fibrous skeleton in relationship to the position of papillary muscles, the commissural chord to the posteromedial commissure usually spreads out wider as it branches and is thicker and longer than the chordae to the anterolateral commissure. This may provide credence for why the leaflet tissue surrounding the anterolateral commissure is less likely to prolapse and therefore at surgery provides a good reference point for demonstrating prolapse for other areas. AL, anterior leaflet; PL, posterior leaflet; PM, papillary muscle; CT, chordae tendineae.

The two leaflets, anterior and posterior, differ in size and shape but share equal leaflet surface area (figure 2.2). The anterior leaflet, also known as the septal or aortic leaflet, is quadrangular or triangular in shape, with a convex free edge. The height or width (base to free edge measurement) of the anterior leaflet is about one third larger than the posterior leaflet. The posterior leaflet (mural or inferolateral) is narrower, attaches to a larger portion of the annulus than the anterior leaflet, and has a concave free edge. Two natural indentations or clefts in the posterior leaflet produce three segments, which subdivide the posterior leaflet, into lateral, central, and medial scallops. The lateral and medial scallops are smaller in surface area than the central scallop. The two leaflets are joined at their lateral free edges near the annulus just above the papillary muscles, to form two hinge points or commissures (figure 2.3). When the mitral valve is closed during systole and viewed enface, the line of valve closure resembles a smile. When the mitral valve is open during diastole and viewed enface, it assumes more of an elliptical shape that gradually tapers like a funnel into the ventricle, and, when imaged sagitally, resembles a trap door with the anterior to posterior leaflet ratio being 2/3 and 1/3 respectively.

The leaflet tissue is thin and transparent near the annulus and the central portion (body) of the valve, gradually thickening near the free edge, becoming opaque and very thick at the opposing surface (rough zone). It is this rough zone that is the point of attachment for the chordae, and which permits a seal between the two leaflets when they approximate during closure. The leaflet edges fold over the chordal attachment (hooding), which somewhat protects the insertion point and provides increased surface area for approximation.

The posterior leaflet, with its narrow height, serves as a valance for the anterior leaflet to swing up and close against promoting a seal during closure. This leads to the concept[8] of the anterior leaflet being the active "velocity leaflet", largely responsible for the dynamics of opening and closing of the mitral orifice. The posterior leaflet is the "passive leaflet" and is the buttress that the anterior leaflet closes against to absorb the strain transmitted to the valve from the pressure generated in the ventricle during systole. The smaller height of the posterior leaflet also defines the orientation of the inflow tract, directing the flow of blood to the posterior aspect of the left ventricle.

Annulus

The two mitral leaflets are attached at their bases to a ring of fibro-muscular tissue in the fibrous skeleton of the heart, called the annulus fibrosus [23,24] (figure 2.1). The fibrous trigones are the major components of the annulus fibrosus and sit adjacent to the commissures. The right trigone or the central fibrous body is the more prominent of the two and is centered between the tricuspid, mitral, and aortic valves. The left trigone is seated between the mitral and aortic valve towards the periphery and most posterior portion of the fibrous skeleton. The two trigones are connected anteriorly with a thick band of collagenous connective tissue (mitralaortic fibrous continuity), which is in between the aortic and mitral valve and which forms the annulus for the entire anterior mitral leaflet. The anterior leaflet occupies only 40% of the total annular perimeter, with the entire basal portion of the anterior leaflet being attached to rigid collagen tissue opposite the aortic valve, which allows commissural attachments to be very close to the trigones. These characteristics allow rigid support of the anterior leaflet. The trigones project connective tissue laterally and posteriorly, surrounding the posterior leaflet to form the remainder of the annulus. The posterior annulus is thinner and weaker than the anterior annulus—as the connective tissue progresses posteriorly it gradually tapers to leave the posterior area around the central scallop with only loose connective tissue almost completely devoid of collagen fibers. This provides less annular support for the posterior leaflet, especially near the central scallop,[25,26] allowing the annulus to stretch in this area.

The dimensions of the annulus are described by a smaller height (anterior–posterior dimension) compared with its width (transverse dimension), with a 3:4 ratio, respectively.[8]

Chordae tendineae

The chordae tendineae are tendinous supporting structures that originate from the tips of the papillary muscles and fan out by branching before inserting onto the ventricular

surface of the leaflet[19] (figure 2.4). Usually, chordal insertion is equally spaced (0.5 mm apart) on the margin of the leaflet edge, which promotes symmetrical motion. Normal chordae tendineae are arranged in an architectural alignment and spacing. Each chord is free from the others, without touching the ventricular myocardium during all phases of the cardiac cycle (figure 2.5). Occasionally, some chordae may originate directly from the ventricular myocardium and insert into the leaflets. Small false chords may originate from the ventricular myocardium and attach to the papillary muscles, which are thought to act as supporting apparatus for the papillary muscles. Aberrant chords are chordae that are attached from myocardium to myocardium, which have unknown significance and probably serve no real purpose. Variations in the number of chords and of the branching or insertion patterns account for the major aberrations of the chordae tendineae.
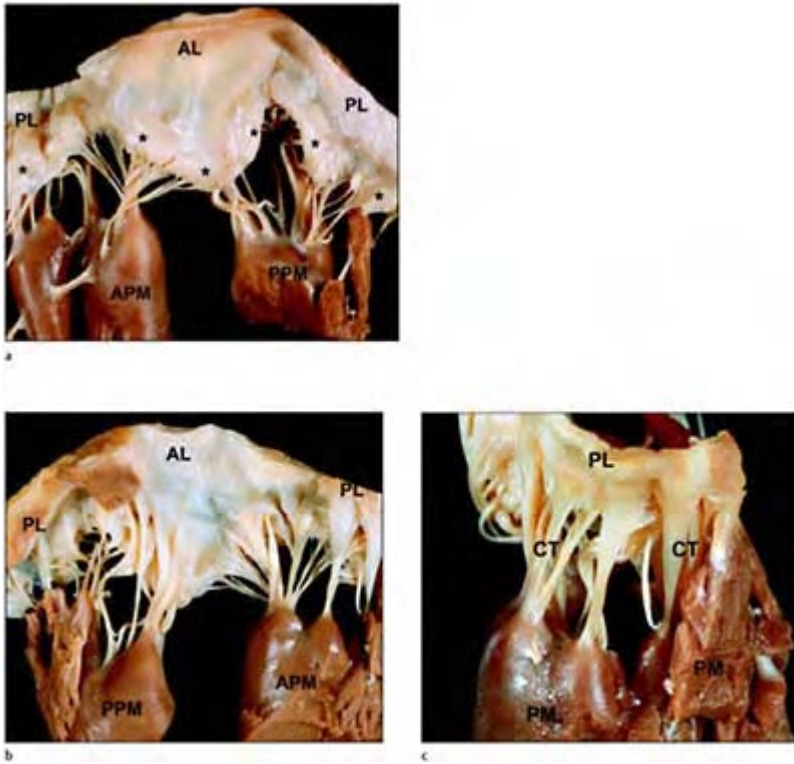
Figure 2.4 Normal mitral valve anatomy. (a) Postmortem mitral valve specimen viewed form the atrial aspect of the leaflets. Chordae tendineae attach to the undersurface of the leaflet margins producing hooding of the leaflet edge for the rough zone (stars).

The greater thickness of the rough zone of the leaflet margin provides greater surface area for leaflet coapation. In addition false chordae tendineae are demonstrated bridging one papillary muscle to another. (b) Postmortem mitral valve specimen viewed from the ventricular aspect of the leaflets. Chordae tendineae insert into the ventricular or undersurface of the leaflet margin. Chordae tendineae only insert to the peripheral margin of the anterior leaflet. (c) Postmortem mitral valve specimen viewed from a lateral ventricular aspect of the posterior leaflet surface. The parallel projection of chordal insertion to the posterior leaflet (c) from the papillary muscles is demonstrated nicely. Chordae tendineae insert to the whole undersurface of the posterior leaflet including the leaflet margin, body of the leaflet and annular insertion portions. This chordal arrangement again lends credence for the pressure support function of the posterior mitral leaflet. AL, anterior leaflet; PL, posterior leaflet; APM, anterior papillary muscle; PPM, posterior papillary muscle; CT, chordae tendineae.

Chordal systems differ according to whether they are attached to the anterior or posterior leaflets.[2–5,7,19] Chordae to the posterior leaflet project and attach to the ventricular surface of the leaflet in a parallel manner. These act as supporting columns to the posterior leaflet and supportthe buttressing theory for closure. Branching posterior leaflet chordae insert into the central scallop free edge, body (mid surface), or basal portion near the annulus. Chordae to the lateral and medial scallops insert in a more variable arrangement. Chordae to the anterior leaflet are projected in an oblique manner, which aids in opening and closing of the leaflet. Anterior leaflet chordae insert onto the ventricular surface of the leaflet directly to the leaflet margin (primary chordae) or

slightly behind the free edge (secondary chordae). Chordae to the anterior leaflet can be further subdivided into paramedial, central strut, or paracommissural, depending on their position on the perimeter of the anterior leaflet free edge margin.

The commissures have a unique chordal system that serves as an anchor to the leaflets hinge point[3,19] (figure 2.3). Each papillary muscle gives rise to one commissural chord. The commissural chord arises in a singular fashion and fans out distally, into about five small chords inserting into the corner of both leaflets, the free edges of the commissural tissue. Due to the slightly oblique position of the valve in the annulus fibrosus in relation to the papillary muscles, the commissural chords to the posterior medial commissure usually spread or fan wider as it branches and are thicker and longer than the chords to the anterior lateral commissure. The proper identification of the commissures can be aided by identifying the respective commissural chord pattern.

Papillary muscles

The papillary muscles originate as muscular projections or columns from the ventricular myocardium, between the apical and middle portion of the ventricular chamber (figure 2.6).[27,28] The exact positioning of both papillary muscles may vary considerably. The anterior papillary muscle usually arises from the lateral border of the anterior wall, and the posterior papillary muscle usually originates from the medial aspect of the posterior wall where it abuts the ventricular septum. There is usually only one anterior papillary muscle, and two or three posterior papillary muscles, but the volume of the anterior and posterior muscle groups are usually equal.

When a papillary muscle group is present the individual muscles wrap around each other in a concave–convex fashion almost acting as a single unit during contraction. The base and body of the papillary muscles are anchored to the ventricular free wall by muscular or tendinous chordae known as false chords, which are believed to serve also as channels for Purkinje fibers. The tips or heads of the papillary muscles taper into tendinous projections to give rise to the chordae tendineae. Each papillary muscle group gives off chordae tendineae in a symmetrical fashion to their respective halves of both the anterior and posterior leaflets (figure 2.4). It is well established that the papillary muscles play a vital part in valve integrity and valve motion.
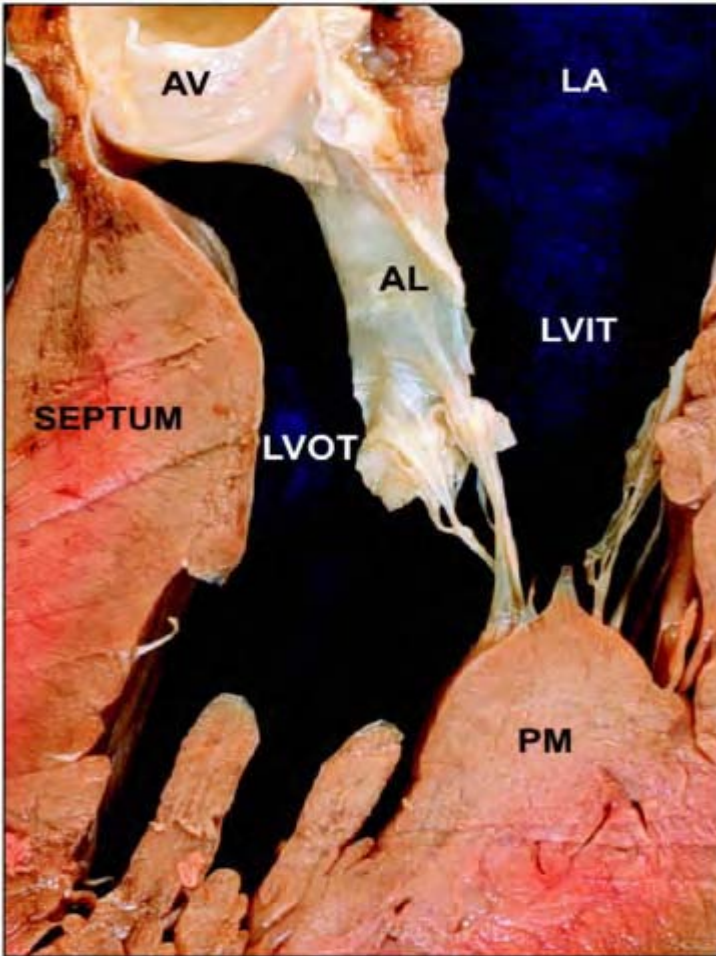
Figure 2.5 Anatomical preparation demonstrating how the mitral valve produces a functional left ventricular inflow tract and left ventricular outflow tract. Unlike the right ventricle there is no true anatomical inflow and outflow tracts. The inflow and outflow tracts are produced by the normal anatomical relationship of the mitral valvular apparatus in its posterior position and orientation in the left ventricle. LA, left atrium; LVIT, left

ventricular inflow tract; PM, papillary muscle; AL, anterior mitral leaflet; AV, aortic valve; Septum; interventricular septum.
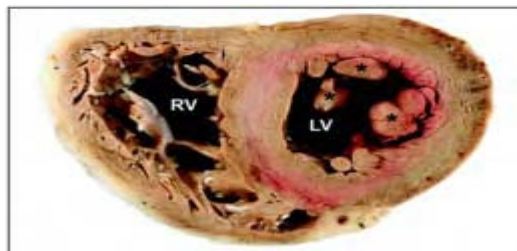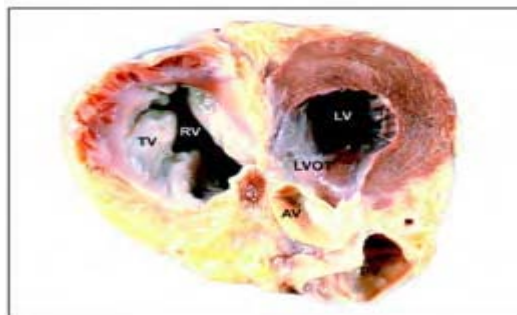
Figure 2.6 Short-axis anatomical preparations corresponding to the standard echocardiographic short-axis views obtained from the gastric window at 0°. (a) Ventricular short axis at the papillary muscle level. (b) Ventricular short axis at the basal level. (c) Short-axis orientation of the

mitral valve as typically projected from the transesophageal gastric window. RV, right ventricle; LV, left ventricle; TV, tricuspid valve; LVOT, left ventricular outflow tract; AV, aortic valve; A1,2,3, anterior mitral leaflet; P1,2,3, posterior mitral leaflet.
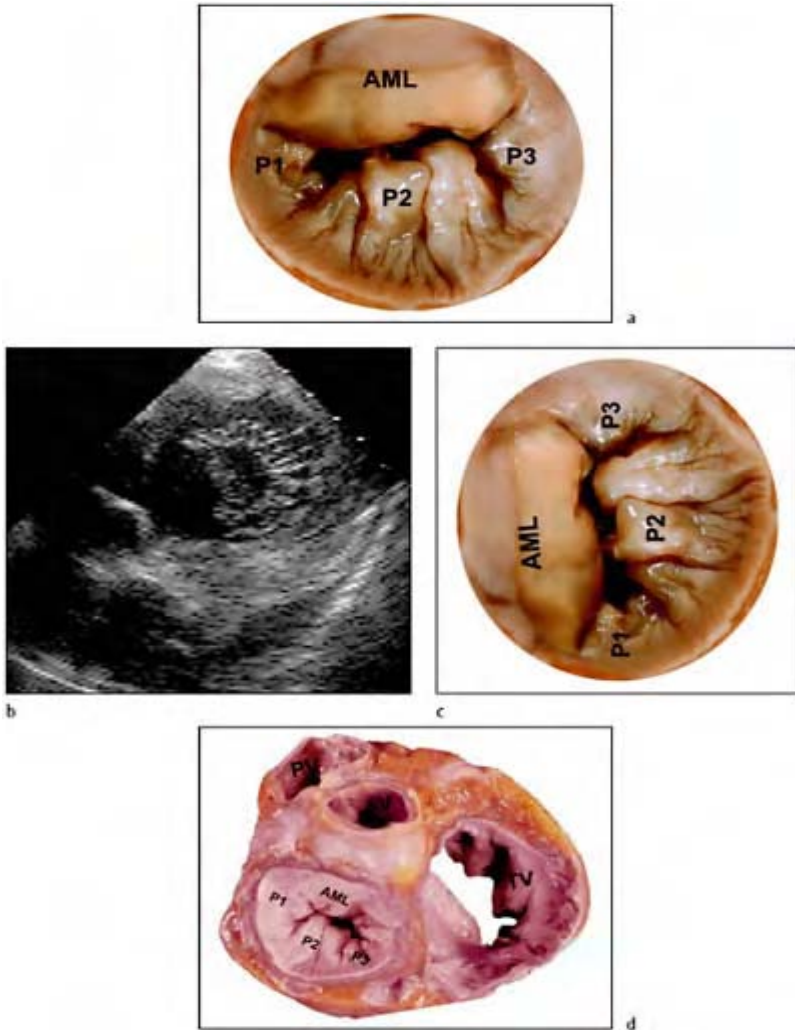
Figure 2.7 Orientation of the mitral valve from different perspectives in the

operating room. It is helpful to understand the orientation of the mitral valve from different perspectives so that meaningful and accurate communication can occur between all three groups especially during mitral valve reparative procedures. (a) Surgeon's anatomical view. (b) Short-axis echo image. (c) Echocardiographer's orientation. (d) Anesthesiologist's anatomical perspective from the head of the operating table. AML, anterior mitral leaflet; P1,2,3, posterior mitral leaflet.
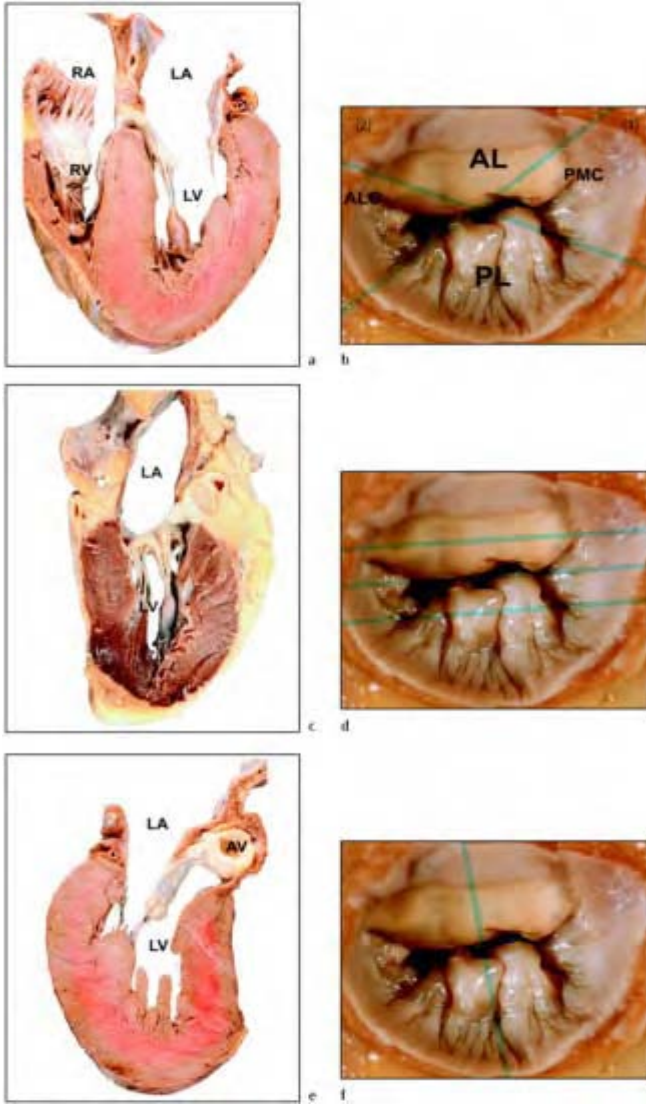
Figure 2.8 Anatomical preparations demonstrating the orientation of the mitral valve depicted in the standard TEE views and short axis plane. Due to the relationship of the esophagus to the heart the mitral valve plane is visualized from many different perspectives, which often produces

confusion in accurately identifying the exact leaflet area visualized. (a) The standard four-chamber, frontal plane at 0° obtained from the mid- to lower esophageal windows. (b) Typically the mitral valve is cut tangentially depending upon the position of the TEE transducer within the esophagus. Lower in the esophagus the valve leaflets are imaged nearer the posteromedial commissure; imaging more of the lateral area of the anterior leaflet and medial area of the posterior leaflet (2). As the probe is slowly withdrawn towards the mid-esophagus the leaflets are imaged nearer the anterolateral commissure; imaging more of the medial area of the anterior leaflet and lateral area of the posterior leaflet (1). (c) The standard two-chamber view at approximately 60°. The transesophageal echocardiography (TEE) imaging plane cuts the mitral valve leaflets parallel to the line of closure. (d) With slight rotational movement of the transducer the plane can be directed through the anterior leaflet, posterior leaflet of line of closure of the leaflets. (e) The standard three-chamber view at 135°. (f) This view produces an imaging plane nearest to truly cutting the mitral valve in an anterior–posterior orientation. RA, right atrium; LA, left atrium; RV, right ventricle; LV, left ventricle; AL, anterior leaflet; PL, posterior leaflet; ALC, anterolateral commissure; PMC, posteromedial commissure.
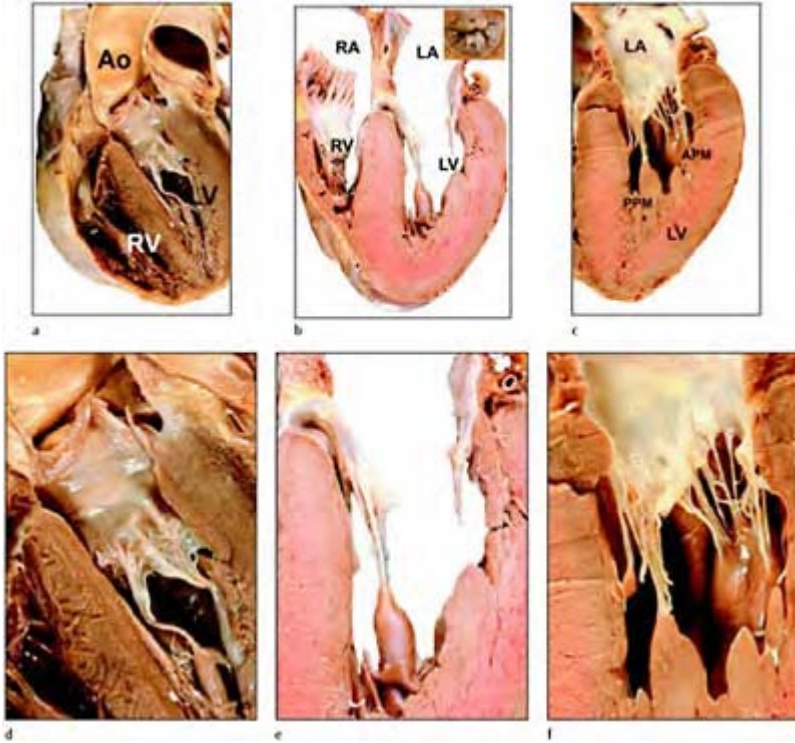
Figure 2.9 Normal echocardiographic anatomy. In the lower esophageal window the mitral valve is imaged in different planes as the transducer is rotated between 0° and 180°. In examining the mitral leaflets and subvalvular apparatus it is important to have a conceptual idea of the true anatomy in each plane in order to mentally construct a three-dimensional perspective of the mitral anatomy. Mitral valve disease or abnormalities can more accurately be described and understood in this manner. Frontal projections. (a) Anatomical preparation of the heart at –10°. (b) Enlargement of mitral apparatus –10°. (c) Anatomical preparation of the heart at 0°. (d)

Enlargement of mitral apparatus 0°. (e)
Anatomical preparation of the heart at
30°. (f) Enlargement of mitral
apparatus 30°.

The blood supply to the papillary muscles is highly variable.[29] The confluence of coronary artery branches joins into a single central artery or meshwork of small branches, which tapers and projects longitudinally in the muscle. This framework of blood supply probably allows the head of the muscle to be more prone to ischemia. The anterior papillary muscle is supplied by the second septal branch of the left anterior descending artery and by a branch of the circumflex artery. The posterior papillary muscle is usually supplied from septal branches of
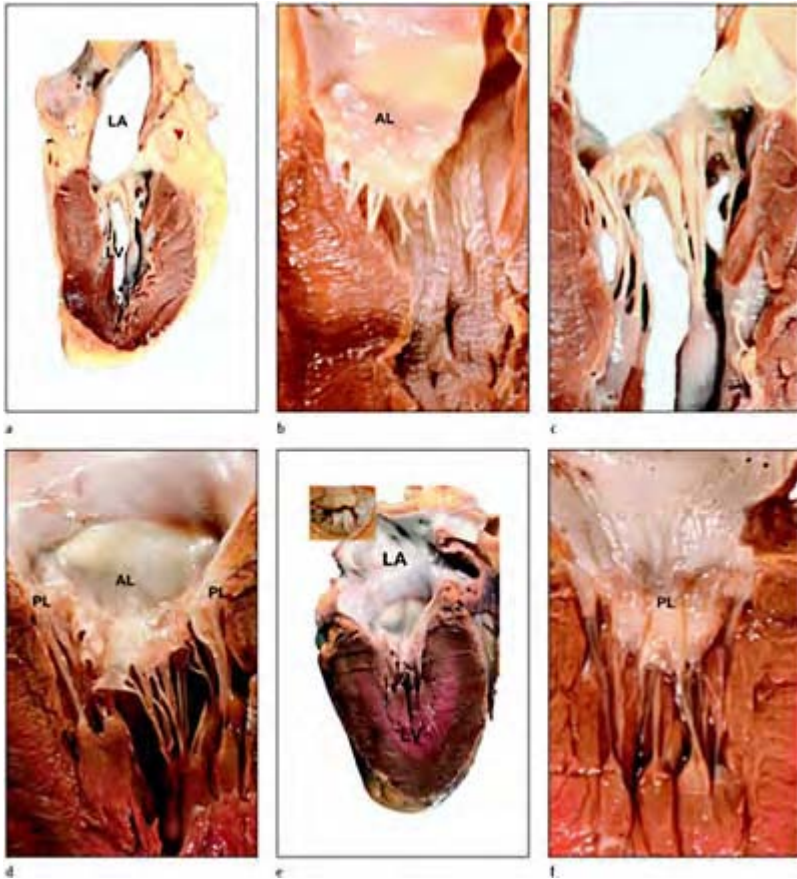
Figure 2.10 Normal echocardiographic
anatomy demonstrating mitral valve

anatomy (continuation of fig. 2.9). Longitudinal projections. (a) Anatomical preparation of the heart at 60° with enlargement of mitral apparatus (b). (c) Anatomical preparation of the heart at 75° with enface view of the mitral leaflets illustrating rotational cuts and corresponding enlargements (d) predominately anterior leaflet, (e) anterior and posterior leaflets near line of closure, (f) predominately posterior leaflet.
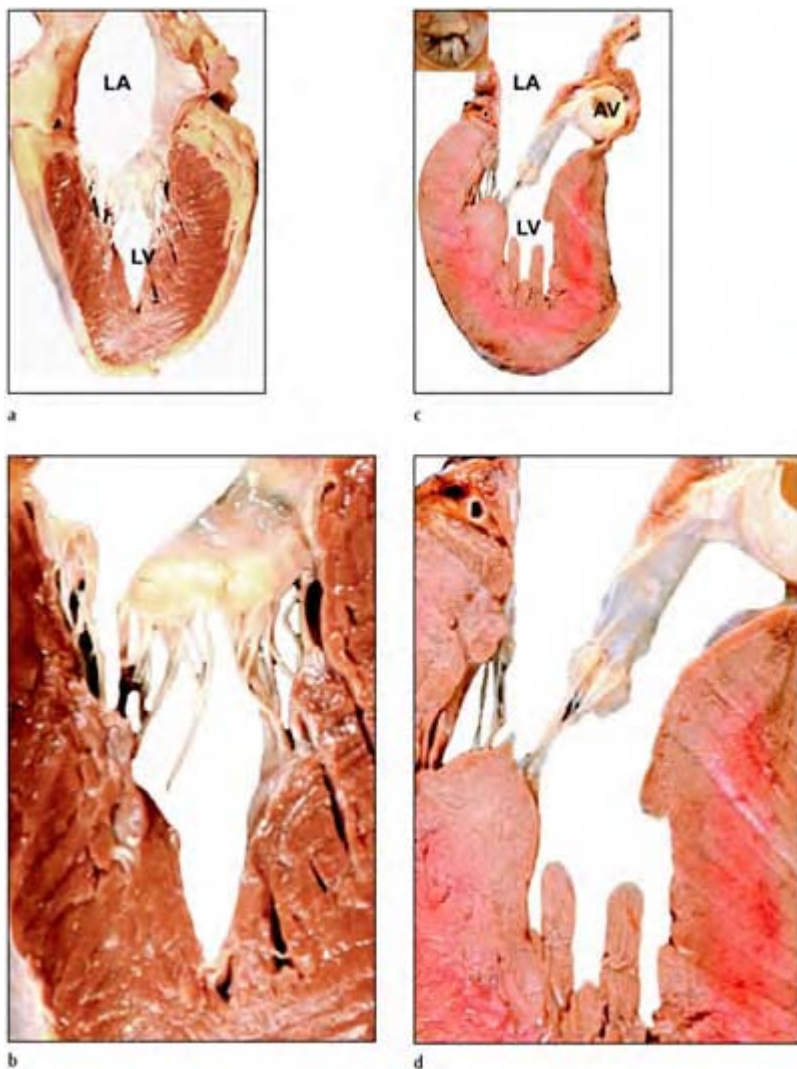
Figure 2.11 Normal echocardiographic anatomy demonstrating mitral valve anatomy (continuation of figures 2.9 and 2.10). (a) Anatomical preparation of the heart at 110° with enlargement of mitral apparatus (b). (c) Anatomical preparation of the heart at 135° with mitral apparatus enlargement (d).

the posterior descending artery, in addition to a small branch of the circumflex artery. When the blood supply is left dominant, the posterior papillary muscle is especially vulnerable to ischemia. Similar to the ventricular endocardium, the papillary muscles are also perfused by the diffusion of oxygen from blood in the ventricular cavity.

Normal multiplane transesophageal echocardiographic valve analysis

Transesophageal echocardiography has allowed many of the intricacies of the mitral valve apparatus to be elucidated.[30-38] It is now widely recognized that proper function of the mitral valve depends on the normal function and integrity of the leaflets, annulus, chordae tendon, papillary muscles, and subjacent left ventricular myocardium. Abnormalities in any of these components, either individually or in combination, produce dysfunction of the mitral valve unit. Multiplane transesophageal echocardiography, can define the mitral valve structure and function. To obtain a comprehensive and accurate description of the whole mitral apparatus it is useful to have a systematic approach in performing the multiplane transesophageal echocardiographic examination (figures 2.7–2.11). With the multiplane transesophageal echocardiographic transducer in the stomach the papillary muscles can be assessed along with their interaction with the left ventricle. With slow withdrawal of the probe into the esophagus the chordae tendineae, and the valve leaflets including commissural areas and annulus, can be assessed in succession (figure 2.6). With a careful systematic transesophageal echocardiographic assessment, a three-dimensional picture of the whole mitral apparatus can be constructed mentally.
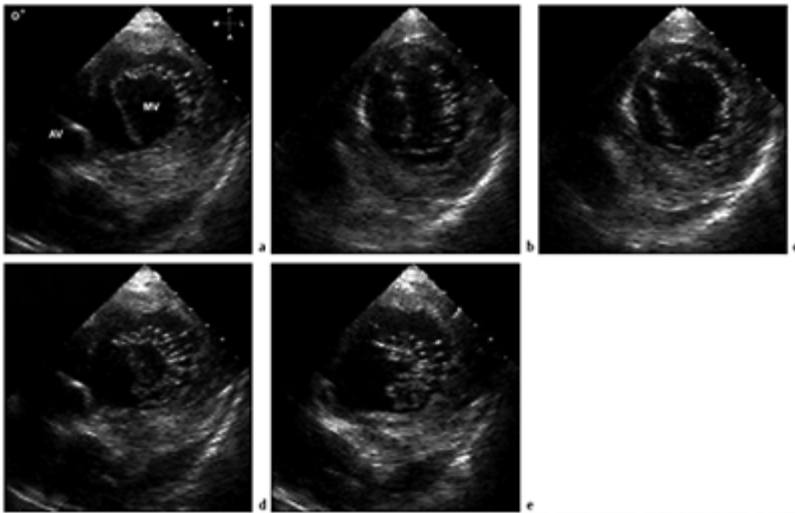
Figure 2.12 Normal mitral valve motion during the cardiac cycle in the

gastric short axis view. In early diastole (a) the open mitral valve conforms to a "D" shape with the anterior leaflet to the right and the posterior leaflet to the left of the echocardiographic image. In mid-diastole (b) the anterior and posterior leaflets drift closer together as left ventricular filling decreases. During atrial systole (c) the valve leaflets again separate to assume a more circular orifice. By late diastole (d) following atrial contraction and end systole (e) the anterior and posterior leaflets approximate into a "C" shape or the typical "smile" as described surgically.

With the multiplane transesophageal echocardiographic transducer at 0°, 40–45 cm from the incisors, in the transgastric position the probe is slightly anteflexed and maneuvered to obtain a short axis view of the left ventricle at the mid papillary muscle level (figures 2.6, 2.12–2.18). Depending on the heart's position in the chest, being either vertical or horizontal the transducer may need to be rotated from 0° to about 15° to obtain a true, non-oblique short axis view of the left ventricle. With the depth of the echocardiographic image set to 12–16 cm, the normal left ventricle should fill most of the image sector and allow good visualization of the papillary muscles for examination. The papillary muscles are visualized in the short axis of the left ventricle in cross-section. The posteromedial papillary muscle is found at the top of the echocardiographic display at approximately 1 O'clock, and the anterolateral papillary muscle is located between 4 and 5 O'clock near the bottom of the display. The exact position of the papillary muscles varies in different patients, which may be better appreciated by transesophageal echocardiographic imaging than by transthoracic echocardiography. However, both papillary muscles
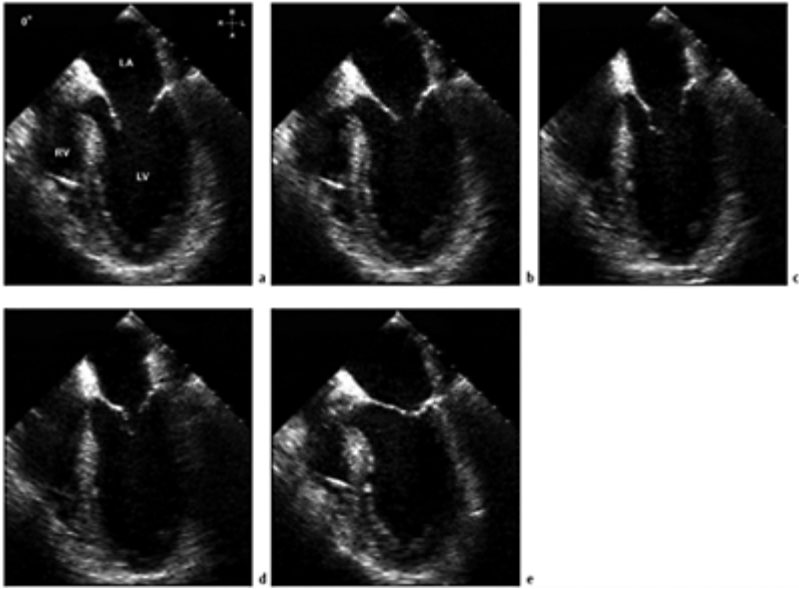
Figure 2.13 Normal mitral valve motion during the cardiac cycle in the lower esophageal view at 0°. The anterior leaflet is in the left of the image sector and the posterior leaflet is on the right. The anterior leaflet appears longer and exhibits greater motion than the posterior leaflet. Both leaflets open and close in a trap door fashion. (a) Early diastole. (b) Mid-diastole. (c) Atrial systole. (d) Late diastole. (e) End systole.

are normally situated in the longitudinal, posterior half of the left ventricle. Therefore in the short axis view the distance between the papillary muscles in the inferior aspect of the left ventricle is less than half the distance around the anterior aspect of the left ventricle. The anterolateral papillary muscle is usually larger than the posteromedial muscle and is usually comprised of one muscle, in contrast to the posteromedial muscle, which is made up of a group of two or more smaller muscles. Both papillary muscles should appear in close approximation with the ventricular myocardium, if not contiguous with it, and should have the same echogenicity or texture as the surrounding muscle. The size or diameter of the papillary muscles should be slightly smaller or approximate the myocardial thickness. Occasionally, both papillary muscles may exhibit isolated hypertrophy,[29] appearing thicker or slightly out of proportion to the ventricular

myocardium, but are in normal positions in the ventricular cavity. In this situation, attention must be paid to the position of the papillary muscles to ensure that there is adequate separation of the muscles along the posterior circumference of the ventricle.

The transducer is then rotated 90° from the true cross-section just obtained to assess the papillary muscles longitudinally (figure 2.19). In the long axis view, with the papillary muscles centered in the middle of the echocardiographic image, the integrity of the papillary muscles to the left ventricular myocardium is readily apparent. In the apex-up orientation, with the transducer at the top of the screen, the posteromedial muscles with multiple heads appear directly at the top of the image and project towards the base of the heart, with the anterolateral muscle at the bottom of the image. Either papillary muscle may be better defined with minor angulations of the probe. The
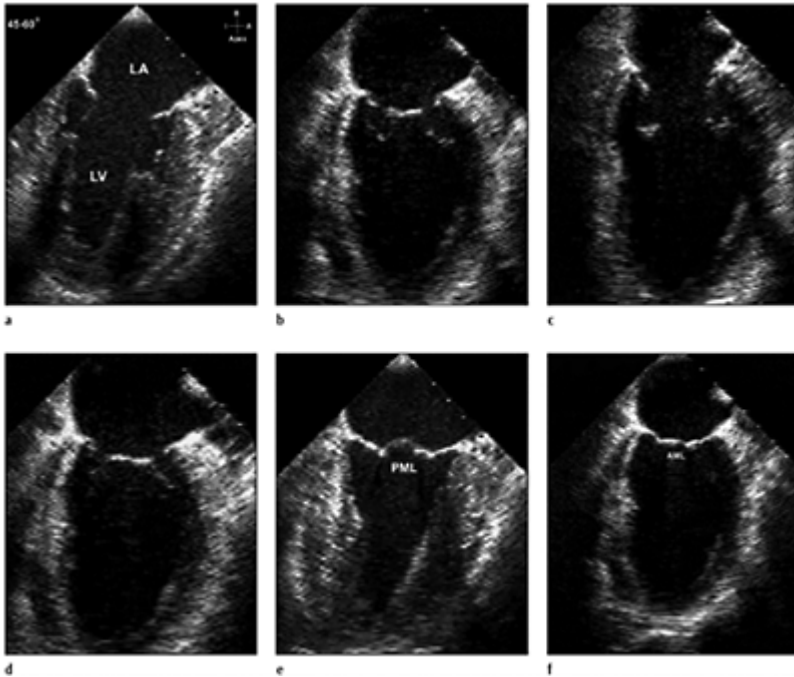
Figure 2.14 Normal mitral valve motion during the cardiac cycle in the lower esophageal view at 60–75°. The anterior leaflet appears in the middle of the annular plane bordered by the posterior leaflet on both sides. The anterior leaflet moves in an out of the mitral plane during the cardiac cycle, while the posterior leaflet swings back

and forth. The probe can be slightly rotated to focus the examination on the anterior or posterior leaflet during closure. (a) Early diastole. (b) Mid-diastole. (c) Atrial systole. (d) Late diastole. (e) Predominately posterior leaflet during end systole, note scalloping of the leaflet. (f) Predominately anterior leaflet during end systole.

papillary muscles should be affixed to the myocardium in the mid third of the ventricle, with the anterolateral muscle generally appearing longer and narrower in the ventricle in the longitudinal projection. In all cases, the papillary muscles should have similar size and motion. The papillary muscles are attached to the ventricle with a broad base and gradually taper to a head in a conical fashion, ending at roughly the same level in the ventricular cavity. Occasionally, a small accessory papillary muscle may be seen emanating from the apex. All muscles should have similar echogenicity, signifying the same muscle texture and density of the surrounding ventricular myocardium. In older patients, however, a small degree of increased echogenicity is frequently observed in the papillary muscle tip, signifying calcification, which probably represents the normal ageing process. Normal motion of the ventricular myocardium should also be observed in relation to normal papillary muscle motion. Fractional shortening of the papillary muscle (FSPM, figure 2.20) can be easily determined in this view by measuring the end-diastolic (EDL) and end-systolic longitudinal lengths (ESL) where FSPM = [{EDL – ESL/EDL} ×100]. Normal papillary muscle fractional shortening in human beings is $30 \pm 8\%$.[29]
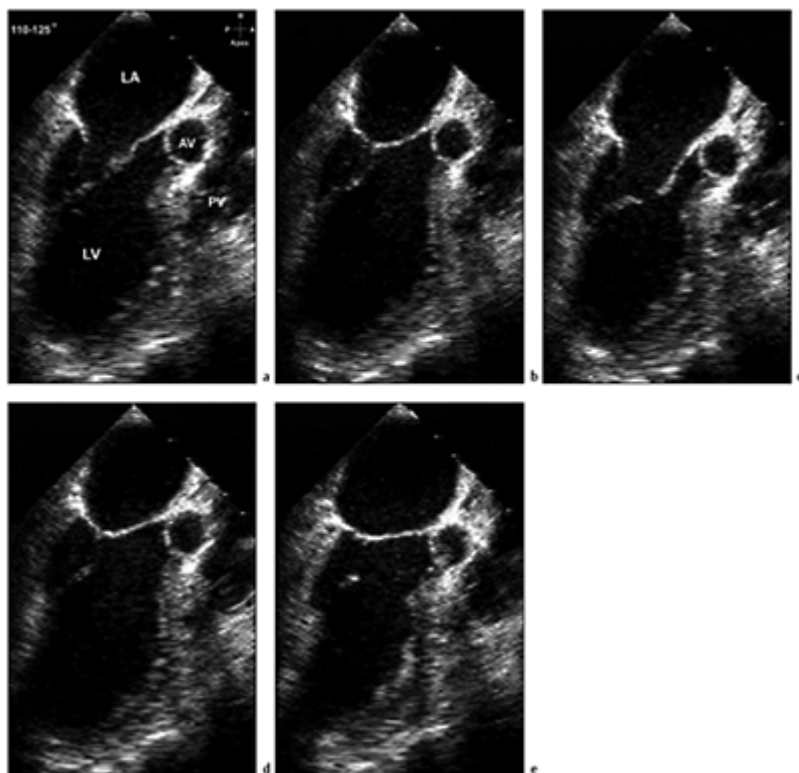
Figure 2.15 Normal mitral valve motion during the cardiac cycle in the lower esophageal view at 135°. The anterior leaflet is on the right of the echo image with the posterior leaflet on the left. As in the 0° orientation the anterior leaflet appears larger and exhibits greater excision. This view however, represents the truest anterior–posterior cut to the mitral valve plane. (a) Early diastole. (b) Mid-diastole. (c) Atrial systole. (d) Late diastole. (e) End systole.

The chordae tendineae are visualized as thin horizontal, continuous structures emanating from the heads of the papillary muscles, projecting towards the annulus (base of the heart) and inserting into the ventricular surface of the leaflets (figure 2.17). The

chordae tendineae appear as multiple, thin linear structures that move in and out of plane with changes in the cardiac cycle between systole and diastole. Normal chordae should all appear to emanate from the apex or head of the papillary muscles and project in a straight, nearly horizontal manner as they fan out towards the leaflets. In the longitudinal projection, the chordae that insert into the posterior leaflet appear
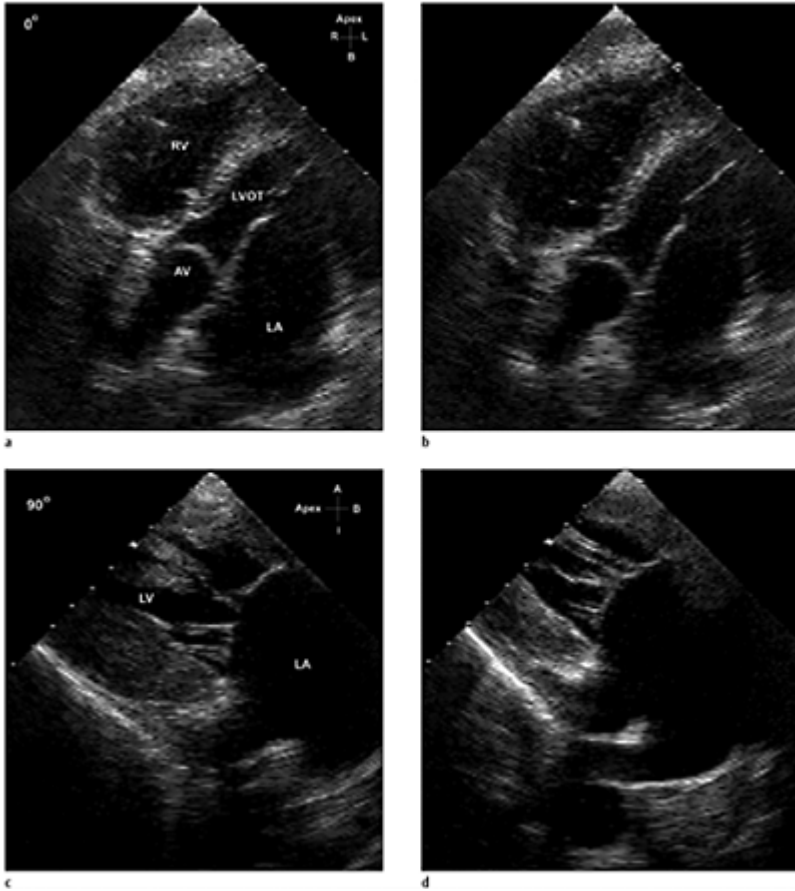
Figure 2.16 Deep transgastric view of the mitral valve. The mitral valve apparatus is nicely demonstrated in the deep transgastric view. The chordae tendineae and papillary muscles are not overshadowed or hidden by coexistent leaflet abnormalities due to the close approximation of the mitral apparatus to the TEE probe. Pathology including

abnormalities in motion of the chordae tendineae and papillary muscles is readily demonstrated during diastole and systole. (a) Diastolic frame at 0°. (b) Systolic frame at 0°. (c) Diastolic frame at 125°. (d) Systolic frame at 125°. The chordae tendineae should appear straight during both diastole and systole. Redundancy or excessive motion of the chordae is easily demonstrated especially during systole suggesting chordal elongation and occasionally SAM (systolic anterior motion).
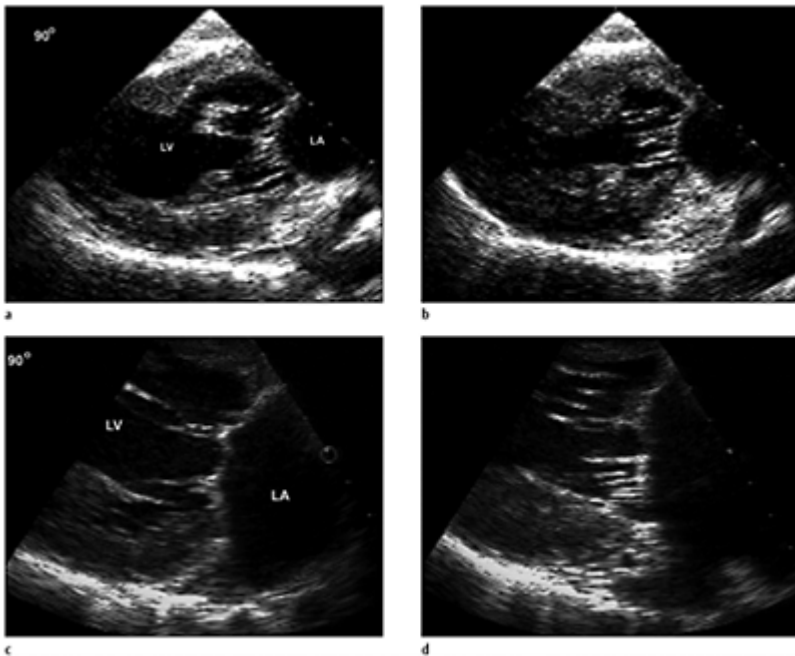
Figure 2.17 Gastric views of the mitral subvalvular apparatus. In the gastric view at 90° the chordae tendineae and papillary muscles are easily demonstrated during diastole and

systole. The chordae to the posterior leaflet appear parallel in orientation during diastole (a) and systole (b). With slight rotation of the probe the chordae to the anterior leaflet are demonstrated with their oblique orientation during diastole (c) and systole (d). With annular dilatation chordae assume an oblique orientation to the posterior leaflet, similar to the anterior leaflet chordae.

nearly horizontal, whereas the chordae to the anterior leaflet are more oblique. It should be noted that all chords, whether they insert into the anterior or posterior leaflet, should appear straight—almost under tension—in both diastole and systole. With the currently available multiplane probes, branching of the chordae tendineae is apparent, but even in the zoom modes the image resolution does not allow for the reliable labeling of chords as primary, secondary, or tertiary branches. Occasionally, chordae may be identified that emanate from the heads of the papillary muscles and insert into the ventricular myocardium. These chordae are frequently identified by transthoracic imaging, but are more readily apparent with transesophageal echocardiography, and have been labeled as ventricular chordae or aberrant chordae.
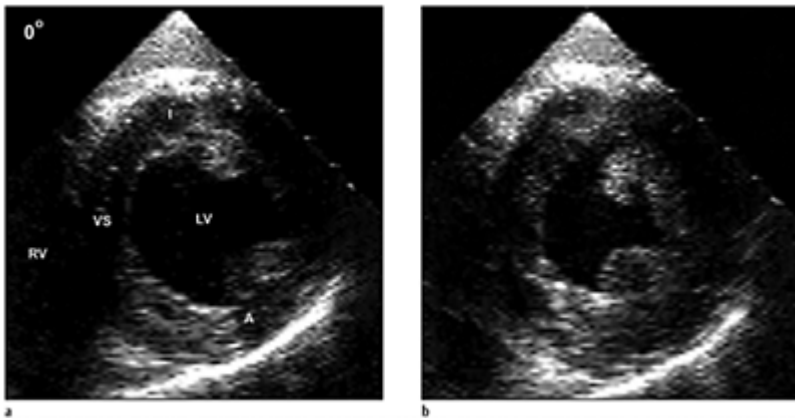
Figure 2.18 Gastric views of the papillary muscle. In the gastric view at 0° at the mid-ventricular level the papillary muscles are seen in short axis. The posterior papillary muscle is

> seen in the top of the image sector and the anterior papillary muscle is seen in the bottom of the image. Both papillary muscles are seated in the posterior third of the ventricle during (a) diastole and (b) systole, which promotes a smaller posterior circumferential dimension than anterior dimension. This dimension is important in that it ensures blood flow in a posterior direction from the left ventricular inflow and also promotes a parallel chordal arrangement to the posterior mitral leaflet.

The probe is slowly advanced to approximately 50 cm at 0° to the deep transgastric level, with anteflexion until the aortic root is imaged obliquely and the mitral subvalvular apparatus is well seen (figure 2.16). The papillary muscles are visualized obliquely with a foreshortened view of the left ventricular apex near the top of the echocardiographic screen. Usually both papillary muscles are visualized between 0° and 20°. The central portions of both papillary muscles are easily inspected along with the chordae tendineae. The chordae tendineae appear straight, all about the same width, and lie in a vertical position in the image. The valve leaflets, however, are too foreshortened to be fully appreciated, especially when they are normal or show hooding, but it is possible to easily determine the anterior from the posterior leaflet. In our experience, this is the best view to assess the chordae tendineae. Elongation of the chords is easily seen, as the chordae appear redundant, bowed, and curvilinear, instead of straight. The chords to the anterior leaflet appear to project at an angle away from the papillary head, and the chords to the posterior leaflet appear to be parallel and vertical. With further rotation of the transducer from 45° to 50°, a sweep of the whole subvalvular apparatus is completed and nearly all of the chords can be assessed.

The multiplane probe is then slightly withdrawn at 90° to center the annulus and leaflets in the echocardiographic image. With slight angulations of the probe, the full breadth of the anterior, posterior, or both leaflets are seen cut vertically, opening and closing with changes in the cardiac cycle. The mitral annular plane is readily apparent, separating the left ventricle (to the left of the image) and the left atrium (to the right of the image), and the normal mitral valve leaflets do not protrude significantly past this imaginary plane towards the left atrium. During diastole when two leaflets are imaged, the posterior leaflet is seen at the top of the echocardiographic image and the anterior leaflet at the bottom of the image. Rotating the transducer from 90° to 135° shifts the image towards the left ventricular outflow tract and the aortic root, displaying the anterior leaflet with much more certainty, being continuous with the aortic root at the bottom of the display. Care should be taken in assessing the thickness of the leaflets at the points of chordal insertion so as not to overestimate leaflet thickness in this area.
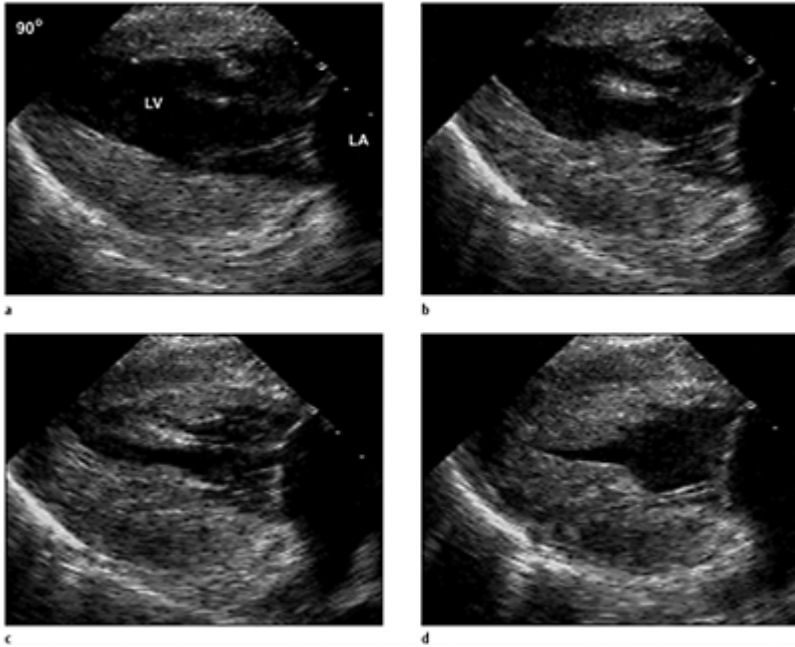
Figure 2.19 Gastric views of the papillary muscle. In the gastric view at 90°the motion of the papillary muscles may be assessed throughout the cardiac cycle. Fractional shortening of the papillary muscle can be measured. (a) Early diastole. (b) Mid-diastole. (c) Atrial contraction. (d) Systole.

The transducer is returned to 0° and the probe is slightly withdrawn towards the lower esophageal level (about 35 cm from the incisors) to image the base of the left ventricle and project the mitral valve leaflets and annular plane enface (figures 2.12, 2.21). The probe is slightly angulated or the transducer is rotated to accommodate the oblique nature of the mitral annulus at this level, until the maximum opening of the valve orifice at the leaflet tips is visualized. The opening and closure of the valve leaflets may be timed with the cardiac cycle and the best appreciation of leaflet motion is obtained in this view. The anterior leaflet will be seen to the left and slightly rotated inferiorly in the image towards the ventricular septum and right ventricle. The posterior leaflet will be displayed directly opposite the anterior leaflet slightly superiorly to the right, towards the left ventricular free wall margin. The commissures are apparent as the points of continuity between the anterior and posterior leaflet. The posteromedial commissure is at the top of the image, roughly in the same orientation as the posteromedial papillary muscle position, and the anterolateral commissure at the bottom of the image corresponds to the position of the
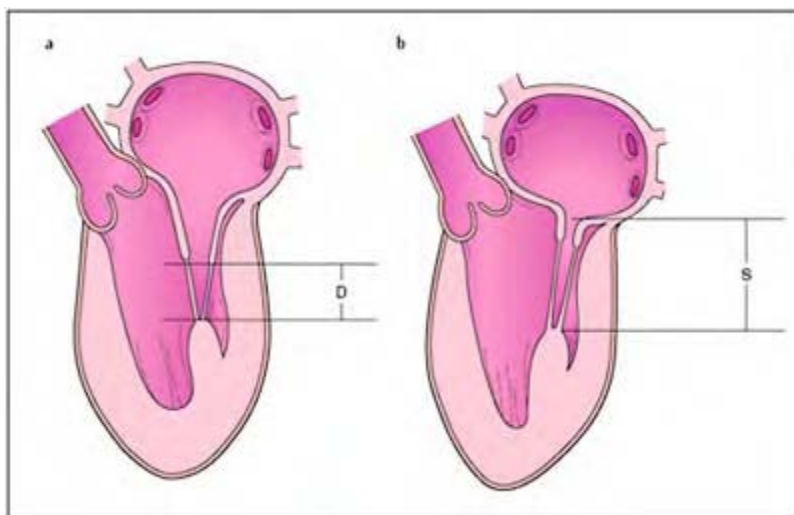
Figure 2.20 Diagram demonstrating measurements of the mitral subvalvular apparatus. Fractional shortening of the papillary muscle can be easily determined by measuring the end-diastolic (a) and end-systolic (b) longitudinal lengths as represented in the diagram. Normal motion of the ventricular myocardium should also be observed in relationship to normal papillary muscle motion.

respective papillary muscle. The leaflets will appear shaggy and non-continuous during movement, due to hooding of the chordal attachments as they move in and out of the imaging plane. The leaflets on cross-section should move appropriately with the cardiac cycle, without areas of chaotic motion. During early diastole when the valve opens, the mitral orifice resembles a letter "D". When the valve leaflets are normal the leaflet margins approximate the shape and dimension of the annulus. If the whole annulus is visualized, the diameter of the annulus can be measured construing a line between the two commissural points. The anterior leaflet appears straight and the posterior leaflet concave, both leaflets join at the commissures. During mid-diastole the leaflets slowly start to approximate in a crescentric fashion, with most motion in the anterior leaflet becoming convex to the posterior leaflet. During atrial systole, both leaflets again open abruptly to form a circular orifice. During ventricular systole both leaflets begin to approximate, as the ventricle becomes smaller, again the anterior leaflet appearing to move more towards the posterior leaflet in a convex manner. When the leaflets are totally closed during systole the line of closure resembles a "smile", with a symmetrical crescent-shaped configuration. During leaflet motion, the individual scallops of the

posterior leaflet may be appreciated. This view represents the typical exposure of the mitral valve as visualized by the cardiac surgeon, and thus is an important view for communicating leaflet abnormalities (figure 2.7). Both leaflets are labeled in three segments according to the normal scallops of the posterior leaflet; P1 is the anterolateral scallop, P2 is the central scallop, and P3 is the posteromedial scallop. The anterior leaflet is subdivided into A1 to A3 based on the segment of leaflet directly opposite the posterior segment.[39]
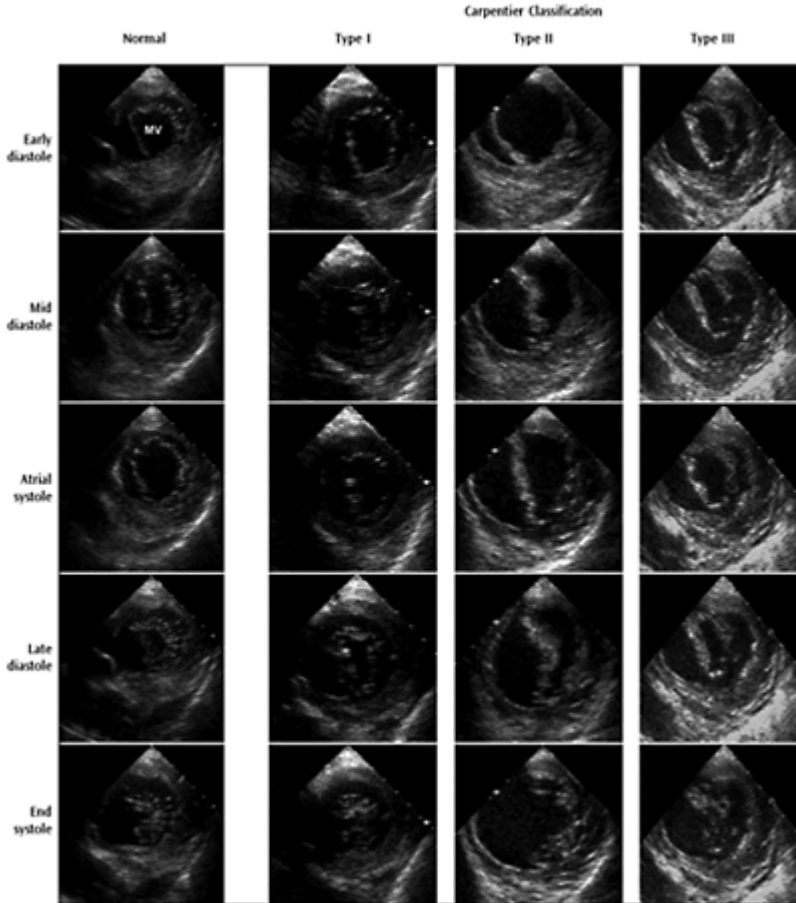
Figure 2.21 Short-axis echocardiographic visualization of mitral valve motion illustrating normal valve motion in comparison to type I, II and III mitral motion according to the Carpentier classification scheme.

The transesophageal echocardiographic probe is then withdrawn at 0° to the mid-esophageal level (30 cm from the incisors), with the tip of the probe in a neutral position with enough flexion to ensure contact between the transducer and the esophageal wall. During withdrawal of the probe, the heart image progresses from a short axis plane of the left ventricle to a four-chamber frontal plane of the heart, then a five-chamber frontal plane of the heart (figure 2.13). The right ventricle is to the left of the image and the left ventricle is to the right of the image. The atrium is displayed to the top of the echocardiography sector with the ventricular apex to the bottom of the image. The mitral valve should be centered in the image with slight rotation of the probe shaft. The depth of the image sector may be decreased between 10 and 12 cm to assess the full linear extent of both leaflets during the cardiac cycle. Occasionally, the zoom feature may provide better resolution and delineation of the leaflet details. The two mitral leaflets open towards the left ventricular apex during diastole, producing a funnel shape to the orifice. Frequently, the subvalvular apparatus, especially the chordae tendineae, will not be visible without increasing the gain settings. The anterior leaflet will be on the left of the echocardiographic image, appear longer, and show the most motion during opening and closure. The posterior leaflet will appear to the right of the echocardiographic image towards the lateral left ventricular wall. The posterior leaflet will appear shorter and move less, with slight but noticeable billowing of the leaflets compared with the anterior leaflet during closure. The rate of movement of the anterior leaflet appears greater than that of the posterior leaflet, with the anterior leaflet opening parallel to the ventricular septum and the posterior leaflet nearly parallel to the posterolateral ventricular wall.

Due to the oblique position of the mitral valve annulus in relation to the transesophageal echocardiographic probe, the valve appears tilted, so that the imaging plane through the valve leaflets cuts the valve tangentially, often producing confusion in accurately identifying the exact area of the leaflet (figure 2.8). When imaging the valve at 0° in the frontal plane, the valve leaflets are imaged nearer the posteromedial commissure at the lower esophageal position, imaging more of the lateral area of the anterior leaflet and medial area of the posterior leaflet (A3, P1). As the probe is slowly withdrawn, the leaflets are transected in a successive manner more towards the middle of the leaflets (A2, P2). With further withdrawal of the probe, the anterolateral commissure portion of the leaflet is reached at the mid-esophageal level, and the medial portion of the anterior leaflet and the lateral region of the posterior leaflet is visualized (A1, P3). With this maneuver, the complete free margins of both leaflets may be inspected in a precise manner. This is most helpful in evaluating the point of closure, or approximation of the leaflets during systole. The frontal plane provides a very good view to visualize the annular plane and excessive motion of the valve leaflets. An imaginary line can be drawn from the points of attachment of both leaflets to the annulus. With normal mitral valve closure the points of approximation of the free edge of both leaflets should not extend past the annular plane or protrude into the left atrium. Due to the saddle shape of the normal mitral valve leaflets during closure, the body of the leaflets may billow or extend minimally past this plane, but the exact point of closure or approximation normally will not. Normal billowing of the body of the leaflet should not protrude more than 1 cm past the annular plane. When evaluating the line of closure in all of these views, the rough zone of the free margins of both leaflets should give the impression that both leaflets coapt, so that the leaflet surface area of contact is at least 1 to 2 mm. Normal valve

leaflets should not appear to barely touch. When the mitral valve is viewed sagitally, the leaflets appear to open into the left ventricle like a trap door, with the anterior leaflet moving predominately. During closure of the valve, the anterior leaflet swings up to meet the posterior leaflet in the plane of the annulus. The anterior leaflet has been referred to as the velocity or active leaflet and the posterior leaflet the passive leaflet.
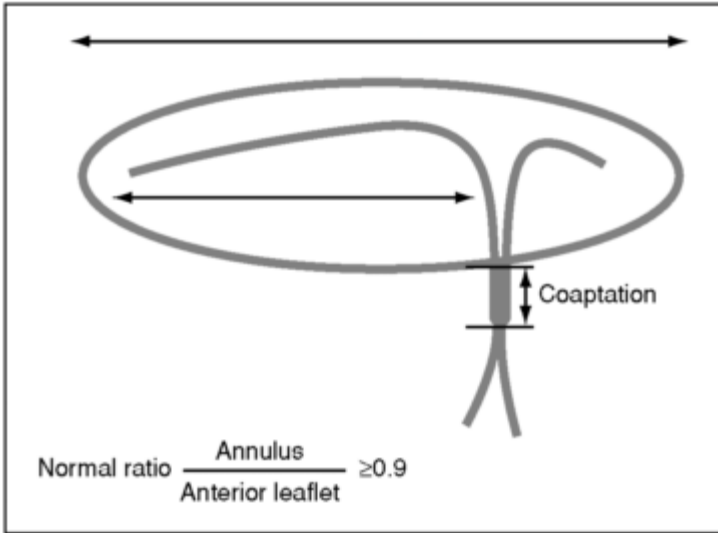
Figure 2.22 Diagram demonstrating measurements with TEE for mitral annular dilatation. When there is dilatation of the annulus, the length of the anterior leaflet may be compared to the length of the annulus and provides an important ratio for evaluating annular dimensions. A ratio less than 0.9 suggest that the annulus is sufficiently dilated so that the anterior leaflet cannot reach the posterior leaflet for adequate closure.

In the five-chamber frontal plane, with the transesophageal echocardiographic probe in the mid-esophagus, approximate dimensional measurements can be made with regard to the mitral valve unit (figure 2.22). When there is subtle dilatation of the annulus, the length of the anterior leaflet may be compared with the length of the annulus, and providing an important ratio to assess normal annulus dimensions.[40] This measurement can be readily made in this view by multiplane transesophageal echocardiography, and

the ratio of the anterior leaflet/annulus length should be about 0.9. A ratio less than 0.9 suggests that the annulus is dilated so that the anterior leaflet cannot reach the posterior leaflet for adequate approximation.

Another important assessment, easily made with transesophageal echocardiography, is the aorto-mitral annulus angle or angle of closure (figure 2.23).[41] In the normal mitral valve, there is an obtuse angle between the anterior mitral leaflet and the aortic root to signify normal annulus size as well as lack of excessive leaflet tissue. This allows forward blood flow during diastole to be oriented toward the ventricular apex, and pushes the line of leaflet closure far from the left ventricular outflow tract, preventing impingement or obstruction by the mitral apparatus.
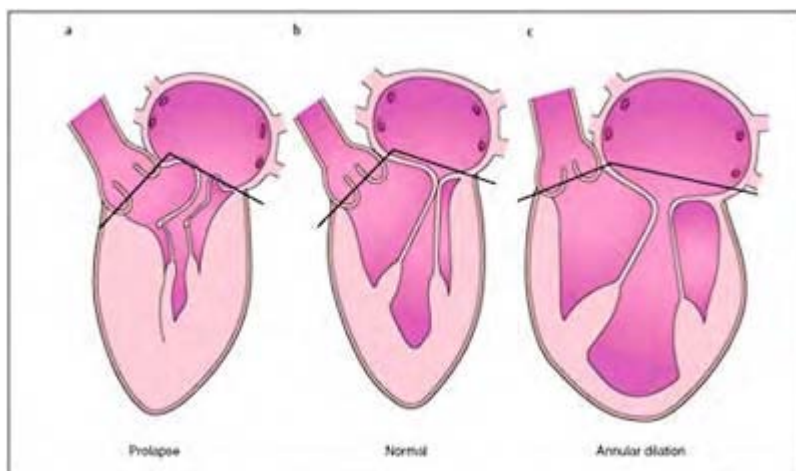
Figure 2.23 Diagram demonstrating the aorto-mitral angle. The aorto-mitral angle may be easily visualized for semi-quantitative or direct measurement with multiple TEE. (a) In mitral valve prolapse the excessive tissue predominately of the posterior leaflet pushes the valvular apparatus towards the left ventricular outflow tract causing the aorto-mitral angle to become more acute. (b) The normal aorto-mitral angle approximately 90°–110°, allows for the functional delineation of the left ventricular inflow and outflow tracts. (c) Annular dilatation of the mitral valve produces

an obtuse angle with the posterior
leaflet being pulled away from the
anterior leaflet reducing leaflet surface
area for coaption.

From 0° the transducer can be rotated slowly to 180° to obtain the full circumference of the mitral annulus and leaflets, exemplifying the true utility of multiplane transesophageal echocardiography (figure 2.8). With some currently available probes the transducer can be rotated past 0° to –10°, which opens into the left ventricular outflow tract or five-chamber view (figure 2.9). Rotating the transducer from 0° to 60° or 75° images the mitral plane in a two-chamber view, with the left atrium in the top of the image sector and the left ventricle to the bottom of the image (figures 2.10, 2.14). The anterior and posterior mitral leaflets will be imaged parallel to the line of closure, and, with slight manipulation of the probe shaft, either the anterior or posterior leaflet will be imaged in its full breadth from commissure to commissure. Either leaflet will appear as a continuous line traversing the annular plane. As the transducer is further rotated through 110°–135°, the mitral leaflets will be imaged in a three-chamber view, with the posterior leaflet now towards the left of the image sector, and the anterior leaflet to the right and continuous with the aortic root to form the left ventricular outflow tract (figures 2.11, 2.15).

Multiplane Doppler examination of the normal mitral valve

The mitral valve directs the flow of blood from the left atrium to the left ventricle. During diastole, the open mitral valve is funnel shaped and gives rise anatomically and physiologically, to the left ventricular inflow tract. During systole, the mitral valve maintains the forward flow of blood by closing, preventing the significant regurgitation of blood into the left atrium. The closed mitral valve leaflets, along with its supporting subvalvular apparatus, protects the left atrium and contiguous pulmonary structures from the high pressures generated in the left ventricle, at the same time not interfering with the outflow tract during left ventricular contraction. The architecture of the mitral valve is well suited to preserve these functions, and when disease affects the mitral apparatus, abnormal hemodynamics are produced that may be identified by Doppler techniques.

Although Doppler recordings may be made in any of the mitral valve views described above, the most important views are those that present the left ventricular inflow tract parallel to the transducer beam. The principles for the transesophageal echocardiographic Doppler assessment of mitral valvular hemodynamics are identical to those for transthoracic measurements and calculations. Routinely, there is no clear advantage in Doppler echocardiography obtained from the transesophageal exam over the transthoracic exam, and rarely would one expect to obtain drastically different information from the transesophageal echocardiogram. One exception may be with the recording of pulmonary venous flow for assessment of mitral insufficiency, which is usually easier with transesophageal windows.
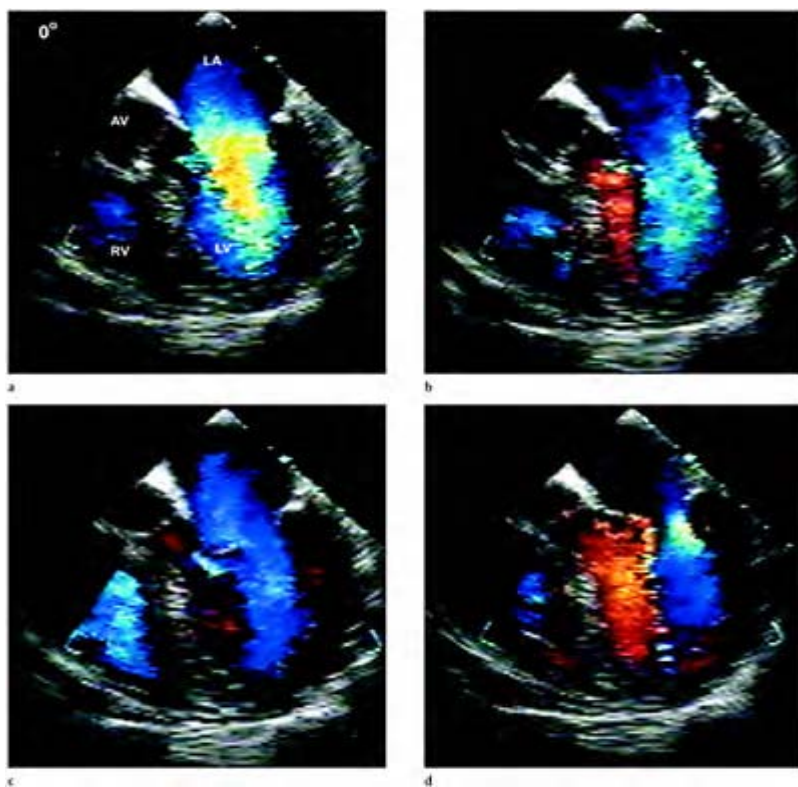
Figure 2.24 Normal color flow Doppler. (a) High velocity color flow Doppler through the open mitral valve leaflets in early diastole recorded in the low esophageal window at 0°. (b) As diastole progresses the velocity of the color flow signal starts to decrease and flow curves around the ventricular apex towards the left ventricular outflow tract. (c) Mid-diastole blood flow velocities decrease substantially as the valve leaflets begin to close further. (d) With atrial systole higher velocity flow is again recorded in the left ventricular inflow tract.
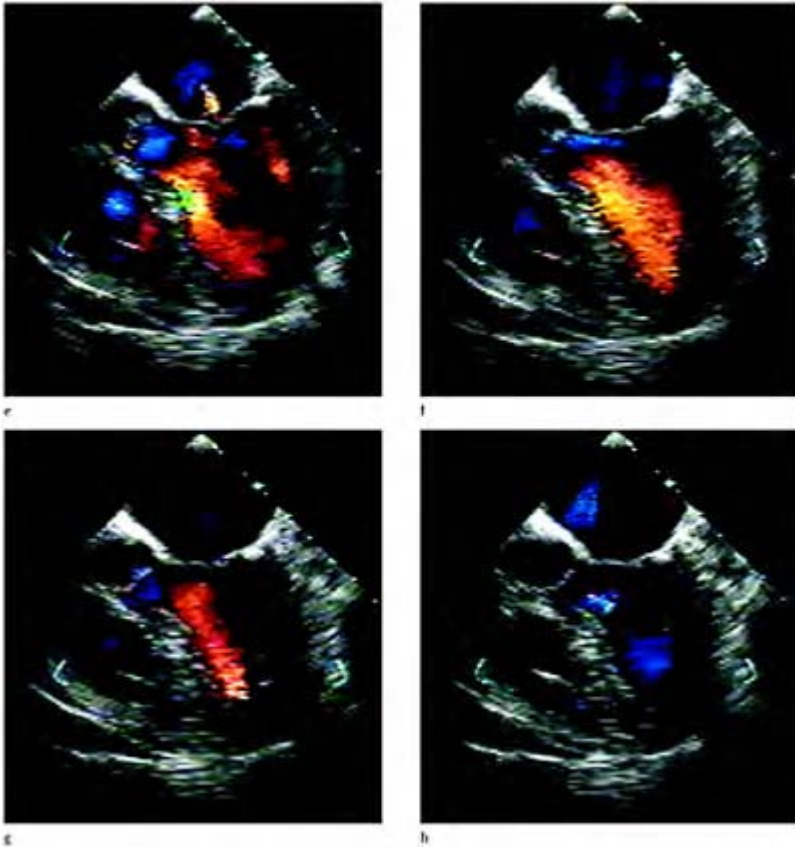
(e) With further closure of the mitral leaflets, reversal of blood flow is noted backward towards the left atrium. (f, g) Complete mitral valve closure and the start of systole higher velocity blood flow is noted in the left ventricular outflow tract towards the aortic valve. (h) At end systole only low velocity flow is detected in the left atrium or left ventricle.
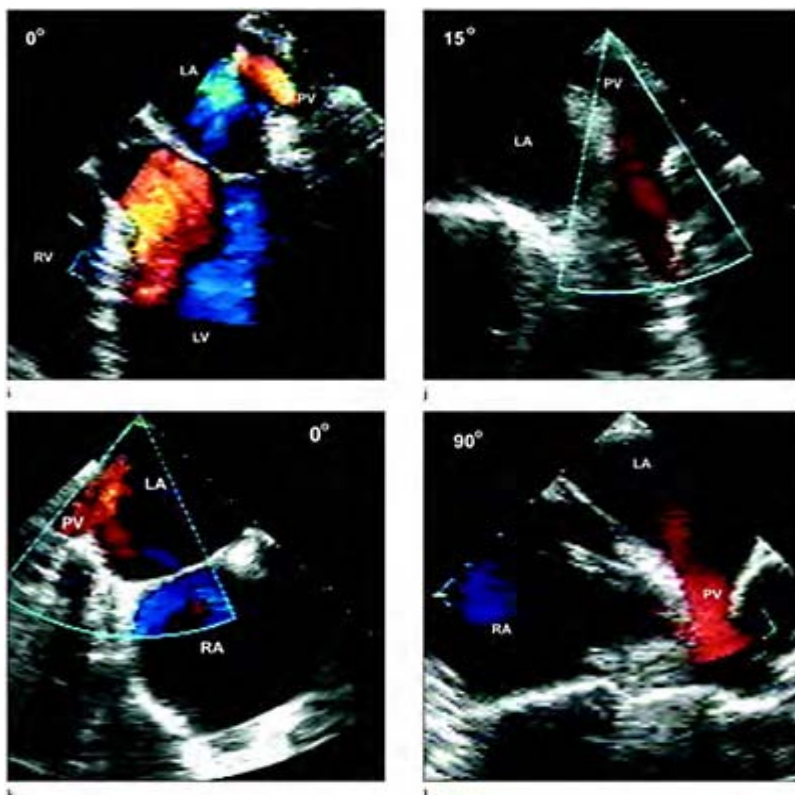
(i) With slight leftward rotation of the probe the orifice of the left pulmonary veins are visualized with low velocity pulmonary venous flow seen entering the left atrium in early diastole. (j) Rotating the transducer to approximately 15° the left pulmonary veins are visualized. Pulsed Doppler can be easily performed in this view to interrogate and record the pulmonary venous flow. (k) Returning the probe to 0° with mild withdrawal and rightward rotation of the probe the origin of the right pulmonary veins are visualized entering the left atrium. (l) At the same level and rotation of the

transducer to 90° the full extent of the
right pulmonary vein and low velocity
color flow is recorded.

Views obtained from the mid- and lower esophagus allow good windows for directing the Doppler beam through the left atrium and the left ventricular inflow tract (figure 2.24). Usually, pulsed Doppler is used to measure the low flow velocities of blood generated from diastole and atrial systole through the left ventricular inflow tract, producing the *e*- and *a*-wave morphology without a detectable gradient. Continuous wave Doppler is usually necessary to measure mitral inflow when increased and disturbed flow is produced, promoting aliasing due to a transmitral gradient. As with transthoracic measuring, color Doppler may help to direct the Doppler beam in a parallel direction toward the inflow tract. Color Doppler; red–blue enhanced maps with flow directed toward the transducer is depicted in red, low velocity flow is detected in the atrium. By contrast, with the transthoracic echocardiogram, in which the atrium is usually black during this part of the cycle, blood flow can be mapped easily with transesophageal echocardiography as it fills the left atrium. Jets of orange–red flow empty from the pulmonary veins, collecting and mixing in the body of the left atrium. Diastolic forward flow increases as it enters the funnel shaped mitral inflow orifice, and the converging flow is shown as patterns of hemispherical aliasing recorded near the open leaflets. As blood flows through the valve and fills the left ventricular cavity undisturbed, red–orange laminar flow is recorded at alternating velocities as the leaflets open with early diastolic filling, and slowly approximate before opening again with atrial systole. Diastolic filling flow is detected as it swirls and turns through 180 degrees at the ventricular apex, before blue laminar flow is again recorded in the left ventricular outflow area. A small area of increased velocity and aliasing is usually detected in the outflow tract, hugging the proximal ventricular septal wall below the aortic valve. During early systole, especially with lower aliasing velocity settings, low velocity backward flow may be recorded initially as the leaflets push blood flow back into the left atrium during closure, to about 1cm from the annulus. At completion of leaflet apposition, blood flow stops completely. Physiological or normal regurgitation is defined by small jets of flow reversal detected close to the mitral annular plane. Single or multiple color flow jets with small jet areas and low flow velocities are imaged without significant turbulence or variance.

Mitral stenosis

Mitral stenosis is the most common cause of left ventricular inflow obstruction. The most common cause of mitral stenosis is rheumatic carditis, despite its decline in developing countries since the introduction of penicillin. Transesophageal echocardiography offers no real advantage over transthoracic techniques in rheumatic mitral stenosis, unless the patient does not have a suitable transthoracic acoustic window. The real advantage of transesophageal echocardiography in mitral stenosis is in diagnosing associated cardiac pathology such as mitral insufficiency, thrombi in the left atrial cavity and appendage, and assessing the integrity of the atrial septum. Transesophageal echocardiography is particularly helpful in assessing the suitability for, and predicting the results of,

percutaneous balloon mitral valvuloplasty, surgical repair and/or commissurotomy. In diagnosing the other causes of mitral or left ventricular inflow obstruction—congenital mitral stenosis, parachute mitral valve, mitral arcade, supravalvular mitral ring, cor triatriatum, left heart or mitral apparatus tumors or thrombi, bacterial or non-bacterial endocarditis, and severe mitral annular calcification—transesophageal echocardiography has a distinct advantage over transthoracic echocardiography.

Rheumatic mitral stenosis in the adult may be categorized by leaflet thickening occurring from fibrosis or calcification, commissural fusion, and stenosis produced in conjunction with fusion, shortening, and calcification of the subvalvular apparatus. These three processes may occur independently but usually occur in combination and various degrees of severity. Commissural fusion is produced from localized inflammation in areas of reduced motion, that occur as a result of annular dilatation during the acute process. Commissural fusion may be isolated, with the other portions of the leaflet remaining totally pliable and free of disease. Leaflet fibrosis, thickening, and calcification, frequently occurs with commissural fusion. Over time, progressive fibrosis occurs leading to restriction, contracture and immobility of the leaflets, starting at the edges and extending to the body of the leaflet. Thickening and fusion of the chordae tendineae follows, producing narrowing and stenosis of the subvalvular area. In many cases this is the predominant pathology of obstruction to inflow.[42,43]

The transesophageal echocardiographic assessment of mitral stenosis includes (1) an anatomic description of the morphology and mobility of the mitral valve and the subvalvular apparatus, (2) an evaluation of the severity of stenosis by estimating the valve orifice area using planimetry and Doppler methods, (3) an evaluation of the effects produced by the hemodynamics of obstruction; left atrial enlargement, pulmonary hypertension, right heart enlargement, and biventricular function, (4) the identification of associated abnormalities; left atrial thrombus, patent foramen ovale or atrial septal defect, and (5) a thorough evaluation of the other valves including the assessment of associated mitral regurgitation.

The best views for assessment of the mitral subvalvular apparatus in mitral stenosis are the deep transgastric frontal (50–55 cm from the incisors, 0°) and the transgastric longitudinal views (40cm from the incisors, 90–120°). In both views the papillary muscles and chordae tendineae are not affected by acoustic shadowing or ghosting from calcified and thickened mitral leaflets. The papillary muscles will appear hypertrophied; and the chordae tendineae should be evaluated for short-ening or retraction, fusion or thickening, and calcification. In mild cases of mitral stenosis the only recognizable differences in the subvalvular apparatus will be slight increases in chordal thickening and minor increase in echogenicity of these structures. Calcification of the subvalvular area may present as small, discrete areas of increased echogenicity. In more severe cases of mitral stenosis the papillary muscles, chordae tendineae and points of chordal insertion to the leaflets can appear as one continuous thick structure without identifiable points of demarcation between them. The chordae tendineae in severe calcific mitral stenosis may be very thick, shortened and fused, and appear to cause retraction or eversion of the leaflets.

The transesophageal echocardiographic probe is then withdrawn to the proximal transgastric position, and the transducer can be rotated between 0° and 20° to try to image the mitral valve enface. This can be difficult, since the valve is frequently oblique to the

probe and the imaging plane from this position in the esophagus. The mitral commissures will be visible and will appear to be thickened and fused, especially near the outer margins. Depending on the degree of fusion and scarring of each individual commissure, the usually central mitral orifice may be displaced or distorted, in addition to being narrowed, producing the classic fish-mouth appearance of the leaflets during diastole. The extent of commissural fusion will determine the severity of mitral stenosis, and in mild and moderate stenosis will cause an abrupt opening movement of the leaflets. With small adjustments in the probe with anteflexion, an assessment of the mitral orifice can be made by planimetry. Accurate planimetry of the valve orifice depends on obtaining a true short-axis of the leaflet tips, viewing the valve as enface as possible and locating the smallest orifice area between the valve leaflets and subvalvular apparatus. Care must be taken to image the valve at the level of the tips of the mitral valve leaflets, and not at the base of the mitral valve funnel; to avoid overestimation of the valve area. Ignoring significant narrowing of the subvalvular area will result in underestimation of the valve area. In heavily calcified valves, again adjustment of the echocardiographic equipment must be set appropriately to avoid blooming of the thickened leaflets and overestimation of the degree of stenosis, with measurements made from the inside edge of the valve leaflets. Stoddard and colleagues[44] have shown an excellent correlation betwen mitral valve areas obtained by planimetry from both the transesophageal and transthoracic echocardiographic approach. Mitral valvotomy or commissurotomy usually produces distortion of the mitral orifice, which may make it difficult to measure accurately the orifice area by planimetry, and is less accurate than other techniques. After valvotomy the valve shows expansion in the orifice dimension along its horizontal axis from commissure to commissure, usually without an obvious change in leaflet opening. In any event, the hallmark of mitral stenosis after valvotomy is that the commissures freely move and are not fused, without significant change in the remainder of the valvular apparatus. Reports have varied about the accuracy of planimetry measurements in mitral stenosis,[44] but in our experience valves can easily and accurately be categorized as mild, moderate, and severe with the transesophageal echocardiographic probes currently available.

With further withdrawal of the probe to the lower and mid-esophageal positions, and with the scope in the neutral or slightly anteflexed position, the mitral valve is imaged in profile in the four-chamber horizontal view at 0°. Thickening and diastolic doming of the anterior and posterior leaflets is readily apparent. Frequently, the subvalvular apparatus will not be visible due to acoustic shadowing from the thickened and calcified leaflets. In mild cases of mitral stenosis, only the distal leaflet tips will appear thickened and appear immobile, sparing the body of the leaflets presenting visually as the "hockey stick or bent-knee deformity" showing diastolic doming. As the disease progresses, the body of the leaflets thickens and becomes visibly less mobile, until the diastolic doming disappears and the valve leaflets show either minimal excursion or appear immobile from diastole to systole. Rotating the transducer from 0° to 135° may adequately assess the anterior and posterior leaflets, along with the commissures.

With the transesophageal echocardiographic probe in the upper esophageal position and continued slight anteflexion at 0°, the basal short-axis plane of the heart visualizes the left atrium, atrial septum, and the left atrial appendage. The left atrium enlarges sequentially with worsening degrees of stenosis, often reaching 6–7 cm in severe mitral

stenosis. Frequently, spontaneous contrast[45–47] or "echo smoke" is visualized in the left atrium and left atrial appendage, characterized by an echocardiographic appearance of swirling and sludging of slowly moving blood cells secondary to rouleaux formation. The left atrium should be carefully inspected for the presence of thrombus. The most frequent site of thrombus[15] is the left atrial appendage, followed by the superior aspect (roof) of the left atrium, the area around the pulmonary vein orifices, and the secundum atrial septum. The left atrium must be fully examined by scanning from 0° to 90° and moving the probe from a somewhat neutral position to full anteflexion, in the upper esophageal position.

It may be helpful to examine the left atrium in stages, starting with the left atrial appendage. The left atrial appendage at 0° has a narrow orifice and projects longitudinally in a twisting, tapering fashion, frequently out of plane. It is necessary to rotate the transducer slowly to 90° to image the full extent of the appendage. When there are prominent pectinate muscles, the appendage may appear cystic and it may be difficult to distinguish the pectinate muscles from thrombi. In this circumstance, it may be helpful to use the zoom feature with or without color Doppler, to observe blood flow in the area in question. Color flow Doppler usually surrounds and enhances a thrombus. It is also occasionally helpful to place the M-mode cursor through the area in question to look for chaotic motion, as seen with some thrombi. With slow withdrawal of the transesophageal echocardiographic probe and rotation of the transducer from 0° to 90°, the body of the left atrium is visible with the areas around the pulmonary veins, atrial septum and foramen ovale, followed by visualization of the roof of the atrium around the level of the aorta and pulmonary artery.

Thrombi vary in size and may appear either well laminated to the atrial wall or freely mobile. It is not uncommon to visualize spontaneous contrast associated with the thrombi, especially in the presence of atrial fibrillation. It is therefore extremely important to carefully observe areas near spontaneous contrast to fully exclude the presence of thrombi.

To complete the examination in mitral stenosis, pulmonary venous flows[48] are evaluated, especially when there is significant mitral insufficiency, the right heart is assessed for chamber enlargement and right ventricular function, and tricuspid and pulmonic flows are assessed to estimate pulmonary artery pressures and to rule out pulmonary hypertension.

Doppler evaluation of mitral stenosis

Accurate estimates of the transmitral gradient and mitral valve orifice area may be made with conventional and color Doppler in the four-chamber esophageal views, using the same techniques as those of transthoracic echocardiography.[49–52] High pulsed repetition frequency or continuous wave Doppler can be used to measure the transmitral gradient. The mitral inflow jet can be easily interrogated and positioned directly parallel to the transducer imaging plane, with the aid of color Doppler and minor adjustments of the transesophageal echocardiographic transducer. The characteristic Doppler features of mitral stenosis are increased peak velocity, reduced rate of decrease in velocity with time, and, in patients in sinus rhythm, augmentation of the velocity signal due to atrial

contraction. The increased transmitral blood flow velocity profile and its slow decline indicate a pressure gradient across the valve continuing throughout diastole. The pressure gradients across the mitral valve at any time are estimated with the modified Bernoulli equation $(P_1 - P_2 = 4[V_{max}]^2)$. Peak and mean transvalvular gradients obtained with the modified Bernoulli formula correlate closely with those calculated at cardiac catheterization using the Gorlin formula, and can be measured online with most of the echocardiographic equipment currently available.[50] Although pressure gradients provide an indication of the presence of obstruction, they are dependent upon the transvalvular volumetric flow and driving pressures through the orifice, which are dictated by the patient's hemodynamic status, therefore they may not accurately reflect the severity of obstruction.[53]

The mitral valve orifice area can be measured with Doppler by estimating the transmitral pressure half-time during diastole.[54–69] In mitral stenosis, the measured transmitral gradient is maximal near the onset of diastole and declines in a linear fashion. The expression of the correlation of time with the falling pressure can be expressed as the time required for the initial maximum gradient to fall by 50%. The more severe the degree of obstruction of the mitral orifice, the longer the time of pressure fall off. The mitral pressure half-time $(t_{1/2})$ can be calculated from the velocity signal as the time interval over which the velocity falls from its maximum to minimum value divided by the square root of 2. The normal pressure halftime is less than 100 msec. Since the transmitral pressure gradient and blood flow velocity are related by a square power function, mitral valve orifice area is calculated as MVA = 220/pressure half-time.[55] Mild mitral stenosis has a pressure half-time of 160 msec or less with a valve area greater than 2 cm^2, and in severe mitral stenosis the pressure half-time is greater than 220 msec with a valve area less than 1 cm^2. There has been concern that the angle of incidence produced by the Doppler interrogation of the mitral valve inflow with transesophageal echocardiography might negatively influence the mitral valve area and maximal gradient. Stoddard and colleagues[56] have shown that Doppler transesophageal echocardiography compares favorably to the transthoracic approach.

Atrioventricular compliance[57,58] and other hemodynamic variables[59] that influence the transmitral gradient may cause inaccurate measurement of the mitral valve area by the pressure half-time method. The pressure halftime method for calculating the mitral valve area results in significant overestimation of the true valve area in situations such as aortic regurgitation,[60–62] mitral regurgitation,[63,64] exercise,[53] pregnancy, decreased diastolic performance of the left ventricle, and immediately after balloon valvuloplasty.[70]

Mitral valve area may also be calculated using the law of continuity.[68] The continuity principle states that volume flow per unit of time through a stenosis is equal to the volume flow either proximal or distal to the stenosis, provided the cardiac output remains constant during both measurements. Volume flow is assessed as the product of the flow velocity integral (FVI) and the cross-sectional area (CSA) of the flow stream. $FVI_1 \times CSA_1$ (normal zone) = $FVI_2 \times CSA_2$ (stenotic zone). In patients with mitral stenosis, the normal zone blood flow velocity and vessel diameter is measured either in the proximal aorta or the proximal pulmonary artery. The blood flow velocity integral across the stenotic mitral valve is obtained with continuous wave Doppler, and the cross-sectional area of the stenosis is calculated. Mitral valve areas calculated from Doppler measurements using the continuity equation correlate closely with those areas calculated

during cardiac catheterization, irrespective of varying hemodynamic conditions or in conditions (as described above) that may affect the pressure half-time. In cases of aortic insufficiency, the normal zone volume flow measurements should be made in the pulmonary artery instead of the aorta to avoid overestimation of the mitral valve area. In patients with significant mitral regurgitation, the increased velocity related to the regurgitant volume tends to underestimate the mitral valve area, limiting the use of the continuity equation in cases of mixed mitral stenosis and regurgitation.

Color Doppler provides other methods for estimating mitral stenosis. It identifies flow convergence surrounding the opening of the mitral orifice on the atrial side, and a characteristic "flame" jet of increased velocity and disturbed forward flow through the stenotic mitral orifice in diastole. The mitral valve orifice may be measured by color Doppler mapping of the proximal isovelocity surface area (PISA) combined with the continuous wave Doppler interrogation of the flow jet through the mitral inflow.[56–60] As flow enters a narrowed orifice from a larger chamber, the convergence of flow is depicted by color flow Doppler as a series of radial, uniform layers or isovelocity surface areas proximal to the stenosis. By identifying PISA and quantifying the volume flow rate, the stenotic area can be calculated using the continuity equation. Initial studies have identified these isovelocity layers as hemispheric, and allow the calculation of flow by the product of the surface area and its aliasing velocity.

The flow convergence region proximal to the stenotic mitral orifice during diastole is easily recorded in the lower esophageal position with the transducer at 0°–90°, to give the best representation of the anterior and posterior leaflets as they form a funnel opening. Flow is recorded at a low aliasing velocity (V_n) by adjusting the color flow baseline to obtain the largest isovelocity from the area, and the radius (r) at peak diastole is measured. Flow rate is corrected by adjusting for the inflow angle formed by the mitral valve leaflets (measured angle α divided by 180°). The peak flow velocity through the mitral valve is recorded with continuous wave Doppler (V_{peak}). Mitral valve area is then calculated as: $MVA = 2\pi r^2 \times \alpha/180° \times V_n/V_{peak}$.

The width of the mitral valve orifice can be measured with biplane or multiplane transesophageal echocardiography in two orthogonal planes, with color Doppler visualization of the flow jet through the mitral inflow. The minor axis of the flow jet can be measured at 0° in the four-chamber view, and the major axis of the flow jet can be measured at 90° in the two-chamber view. The mitral valve area (MVA) can be measured simply by calculating the shape of the mitral valve orifice as an ellipse, using the major (M1) and minor axis (M2) of the flow jet: $MVA = \pi \times (M1)/2 \times (M2)/2$. Chen and colleagues[78] reported in patients with mitral stenosis that there was a very strong correlation between the transesophageal echocardiographic mitral valve area and those derived by the Gorlin formula using cardiac catheterization data (r = 0.94; standard error of estimate = 0.13 cm^2).

Percutaneous balloon mitral valvuloplasty

Although mitral stenosis is usually adequately defined by transthoracic echocardiography, transesophageal echocardiography is usually necessary for patients undergoing percutaneous mitral valvotomy.[79–87] Transesophageal

Table 2.1 Echocardiographic grading of valvular characteristics in mitral stenosis

Grade	Mobility	Subvalvular thickening	Leaflet thickening	Calcification
1	Highly mobile valve with only leaflet tips restricted	Minimal thickening just below the mitral leaflets	Leaflets near normal in thickness (4–5 mm)	A single area of increased echo brightness
2	Leaflet mid and base portions have normal mobility	Thickening of chordal structures extending up to one third of the chordal length	Mid-leaflets normal, considerable thickening of margins (5–8 mm)	Scattered areas of brightness confined to leaflet margins
3	Valve continues to move forward in diastole, mainly from the base	Thickening extending to the distal third of the chords	Thickening extending through the entire leaflet (5–8 mm)	Brightness extending into the mid-portion of the leaflets
4	No or minimal forward movement of the leaflets in diastole	Extensive thickening and shortening of all chordal structures extending down to the papillary muscles	Considerable thickening of all leaflet tissue (>8–10 mm)	Extensive brightness throughout much of the leaflet tissue

From Wilkins GT, et al. Percutaneous balloon dilatation of the mitral valve: analysis of echocardiographic variables related to outcome and the mechanism of dilatation. *Br Heart J* 1988;60:299.

echocardiography may be helpful to identify an occasional case of congenital mitral stenosis that has emerged in adulthood and might not be ideal for valvuloplasty. Transesophageal echocardiography is extremely helpful in ruling out left atrial thrombi, which are the main contraindication to balloon valvuloplasty.[88,89] Atrial thrombi are not routinely visualized by transthoracic echocardiographic imaging. These thrombi may be dislodged during the manipulation of the catheter hardware during the procedure, and are a source of cerebral or systemic embolization and untoward complications.[90]

Transesophageal echocardiography is also necessary to adequately evaluate mitral insufficiency that may not be fully appreciated on transthoracic imaging.[91–93] Moderate to severe mitral regurgitation is considered a contraindication since this can be made worse with balloon dilatation. As a rule of thumb, mitral regurgitation increases by at least 1° of severity with balloon dilatation. Due to acoustic shadowing that is usually present on transthoracic imaging by a calcified mitral valve or the eccentricity of a regurgitant jet, mitral regurgitation can easily be overlooked. Mitral regurgitant jets may be difficult to detect, by transthoracic echocardiography especially in cases of previous commissurotomy.

Although transesophageal echocardiographic imaging is well suited to describe these contraindications, transthoracic echocardiography is adequate for most patients in determining the echocardiographic score index for mitral stenosis. In a few patients with poor transthoracic windows, transesophageal echocardiography may be helpful in predicting the anticipated success of the balloon valvuloplasty by accurately defining the extent of the stenotic pathology.[94–96] Wilkins and colleagues[79] have described an echocardiographic scoring system in an attempt to predict which patients would benefit

from this procedure (table 2.1). The score index grades stenotic pathology on a scale of 0–4, higher scores representing more abnormal structures. Valve mobility, thickness, calcification, and subvalvular thickening are all graded echocardiographically and added together for a score index between 1 and 16. Patients with a score of 8 or less have a greater than 90% likelihood of a satisfactory result with balloon dilatation. The predictors that correlate best with mitral valve splitability or subsequent area improvement are the severity of leaflet thickness, pliability, and degree of valve calcification. Cannan and colleagues[97] have shown that the echocardiographic assessment of commissural calcium is a simple predictor of outcome after percutaneous mitral valvotomy. If there is calcium detected in either one of the medial or lateral commissures, survival, the incidence is repeat balloon valvotomy, or mitral valve replacement was significantly different between patients without commissural calcium. That study also showed by Cox regression that commissural calcium together with the mitral echo score was the only significant variable for predicting outcome. Although the individual decision to proceed to valvotomy must be based on clinical considerations, the echocardiographic characteristics of the mitral apparatus may be a useful guide for deciding further treatment.

Transesophageal echocardiographic imaging may be used during the balloon valvuloplasty procedure for the positioning of catheters, puncturing the atrial septum, determining balloon sizing, and evaluating the worsening of any regurgitation after the procedure. In many interventional cardiac laboratories, transesophageal echocardiography is done routinely during the procedure in conjunction with fluoroscopy. It is also possible to undertake balloon valvuloplasty with transesophageal echocardiography alone, especially for laboratories familiar with the procedure.[90]

Transesophageal echocardiography is surprisingly well tolerated by patients during balloon valvuloplasty. In most laboratories, intravenous sedation is given during the procedure, which also allows the patient to tolerate the transesophageal echocardiographic procedure. The transesophageal echocardiographic probe should be left in place only for as long as necessary to allow visualization of the procedure. It is helpful to support the scope in the mouth, not allowing the scope to slacken or move frequently, which prevents gagging and minimizes aspiration. A clear advantage of multiplane transesophageal echocardiographic imaging is that it allows for less probe manipulation, which may be tolerated better by the patient. It is also important to monitor the patient's airway, making sure it is clear at all times, suctioning frequently, and that oral and topical anesthesia does not wear off during an occasionally long procedure. The transesophageal echocardiographic procedure allows a physician to be at the head of the table, much like an anesthesiologist during surgery, which is often appreciated by the patient.

To aid in puncturing and crossing the atrial septum with the catheter hardware, the foramen ovale area is visualized in the lower esophageal position between 0° and 45° or the mid-esophageal position at 90°–130°. In both views, a large portion of the bodies of both the left and right atrium are visualized with the foramen ovale area positioned in the middle of the echocardiographic display. Using this approach, the atrial septum is nearly perpendicular to the imaging plane and allows the visualization of typical catheter artifact as the hardware is introduced into the appropriate position. With minor angulations, the orifice of the inferior vena cava, superior vena cava, tricuspid valve, or coronary sinus

should be easily visualized to allow proper direction of the catheter in the appropriate position.

To visualize the catheter and the balloon as it crosses the mitral valve, standard four or two chamber views concentrating on imaging the left atrium and ventricle are obtained from the mid- to lower esophageal positions. The catheter hardware is readily identified by transesophageal echocardiography in both the left atrium and left ventricle. The size of the mitral annulus may be estimated by measuring diameter or the length of the annulus between the posterior wall of the aortic root and the junction of the left atrium and ventricle. Imaging during the seating of the balloon with inflation gives confidence during the procedure that the balloon is in the best position. Success is shown by increased leaflet motion after balloon deflation. Doppler interrogation of the mitral inflow is unrewarding in assessing valve orifice area, immediately following the procedure.

After balloon deflation, the mitral valve is carefully assessed for the development or worsening of mitral regurgitation.[91–93] With balloon dilatation, the valve should split and open along both commissures, in a similar fashion to surgical commissurotomy. The mitral valve area can be calculated from the measurement of the major and minor axis of the flow jet through the mitral orifice in two orthogonal views, or by planimetry of the mitral orifice in the short axis views.

Mitral regurgitation is readily apparent by color Doppler after the procedure, and a structural defect may be attributed to the cause of the regurgitation with the careful interrogation of valve anatomy. Mitral regurgitation can be measured quickly by the modified flow convergence or the vena contracta method, as long as significant distortion of the valve orifice has not been produced during the procedure.

The pulmonary venous flow pattern may be assessed by pulsed Doppler methods.[98] In mitral stenosis, the pulmonary venous systolic flow is decreased and the pulmonary diastolic flow is prolonged. Immediately after mitral valvuloplasty there is an immediate increase in pulmonary venous systolic forward flow in patients with sinus rhythm.

Echocardiographically, the procedure is successful if the mitral valve area is 1.5 cm^2 or more and mitral regurgitation is 2+ or less. Lung and colleagues[85,86] reported that the independent predictors of good functional results 5 years after mitral valvuloplasty were the mitral echo score, functional class and cardiothoracic index before the procedure, and the resultant valve area after balloon dilatation. Although most patients benefit from this procedure, due to the inherent nature of the disease process alluded to by the echocardiography score index, results in individual patients are variable. In selected patients with pliable valves, non-calcified leaflets with minimal subvalvular involvement, and little or no mitral regurgitation, the results of balloon valvotomy are similar to the surgical commissurotomy approach.[99,100] After the procedure, imaging of the atrial septum and Doppler techniques may be used to determine the persistence and size of a residual atrial septal defect, which usually disappears over time.[101–103] In our experience, the information obtained during the balloon procedure with transesophageal echocardiography may be used to interpret subsequent transthoracic echocardiograms done in the follow-up period, as long as acceptable transthoracic images are obtained.[104]

Mitral regurgitation

Mitral regurgitation is a very complex disease and has been poorly understood in the past. Unlike mitral stenosis, for which the cause is almost always rheumatic disease resulting in predictable mitral valve lesions, there are many disease processes that may render a mitral valve incompetent (table 2.2). With the eradication of rheumatic disease in most parts of the world, degenerative valve disease, bacterial and non-bacterial endocarditis, congenital heart disease, and diseases of the left ventricle including ischemia and cardiomyopathy are increasingly implicated as the cause of mitral regurgitation. In addition, each disease process may cause a variety of mitral lesions that can singly or in combination adversely affect the structural integrity of the mitral valve apparatus. To complicate the disease further, there are numerous theories and great debate over the intricacies of the interactions between the valve leaflets and subvalvular apparatus. Mitral regurgitation is common in cardiac patients on an acute or chronic basis. The natural history of mitral insufficiency is highly variable, dependent upon the etiology and the rate of progression of mitral lesions in an individual patient. Survival is largely dependent on the rate of deterioration of left ventricular function and the development of other co-morbid factors.[105] Recently, Ling and colleagues[106,107] have described the natural history of mitral regurgitation due to flail mitral leaflets. Patients with flail mitral leaflets that are managed medically have a 6.3% yearly mortality, and early surgical correction reduces mortality by almost 70%.

Table 2.2 Etiology ofmitral regurgitation

N = 520	%
Degenerative	63
Ischemic	14
Rheumatic	13
Endocarditis	6
Congenital	4
From Cosgrove DM, Stewart WJ. Mitral valvuloplasty. *Curr Prob Cardiol* 1989;14(7):353–416.	

In the past mitral valve replacement was the only option for treating patients with severe symptoms who failed medical therapy. Irrespective of the cause, mitral valve replacement has not been the panacea for the treatment of mitral regurgitation, because of high morbidity and mortality.[108] Despite the progress made in other open-heart procedures, significant improvement in survival for patients with mitral regurgitation and mitral valve replacement has not occurred. Valvular reconstructive techniques have been developed to treat mitral regurgitation, stemming from the need to avoid anticoagulation and the relatively high cost of mitral valve replacement.[10–13] Enthusiasm for mitral valve repair has quickly grown because of a low operative risk, and excellent short-term and long-term results, without the need for anticoagulation. With the introduction and success of mitral valve reconstructive techniques, patients with severe mitral regurgitation are now being considered as surgical candidates at a younger age, before they develop symptoms and have irreversible cardiac dysfunction. It is not a coincidence that many of

the strides made in better appreciating and treating mitral disease, particularly regurgitation, have paralleled the development and improvements in echocardiographic technology. As image resolution and Doppler techniques have improved, especially with the introduction of transesophageal echocardiography, mitral valve anatomy and function can be visualized in detail.

Mitral regurgitation can result from primary disease in any one of the component parts of the mitral valve leaflets or subvalvular apparatus.[109] Rheumatic disease, bacterial endocarditis, non-bacterial endocarditis (lupus erythematosus), myxomatous degeneration, fibroelastic deficiency, or trauma may damage the mitral leaflets, or elongate or rupture the chordae tendineae. The papillary muscles may malfunction transiently or permanently secondary to ischemia, infarction, or infiltrative disease. The mitral valve annulus may dilate secondary to ventricular enlargement, or calcify secondary to degenerative disease, preventing normal annular motion. Mitral regurgitation may also result from the disruption of the valvular structures, which may occur with increased muscle mass or hypertrophy commonly associated with increased ventricular pressures during systole, such as in aortic stenosis and obstructive hypertrophic cardiomyopathy. In dilated cardiomyopathy, mitral regurgitation may result from changes in left ventricular cavity shape, with the ventricle becoming more spherical than ellipsoid. Distorted ventricular geometry produces multiple abnormalities in mitral architecture. The papillary muscles are displaced along the long axis of the heart so they are further apart than normal. Since there is no change in chordae tendineae length, leaflet motion is altered and the leaflets are unable to coapt normally.
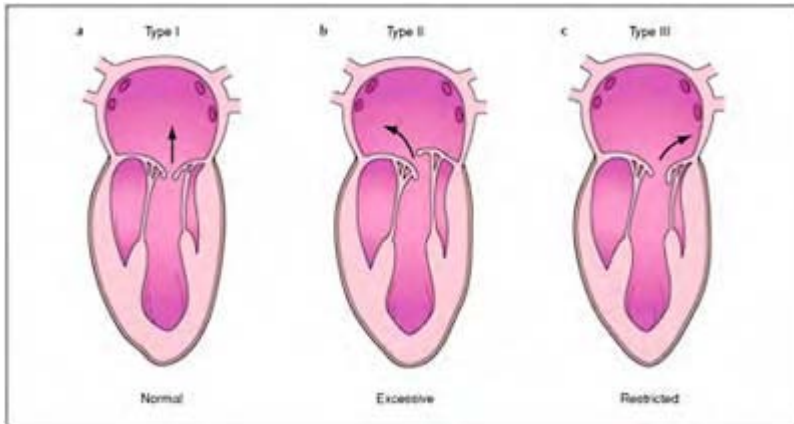
Figure 2.25 Mitral valve motion in mitral regurgitation has been classified by Carpentier and colleagues into three groups. This is a useful method for describing the abnormality responsible for mitral regurgitation, often eluding to the pathology, as well as in

> communicating mitral valve structural abnormalities to the surgeon in the operating room. Mitral valve motion is described according to the predominate abnormality noted since mitral dysfunction is often caused by coexisting abnormalities. (a) Type I mitral regurgitation results from annular dilatation. (b) Type II mitral regurgitation results from excessive leaflet motion during closure producing prolapse during diastole. (c) Type III mitral regurgitation is produced by restrictive motion of one or both leaflets.

Transesophageal echocardiography has therefore enabled:

• Establish the presence of mitral regurgitation
• Determine the patho-etiology of mitral regurgitation
• Quantification of the severity of mitral regurgitation
• Determination of the severity of left ventricular dysfunction and pulmonary hypertension
• Preoperative and postoperative evaluation of mitral valve surgery.

To provide a consistent and a logical framework for defining the pathology of mitral regurgitation, it is helpful to describe mitral valve lesions with echocardiography on the basis of a functional approach rather than specifically describing each particular abnormality.

Classification of mitral regurgitation

Abnormal structural integrity of the mitral valve can be easily categorized according to the classification described by Carpentier,[10] defining the leaflet motion responsible for the lack of leaflet approximation during systole. Mitral valve motion in mitral regurgitation may be simply and logically described as: type I, normal valve mobility; type II, increased leaflet mobility; and type III, restricted valve mobility (figure 2.25). In conjunction with this classification, specifics of mitral anatomy can be defined echocardiographically or visually at the time of surgery to elucidate further the cause of mitral insufficiency (table 2.3). Adopting this classification of mitral regurgitation helps establish effective communication between the echocardiographer and the surgeon, helping to define the surgical methods necessary for a successful repair.

Table 2.3 Carpentier's functional classification of mitral valve disease

Type	Description
Type I	Annular dilatation
Normal leaflet motion	Leaflet perforation
	Cleft leaflet
Type II	Chordal rupture
Leaflet prolapse	Chordal elongation
	Papillary muscle rupture
	Papillary muscle elongation
Type III	Commissure fusion, leaflet (thickening)
Restricted leaflet motion	Chordal fusion/thickening
	RWMA/LV aneurysm

From Carpentier A. Cardiac valve surgery—the "French correction". *J Thorac Cardiovasc Surg* 1983;86:323–37.

There have been many studies comparing the results of transesophageal echocardiography, transthoracic echocardiography, and epicardial echocardiography with surgical valve analysis that have used this functional classification of mitral valve disease. The ESMIR group[110] recently reported that the correct prediction of surgical strategy in mitral regurgitation was 86% with transthoracic echocardiography, and 89% with monoplane transesophageal echocardiography. These findings are similar to those reported by Stewart and colleagues,[111] who accurately defined mitral regurgitation by epicardial and transesophageal echocardiography. Two-dimensional imaging and Doppler accurately diagnosed 93% of surgical patients with posterior leaflet prolapse or flail, 94% of anterior leaflet prolapse or flail, 44% of bileaflet prolapse or flail, 75% of papillary muscle elongation or rupture, 91% of restricted leaflet motion or rheumatic thickening, 72% of ventricular–annular dilation, and 62% of leaflet perforation or cleft.

Type I

In type I mitral regurgitation, the valve motion is normal, and most of the regurgitation is produced by annular dilatation. Although the valve leaflets are normal they are not long enough to adequately produce the required surface area for approximation of the rough edges of both leaflets. Therefore regurgitation is produced from inadequate sealing of the leaflets during systole. Other causes of type I mitral regurgitation include discrete leaflet perforation and cleft mitral valve.

Annular dilatation usually occurs as a result of an enlarging left ventricle (ventriculo–annular dilatation).[112–115] Studies of the mitral annulus have shown it to be dynamic rather than a fixed structure, normally changing its orifice shape and chamber dimensions during systole and diastole. Most of the motion in the annulus occurs in its posterior circumference situated in the atrioventricular groove. Histologically, the posterior aspect of the annulus is composed of loose connective tissue, devoid of collagen, since the

collagen fibers that project posteriorly from the trigones, taper and thin out before reaching the entire circumference of the annulus. Therefore the posterior region is the weakest and most vulnerable aspect when stretching under tension compared with the remainder of the annulus. With excessive dilatation of the ventricle, the mitral annulus enlarges or "gives" in the posterior aspect, allowing the annulus to assume a more geometrically circular shape, rather than the normal D shape during systole. This dilatation means that the anterior leaflet does not approximate to the posterior leaflet on the basis of a fixed leaflet length. The chordae tendineae to the posterior leaflet may be slightly elongated and assume a more oblique angle, rather than having their normal parallel orientation, thus tethering the posterior leaflet and not allowing the necessary motion for both leaflets to coapt properly. With transesophageal echocardiography, the annulus appears enlarged with normal leaflet motion. The loss of surface area for coaptation of the leaflets is readily appreciated in the lower esophageal position, when imaging the mitral level from the four-chamber and two-chamber views obtained from 0° to 135°. In addition to evaluating leaflet approximation with these views, a ratio of the length of the annular ring diameter can be compared with the height of the anterior leaflet, and annular dilatation exits with ratios less than 0.9. Imaging from the transgastric position with the transducer at 0°, the mitral annulus has a D shape in normal patients and a circular shape when dilated (figure 2.21). The posteromedial commissure is directly at the top of the image sector, and the anterolateral commissure at the bottom of the screen. The anterior leaflet appears to the left, next to the septum, and is geometically convex, with the posterior leaflet appearing to the right and geometrically concave. The pattern of leaflet opening and closing is readily distinguishable from normal when annular dilatation occurs, when visualizing the valve enface by transesophageal echocardiography in the horizontal transgastric view. Normally during systole, the line of leaflet approximation or closure illustrates a "smile shape" which is distorted when dilatation occurs. Opening is more circular in shape, as described above. The posterior position of the line of closure should be easily appreciated relative to the center of the valve plane, which shifts centrally with dilatation. Color flow Doppler imaging from the lower esophageal position, in the horizontal or longitudinal views of the left heart, usually helps to show a centrally projected regurgitant jet(s) into the left atrium, with annular dilatation.

Papillary muscle dysfunction has been noted in patients with dilated and poorly contracting left ventricles.[116] Papillary-muscle abnormalities have also been described in cardiomyopathic diseases involving the left ventricle. There is significant elongation and thinning of papillary muscle in idiopathic dilated cardiomyopathy. Left ventricular enlargement tends to alter the spatial relation between the papillary muscles rather than affecting their motion. With significant dilatation, the papillary muscles are pulled further into the left ventricular cavity, producing incompetence of the mitral valve by affecting the apposition of the leaflets during systolic closure. In cases of cleft mitral valve or leaflet perforation, mitral valve leaflet opening and closing are normal and the specific defect may not be readily apparent. Cleft mitral valves are occasionally observed in the adult as an isolated finding, not associated with atrioventricular canal defects.[117–120] The clefts may be partial or complete, and when complete, may be confused with an accessory leaflet or an anatomic tricuspid leaflet. Associated with the cleft deformity in the leaflet are accessory chordae, which insert into the margins of the cleft and originate

from the ventricular septum. The cleft is usually found in the anterior leaflet, and, viewing the valve enface in short axis, appears as a line of opening perpendicular to the usual line of leaflet closure during diastole. This finding may be confused with scalloping of the leaflet. In transverse or longitudinal long axis views, the cleft in the leaflet can be confused with the normal orifice opening during diastole or mild prolapse with billowing during systole, if careful scanning is not performed. Another characteristic of a cleft leaflet that distinguishes it from a prolapsed leaflet, is that there is minor leaflet thickening in comparison to that which occurs in mitral valve prolapse from myxomatous degeneration. While scanning between 0° and 135°, the cleft should be distinguishable from the normal orifice by demonstrating both openings and by the fact that the cleft is usually eccentric to the normal location of the orifice in respective views. Color Doppler is usually very helpful in demonstrating systolic and diastolic turbulent high-velocity flow through the cleft orifice, which is readily distinguishable from normal.

Leaflet perforations usually occur as a result of trauma (wrongly placed catheters) or as a common consequence of bacterial endocarditis. The cause is usually apparent from the patient's clinical history and not readily distinguishable on echocardiography, unless obvious vegetation is present. Leaflet perforations may occur on either leaflet, and may or may not be involved with the line of leaflet closure. Leaflet perforations are visualized echocardiographically in long-axis views as small areas of leaflet prolapse, or with color Doppler as high velocity jets in non-suspect areas of the mitral valve plane with no obvious defect.

Type II

Type II motion is shown by leaflet prolapse and is present when the free edge of either leaflet overrides the annular plane and orifice during systole, resulting in lack of coaptation of the leaflets.[14,121–127] This is in direct comparison with billowing or floppy mitral leaflets, in which excessive leaflet tissue protrudes or prolapses beyond the annular plane into the left atrium, with the point of leaflet coaptation is below the plane of annulus (figure 2.26). It is not unusual, however, to observe billowing valve leaflets associated with prolapse, causing lack of apposition of the leaflets. This type of valve motion is frequently produced by degeneration of the valve structures from chronic rheumatic disease or, with myxomatous degeneration, fibroelastic deficiency, or a combination of the above. The hallmark of degenerative valve disease is excessive leaflet tissue, shown echocardiographically by altered leaflet thickening and increased length, resulting in redundant leaflet motion.[126] With the progression of degenerative disease, isolated annular dilatation[121] without ventricular enlargement can result, and with subsequent mitral annular calcification. Type II motion may also be caused by isolated chordal or papillary muscle elongation and/or rupture.[128–133]

Prolapse   Billowing   Prolapse and billowing
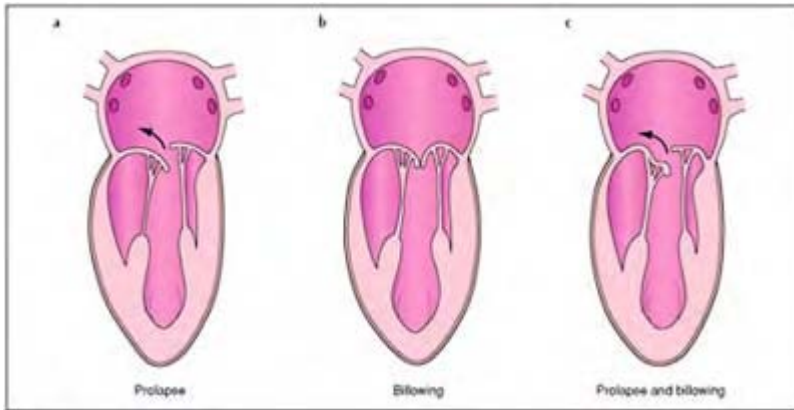
Figure 2.26 Diagram demonstrating mitral valve motion with prolapse. Mitral valve prolapse is produced when the mitral valve apparatus allows for excessive leaflet motion during diastole promoting the lack of leaflet coaption during closure. Billowing of the leaflet due to excessive tissue produces protrusion of the body of the leaflet, into the left atrium during diastole without affecting leaflet closure. Mitral valve prolapse of myxomatous origin often produces prolapse and billowing of the mitral apparatus. It is important to distinguish true prolapse from billowing in the diagnosis of mitral regurgitation, especially when defining valvular abnormalities prior to mitral valve repair.

Mitral valve prolapse is now a well-recognized cause of mitral regurgitation, largely due to improvements in echocardiography. In the early history of mitral valve prolapse, diagnosis was difficult because of the poorer imaging resolution of earlier echocardiographic equipment. With transthoracic echocardiography, the mitral valve depth is usually out of the range for good visualization of the leaflets. Pronounced billowing of the leaflets is commonly misdiagnosed as prolapse with transthoracic imaging, even under multiple views. Only in the patient with excellent images can one be sure which leaflet is prolapsing. Coexisting abnormalities, such as elongated chordae and

ruptured small chords, can be very difficult to see if examination is not thorough and meticulous. A definitive diagnosis can usually be made with transesophageal echocardiographic imaging from the esophagus under higher imaging frequencies. It is paramount, however, even with transesophageal echocardiographic imaging, that a systematic approach be followed in analyzing the full mitral valve unit in patients with prolapse, to follow the progression of disease, or to give the cardiac surgeon the necessary information for a successful repair when the disease has reached that stage.

The transgastric and deep transgastric views are ideal to assess the subvalvular apparatus in mitral valve prolapse and to establish continuity for the papillary muscles, chordae tendineae, and valve leaflets (figure 2.21). The papillary muscles and chordae tendineae should be scanned from 0° to 135° in both views to identify focal areas of echogenicity, indicating fibrosis or calcific lesions, representing friction-type lesions when either are elongated, redundant, or displaced. Areas with high frequency or vibratory movement in the chords or papillary muscles during the cardiac cycle suggest rupture of the supporting apparatus. In the deep transgastric views, sweeping from 0° to 45°, the papillary muscles are imaged obliquely, but the chordal apparatus are well visualized. Elongation and redundancy of the chords may be noted by comparing chordal length among the chordal groups—in many cases significant bowing of the chords can be seen during the cardiac cycle.

The four-chamber and two-chamber left ventricle views from the lower and mid-esophageal position from 0° to 110° enable the best evaluation of the valve leaflets. The leaflets are easily identified as anterior and posterior, in relation to both commissures. In the four-chamber view slowly withdrawing the scope, the posterior commissural area is shown from the lower esophageal position; the mid-portion of the leaflets is seen in the mid-esophagus and the anterior commissural area in the upper esophageal position. Rotating the transducer from 0° to 90° images both leaflets in relation to each other, or in full-length individual cuts of each particular leaflet. The mitral annular plane should be constructed mentally, and leaflet motion should be labeled as excessive, normal, or restricted for each segment of the anterior and posterior leaflets in relation to the ventricular side of the annulus. By contrast with transthoracic echocardiography, billowing or prolapse of the leaflet margins are distinguishable from the many views obtained with multiplane transesophageal echocardiography. At about 45° to 90°, the mitral leaflets are imaged parallel to the line of closure. Either leaflet will appear as a continuous echocardiographic line traversing the annular plane. With subtle medial or lateral rotation of the probe, either the anterior or posterior leaflet will be visualized. The posterior leaflet will be essentially linear with minor bulging illustrating the three scallops. The anterior leaflet will appear more curvilinear in the center of the valve plane, with the lateral and medial scallops of the posterior leaflet on either side of the anterior leaflet—especially apparent when the leaflets are open during diastole. In this view, prolapse or flail of the opposite leaflet will usually appear as a smaller, free linear or curvilinear echo, superior to the annulus and the other leaflet on the atrial side. Flail segments are easily noted and are represented by the leaflet overriding the other leaflet in the frontal planes, generally with short segments of the ruptured chord attached, showing either high-frequency movement or actual prolapse back and forth between the atrial and ventricular cavities during the cardiac cycle. Leaflet thickness[134] may also be assessed in this view. In degenerative mitral-valve prolapse the leaflets may thicken in diastole when

they are slack and unstressed as the result of leaflet redundancy, overlap, prominent interchordal hooding, and the presence of excessive tissue. In systole, when the leaflets are under tension from ventricular forces, the leaflets appear thinner. Leaflet thickness can be assessed by measuring the percentage change in leaflet width from diastole to systole, which is normally 22–34%. In patients with mitral valve prolapse, the percentage change in leaflet thickness from diastole to systole averages 54–62%.

With all of these views, the direction of the regurgitant jet(s) is illustrated using color Doppler. The long-axis planes are ideal for determining which leaflet is involved, although the short axis planes are better for determining the specific segment of the abnormal leaflet.[111] The general direction and origin of the regurgitant jet should be noted as posteriorly, anteriorly, or centrally, and if there is one or more jets. Careful scanning prevents the improper labeling of the jet as multiple when tangentially cut out of plane. In large jets that fill the left atrium, it may be necessary to decrease the color and image gain so as to identify properly the origin of the jet. The origin of the jet should be described as towards one or the other commissure, or having a central location along the line of leaflet coaptation during closure or emanating from outside of this plane. Color Doppler flow mapping may also be helpful to define prolapsing leaflet tissue, showing an eccentric regurgitant flow jet, in the opposite direction of the leaflet that is prolapsing.[135] With degenerative prolapse of the anterior leaflet, the regurgitant jet is directed posteriorly, and with posterior leaflet prolapse the regurgitant jet is directed anteriorly. By contrast, rheumatic prolapse results in the predominant fibrosis of one leaflet, the normal leaflet protrudes above the abnormal one, and the regurgitant jet is directed toward it. When there is bileaflet rheumatic or degenerative disease involvement producing prolapse of both leaflets, the jet is directed centrally into the left atrium, or is slightly eccentric if one leaflet prolapses more than the other one. There may be many jets, showing that there are multiple discrete areas that do not approximate properly. It is important to identify the presence of multiple jets in more than one view.

Echocardiographically, it is also possible to derive the pathological cause of prolapse by noting mitral lesion patterns common to specific disease states. In rheumatic prolapse, the predominant lesion in most cases is isolated prolapse of the anterior leaflet secondary to elongated or ruptured chordae tendineae or papillary muscles. Both leaflets may be slightly thickened or retracted with shortening and fusion of the chords, and only a few show annular dilatation.[136–138] Myxomatous degeneration is characterized by excessive tissue of all the scallops of theposterior leaflet.[139,140] When there is associated anterior leaflet prolapse, it is most prominent in the posteromedial half of the leaflet (A2, A3). Myxomatous degeneration is frequently observed in younger patients, and as the disease progresses both leaflets appear thickened, with extensive hooding of the rough zone. Chordae to both leaflets elongate and appear thickened and redundant. Excessive tissue of the posterior leaflet tends to push the anterior leaflet and line of closure forward, which in small ventricles narrows the aorto-mitral angle, to produce systolic anterior motion (SAM) of the valve leaflets and chordal apparatus. Patients with fibroelastic deficiency and prolapse have thinner leaflets, lack of billowing. Prolapse is usually limited to the central scallop (P2) of the posterior leaflet with some degree of annular dilatation. The chordae appear thinner but redundant, with or without minor ruptures, and the left ventricle is commonly hypertrophic. Prolapse of ischemic origin usually results in thickening and increased echogenicity of the chordae tendineae and papillary muscles.

Normal appearing leaflets are associated occasionally, with ruptured chordae near the leaflet edge insertion points.

Papillary muscle rupture, either partial or complete, is an uncommon complication of acute myocardial infarction, and is associated with high mortality.[141–145] There is a significant increase in the incidence of posteromedial papillary muscle rupture compared with anterolateral muscle rupture in myocardial infarction. Rupture may occur near the head of the papillary muscle partially involving the chordal attachments. Rupture of the whole muscle results in complete detachment of the papillary muscle from the ventricular myocardium, producing a flail mitral leaflet. Regional wall motion abnormalities are usually detected in the myocardium subjacent to the papillary muscle, and are hypokinetic, rather than akinetic or dyskinetic as might be expected. Transthoracic echocardiography imaging is usually adequate for the diagnosis of papillary muscle rupture, but transesophageal echocardiography may be required in patients with poor acoustic windows, in cases of partial rupture, or when the ruptured papillary muscle head does not prolapse into the left atrium. Transesophageal echocardiography is also useful to diagnose papillary muscle hemorrhage[146,147] in acute mitral regurgitation by observing a markedly irregular echolucency in a papillary muscle, with ventricular systolic thinning of the myocardium, preventing the lack of coaptation of the mitral leaflets.

Transesophageal echocardiography illustrates the anatomical abnormalities of papillary muscle rupture with more certainty than transthoracic echocardiography, but both techniques adequately define abnormal regional wall motion involvement, and the use of Doppler with either technique defines the severity of the resultant mitral regurgitation. Moursi and colleagues[145] have shown that with biplane or multiplane transesophageal echocardiography an accurate diagnosis of ruptured papillary muscle can be made with certainty. In 90% of their patients, the ruptured papillary muscle head showed relatively large-amplitude erratic motion in the left ventricular cavity even when the ruptured muscle did not prolapse into the left atrium. In 70% of the patients the residual papillary muscle still attached to the ventricular wall also showed a prominent but less erratic motion than the free papillary muscle head portion. From these findings, transesophageal echocardiography reliably detected all patients with papillary muscle rupture in a retrospective analysis. When there is partial rupture of the papillary muscle, the involved leaflet still appears flail, but the muscle does not prolapse into the left atrium. Careful inspection of the papillary muscle in multiple planes usually shows partial attachment of the papillary muscle to the ventricular myocardium. Prominent mitral leaflet prolapse occurs in all patients with papillary muscle rupture. Even though each leaflet receive support from both papillary muscles, one leaflet is usually observed to prolapse more than the other. When the pulmonary veins are interrogated with Doppler, systolic flow reversal is recorded. With color Doppler, the mitral regurgitant jet usually fills the entire atrium.

Type III

Type III motion is shown by restricted leaflet motion in which a leaflet does not open normally during diastole. Echocardiographically, it appears that only one leaflet is moving and the other leaflet is fixed in a diastolic position, producing lack of coaptation (figure 2.21). This type of leaflet motion may result from commissure fusion or

thickening, from chordal fusion or thickening, or, more commonly, from left ventricular infarction with or without aneurysm formation. As with type II motion, annular dilatation may be present as well, since one leaflet may be restricted and the other leaflet prolapsing.

Even though mitral regurgitation has been readily attributed to ischemic papillary muscle dysfunction, the functional consequence of mitral regurgitation secondary to isolated ischemic papillary muscle dysfunction is unclear.[148–150] Regional wall motion abnormalities of the left ventricle are frequently observed in cases of papillary muscle dysfunction. It has been suggested that papillary muscle motion or function should be assessed together with the motion of the left ventricular wall subjacent to the particular papillary muscle. In patients with prior myocardial infarctions[29] a reduction in percentage of papillary muscle fractional shortening to $15 \pm 14\%$ was observed, compared with normal patients ($30 \pm 8\%$). In patients with posterior myocardial infarction, the posteromedial papillary muscle motion was reduced, and appeared more echodense than the anterolateral muscle. Mintz and colleagues[141] reported that the posterior leaflet was retracted, rigid, and non-mobile in patients with a prior infarct and severe mitral regurgitation. The severity of associated mitral regurgitation is related to degree of contractility and dilation of the left ventricle. Significant mitral regurgitation is rare with normal left ventricular systolic function. Kaul and colleagues[150] showed that ischemic mitral regurgitation is not related to acute papillary muscle dysfunction or to regional wall motion abnormality produced experimentally in the laboratory, but rather to global left ventricular dysfunction. The prevalence of severe mitral regurgitation is greater when there is both anterior and posterior papillary muscle dysfunction.

Coexistent with all three types of valve motion may be sporadic or diffuse mitral annular calcification (MAC).[151] MAC occurs in degenerative disease irrespective of annular dilatation. MAC probably represents the breakdown and degeneration of the annulus, followed by calcification, especially in the posterior segment composed of loose connective tissue. Sporadic or extensive annular calcification may occur, may distort the orifice, and can influence results unfavourably.

Quantification of mitral regurgitation

It has become increasingly important and it is certainly a challenge to accurately define the severity of mitral regurgitation. Even though there are methods to describe the quantity of mitral insufficiency, none is totally acceptable. The difficulty in evaluating mitral regurgitation stems mostly from its variable presentations attributable to different mitral lesions; the inability to detect accurately and assign a meaningful value to the true quantity of regurgitant flow, and the inability to define precisely the hemodynamic significance imposed by regurgitation in individual patients with different disease states. Echocardiography provides an easy, accurate, and non-invasive method to identify and serially quantify mitral regurgitation. Either method, transthoracic or transesophageal, may be used to quantify mitral regurgitation, since the same technical and physiological factors limit both echocardiographic and Doppler techniques (table 2.4). In individual patients, however, transesophageal echocardiography may provide additional information via better imaging from the esophageal window. Due to the excellent quality of the

images obtained of the valve apparatus and the color flow jets with transesophageal echocardiography, an experienced echocardiographer may be able to provide much more accurate information just through intuition than can be obtained from other more sophisticated methods. The information obtained from transesophageal echocardiography may aid in the recognition and interpretation of subsequent transthoracic studies.

Patients often develop severe mitral regurgitation and left ventricular dysfunction before the onset of symptoms, highlighting the importance of accurately assessing the degree of regurgitation by an accurate and reproducible method. Currently, we can at best semiquantify the hemodynamic significance of mitral regurgitation, which has serious implications for patients with mitral regurgitation. In patients with suspected mitral regurgitation, echocardiography is primarily used to identify regurgitant jets by color flow or conventional Doppler techniques (table 2.4). Once mitral regurgitation is documented, severity is estimated by correlating the total quantity of regurgitant flow to an assessment of ventricular performance and reserve (table 2.5). In this way, patients with mitral regurgitation can be successfully managed with surgery, which presently offers the best outcome for patient management.

Table 2.4 Echocardiographic quantification of mitral regurgitation

	Sellers grade			
	Mild 1+	Moderate 2+	Mod/Sev 3+	Severe 4+
Max regurg jet area[171]	$1.5–4\ cm^2$ (82,95)	$4–7\ cm^2$ (100,95)		$> 7\ cm^2$ (83,100)
Mosaic jet[172]	$< 3\ cm^2$ (96,100,98)			$> 6\ cm^2$ (91,100,98)
Jet area/left atrial area ratio[169]	< 20% (96,91,94)		> 35% (64,93,85)	
Pulmonary venous flow[180]	Normal	Blunted systolic flow (61,97)		Systolic flow reversal (93,100)
PISA (ROA)[TTE (199)]	$< 0.1\ cm^2$		$0.3–4.9\ cm^2$	$\geq 0.5\ cm^2$
Vena contracta[mono] [(183)]	$2.6 \pm 1.0\ mm$	$4.2 \pm 1.2\ mm$	$6.3 \pm 1.2\ mm$	$8.6 \pm 2.2\ mm$
ROA				$> 5.5\ cm^2$ (92,92,88)
RSV				> 60 cc (88,93,94)
Vena contracta[multi] [(185)]				> 6 mm (95,98,95)
RSV				> 80 cc (86,95,92)

ROA = regurgitant orifice area; RSV = regurgitant stroke volume; PISA = proximal isovelocity surface area; mono = monoplane transesophageal echocardiography; multi = multiplane transesophageal echocardiography; TTE = transthoracic echocardiography; numbers in parentheses (sensitivity, specificity, positive predictive value).

In valvular stenosis, it is widely accepted that the reduction of valve opening or the size of the hole as described by the stenotic orifice area determines the severity of valve

disease. The stenotic orifice area is conceptually easier to understand and accepted by clinicians, since it may be directly measured or calculated. Unlike stenotic valve disease, the effective regurgitant orifice, or the hole in the valve produced by valve lesions, especially atrioventricular valves, is difficult to conceptualize since it is not readily appreciated by any method. In mitral regurgitation, the hole produced during systole by the lack of approximation during closure of the valve leaflets can be better appreciated, especially when using the functional classification. It is easy to deduce—the larger the regurgitant hole, the greater the regurgitant volume. Recently, echocardiographic and Doppler methods have been developed to measure and calculate the regurgitant orifice area. In addition to these methods, the better image resolution and multiple views of multiplane transesophageal echocardiography have all led to a better appreciation of the regurgitant orifice area concept.

Table 2.5 Echocardiographic findings suggesting severe mitral regurgitation

1. Progressive end-systolic ventricular enlargement > 4 cm
2. Left ventricular end-diastole dimension ≥ 7 cm
3. Ejection fraction < 60%
4. ROA > 0.5 cm^2
5. Regurgitant volume $60 \geq$ cc
6. Regurgitant fraction > 55%
7. Flail leaflet
8. Color flow max regurgitant jet area > 7 cm^2
9. Regurgitant jet area/left atrial area > 35%
10. Pulmonary venous systolic flow reversal
11. Left atrial diameter > 30 mm per square meter of BSA

It is well accepted that the degree of severity of mitral regurgitation is associated with the regurgitant volume. A regurgitant volume less than 35% of the total left ventricular stroke volume can be well tolerated for long periods and does not result in the significant progression of left ventricular dysfunction. Rather, regurgitant volumes greater than 50% seem to lead almost invariably to quicker clinical deterioration. Mitral regurgitation with volumes of 35–50% presents a clinical dilemma, and may or may not cause a problem depending on other coexistent conditions. In most cases, ejection fraction and the serial measurements of end-systolic and end-diastolic ventricular volumes can be used to assess the ventricular performance. However, because of its high dependence on loading conditions, the ejection fraction may not reflect the intrinsic left ventricular performance. The end-systolic and end-diastolic volumes are markers that can predict a poor outcome after surgery in terms of perioperative mortality and morbidity, but they lack adequate sensitivity and specificity. The risk of early and late postoperative morbidity and mortality is increased in patients with impaired left ventricular performance. The potential for postoperative improvement is limited as ventricular reserve diminishes. Therefore, the ideal timing for surgical intervention probably occurs at the onset of left

ventricular impairment to circumvent the small risk of perioperative events associated with current surgical techniques.

Echocardiographic diagnosis of mitral regurgitation

Conventional and color Doppler methods allow the detection of mitral regurgitation with a high degree of accuracy (table 2.4). Positioning the pulsed Doppler sample volume on the left atrial side of the mitral annulus, below the leaflet tips during systole, permits sensitive identification of backward systolic flow, which is diagnostic of mitral regurgitation. Pulsed wave Doppler mapping of the left atrium to determine the extent of the regurgitant jet is not routinely performed and really is superfluous with transesophageal echocardiography. The color Doppler flow method is the preferred technique in combination with transesophageal echocardiography, and is extremely sensitive in detecting and illustrating regurgitant flow from the left ventricle to the atrium during systole.

Through the use of Doppler techniques it is now widely recognized that all valves leak slightly, due to the displacement of blood from the normal motion of the valve during closure, and trivial or physiological regurgitation is frequently shown in normal patients. Physiological regurgitation,[152] which is most commonly defined with transesophageal echocardiography and color flow Doppler, is defined by small jets of flow reversal detected in close approximation to the mitral annular plane, usually during the early phase of systole, when the leaflets are closing. Pulsed Doppler sampling shows these jets usually within a 1cm area about the annular plane. Single or multiple color flow jets with small jet areas and low flow velocities are imaged without significant turbulence or variance.

With transesophageal echocardiography and color flow Doppler, significant regurgitant flow jets are readily visualized, emanating from a closed mitral valve orifice as high velocity systolic jets of flow.[153–155] Regurgitant flow jets are easily recognized by their mosaic or green appearance produced by turbulence and variance maps recorded against the background of low velocity blood flow filling the atrium (figure 2.27). Transesophageal echocardiography has a clear advantage over transthoracic imaging in mitral regurgitation. Eccentric regurgitant jets are easier to visualize from the multiple views provided by the esophageal window, and may be easily followed in their full extent throughout the atrium with minor changes in probe positioning. Generally, the regurgitant jets appear larger than they do from the transthoracic approach, with imaging from the esophageal window. The left atrium is physically closer to the transducer, which permits better resolution by taking full advantage of the transducer frequency and eliminating the acoustic shadowing from the valve apparatus that occurs in the apical windows with transthoracic imaging.

It is important to describe fully regurgitant flow jets when classifying mitral regurgitation by transesophageal echocardiography. Regurgitant jets are composed of an area of flow convergence on the ventricular surface of the regurgitant mitral orifice that narrows as it proceeds through the mitral orifice (vena contracta). The flow rapidly spreads out like a flame (maximal jet area) and mixes with blood flow in the left atrium.

Regurgitant jet flow may be directed centrally into the left atrium, or may take an eccentric path as it originates from the regurgitant orifice.

Diastolic mitral regurgitation

Mitral regurgitation or retrograde blood flow can occasionally be recorded during diastole as well as in systole, even though there is proper closure of the valve.[156–158] A positive pressure gradient develops between the left atrium and left ventricle due to improper timing of atrial-ventricular relaxation and contraction cycles. Doppler recordings of diastolic regurgitation consist of low volume, high velocity flow jets that diminish abruptly when the valve becomes completely competent during ventricular systole. Diastolic mitral regurgitation may be seen in cases of conduction disturbance as in atrioventricular block, atrial flutter, atrial fibrillation, in severe aortic regurgitation, or with decreased ventricular compliance and distensibility.

Estimation of the severity of mitral regurgitation

Measurement of regurgitant jet area

Doppler color flow mapping, in addition to identifying regurgitant jets, may also provide a semiquantitative method to estimate the volume of the regurgitant jet.[159–163] Planimetry of the cross-sectional jet area visualizes the extent of the maximal regurgitant signal. The maximal jet area must be optimally visualized by adjustment of the transducer, which improves by using the transesophageal approach, since jets do not need to be centrally oriented from the orifice to be seen adequately.[164] The sensitivity of this method, using transthoracic echocardiography rather than angiographic ventriculography, has been reported[165] to be about 86%, with a specificity of 100% and a correlation coefficient of 0.83. The severity is graded from mild to severe according to the jet area measured. Mild regurgitation has a jet area of less than 1.5 cm^2, moderate jet areas 1.5–3.0 cm^2, moderate to severe jet areas 3.0–4.5 cm^2, and severe regurgitation jets, larger than 4.5 cm^2. Due to the technical factors involved in Doppler imaging, involving the spatial relations of flow jets, better results may not be possible with this method. The spatial distribution of the regurgitant jet imaged by color Doppler flow mapping is highly dependent on the velocity of the driving pressure transmitted from the left ventricle to produce regurgitation, rather than on the regurgitant volume. Under constant flow conditions in vitro, the spatial distribution of a regurgitant jet increases with increasing flow rate producing a larger regurgitant jet on color Doppler flow mapping, which leads to overestimation of the severity of regurgitation. Similarly, if the flow rate remains constant and the regurgitant jet orifice is modified,[166] the spatial distribution of the jet will decrease as the orifice size is increased, despite identical flow rate and regurgitant volume. In these situations, measurement of the jet area will underestimate the severity of mitral regurgitation. The jet area depends not only on the regurgitant volume, but also on the regurgitation orifice and the velocity of blood flow.
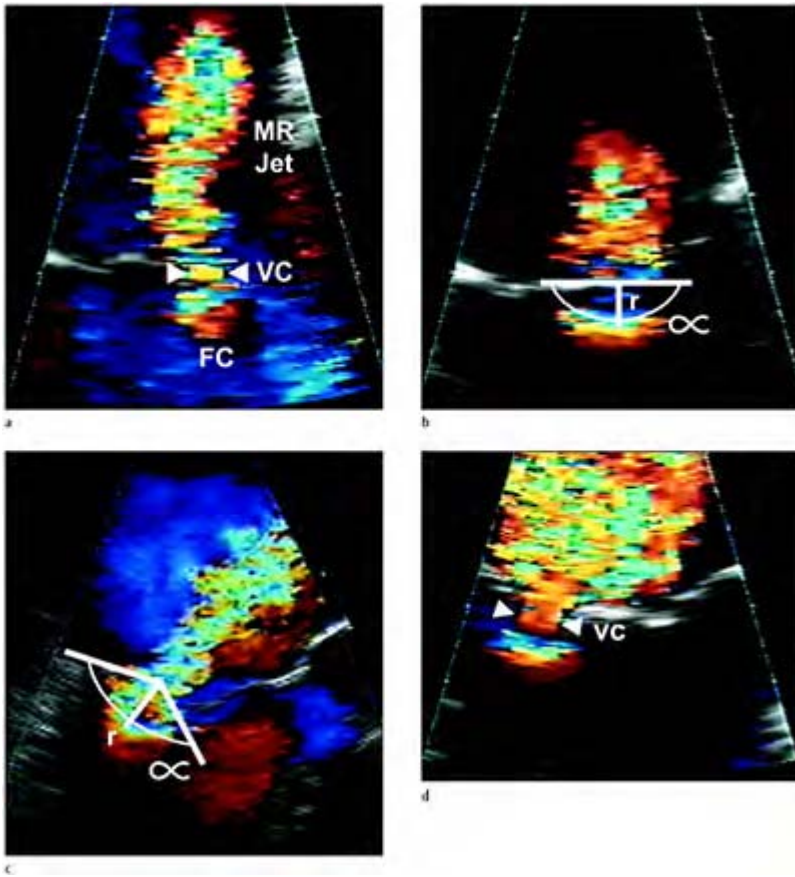
Figure 2.27 Color flow Doppler of the
flow jet in mitral regurgitation
demonstrating flow convergence and
vena contracta, which may be utilized
for determining the severity of mitral
regurgitation. (a) Typical central color
flow jet of mitral regurgitation
extending into the body of the let
atrium. (b) Enlarged view of the flow
convergence in a central directed jet,
illustrating an angle of closure of 180°
as utilized in the proximal isovelocity
surface area (PISA) method. (c) When
an eccentric mitral regurgitant jet is

detected the angle of leaflet closure
may not be 180° and the angle must be
corrected and measured for proper
utilization in the PISA method. (d)
Enlarged view of a mitral regurgitant
jet illustrating the proper point
(arrows) of measurement for the vena
contracta method.

There is also wide variation in the spatial characteristics of regurgitant jets in patients with mitral regurgitation. Distortion of the spatial pattern of the regurgitant jet may occur, with collision of multiple and multi-directed jets or by jets directed towards and impacting the left atrial wall or Coanda effect,[167] all of which complicate the estimation of jet area. Pulmonary venous flow[168] directed towards the mitral regurgitant jet may produce smaller jet areas (through distortion and flattening) than may occur when the pulmonary venous flow is directed away from the regurgitant jet. The estimation of regurgitant areas can be modified by many hemodynamic variables, such as the level of the left atrial pressure, and by changes in heart rate, most pronounced in patients with acute severe mitral regurgitation. Considering all the factors that may influence the true measurements and calculations of mitral regurgitation, an experienced echocardiographer may be able to construct an accurate assessment of mitral regurgitation from visual impression alone.

To assess mitral regurgitation more precisely, the maximum jet area relative to the left atrial size can be determined also measuring the jet area in three orthogonal planes. With transthoracic imaging,[169] a ratio of the jet area to the left atrial area of less than 0.2 shows mild regurgitation, 0.2–0.4 moderate regurgitation, and greater than 0.4 severe regurgitation, as obtained with angiography. Unfortunately, these techniques have not increased the statistical correlation with angiography, supporting the fact that the Doppler method provides better information on the velocity of flow than on the regurgitant volume.

Many reports that compared transesophageal echocardiography with color flow Doppler and ventriculography have shown an excellent correlation between the two methods for quantifying mitral regurgitation.[170] With transesophageal echocardiography, the absolute jet area may be calculated with good results. Color Doppler mapping of the area of the regurgitant jet[171] is around 95% sensitive and 100% specific, with a predictive accuracy of 98%.

It has been suggested that the area calculation of only the mosaic portion (variance) of the regurgitant jet is enough to quantify severity.[172] A maximal mosaic area of less than 3 cm^2 showed mild regurgitation with a sensitivity of 96%, a specificity of 100%, and a predictive accuracy of 98%. A maximal mosaic jet area of greater than 6 cm^2 predicted severe regurgitation, with a specificity of 91%, a specificity of 100%, and a predicted accuracy of 98%.

Transesophageal echocardiographic comparison of the regurgitant jet area as a percentage of the left atrial area is accurate, despite limitations in visualizing the full atrial dimension.

Measurement of regurgitant volume and regurgitant fraction

Mitral regurgitant volumes can be calculated echocardiographically by comparing the difference between mitral and aortic stroke volumes, and expressing the regurgitant volume as a fraction of the total mitral inflow.[173,174] Aortic outflow volume is derived from the product of aortic cross-sectional area multiplied by the flow velocity integral and heart rate. The aortic cross-sectional area is obtained by measuring the diameter of the aortic annulus just proximal to the point of insertion of the aortic cusps, and using $2\pi r^2$, assuming that the aortic orifice is circular. The aortic stroke volume is obtained by calculating the area under the flow velocity time integral curve. The aortic outflow can be obtained from the deep transgastric position at 0° or from the lower esophageal position at 0° using a five-chamber view. The aortic annulus diameter is usually best taken from the lower esophageal position at 135°–150°. This determination of aortic outflow by the pulse Doppler method is fairly accurate compared with the thermodilution technique.

The mitral inflow volume is calculated in a similar manner, but the mitral orifice probably should be considered elliptical instead of circular. The long axis of the mitral orifice can be measured in the transgastric view at about 90°, during mid-diastole. The short axis dimension can be taken from the transgastric short axis view at 0° to 15° to present the valve enface and again is measured at mid-diastole. The mitral valve area is calculated by: $MVA = (\pi/4) \times L \times S$. Pulsed Doppler measures the mitral inflow velocity in the lower esophageal position from 0° to 90° in four- or two-chamber views, placing the sample volume at the leaflet tips. With this method, using transthoracic echocardiography, a correlation coefficient of 0.92 has been obtained compared with angiographic methods.

Obviously, the measurement of the regurgitant volume in this manner is cumbersome and time-consuming. Accurate measurement of the aortic and mitral annulus is vital for adequate results, which should give multiplane transesophageal echocardiography an advantage since it gives more accurate results. In patients with atrial fibrillation and mitral regurgitation, numerous measurements must be taken of the flow velocity time integrals, averaged to compensate for variation in diastolic filling times.

Measurement of regurgitant orifice area

One of the first methods to calculate the effective regurgitant orifice area was described by the Mayo Clinic.[175] The effective regurgitant orifice area may be calculated by pulsed and continuous wave Doppler, as the ratio of regurgitant volume/regurgitant jet time–velocity integral. Mitral and aortic stroke volumes are estimated by pulsed wave Doppler, calculating the orifice flow for each (the orifice area times the velocity), and the regurgitant volume is calculated from the difference of the mitral inflow and aortic inflow. The time–velocity integral is obtained by continuous wave Doppler of the mitral regurgitant jet. The effective regurgitant orifice area obtained in this manner is strongly predictive of the severity of mitral regurgitation. Surgical observations have suggested

that there is a marked difference between the mitral regurgitant orifice area of moderate and severe lesions (35 ± 12 mm^2 and 75 ± 33 mm^2, respectively, p = 0.009), underlining the importance of this measurement.

Quantification of regurgitation from pulmonary venous flow patterns

Some authors suggest the use of the pulmonary venous flow pattern to predict the severity of mitral regurgitation. By definition, severe (4+) mitral regurgitation produces the systolic reflux of contrast media into the pulmonary veins during angiographic ventriculography. In animal models and patients, pulmonary venous flow patterns may be altered by regurgitant volume, left atrial compliance, left ventricular systolic and diastolic function, systolic blood pressure, and peripheral vascular resistance. Despite all of these factors, however, regurgitant volume is largely responsible for producing negative systolic pulmonary venous flow. Multiplane transesophageal echocardiography has provided an excellent non-invasive means to interrogate the pulmonary veins using pulsed wave and color flow Doppler to describe abnormal pulmonary venous flows (figure 2.28). Recently, transesophageal echocardiographic Doppler studies have shown that increases in severity of mitral regurgitation produces characteristic pattern changes in pulmonary venous flow (table 2.6).

Table 2.6 Pulmonary venous flow indices in mitral regurgitation

Sellers MR grade	1+	2+	3+	4+
Patients (no.)	1	12	8	22
Peak systolic velocity (S) (cm/s)	44	37 ± 20†	26 ± 28*	14 ± 20‡
Peak diastolic velocity (D) (cm/s)	53	53 ± 22	52 ± 26	61 ± 18
Systolic/diastolic (S/D) ratio	0.8	0.8†	0.5*	0.3‡

*$p< 0.05$ peak S, D, S/D ratio for 3+ versus 4+ mitral regurgitation;
†$p< 0.05$ peak S, D, S/D ratio for 2+ versus 4+ mitral regurgitation;
‡$p< 0.05$ peak S, D, S/D ratio for 4+ versus (2+, 3+) mitral regurgitation.
From Klein AL, Obarski TP, Stewart J, et al. Transesophageal Doppler echocardiography of pulmonary venous flow: a new marker of mitral regurgitation severity. *J Am Coll Cardiol* 1991;18:518–26.

Normal pulmonary venous flow is pulsatile, and corresponds to the X and Y descent of the left atrial pressure curve. Normal flow emptying into the left atrium from either the right or left pulmonary vein is easily visualized by multiplane transesophageal echocardiography, and appears non-turbulent and reddish orange in color on standard color flow velocity maps. With pulsed wave Doppler, normal pulmonary venous flow appears as biphasic waves above the Doppler baseline, with forward flow recorded during systole and diastole. Occasionally, a small wave of reversed atrial flow is noted immediately after diastolic forward flow, corresponding to mitral valve closure. The peak velocity of the systolic integral is greater than the diastolic peak velocity, with a ratio of about 2:1. When recording pulmonary venous flow with pulsed Doppler, the sample volume must be placed at least 1–2 cm into the pulmonary vein to eliminate extraneous
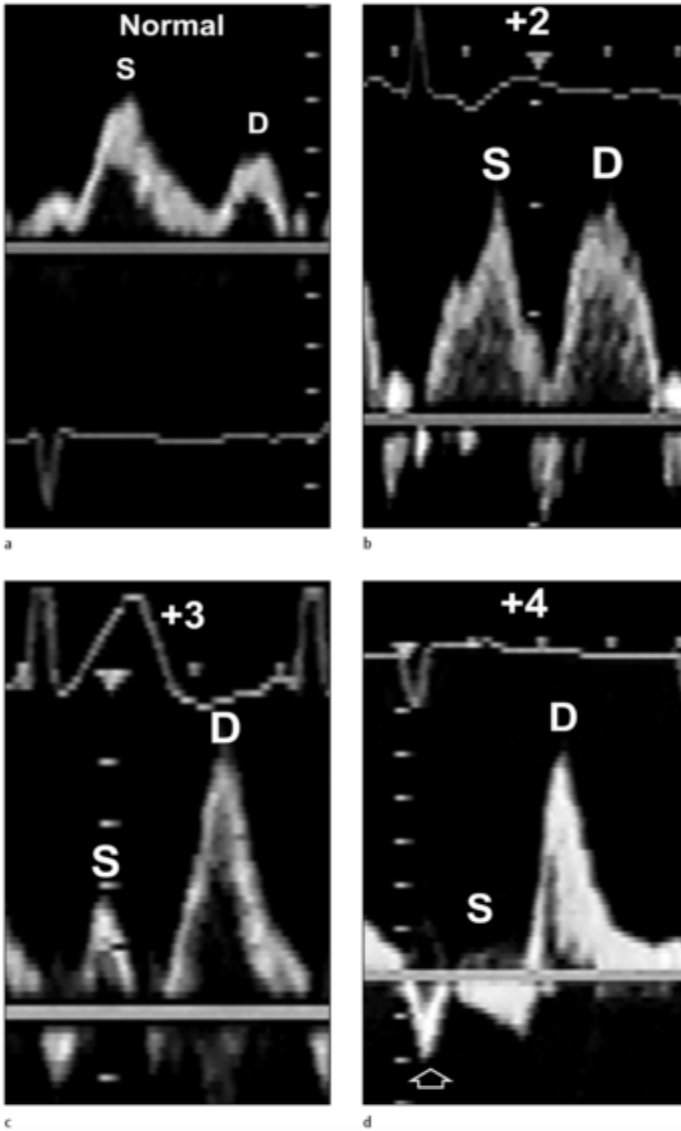
Figure 2.28 Pulmonary venous flow. Pulsed Doppler pulmonary venous flow patterns recorded with mitral regurgitation. (a) Normal pulsed Doppler pulmonary venous flow pattern, with systolic flow (S) component greater than the diastolic flow (D) component. (b) In mild mitral

regurgitation the systolic flow component is equal to the diastolic flow component. (c) In moderate mitral regurgitation the systolic forward flow component becomes less than the diastolic flow component and flow reversal is detected. (d) In severe mitral regurgitation forward systolic flow ceases and flow reversal is noted during systole with forward flow only occurring during diastole. (e) Echocardiographic visualization of the pulmonary vein illustrating various pulse Doppler sampling points for recording pulmonary venous flow. Pulsed Doppler sampling for pulmonary venous flow should be performed within 1cm of the vein orifice (g) for the most accurate results. (f) Pulsed Doppler with the sample volume at the orifice. (h) Pulsed Doppler with the sample volume deep in the pulmonary vein.

In mitral regurgitation different flow profiles between the left (i) and right (j) pulmonary veins are recorded in a patient with an eccentric mitral regurgitant jet. The flow profile in (i) suggests normal-to-mild mitral regurgitation and the profile in (j) suggests mild-to-moderate mitral regurgitation. This example underlines the importance of measuring both the right and left pulmonary veins and illustrates the limitations of this method when evaluating the severity of mitral regurgitation.

atrial flow turbulence near the orifice of the vein or venous movement as a result of respiration. The angle of incidence of the Doppler sample can usually be made negligible by rotating the transducer of the multiplane probe. Discordant pulmonary venous flow has been described between the right and left pulmonary veins, so both veins should be sampled to ensure accurate results. It should also be noted that pulmonary venous systolic peak velocities and systolic flow integrals can increase in the left pulmonary vein in normal patients lying in the left lateral decubitus position.[176]
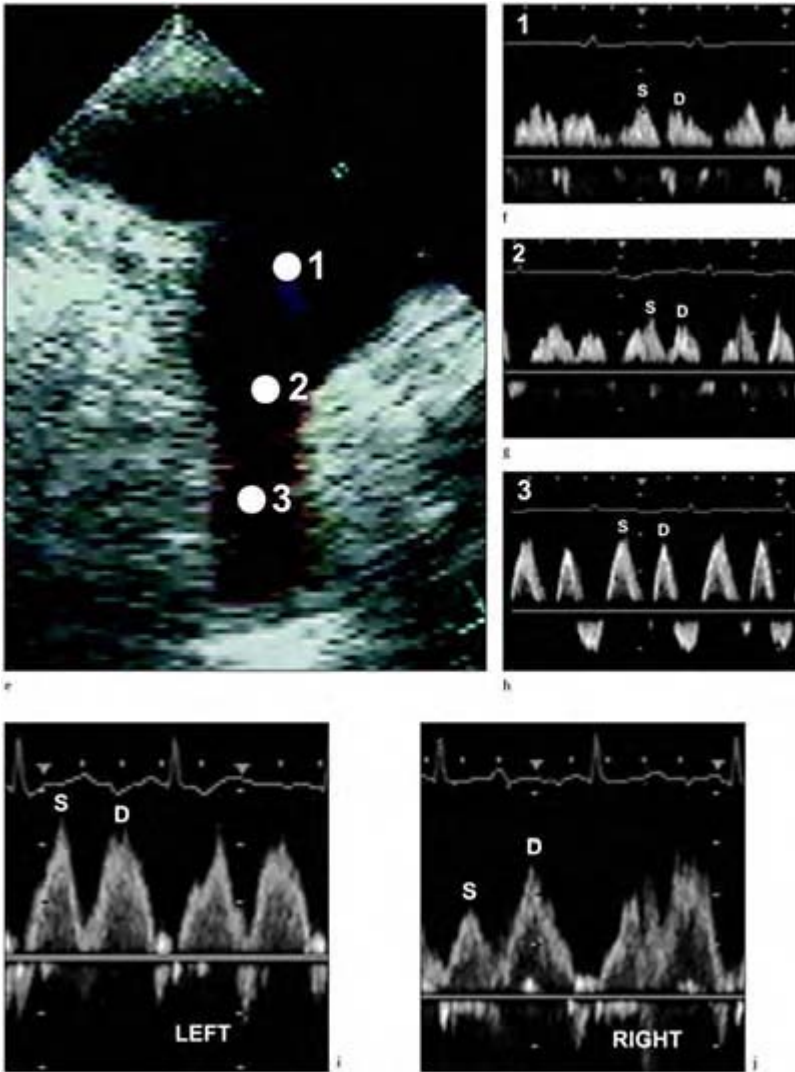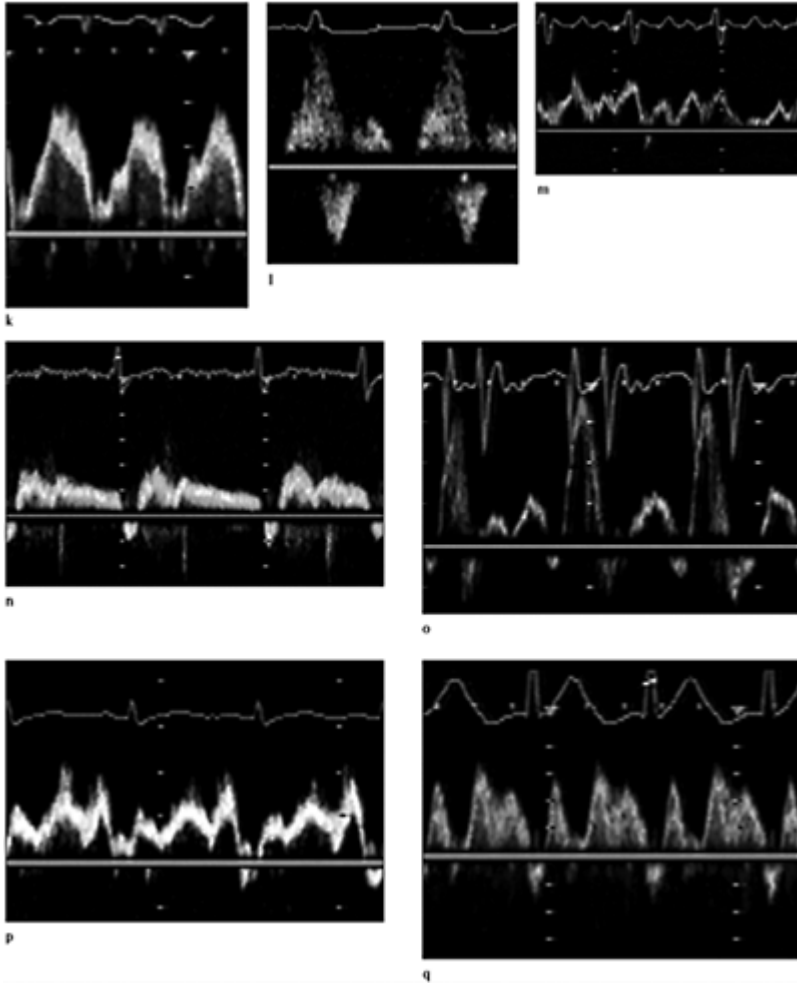
The pulmonary venous flow profile may also be affected by the underlying cardiac rhythm. (k) Supraventricular tachycardia. (l) Ventricular pacing. (m) Atrial flutter. (n) Atrial fibrillation. (o) A–V sequential pacing. (p) 1° heart block. (q) Junctional rhythm.

With varying degrees of mitral regurgitant volumes, pulmonary venous flow patterns have been described as normal, blunted, or reversed in systolic flow, whereas diastolic forward flow generally remains the same.[177–182] Klein and colleagues[180] have found that 98% of patients with severe (4+) mitral regurgitation show systolic flow reversal, with a sensitivity of 93% and a specificity of 100% compared with other transesophageal

echocardiographic color flow mapping methods. Patients who had moderate regurgitation (3+) had blunted systolic flow, with a sensitivity of 61% and a specificity of 97%. Patients with milder mitral regurgitation (2+ or 1+) had normal or equiphasic flow. Similarly, there were significant differences in peak systolic flow velocities and systolic/diastolic flow ratios between each grade of mitral regurgitation. Additionally, the presence of atrial fibrillation did not alter the significance of results in patients with different grades of mitral regurgitation. Discordant venous flow was seen between the right and left pulmonary veins, and was attributable to the direction and orientation of the mitral regurgitant jet, illustrating the importance of sampling both right and left pulmonary veins and using the most significant pattern. In a follow-up study, the same group showed that pulmonary venous flow reflects the severity of mitral regurgitation on the left atrial pressure *a* and *v* waves.

Therefore, with care, the transesophageal echocardiographic findings of the combination of reversed and blunted systolic flow is useful to differentiate clinical significant mitral regurgitation (4+ or 3+) from clinically insignificant regurgitation (2+ or 1+), to further aid in the classification of mitral regurgitation.

Measurement of proximal jet width and vena contracta

Measurement with transesophageal echocardiography of the width of the proximal regurgitant jet just above the valve orifice is also promising.[183] When the width of the regurgitant jet orifice is greater than 5.5 mm, it correlates nicely with severe regurgitation on angiography and a regurgitant stroke volume of more than 60ml. An advantage to the measurement of the jet width orifice is that it should not be as susceptible to most of the physiological factors that plague measurements of the jet area. The vena contracta method does assume that the mitral regurgitant orifice does not change shape during systole, which may not be valid in patients with mitral valve prolapse.[184]

In a somewhat further refinement of this technique, measurement of the vena contracta portion of the regurgitant jet can be made quickly with accurate results, that are independent of hemodynamics and orifice geometry. The diameter of the vena contracta or narrowest extent of the regurgitant jet as it passes through the valve orifice may be measured in one or two orthogonal echocardiographic planes.[186–188] Studies have shown that the vena contracta width measured by transthoracic and transesophageal echocardiography correlates well with the angiographic grading of mitral regurgitation.[185]

In a subsequent study,[188] vena contracta measurements by transthoracic echocardiography accurately predicted regurgitant volume ($r = 0.85$, SEE = 20 ml) and regurgitant orifice area ($r = 0.86$, SEE = 0.15 cm^2). In addition, the vena contracts width was the only independent predictor of the severity of mitral regurgitation by multivariate analysis when considering pulmonary venous flow reversal, maximal jet area, and left atrial size. A vena contracta width of 0.5 cm or more in the parasternal long-axis view was always associated with severe mitral regurgitation, a regurgitant volume of 60 ml, and a regurgitant orifice area of 0.4 cm^2. A vena contracta width of 0.3 cm or less was associated usually with mild mitral regurgitation, and predicted a regurgitant volume of less than 60ml and regurgitant orifice area of less than 0.4 cm^2.

Regurgitant volumes obtained by multiplane transesophageal echocardiography measurement of vena contracta width correlate nicely with regurgitant volumes obtained angiographically using the thermodilution technique.

Potential limitations of vena contracta width measurements are related to assumptions of the mitral orifice and validation in different clinical states. The mitral orifice is assumed to be circular or elliptical with this method, when it is usually irregular in shape. Another error may occur in assuming that the mitral regurgitant orifice is fixed and not dynamic. A technical consideration is that it is generally difficult to distinguish the narrowest flow zone corresponding to the vena contracta. Resolution of the vena contracta is highly dependent on the spatial resolution of the view and the echocardiographic equipment. At present, this method has not been validated for patients with coexistent aortic insufficiency or atrial fibrillation, but the vena contracta method should not be affected by the presence of aortic insufficiency.

Measurement of flow convergence (PISA)

Color flow Doppler mapping makes it possible to evaluate the acceleration of blood flow as it converges toward a regurgitant orifice. A zone of flow acceleration can be visualized proximal to the regurgitant orifice in almost all patients under transesophageal echocardiography, and it correlates well with the severity of mitral regurgitation.[189–192]

As blood flow accelerates toward the regurgitant orifice, concentric rings of isovelocity regions are produced in a radial fashion, decreasing in size as they approach the mitral orifice. Successive layers of isovelocity hemispheres are shown with color Doppler, and may be enlarged and enhanced with the zoom mode of the echocardiographic instrument. On velocity maps, aliasing layers of flow appear as alternating shades of red and blue, much like a rainbow. The velocity increases as flow converges on the mitral orifice, with the smallest hemisphere nearest the orifice having the highest velocity.

The zone of flow convergence proximal to a mitral regurgitant orifice is described mathematically as hemispherical. If all the blood flow within the convergence region passes through the regurgitant orifice, and the product of flow area times spatial velocity is constant at any position within the flow stream (law of continuity), then these data can be used to calculate the regurgitant flow rate. The flow rate Q (ml/sec) is equal to the velocity of blood flow multiplied by the cross-sectional area of the first isovelocity ring: $Q = 2\pi r^2 v$, where r is the radial distance of the first alias from the regurgitant orifice, $2\pi r^2$ is the area of the hemisphere at radial distance r, and v is the aliasing velocity in cm/sec at radial distance r.

The effective regurgitant orifice area can be calculated by dividing the flow rate Q by the maximal velocity of the mitral regurgitant jet through the orifice, as recorded with continuous wave Doppler. Next, the regurgitant volume may be calculated by multiplying the effective regurgitant orifice area by the time velocity integral of the mitral regurgitant jet.

Many studies have been done in both models and clinical patients, to validate the utility of the flow convergence method for mitral regurgitation. These studies have addressed the potential limitations of flow convergence relating to the mathematical calculations, and the geometric assumptions made about the flow orifice and interaction

of flow about the orifice.[194–201] When the proximity to the orifice causes the isovelocity surfaces to flatten out, the flow regions cannot be assumed to be hemispherical, and therefore it is necessary to lower color aliasing velocities, which increases the radius to allow for better measurement.[194]

Occasionally, mitral lesions produce an eccentrically placed regurgitant orifice in relation to the valve plane, which may distort the shape of the proximal flow convergence contour.[197,198] Clinically, with a flail or severely prolapsing posterior leaflet the flow convergence angle may be constrained by the posterior wall of the left ventricle. If the velocity contour in error is considered hemispherical, the mitral flow rates are grossly overestimated by the flow convergence method. In this instance, the proximal flow contour can not be considered hemispherical and the flow equation must be corrected by the true convergence angle. There are two ways to correct for this: (1) involves measuring the true angle (αon the image sector with a protractor and correcting the calculated regurgitant flow volume or regurgitant orifice area by multiplying by $\alpha/180$; or (2) substituting $2\pi r$ in the flow convergence by the true area of $\pi = \tau + 2 \tan^{-1} d/r$, where d is the measured distance from the constraining wall to the radian of the regurgitant orifice. Good results have been obtained with both methods, eliminating the gross overestimation of regurgitant flow volumes.

The severity of mitral regurgitation can be described through the use of the regurgitant orifice area, since fundamentally its size is the major determinant of regurgitant volume and thus regurgitant fraction. As validated by angiographic and echocardiographic methods,[199] a calculated regurgitant orifice area of more than 0.5 cm^2 correlates with severe (4+) mitral regurgitation, greater than 0.3 cm^2 but less than 0.5 cm^2 correlates with moderate (3+) regurgitation, and less than 0.1 cm^2 corresponds to mild or trace regurgitation.

In an effort to shorten the time required for the flow convergence method, the Cleveland Clinic has simplified the formula by making various assumptions.[202] The regurgitant orifice area may be simplified and calculated as ROA = $r^2/2$, where r is the distance of the aliasing contour when the aliasing velocity is set to 40 cm/s, and it is assumed that the pressure difference between the left ventricle and the left atrium in systole is 100 mmHg (as produced by a 5 m/s regurgitant jet).

Prediction of ventricular function after surgical correction

Left ventricular dysfunction is the most common cause of morbidity and mortality after the successful surgical correction of mitral regurgitation. Although the operative mortality for mitral repair or replacement has fallen in the 1990s, patients that present with left ventricular dysfunction still have a poor long-term prognosis. For this reason many asymptomatic patients are being considered as surgical candidates for the treatment of mitral regurgitation, to prevent the development of significant left ventricular dysfunction.[203–212]

The operative mortality for the surgical correction of mitral regurgitation is related to age and functional class.[206] The operative mortality for surgical correction of mitral regurgitation is 1.3% in patients less than 75 years old and 5.7% in patients over 75 years old. The operative mortality for mitral regurgitation is 9% for patients in functional

classes III and IV, versus 1.5% for functional classes I and II. Mitral valvular repair has had a significant effect on the operative mortality of mitral regurgitation, with or without other cardiac surgery. In most institutions currently undertaking mitral valve repair for the treatment of organic mitral regurgitation, the operative mortality is approaching 0%.

Late survival after the surgical correction of mitral regurgitation is related to preoperative left ventricular function, and echocardiographic measurement of ejection fraction (EF) is an excellent predictor of late survival.[207] Late survival at 10 years is 32% with an echocardiographic EF of less than 50%. Survival is about 53% with an EF between 50 and 60%, and a 72% survival can be expected with an EF of 60% or more. End-systolic ventricular enlargement is also an excellent echocardiographic predictor of poor left ventricular contractile reserve for the development of postoperative ventricular dysfunction. The demonstration of an end-systolic ventricular dimension after exercise of more than 40–45 mm with stress exercise echocardiography reliably predicts poor left ventricular function after valve repair.

Papillary muscle dysfunction

The papillary muscles contribute to the functional integrity of the mitral valve unit. Dysfunction of the papillary muscles may result in regurgitation, obstruction, or both. Transesophageal echocardiography has led to significant advances in the visualization and diagnosis of papillary muscle abnormalities. Papillary muscle dysfunction may be the result of morphological, positional, or functional changes due to acquired or congenital heart disease. In some patients there is severe calcification of the whole papillary muscle extending into the ventricular myocardium and/or the chordae tendineae, by contrast with the normal age-related changes of calcification of the head of the papillary muscle in elderly patients. Papillary muscle dysfunction can be catastrophic, such as in muscle rupture associated with acute myocardial infarction, or can be of lesser or unknown significance in many other clinical circumstances.

Papillary muscle enlargement occurs together with ventricular hypertrophy states.[212] In cases of hypertrophic cardiomyopathy, the papillary muscles may be hypertrophic to the extent that they cause mid-ventricular obstruction, especially when the ventricular cavity is small as occurs in low volume states. The location of the papillary muscles may also be an issue in hypertrophic cardiomyopathy, particularly when there is non-concentric left ventricular hypertrophy, and may produce systolic anterior motion (SAM) of the subvalvular apparatus.[213] SAM plus mitral insufficiency without the presence of septal hypertrophy has been shown using echocardiography to displace papillary muscles in dogs. Studies have also shown reduced papillary muscle fractional shortening due to the increased width of the papillary muscle, despite normal papillary muscle length.

Mitral annular calcification

Mitral annular calcification is frequently observed in patients with or without significant mitral valvular disease. Degenerative disease occurs frequently in the mitral annulus and the fibromuscular skeleton of the heart, in association with other disease entities or as a

consequence of ageing. Annular calcification is common in the elderly without disease of the chordae or leaflets, especially in women over 70 years old.[214] Calcification of the mitral annulus is one of the most common abnormalities found at necropsy, occurring in 10% of necropsies in patients over 50 years old.[214–216] Mitral annular calcification is frequently associated with disorders that produce mitral regurgitation, such as myxomatous degeneration.[217] Mitral annular calcification is also common in several metabolic disorders involved with calcium deposition,[218] such as Hurler's syndrome,[219] Paget's disease, and bone dystrophy of chronic renal failure.[220]

Calcium deposition is commonly encountered in the loose connective tissue of the posterior aspect of the mitral annulus, especially near the central scallop of the posterior leaflet. In addition, degenerative calcium deposits may be found in the junction formed by the ventricular surface of the posterior leaflet and the posterior left ventricular wall (posterior submitral angle). When severe calcium deposition totally surrounds the annulus and extends into the posterior leaflet tissue and proximal ventricular myocardium, obstruction of the left ventricular inflow tract may occur.[221] Mitral annular calcification is usually limited to the posterior annulus, and extends medially and laterally towards the fibrous trigones. The anterior aspect of the annulus is usually unaffected, unless there is associated aortic sclerosis or calcific aortic stenosis that extends into the aorto-mitral fibrosa. When there is calcification of the medial margin of the annulus, the conduction system may be involved, resulting in conduction disturbances. When the width of the calcific annular band exceeds 5 mm, there is a significant increase in the incidence of conduction defects, atrial fibrillation, and heart failure.[222–224]

In patients with mitral annular calcification, transthoracic echocardiography has a sensitivity of 76% and a specificity of 94% compared with fluoroscopy.[225] Echocardiography is less sensitive if thickening of the annulus is due to sclerosis or fibrosis and not calcification. Although not reported, transesophageal echocardiography with its improved image resolution from the esophagus is beneficial in cases that are not clear using transthoracic imaging. Transesophageal echocardiography is extremely helpful in moderate to severe cases of mitral annular calcification, since with transthoracic echocardiography the mitral valve leaflets and subvalvular apparatus may be overshadowed by the dense calcium deposits similar to the acoustic shadowing produced by a prosthetic valve. Extensive mitral annular calcification occasionally produces an irregular or raised margin in the annulus, to form a crevice or potential space between the annulus and atrial wall. These types of deformities with the annulus are associated with bacterial endocarditis and thrombus formation, which are more easily shown with transesophageal echocardiography. Extensive mitral annular calcification is associated with a greater incidence of cerebral and retinal embolism than age-matched wounds.[223]

The deep transgastric views allow good visualization of the mitral valve unit without acoustic shadowing. The short axis and longitudinal transgastric views allow good visualization of the entire annulus to determine the full extent of annular involvement. The four-chamber and two-chamber lower esophageal views (0°–180°) allow full evaluation of the mitral valve and surrounding left ventricular myocardium to identify calcific extension to the leaflets and myocardial wall.

Echocardiographically, mitral annular calcification appears as highly reflective areas of increased echogenicity. Calcification may occur as single or multiple small discrete

areas (1.5 mm or more), or as larger semicircular linear bands in the area of the annulus adjacent to the posterior mitral leaflet at the atrioventricular junction. Mitral annular calcification may extend into the posterior leaflet and render the leaflet immobile. When annular calcification extends and involves the body and tip of the anterior leaflet and chordae tendineae, left ventricular inflow obstruction may be produced, as shown with Doppler echocardiography.[221]

The echocardiographic identification of mitral annular calcification is extremely important in patients who present for mitral valve repair, as well as for mitral valve replacement, since annular calcification is not always readily appreciated by the cardiac surgeon. Paraprosthetic leaks are technically unavoidable during valve replacement in patient with significant annular calcification. Small or large areas of calcification interfere with the ability to adequately suture or secure rigid prosthetic sewing rings to the fibrous skeleton. In patients with significant annular calcification, mitral repair appears to be a better option than mitral replacement. Newer techniques in mitral repair allow for the near total debridement of the mitral annulus with good results.[226] Removing annular calcium allows for easier suture placement with better tissue approximation, easier placement of the annuloplasty ring, less annular distortion (better geometry avoids regurgitation or obstruction), better leaflet mobility, and the theoretical advantage of allowing annular remodeling and restoration of annular motion.

Mitral valve endocarditis

Infective endocarditis is caused by a microbial infection of the endocardial lining of the heart, which is difficult to diagnose and treat. Infectious endocarditis generally results in permanent damage, even with successful antibiotic treatment. The characteristic lesion of infective endocarditis is a vegetation. Transesophageal echocardiography is arguably the procedure of choice and is the gold standard for detection of mitral valve vegetations.[227–232] Transthoracic echocardiography reliably detects vegetations about 3 mm in size.[233] In a study comparing transesophageal echocardiography with transthoracic echocardiography for detecting vegetations between 2 and 5 mm, the sensitivity of monoplane transesophageal echocardiography was 90% and 58% for transthoracic echocardiography.[234] The diagnosis of infective endocarditis is still primarily a clinical diagnosis, since pathological studies show that up to 50% of patient who die of acute endocarditis do not have vegetations.[235] However, Shively and colleagues[236] suggested that the absence of the characteristic abnormalities by transesophageal echocardiography indicate a low probability of disease in a patient with intermediate pre-test likelihood of endocarditis.

Mitral valve vegetations impair the functional integrity of the mitral valve apparatus through destruction of the annulus, leaflets, or chordae. With transthoracic echocardiography, vegetation size and appearance are highly variable. They may be nodular or resemble irregular echogenic masses attached to one or both of the valve leaflets, or, occasionally, to the chordae tendineae. With multiplane transesophageal echocardiography, vegetation morphology may be better defined and vegetations can be categorized as nodular, globular, shaggy, frond-like, polypoid, or tubular.[237–240] When vegetations appear tubular they may be confused with senescent valvular thickening,

papillomas, or papillary fibroelastomas of the mitral valve, that frequently appear as thin, multiple hairlike projections on the leaflet margins or chordal structures. Vegetations may be sessile or pedunculated, and may be as large as 40mm in diameter. Placing the M-mode cursor on the vegetation in the zoom mode, sessile vegetations may show fine vibratory movements. Vegetations move in concert with the leaflet when firmly adherent to it, or almost independent of valve motion or chaotic when pedunculated. Pedunculated vegetations usually appear larger with multiplane transesophageal echocardiography, and are frequently noted to prolapse between the left ventricular outflow tract and left atrial cavity during the cardiac cycle.[241,242] Even with transesophageal echocardiography, it may not be easy to distinguish vegetation from small ruptured chords and prolapsing leaflet with myxomatous degeneration. With transesophageal echocardiography, vegetations may be distinguishable from senescent valvular thickening, discrete calcifications, or annular calcification as relatively fixed, symmetrical, or variably hyper-refractile masses. Vegetations usually occur on previously deformed valves, but depending on the offending bacterial organism, vegetations may be produced on normal valves or may spread to produce satellite vegetations. The size or morphology of vegetations bears no correlation with the location or specific causative organism.[234,240,243] Newer or acute vegetations may appear less dense or hypo-refractile in echogenicity compared with chronic lesions that appear more echodense and less mobile, but this finding is clearly subjective.[244–246]

Vegetations usually occur on the atrial surface of the leaflet tips, where they prevent the normal coaptation and approximation of the leaflets during systole, and cause mitral regurgitation. In abnormal mitral valves, vegetations may occur at friction sites or jet lesions, such as the body of the leaflets and atrial wall, the basal surface of the ventricular septum, or on chordae showing systolic anterior motion.[242] Complications of vegetations or infective endocarditis of the mitral valve may produce perforation in the body of the leaflet, or result in ruptured chordae and flail or prolapsing leaflets, or disruption of the mitral annulus from a perivalvular abscess.[247] Perivalvular abscesses appear as distinct echodense (signifying purulent debris) or echolucent (sterile cavity) areas near the annular ring or annular attachment of the leaflet, and are found in about 20–30% of patients in surgical or necropsy studies.[248,249] Careful scanning with multiplane transesophageal echocardiography is ideal to identify perivalvular abscess and to distinguish abscess from lipomatous tissue, which may be frequently observed in the region of the annulus and the primum area of the atrial septal wall and is not generally echolucent. With color Doppler, flow jets may appear moving in and out of the echolucent area with systolic expansion or diastolic collapse. Sub-aortic extension of aortic valve endocarditis may affect the anterior mitral leaflet, leading to an aneurysm or perforation of the leaflet.[250–255] Echocardiographically, an aneurysm of the leaflet appears as a bulge in the leaflet during systole and diastole, and is an ominous sign since there appears to be a high rate of rupture.

There is a 25% embolization rate with mitral valve endocarditis. Rohmann and colleagues[243] found that mitral valve vegetations were an independent predictor of embolic complications with multivariate analysis, especially in vegetations larger than 10 mm. Mobility of the vegetation has also been associated with an increased risk of embolization and death in endocarditis. When transesophageal echocardiography is done for the diagnosis of endocarditis and before a recognized embolic event especially with

native mitral valve vegetation, 85% of large vegetations are mobile, in contrast with only 48% of small vegetations smaller than 10 mm.[234] Embolic episodes are more common with mobile vegetations (38%) than sessile vegetations (19%).[234] The visualization of spontaneous echocontrast or smoke on transesophageal echocardiography is also a risk factor for embolization, prolonged vegetation healing, and surgical intervention, under multivariate analysis.[256–259]

Serial examination during treatment of infective endocarditis with transesophageal echocardiography shows that vegetations may regress or grow larger.[256–259] In a study of vegetation size during treatment, only 39% of vegetations decreased in size, with 47% not significantly changing and 14% of vegetations increasing in size. A significant increase in vegetation size after 2 weeks of effective antibiotic therapy is a medical therapeutic failure for infectious endocarditis.

Non-bacterial endocarditis

Transesophageal echocardiography has sparked a considerable interest in the recognition of non-bacterial endocarditis.[260–265] Non-bacterial vegetations are more common in left sided cardiac valves, especially the mitral valve. Non-bacterial thrombotic endocarditis has been associated with malignancy (marantic endocarditis), uremia, and connective tissue disorders. Non-bacterial vegetations usually appear as small, sessile, and verucous lesions on the valve leaflets. Prominent valvular vegetations may be shown in patients with lupus erythematosus who have high anticardiolipin (anti-phospholipid) antibody titers.[263] In the antiphospholipid syndrome, vegetations can be either primary, occurring in the absence of an underlying disorder, or secondary, in association with lupus erythematosus. Libman–Sacks endocarditis has been identified in about one-third of patients with primary involvement, and in increased frequency in patients with systemic lupus erythematosus and high anti-phospholipid antibody titers compared with patients with low titers. Although Libman–Sacks vegetations have been found in 35–65% of lupus patients in early necropsy studies, they are usually clinically silent or show only minor hemodynamic abnormalities.[260] Libman–Sacks lesions are described in pathological studies as sterile fibrofibrinous vegetations 3–4 mm in size that may develop anywhere on the endocardial surface, with a propensity for the ventricular surface of the mitral valve. Healed Libman-Sacks lesions show a fibrous plaque pathologically, sometimes with focal calcification. In extensive lesions or with corticosteroid therapy, healing may produce valve dysfunction as a result of valve deformities secondary to marked scarring or thickening. Libman–Sacks lesions may serve as a nidus for bacterial endocarditis or valve thrombi. Vegetations are frequently diagnosed by transesophageal echocardiography in patients with systemic lupus erythematosus. In an analysis of lupus patients with transesophageal echocardiography, valvular lesions were found in 61%, predominantly as valvular thickening in 51%, or as leaflet masses or vegetation in 43%. The lesions produced hemodynamics for regurgitation in 25%, and stenosis in 4% of patients.[264]

Echocardiographically, vegetations appear as thickening or masses of varying size and shape, with irregular borders and echodensity, firmly attached to the valve surface of the leaflet body or margins. Vegetations show relatively little motion. Roldan and

colleagues[264] reported that on serial transesophageal echocardiographic examinations done almost 2.5 years apart, valvular abnormalities frequently resolved, appeared for the first time, or persisted but changed in appearance or size between the two studies. Mild or moderate valvular regurgitation did not progress to become severe, and new stenoses did not develop. Neither the presence of valvular disease nor changes in the echocardiographic findings were temporally related to the duration, activity, or severity of lupus, or to its treatment. The presence of valvular lesions is related to increased morbidity and mortality.

Echocardiographic analysis in the Antiphospholipid Antibodies in Stroke Study Group disclosed mitral valve abnormalities in 22.2% of patients with cerebral ischemic events and high antiphospholipid antibody titers.[265] Antithrombotic therapy is indicated for secondary prevention in patients with antithrombotic associated valvular disease who have already had a thromboembolic event.

Indications for transesophageal echocardiography in endocarditis

The indications of transesophageal echocardiography in suspected mitral valve endocarditis are a negative transthoracic echocardiogram in the setting of persistent bacteremia, without another obvious detected source of infection constituting a high probability of infectious endocarditis. If transthoracic echocardiography is diagnostic for vegetation and regurgitation is adequately defined, a transesophageal echocardiogram is usually not necessary and does not supply additional information, especially if there are no complications and the patient is clinically stable and responding to therapy. If these conditions are not met, however, transesophageal echocardiography is especially helpful in the diagrams of mitral valve endocarditis (table 2.7). Serial examinations either by transesophageal echocardiography or transthoracic echocardiography should be done to follow the vegetation size, and to assess intracardiac hemodynamics including left ventricular function. Transthoracic echocardiography usually enables assessment of regurgitation and cardiac hemodynamics even if the specific vegetation is not seen. Subsequent examinations may be done on a weekly basis by transthoracic echocardiography and every 2 weeks by transesophageal echocardiography if that was the diagnostic study. With the clinical presentation of new physical signs, complications, or hemodynamic instability, transesophageal echocardiography should be performed in all patients with mitral valve endocarditis.

Table 2.7 Indications for transesophageal echocardiography (TEE) in endocarditis

Initial baseline study (diagnostic)
Strong clinical suspicion with negative or poor images on transthoracic echo
Clinical picture different from transthoracic echo findings
Suspected prosthetic valve endocarditis
During course of therapy (2 to 4 weeks)*

Evaluate vegetation size and appearance on therapy

Evaluate abscess or valve destruction noted on baseline study

Rule out new complications

Acute complications

Change in clinical picture

Worsening hemodynamics

Persistently positive blood cultures

*TEE is often not necessary even if it was the baseline study, if the transthoracic image quality was adequate and TTE findings are interpretable in view of the initial TEE findings.

Congenital mitral disease

Developmental abnormalities of one or more components of the mitral valve constitute congenital mitral valve disease as an isolated finding or in combination with other

Table 2.8 Congenital lesions ofthe mitral valvular unit

Valvular apparatus	Abnormality
Annulus	Dilatation – deformity
Commissure	Fusion
	Double orifice
Leaflets	Cleft
	Agenesis
Chordae	Absent
	Fusion
	Elongation
Papillary muscle	Malposition
	Elongation
	Arcade
	Parachute valve
From Carpentier A. Cardiac valve surgery—the "French correction". *J Thorac Cardiovasc Surg*1983;86:323–37.	

congenital malformations of the heart. Congenital mitral valvular disease may result in stenosis, incompetence, or both. Occasionally, congenital mitral valvular disease, with minor hemodynamic abnormalities, can go undetected or be confused with other forms of acquired disease and not be discovered until the patient is a young adult. In our experience, it is not unusual that in the occasional young patient presenting for assessment of mitral stenosis before valvuloplasty or for the feasibility of surgical repair of mitral valve prolapse, congenital abnormalities are discovered using transesophageal echocardiography. To better understand congenital mitral disease in the young adult, it is

helpful to be familiar with the specific congenital abnormalities that may occur for each component of the mitral unit (table 2.8), rather than trying to label a specific syndrome based on image recognition.[266–268] By the time the congenital patient reaches adulthood the lesion has degenerated (wear and tear), and does not always appear as initially described, which generates confusion and perhaps a wrong diagnosis with transthoracic echocardiography. Also, evaluating congenital mitral disease by its component parts may offer the patient an opportunity for repair rather than valve replacement, which is usually the first choice.[269–273]

Papillary muscle abnormalities

Congenital abnormalities of the papillary muscles include the malposition of the muscles in the ventricular cavity, elongation of the muscles, accessory muscles, a single muscle with or without an accessory muscle, or muscles associated with extensive fibrotic tissue.

Probably the most recognized congenital papillary muscle abnormality occurs in the parachute mitral valve.[274,275] In the parachute valve, there is only one single, long papillary muscle—usually the posteromedial muscle that originates closer to the ventricular apex. If an anterolateral muscle is present, it is an accessory muscle, and is small and chordae are usually aberrantly connected to the ventricle: the chordae are shortened and thickened. The leaflets are normal at birth, and by adulthood may become thickened as a result of degenerative changes or the development of excessive leaflet tissue. All chordae emanate from the leaflets and converge into the single papillary muscle, which narrows the inflow tract, restricts normal leaflet motion, and produces an eccentric orifice opening. In this manner, stenosis or obstruction to flow is produced in the subvalvular region as flow is directed into a posteriorly oriented inflow tract towards the closely grouped and crowded chordae tendineae. Secondarily, regurgitation may also occur due to the restricted leaflet motion interfering with the approximation of the leaflets during systole.[276] These findings, especially the visualization of one centrally placed papillary muscle in the transgastric short axis view of the left ventricle, are easily seen with transesophageal echocardiography.

Mitral arcade may also be occasionally seen in the young adult.[277] Transesophageal echocardiography in mitral arcade shows a bridge of fibrous tissue in between the papillary muscles that directly attaches to the anterior leaflet. The commissures are rudimentary and therefore distinct separation is not seen. The anterior leaflet may be rudimentary with a normal posterior leaflet. The chordae are short and thickened, giving the appearance that the papillary muscles extend directly to the leaflets. The papillary muscles are large and elongated, and may be displaced anteriorly. These lesions predominantly produce regurgitation, and secondarily produce obstruction of flow.

The posterior placement of two hypertrophied papillary muscles may also cause subvalvular stenosis.[278] On transgastric short axis views, the papillary muscles are obviously thickened and abnormally placed in the left ventricular cavity with a small posterior interpapillary muscle dimension. Rotation of the transducer to 90° shows the chordae to be thickened, and anomalous thick muscular bands are common. Hypoplastic papillary muscles may occur, often in groups of three or more with thickened chordae, and may cause subvalvular obstruction.[279, 280]

Chordal anomalies

Congenital chordal anomalies may cause mitral insufficiency or stenosis.[270,278] Chordae may be fused or totally absent in congenital mitral stenosis. Chordae may be abnormally placed to the whole body of anterior leaflet instead of just to the free edge, in a pattern similar to that of the posterior leaflet. Chordae may be elongated and may result in significant leaflet prolapse.

Leaflet anomalies

Leaflet clefts may occur mainly in the anterior leaflet and rarely in the posterior leaflet as previously described, with or without an AV canal defect.[117–120,281,282] In the isolated cleft of the anterior leaflet, an additional smaller leaflet may be formed by an accessory commissure with or without accessory chordal attachment, which produces mitral insufficiency. Careful scanning is required so that this is not confused with myxomatous degeneration and a ruptured posterior leaflet or a perforated leaflet.

The orifice formed by the mitral leaflets may be narrowed by agenesis of the leaflets, absence of the commissures, or congenital thickening or fibrosus of the leaflets, which appears similar echocardiographically to rheumatic stenosis without the presence of calcification.[283]

Congenital mitral insufficiency may be caused by hypoplastic leaflets that appear as small, fibrous, stubby leaflets. One or both commissures may be absent, producing multiple orifices.[278,283,285]

Annular anomalies

The mitral annulus may be dilated congenitally due to the deficiency of commissural tissue, usually in association with other anomalies of the valve unit.[278] The mitral annulus may be small, as an isolated finding with obstruction or without obvious obstruction in association with coarctation of the aorta.[274,283] Supravalvular rings may be present, consisting of thick fibrous rings on the left atrial side of the annulus, with the normal connections to the left atrium.[284] Non-obstructive rings may present as an incidental finding during transesophageal echocardiography, in association with other anomalies of the mitral unit.[285]

Techniques of mitral repair

It is helpful for the echocardiographer to have a cursory understanding of the techniques of mitral repair, to collect all of the information that will be needed by the cardiac surgeon. Carpentier and Duran have developed most of the techniques used in mitral valve repair, with some modifications by other institutions.[8,10,287–309] For this short review, the techniques of Carpentier will be highlighted.

Mitral reconstructive surgery requires optimum exposure and visualization of the mitral leaflets and subvalvular apparatus. A median sternotomy is done and the left atrium is opened longitudinally from the patient's right side, posterior to the interatrial groove beneath both vena cavae, anterior to the right superior and inferior pulmonary

veins (figure 2.29). The heart is held open with special self-retaining retractors. The surgeon visualizes the mitral valve through the left atrium with a perspective similar to the transgastric short axis view at the base of the heart, with the echo image rotated 90° clockwise. Inspection of the mitral valve (table 2.9) suggests obvious enlargement or deformity of the annulus, prolapse or overriding of the leaflets, jet lesions, or foci of infection. An asymmetric line of closure suggests leaflet prolapse or restriction. Thickening of the leaflets and restriction is apparent by their lack of pliability. Mobility of the leaflets is checked with the use of nerve hooks wrapped around the chords at their marginal insertion, to retract gently the leaflet edges in an open and closed maneuver assessing normal, prolapse, or restricted motion. Prolapse and elongation of the chordae can be assessed by retracting corresponding segments for both leaflets with nerve hooks, observing the difference between the two leaflets (figure 2.30). The P1 segment of the posterior leaflet or the posterior leaflet segment closest to the anterior commissure usually serves as a normal reference point for comparison of other leaflet areas, since this segment is least prone to prolapse. Direct surgical observation in this manner is usually better than echocardiography in identifying the specific segment of leaflet pathology.

Table 2.9 Anatomic lesions for valve repair

Lesion	Number	%
Annulus dilatation/deformation	171	87.6
Posterior leaflet prolapse	111	56.9
Anterior leaflet prolapse	78	40.0
Chordal elongation	128	65.6
Chordal rupture of anterior leaflet	29	14.8
Chordal rupture of posterior leaflet	98	50.2
Commissural fusion	11	5.2
Chordal fusion	16	8.2
Papillary muscle rupture	2	1.1
From Deloche A, et al. Valve repair with Carpentier techniques: the second decade. *J Thorac Cardiovasc Surg* 1990;99:990–1002.		
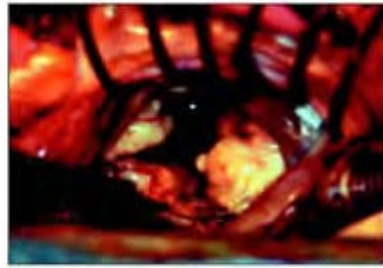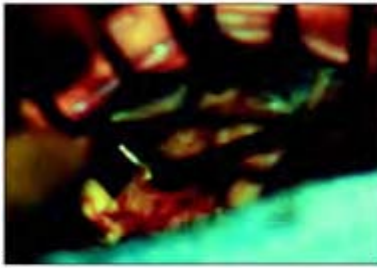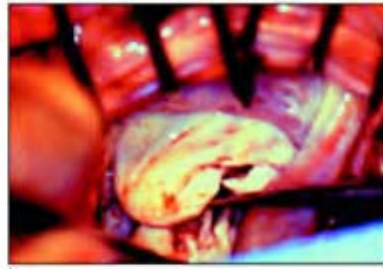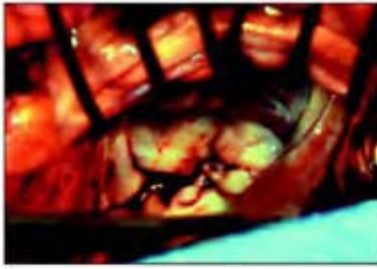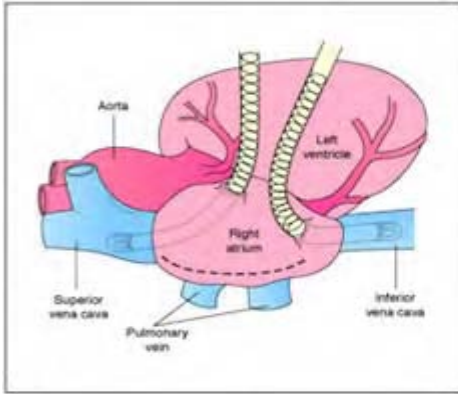
Figure 2.29 Diagram depicting the surgical exposure of the heart during mitral valvular repair from the surgeon's perspective. Surgical exposure of the left atrium (LA) and mitral valve is provided by a surgical incision extending from the superior (SVC) and inferior vena cava (IVC), adjacent to the interatrial groove situated in the posterior aspect of the

right atrium (RA), anterior to the insertion of the right pulmonary veins (PV). LV, left ventricle; Ao, aorta. (a–g) Photographs during various stages of a mitral valve repair. (a) Initial exposure of the mitral valve. (b) Evaluation of the anterior mitral leaflet. (c) Evaluation of the posterior mitral leaflet with prolapse of the central scallop due to a ruptured chordae. (d) Excision of the central scallop of the posterior leaflet.
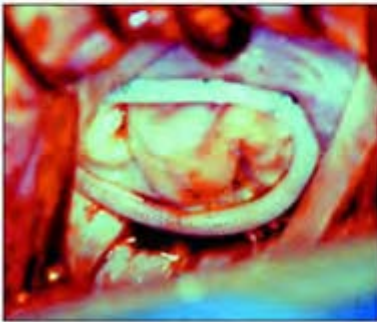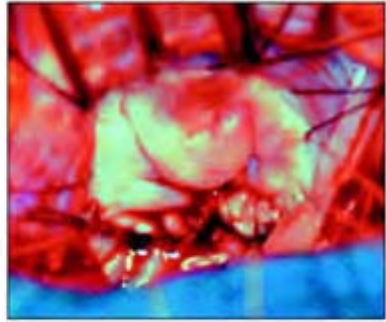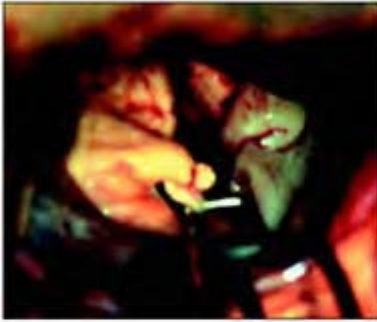
(e) Re-approximation of the posterior leaflet with a sliding repair. (f) View of the repaired posterior leaflet before ring placement. (g) Finished mitral repair with annuloplasty ring sewn in place.

The distribution of lesions in patients with degenerative disease has been described by the Cleveland Clinic for 458 surgical patients.[109] Ruptured chordae tendineae to the mitral leaflets is certainly the most common finding in surgical patients with degenerative prolapse. Posterior chordae ruptures occurred in 41% of patients, with anterior chordae rupture in 10%, and anterior and posterior chordal rupture in 4%.

The type of pathology that is observed dictates the mitral reparative technique used. To achieve successful surgery, all abnormalities of the mitral apparatus must be repaired. Frequently, the mitral pathology will require more than one technique to obtain a satisfactory and complete repair (table 2.10).

Table 2.10 Mitral reparative technique*

Procedure	Number	%
Carpentier ring annuloplasty	185	95.5
Resection of posterior leaflet	121	62.0
Resection of anterior leaflet	37	18.9
Chordal shortening	89	45.6
Leaflet mobilization	10	5.1
Associated commissurotomy	11	5.2
Papillary muscle reimplantation	2	1.1
Tricuspid annuloplasty	32	16.4
*Average number of techniques per patient = 2.35. From Deloche A, et al. Valve repair with Carpentier techniques: the second decade. *J Thorac Cardiovasc Surg* 1990;99:990–1002.		
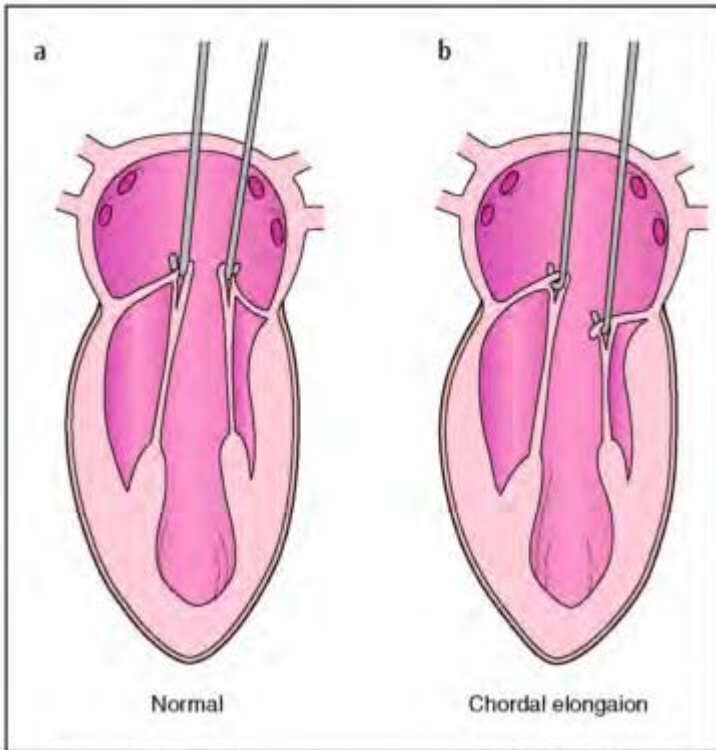
Figure 2.30 Diagram illustrating the surgical technique for testing chordal length. Chordae hooks are utilized to apply traction on different leaflet segments in order to demonstrate differences in chordal length contributing to leaflet prolapse. Although commonly performed in mitral valve evaluation during surgical repair, the limitations of this technique are obvious, especially when the heart is collapsed on cardiopulmonary bypass.
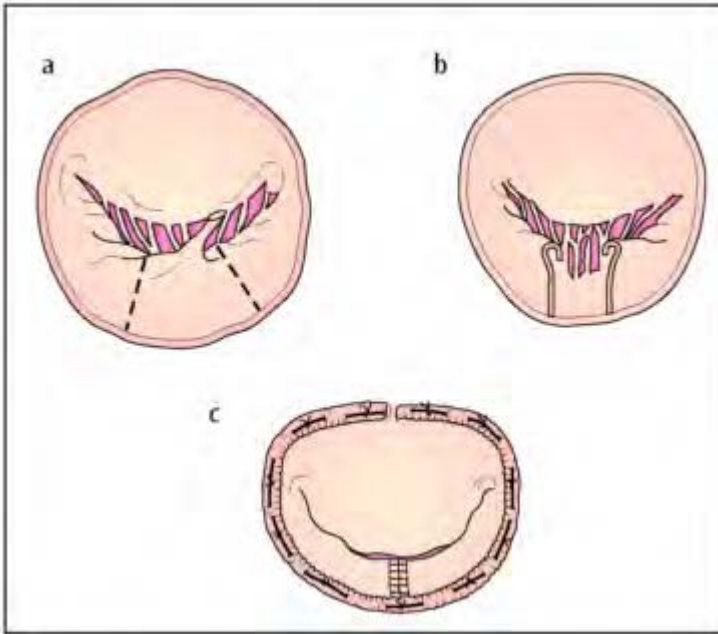
Figure 2.31 Posterior leaflet quadrangular resection. Surgical repair of a ruptured chord to the posterior leaflet (a) involves resecting the excessive leaflet tissue along with the ruptured and elongated chords. In cases requiring less than a quarter resection of the total leaflet and when there is not excessive height to the remaining posterior leaflet, a simple quadrangular resection can be performed (b). Following resection of the leaflet tissue (c) the remaining leaflet tissue is sewn together and an annuloplasty ring is placed.
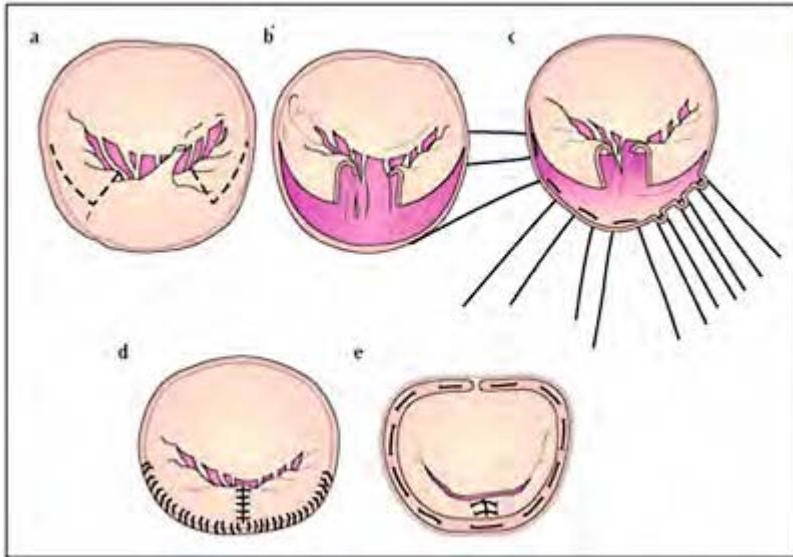
Figure 2.32 Sliding resection of the posterior leaflet. When there is excessive posterior leaflet tissue and/or ruptured chordae involving a large resection a sliding repair is performed to decrease leaflet height and allow reduction of the annulus. (a) Area of the posterior leaflet to be resected. (b) Leaflet tissue removed. (c) Annular ring reduction sutures in place utilized to plicate the posterior annulus. (d) Reattachment of the posterior leaflet. (e) Final repair after annuloplasty ring placement.
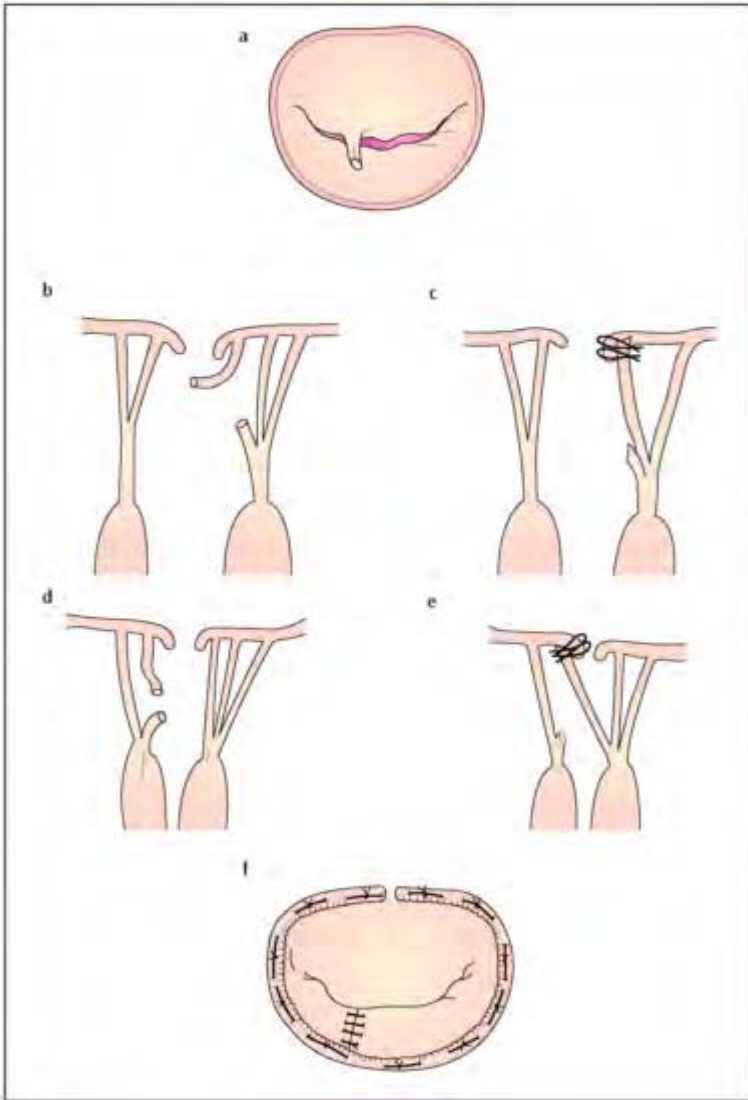
Figure 2.33 Diagram illustrating chordal transfer. Chordae may be transferred from one segment of the same leaflet or from the opposite leaflet to repair a ruptured chordae tendineae. (a) Rupture chordae tendineae of the anterior mitral leaflet. (b) Longitudinal view of the ruptured

chordae and attached normal secondary chordae in close approximation to the ruptured chordae. (c) The ruptured chordae is surgically removed and a neighboring secondary chordae is excised at its leaflet insertion and transferred to the leaflet edge providing leaflet support in order to prevent prolapse of that segment.

In some cases when a secondary chord from the same leaflet may not be sufficient to transfer, a corresponding chord from the posterior leaflet (d) may be excised and transferred to the anterior leaflet. (e) The posterior leaflet is then repaired (f) after the chordae is removed and transferred similarly to a posterior leaflet resection. The repair is then completed with an annuloplasty ring.

Surgical repair of a ruptured chord to the posterior leaflet involves resecting the excessive leaflet tissue along with the ruptured and elongated chords. In cases requiring less than 1/4 resection of the total leaflet, and when there is not excessive height to the remaining posterior leaflet, a simple quadrangular resection can be done (figure 2.31). Two perpendicular incisions are made from the leaflet margins to the annulus, on either side of the involved segment. The leaflet segment is removed by an incision along the base of the leaflet following the border of the annulus. The associated chords are then cut near their origin at the tips of the papillary muscles. Resection is completed by surgical plication of the annulus and approximating the remaining two edges of the remnant posterior leaflet with intermittent sutures, so the knots are on the ventricular side of the leaflets. In cases requiring up to 60% leaflet resection, and when there is excess tissue of the posterior leaflet, a sliding leaflet technique is required (figure 2.32). This involves incisions similar to a quadrangular resection, with the addition of two triangular resections at the base of the posterior leaflet remnants to correct for excess tissue height. All secondary and basal chords are removed from the leaflet remnants so that they are free of restriction and tension when they are approximated later. Mattress sutures are passed through the annulus, which circumferentially decreases the annulus by compressing the posterior aspect of the annulus, bringing the leaflet remnants into approximation. Each leaflet remnant is then reattached by suturing to the compressed annulus. The two leaflet remnants are then sewn together with inverted, interrupted sutures. The repair is completed by the insertion of a prosthetic ring.
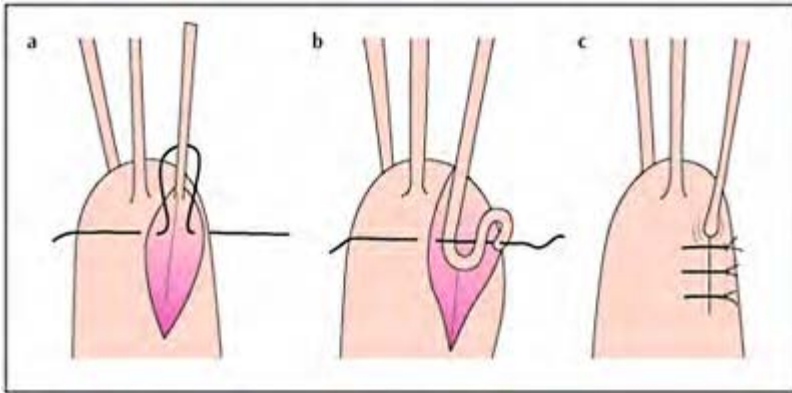
Figure 2.34 Diagram illustrating a surgical method of shortening elongated chordae tendineae. The chordae is shortened by burying a small length within the papillary muscle. (a) A trench is created in the papillary muscle. (b) With a suture an appropriate length of the chordae is pulled and buried in the trench created in the papillary muscle. (c) After burying the chordae the trench is sutured closed.

Ruptured chordae and prolapse of the anterior leaflet are never repaired by resection, so that the integrity and length of the anterior leaflet is preserved to ensure proper closure against the opposing posterior leaflet. Anterior chordal ruptures are repaired by secondary chordal transfer or transposition of chordae. In secondary chordal transfer, normal secondary chordae from the anterior leaflet close to the ruptured chord leaflet are removed and reattached to the margin of the leaflet to act as a primary chord (so as to spread out the existing chords to provide leaflet integrity). Marginal or primary chords are the most important and must be spaced about every 5 mm along the leaflet edge. Secondary chords are of less importance and may be sacrificed to replace marginal chords. Transposition of chordae is done by transferring chords from the posterior leaflet to the anterior leaflet (figure 2.33). Secondary chords are removed from the posterior leaflet by resecting a small triangular portion from the free edge of the posterior leaflet, directly opposite the lesion of the anterior leaflet. The posterior leaflet segment and attached chordae are sutured to the anterior leaflet edge, and the posterior leaflet is repaired if necessary.

When there is chordal rupture of both leaflets it usually is a result of one leaflet chord rupturing due to strain from rupture of the opposite leaflet chord. This usually involves using both secondary chordal transfer and transposition of chordae. When chordae

rupture near the commissures it usually involves the anterolateral commissure, and the commissure is reconstructed by transplanting chords and surgically making a new commissure "magic suture" stitch.

In 30% of patients, the chords are just elongated, and are not ruptured. In these instances, a shortening plasty may be done, which entails shortening of the chords by folding a small portion of the chord on itself and burying that portion into an incision made longitudinally, creating a trough in the papillary muscle from which it originates (figure 2.34). Chords may be shortened in small groups by this method, and multiple groups may need to be shortened. Occasionally, prolapsed segments with elongated chords may be corrected by chordal transfer techniques.

When chordae are thickened, areas of thickening can be trimmed or shaved. When chordae are fused they can be split or debrided with a scalpel or rongeur.[310–312] In fusion of the centrally placed chords, fenestration or the removal of triangular wedges of tissue is done (figure 2.35). When retraction of the posterior leaflet occurs, secondary and tertiary chords may be removed to permit better pliability of the leaflet. In cases of subvalvular stenosis, the chords may need to be shaved to the level of the papillary muscles, and occasionally the papillary muscles may need to be split and divided. Although not a Carpentier technique, artificial chords have been constructed with Gore-Tex or suture material to replace existing natural chordae.[313–315]
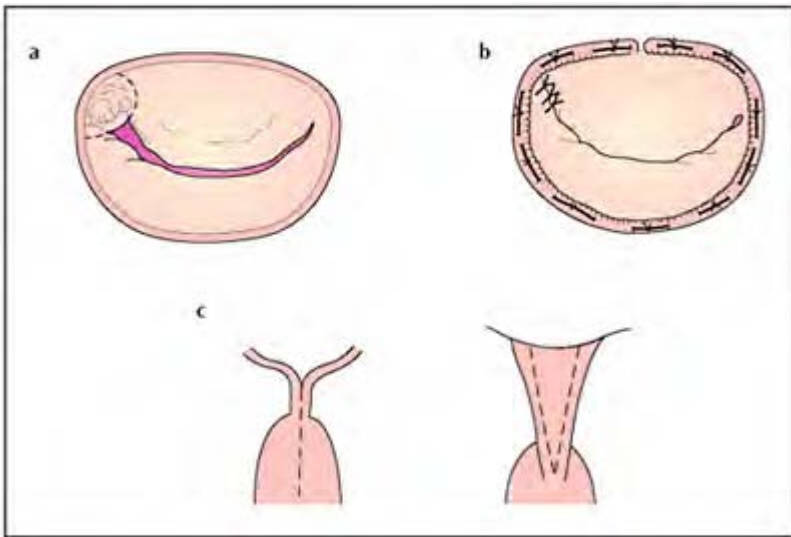
Figure 2.35 Surgical techniques used for repair in mitral stenosis. (a) Commissural fusion or focal areas of calcification may be removed by debridement or excision as illustrated in (b). The need for placement of a

mitral annular ring is somewhat controversial although it provides support to the valve after the repair. When chordae are thickened and fused, areas of thickening can be trimmed or shaved or when fused can be split or debrided with a scalpel. In fusion of the centrally placed chords, fenestration or the removal of triangular wedges of tissue is performed. In cases of subvalvular stenosis the chords may need to be shaved to the level of the papillary muscles and occasionally the papillary muscles may need to be split and divided (c) to relieve obstruction with unrestricted valve motion.
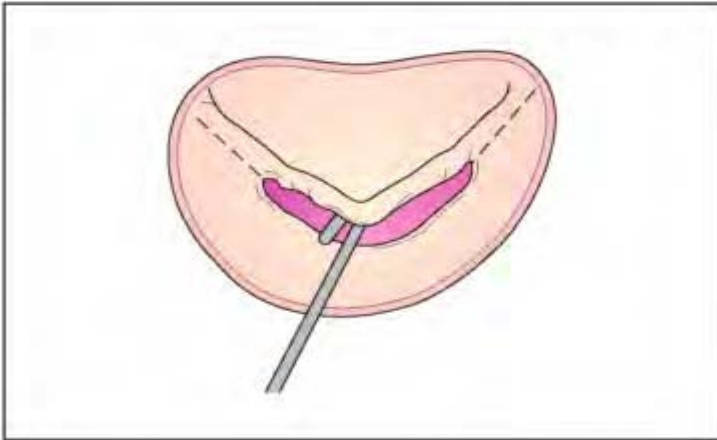
Figure 2.36 Mitral commissurotomy. During open mitral commissurotomy, gentle traction is applied to the anterior mitral leaflet to delineate further the line of fusion allowing a more accurate placement of the surgical incision. It is important that the leaflets are separated

with chordae intact to each respective
leaflet producing the best results.

In stenotic valves with commissural fusion, the commissural furrow is incised with a scalpel blade (figure 2.36). The line of commissural fusion may be identified by placing vertical traction on the free edge of both leaflets with nerve hooks, or by distending the ventricle with saline. The fused commissures are incised centrally from the valve orifice along the furrow, and should divide and spare the attached chordae to approximately a few mm from the annulus. The chordae exposed after the separation of the commissures are repaired in the manner previously described.

Clefts of leaflets or perforations in leaflets can be repaired by simple closing stitches or by patches made from the patient's own glutaraldehyde-treated pericardium (figure 2.37).[316] Complete or partial papillary muscle rupture is repaired by sewing the papillary muscle back in place, which works surprisingly well (figure 2.38). In cases of restricted motion due to ischemic papillary muscle dysfunction, the papillary muscles may be removed at their base, repositioned, and re-implanted in the ventricle,
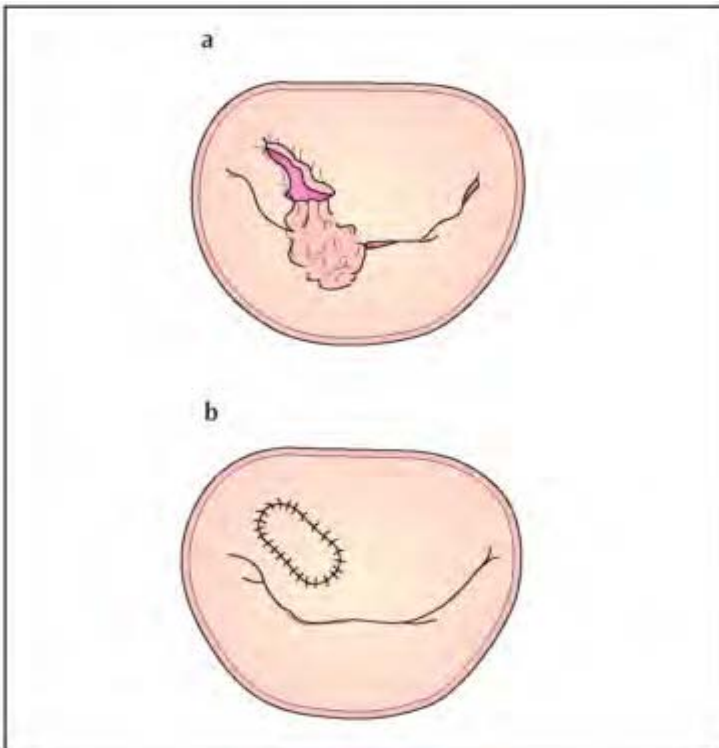
Figure 2.37 Diagram illustrating
surgical repair methods utilized in
infective endocarditis. In selected

cases, valvular vegetations (a) can be surgically excised as long as the underlying tissue has not been destroyed. When perforations develop as a result of endocarditis, the infected tissue may be debrided and a pericardial patch (b) may be utilized to close the remaining small hole.
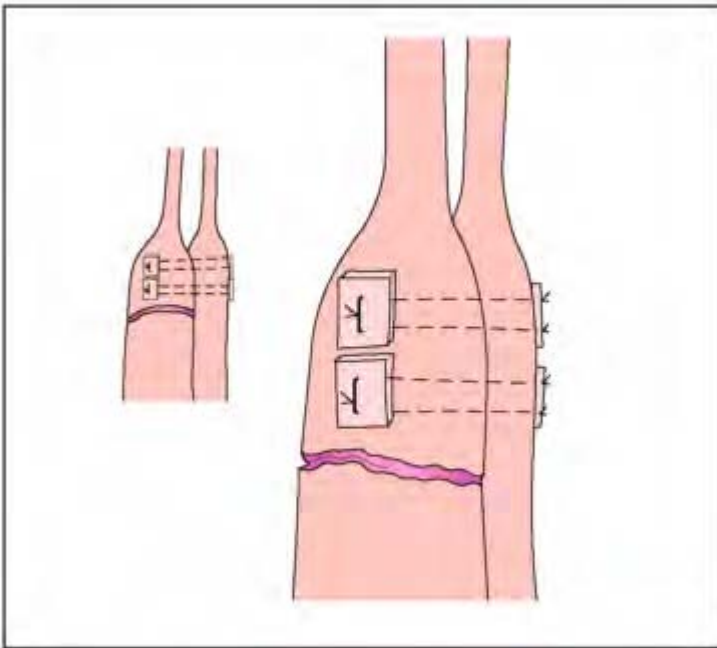
Figure 2.38 Diagram illustrating the reattachment of a ruptured papillary muscle. In selected cases of partial or complete rupture the papillary muscle can be reattached surgically particularly when there is good tissue to support the sutures used in the re-anastomosis.

usually in a more superior position. In the purest form of Carpentier's techniques, pledgets are not used for the repair. Instead, a larger suture specifically designed for reconstruction is used. Pledgets are small pieces of Teflon used to reinforce suture

material, and are widely used in North American cardiac surgery. Pledgets are thought to make the repair bulky, limiting mobility, and promoting thrombus formation and potential infection. Although pledgets should be avoided, papillary muscle surgery may require reinforcement with pledget material.

Mitral valve repair has also been extremely successful in acute and chronic cases of bacterial endocarditis, with a low operative morbidity and mortality, and with the same durability for the mitral reconstruction.[317–319] Mitral valve repair is done with the usual techniques including debridement of all infected tissue and placement of an annuloplasty ring. With mitral valve replacement in the setting of bacterial endocarditis there is a 10–15% risk of subsequent endocarditis in 5 years, with the greatest risk occurring in the first 6 months postoperatively. It appears that as long as the patient has been pretreated with adequate antibiotics and all of the infected tissue is removed, mitral valve repair is associated with a lower re-infection rate than mitral valve replacement (operative mortality 7.4%; by actuarial methods $61 \pm 6\%$ of patients are alive at 10 years and there is no recurrence of endocarditis). Mitral valve repairs associated with a paravalvular abscess carry the highest risk of reinfection. d'Udekem and colleagues,[320] have reported on 122 consecutive patients with active infective endocarditis and paravalvular abscess, treated with the usual reparative techniques plus wide excision of the abscess and reconstruction of the heart with glutaraldehyde-fixed bovine pericardium. There were nine operative deaths (7.4%) and only one patient had persistent infection that required re-operation. Freedom from recurrent endocarditis was $79 \pm 9\%$ at 10 years.
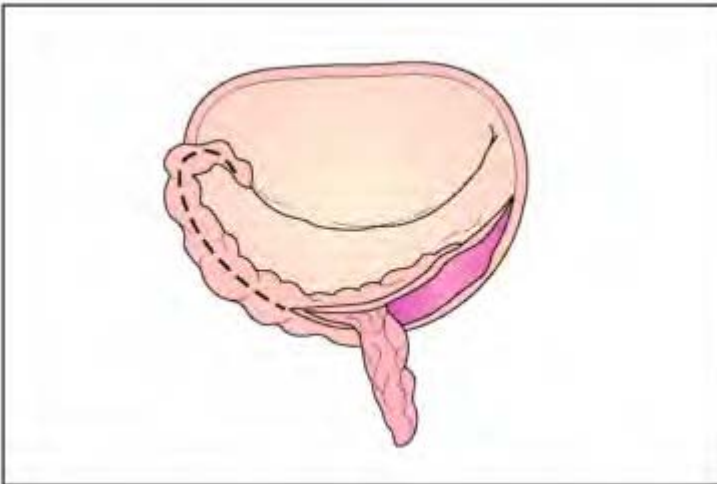
Figure 2.39 Excision of mitral annular calcification. When calcification predominately occurs in the posterior region of the annulus, exposure of the posterior annulus is accomplished by

initially detaching the posterior leaflet from the annulus. The ventricular endothelium is then incised around the borders of the area of calcification. The bar of calcium is then removed in one piece if possible to avoid fragmentation and embolization. Following the removal of calcium, the trench is sutured closed and the posterior leaflet is re-attached.

Mitral annular calcification (MAC) has been described in association with most of the disease processes that cause mitral disease.[226] Mitral valve replacement with extensive MAC is associated with an increased risk of ventricular rupture (18%), which has not been reported with mitral repair. Extensive annular calcification may occur, which can distort the orifice and can influence mitral repair results unfavorably. When significant MAC is present, dissection and debridement is done in the affected areas of the annulus to remove it (figure 2.39). When calcification predominantly occurs in the posterior region, exposure of the posterior annulus is accomplished by detaching the posterior leaflet from the annulus. The ventricular endothelium is then incised around the borders of the area of calcification. The bar of calcium is then removed in one piece if possible, with fine dissection using scissors, creating a trench in the annulus. Careful attention must be paid not to expose the circumflex artery or weaken the annulus by going too far into the atrioventricular groove or the ventricular myocardium. When calcium extends to the posterior leaflet, it is removed from the leaflet by shaving with a scalpel or debriding with a rongeur. Following the removal of calcium, the trench is sutured closed, and the posterior leaflet is reattached.

Whether there is associated annular dilatation or not, the surgical repair is completed with the placement of an annuloplasty ring (figure 2.40). In cases of type I and especially type III motion, an annuloplasty ring is usually all that is required for a successful repair. The annuloplasty ring promotes remodelling of the mitral annulus, provides support for the chordal and leaflet repairs, and promotes coaptation of the anterior and posterior leaflets. The annuloplasty ring also promotes remodelling by providing a measured plication of the posterior annulus and a decrease in the anterior–posterior dimension. In this manner, the annulus is returned to its normal physiological size and shape, and should not be restrictive to the inflow tract. Stenosis produced by the annuloplasty ring is unacceptable, producing obstruction to inflow, and promoting systolic anterior motion of the mitral valve and thromboembolic complications.
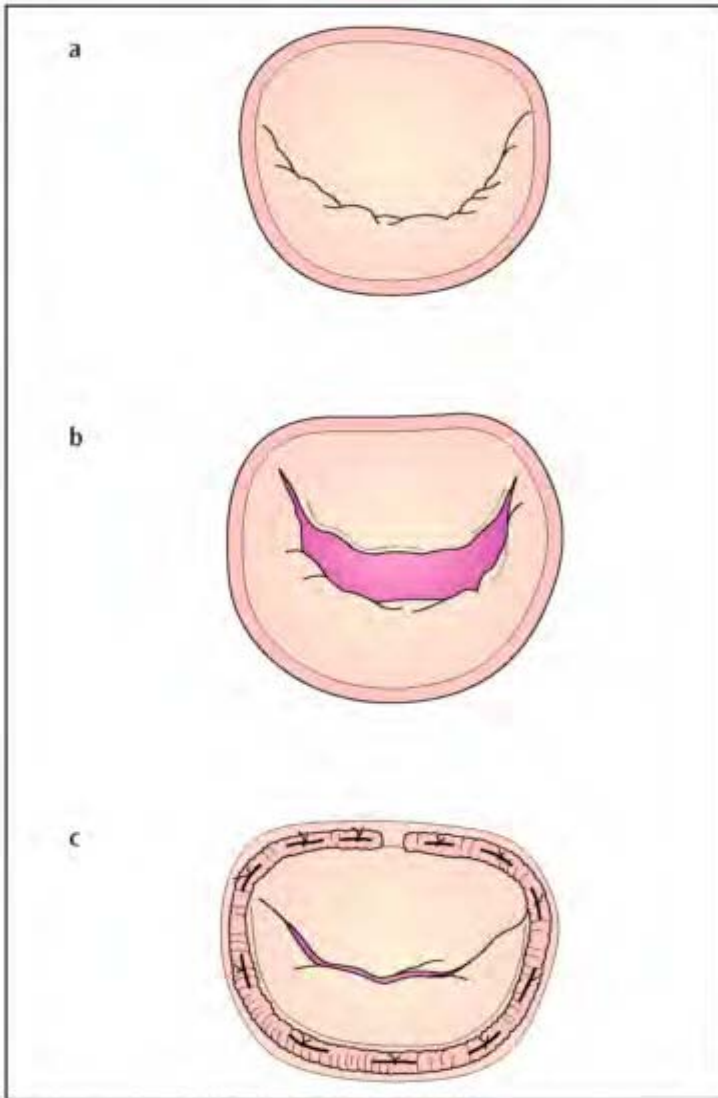
Figure 2.40 Mitral valve drawing
illustrating annular dilatation. (a)
Normal mitral valve as viewed enface.
Note the normal dimensions and shape
of the mitral valve and annulus. The
width of the anterior leaflet is greater
than the posterior leaflet, which
produces a line of closure towards the

posterior aspect of the annulus. The normal annulus dimensions are described by a smaller height (anterior–posterior diameter) in comparison to the width (transverse diameter) with a 3:4 ratio, respectively. (b) With annular dilatation the height of the annulus enlarges becoming greater than the transverse diameter. The length, as well as the width of the posterior leaflet enlarges which shifts the line of closure of the mitral valve to the center of the annulus. Annular dilatation may occur as a consequence of the disease process as in acute rheumatic mitral regurgitation or occurs as a result of secondary ventricular enlargement. Dilatation occurs predominantly in the posterior aspect of the mitral annulus due to the makeup of the annular tissue. (c) Surgical placement of a mitral annular ring returns the normal shape and dimensions to the mitral valve.

When measuring for ring size it is usually best to select a larger ring size for type I and II motion, and a smaller ring size for type III motion. Ring size is measured with a sizer supplied by the manufacturer of the ring, as the distance between the two commissures or at the height of the mid portion of the anterior leaflet, to select a ring whose surface area most closely matches the surface area of the anterior leaflet (figure 2.41). On average, in adults a 32–34 mm ring is used for men and a 30–32 mm ring for women. A properly positioned annular ring provides the normal apposition of the leaflets and avoids obstruction. To ensure proper alignment and geometric positioning without distortion, the natural mitral commissures must be correctly identified, and the commissure markings on the ring must be anchored appropriately at each commissure. The midpoints of the anterior and posterior leaflets should be oriented so that they are directly opposite each other, making sure that the leaflets' line of closure is parallel to the annulus of the posterior leaflet. After placement of the ring, visual inspection yields good symmetrical geometry of the line of closure ("smile") for the mitral valve leaflets with respect to the annulus.
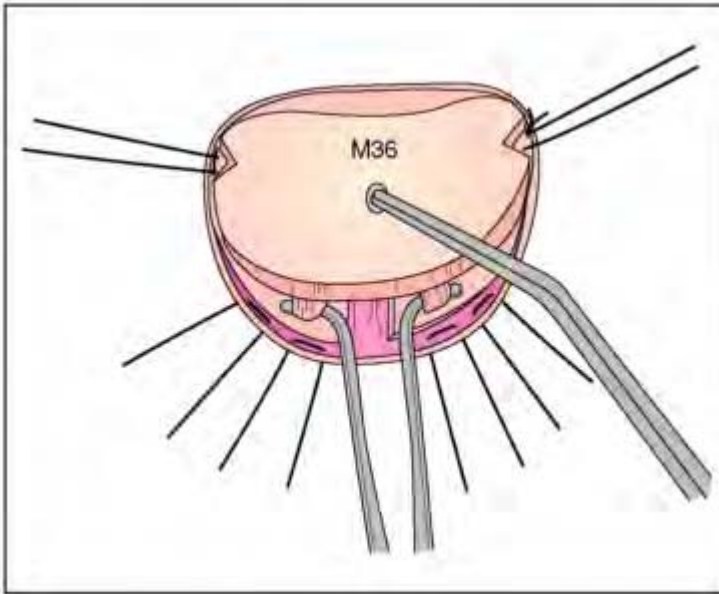
Figure 2.41 Diagram illustrating the surgical measurement of the mitral annulus for sizing the mitral annular ring. The ring size is based on the size and area of the anterior mitral leaflet. Markings or grooves on the sizer corresponds to points for matching up to the commissures. On average 32–34 mm rings are used in males and 30–32 mm rings are used in females. According to surgeon preference downsizing the dimension of the mitral annular ring may be performed in patients with left ventricular enlargement. Since mitral rings will not allow for dilatation during diastole caution must be exercised so as not to cause stenosis and a significant transvalvular gradient following the repair.
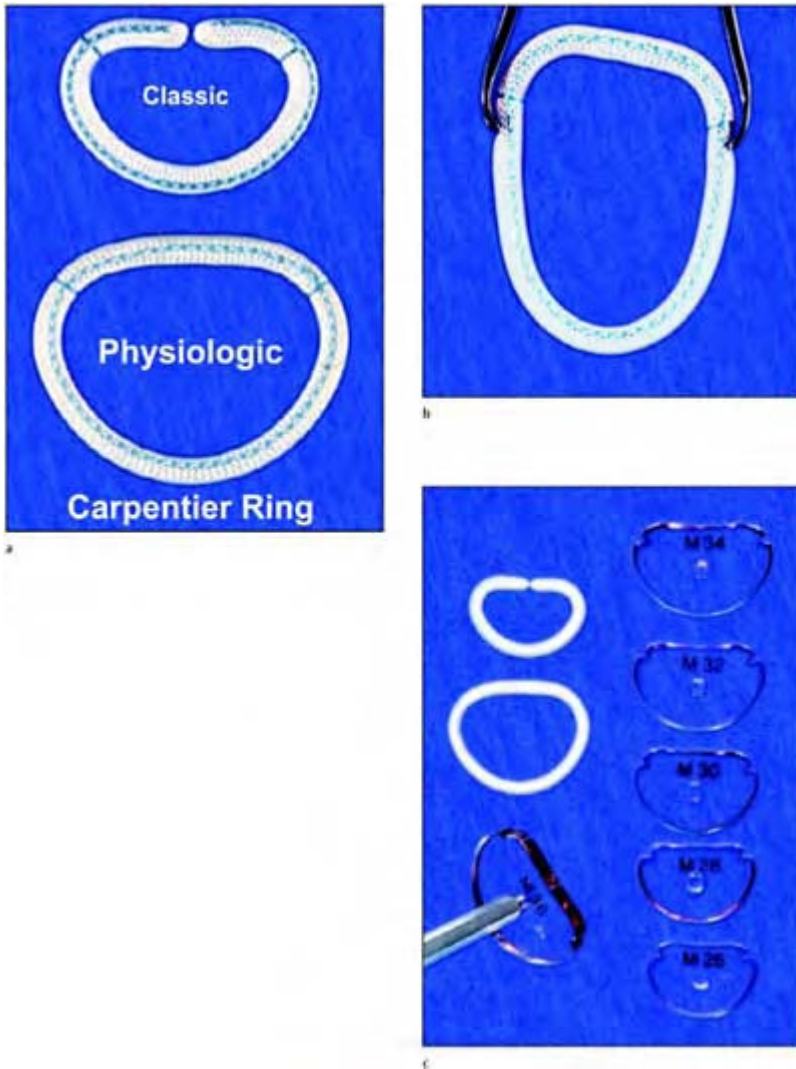
Figure 2.42 Mitral valve annuloplasty rings. (a) Carpentier–Edwards classic (fixed) and physiological (semi-flexible) rings. Both rings are D-shaped imitating the normal shape of the mitral annulus which allows for proper closure and approximation of the leaflets during systole through remodeling of the distorted mitral

annulus. To avoid annular distortion from improper alignment of the valve ring, markings indicate the fixation points for respective commissures. The fixed ring preserves the width of the annulus and will maintain annular size and shape during both diastole and systole. Some flexibility is provided by the split of the ring anteriorly. (b) The Carpentier–Edwards physiological ring follows the same principle as the fixed ring in preserving the anterior aspect of the annulus by being fixed, however, the posterior portion allows for more flexibility allowing the annulus to change shape during the cardiac cycle. (c) Mitral ring sizers are specifically designed for measurement of the proper ring size used during mitral valve repair surgery. The ring size is based on the size and area of the anterior mitral leaflet.
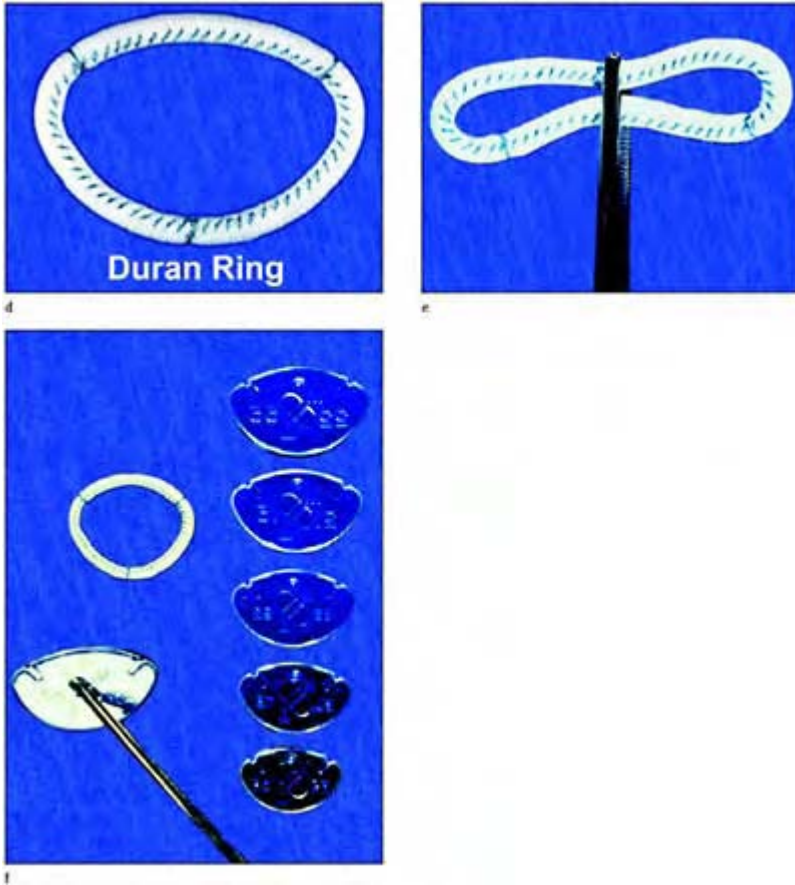
(d) Duran mitral valve ring and Duran mitral annular band. Both rings are extremely flexible and are not pre-shaped. (e) Flexible Duran mitral ring assumes the proper shape of the annulus by surgical repair of the valve after it is sewn in place. Controversy exists over the type of ring utilized during the repair and is generally based upon the surgeons preference. (D) Duran measurements ring sizers.
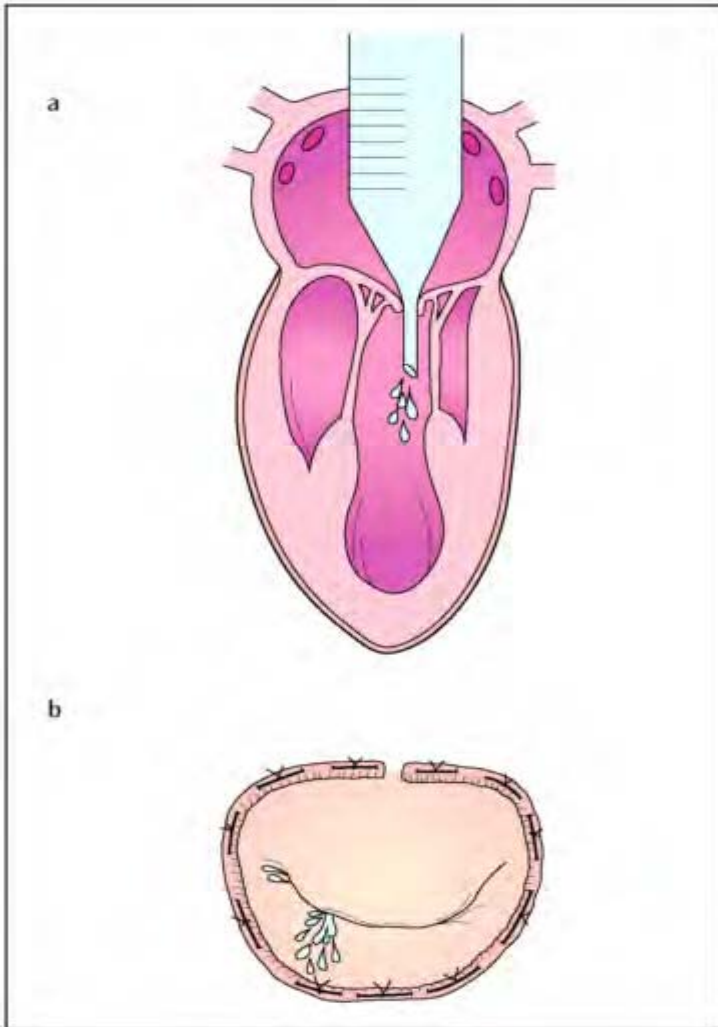
Figure 2.43 Surgical testing for
residual mitral regurgitation. (a)
Competence of the mitral valve is
tested by inserting a syringe or catheter
through the valve and fluid is injected
filling the left ventricle. (b) Valve
leaks corresponding to mitral
regurgitation are detected when the
leaflets coapt with ventricular filling.

Two types of annuloplasty ring are currently available, a fixed ring and flexible ring (figure 2.42).[321,322] There are two Carpentier rings—the fixed "classic" ring and the semi-flexible "physiological ring". Both rings have a rather fixed "D" shape which promotes remodeling of the distorted annulus to the typical systolic shape allowing proper closure and approximation of the leaflets. With the fixed ring, the width of the annulus is preserved and the mitral annulus will maintain its size and shape during the entire cardiac cycle. The flexible Carpentier ring follows the same principle, in that the anterior aspect of the ring is fixed and the posterior aspect is flexible. The anterior leaflet height dictates the use of one ring over another. If the length is larger (excessive tissue) than the sizer, then a "classic" fixed ring should be used, otherwise

Table 2.11 Echocardiographic findings needing a second pump run

• Residual mitral regurgitation $\geq$ 2+
No change or worsening MR
Color flow maximum jet area > 4 cm^2
PVF blunted systolic forward flow
PVF systolic flow reversal
• Mitral inflow obstruction
Increased peak gradient across mitral valve
• Left ventricular outflow tract obstruction
SAM
Increased peak gradient in LVOT
• Flail leaflet
• Suture dehiscence
• Ring dehiscence
• Incomplete repair

ring choice should probably favor the physiologic ring. The Duran ring is completely flexible, theoretically allowing for a normal elliptical annular shape during systole and a circular shape without obstruction during diastole, and does not produce left ventricular outflow obstruction during systole. The type of annuloplasty ring used depends on the type of repair, valvular anatomy, or preference of the surgeon.

After placement of the annular ring and before the sutures are tied in place, the competency of the valve is tested. Saline is injected into the left ventricular cavity. When the cavity is filled, the mitral leaflets expand and assume their normal position. Occasionally, the anterior leaflet may require slight unfurling, by manipulation with a nerve hook, to expand fully. Areas of prolapse and mitral regurgitation may be visualized in this manner (figure 2.43).

After mitral valve repair, patients receive anticoagulation for 2 months to promote good healing and fibrosis between the repaired tissue and the exposed cloth and sutures of the annular ring.

Intraoperative echocardiographic evaluation of the mitral valve after repair

After surgical repair of the mitral valve, echocardiographic analysis is done intraoperatively, immediately after weaning of cardiopulmonary bypass, to evaluate the success of the repair. Immediate echocardiographic evaluation is important since the conventional surgical assessment of mitral regurgitation (filling the arrested ventricle

Table 2.12 Post pump intraoperative echocardiography at the Cleveland clinic

Lesion (n = 611)	Number (%)
Successful repair	557 (91.2)
Failed repairs	54 (8.8)
LVOT obstruction	14 (2.2)
Persistent MS	1 (0.2)
Persistent flail	2 (0.4)
Persistent MR	33 (5.4)
Other	4 (0.6)
From Stewart WJ, et al. The value of echocardiography in mitral valve repair. *Cleveland Clin J Med* 1991;58(2):177–83.	

with saline to look for a leak) is a cursory technique at best, and has not been proven reliable compared with intraoperative echocardiography. The immediate intraoperative transesophageal echocardiographic evaluation of the repair, assessing the degree of residual mitral regurgitation accurately predicts the results of mitral valve repair compared with postoperative angiographic evaluation. Assessment of the severity of mitral regurgitation immediately after the repair gives an accurate reflection of the results, and does not change significantly on subsequent postoperative follow-up (table 2.11).

The mitral leaflet motion is evaluated in the same manner postoperatively, to determine the resolution of defects, and including the development of any new abnormalities as a result of the repair. Before visualization of the heart, it is extremely helpful to compare the preoperative echocardiographic assessment with the surgical findings and to know what techniques were used in the mitral valve reconstruction. In this manner, a quicker and more thorough echocardiographic evaluation of the leaflets and subvalvular apparatus can be made, immediately after the cessation of cardiopulmonary bypass and before decannulation. Findings that require the reinstitution of cardiopulmonary bypass and repeat of a repair are very subjective (table 2.12). Careful consideration and discussion with the surgeon and anesthesiologist must be made before the initial repair is judged inadequate. Although there is a learning curve for the surgeon for valve reconstruction, a considerable degree of experience is required by the echocardiographer as well. Some findings are obvious, and need further surgery, especially if the patient develops poor hemodynamics and the regurgitation or stenosis is worse or unchanged. Less clear are cases in which, for example, the mitral regurgitation

was severe preoperatively and after the repair there is moderate mitral regurgitation. Depending on many factors—the age of the patient, the time already spent on bypass and

Table 2.13 Reoperations in mitral valve repair

Causes of reoperation	Number
Early reoperation (<2 yr)	*10*
Ring dehiscence	1
Recurrent annular distention*	2
Triangular resection	3
Residual prolapse	4
Late reoperation (>2 yr)	*13*
Recurrent prolapse	4
Leaflet retraction	6
Valve stenosis	3
*No ring was used	
From Deloche A, et al. Valve repair with Carpentier techniques: the second decade. *J Thorac Cardiovasc Surg* 1990;99:990–1002.	

cross-clamp time, the severity of pathology, the improve ment in hemodynamics, the experience of the echocardiographer and the surgeon etc—residual moderate regurgitation may be acceptable. Other questions, such as whether to perform a second repair or valve replacement, require the consideration of many of the same factors (table 2.13).

The mitral apparatus should be scanned in multiple planes to assess the continuity of the papillary muscles, chordae, and leaflets. Occasionally, small chordae remnants that were removed may be seen fluttering in close proximation to the papillary muscles, but there should not be any chordae of significant length with large chaotic motion. If chordae were shortened too much the leaflets should show restricted motion. If the chordae remain elongated, there will be prolapse of the leaflets. Visualization of the posterior leaflet is limited due to the presence of the annular ring after leaflet resection. In most cases, the posterior leaflet should appear immobile and fixed in its diastolic position. The posterior leaflet usually regains its motion within 1–6 months. There should be no obvious prolapse of the leaflet margins in line of approximation in long axis views, and depending on the adequacy of repair the leaflets should show their normal height ratio (2/3 anterior to 1/3 posterior). If the line of closure is visualized in the short axis plane, it should be placed posteriorly in the ventricle and follow the line of the posterior annulus. Small suture ends may be seen around the annular ring in long axis or short axis views. Suture dehiscence is characterized by long sutures that show obvious chaotic motion throughout the cardiac cycle. Use of the zoom feature or decreasing the echocardiographic field depth may help resolve the normality or abnormality of these findings.

Usually a remodelling annuloplasty ring may be visualized in the region of the mitral annulus, in the short axis proximal transgastric view at 0°–30°, as represented by
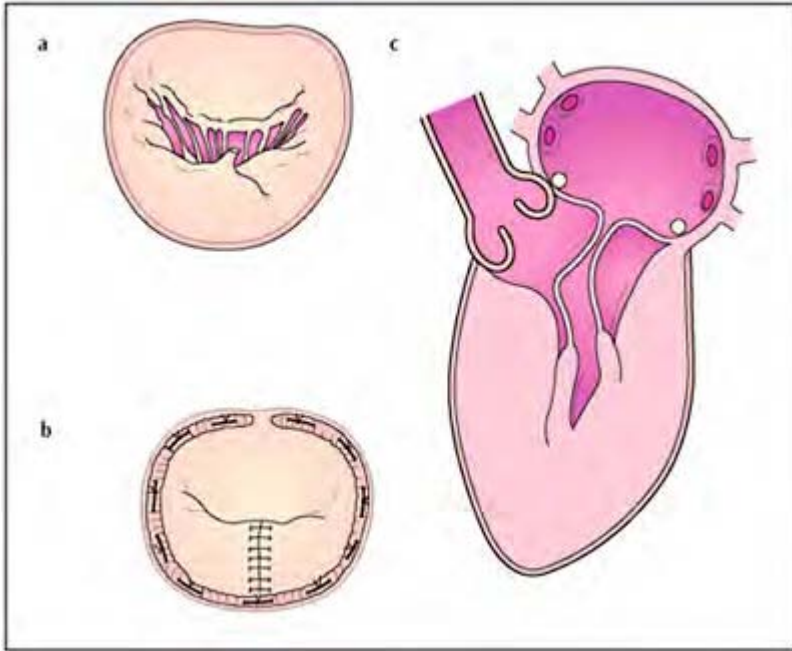
Figure 2.44 Systolic anterior motion (SAM) following repair. SAM of the mitral valve may be produced following mitral repair due to excessive height of the posterior leaflet, which pushes the line of closure anteriorly towards the left ventricular outflow tract. SAM may also be produced when too small an annuloplasty ring is utilized for the repair, especially in hypertrophic ventricles with small cavity dimensions.

increased echogenicity, hyper-reflectivity, and shadowing similar to a prosthetic valve, with the shape of ring and the annulus approximating its normal D-shape. A small decrease in the mitral valve area will be observed by the Doppler pressure half-time method, for both the Carpentier rings or flexible Duran ring.[322] There should not be a significant increase, however, in the peak transmitral diastolic velocity, peak transmitral diastolic gradient (8 ± 4 mmHg), mean transmitral diastolic gradient (3 ± 2 mmHg), or the grade of mitral regurgitation despite the reduction in valve area for any of the ring

types. Although patients with flexible rings have better left ventricular function initially after the repair, no significant difference is shown at 1 year after surgery. When suture dehiscence is present about the annular ring, the annular ring will have a rocking motion, back and forth throughout the cardiac cycle.

Color flow mapping is done to determine a reduction in the severity of mitral regurgitation compared with preoperative values. Residual mitral insufficiency is frequently directed in a different direction after the repair, but the maximum jet area or the jet area/left atrial area ratio should be decreased in comparison to preoperative measurements. If necessary, the regurgitant orifice area may be calculated from the vena contracta or flow convergence method. Pulsed Doppler interrogation of the pulmonary veins should show improvement or increase in the systolic forward flow, normalizing the systolic : diastolic ratio, and preoperative systolic flow reversal should be eliminated.

In about 80% of cases, successful valve repair results in trivial or no mitral regurgitation (at experienced centers), and an acceptable result should yield below 2+ mitral regurgitation.[109] Mild or trivial mitral regurgitation after mitral valve repair may be related to left ventricular function or persistent abnormality of the mitral apparatus. Patients with chronic heart disease and severe left ventricular failure may show residual mitral regurgitation immediately after heart activity has resumed, secondary to increased afterload. Type III or restricted leaflet motion may be observed after ischemic arrest due to transient left ventricular dysfunction. With continued monitoring during the completion of surgery, leaflet motion normalizes, coinciding with the return of left ventricular function. Occasionally, patients receiving inotropic and vasodilatory drugs who have reduced ventricular filling (as seen immediately after weaning from bypass) may develop left ventricular outflow obstruction with mild to moderate mitral regurgitation after repair. Correction of hemodynamics usually results in the disappearance of left ventricular outflow obstruction and mitral regurgitation. Other causes of mild regurgitation not specifically related to the mitral repair may be abnormal cardiac rhythms, such as ventricular tachycardia or paced rhythms.

A failed mitral valvular repair should be considered when there is no detectable change in the severity of mitral regurgitation from preoperative values, or there is 2+ or greater mitral insufficiency in the setting of normal left ventricular function. The prevalence of failed mitral valvular repair resulting in a second pump-run is about 8% as reported by the Cleveland Clinic, and may be slightly higher depending on the experience of the surgical team (table 2.13).[109] Immediate failures may be the result of left ventricular outflow tract obstruction (3%), incomplete correction, and suture dehiscence of the annular ring or valve repair. Late failure after mitral repair is primarily due to progression of the underlying disease, especially with degenerative disease. Late failure may also be attributable to the degree of surgical experience and the difficulty of the techniques used during the repair. Chordal shortening techniques and repairs of the anterior leaflet with redundant excessive tissue are technically difficult since they require the proper assessment of length and elongation in the arrested and empty heart. Suturing the papillary muscle may be difficult in cases of reattachment after muscle rupture and burying chords in the papillary muscle for chordal shortening, which may result in early or late suture dehiscence.
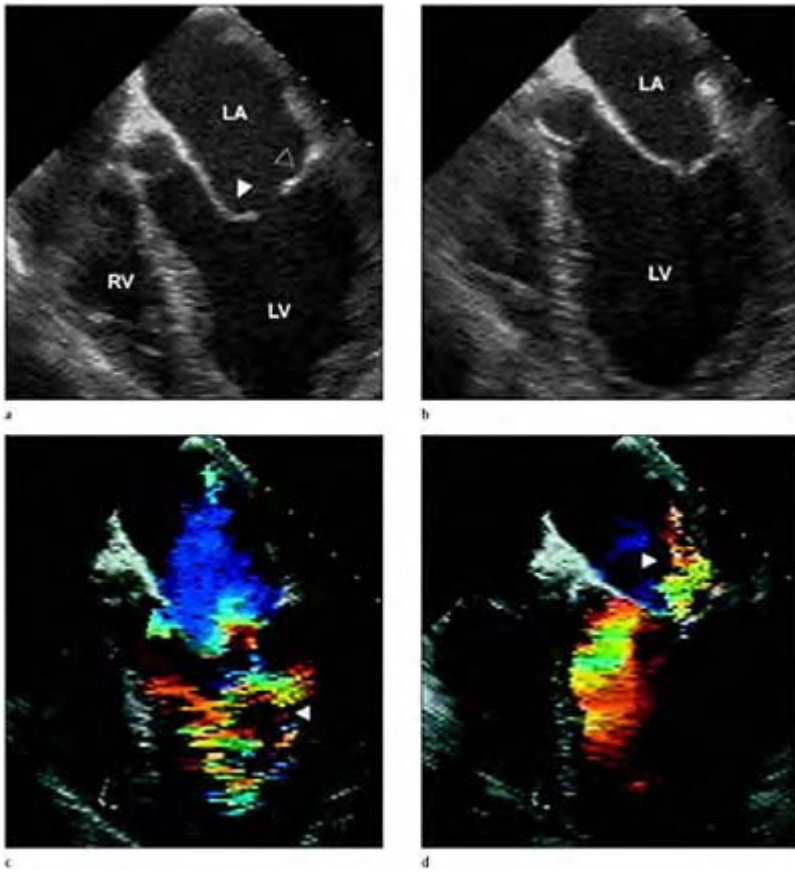
Case 2.1 Mild mitral stenosis. The structural and functional abnormalities of mitral stenosis can be easily demonstrated with multiplane TEE including fibrosis, calcification and restriction of motion (diastolic doming) in multiple scanning planes obtained from the lower esophageal window. Conventional and color Doppler evaluation of the left ventricular inflow tract is easily performed with a parallel plane to mitral flow. (a) Diastolic frame obtained at 0°illustrating mildly

thickened mitral leaflets and diastolic doming (arrow). The anterior leaflet is towards the septum and the left of the image with the posterior leaflet to the right of the image. Valve opening can also be visually assessed during diastole as well as valve closure during (b) systole. (c) Color flow Doppler in diastole demonstrating a stenotic jet (arrow) through the mitral valve. (d) Color flow Doppler during systole demonstrates a small regurgitant jet (arrow). Rheumatic disease often presents as a mixed lesion with both stenosis and regurgitation.

Left ventricular outflow tract obstruction complicates mitral valve repair in 3–5% of cases, with or without residual mitral regurgitation (figure 2.44).[323–326] After mitral repair, resting gradients in the left ventricular outflow have been measured from 0 to 44 mm Hg, which may significantly increase with isoproterenol stimulation. Left ventricular outflow tract obstruction is most common in degenerative posterior leaflet prolapse, and has not been reported after the repair of type I mitral regurgitation or rheumatic disease producing restrictive or prolapsed leaflets. The development of outflow tract obstruction has been eliminated largely with the second generation of Carpentier repair techniques.[40,41] In the first decade of repair, smaller rings were used more frequently, and resection of the posterior leaflet was not accompanied by shortening of the height of the leaflet. Left ventricular outflow tract obstruction has been attributed to reduction in size of the mitral annulus, secondary to the annuloplasty ring. With the placement of the annular ring, the posterior left ventricular wall and the posterior mitral leaflet are directed anteriorly towards the aorta, resulting in significant narrowing of the mitro-aortic angle to 120°–100°. Additionally, both leaflets were displaced into the left ventricular outflow tract. This distortion in ventricular geometry pushes the left ventricular inflow into the left ventricular outflow tract, with forward diastolic flow directed toward the ventricular septum instead of toward the ventricular apex. Excess tissue of the posterior leaflet (> 1 cm height) in conjunction with the annular ring causes the posterior leaflet to close first, and pushes the anterior leaflet and thus the line of leaflet closure towards the left ventricular outflow tract, producing systolic anterior motion (SAM). The left ventricular outflow tract and mitral valve leaflet motion should be carefully assessed in the deep transgastric view at 0°, or in the lower esophageal position between 90° and 180°, to assess proper leaflet aspect during systole and diastole, and the presence of SAM. Using these same views, color flow Doppler imaging of the inflow and outflow jets shows the direction and orientation of blood flow. Forward diastolic flow from the mitral orifice is directed anteriorly in the ventricle, while the reverse flow is deflected along the posterobasal wall and upward toward the mitral valve and aorta.
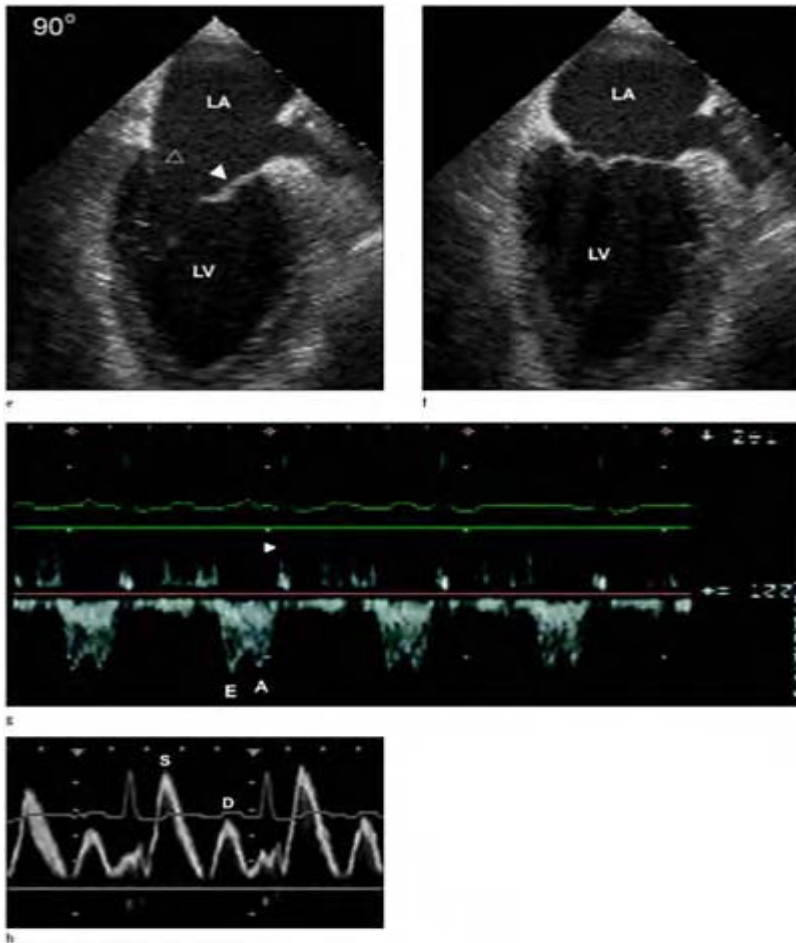
Rotating the transducer to 90° (e) diastolic doming
(arrows), with restricted opening is again demonstrated,
with valve closure during (f) systole. (g) Continuous
wave Doppler through a mildly stenotic mitral valve
orifice demonstrates increased E and A wave
velocities, with a normal pressure half-time. (h) At 90°
left pulmonary venous Doppler is performed
demonstrating normal systolic (S) and diastolic (D)
flow profiles. LA, left atrium; LV, left ventricle; RV,
right ventricle.
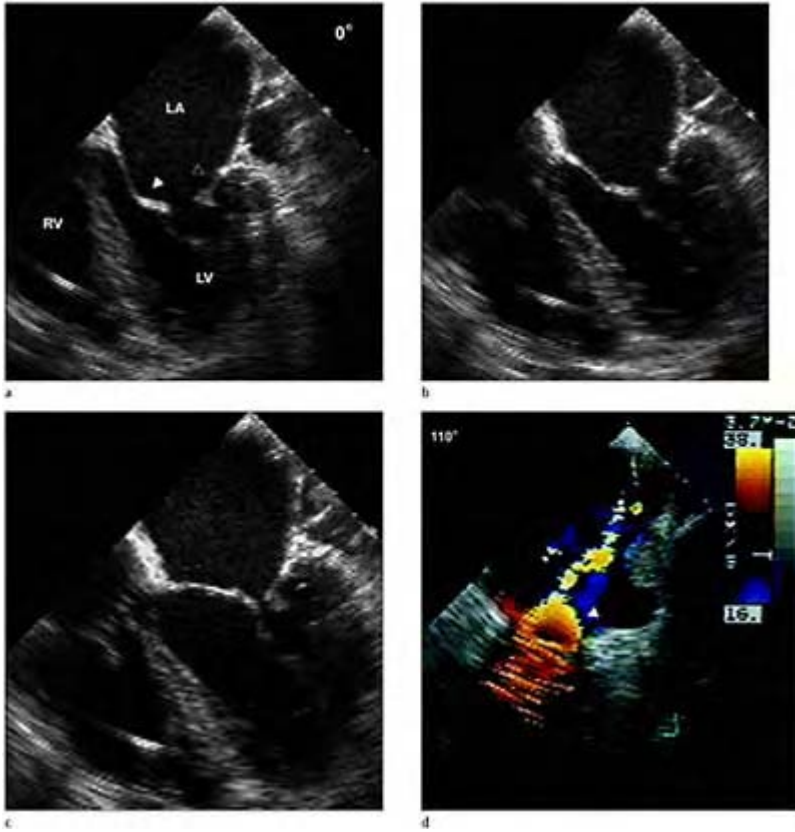
Case 2.2 Mild mitral stenosis and regurgitation. Thickening and diastolic doming of the mitral valve leaflets with mild restriction of opening during early diastole (a) and end diastole (b) at 0° in the lower esophageal window. (c) Systolic frame demonstrating leaflet closure. (d) Color flow Doppler performed with the transducer rotated to 110° demonstrating flow convergence through the stenotic mitral orifice. Flow convergence can be best visualized through adjusting the aliasing velocity.
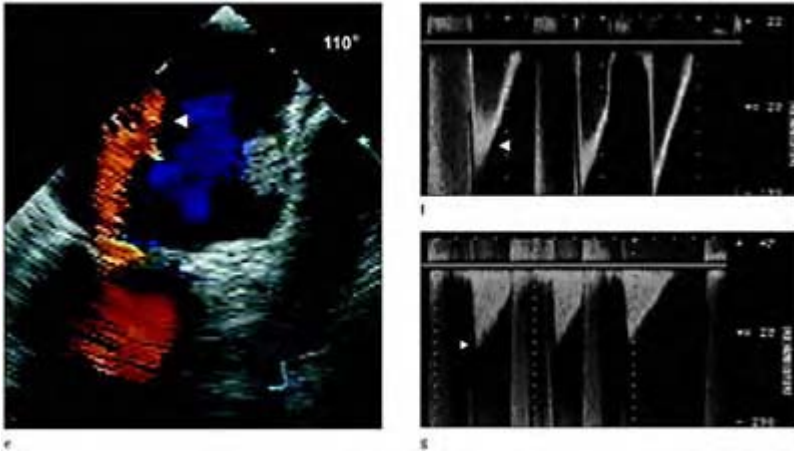
(e) Systolic frame demonstrating a
mild mitral regurgitant jet. Color flow
Doppler can also be useful for
directing conventional Doppler (f)
pulsed wave or (g) continuous wave
through the stenotic valve orifice.
Conventional Doppler demonstrating
increased velocity of the *e* wave
(arrows) and lack of an *a* wave during
atrial fibrillation. Pressure half-time
can be estimated with continuous wave
Doppler. LA, left atrium; LV, left
ventricle; RV, right ventricle.
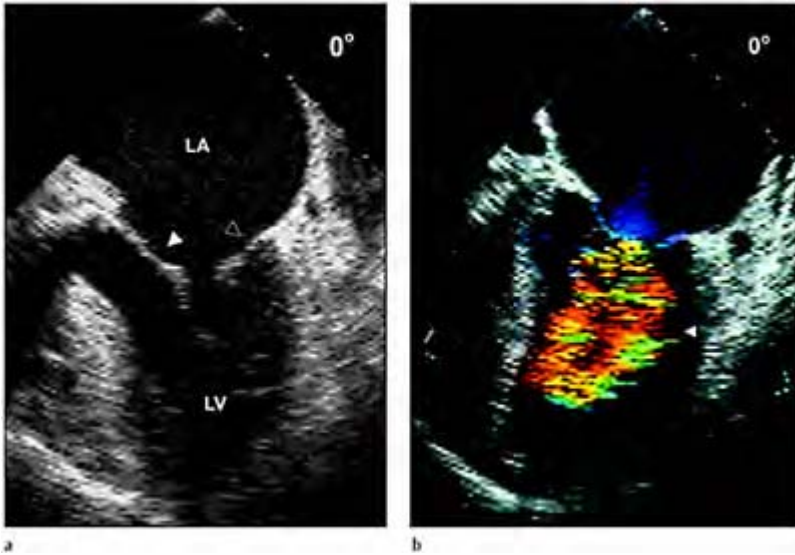
Case 2.3 Moderate mitral stenosis and mild regurgitation. The mitral leaflets are thickened and restricted with decreased amplitude of opening during diastole (a) and with color flow Doppler a stenotic jet (b) is demonstrated. Note diastolic doming is often less noticeable as the severity of mitral stenosis increases.
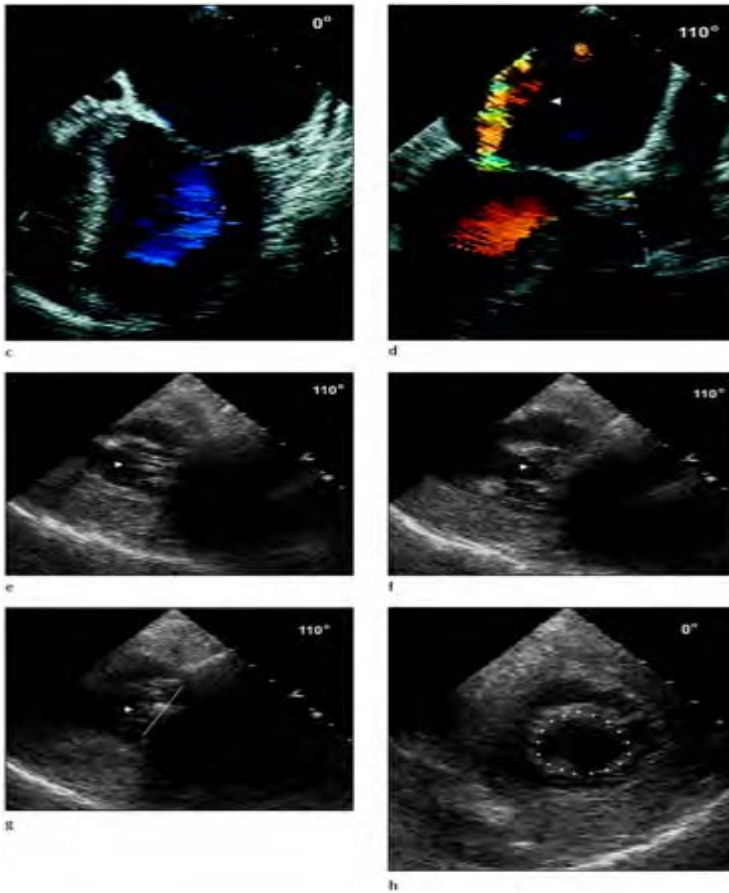
In systole (c) the mitral regurgitant jet is not identified until the transducer is rotated to 110° (d). With thickening and calcification of the mitral leaflets the subvalvular apparatus may not be visualized requiring additional echocardiographic views. Marked thickening and calcification and shortening of the chordae tendineae and papillary muscles are appreciated during systole (e) and diastole (f) in the gastric view in the horizontal projection at 90° in the same patient. The annular dimension and extent of calcification can also be seen in these views to assist in determining the proper plane for planimetry of the valve orifice when the transducer is rotated back to 0°. LA, left atrium; LV left ventricle.
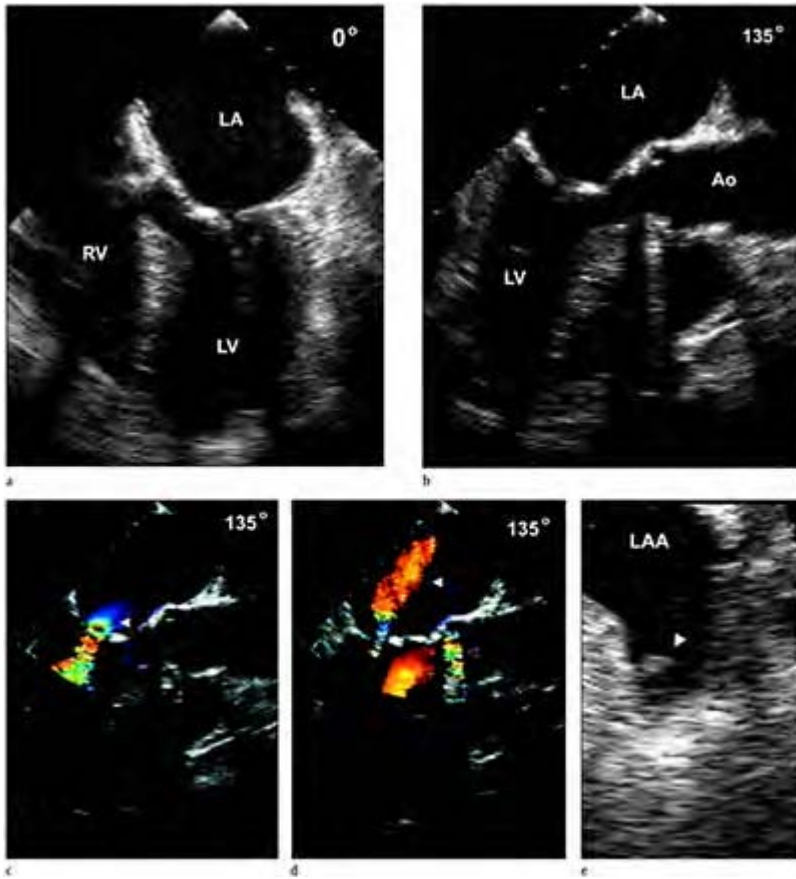
Case 2.4 Severe mitral stenosis. Marked thickening and calcification of the mitral valve leaflets with significantly restricted opening in diastole (a) at 0° in the lower esophageal views. Rotating the transducer to 135° (b) allows further interrogation of the mitral valve and in addition illustrates a stenotic aortic valve. Color flow Doppler at 135° demonstrating flow convergence of the mitral stenotic jet during diastole (c) and a mitral regurgitant jet (d) with turbulent and stenotic flow across the aortic valve during systole. (e) Visualizing the left atrial appendage demonstrates a thrombus at 10° in the upper esophageal view. LA, left atrium; LV, left ventricle; RV, right ventricle; LAA, left atrial appendage.
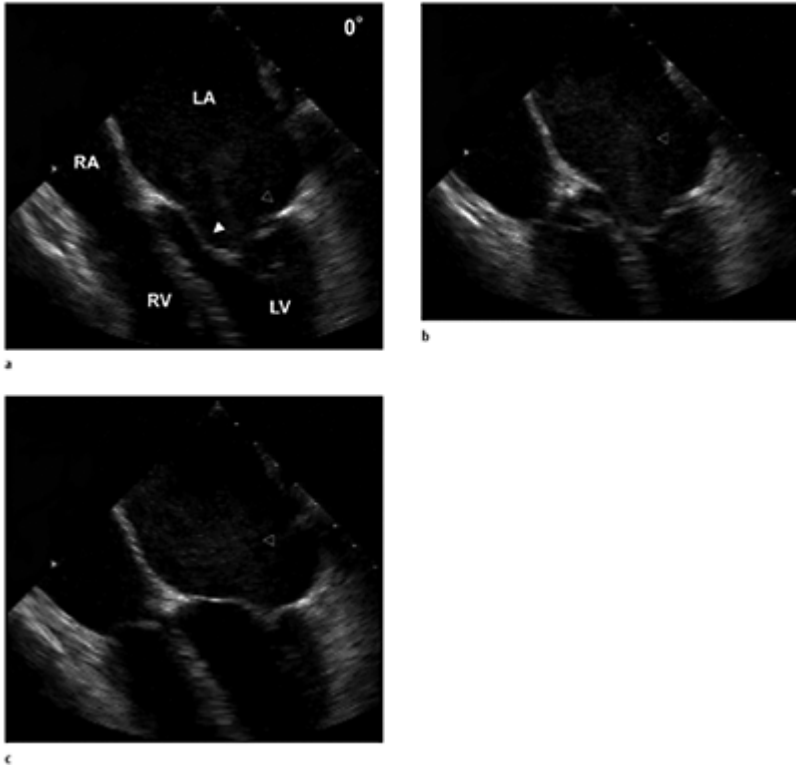
Case 2.5 Moderate mitral stenosis. (a) Marked left atrial enlargement with diastolic doming of the restricted and thickened leaflets. The posterior leaflet is heavily calcified and exhibits severely restricted motion. (b) Echocardiographic smoke (arrow) identified in the body of the left atrium denoting sluggish blood flow due to the restricted mitral valve opening. (c) Closure of the mitral valve leaflets. Echocardiographic smoke (arrow). LA, left atrium; LV, left ventricle; RA, right atrium; RV right ventricle.
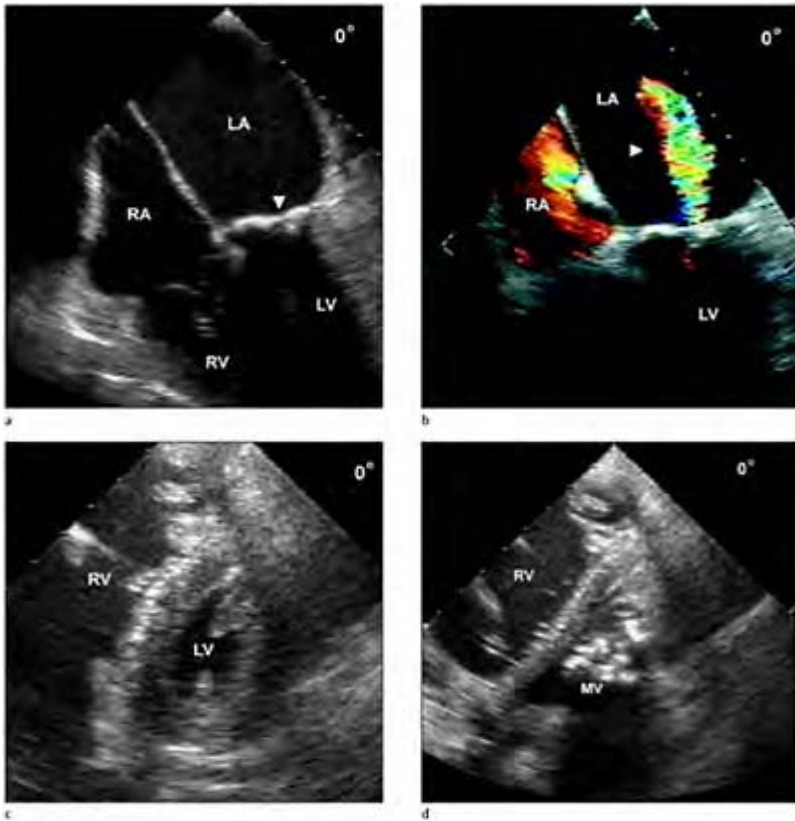
Case 2.6 Severe mitral stenosis. (a) Marked annular calcification and calcified mitral leaflets. (b) During systole a mitral regurgitant jet (arrow) is demonstrated. (c) Gastric transducer position at 0°at the ventricular basal level demonstrates the typical small left ventricle (LV) of severe mitral stenosis with a flattened septum and a dilated right ventricle (RV) consistent with right ventricular pressure overload. (d) With slight withdrawal of the transducer to the esophagus the mitral valve (MV) orifice may be visualized for estimation of orifice area.
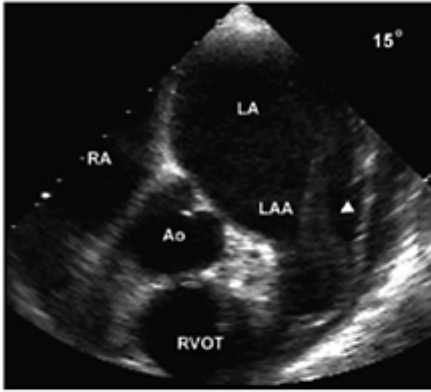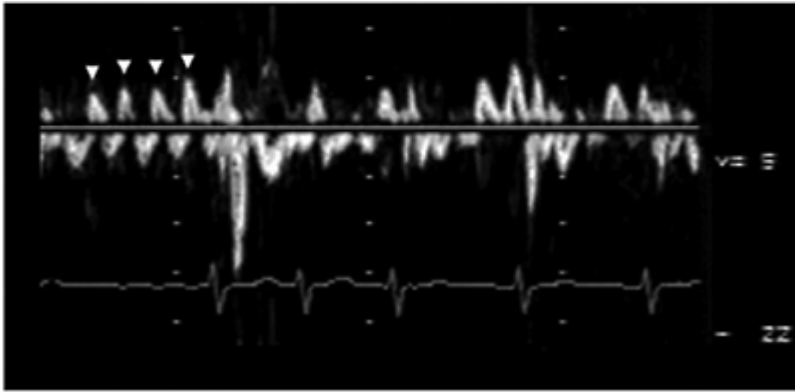
(e) Views of the left atrial appendage (LAA) demonstrate a thrombus and echocardiographic smoke. Pulsed wave Doppler interrogation of the left atrial appendage (f) demonstrates fibrillatory waves (arrows) with atrial fibrillation and diminished flow velocity in the appendage as a precursor for smoke and thrombus formation. LA, left atrium; RA, right atrium, RVOT, right ventricular outflow tract; AV, aortic valve.
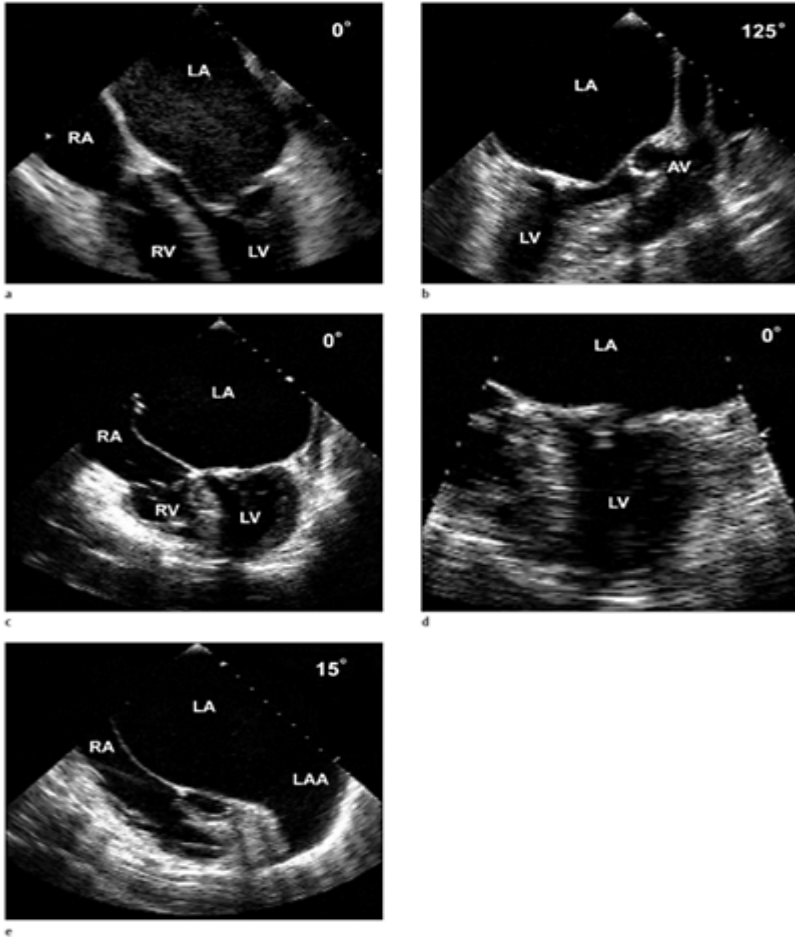
Case 2.7 Severe mitral stenosis. (a) Left atrial enlargement with diastolic doming of the mitral leaflets with restricted opening. (b) Markedly enlarged left atrium in comparison to a small left ventricle with rotation of the transducer to 125°. (c) Bi-atrial enlargement with small ventricular cavities in a patient with rheumatic disease illustrating a restrictive component from associated pericardial involvement. (d) Annular plane exhibiting marked calcification. (e) Marked left atrial enlargement including the left atrial appendage (LAA). LA, left atrium; LV, left ventricle; RA, right atrium; RV, right ventricle; AV, aortic valve.
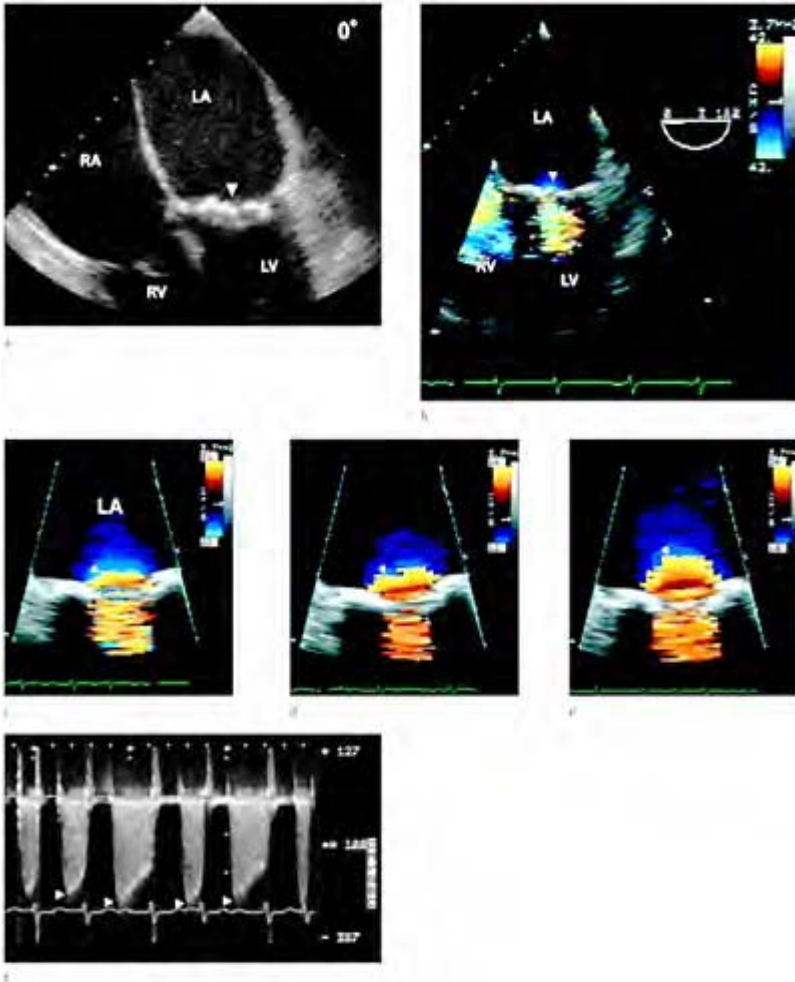
Case 2.8 Calculation of the mitral
valve orifice in mitral stenosis. The
PISA method can be utilized to
measure the stenotic valve orifice area.
(a) Stenotic mitral valve obtained in
the lower esophageal view at 0°. The
leaflets are thickened and calcified and
mitral valve opening is not readily
identified. (b) Color flow Doppler
demonstrating the mitral stenotic jet
during diastole. With normal aliasing

velocity and standard echocardiographic depth settings the proximal flow convergence is not well visualized. Utilizing the zoom or RES feature of the echocardiographic equipment this area can be magnified for measurement. Decreasing the color flow aliasing velocity and shifting the baseline allows for better visualization (c,d,e) of the area of first alias (arrow) allowing more accurate measurement of the radius and determining the angle of the mitral leaflets. (f) Continuous wave Doppler recording of mitral stenosis, demonstrating an averaged maximum velocity (arrows) of 2.9 m/sec. Mitral regurgitation is also demonstrated above the baseline during systole. LA, left atrium; RA, right atrium; LV, left ventricle; RV, right ventricle
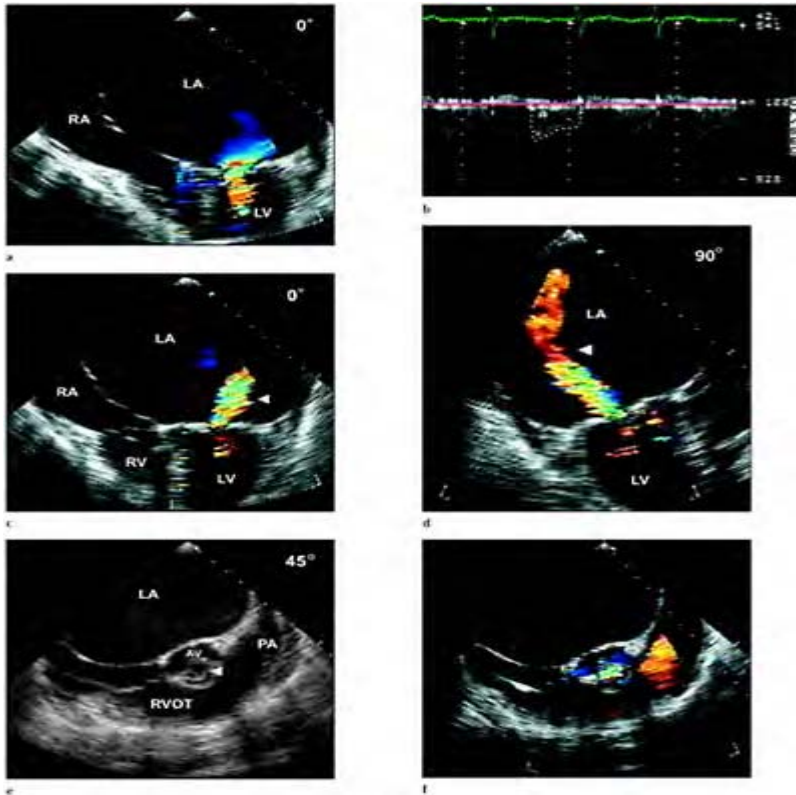
Case 2.9 Severe rheumatic mitral stenosis. (a) Marked left atrial enlargement, with color flow Doppler demonstrating a mitral stenotic jet. (b) Continuous wave Doppler directed by the color flow stenotic jet in (a), exhibits increased maximal gradient and a prolonged pressure half-time. (c) Color flow Doppler demonstrating an associated mitral regurgitant jet (arrow). (d) The same color flow Doppler regurgitant jet visualized in (c) as visualized at 90°. (e) Visualization of the aortic valve in the upper esophageal view at 45°. The aortic valve is stenotic with reduction of valve area during systole. Multiple valvular lesions frequently occur in rheumatic disease. (f) The aortic valve during diastole exhibits marked calcification during closure. LA, left atrium; PA, pulmonary artery.
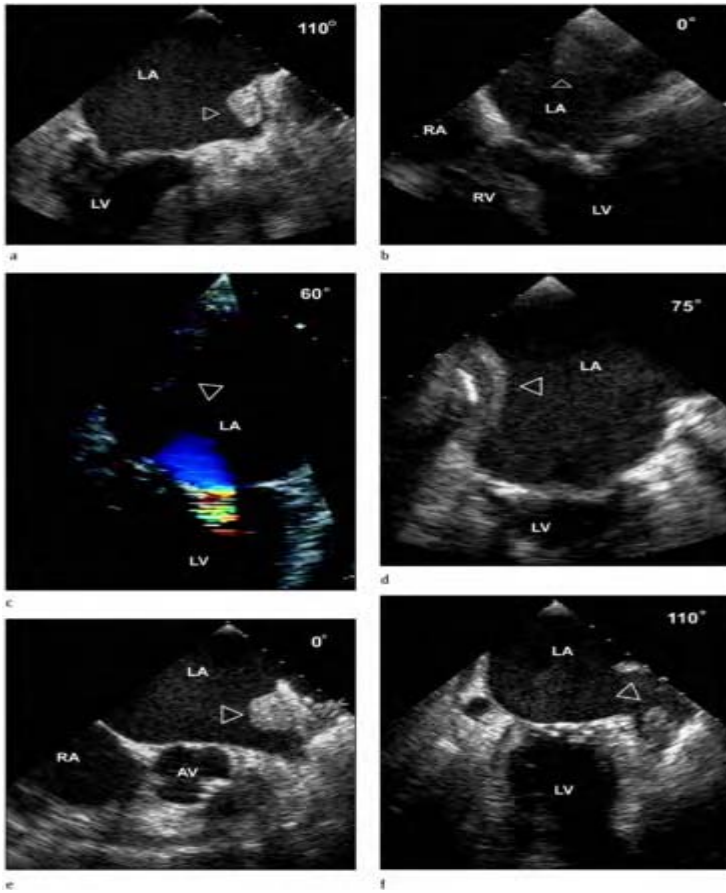
Case 2.10 Left atrial thrombi are frequently associated with mitral stenosis. (a) Left atrial thrombus at the origin or left atrial appendage (arrow). (b) Left atrial thrombus (arrow) attached to the superior, posterior wall of the left atrium. (c) Left atrial thrombus (arrow) projecting into the left atrial cavity visualized at 60° from the lower esophageal window. (d) A laminated left atrial thrombus (arrow) attached to the posterior wall of the left atrium visualized at 75°. (e) A left atrial appendage thrombus (arrow) protruding into the body of the left atrium. (f) Left atrial thrombus buried in the apex of the left atrial appendage. LA, left atrium; LV, left ventricle; LAA, left atrial appendage.
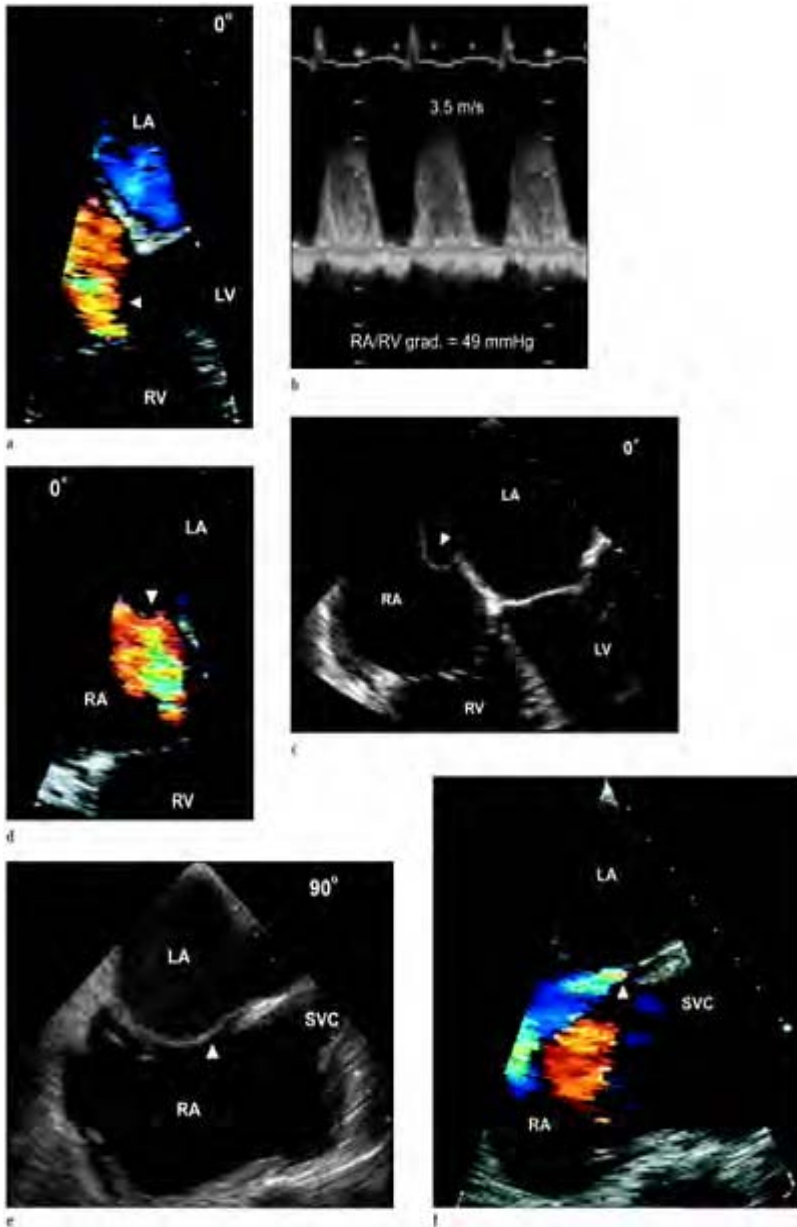
Case 2.11 Coexistent abnormalities
associated with mitral stenosis. (a)
Tricuspid regurgitation demonstrated
by color flow Doppler. (b) Continuous

wave Doppler guided by the color flow regurgitant jet in (a). The maximum velocity recorded is greater than 3 m/sec consistent with pulmonary hypertension. (c) Atrial septal aneurysm (arrow). (d) Tricuspid regurgitation jet in the same patient wraps around and outlines the atrial septal aneurysm. (e) The bi-caval view obtained at 90° in the upper esophageal position, visualizing the atrial septum. Thinning of the atrial septum is noted in the region of the foramen ovale. (f) Color flow Doppler in the same patient demonstrating a left to right shunt (arrow) in the region of the atrial septum. LA, left atrium; RA, right atrium; SVC, superior vena cava.
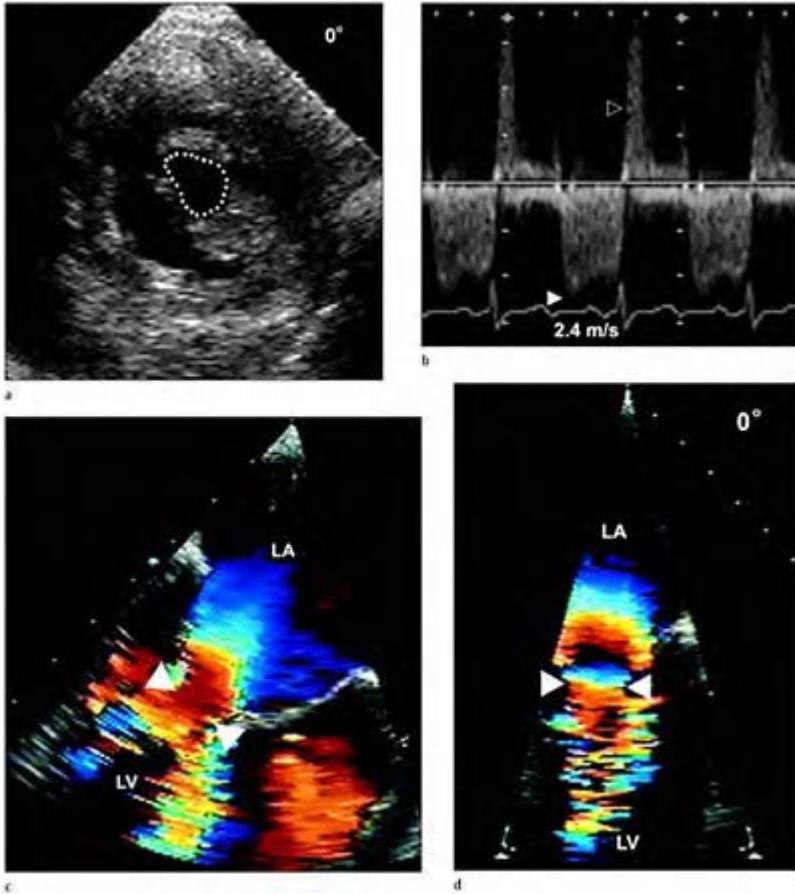
Case 2.12 Measurement of mitral valve area in mitral stenosis. (a) Planimetery of the valve orifice (dotted circle) can be performed in the short-axis views. Care must be taken in order to measure the valve area at the appropriate plane. In addition, heavily calcified valves may produce blooming of the echo interface and obscure the true valve opening, overestimating the severity of stenosis. (b) Continuous wave Doppler through the mitral valve orifice. The maximum and mean gradient, as well as the pressure half-

time may be measured with continuous wave Doppler. A newer method for calculating mitral valve areas utilizes the vena contracta of the stenotic color flow jet. With the vena contracta method, the mitral valve area is calculated by measuring the width of the color flow jet at the level of the stenotic valve orifice (vena contracta) in one (c) or two perpendicular planes (d). LA, left atrium; LV, left ventricle.
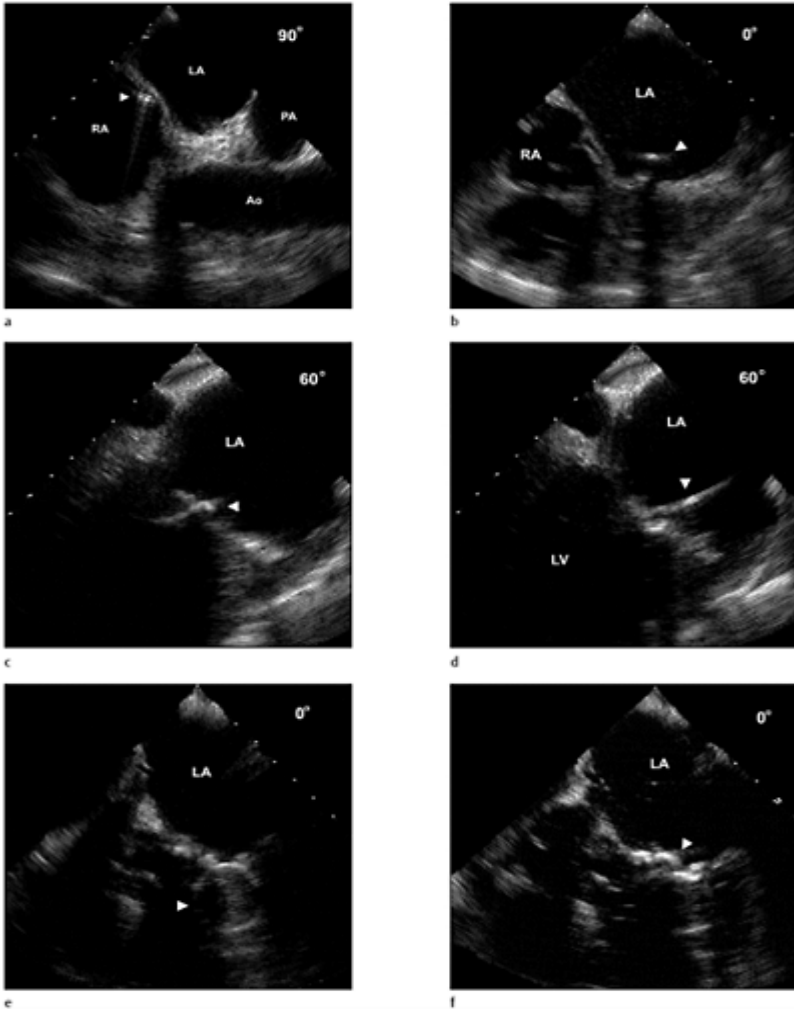
Case 2.13 Multiplane TEE during mitral valvuloplasty.
TEE imaging may be utilized during the balloon
valvuloplasty procedure for the positioning of
catheters, puncturing the atrial septum, determining
balloon sizing and evaluating valve opening and mitral
regurgitation after balloon dilatation. A clear advantage
of multiplane TEE imaging is afforded by rapidly
obtaining multiple views
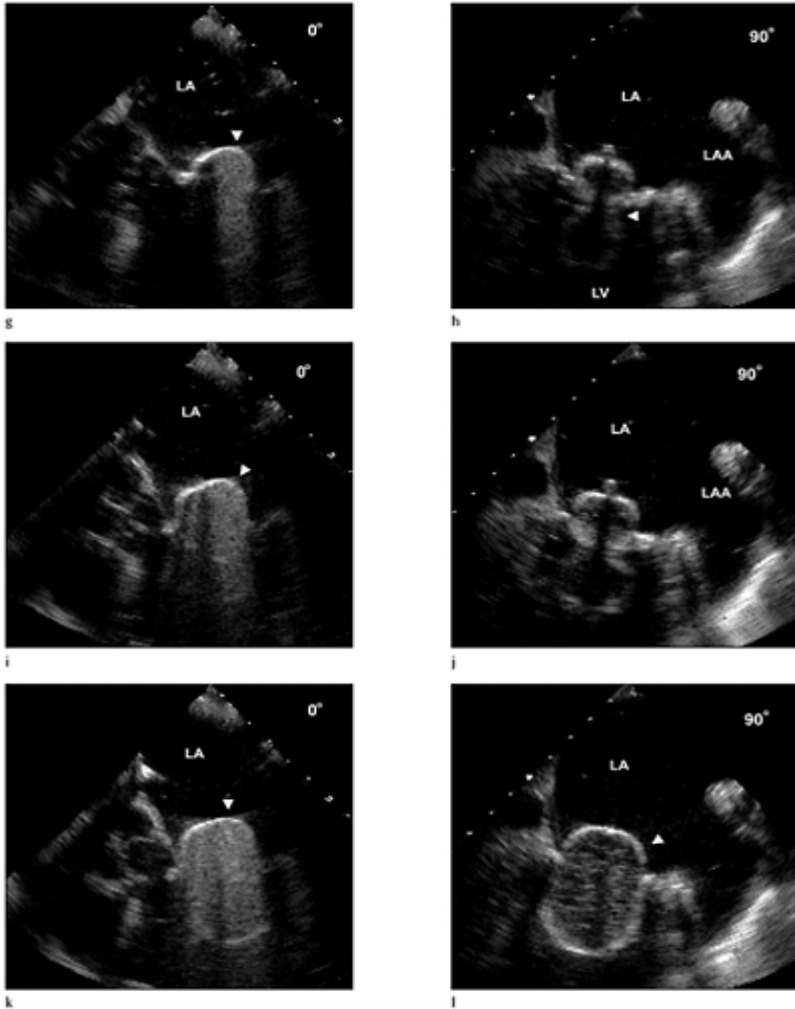
with the least probe manipulation. (a) View of the atrial septum and ideal catheter position (arrow) for crossing the atrial septum. The balloon catheter (arrow) is advanced into the left atrium (b), and across the mitral valve (c) and (d). Proper balloon position (arrow) is confirmed in the stenotic orifice (e) and (f). Progressive inflation of the balloon at 0° and 90° (g–l).
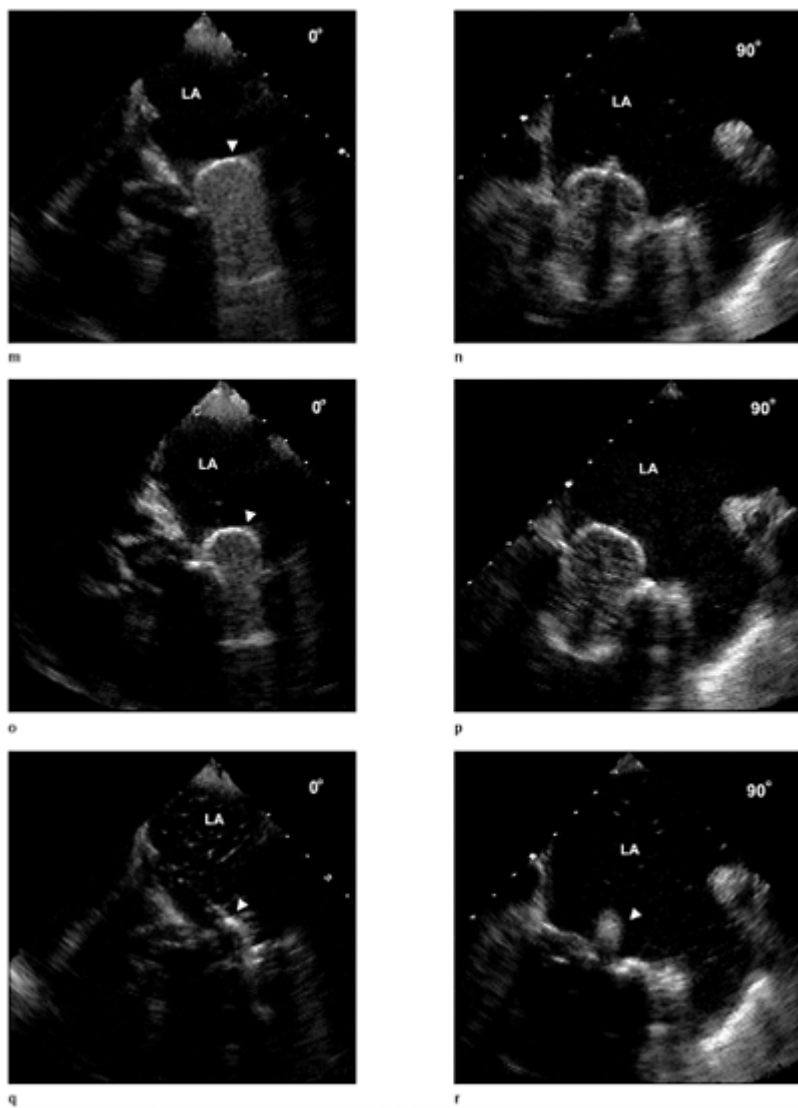
Deflation of the balloon at 0° and 90° (m–r). LA, left atrium; RA, right atrium; Ao, aorta; LV, left ventricle; LAA, left atrial appendage.
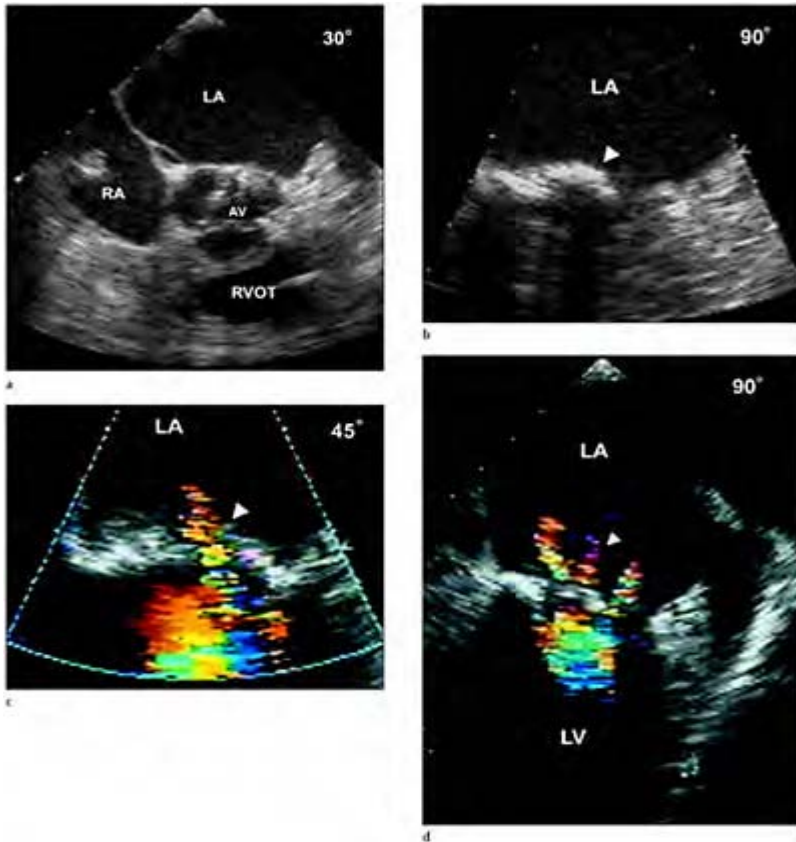
Case 2.14 Following the procedure, a
TEE examination is performed to
determine the development of new
mitral regurgitation and residual
shunting across the atrial septum
following of the catheters. (a) Small
defect in the atrial septum following
the removal of the balloon catheter. (b)
Mitral valve closure, point of leaflet
coaption (arrow). Heavy calcification
is noted in the annular plane. Color
flow doppler demonstrating new mitral
regurgitation at 45° (c) and 90° (d).
LA, left atrium; RA, right atrium;
RVOT, right ventricular outflow tract.
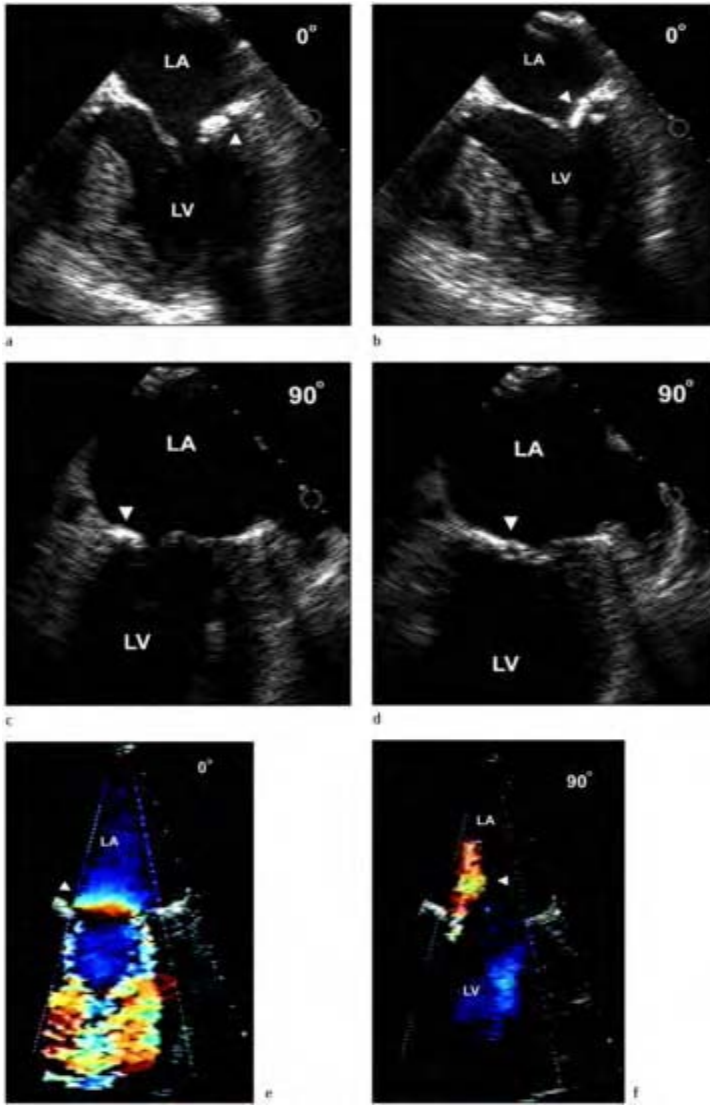
Case 2.15 Mitral annular calcification. Calcification of the posterior mitral annulus (arrow) during diastole (0° (a) and 90° (c)) and systole (0° (b) and 90° (d)). (e) Color flow Doppler through the mitral valve orifice during diastole demonstrating turbulence (arrow) and mild mitral regurgitation (arrow) during systole (f). LA, left atrium; LV, left aventricle.
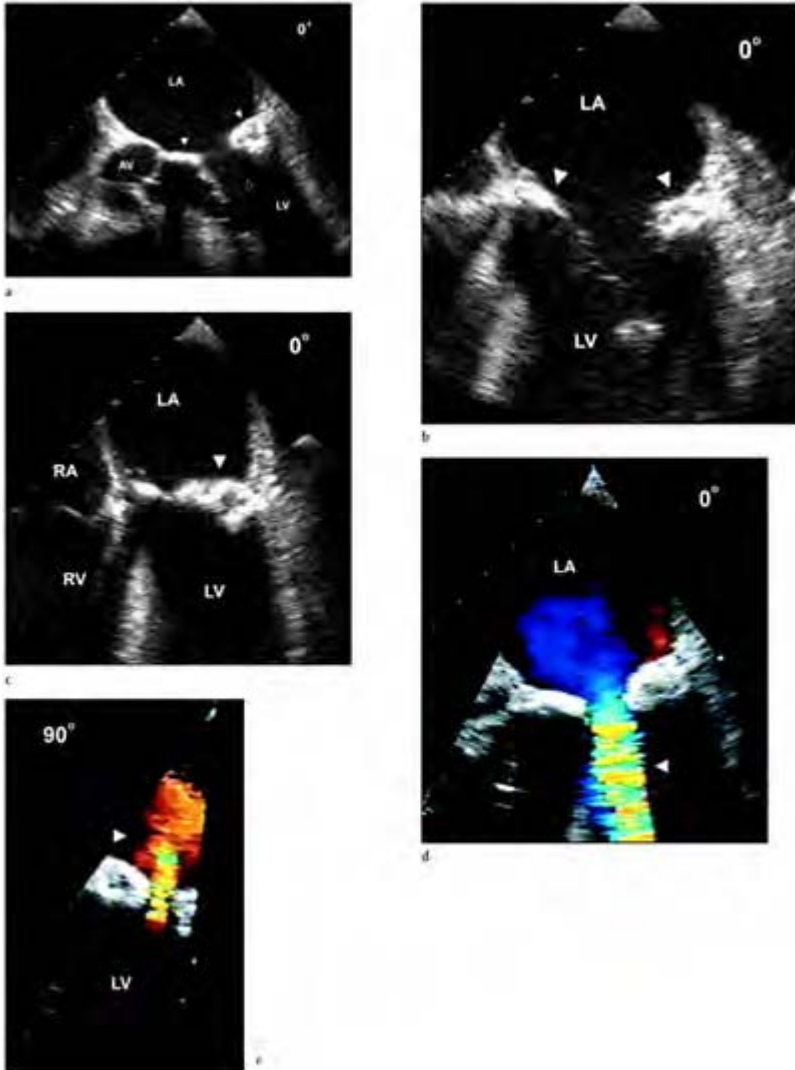
Case 2.16 Severe mitral annular
calcification. (a) Severe calcification of
the anterior and posterior annulus of
the mitral valve (arrows). Calcification
extends in the posterior leaflet. (b)
Adequate motion is exhibited by the
anterior leaflet during diastole,
however, the posterior leaflet appears
severely restricted. (c) During systole

only the annulus is visualized during valve closure. (d) Color flow Doppler recorded during diastole demonstrates a high velocity turbulent jet (arrow), resembling the flow jet of mitral stenosis. (e) Color flow Doppler demonstrating a mitral regurgitant jet (arrow) during systole. LA, left atrium.
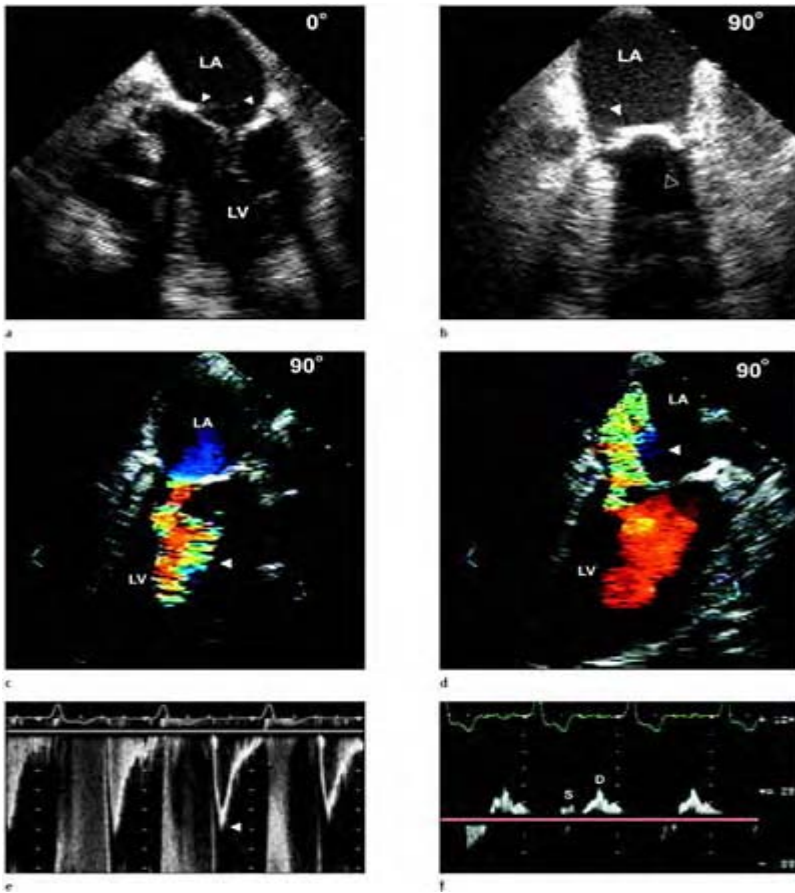
Case 2.17 Severe mitral annular calcification. (a) Severe calcification of the anterior and posterior annulus of the mitral valve (arrows). (b) During systole only the annulus is visualized during valve closure. (c) Color flow Doppler recorded during diastole

demonstrates a high velocity turbulent jet (arrow). (d) Color flow Doppler demonstrating mitral regurgitant jet (arrow) during systole. (e) Pulsed wave Doppler directed by the color flow jet demonstrating increased *e* wave velocity and mitral regurgitation. (f) Pulsed wave Doppler of pulmonary venous flow demonstrating flow reversal during systole suggesting significant mitral regurgitation. S, systolic flow; D, diastolic flow.
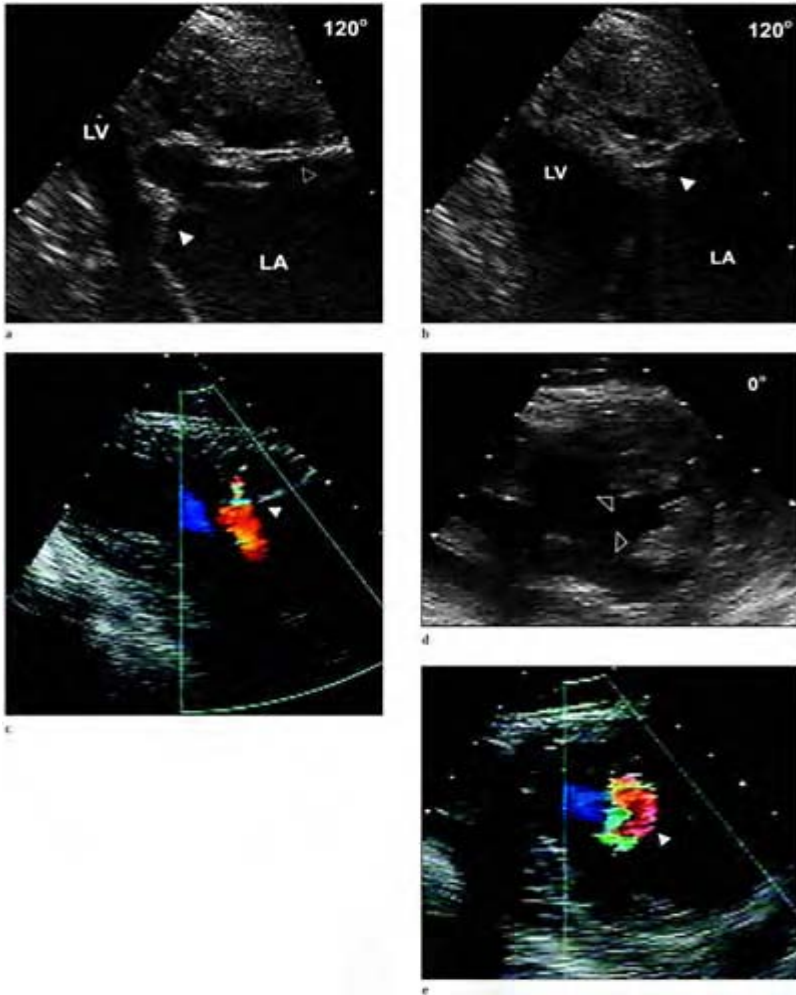
Case 2.18 Parachute mitral valve. Deep transgastric view of the subvalvular apparatus during diastole (a)

and systole (b). Chordae tendineae appear to be attached from only one papillary muscle that originates from the ventricular apex. (c) Color flow Doppler during systole demonstrating the direction of forward flow (arrow) through the mitral apparatus. (d) Short-axis view of the left ventricle at the mid-ventricular level. The papillary muscles are grouped tightly together and originate from the inferior wall. (e) Color flow Doppler demonstrating flow during systole.
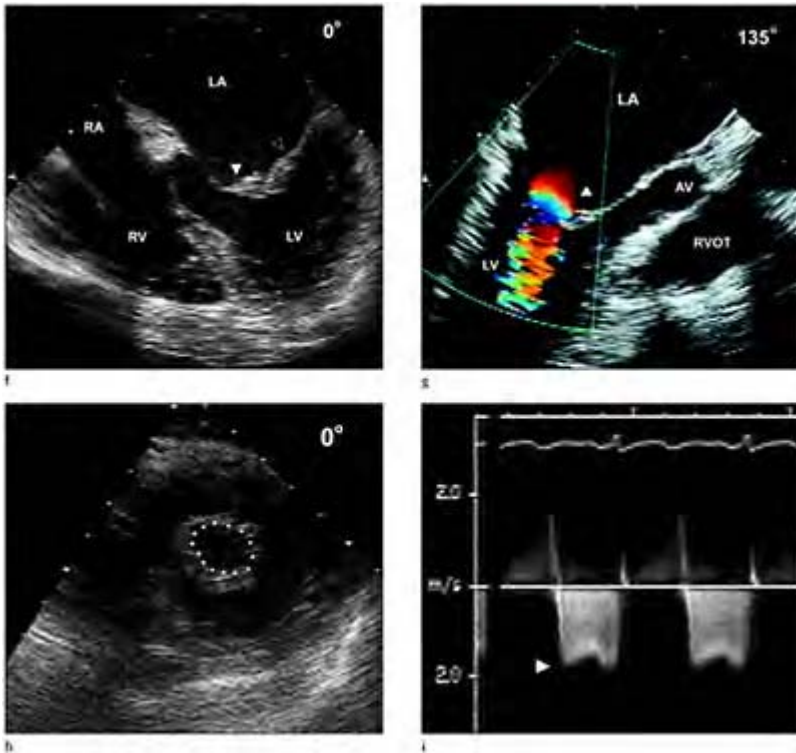
(f) Thickening of the mitral valve leaflets tips is demonstrated during systole. (g) Restricted opening of the mitral valve leaflets demonstrated by diastolic doming and high velocity color flow through the mitral valve orifice. (h) Short axis demonstrating the restricted valve area of the mitral

valve. (i) Continuous wave Doppler of the left ventricular inflow tract demonstrating a 2m/sec flow velocity across the mitral valve. LA, left atrium; LV, left ventricle; AL, anterior leaflet; PL, posterior leaflet.
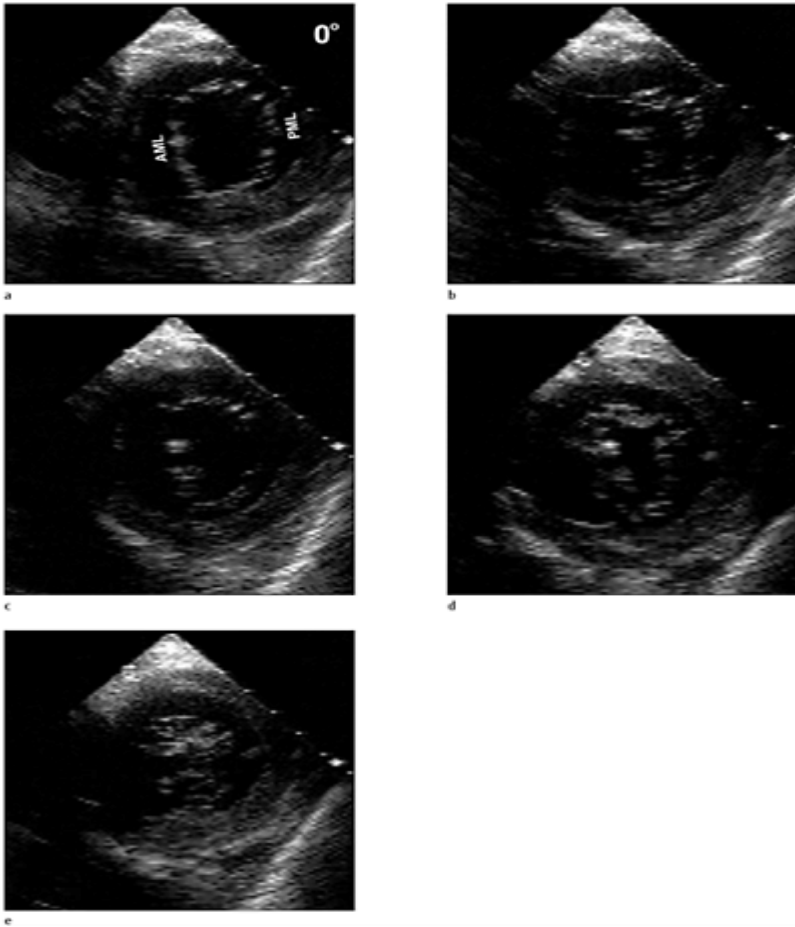
Case 2.19 Mitral annular dilatation. Short-axis echocardiographic images of the mitral valve recorded through diastole to systole. (a) Early diastole. (b) Mid diastole. (c) Atrial systole. (d) End diastole. (e) End systole. AML, anterior leaflet; PML, posterior leaflet.
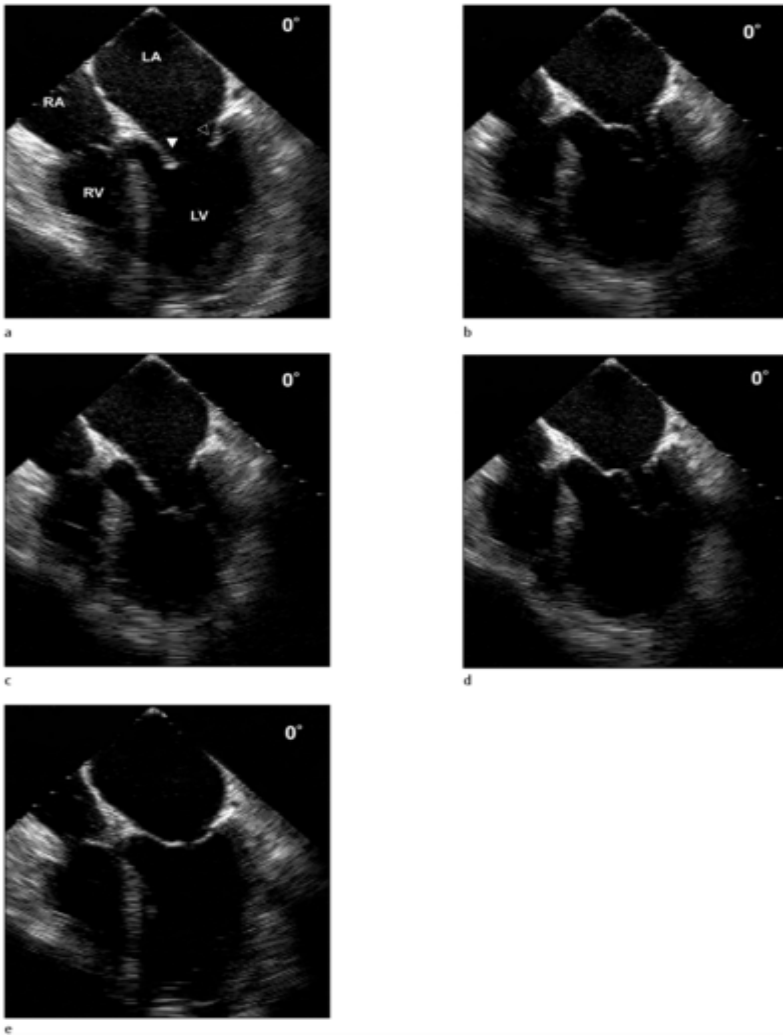
Case 2.20 Mitral annular dilatation. Four-chamber view from the lower esophageal window at 0°. Note mitral valve leaflet motion appears normal in this view, anterior leaflet (solid arrow) and posterior leaflet (open arrow). The only noticeable abnormality is mild annular dilatation. (a) Early diastole. (b) Mid diastole. (c) Atrial systole. (d) End diastole. (e) End systole. RA, right atrium; LA, left atrium; RV, right ventricle; LV, left ventricle.
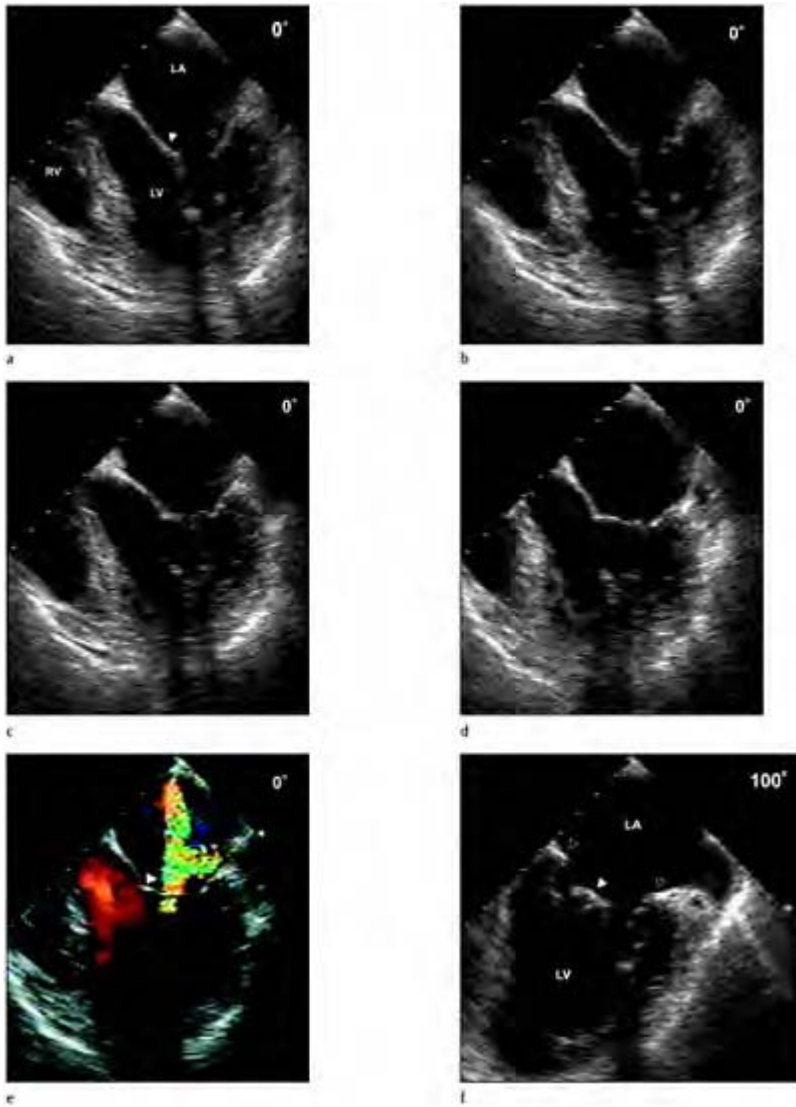
Case 2.21 Mitral annular dilatation. Mitral leaflet motion appears normal, however the leaflets appear small during closure in relation to the enlarged mitral annulus. (a) Early diastole. (b) Mid diastole. (c) End diastole. (d) End systole. (e) Systolic frame demonstrating a centrally directed mitral regurgitation (arrow) jet with color flow Doppler. (f) Early diastole.
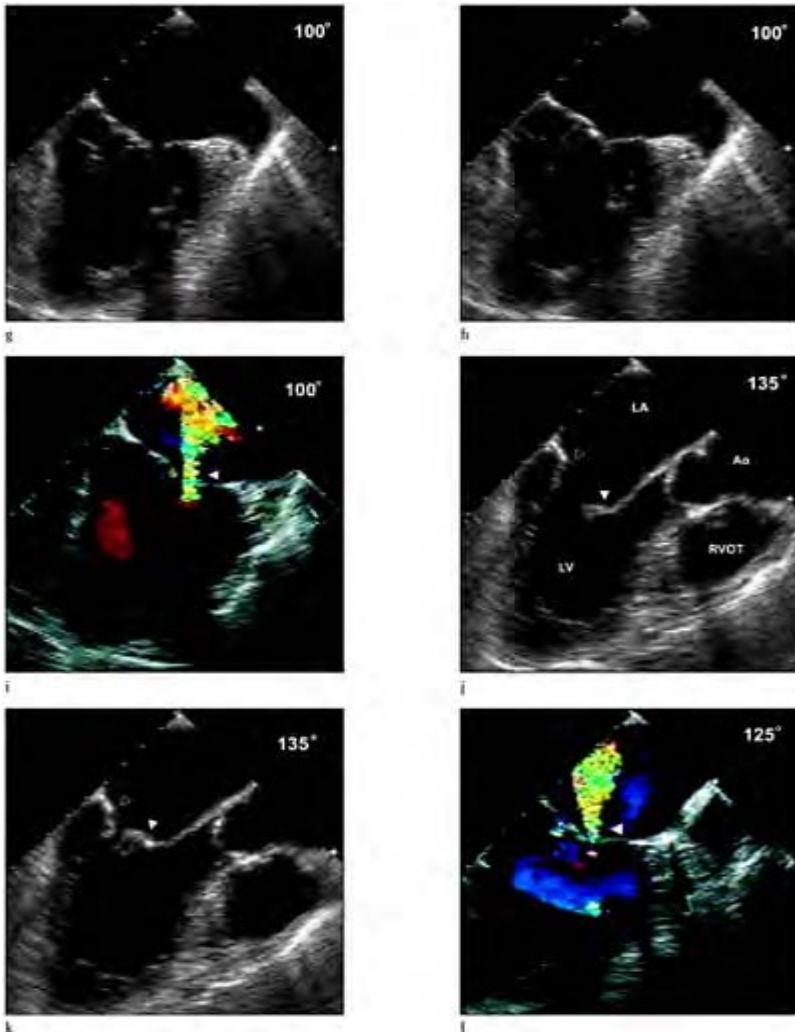
(g) Mid diastole. (h) Systole. (i) Color Doppler during systole demonstrating a central mitral regurgitant jet. (j) Diastolic frame at 125°. (k) Systolic frame at 125°. (l) Color Doppler during systole demonstrating a central mitral regurgitant jet. A, anterior leaflet (solid arrow); P, posterior leaflet (open arrow); LV, left ventricle; LA, left atrium; Ao, aorta; RVOT, right ventricular outflow tract; RV, right ventricle.
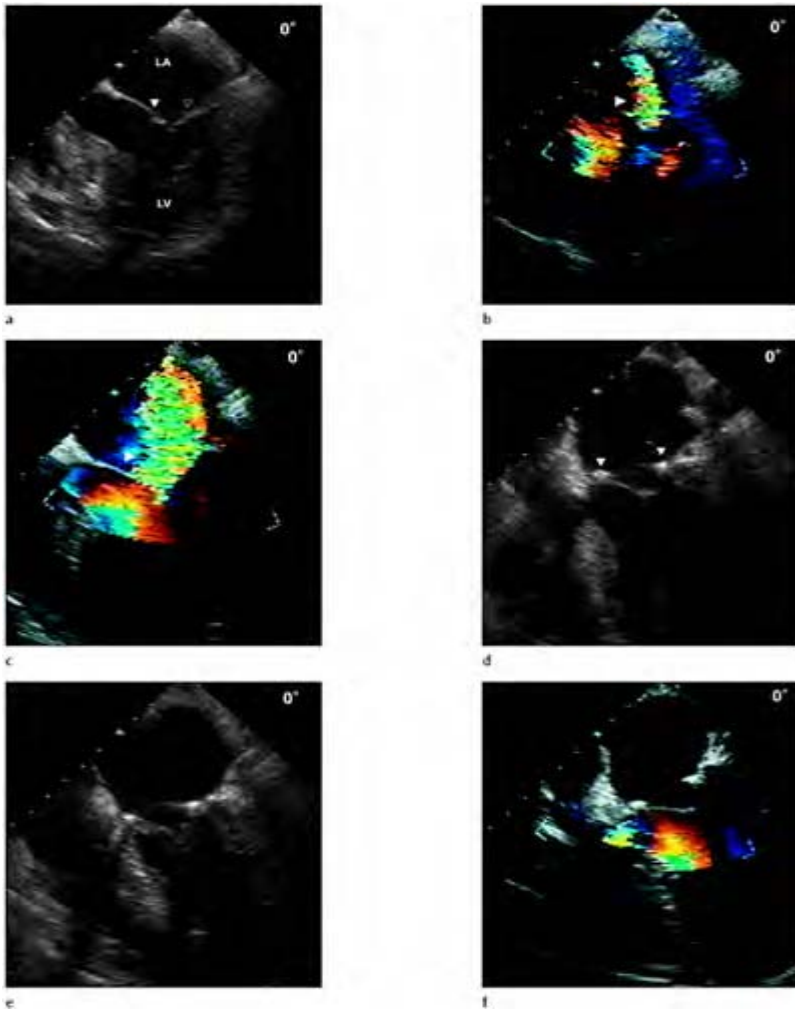
Case 2.22 Mitral annular dilatation. (a) Systolic frame demonstrating annular dilatation. (b) Mild mitral regurgitation (arrow). (c) Severe mitral regurgitation (arrow) with pharmacological provocation. (d) Diastolic frame of mitral annuloplasty ring (arrows) following mitral repair. (e) Systolic frame following mitral repair. (f) Color flow Doppler recorded during systole with trace mitral regurgitation (arrow). LA, left atrium; LV, left ventricle; AML, anterior leaflet (solid arrow); PML posterior leaflet (open arrow).
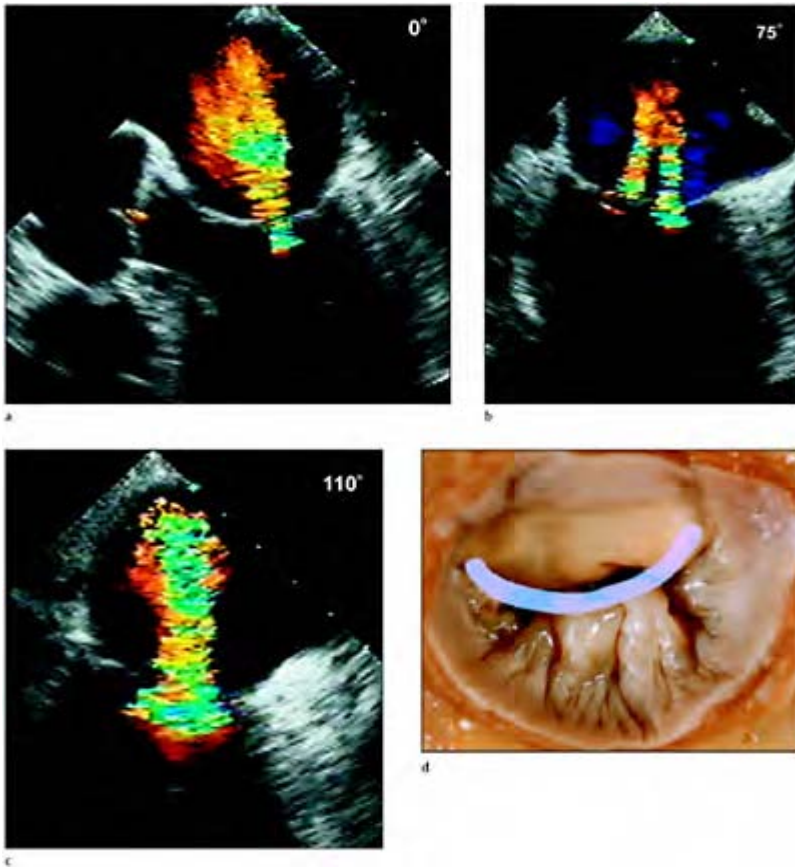
Case 2.23 Mitral annular dilatation and mitral regurgitation. (a) Color flow Doppler demonstrating a centrally directed regurgitant jet with annular dilatation viewed at 0°. (b) When viewed at 75°, the centrally directed jet is demonstrated as two separate jets. With annular dilatation two regurgitant jets are frequently seen originating from both corners of the valve. (c) A single regurgitant jet is again visualized at 110°. (d) Anatomical specimen of the mitral valve illustrating the line of closure. With annular dilatation, one or multiple jets can originate anywhere along the line of closure most frequently in the corners of the leaflets near the commissures.
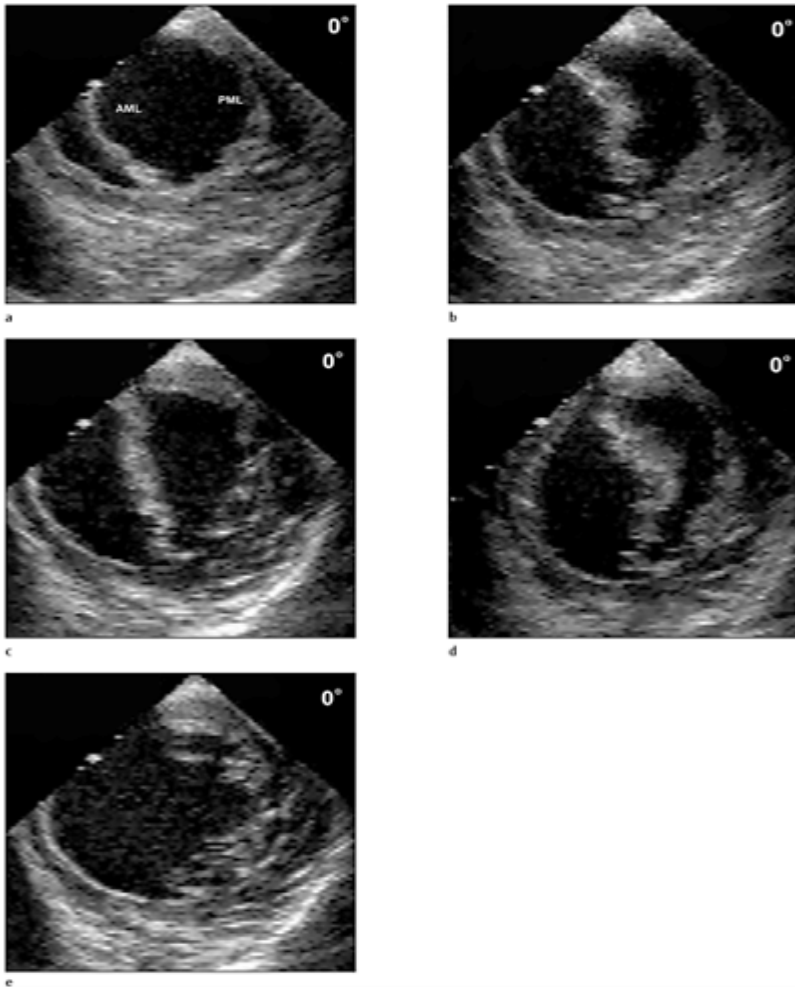
Case 2.24 Mitral valve prolapse. Short-axis echocardiographic images of the mitral valve recorded from diastole through systole. In all stages of the cardiac cycle the valve motion appears distorted and valve opening more circular than with normal motion. This may also be attributed to annular dilatation, which frequently accompanies prolapse. Maximum valve opening occurs during early diastole and not during atrial systole. (a) Early diastole. (b) Mid diastole. (c) Atrial systole. (d) End diastole. (e) End systole. AML, anterior leaflet; PML, posterior leaflet.
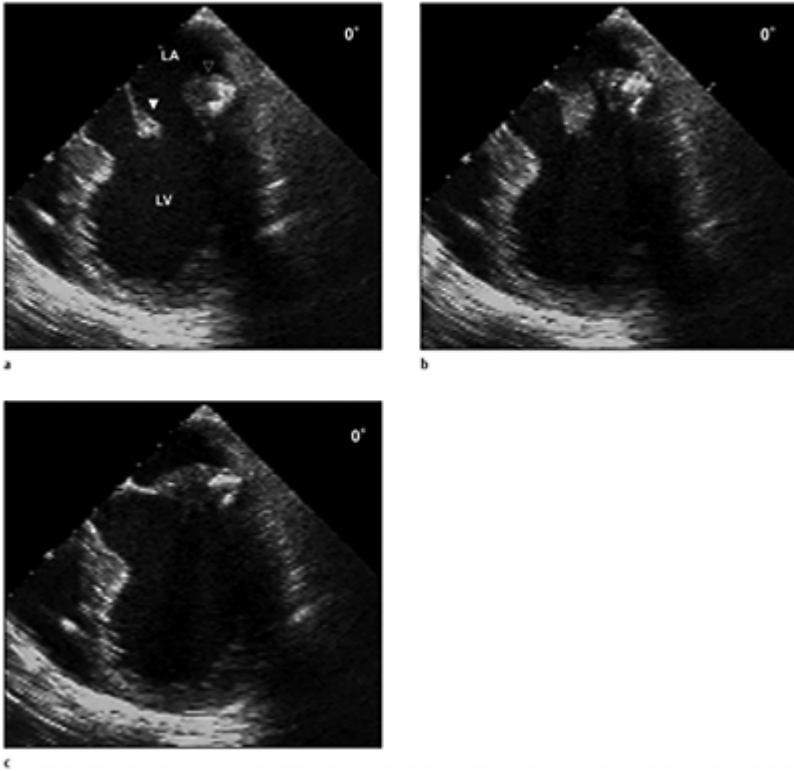
Case 2.25 Mitral valve prolapse. Views obtained from the lower esophageal window at 0° from diastole to systole. (a) Early diastole. (b) End diastole. (c) Systole. The mitral valve appears thickened especially near the leaflet tips throughout the cardiac cycle, consistent with myxomatous degenerative changes in the leaflet tissue. In addition there is mild mitral annular calcification noted in the posterior annulus. LA, left atrium; LV, left ventricle.
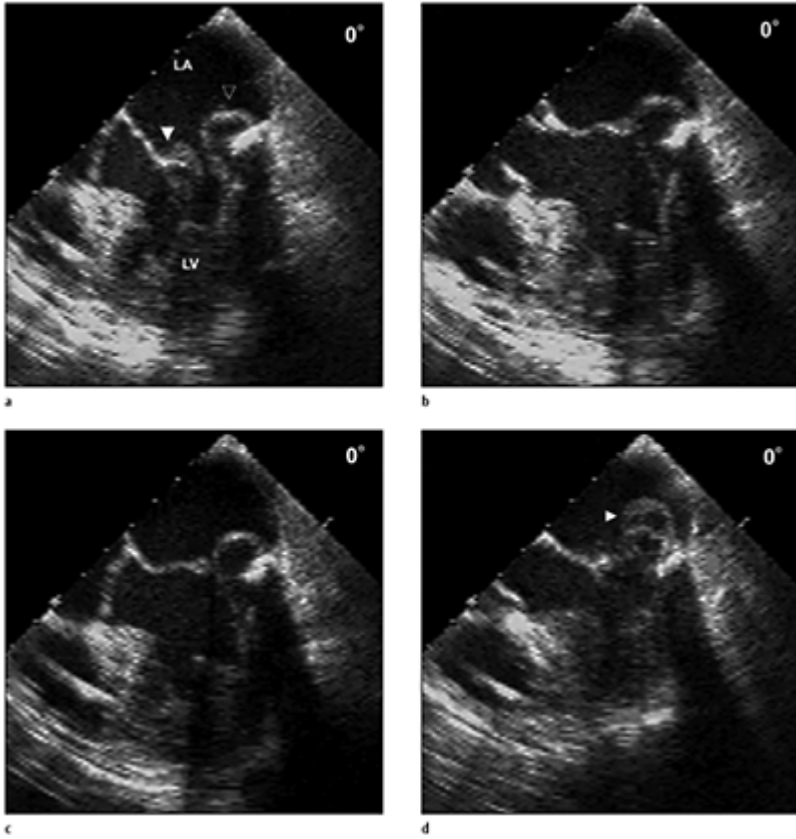
Case 2.26 Mitral valve prolapse.
Views obtained from the lower
esophageal window at 0° from diastole
to systole (a–d). The mitral leaflets
appear markedly thickened in all
views, with billowing of the leaflet
tissue into the left atrium. The lack of
leaflet coaption or prolapse of the
posterior leaflet is demonstrated in the
systolic frame (d). LA, left atrium; LV,
left ventricle; AML, anterior leaflet
(closed arrow); PML, posterior leaflet
(open arrow).
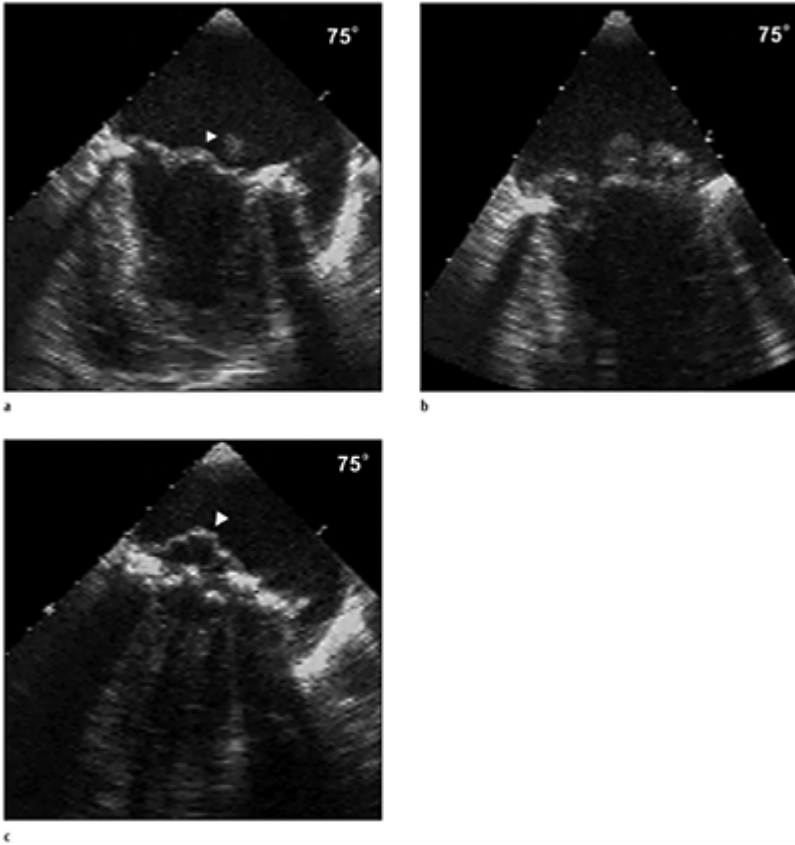
Case 2.27 Mitral valve prolapse. Views obtained from the lower esophageal window at 75° from diastole to systole (a–c), in the same patient as in Case 26. Marked billowing (arrows) of the posterior leaflet superimposed on the plane of the anterior mitral leaflet.
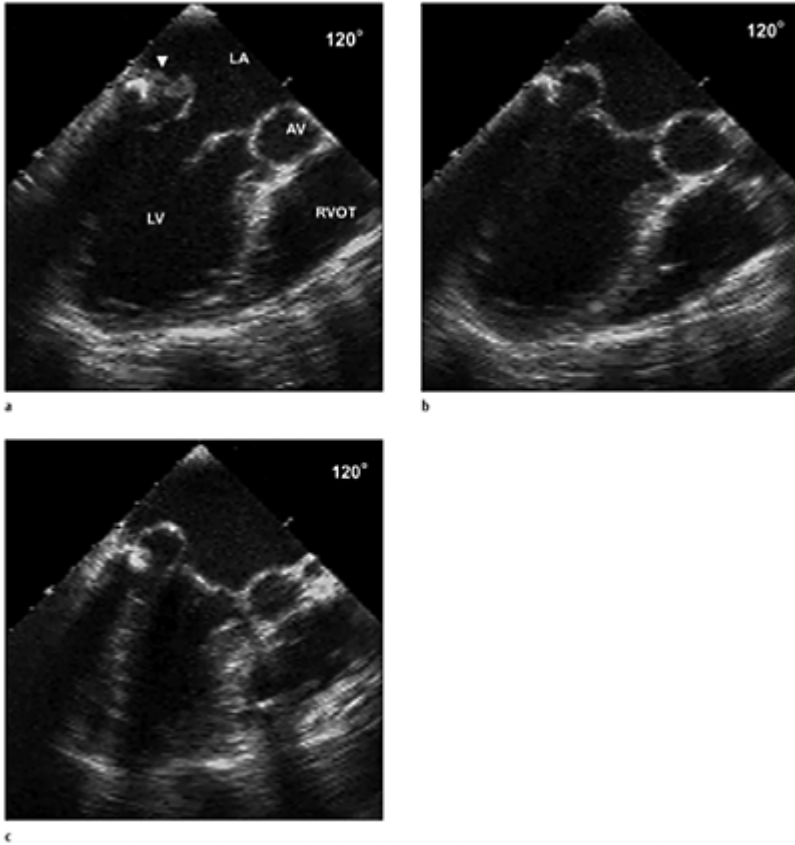
Case 2.28 Mitral valve prolapse. Views obtained from the lower esophageal window at 120° from diastole to systole (a–c), in the same patient as in Case 26. Marked billowing (arrows) of the posterior leaflet superimposed on the plane of the anterior mitral leaflet. LA, left atrium; LV, left ventricle; RV, right ventricle.
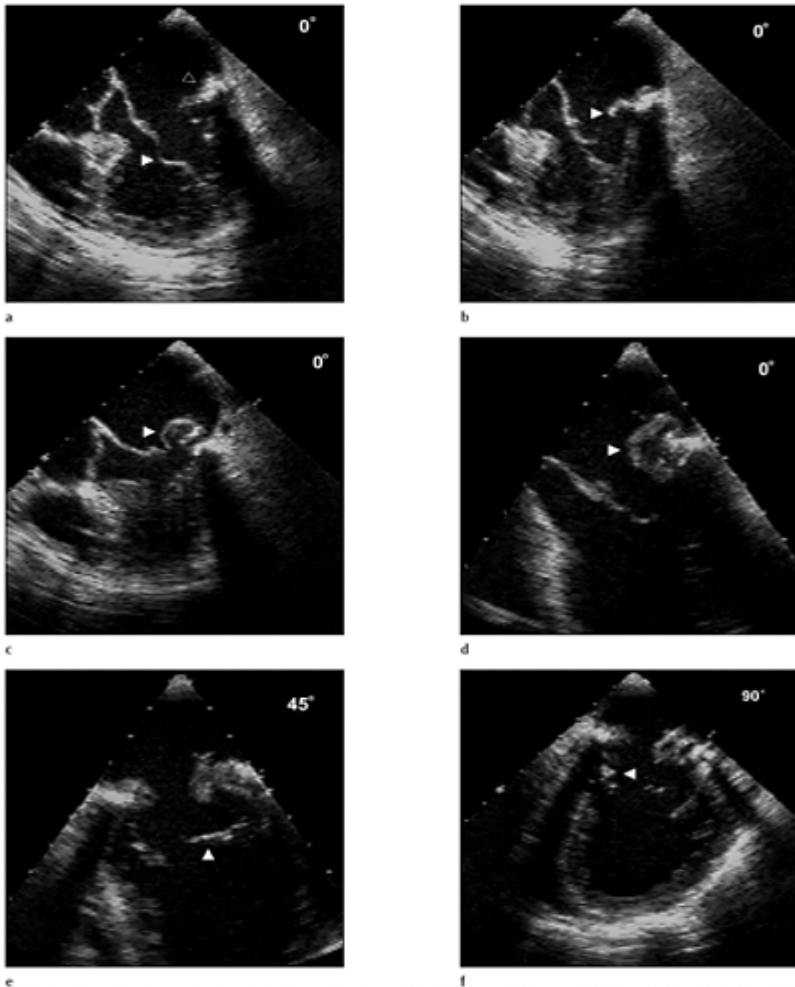
Case 2.29 Associated findings in mitral valve prolapse. (a) Mitral annular calcification (solid arrow) and elongated redundant chordae of the anterior leaflet (open arrow). (b–d) Ruptured chordae tendineae and flail posterior leaflet segment (arrows). (e) Ruptured chordae (arrow) noted in the left ventricle. (f) Calcified chordae tendineae (arrow) of the posterior leaflet. LA, left atrium; LV, left ventricle; AV, aortic valve; RVOT, right ventricular outflow tract.
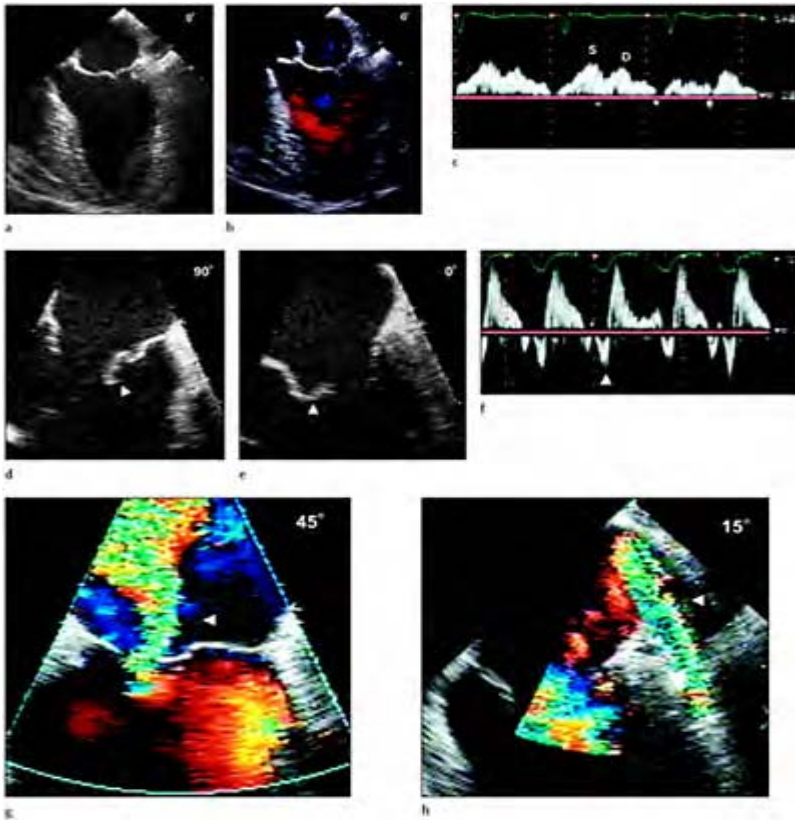
Case 2.30 Mitral valve prolapse with a ruptured
anterior leaflet chordae tendineae occurring
immediately following cardiopulmonary bypass. (a)
Systolic frame demonstrating valve closure. (b) Color
flow Doppler demonstrating mild regurgitation. (c)
Pulsed Doppler recording the pulmonary vein
demonstrating normal systolic (S) and diastolic (D)
flow profiles. Immediately following weaning from
cardiopulmonary bypass, enlarged views of the anterior
mitral leaflet at 0° (d) and 90° (e) demonstrating a
ruptured chordae (arrow). (f) Pulsed Doppler recording
of the pulmonary vein demonstrating systolic flow
reversal (arrow) and predominance of diastolic flow,
suggesting severe regurgitation. Color flow Doppler of
a new posteriorly directed mitral regurgitant jet at 45°
(g) and 15° (h).
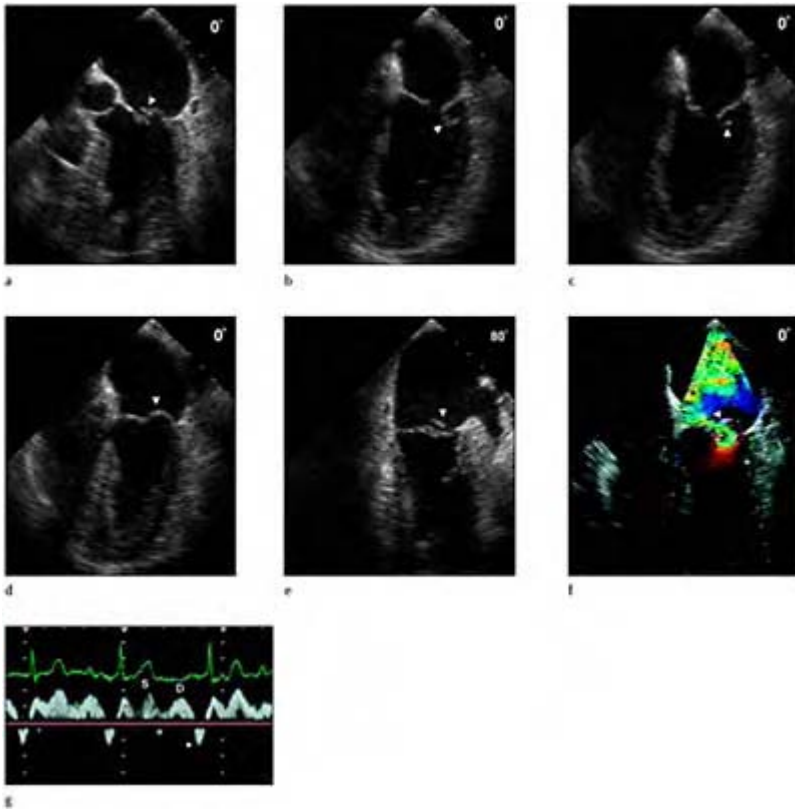
Case 2.31 Ruptured chordae tendineae to the posterior leaflet. The ruptured chordae (arrow) is demonstrated freely moving from the left ventricle to the left atrium during the cardiac cycle. Views obtained from systole to diastole (a–d) at 0°. (e) Systolic frame at 90° demonstrating the rupture chord prolapsing freely into the left atrium. (f) Color flow Doppler at 0° demonstrating an anterior directed mitral regurgitant jet (arrow). (g) Pulsed wave Doppler recording of pulmonary venous flow demonstrating a nearly normal pulmonary venous flow despite a significant regurgitant jet. S, systolic flow; D, diastolic flow.
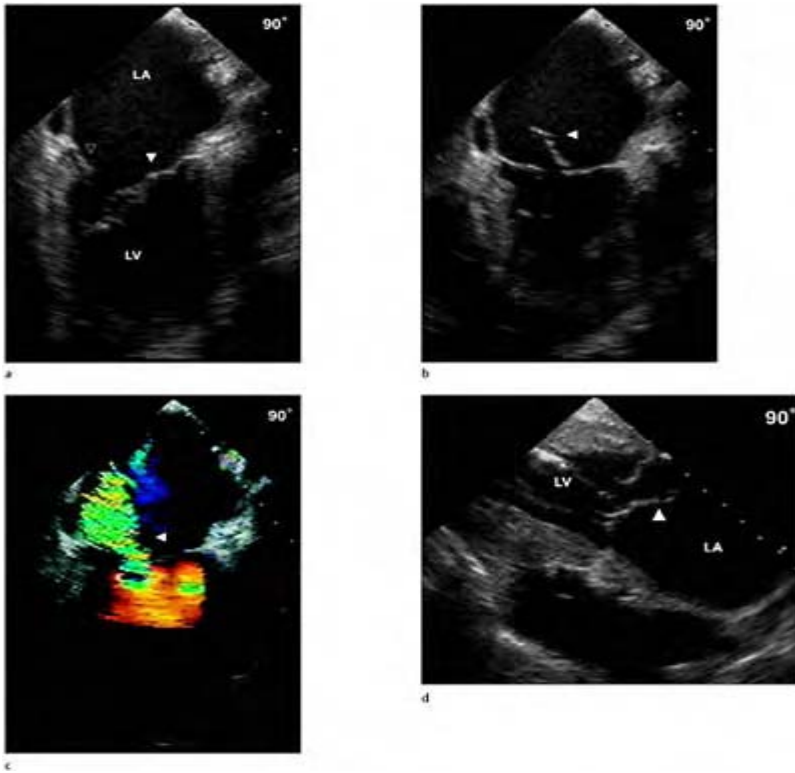
Case 2.32 Ruptured chordae tendineae. (a) Diastolic frame from the lower esophageal window at 90° demonstrates a large left atrium and normal valve opening. (b) Systolic frame demonstrates the ruptured chord (arrow) projecting into the left atrium. (c) Systolic frame with color flow Doppler yields moderate mitral regurgitation (arrow). Although the jet appears to be directed posteriorly in this view, it is tempting to label the ruptured chord to the anterior leaflet, however the ruptured chord was attached to the posterior leaflet. (d) Gastric view at 90° demonstrates the ruptured chord projecting into the left atrium. The gastric and deep transgastric views are extremely useful for evaluating the subvalvular apparatus when there are questions from the other views. LA, left atrium; LV, left ventricle; AML, Anterior leaflet (closed arrow); PML, Posterior leaflet (open arrow).
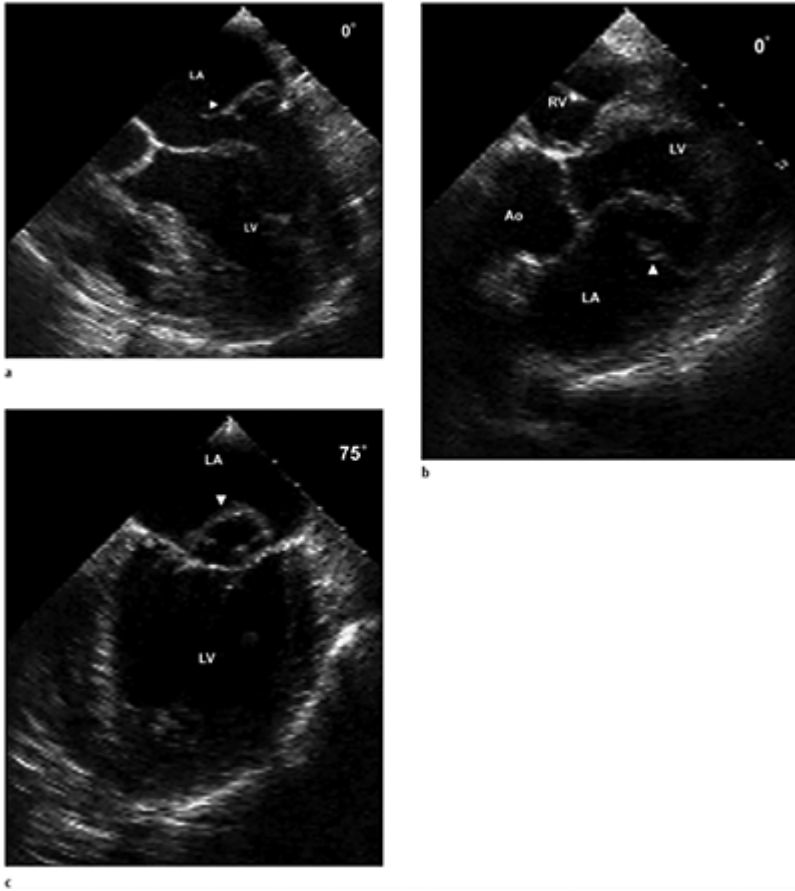
Case 2.33 Ruptured chordae tendineae with a flail posterior leaflet. To construct a mental three-dimensional image, multiple views may be necessary to demonstrate all of the associated pathology especially when describing the abnormalities prior to mitral valve repair. (a) Systolic frame from the lower esophageal window at 0° demonstrating a ruptured chordae and flail posterior leaflet (arrow). (b) Systolic frame from the deep transgastric window at 0° demonstrating the ruptured chordae. (c) Systolic frame from the lower esophageal window demonstrating marked billowing of the P2 or central scallop (arrow) of the posterior leaflet superimposed on a normal anterior leaflet.
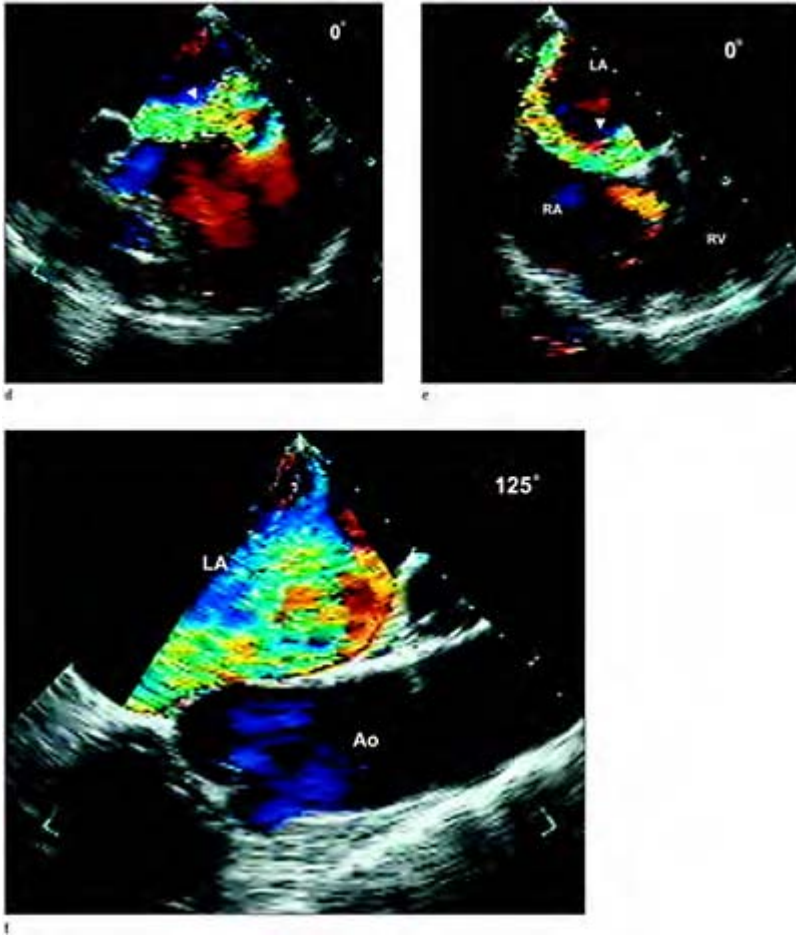
(d) Color flow Doppler from the lower esophageal window at 0° demonstrating severe mitral regurgitation directed anteriorly towards the atrial septum. (e) Color flow Doppler after sight withdrawal and rightward rotation of the probe demonstrates the mitral regurgitant jet hugging the atrial septum and wrapping around the atrium. (f) Color flow Doppler of the severe mitral regurgitant jet obtained at 125°. LA, left atrium; LV, left ventricle; Ao, aorta; RA, right atrium; RV, right ventricle.
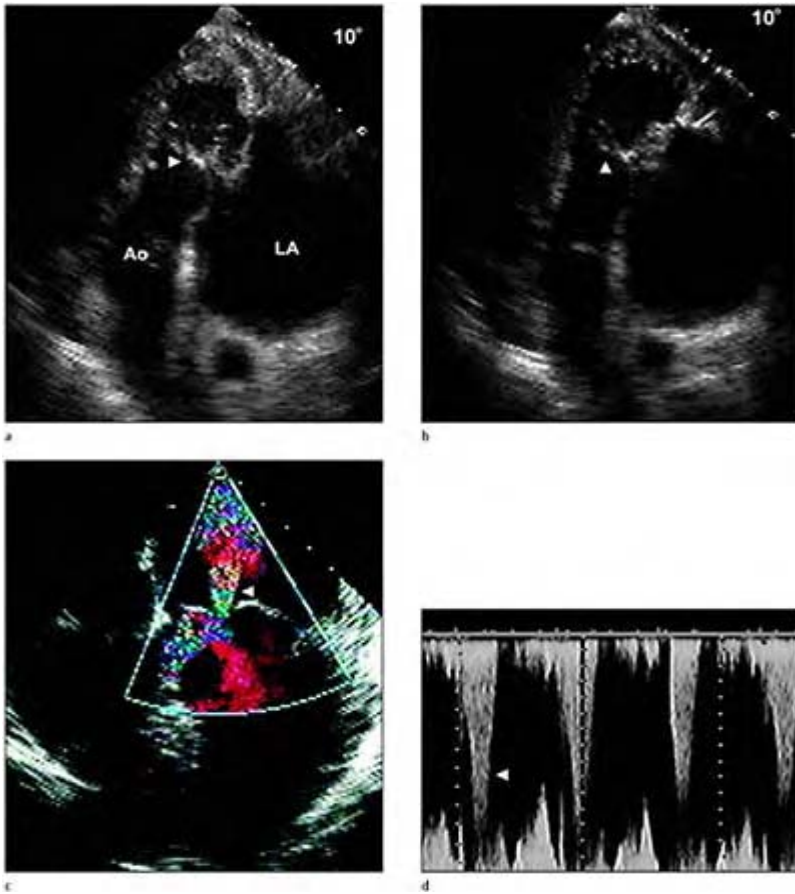
Case 2.34 Mitral valve prolapse and SAM. (a) End-diastolic frame from the deep transgastric window at 10°, demonstrating elongated and thickened chords (arrow). (b) Systolic frame demonstrating systolic anterior motion or SAM (arrow). (c) Color flow Doppler from the lower esophageal window at 0° demonstrating billowing and prolapse of the mitral valve leaflets with associated mitral regurgitation and accelerated and disturbed flow in the left ventricular outflow tract. (d) Continuous wave Doppler obtained from the deep transgastric window demonstrating high velocity flow in the outflow tract.
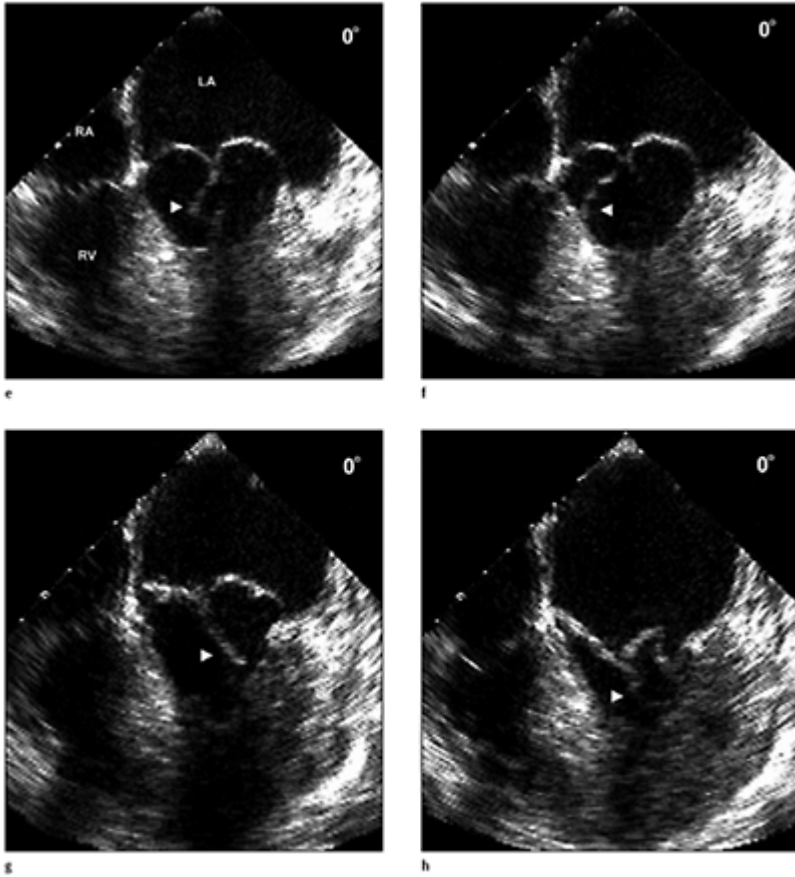
(e–h) Systolic frames obtained from
the lower esophageal window at 0°
with anteflexion of the probe
highlights the systolic motion of the
chordae tendineae throughout systole
(arrows). Marked billowing of both
mitral leaflets is noted in all frames
with prolapse of the posterior leaflets
demonstrated in (h).
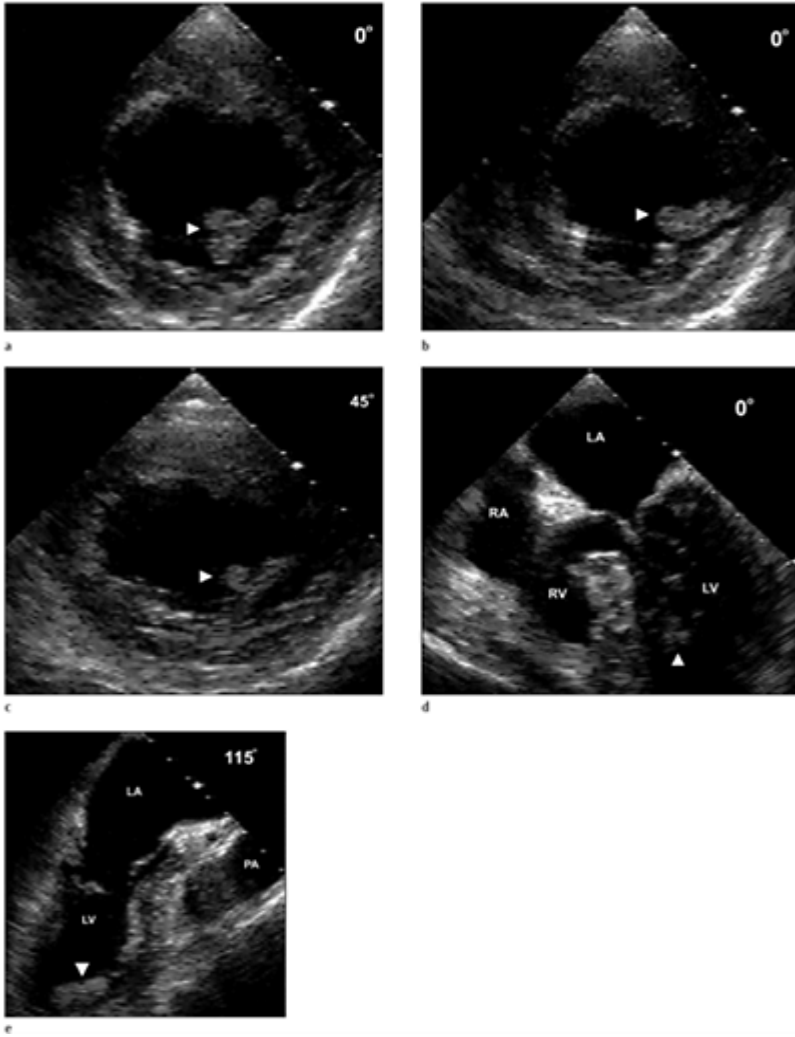
Case 2.35 Ruptured papillary muscle. (a) Diastolic frame from the short axis view at the mid ventricular level, 0°, demonstrates partial rupture of the anterior papillary muscle. (b) Systolic frame demonstrating partial rupture of the papillary muscle. (c) Diastolic frame at 45° demonstrates the chaotic motion of the papillary muscle. Systolic frame from the lower esophageal window at 0° (d), 110° (e) and 90° (f) demonstrates multiple echodensities (arrow) near the papillary muscle.
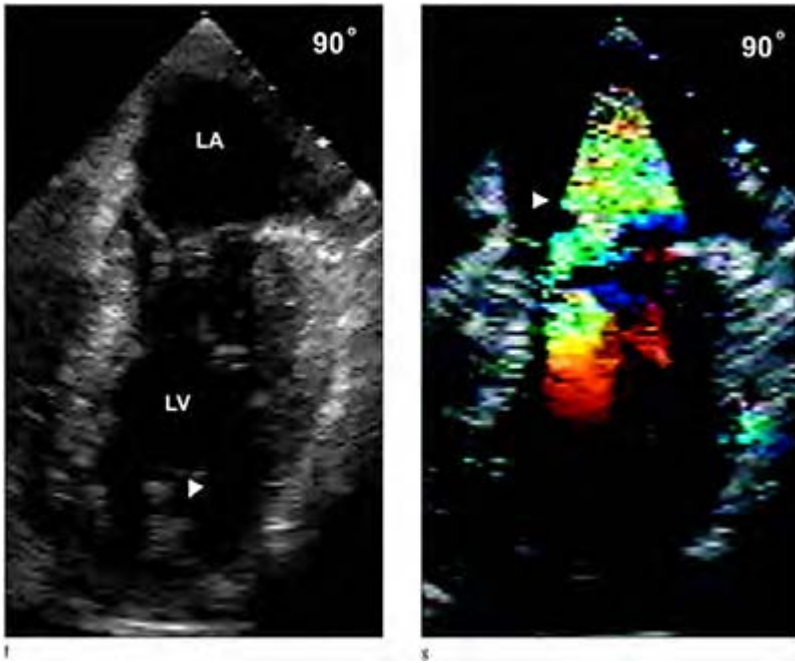
Although partial rupture of the papillary muscle usually produces dramatic mitral regurgitation (g), careful inspection of the papillary muscles must be performed in multiple views to document the defect. In addition to the papillary muscle abnormality, the anterior left ventricular wall was noted to be severely hypokinetic. Although partial rupture of a papillary muscle may be suggested by transthoracic imaging, the definitive diagnosis of partial rupture of a papillary muscle is made with TEE. LA, left atrium; LV, left ventricle; RA, right atrium; RV, right ventricle.
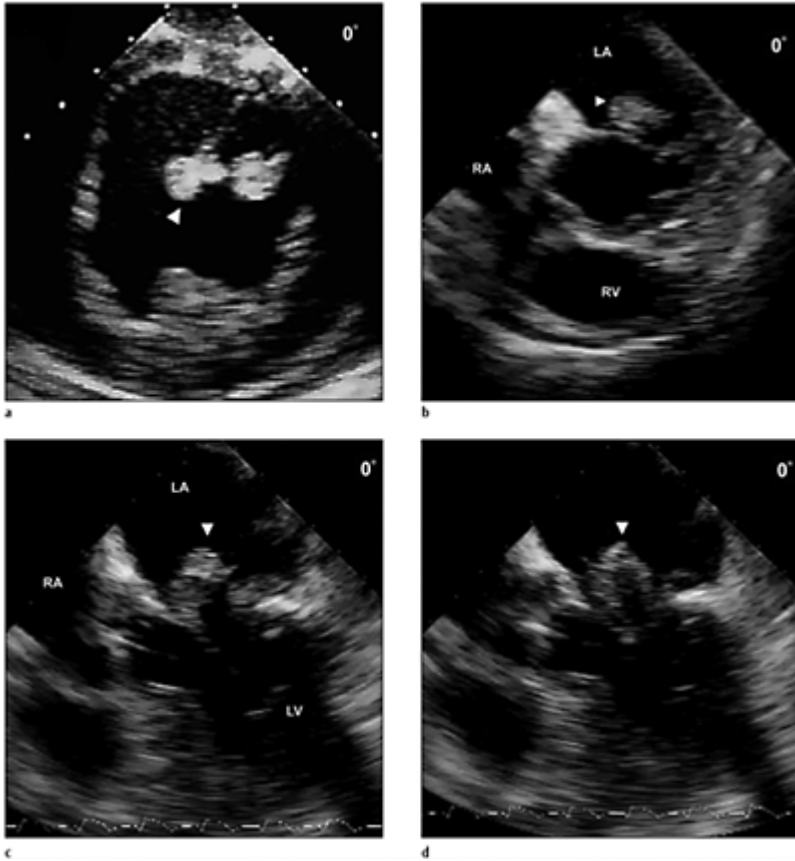
Case 2.36 Ruptured papillary muscle. (a) Mid-ventricular short-axis view demonstrates a freely, floating posterior papillary muscle in diastole. (b) Systolic frame from the mid-esophageal window of the base of the heart demonstrates the papillary muscle (arrow) prolapsing into the left atrium above the mitral valve annular plane. (c,d) Systolic frames from the lower esophageal window at 0° illustrating the ruptured papillary muscle (arrow) prolapsing through the mitral valve plane.
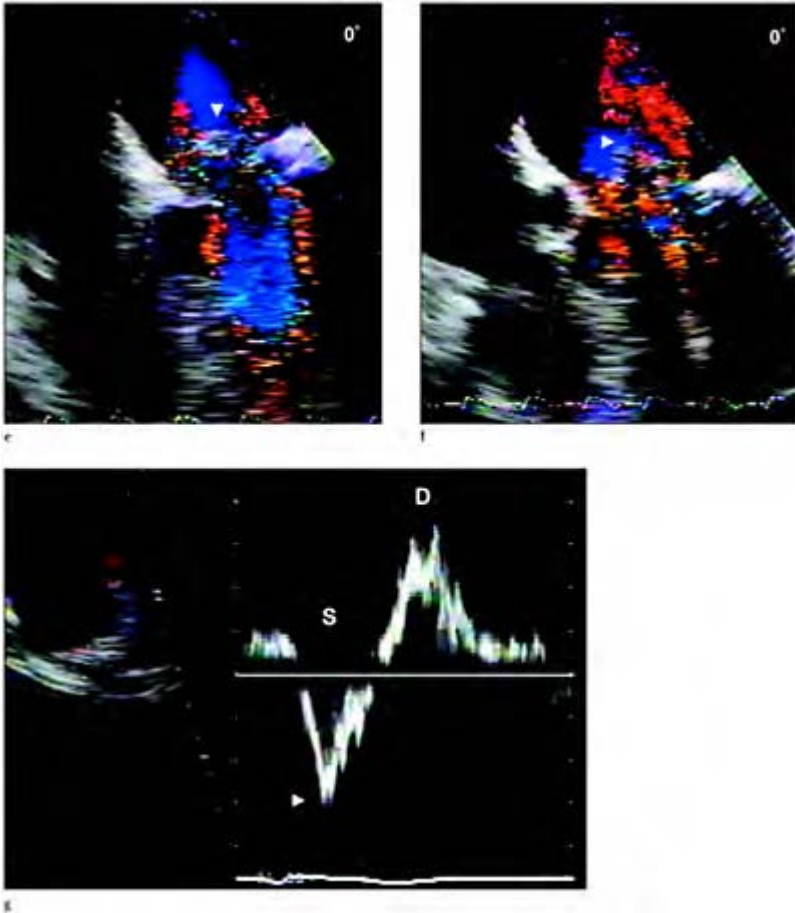
(e,f) Color flow Doppler demonstrating mitral regurgitation associated with the ruptured papillary muscle. (g) Pulsed wave Doppler of the left upper pulmonary vein demonstrating systolic (S) flow reversal (arrow) and diastolic (D) flow predominance suggesting severe mitral regurgitation. LA, left atrium; LV, left ventricle; RA, right atrium.
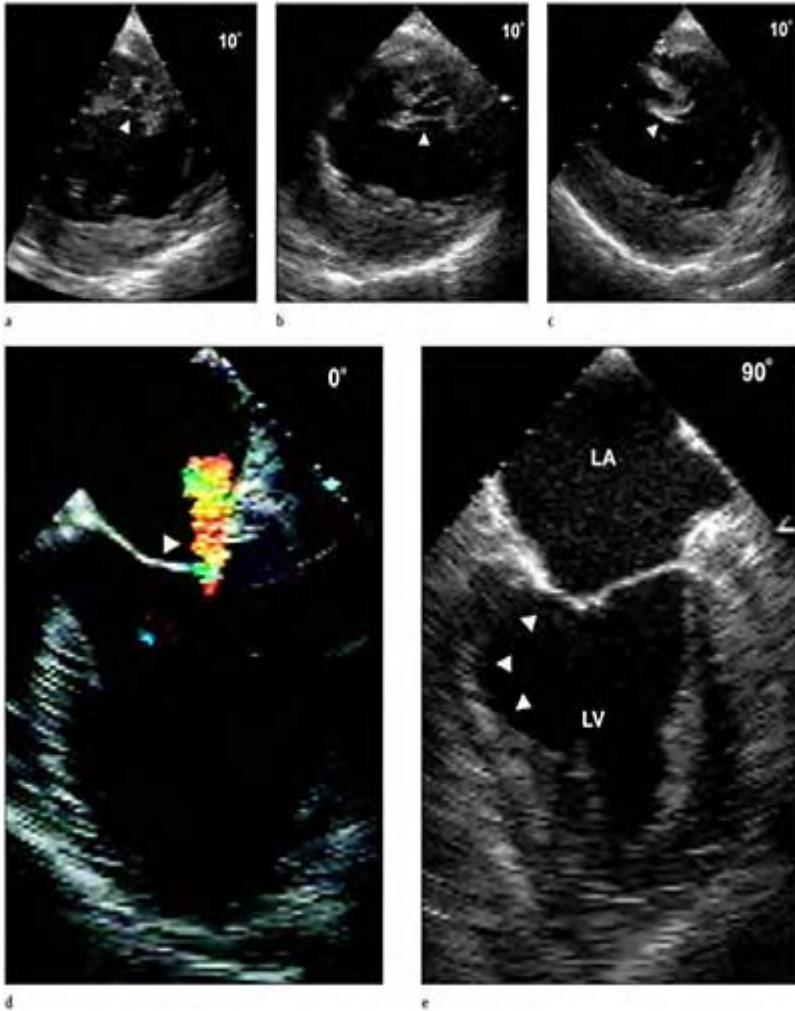
Case 2.37 Papillary muscle
hemorrhage. (a–c) Short-axis views at
the mid-ventricular level at 10°
demonstrating hemorrhage of the
posterior papillary muscle during the
cardiac cycle. The papillary muscle
appears enlarged with multiple cystic,
echo free areas within the confines of
the papillary muscle. (d) Color flow
Doppler demonstrating mitral

regurgitation associated with the dysfunction of the papillary muscle. (e) Systolic frame from the lower esophageal window at 90° highlights a posterior wall infarction and small ventricular aneurysm (arrows) of that area. Papillary muscle hemorrhage usually produces mitral regurgitation through restriction of leaflet motion (type III) rather than by prolapse of the leaflet as associated with rupture or partial rupture of the papillary muscle. Similarly to partial rupture of a papillary muscle, the resolution provided with TEE is needed for a definitive diagnosis. LA, left atrium; LV, left ventricle.
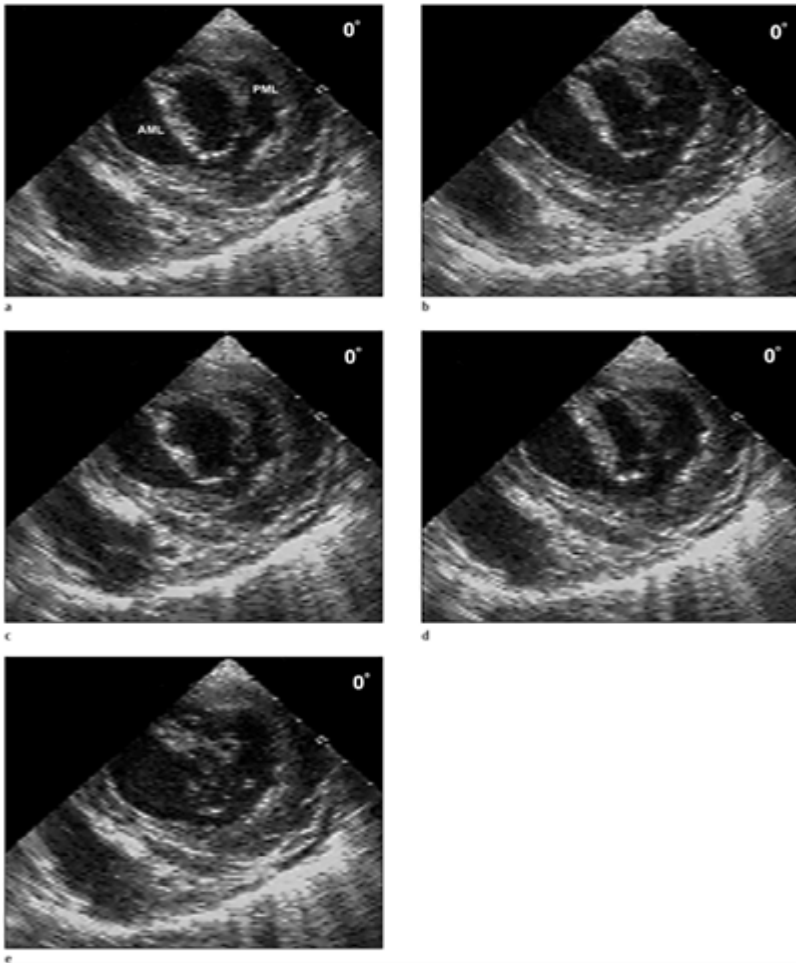
Case 2.38 Type III, restricted mitral regurgitation. Short-axis echocardiographic images of the mitral valve recorded from diastole through systole. (a) Early diastole. (b) Mid diastole. (c) Atrial systole. (d) End diastole. (e) End systole. Note all leaflet motion is produced by the anterior leaflet, with the posterior leaflet remaining fixed and non-mobile during the entire cardiac cycle. With type III restricted motion, severe mitral regurgitation usually does not occur until there is co-existent annular dilatation. AML, anterior leaflet; PML, posterior leaflet.
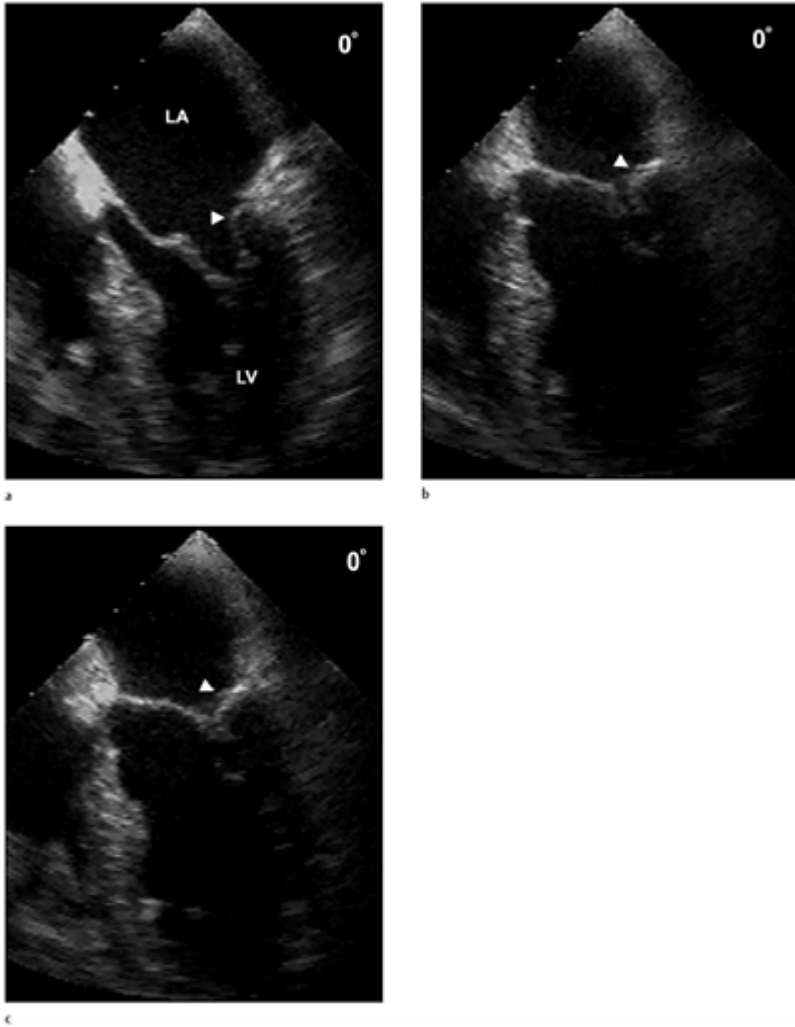
Case 2.39 Type III mitral regurgitation. (a–c) Frontal views of the mitral valve obtained from the lower esophageal window at 0°from diastole to systole in the same patient in Case 38. The anterior mitral leaflet is on the left and the posterior leaflet (arrow) is on the right. The posterior leaflet is thickened with mild calcification and is relatively immobile during the cardiac cycle. LA, left atrium; LV, left ventricle.
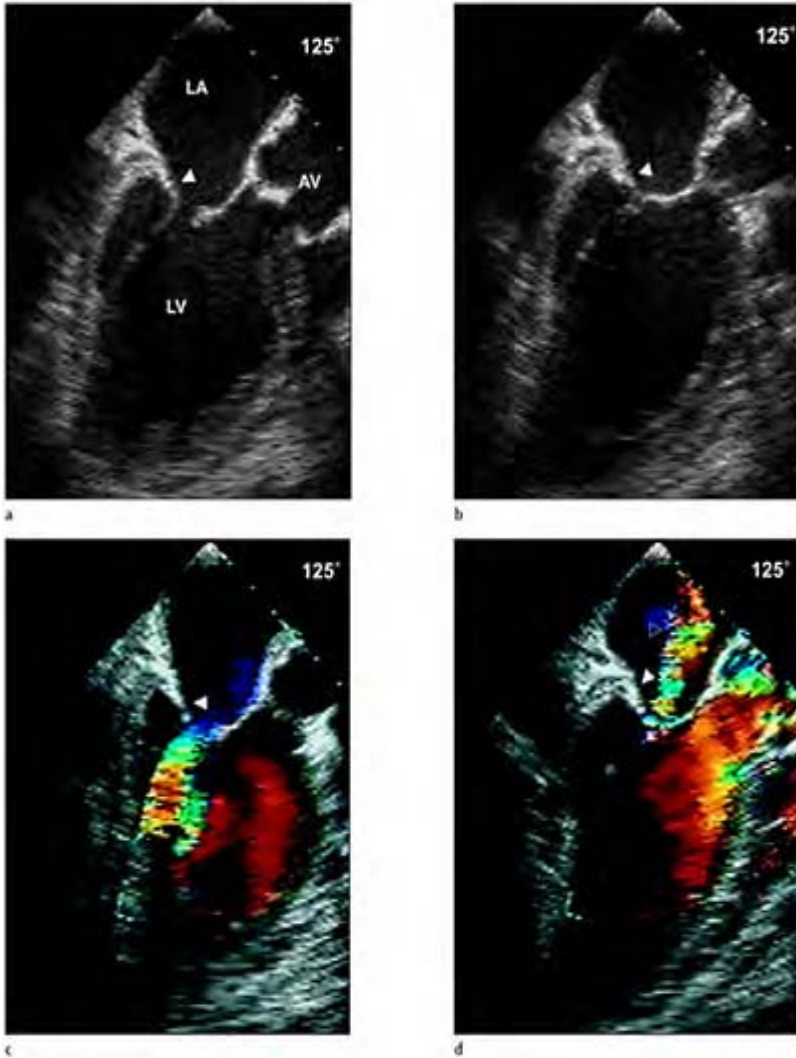
Case 2.40 Type III mitral regurgitation. Mitral valve images obtained from the lower esophageal window at 125° in diastole (a) and systole (b), demonstrating an immobile, fixed posterior leaflet throughout the cardiac cycle. (c) Color flow Doppler of the left ventricular inflow tract depicting high velocity

flow (arrow) across the mitral orifice suggesting a mild degree of obstruction associated with the fixed leaflet. (d) Color flow Doppler during systole demonstrating mitral regurgitation (arrow). Restriction to the posterior leaflet may not necessarily be symmetrical or involve the entire leaflet. Obviously since there are three scallops and intervention by two papillary muscles from different regions of the myocardium, depending on the pathology responsible for the restrictive process only part of the posterior leaflet may be involved. It is important to view the entire posterior leaflet in multiple views in order to diagnosis type III motion. LA, left atrium; LV, left ventricle; AV, aortic valve.
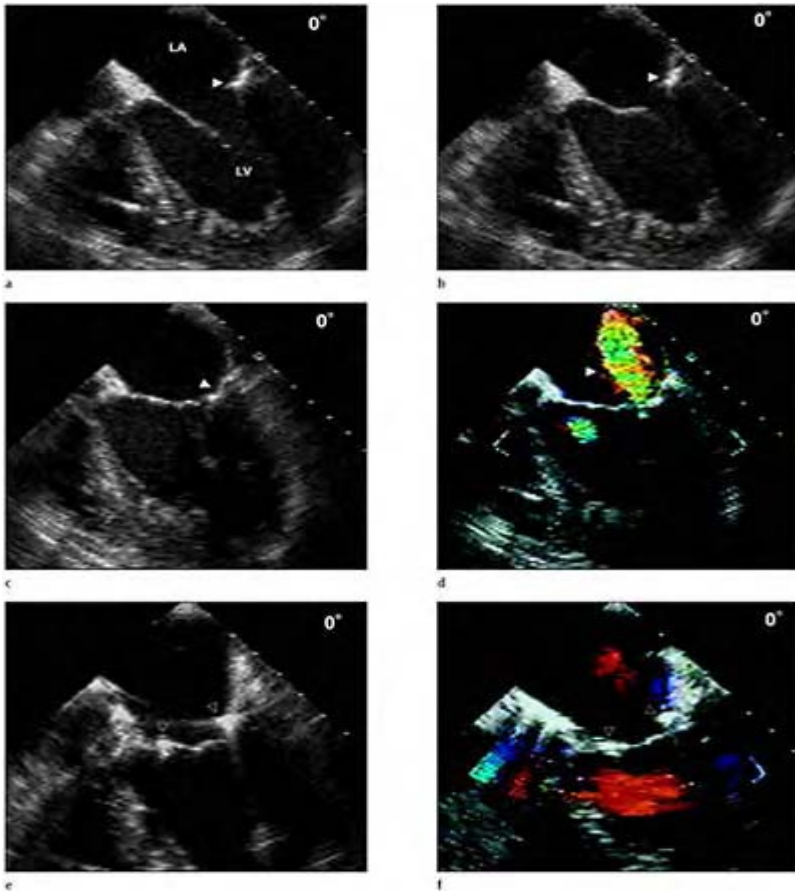
Case 2.41 Type III mitral regurgitation. Mitral valve images obtained from the lower esophageal window at 0° in diastole (a), mid-diastole (b) and systole (c) demonstrating an immobile posterior leaflet (arrow). (d) Color flow Doppler demonstrating significant mitral regurgitation. Often, type III mitral regurgitation only requires an annuloplasty ring during repair to eliminate the regurgitation. Postoperative views in the same patient, (e) demonstrating a mitral annuloplasty ring (arrows), (f) color flow Doppler demonstrating the absence of mitral regurgitation. LA, left atrium; LV, left ventricle.
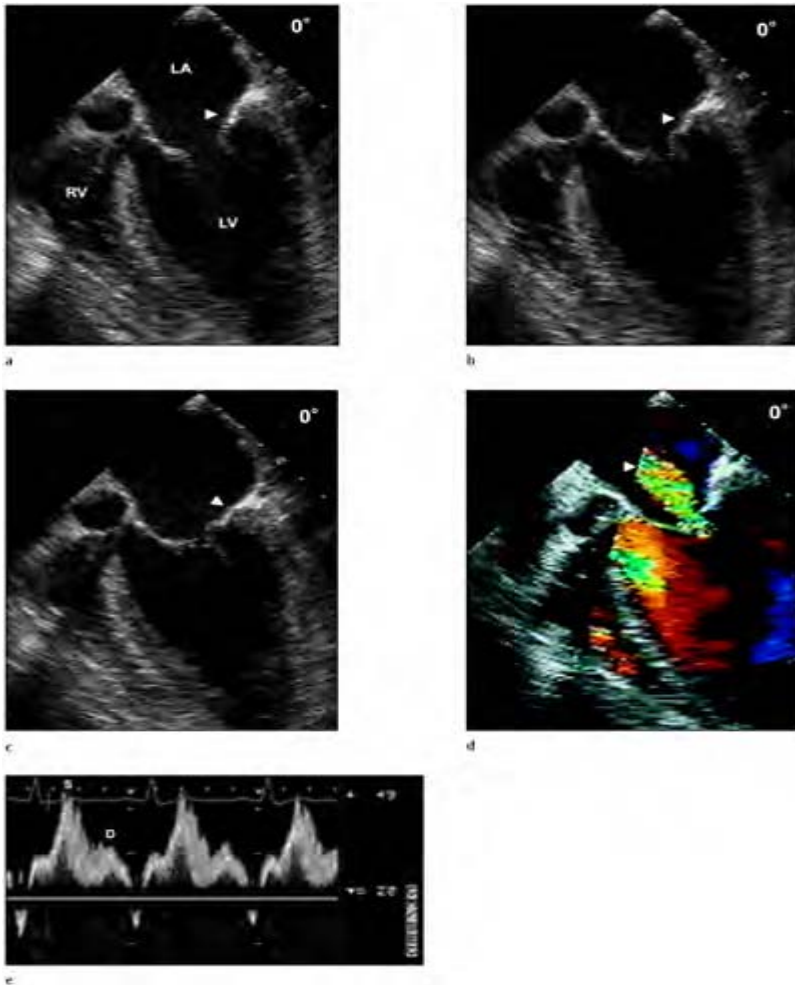
Case 2.42 Type III mitral regurgitation. (a,b) Mitral valve images obtained from the lower esophageal window at 0°. The posterior leaflet is immobile throughout the cardiac cycle. In systole (c) a small portion of the leaflet prolapses past the anterior leaflet. At the time of surgery there was a small flail segment, although the major pathology was restrictive. (d) Color flow Doppler demonstrating mitral regurgitation. (e) Pulsed wave Doppler of pulmonary venous flow. LA, left atrium; LV, left ventricle; RV, right ventricle; S, systolic; D, diastolic.
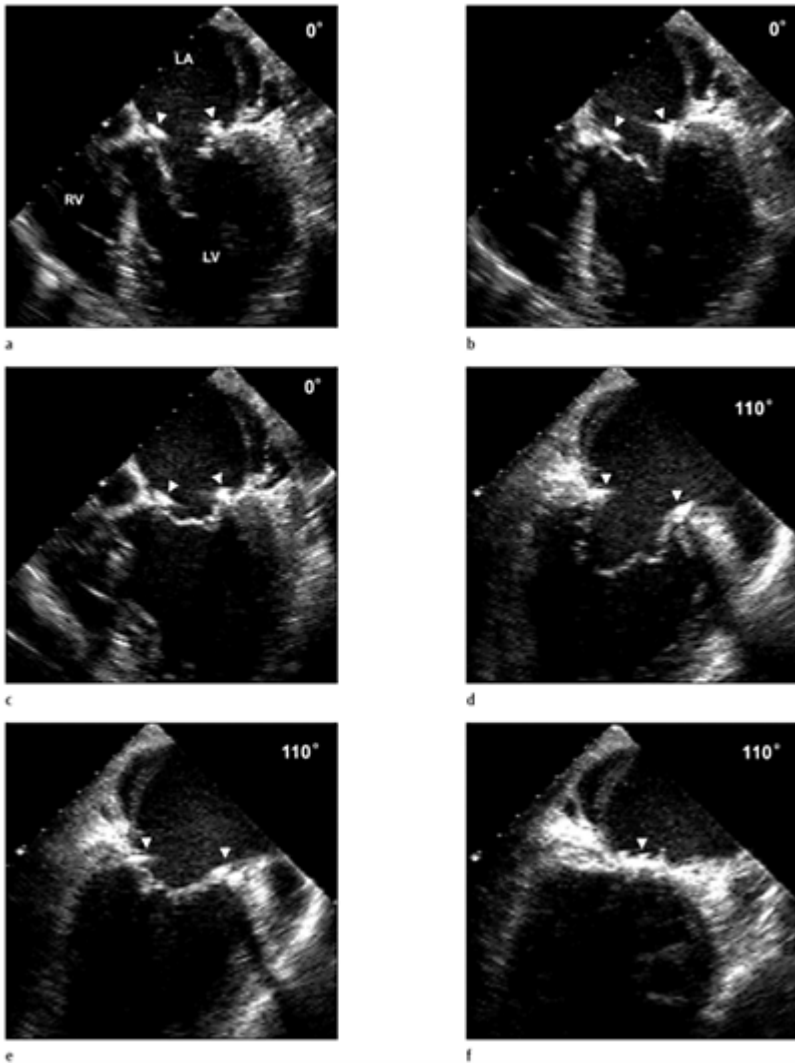
Case 2.43 Mitral valve repair. Mitral valve analysis post repair. Lower esophageal window at 0° (a–c) and 110° (d–f) from diastole through systole. The mitral annuloplasty ring is well visualized in cross-section (arrows). The anterior leaflet exhibits most of the leaflet motion. The posterior leaflet often appears fixed and does not exhibit significant motion for a period of 6–8 weeks following the repair. There is no obvious prolapse and leaflet motion appears normal. In addition to valve leaflet motion, left ventricular wall motion should be assessed, to rule/out inferior and/or posterior wall hypokinesis or akinesis resulting from an annular suture involving the circumflex artery. LA, left atrium; LV, left ventricle; RV, right ventricle.
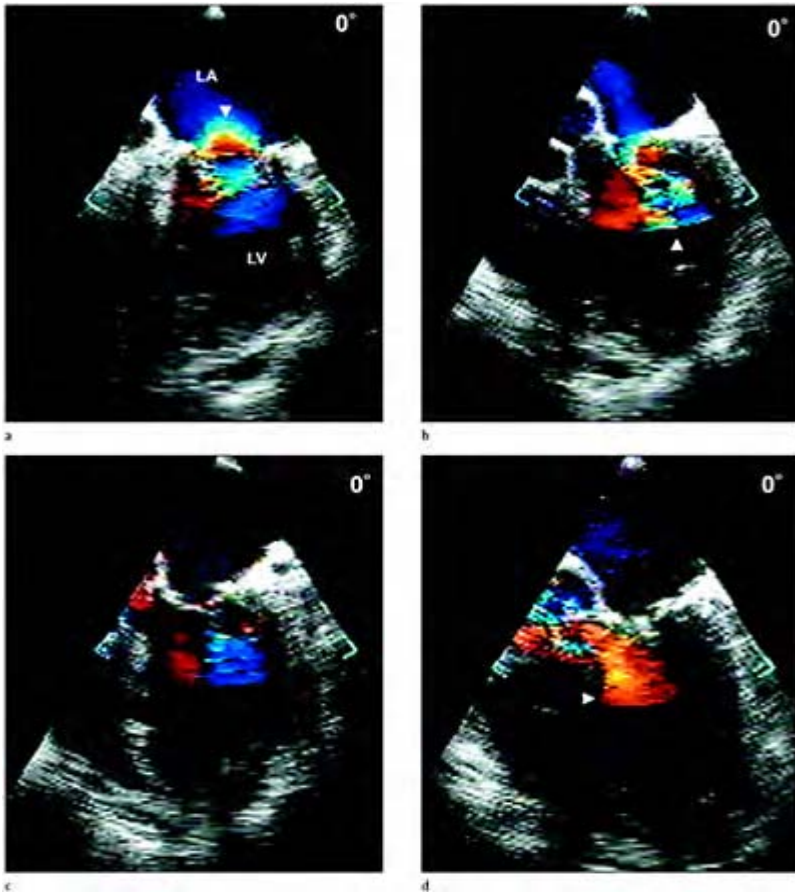
Case 2.44 Color flow Doppler following a successful mitral valve repair. Color flow Doppler from diastole through systole (a–d) recorded at 0° and corresponding views at 115° (e–h). In early diastole (a, e) flow convergence is noted above the annuloplasty ring. During mid-diastole (b, f) slightly accelerated flow velocity is noted and the inflow jet should be directed posteriorly into the left ventricle. With closure of the leaflets (c, g) flow should diminish in the left ventricular inflow tract and start to appear in the outflow tract. In systole normal velocity flow is recorded in the outflow tract and mitral regurgitation should not be detected.
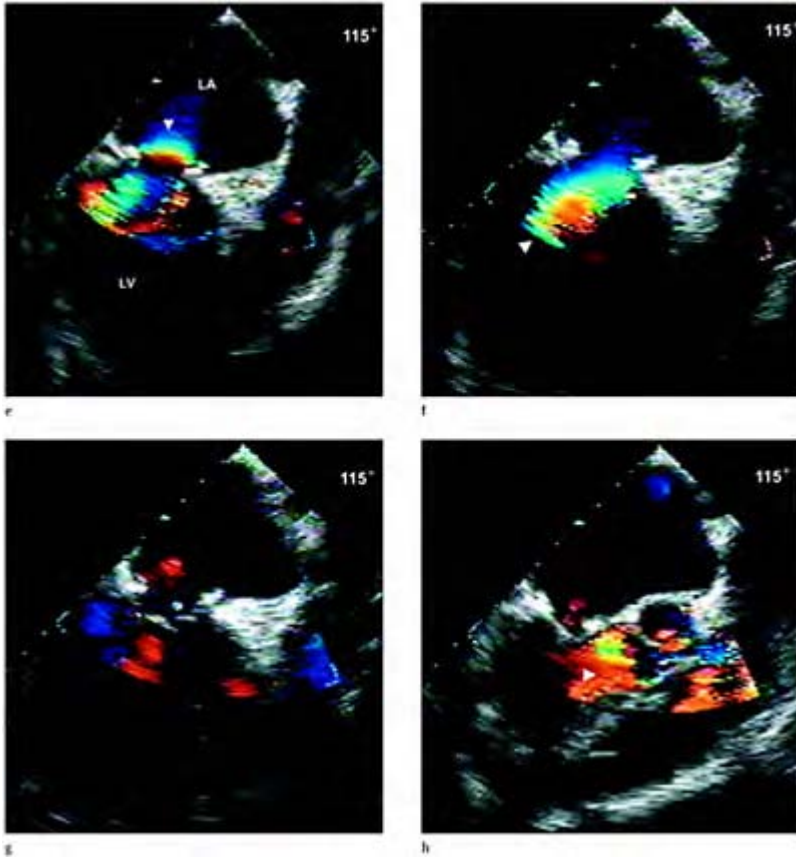
Pulsed and continuous wave Doppler may be guided by color flow to rule out a significant gradient across the annuloplasty ring suggestion restriction of the mitral orifice by the repair or in the outflow tract in relation to SAM. LA, left atrium; LV, left ventricle.
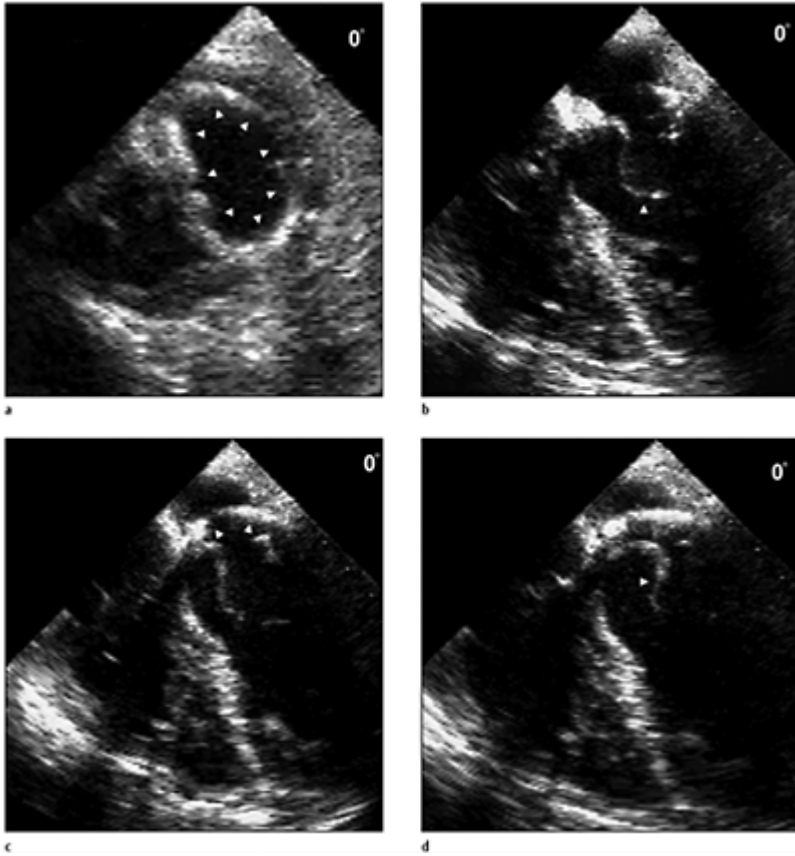
Case 2.45 Mitral valve repair. (a) Short-axis echocardiographic image illustrating the full extent of the mitral annuloplasty ring. (b–d) Serial echocardiographic images obtained from the lower esophageal window at 0° with mild anteflexion of the probe, demonstrating chordal analysis following the repair. Redundant chordae are noted to the anterior leaflet illustrated as an undulating motion from diastole to systole, in an unsuccessful repair and was the only obvious abnormality visualized. Echogenicity of the annuloplasty ring leaflet may deter analysis of leaflet motion following the repair, making it important to perform a complete analysis from multiple views of the mitral leaflets and subvalvular apparatus.
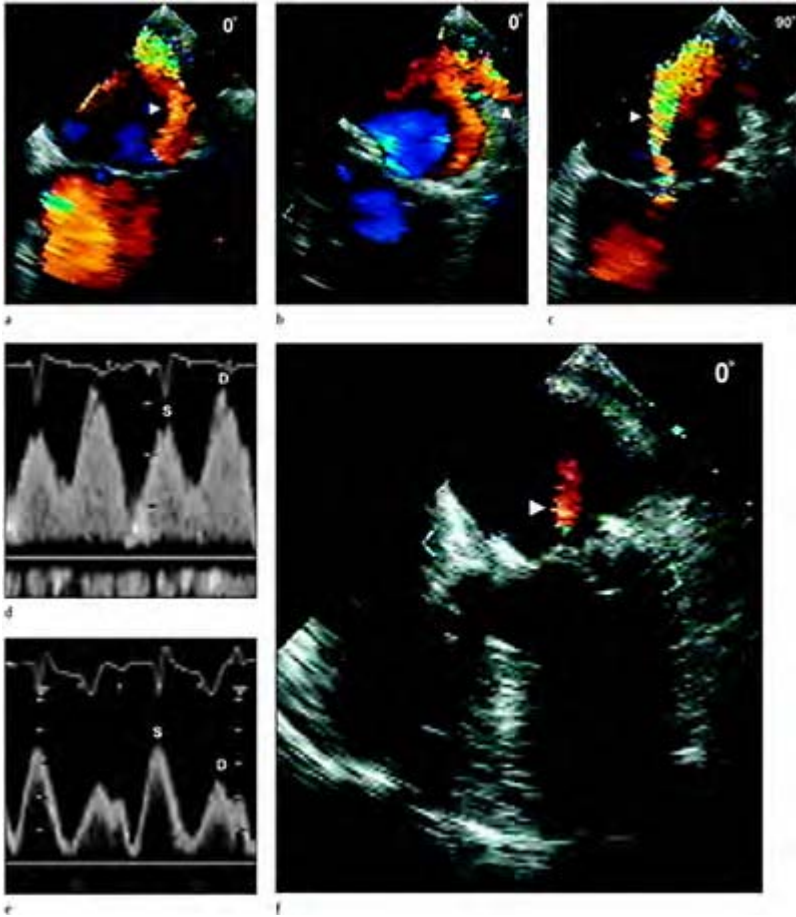
Case 2.46 Successful mitral repair of mitral valve prolapse and annular dilatation. (a–c) Color flow Doppler illustrating significant mitral regurgitation before mitral repair. (d) Pulsed wave Doppler of the right upper pulmonary vein illustrating decreased systolic flow in comparison to diastolic flow. Following successful mitral valve repair (e) systolic flow has normalized in relationship to diastolic flow as represented by no significant mitral regurgitation demonstrated in (f) S, systolic flow; D, diastolic flow.
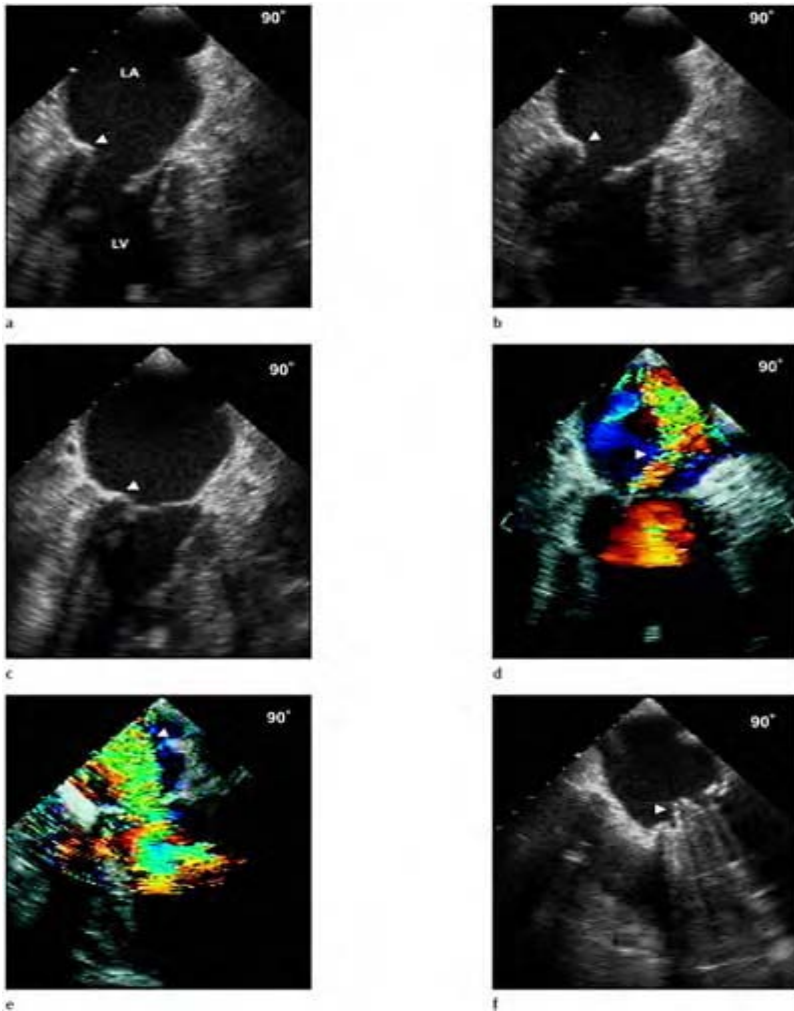
Case 2.47 Unsuccessful mitral repair of type III restrictive mitral regurgitation. (a–c) Diastolic through systolic frames demonstrating an immobile posterior leaflet. In addition there was a small posterior wall aneurysm. (d) Color flow Doppler demonstrating significant mitral regurgitation. (e) Immediately following the repair severe mitral regurgitation is noted almost entirely filling the left atrium. (f) St. Jude prosthesis replacing the repair. LA, left atrium; LV, left ventricle.
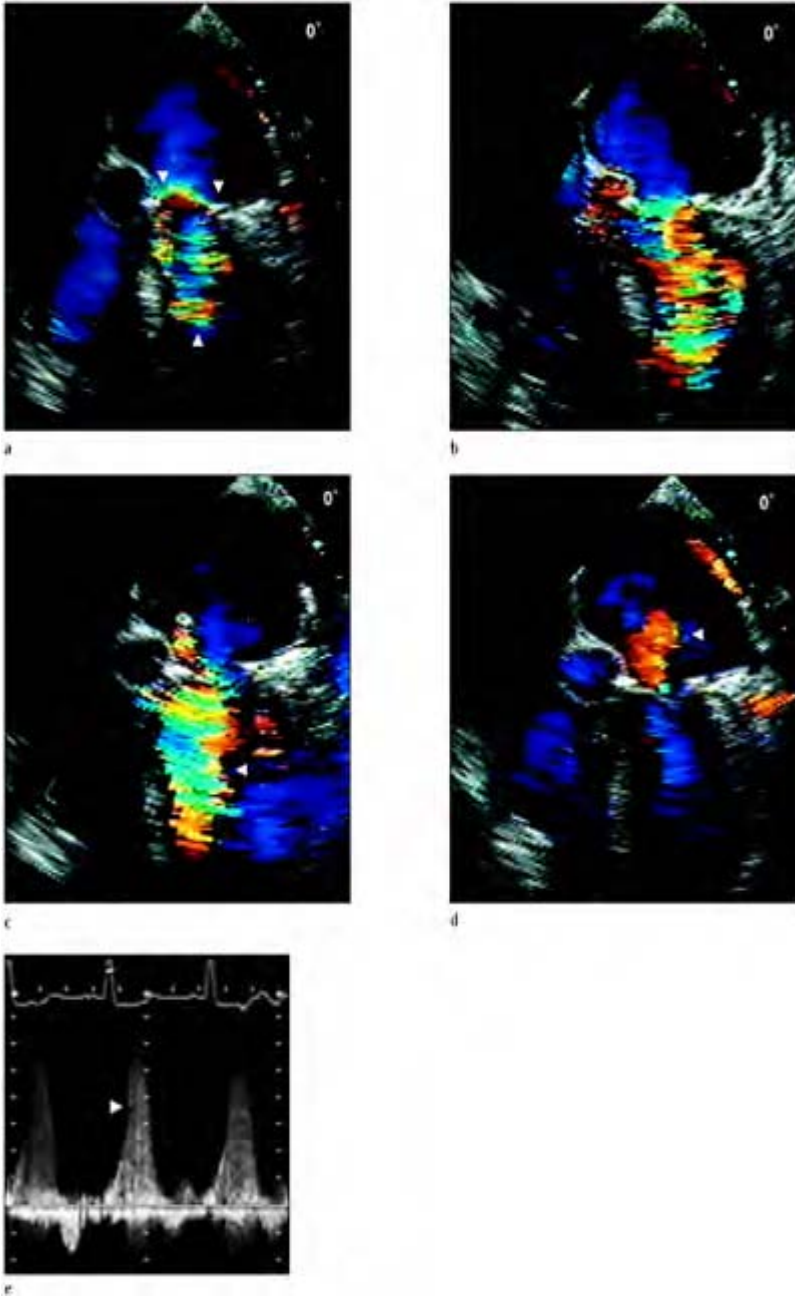
Case 2.48 Doppler illustration of SAM
post mitral repair. (a) End-systolic
frame obtained from the lower

esophageal window at 0°. Note the tilt of the mitral annuloplasty ring (arrows) in relation to the aortic valve. This finding corresponds to a decreased aorto-mitral angle. There is high velocity flow demonstrated in the left ventricular outflow tract by color Doppler. (b) Subsequent diastolic frame demonstrating left ventricular inflow color flow jet directed anteriorly towards the left ventricular outflow tract. (c) Early systolic frame demonstrating high velocity flow in the left ventricular outflow tract. (d) End-systolic frame demonstrating mitral regurgitation. (e) A 5 m/sec high velocity jet recorded with continuous wave Doppler of the left ventricular outflow tract suggesting significant SAM and failed repair.
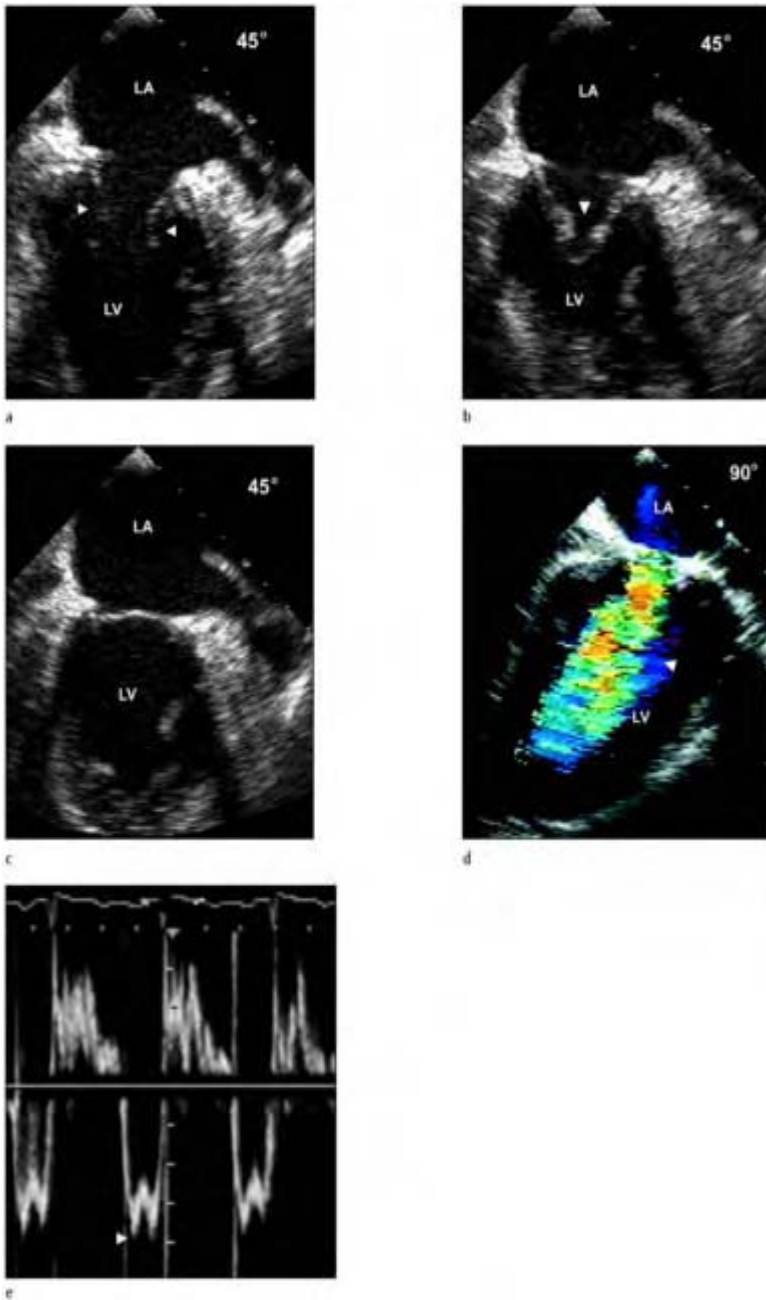
Case 2.49 Left ventricular inflow
obstruction post mitral repair
secondary to a small mitral

annuloplasty ring. (a) Diastolic frame obtained from the lower esophageal window at 90° exhibiting restricted anterior mitral valve motion following repair. Note the annular diameter, which appears significantly smaller or "pinched" in reference to the left atrium and left ventricle at that level. (b) Thickened anterior and posterior leaflets during mid-diastole. The posterior leaflet exhibits much more motion than usual following mitral repair, which is consistent with excessive remaining tissue. (c) Systolic frame suggesting normal leaflet closure. (d) Color flow Doppler demonstrating high velocity flow during diastole in the left ventricular inflow tract. (e) Pulse wave Doppler during diastole. The flow across demonstrates a 1.75 m/sec flow jet and a 12 mmHg gradient across the mitral valve.
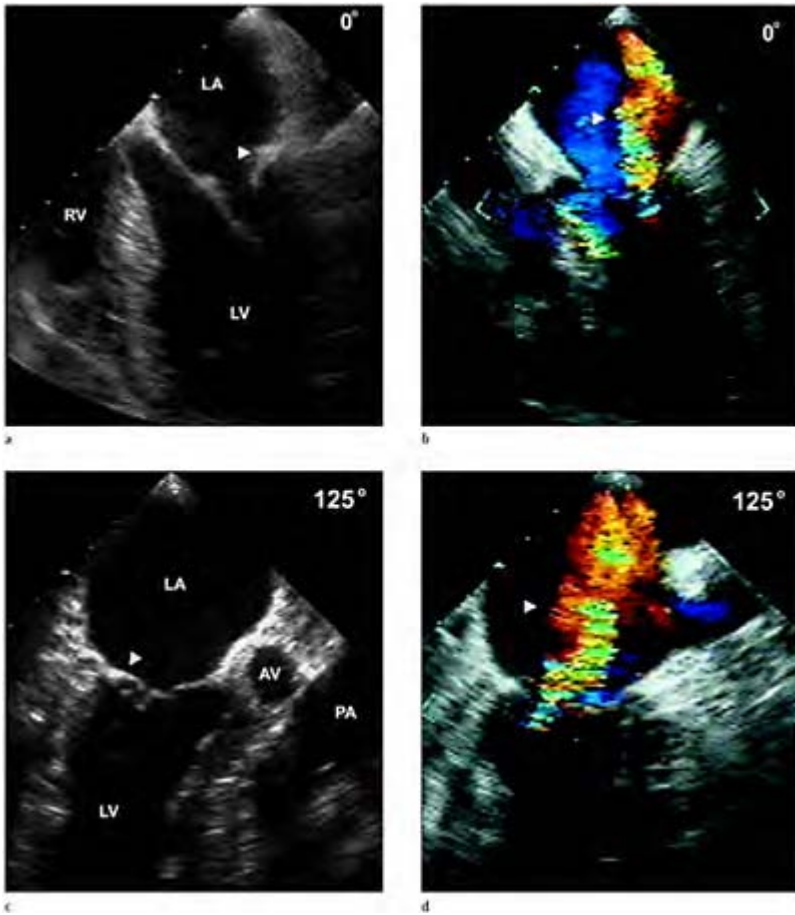
Case 2.50 Failed mitral valve repair. (a) Mitral regurgitation secondary to mitral annular calcification (arrow) and prolapse of the posterior leaflet secondary to excessive leaflet tissue, recorded from the lower esophageal window at 0° and at 125° (c). (b) Corresponding color flow Doppler image demonstrating a mitral regurgitant jet (arrow) at 0° and 125° (d). Post repair involving a triangular resection of the posterior leaflet without removal of the mitral annular calcification.
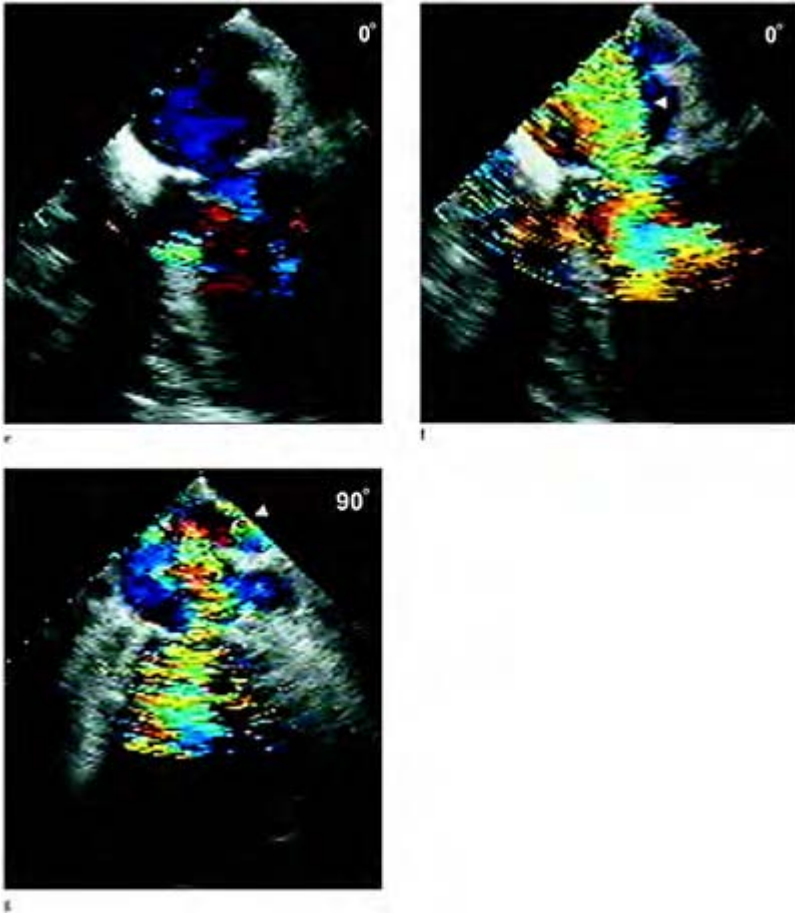
(e) The mitral annuloplasty ring is readily apparent and appears small in relation to the mitral annulus although color flow Doppler does not demonstrate significant flow obstruction during diastole. (f) Severe mitral regurgitation (arrow) demonstrated in diastole at 0° and with reversal of flow in the pulmonary veins at 90° (g). LA, left atrium; LV, left ventricle; RV, right ventricle; AV, aortic valve; PA, pulmonary artery.
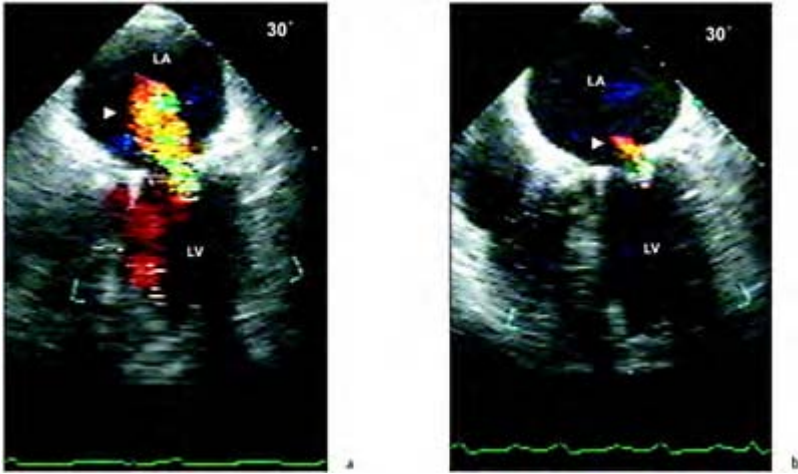
Case 2.51 Mitral valve repair.
Immediately following weaning from
cardiopulmonary bypass a fairly large
mitral regurgitant jet (a) is suggested
with ventricular pacing. With
resumption of sinus rhythm (b) the
mitral regurgitant jet is dramatically
reduced and represents the true result
of the mitral repair.
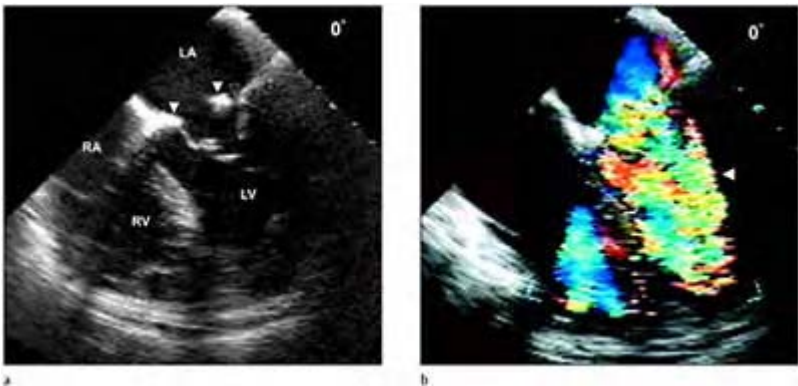
Case 2.52 Ring dehiscence post mitral
repair. (a) Mid-diastolic frame
obtained from the lower esophageal
window at 0°. There is an echo free

space between the mitral annuloplasty ring and the valve annulus. Color flow Doppler during systole (b) and diastole (c) demonstrating abnormal flow in the region of the space and a significant mitral regurgitant jet originating between the mitral annuloplasty ring and the mitral annulus. (d) With anteflexion of the probe at 75° the annuloplasty ring is demonstrated again with an echo free space suggesting ring dehiscence. (e) Continuous wave Doppler through the mitral valve demonstrating high velocity flow during diastole in the range of 1.3 m/sec. (f) Echo free space demonstrated between the annuloplasty ring and the annulus at 115°, with color flow Doppler again demonstrating significant mitral regurgitation (g) and high velocity flow during systole (h). During the second cardiopulmonary bypass run, the mitral annuloplasty ring was determined to be too small and had separated from the annulus. LA, left atrium; LV, left ventricle; RA, right atrium; RV, right ventricle; AV, aortic valve.
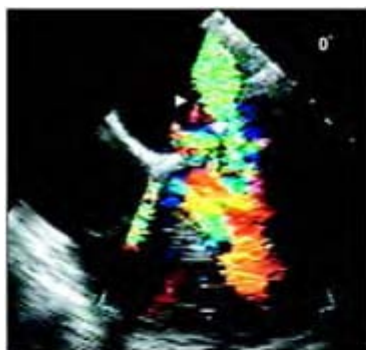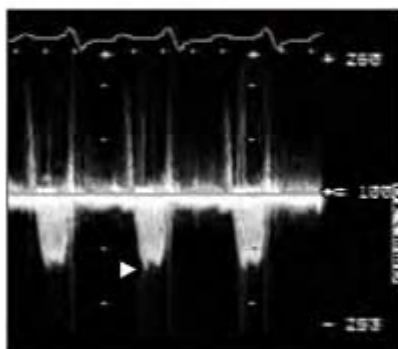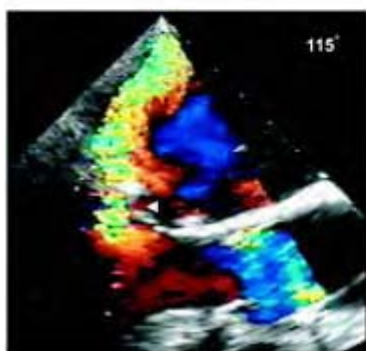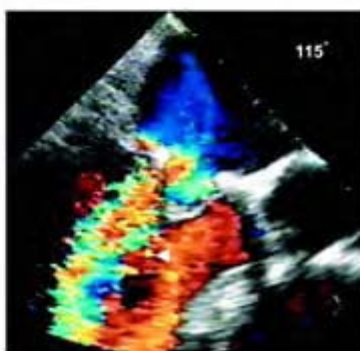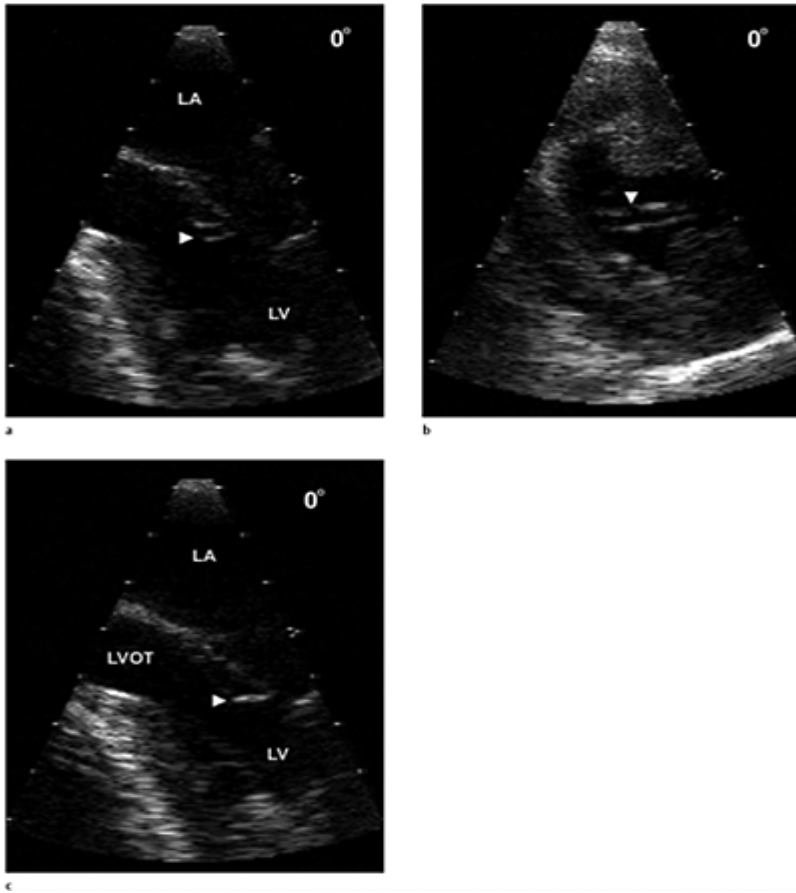
Case 2.53 Papillary fibroelastoma of the mitral valve. Papillary fibroelastomas of the mitral valve frequently appear as thin, multiple hairlike projections emanating from the leaflet margins or chordal structures and therefore are frequently confused with valvular vegetations. Echocardiographic images of a patient with two small papillary fibroelastomas (arrows) attached to chordae tendineae, recorded at the lower esophageal (a) and gastric windows (b) at 0°. (c) Papillary fibroelastoma attached to the anterior mitral leaflet that appeared to flip in and out the left ventricular outflow tract during systole. LA, left atrium; LV, left ventricle; LVOT, left ventricular outflow tract.
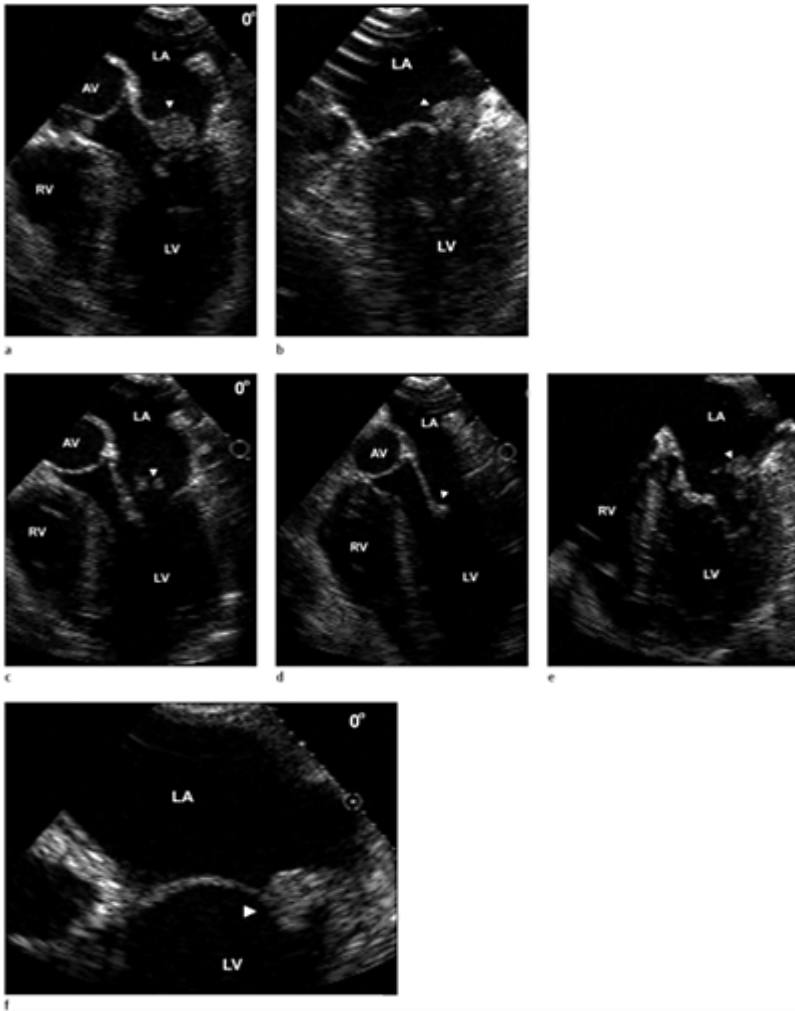
Case 2.54 Mitral valve vegetation. A medium sized multilobular, *Staphylococcus aureus* vegetation (arrow) attached to the posterior leaflet as recorded from the lower esophageal window at 0° during the cardiac cycle (a–e). (f) Enlarged view of the vegetation (arrow). Although visualized in multiple views the vegetation was rather sessile and did not exhibit excessive motion. LA, left atrium; LV, left ventricle; AV, aortic valve; RV, right ventricle.
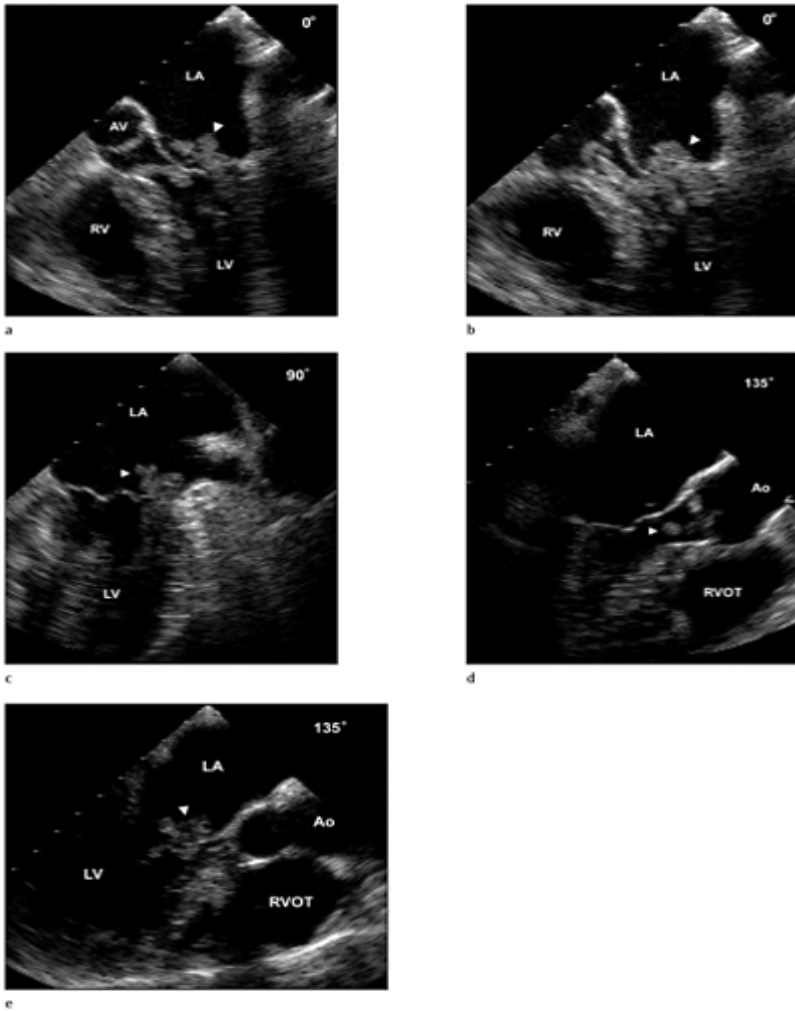
Case 2.55 Mitral valve vegetation. A large multilobular vegetation (arrows) attached predominately to the anterior leaflet with segments noted on the atrial and ventricular surface of the leaflet. During the cardiac cycle the vegetation flipped in and out of the left ventricular outflow tract. Viewing the vegetation from 0° to 135° (a–e) gives full appreciation of the size and mobility of the vegetation. LA, left atrium; LV, left ventricle; AV, aortic valve; RV, right ventricle; RVOT, right ventricular outflow tract; Ao, aorta.
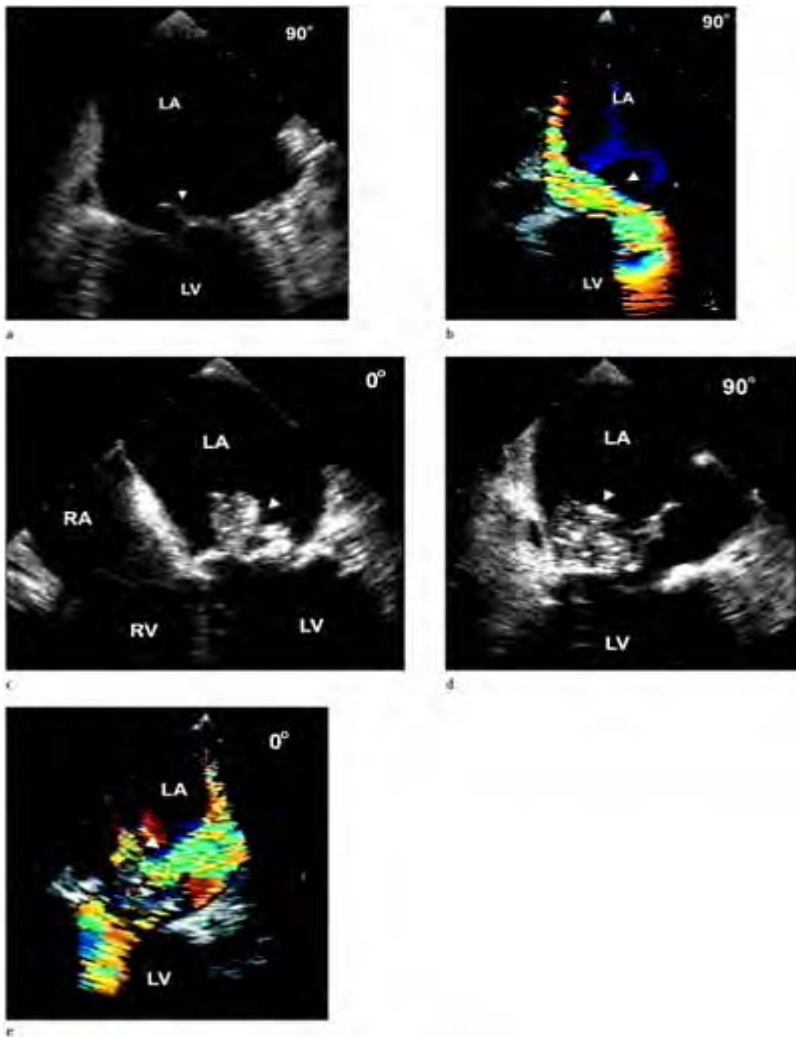
Case 2.56 Mitral valve vegetation with extensive
destruction of the mitral apparatus. (a) Flail anterior
leaflet (arrow) producing severe mitral regurgitation (b)
with a posterior directed color flow jet recorded at 90°.
Visualization of the vegetation (arrow) from the lower
esophageal window at 0° (c) and 90° (d). (e) Color
flow Doppler demonstrating disturbed flow (arrow) in
the area of the vegetation. LA, left atrium; LV, left
ventricle; RV, right ventricle; RA, right atrium.
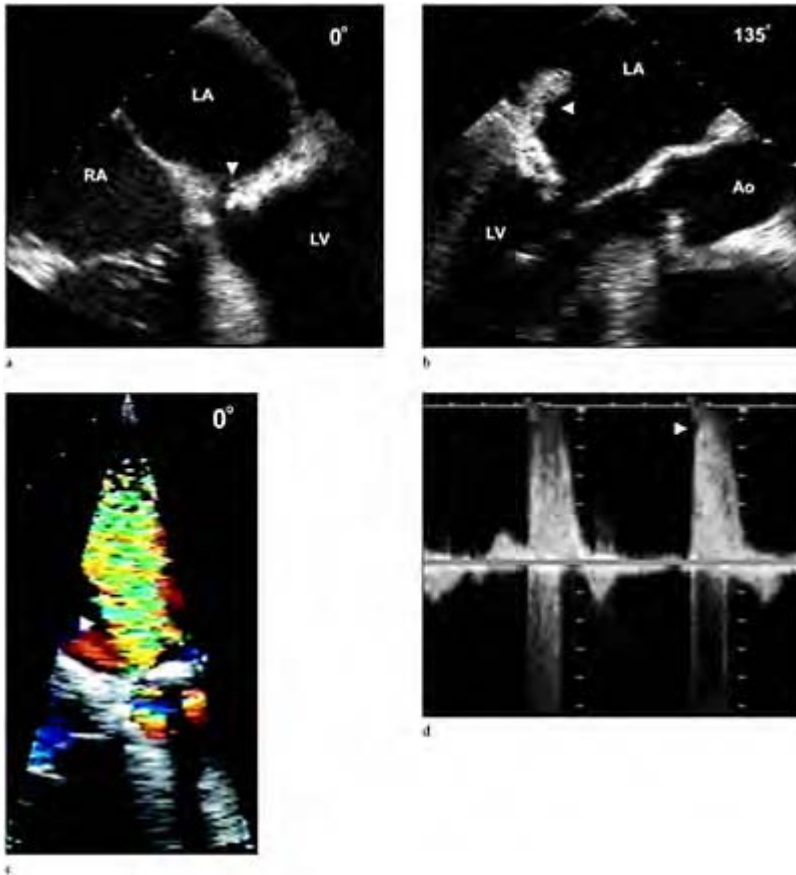
Case 2.57 Mitral valve vegetation producing a perforated leaflet with severe mitral annular calcification. (a) Mitral annular calcification denoted by thick echodensity extending along the annular plane. The probe is retroflexed at 0° in the lower esophageal window to visualize the posterior plane of the heart. Small echo free space (arrow) representing a perforation in the base of the valve leaflet. (b) With rotation of the transducer to 130° the vegetation is illustrated as a globular mass hugging the posterior wall of the left

atrium. Color flow (c) and continuous wave Doppler (d) demonstrating severe mitral regurgitation. Flow through a perforation is often recorded in both phases of the cardiac cycle in a to and fro manner. LA, left atrium; LV, left ventricle; RA, right atrium; Ao, aorta.
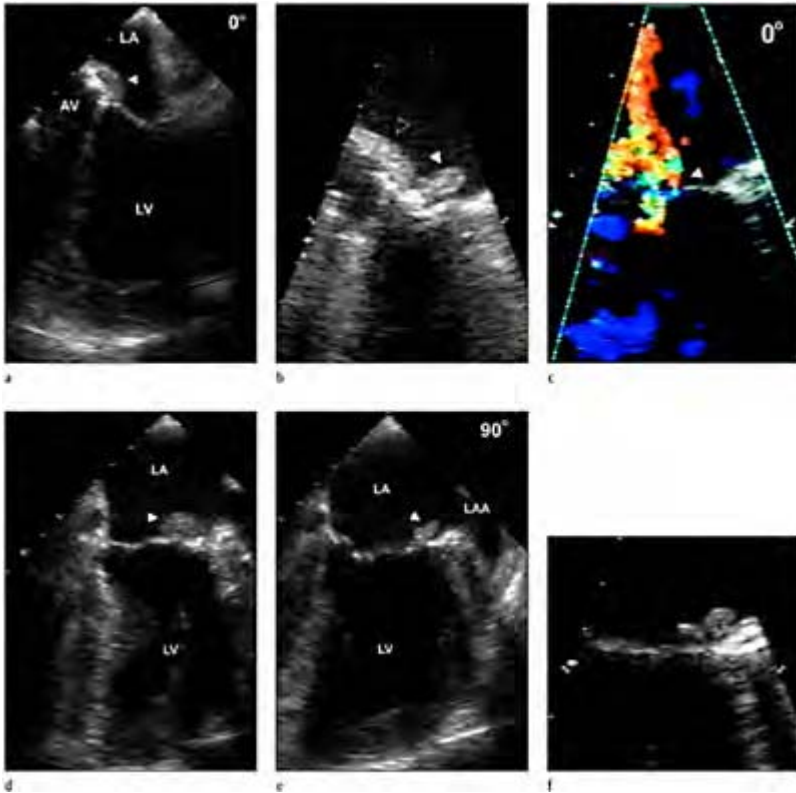
Case 2.58 Mitral valve vegetation with an annular abscess. (a) Small annular abscess (arrow) visualized near the aorto-mitral fibrosa from the lower esophageal view at 0°. (b) Slight retroflexion of the probe demonstrates a small vegetation (arrow) in close

proximity to the abscess in an enlarged view. (c) Color flow Doppler demonstrates a mitral regurgitant jet emanating from the same area as the vegetation and the abscess, which is not allowing apposition of the leaflets near the area of the posterior commissure. (d, e)Rotating the transducer to approximately 90° demonstrates the full extent of the abscess and the vegetation (arrow). (f) Enlarged view of the vegetation (arrow). LA, left atrium; LV, left ventricle; LAA, left atrial appendage.
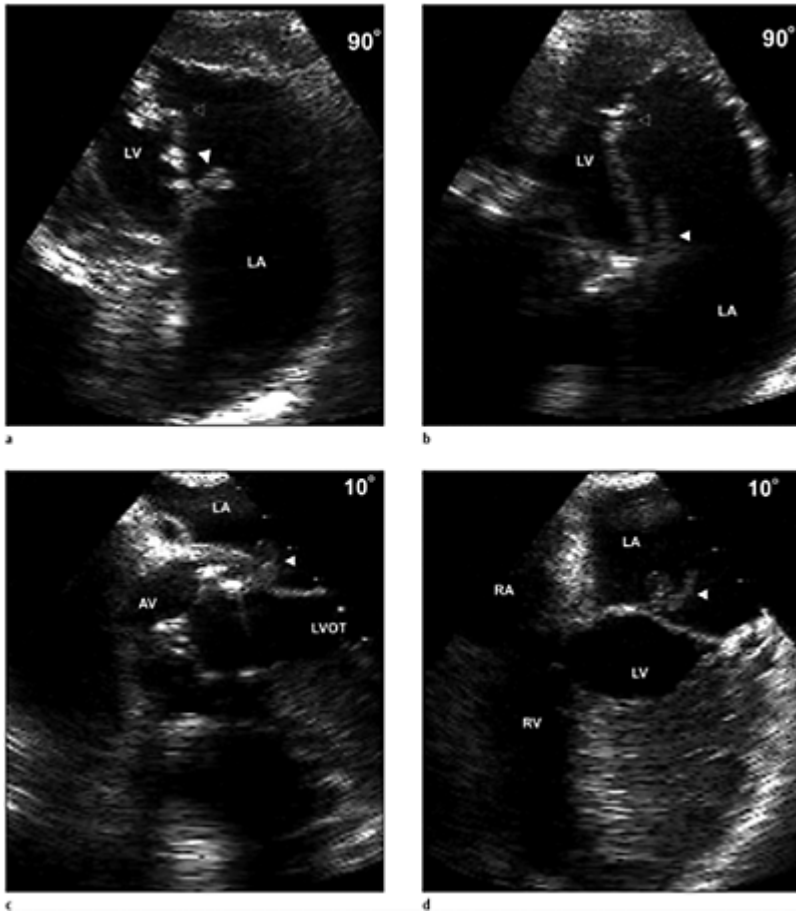
Case 2.59 Sub-aortic extension of prosthetic valve endocarditis with an associated mitral valve vegetation. Careful scanning with multiplane TEE is ideal for identifying perivalvular abscess. Deep transgastric view at 0° demonstrates a mobile vegetation attached to the anterior leaflet during systole (a) and diastole (b), vegetation (open arrow), chords (solid arrow). In the lower esophageal view at 10° (c,d) an aortic prosthetic valve is seen with an associated small annular abscess. With rotation of the transducer to 45° the same vegetation demonstrated in (a) and (b) is seen.
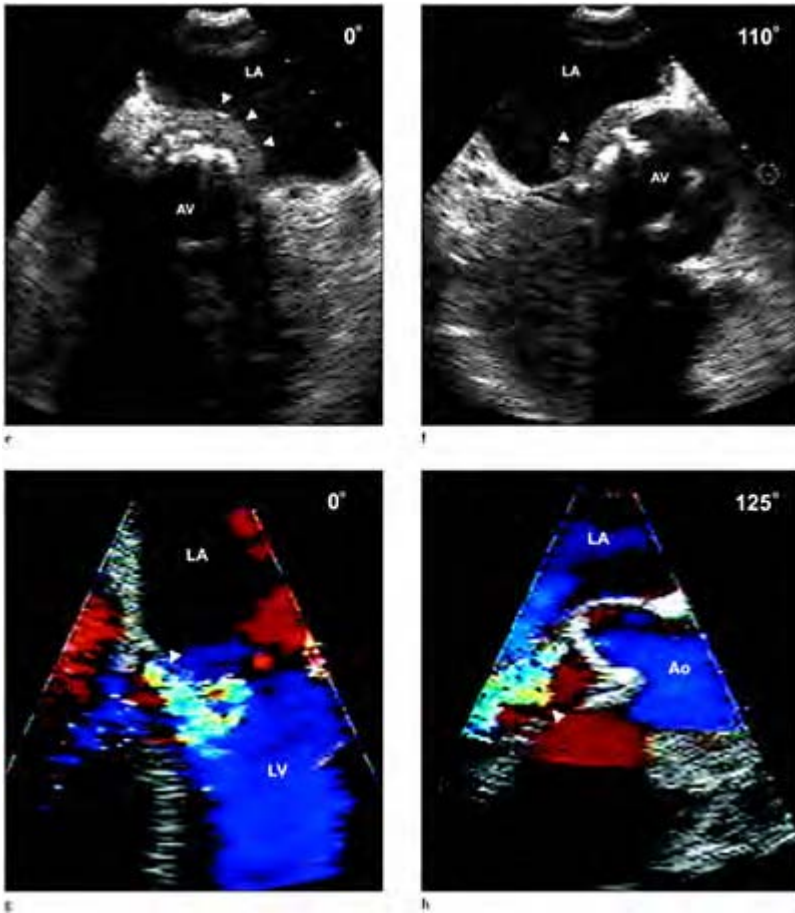
(e) At 0° the abscess (arrow) is seen wrapping around the aortic prosthetic ring. (f) With further rotation of the transducer to 110° the abscess and the vegetation are demonstrated in close proximity to each other.

Aortic regurgitation is demonstrated with color flow Doppler at 0° (g) and 125° (h). LA, left atrium; LV, left ventricle; RA, right atrium; RV, right ventricle; Ao, aorta; AV, aortic valve; LVOT, left ventricular outflow tract.
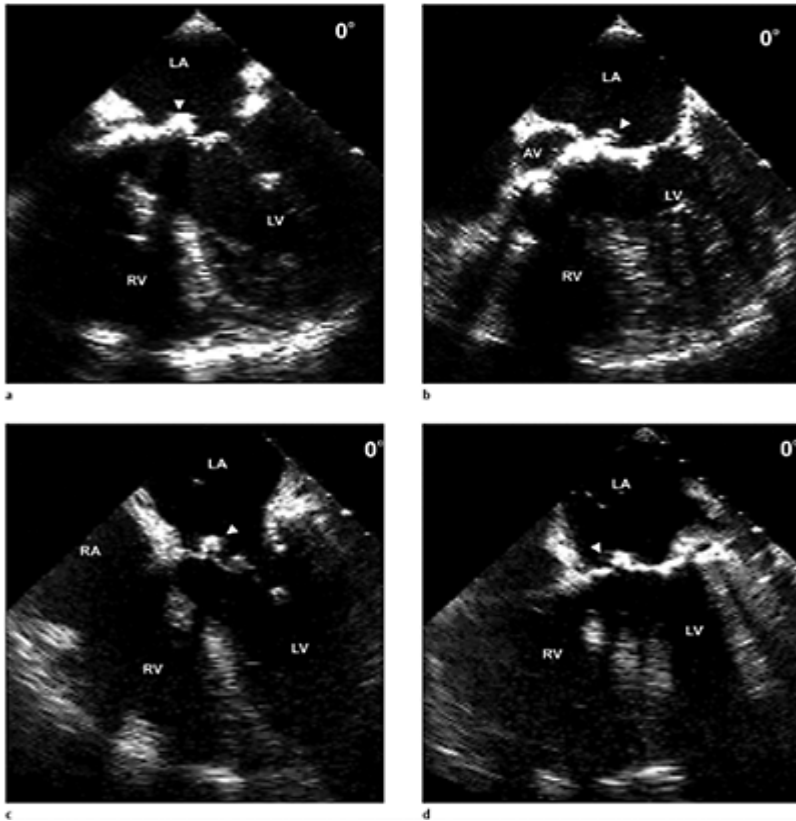
Case 2.60 (a–d) Sub-aortic extension of aortic
prosthetic valve endocarditis causing a mycotic
aneurysm of the mitral valve which appears as a bulge
in the anterior mitral leaflet expanding and contracting
during systole through diastole. (e) Small vegetation
(arrow) associated with a prosthetic aortic valve. (f)
Color flow Doppler demonstrating flow into an aortic
annular abscess at 125° during systole. (g) At 0° a color
flow jet (arrow) is demonstrated in the left atrium
demonstrating perforation. During diastole color flow
does not demonstrate flow into the abscess cavity at 0°
(h) or 125° (i). (j) Enlarged view demonstrating a
collapsed abscess cavity during diastole. LA, left
atrium; LV, left ventricle; RA, right atrium; RV, right
ventricle; AV, aortic valve; Ao, aorta.
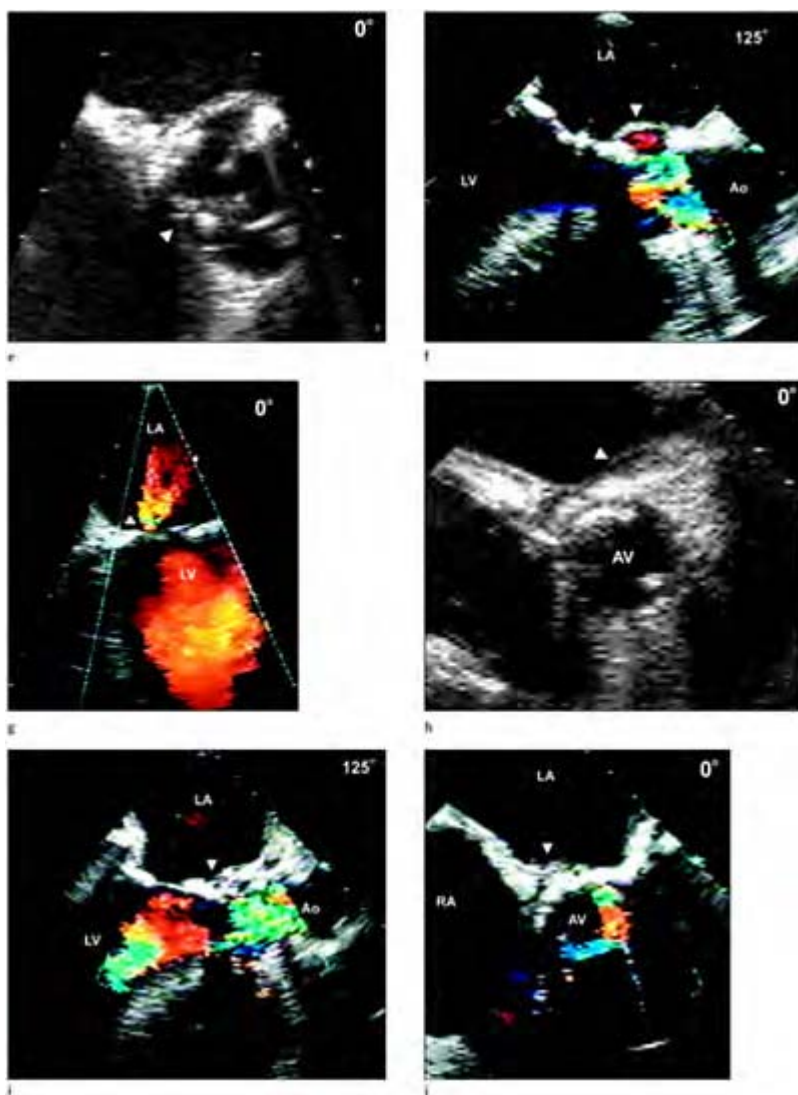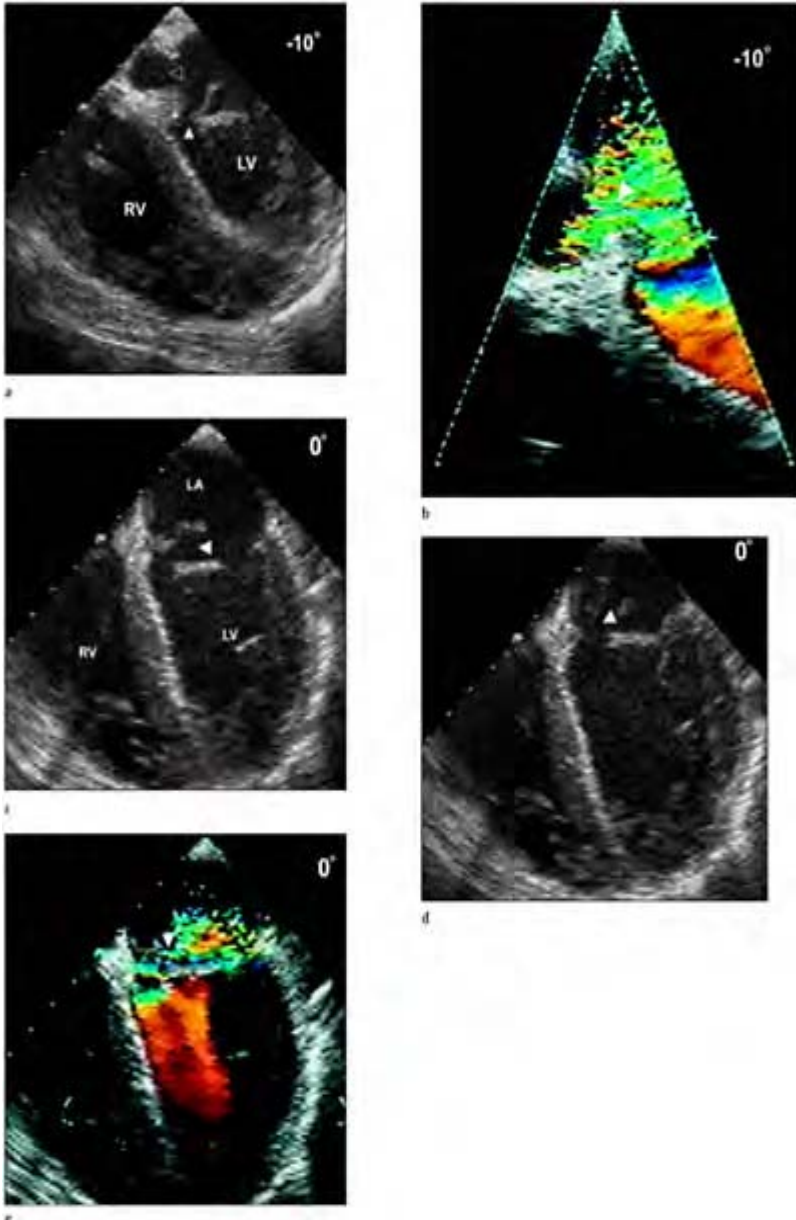
Case 2.61 Mitral valve endocarditis producing a perforated leaflet with an annular abscess. (a) View of the mitral valve with the probe in the gastroesophageal junction at

approximately –10°. The posterior aspect of the mitral valve annulus is seen with a small submitral aneurysm (open arrow). A perforation is visualized in the mitral leaflet (closed arrow) with vegetative debris noted near the perforation. (b) Color flow Doppler demonstrates flow (arrow) in the aneurysm and through the perforation. Views obtained from the lower esophageal window at 0° demonstrate mobility of the vegetation during diastole (c) and systole (d), and color flow Doppler demonstrates flow (arrow) through the perforation (e). LA, left atrium; LV, left ventricle; RV, right ventricle.
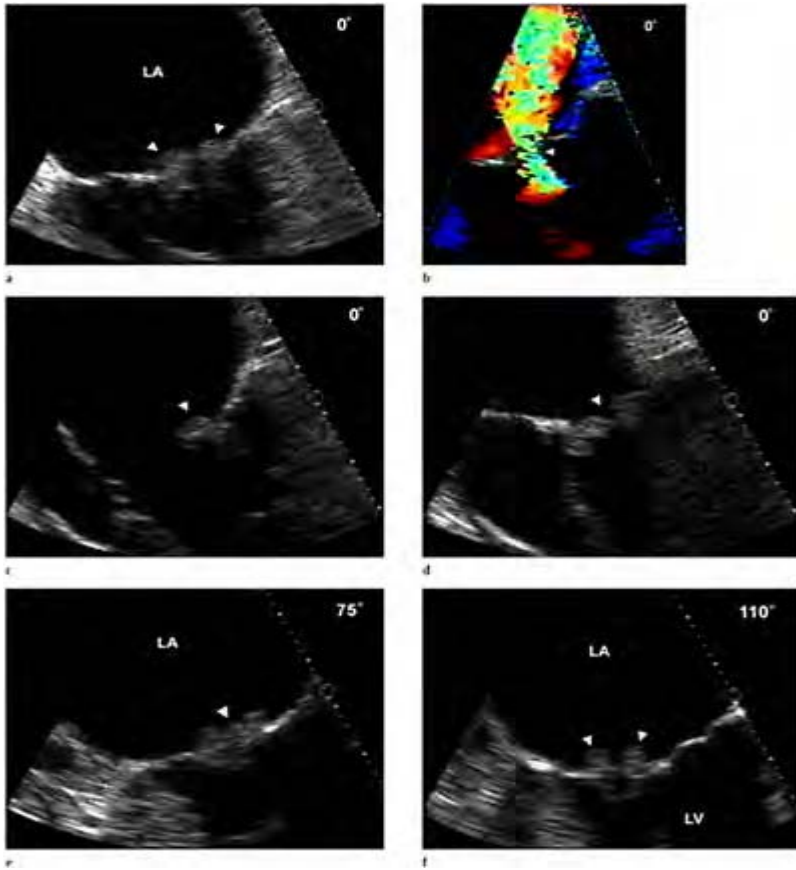
Case 2.62 Non-bacterial endocarditis in a patient with lupus erythematosus; the TEE indication was rule out cardiac source of embolus. (a) Thickening of both leaflet tips is seen (arrows). (b) Significant mitral regurgitation is demonstrated by color flow Doppler. Angulation of the probe, with enlarged views visualizes the posterior leaflet (c) and anterior leaflet (d), both leaflets (e,f) with thickening and shaggy echoes noted on the leaflet margin. It is not unusual to see this picture of "kissing vegetations" on both leaflet margins in non-bacterial endocarditis. LA, left atrium; LV, left ventricle.
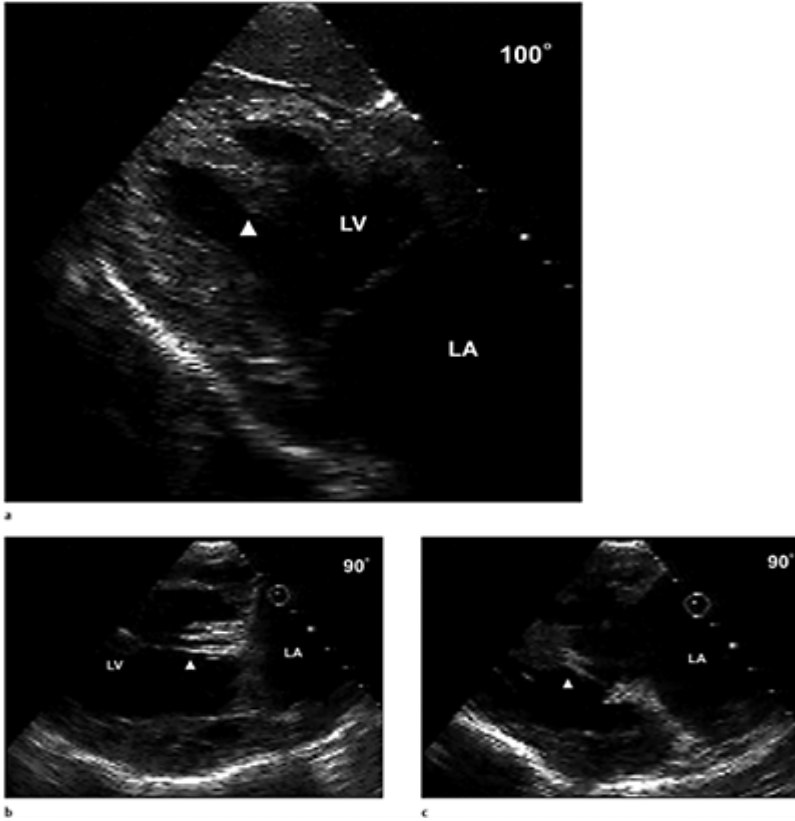
Case 2.63 Congenital mitral stenosis. (a) Deep transgastric view obtained at 100° demonstrates an abnormally placed papillary muscle emanating from the ventricular apes. In the longitudinal gastric views at 90° in systole (b) and (c) diastole abnormal chordal orientation is noted with the single papillary muscle-giving rise to both leaflets. During diastole the limited range of chordal motion is demonstrated due to restricted leaflet opening. (d) Marked thickening of both leaflets is noted, and with angulation of the probe (e) excessive tissue associated with the posterior leaflet and prolapse (arrow) is demonstrated. (f) Color flow Doppler demonstrates severe mitral regurgitation (arrow). (g) Restricted and abnormal motion of the anterior leaflet is demonstrated. LA, left atrium; LV, left ventricle; RV, right ventricle; AV, aortic valve.
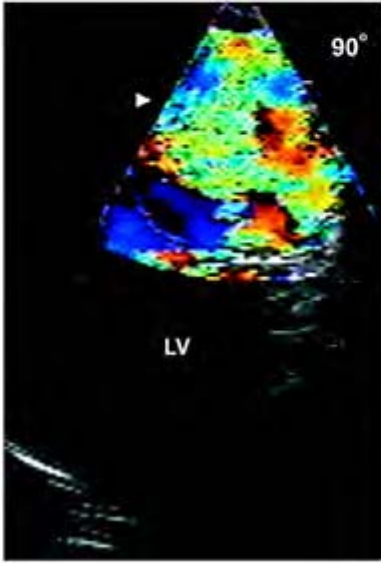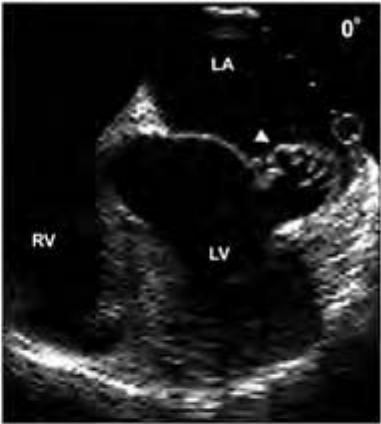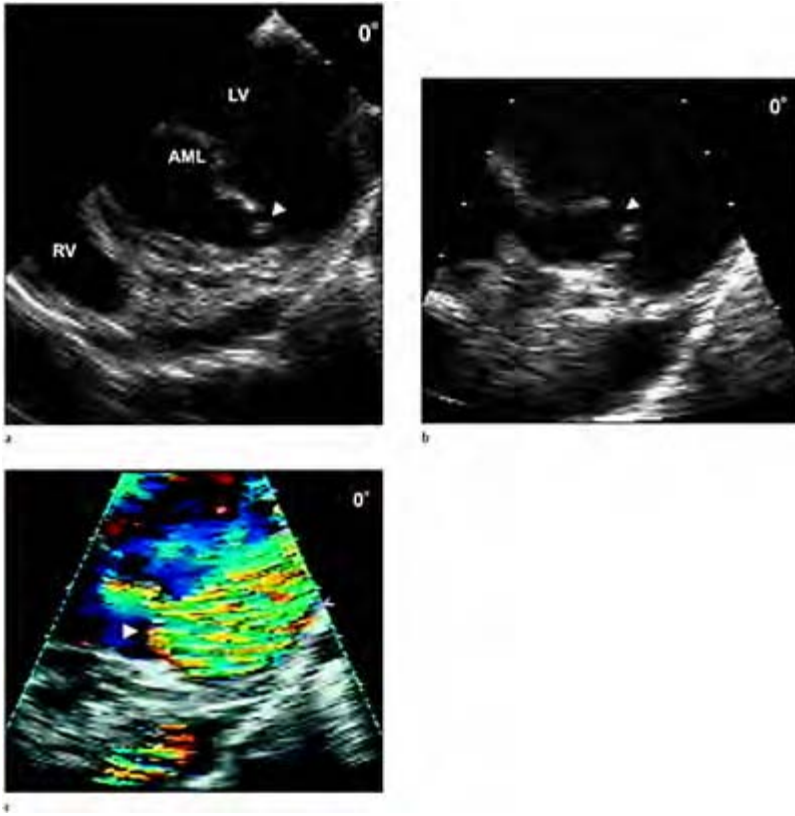
Case 2.64 Partial cleft mitral valve. (a–c) Gastric short-axis views with slight anteflexion of the probe demonstrates a break in the continuity of the anterior leaflet (echo free space), with color flow Doppler (c) demonstrating flow (arrow) through the cleft. (d) View obtained from the gastroesophageal junction with anteflexion of the probe demonstrates a cleft of the anterior leaflet margin (arrow) and with (e) color flow Doppler a mitral regurgitant jet (arrow) is demonstrated in the left atrium. With rotation of the transducer to 75° the cleft is noted (f) with mitral regurgitation filling the left atrial appendage (g). Multiplane TEE allows visualization of the cleft in multiple views allowing the diagnosis be made with confidence. AML, anterior leaflet; LA, left atrium; LV, left ventricle; RA, right atrium; RV, right ventricle; LAA, left atrial appendage.
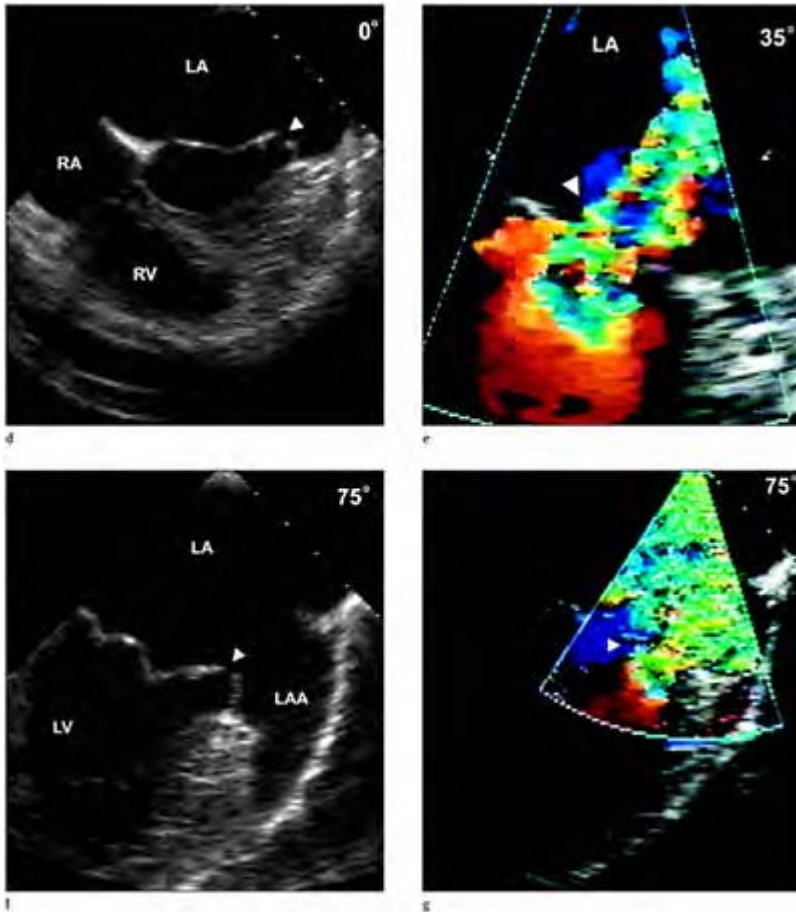
References

1. Edler I. Ultrasound cardiogram in mitral valve disease. *Acta Chir Scand* 1956;3:230.
2. Brock RC. The surgical and pathological anatomy of the mitral valve. *Br Heart J* 1952;14:489.
3. Rusted IE, Scheifley CH, Edwards JE. Studies of the mitral valve. I. Anatomic features of the normal mitral valve and associated structures. *Circulation* 1952;6:825.
4. Chiechi MA, Lees WM, Thompson R. Functional anatomy of the normal mitral valve. *J Thorac Surg* 1956;32:378.
5. Van der Spuy JC. The functional and clinical anatomy of the mitral valve. *Br Heart J* 1958;20:471.
6. Du Plessis LA, Marchand P. The anatomy of the mitral valve and its associated structures. *Thorax* 1964 ;19:221.
7. Silverman ME, Hurst JW. The mitral complex. Interaction of the anatomy, physiology and pathology of the mitral annulus, mitral valve leaflets, chordae tendineae and papillary muscles. *Am Heart J* 1968;76:399–418.

8. Carpentier A, Deloche A, Dauptain J, et al. A new reconstructive operation for correction of mitral and tricuspid insufficiency. *J Thorac Cardiovasc Surg* 1971;61:1–13.

9. Kinsley RH. Valve replacement. *Ann Life Ins Med* 1980;6:185.

10. Carpentier A. Cardiac valve surgery—the "French correction". *J Thorac Cardiovasc Surg* 1983;86:323–37.

11. Bonchek LI. Correction of mitral valve disease without valve replacement. *Am Heart J* 1982;104:865–8.

12. Antunes MJ, Colsen PR, Kinsley RH. Mitral valvuloplasty: a learning curve. *Circulation* 1983;68: II-70–5.

13. Cosgrove DM, Chavez AM, Lytle BW, et al. Results of mitral valve reconstruction. *Circulation* 1986;74:1-82–7.

14. Becker AE, De Wit APM. Mitral valve apparatus. A spectrum of normality relevant to mitral valve prolapse. *Br Heart J* 1979;42:680–9.

15. Roberts WC. Morphologic features of the normal and abnormal mitral valve. *Am J Cardiol* 1983;51:1005–28.

16. Perloff JK, Roberts WC. The mitral apparatus. Functional anatomy of mitral regurgitation. *Circulation* 1972;46:227–39.

17. Ranganathan N, Lam JHC, Wigle ED, Silver MD. Morphology of the human mitral valve. II. The valve leaflets. *Circulation* 1970;41:459–67.

18. Edwards JE, Burchell HB. Pathologic anatomy of mitral insufficiency. *Proc Staff Meet Mayo Clin* 1958;33:497.

19. Lam JHC, Ranganathan N, Wigle ED, Silver MD. Morphology of the human mitral valve. II. Chordae tendineae: a new classification. *Circulation* 1970;41:449–58.

20. Olson LJ, Subramanian R, Ackermann DM, et al. Surgical pathology of the mitral valve: a study of 712 cases spanning 21 years. *Mayo Clin Proc* 1987;62:22–34.

21. Dean AI Jr. The movements of the mitral cusps in relation to the cardiac cycle. *Am J Physiol* 1916;40:206.

22. Rushmer RF, Finlayson BL, Nash AA. Movements of the mitral valve. *Circ Res* 1956;4:337.

23. Zimmerman J, Bailey CP. The surgical significance of the fibrous skeleton of the heart. *J Thorac Cardiovasc Surg* 1962 ;44:701.

24. Komeda M, Glasson JR, Bolger AF, et al. Three-dimensional dynamic geometry of the normal canine mitral annulus and papillary muscles. *Circulation* 1996;49:II159–63.

25. Titus JL. Anatomy and pathology of the mitral valve. In: Surgery for acquired mitral valve disease. Ellis FH Jr. (ed). Philadelphia: Saunders, 1967.

26. Little RC. Effect of atrial systole on ventricular pressure and closure of the A-V valves. *Am J Physiol* 1951;166:289.

27. Sarris GE, Miller DC. Role of the mitral subvalvular apparatus in left ventricular systolic mechanics. *Sem Thorac Cardiovasc Surg* 1989;1:133–43.

28. Roberts WC, Cohen LS, Left ventricular papillary muscles. *Circulation* 1972;46:138–53.

29. Madu EC, D'Cruz IA. The vital role of papillary muscles in mitral and ventricular function: Echocardiographic insights. *Clin Cardiol* 1997;20:93–8.

30. Pandian NG, Hsu TL, Schwartz SL, et al. Multiplane transesophageal echocardiography. Imaging planes, echocardiographic anatomy, and clinical experience with a prototype phased array OmniPlane probe. *Echocardiography* 1992;9:649–66.

31. Bansal RC, Shakudo M, Shah PM, Shah PM. Biplane transesophageal echocardiography: Technique, image orientation, and preliminary experience in 131 patients. *J Am Soc Echocardiogr* 1990;3:348–66.

32. Pai RG, Tanimoto M, Jintapakorn W, et al. Volume rendered three-dimensional anatomy of the mitral annulus using transesophageal echocardiography. *Circulation* 1993;88:341–9.

33. Stumper O, Fraser AG, Ho SY, et al. Transesophageal echocardiography in the longitudinal axis: correlation between anatomy and images and its clinical implications. *Br Heart J* 1990;64:282–8.

34. Schneider A, Schwartz S, Pandian N, et al. Multiplane transesophageal echocardiography provides more precise echocardiography-anatomic definition and functional assessment of the normal and pathologic mitral valve and its apparatus. *J Am Coll Cardiol* 1993;21:83A.
35. Salutri A, Becker AE, Van Herwerden L, et al. Three-dimensional echocardiography of normal and pathologic mitral valve: a comparison with two-dimensional transesophageal echocardiography. *J Am Coll Cardiol* 1996;27:1502–10.
36. Chandraratna PAN, Aronow WS. Mitral valve ring in normal versus dilated left ventricle. Cross-sectional echocardiographic study. *Chest* 1981;79:151–4.
37. Come PC, Riley MF. M-mode and cross-sectional echocardiographic recognition of fibrosis and calcification of the mitral valve chordae and left ventricular papillary muscles. *Am J Cardiol* 1982;49:461–6.
38. Glasson JR, Komeda M, Daughters GT, et al. Loss of three-dimensional canine mitral annular systolic contraction with reduced left ventricular volumes. *Circulation* 1996;94:II152–8.
39. Deloche A, Jebara VA, Relland JYM, et al. Valve repair with Carpentier techniques. The second decade. *J Thorac Cardiovasc Surg* 1990;99:990–1001.
40. Assoun B, Diebold B, Abergel E, et al. Morphology-function relationship after mitral valve repair (abstr). *Circulation* 1992;86 (suppl I):I-724.
41. Mihaileanu S, Marino JP, Chauvaud S, et al. Left ventricular outflow obstruction after mitral valve repair (Carpentier's Technique): Proposed mechanisms of disease. *Circulation* 1988;78 (suppl I):I-78–84.
42. Gordon SPF, Douglas PS, Come PC, Manning WJ. Two-dimensional and Doppler echocardiographic determinants of the natural history of mitral valve narrowing in patients with rheumatic mitral stenosis: implications for follow-up. *J Am Coll Cardiol* 1992;19:968–73.
43. Sagie A, Freitas N, Padial LR, et al. Doppler echocardiographic assessment of long-term progression of mitral stenosis in 103 patients: valve area and right heart disease. *J Am Coll Cardiol* 1996;28:472–9.
44. Stoddard MF, Prince CR, Ammash NM, Goad JL. Two-dimensional transesophageal echocardiographic determination of mitral valve area in adults with mitral stenosis. *Am Heart J* 1994;127:1348–53.
45. Chen Y-T, Kan M-N, Chen J-S, et al. Contributing factors to formation of left atrial spontaneous echo contrast in mitral valvular disease. *J Ultrasound Med* 1990;91:51–5.
46. Daniel WG, Nellessen U, Shroder E, et al. Left atrial spontaneous echo contrast in mitral valve disease: an indicator for an increased thromboembolic risk. *J Am Coll Cardiol* 1988;11:1204–11.
47. Yamamoto K, Ikeda U, Seino Y, et al. Coagulation activity is increased in the left atrium of patients with mitral stenosis. *J Am Coll Cardiol* 1995;25:107–12.
48. Klein AL, Bailey AS, Cohen GI, et al. Effects of mitral stenosis on pulmonary venous flow as measured by Doppler transesophageal echocardiography. *Am J Cardiol* 1993;72:66–72.
49. Currie PJ, Hagle DJ, Seward JB, et al. Instantaneous pressure gradient: a simultaneous Doppler and dual catheter correlative study. *J Am Coll Cardiol* 1986;7:800–6.
50. Nishimura RA, Rihal CS, Tajik AJ, Holmes DR. Accurate measurement of the transmitral gradient in patients with mitral stenosis: a simultaneous catheterization and Doppler echocardiographic study. *J Am Coll Cardiol* 1994;24:152–8.
51. Kim WY, Bisgaard T, Nielsen SL, et al. Two-dimensional mitral flow velocity profiles in pig models using epicardial Doppler echocardiography. *J Am Coll Cardiol* 1994;24:532–45.
52. Pu M, Griffin BP, Vandervoort PM, et al. Intraoperative validation of mitral inflow determination by transesophageal echocardiography: comparison of single-plane, biplane and thermodilution techniques. *J Am Coll Cardiol* 1995;26:1047–53.
53. Dahan M, Paillole C, Martin D, Gourgon R. Determinants of stroke volume response to exercise in patients with mitral stenosis: a Doppler echocardiographic study. *J Am Coll Cardiol* 1993;21:384–9.

54. Libanoff AJ, Rodbard S. Atrioventricular pressure half-time: measure of mitral valve orifice area. *Circulation* 1968;38:144–50.
55. Hatle L, Angelsen B, Tromsdal A. Noninvasive assessment of atrioventricular pressure half-time by Doppler ultrasound. *Circulation* 1979;60:1096–104.
56. Stoddard MF, Prince CR, Tuman WL, Wagner SG. Angle of incidence does not affect accuracy of mitral stenosis area calculation by pressure half-time: application to Doppler transesophageal echocardiography. *Am Heart J* 1994;127:1562–72.
57. Triposkiadis F, Wooley CF, Boudoulas H. Mitral stenosis: left atrial dynamics reflect altered passive and active emptying. *Am Heart J* 1990;120:124–32.
58. Karp K, Teien D, Bjerle P, Eriksson P. Reassessment of valve area determinations in mitral stenosis by the pressure half-time method: impact of left ventricular stiffness and peak diastolic pressure difference. *J Am Coll Cardiol* 1989;13:594–9.
59. Braverman AC, Thomas JD, Lee RT. Doppler echocardiographic estimation of mitral valve area during changing hemodynamic conditions. *Am J Cardiol* 1991;68:1485–90.
60. Moro E, Nicolosi GL, Zanuttini D, et al. Influence of aortic regurgitation on the assessment of the pressure half-time and derived mitral-valve area in patients with mitral stenosis. *Eur Heart J* 1988;9:1010–17.
61. Flachskampf FA, Weyman AE, Gillam L, et al. Aortic regurgitation shortens Doppler pressure half-time in mitral stenosis: clinical evidence, in vitro simulation and theoretic analysis. *J Am Coll Cardiol* 1990;16:396–404.
62. Grayburn PA, Smith MD, Gurley J, et al. Effect of aortic regurgitation on the assessment of mitral valve orifice area by Doppler pressure half-time in mitral stenosis. *Am J Cardiol* 1987;60:322–6.
63. Bryg RJ, Williams GA, Labovitz AJ, et al. Effect of atrial fibrillation and mitral regurgitation on calculated mitral valve area in mitral stenosis. *Am J Cardiol* 1986;57:634–8.
64. Fredman CS, Pearson AC, Labovitz AJ, Kern MJ. Comparison of hemodynamic pressure half-time method and Gorlin formula with Doppler and echocardiographic determinations of mitral valve area in patients with combined mitral stenosis and regurgitation. *Am Heart J* 1990;119:121–9.
65. Wranne B, Ask P, Loyd D, Eng D. Analysis of different methods of assessing the stenotic mitral valve area with emphasis on the pressure gradient half-time concept. *Am J Cardiol* 1990;66: 614–20.
66. Knutsen KM, Bae EA, Sivertssen E, Grendahl H. Doppler ultrasound in mitral stenosis. Assessment of pressure gradient and atrioventricular pressure half-time. *Acta Med Scand* 1982;211:433–6.
67. Lloyd D, End D, Ask P, Wranne B. Pressure half-time does not always predict mitral valve area correctly. *J Am Soc Echocardiogr* 1988;1:313–21.
68. Nakatani S, Masuyama T, Kodama K, et al. Value and limitations of Doppler echocardiography in the quantification of stenotic mitral valve area: comparison of the pressure half-time and the continuity equation methods. *Circulation* 1988;77:78–85.
69. Faletra F, Pezzano A, Rossana F, et al. Measurement of mitral valve area in mitral stenosis: Four echocardiographic methods compared with direct measurement of anatomic orifices. *J Am Coll Cardiol* 1996;28:1190–7.
70. Thomas JD, Wilkins GT, Choong CY, et al. Inaccuracy of mitral pressure half-time immediately after percutaneous mitral valvotomy. Dependence on transmitral gradient and left atrial and ventricular compliance. *Circulation* 1988;78:980–93.
71. Ascah KJ, Stewart WJ, Gillam LD, et al. Calculation of transmitral flow by Doppler echocardiography: a comparison of methods in a canine model. *Am Heart J* 1989;117:402–10.
72. Kawahara T, Yamagishi M, Seo H, et al. Application of Doppler color flow imaging to determine valve area in mitral stenosis. *J Am Coll Cardiol* 1991;18:85–92.

73. Deng Y-B, Matsumoto M, Wang X-F, et al. Estimation of mitral valve area in patients with mitral stenosis by the flow convergence region method: selection of aliasing velocity. *J Am Coll Cardiol* 1994;24:683–9.

74. Rifkin RD, Harper K, Tighe D. Comparison of proximal isovelocity surface area method with pressure half-time and planimetry in evaluation of mitral stenosis. *J Am Coll Cardiol* 1995;26:458–65.

75. Rodriquez L, Monterroso V, Mueller L, et al. Validation of a new method for valve area calculation using the proximal isovelocity surface area in patients with mitral stenosis. *J Am Coll Cardiol* 1990;15:109A.

76. Moises VA, Chao K, Shandas R, et al. Effects of orifice size and shape on flow rate estimated from flow convergence region imaged by color Doppler flow mapping proximal to restrictive orifices: an in vitro study. *J Am Coll Cardiol* 1990;15:109A.

77. Utsunomiya T, Ogawa T, Tang HA, et al. Doppler color flow mapping of the proximal isovelocity surface area: a new method for measuring volume flow rate across a narrowed orifice. *J Am Soc Echocardiogr* 1991;4:338–48.

78. Chen C, Schneider B, Koschyk D, et al. Biplane transesophageal color Doppler echocardiography for assessment of mitral valve area with mitral inflow jet widths. *J Am Soc Echocardiogr* 1995;8:121–31.

79. Wilkins GT, Weyman AE, Abascal VM, et al. Percutaneous balloon dilatation of the mitral valve: an analysis of echocardiographic variables related to outcome and the mechanism of dilatation. *Br Heart J* 1988;60:299–308.

80. Condit JR, Benoit SB, Gottdiener JS. Transesophageal echocardiography is of no additional diagnostic value to transthoracic echocardiography in the evaluation of mitral stenosis for balloon mitral valvuloplasty. *Circulation* 1993;88:I-351.

81. Jaarsma W, Visser CA, Suttorp MJ, et al. Transesophageal echocardiography during percutaneous balloon mitral valvuloplasty. *J Am Soc Echocardiogr* 1989;2:380–5.

82. Cormier B, Vahanian A, Michel P-L, et al. The contribution of transesophageal echocardiography in the ultrasound assessment of percutaneous mitral valvuloplasty (abstr). *J Am Coll Cardiol* 1989;13:51-A.

83. Otto CM, Davis KB, Holmes DR, et al. Methodologic issues in clinical evaluation of stenosis severity in adults undergoing aortic or mitral balloon valvuloplasty. *Am J Cardiol* 1992;69:1607–16.

84. Casale PN, Whitlow P, Currie PJ, Stewart WJ. Transesophageal echocardiography in percutaneous balloon valvuloplasty for mitral stenosis. *Cleve Clin J Med* 1989;56:597–600.

85. Lung B, Cormier B, Ducimetiere P, et al. Immediate results of percutaneous mitral commissurotomy. A predictive model on a series of 1514 patients. *Circulation* 1996;94:2124–30.

86. Lung B, Cormier B, Ducimetiere P, et al. Functional results 5 years after successful percutaneous mitral commissurotomy in a series of 528 patients and analysis of predictive factors. *J Am Coll Cardiol* 1996;27:407–14.

87. Orange SE, Kawanishi DT, Lopez BM, et al. Actuarial outcome after catheter balloon commissurotomy in patients with mitral stenosis. *Circulation* 1997;95:382–9.

88. Manning WJ, Reis GJ, Douglas PS. Use of transesophageal echocardiography to detect left atrial thrombi before percutaneous balloon dilatation of the mitral valve: a prospective study. *Br Heart J* 1992;67:170–3.

89. Kronzon I, Tunick PA, Glassman E, et al. Transesophageal echocardiography to detect atrial clots in candidates for percutaneous transseptal mitral balloon valvuloplasty. *J Am Coll Cardiol* 1990;16:1320–2.

90. Orme EC, Wray RB, Mason JW. Balloon mitral valvuloplasty via retrograde left atrial catheterization. *Am Heart J* 1989;117:680–3.

91. Abascal VM, Wilkins GT, Choong CY, et al. Mitral regurgitation after percutaneous balloon mitral valvuloplasty in adults: evaluation by pulsed Doppler echocardiography. *J Am Coll Cardiol* 1988;11:257–63.
92. Mahan EF III, Ballal RS, Nanda NC. Mitral valve tear complicating percutaneous valvuloplasty: diagnosis by transesophageal Doppler color flow mapping. *Am Heart J* 1991;122:238–41.
93. O'Shea JP, Abascal VM, Wilkins GT, et al. Unusual sequelae after percutaneous mitral valvuloplasty: a Doppler echocardiographic study. *J Am Coll Cardiol* 1992;19:186–91.
94. Reid CL, McKay CR, Chandraratna PAN, et al. Mechanisms of increase in mitral valve area and influence of anatomic features in double-balloon, catheter balloon valvuloplasty in adults with rheumatic mitral stenosis: a Doppler and two-dimensional echocardiographic study. *Circulation* 1987;76:628–36.
95. Marwick Th, Torelli J, Obarski T et al. Assessment of the mitral valve splitability score by transthoracic and transesophageal echocardiography. *Am J Cardiol* 1994;22:194A.
96. Levin TN, Feldman T, Balasia B, et al. Commissural morphology to predict outcome after balloon mitral valvotomy. *Circulation* 1993;88:I-35.
97. Cannan CR, Nishimura RA, Reeder GS, et al. Echocardiographic assessment of commissural calcium: a simple predictor of outcome after percutaneous mitral balloon valvotomy. *J Am Coll Cardiol* 1997;29:175–80.
98. Jolly N, Arora R, Mohan J, Khalilullah M. Pulmonary venous flow dynamics before and after balloon mitral valvuloplasty as determined by transesophageal Doppler echocardiography. *Am J Cardiol* 1992;70:780–4.
99. Farhat MB, Boussadia H, Gandjbakhch I, et al. Closed versus open mitral commissurotomy in pure noncalcific mitral stenosis: Hemodynamic studies before and after operation. *J Thorac Cardiovasc Surg* 1990;99:639–44.
100. Lau K-W, Ding Z-P, Hung J-S. Percutaneous transvenous mitral commissurotomy versus surgical commissurotomy in the treatment of mitral stenosis. *Clin Cardiol* 1997;20:99–106.
101. Vasan RS, Shrivastava S, Kumar MV. Value and limitations of Doppler echocardiographic determination of mitral valve area in Lutembacher syndrome. *J Am Coll Cardiol* 1992;20:1362–70.
102. Yoshida K, Yoshikawa J, Akasaka T, et al. Assessment of left-to-right atrial shunting after percutaneous mitral valvuloplasty by transesophageal color Doppler flow-mapping. *Circulation* 1989;80:1521–6.
103. Kronzon I, Tunick PA, Goldfarb A, et al. Echocardiographic and hemodynamic characteristics of atrial septal defects created by percutaneous valvuloplasty. *J Am Soc Echocardiogr* 1990;3:64–71.
104. Palacios IF, Tuzcu ME, Weyman AE, Newell JB, Block PC. Clinical follow-up of patients undergoing percutaneous mitral balloon valvotomy. *Circulation* 1995;91:671–6.
105. Peterson KL. Timing of cardiac surgery in chronic mitral valve disease: implications of natural history studies and left ventricular mechanics. *Sem Thorac Cardiovasc Surg* 1989;1:106–17.
106. Ling LH, Enriquez-Sarano M, Seward JB, et al. Clinical outcome of mitral regurgitation due to flail leaflet. *N Engl J Med* 1996;335:1417–23.
107. Ling LH, Enriquez-Sarano M, Seward JB, et al. Early surgery in patients with mitral regurgitation due to flail leaflets. A long-term outcome study. *Circulation* 1997;96:1819–25.
108. Sand ME, Naftel DC, Blackstone EH, Kirklin JW, Karp RB. A comparison of repair and replacement for mitral valve incompetence. *J Thorac Cardiovasc Surg* 1987;94:208–19.
109. Cosgrove DM, Stewart WJ. Current problems in cardiology: mitral valvuloplasty. 1989;14(7):353–416.
110. Hellemans IM, Pieper EG, Ravelli ACJ, et al. Prediction of surgical strategy in mitral valve regurgitation based on echocardiography. *Am J Cardiol* 1997;79:334–8.

111. Stewart WJ, Currie PJ, Salcedo EE, et al. Intraoperative Doppler color flow mapping for decision-making in valve repair for mitral regurgitation. Technique and results in 100 patients. *Circulation* 1990;81:556–66.
112. Oki T, Fukuda N, Iuchi A, et al. Possible mechanisms of mitral regurgitation in dilated hearts: a study using transesophageal echocardiography. *Clin Cardiol* 1996;19:639–43.
113. Chandraratna PAN, Aronow WS. Mitral valve ring in normal vs. dilated left ventricle. Cross-sectional echocardiographic study. *Chest* 1981;79:151–4.
114. Tsakiris AG, von Bernuth G, Rastelli GC, et al. Size and motion of the mitral valve annulus in anesthetized intact dogs. *J Appl Physiol* 1971;30:611–18.
115. Bulkley BH, Roberts WC. Dilatation of the mitral annulus: a rare cause of mitral regurgitation. *Am J Med* 1975;59:457–63.
116. Madu EC, Reddy RC, D'Cruz IA. Papillary muscle morphology and function in LV systolic dysfunction and dilated cardiomyopathy: a transesophageal echocardiographic study (abstr). *J Am Soc Echocardiogr* 1996;9:371A.
117. Sigfusson G, Ettedgui JA, Silverman NH, Anderson RH. Is a cleft in the anterior leaflet of an otherwise normal mitral valve an atrioventricular canal malformation? *J Am Coll Cardiol* 1995;26:508–15.
118. Creech O, Ledbeter MK, Reemtsma K. Congenital insufficiency with a cleft in the posterior leaflet. *Circulation* 1962;25:390.
119. DiSegni E, Edwards JE. Cleft anterior leaflet of the mitral valve with intact septa. A study of twenty cases. *Am J Cardiol* 1983;51:915.
120. DiSegni E, Bass JL, Lucas RV Jr, et al. Isolated cleft mitral valve: a variety of congenital mitral regurgitation identified by 2-dimensional echocardiography. *Am J Cardiol* 1983;51:927–31.
121. Levine RA, Triulzi MO, Harrigan P, Weyman AE. The relationship of mitral annular shape to the diagnosis of mitral valve prolapse. *Circulation* 1987;75:756–67.
122. Levine RA, Handschumacher MD, Sanfilippo AJ, et al. Three-dimensional echocardiographic reconstruction of the mitral valve, with implications for the diagnosis of mitral valve prolapse. *Circulation* 1989;80:589–98.
123. Zuppiroli A, Rinaldi M, Kramer-Fox R, et al. Natural history of mitral valve prolapse. *Am J Cardiol* 1995;75:1028.
124. Boudoulas H, Kolibash AJ, Baker P, et al. Mitral valve prolapse and the mitral valve prolapse syndrome: a diagnostic classification and pathogenesis of symptoms. *Am Heart J* 1989;118:796–817.
125. Joh Y, Yoshikawa J, Yoshida K, et al. Transesophageal echocardiographic finding of mitral valve prolapse. *J Cardiol* 1989;19(suppl 21):85–95.
126. Titus JL, Edwards J. Mitral insufficiency other than rheumatic, ischemic, or infective: Emphasis on mitral valve prolapse. *Sem Thorac Cardiovasc Surg* 1989;1:118–28.
127. Pini R, Greppi B, Kramer-Fox R, et al. Mitral valve dimensions and motion and familial transmission of mitral valve prolapse with and without mitral leaflet billowing. *J Am Coll Cardiol* 1988;12:1423–31.
128. Turabian M, Chan K-L. Rupture of mitral chordae tendineae resulting from blunt chest trauma: diagnosis by transesophageal echocardiography. *Can J Cardiol* 1990;6:180–2.
129. Alam M, Sun I. Superiority of transesophageal echocardiography in detecting ruptured mitral chordae tendineae. *Am Heart J* 1991;121:1819–21.
130. Roth SL, Friedman GH, Bodenheimer MM, Chasanoff H. Redundant loops of chordae tendineae: a new potential cardiac source of embolism detected by transesophageal echocardiography. *J Am Coll Cardiol* 1994;22:75A.
131. Hozumi T, Yoshikawa J, Yoshida K, et al. Direct visualization of ruptured chordae tendineae by transesophageal two-dimensional echocardiography. *J Am Coll Cardiol* 1990;16:1315–19.
132. Schlueter M, Kremer P, Hanrath P. Transesophageal 2-D echocardiographic feature of flail mitral leaflet due to ruptured chordae tendineae. *Am Heart J* 1984;108:609–10.

133. Himelman RB, Kusumoto F, Oken K, et al. The flail mitral valve: echocardiographic findings by precordial and transesophageal imaging and Doppler color flow imaging. *J Am Coll Cardiol* 1991;17:272–9.

134. Louie EK, Langholz D, Mackin WJ, et al. Transesophageal echocardiographic assessment of the contribution of intrinsic tissue thickness to the appearance of a thick mitral valve in patients with mitral valve prolapse. *J Am Coll Cardiol* 1996;28:465–71.

135. Stewart WJ, Currie PJ, Salcedo EE, et al. Evaluation of mitral leaflet motion by echocardiography and jet direction by Doppler color flow mapping to determine the mechanism of mitral regurgitation. *J Am Coll Cardiol* 1992;20:1353–61.

136. Eliot RS, Edwards JE. Pathology of rheumatic fever and chronic valvular disease. In: Hurst JW (ed). *The Heart*(3rd edn) New York: McGraw-Hill, 1974.

137. McDonald L, Dealy JB, Rabinowitz M, et al. Clinical, physiological and pathological findings in mitral stenosis and regurgitation. *Medicine* 1957;36:237.

138. Perloff JK, Roberts WC. The mitral apparatus functional anatomy of mitral regurgitation. *Circulation* 1972;46:227.

139. Davies MJ, Moore BP, Brainbridge MB. The floppy mitral valve study of incidence, pathology and complications in surgical, necropsic and forensic material. *Br Heart J* 1978;40:468.

140. Guthrie RG, Edwards JE. Pathology of the myxomatous mitral valve. Nature, secondary changes and complications. *Minn Med* 1976;59:637.

141. Mintz GS, Victor MF, Kotler MN, et al. Two-dimensional echocardiographic identification of surgically correctable complications of acute myocardial infarction. *Circulation* 1981;64:91–6.

142. Come PC, Riley MF, Weintraub R, Morgan JP, Nakao S. Echocardiographic detection of complete and partial papillary muscle rupture during acute myocardial infarction. *Am J Cardiol* 1985;56:787–9.

143. Sakai K, Nakamura K, Hosoda S. Transesophageal echocardiographic findings of papillary muscle rupture. *Am J Cardiol* 1991;68:561–3.

144. Manning WJ, Waksmonski CA, Boyle NG. Papillary muscle rupture complicating inferior myocardial infarction: identification with transesophageal echocardiography. *Am Heart J* 1995;129:191–3.

145. Moursi MH, Bhatnagar SK, Vilacosta I, et al. Transesophageal echocardiographic assessment of papillary muscle rupture. *Circulation* 1996;94:1003–9.

146. Cerza RF. Echocardiography of papillary muscle hemorrhage. *J Cardiothor Vasc Anesth*1994;8:446–7.

147. Hauser A, Rathod K, McGill J, et al. Blood cysts of the papillary muscle. *Am J Cardiol* 1983;51:612–13.

148. Fishbein MC. Mitral insufficiency in coronary artery disease. *Sem Thorac Cardiovasc Surg* 1989;1:129–32.

149. Voci P, Bilotta F, Catetta Q, et al. Papillary muscle perfusion pattern. A hypothesis for ischemic papillary muscle dysfunction. *Circulation* 1995;91:1714–18.

150. Kaul S, Sponitz WD, Glasheen WP, Touchstone DA. Mechanism of ischemic mitral regurgitation: an experimental evaluation. *Circulation* 1991;84:2167–80.

151. Byram MT, Roberts WC, Frequency and extent of calcific deposits in purely regurgitant mitral valves: analysis of 108 operatively excised valves. *Am J Cardiol* 1983;52:1059–61.

152. Akamatsu S, Uematsu H, Yamamoto M, et al. Evaluation of physiological mitral regurgitant flow with transesophageal Doppler echocardiography (abstr). *Jpn Circulation J* 1989;53:663.

153. Omoto R, Kyo S, Matsumura M, et al. Evaluation of biplane color Doppler transesophageal echocardiography in 200 consecutive patients. *Circulation* 1992;85:1237–47.

154. Matsumara M, Kyo S, Shah P, et al. A new look at mitral valve pathology with bi-plane color Doppler transesophageal probe (abstr). *Circulation* 1989;80 suppl 2:II–579.

155. Yoshida K, Yoshikawa J, Yamaura Y, et al. Assessment of mitral regurgitation by biplane transesophageal color Doppler flow mapping. *Circulation* 1990;82:1121–6.

156. Schnittger I, Appleton CP, Hatle LK, Popp RL. Diastolic mitral and tricuspid regurgitation by Doppler echocardiography in patients with atrioventricular block: new insight into the mechanism of atrioventricular valve closure. *J Am Coll Cardiol* 1988;11:83.

157. Rokey R, et al. Detection of diastolic atrioventricular valvular regurgitation by pulse Doppler echocardiography and its association with complete heart block. *Am J Cardiol* 1986;57:692.

158. Clyne CA, Cuenoud HF, Pape LA. Diastolic mitral regurgitation occurring with complete atrioventricular block detected by Doppler color flow mapping. *Echocardiography* 1989;6:543.

159. Sadoshima J-I, Koyanagi S, Sugimachi M, et al. Evaluation of the severity of mitral regurgitation by transesophageal Doppler flow echocardiography. *Am Heart J* 1992;123:1245–51.

160. Cooper JW, Nanda NC, Philpot EF, Fan P. Evaluation of valvular regurgitation by color Doppler. *J Am Soc Echocardiogr* 1989;2:56–66.

161. Wang SS, Rubenstein JJ, Goldman, Sidd JJ. A new Doppler-echocardiography method to quantify regurgitant volume. *J Am Soc Echocardiogr* 1992;5:107–14.

162. Walker PG, Oyre S, Pedersen EM, et al. A new control volume method for calculating valvular regurgitation. *Circulation* 1995;92:579–86.

163. Kleinman JP, Czer LSC, DeRobertis M, et al. A quantitative comparison of transesophageal and epicardial color Doppler echocardiography in the intraoperative assessment of mitral regurgitation. *Am J Cardiol* 1989;64:1168–72.

164. Enriquez-Sarano M, Tajik AJ, Bailey KR, Seward JB. Color flow imaging compared with quantitative Doppler assessment of severity of mitral regurgitation: influence of eccentricity of jet and mechanism of regurgitation. *J Am Coll Cardiol* 1993;21:1211–19.

165. Miyatake K, Izumi, Okamoto M, et al. Semiquantitative grading of severity of mitral regurgitation by real-time two dimensional Doppler flow imaging technique. *J Am Coll Cardiol* 1986;7: 82–88.

166. Shiota T, Jones M, Teien DE, et al. Dynamic change in mitral regurgitant orifice area: Comparison of color Doppler echocardiographic and electromagnetic flowmeter-based methods in a chronic animal model. *J Am Coll Cardiol* 1995;26:528–36.

167. Sahn DJ. Instrumentation and physical factors related to visualiza-tion of stenotic and regurgitant jets by Doppler color flow mapping. *J Am Coll Cardiol* 1988;12:1354–65.

168. Mizushige K, Shiota T, Paik J, et al. Effects of pulmonary venous flow direction on mitral regurgitation jet area as imaged by color Doppler flow mapping. An in vitro study. *Circulation* 1995;19:1834–9.

169. Helmcke F, Nanda NC, Hsiung MC, et al. Color Doppler assessment of mitral regurgitation with orthogonal planes. *Circulation* 1987;75:175–83.

170. Castello R, Lenzen P, Aquirre F, Labovitz A. Variability in the quantitation of mitral regurgitation by Doppler color flow mapping: comparison of transthoracic and transesophageal studies. *J Am Coll Cardiol* 1992;20:433–8.

171. Smith MD, Harrison MR, Pinton R, et al. Regurgitant jet size by transesophageal compared with transthoracic Doppler color flow imaging. *Circulation* 1991;83:79–86.

172. Castello R, Lenzen P, Aguirre F, Labovitz A. Quantitation of mitral regurgitation by transesophageal echocardiography with Doppler color-flow mapping: correlation with cardiac catheterization. *J Am Coll Cardiol* 1992;19:1516–21.

173. Enriquez-Sarano M, Bailey KR, Seward JB, et al. Quantitative Doppler assessment of valvular regurgitation. *Circulation* 1993;87:841–8.

174. Rokey R, Sterling LL, Zoghbi WA, et al. Determination of regurgitant fraction in isolated mitral or aortic regurgitation by pulsed Doppler two-dimensional echocardiography. *J Am Coll Cardiol* 1986;7:1273–8.

175. Enriquez-Sarano M, Seward JB, Bailey KR, Tajik AJ. Effective regurgitant orifice area: a noninvasive Doppler development of an old hemodynamic concept. *J Am Coll Cardiol* 1994;23:443–51.

176. Tanabe K, Yoshitomi H, Oyake N, et al. Effects of supine and lateral recumbent positions on pulmonary venous flow in healthy subjects evaluated by transesophageal Doppler echocardiography. *J Am Coll Cardiol* 1994;24:1552–7.

177. Teien DE, Jones M, Shiota T, et al. Doppler evaluation of severity of mitral regurgitation: relation to pulmonary venous flow patterns in an animal study. *J Am Coll Cardiol* 1995;25:264–8.

178. Passafini A, Shiota T, Depp M, et al. Factors influencing pulmonary venous flow velocity patterns in mitral regurgitation: an in vitro study. *J Am Coll Cardiol* 1995;26:1333–9.

179. Klein AL, Obarski TP, Calafiore PC, et al. Reversal of systolic flow in pulmonary veins by transesophageal Doppler echocardiography predicts severity of mitral regurgitation (abstr). *J Am Coll Cardiol* 1990;15:74A.

180. Klein AL, Obarski TP, Stewart J, et al. Transesophageal Doppler echocardiography of pulmonary venous flow: a new marker of mitral regurgitation severity. *J Am Coll Cardiol* 1991;18:518–26.

181. Klein AL, Tajik AJ. Doppler assessment of pulmonary venous flow in healthy subjects and in patients with heart disease. *J Am Soc Echocardiogr* 1991;4:379–92.

182. Castello R, Pearson AC, Lenzen P, Labovitz AJ. Effect of mitral regurgitation on pulmonary venous velocities derived from transesophageal echocardiography color-guided pulse Doppler imaging. *J Am Coll Cardiol* 1991;17:1499–506.

183. Tribouilloy C, Shen WF, Quere JP, et al. Assessment of severity of mitral regurgitation by measuring regurgitating jet width at its origin with transesophageal Doppler color flow imaging. *Circulation* 1992;85:1248–53.

184. Baumgartner H, Schima H, Kuhn P. Value and limitations of proximal jet dimensions for the quantitation of valvular regurgitation: an in vitro study using Doppler flow imaging. *J Am Soc Echocardiogr* 1991;4:57–66.

185. Grayburn PA, Fehske W, Omran H, et al. Multiplane transesophageal echocardiographic assessment of mitral regurgitation by Doppler color flow mapping of the vena contracta. *Am J Cardiol* 1994;74:912–17.

186. Mele D, Vandervoort P, Palacios I, et al. Proximal jet size by Doppler color flow mapping predicts severity of mitral regurgitation. *Clinical Studies Circ* 1995;91:746–54.

187. Hall SA, Brickner E, Willet DL, et al. Assessment of mitral regurgitation severity by Doppler color flow mapping of the vena contracta. *Circulation* 1997;95:636–42.

188. Simpson IA, Sahn DJ. Hydrodynamic investigation of a hemodynamic problem: a review of the in vitro evaluation of mitral insufficiency by color Doppler flow mapping. *J Am Soc Echocardiogr* 1989;2:67–72.

189. Recusani F, Bargiggia GS, Yoganathan AP, et al. A new method for quantification of regurgitant flow rate using color Doppler flow imaging of the flow convergence region proximal to a discrete orifice: an in vitro study. *Circulation* 1991;83:594–604.

190. Utosonomiya T, Ogawa T, Tang HA, et al. Doppler color flow mapping of the proximal isovelocity surface area: a new method for measuring volume flow rate across a narrowed orifice. *J Am Soc Echocardiogr* 1991;4:338–48.

191. Giesler MO, Stauch M. Color Doppler determination of regurgitant flow: from proximal isovelocity surface areas to proximal velocity profiles. *Echocardiography* 1992;9:51–62.

192. Geisler M, Grossmann G, Schmidt A, et al. Color Doppler echocardiographic determination of mitral regurgitant flow from the proximal velocity profile of the flow convergence region. *Am J Cardiol* 1993;71:217–24.

193. Chen C, Koschyk D, Brockhoff C, et al. Noninvasive estimation of regurgitant flow rate and volume in patients with mitral regurgitation by Doppler color mapping of accelerating flow field. *J Am Coll Cardiol* 1993;21:374–83.

194. Deng Y-B, Matsumoto M, Wang X-F, et al. Estimation of mitral valve area in patients with mitral stenosis by the flow convergence region method: selection of aliasing velocity. *J Am Coll Cardiol* 1994;24:683–9.

195. Enriquez-Sarano M, Miller FA, Hayes SN, et al. Effective mitral regurgitant orifice area: clinical use and pitfalls of the proximal isovelocity surface area method. *J Am Coll Cardiol* 1995;25:703–9.
196. Enriquez-Sarano M, Sinak LJ, Tajik AJ, et al. Changes in effective regurgitant orifice throughout systole in patients with mitral valve prolapse. A clinical study using the proximal isovelocity surface area method. *Circulation* 1995;92:2951–8.
197. Pu M, Vandervoort PM, Griffin BP, et al. Quantification of mitral regurgitation by the proximal convergence method using transesophageal echocardiography. Clinical validation of a geometric correction for proximal flow constraint. *Circulation* 1995;92:2169–77.
198. Pu M, Vandervoort PM, Greenberg NL, et al. Impact of wall constraint on velocity distribution in proximal flow convergence zone. Implications for color Doppler quantification of mitral regurgitation. *J Am Coll Cardiol* 1996;27:706–13.
199. Vandervoort PM, Rivera JM, Mele D, et al. Application of color Doppler flow mapping to calculate effective regurgitant orifice area: an in vitro study with initial clinical observations. *Circulation* 1993;88:1150–6.
200. Shiota T, Sinclair B, Ishii M, et al. Three-dimensional reconstruction of color Doppler flow convergence regions and regurgitant jets: an in vitro quantitative study. *J Am Coll Cardiol* 1996;27:1511–18.
201. Simpson IA, Shiota T, Gharib M, Sahn D. Current status of flow convergence for clinical applications: is it a leaning tower of "PISA"? *J Am Coll Cardiol* 1996;27:504–9.
202. Thomas JD. How leaky is that mitral valve? Simplified Doppler methods to measure regurgitant orifice area. *Circulation* 1997;95:548–50.
203. Stoddard MF, Prince CR, Dillon S, et al. Exercise-induced mitral regurgitation is a predictor of morbid events in subjects with mitral valve prolapse. *J Am Coll Cardiol* 1995;25:693–9.
204. Kontos GJ, Schaff HV, Gersh BJ, Bove AA. Left ventricular function in subacute and chronic mitral regurgitation. Effect on function early postoperatively. *J Thorac Cardiovasc Surg* 1989;98:163–9.
205. Starling MR. Effects of valve surgery on left ventricular contractile function in patients with long-term mitral regurgitation. *Circulation* 1995;92:811–18.
206. Enriquez-Sarano M, Schaff HV, Orszulak TA, et al. Valve repair improves the outcome of surgery for mitral regurgitation. A multi-variate analysis. *Circulation* 1995;91:1022–8.
207. Enriquez-Sarano M, Tajik AJ, Schaff HV, et al. Echocardiographic prediction of left ventricular function after correction of mitral regurgitation: results and clinical implications. *J Am Coll Cardiol* 1994;24:1536–43.
208. Goldman ME, Mora F, Guarino T, Fuster V, Mindich BP. Mitral valvuloplasty is superior to valve replacement for preservation of left ventricular function: an intraoperative two-dimensional echocardiographic study. *J Am Coll Cardiol* 1987;10:568–75.
209. Rahko PS, Berkoff HA. Echocardiographic comparison of cardiac size and function before and after surgery for isolated mitral valve repair versus mitral valve replacement. *Acta Cardiologica* 1990;3:189–94.
210. Enriquez-Sarano M, Schaff HV, Orszulak TA, et al. Congestive heart failure after surgical correction of mitral regurgitation. A long-term study. *Circulation* 1995;92:94–6.
211. Corin WJ, Sutsch G, Murakami T, Krogmann ON, Turina M, Hess OM. Left ventricular function in chronic mitral regurgitation: preoperative and postoperative comparison. *J Am Coll Cardiol* 1995;25:113–21.
212. Madu EC, Reddy RC, D'Cruz IA. Transesophageal echocardiography assessment of papillary muscle anatomy and contraction in patients with and without left ventricular hypertrophy. *J Am Coll Cardiol* 1996;27(suppl A):350A.
213. Levine RA, Vlahakes GJ, Lefebvre X, et al. Papillary muscle displacement cause systolic anterior motion of the mitral valve. Experimental validation and insights into the mechanism of subaortic obstruction. *Circulation* 1995;91:1189–95.

214. Pomerance A. Pathological and clinical study of calcification of the mitral valve ring. *J Clin Pathol* 1970;23:354–60.

215. Roberts WC. Morphological features of the normal and abnormal mitral valve ring. *Am J Cardiol* 1983;51:1005–28.

216. Pomerance A, Davies MJ. The pathology of the heart. Oxford: Blackwell Scientific Publication, 1975.

217. Criley JM, Lewis K, Humphries JO, Ross RS. Prolapse of the mitral valve; clinical and cineangiographic findings. *Br Heart J* 1966;28:488–96.

218. Schieken R, Kerber RE, Ionasescu W, Zellweger H. Cardiac manifestations of the mucopolysaccharidoses. *Circulation* 1975;52:700–5.

219. Harrison CV, Lennox B. Heart block in osteitis deformans. *Br Heart J* 1948;10:167–73.

220. Nestico PF, Depace NL, Morganroth J, et al. Mitral annular calcification: clinical pathophysiology and echocardiographic review. *Am Heart J* 1984;107:989–96.

221. Hammer WJ, Roberts WC, deLeon AC Jr. "Mitral stenosis" secondary to combined "massive" mitral annular calcific deposits and small, hypertrophied left ventricles: hemodynamic documentation in four patients. *Am J Med* 1978;64:371–6.

222. Mellino M, Salcedo EE, Lever HM, et al. Echocardiographic quantified severity of mitral annulus calcification. *Am Heart J* 1982;103:222–5.

223. DeBono DP, Warlow CP. Mitral annulus calcification and cerebral or retinal ischemia. *Lancet* 1979;2:383–5.

224. Meltzer RS, Martin RP, Robbins BS, Popp RL. Mitral annular calcification: clinical and echocardiographic features. *Acta Cardiol (Brux)* 1980;35:189–202.

225. Wong M, Tei C, Shah PM. Sensitivity and specificity of two-dimensional echocardiography in the detection of valvular calcification. *Chest* 1983;84:423–7.

226. Asmar BE, Acker M, Couetil JP, et al. Mitral valve repair in the extensively calcified mitral valve annulus. *Ann Thorac Surg* 1991;52:66–9.

227. Erbel R, Rohmann S, Drexler M, et al. Improved diagnostic value of echocardiography in patients with infective endocarditis by transesophageal approach. A prospective study. *Eur Heart J* 1988;9:45–53.

228. Daniel WG, Shroder E, Mugge A, Lichtlen PR. Transesophageal echocardiography in infective endocarditis. *Am J Card Imaging* 1988;2:78–85.

229. Daniel WG, Schroder E, Nonnast-Daniel B, Lichtlen PR. Conventional and transesophageal echocardiography in the diagnosis of infective endocarditis. *Eur Heart J* 1987;8 (suppl J):287–92.

230. Klodas E, Edwards WD, Khandheria BK. Use of transesophageal echocardiography for improving detection of valvular vegetations in subacute bacterial endocarditis. *J Am Soc Echocardiogr* 1989;2:386–9.

231. Birmingham GD, Rahko PS, Ballantyne F III. Improved detection of infective endocarditis with transesophageal echocardiography. *Am Heart J* 1992;123:774–81.

232. Khandheria BK. Suspected bacterial endocarditis: to TEE or not to TEE. *J Am Coll Cardiol* 1993;21:222–4.

233. Martin RP, Meltzer RS, Chia BL, et al. Clinical utility of two dimensional echocardiography in infective endocarditis. *Am J Cardiol* 1980;46:379–85.

234. Mugge A, Daniel WG, Frank G, Lichtlen PR. Echocardiography in infective endocarditis: reassessment of prognostic implications of vegetation size determined by the transthoracic and the transesophageal approach. *J Am Coll Cardiol* 1989;14:631–8.

235. Sochowski RA, Chan K-L. Implications of negative results on a monoplane transesophageal echocardiographic study in patients with suspected infective endocarditis. *J Am Coll Cardiol* 1993;21:216–21.

236. Shively BK, Gurule FT, Roland CA, et al. Diagnostic value of transesophageal compared with transthoracic echocardiography in infective endocarditis. *J Am Coll Cardiol* 1991;18:391–7.

237. Taams MA, Gussenhoven EJ, Bos E, et al. Enhanced morphological diagnosis in infective endocarditis by transesophageal echocardiography. *Br Heart J* 1990;63:109–13.
238. Dillion JC, Feigenbaum H, Konecke LL, et al. Echocardiographic manifestations of valvular vegetations. *Am Heart J* 1973;86:698–704.
239. Roy P, Tajik AJ, Giuliani ER, et al. Spectrum of echocardiographic findings in bacterial endocarditis. *Circulation* 1976;53:474–82.
240. Sanfilippo AJ, Picard MH, Newell JB, et al. Echocardiographic assessment of patients with infectious endocarditis: prediction of risk for complications. *J Am Coll Cardiol* 1991;18:1191–9.
241. Job FP, Lethen H, Franke S, et al. Benefit of bi- or multiplane versus monoplane TEE for the assessment of endocarditic lesions (abstr). *J Am Coll Cardiol* 1993;21:488A.
242. Schwinger ME, Tunick PA, Freedberg RS, Kronzon I. Vegetations on endocardial surfaces struck by regurgitant jets: diagnosis by transesophageal echocardiography. *Am Heart J* 1990;119:1212–15.
243. Rohmann S, Erbel R, Gorge G, et al. Clinical relevance of vegetation localization by transesophageal echocardiography in infective endocarditis. *Eur Heart J* 1992;13:446–52.
244. Stafford A, Wann LS, Dillion JC, et al. Serial echocardiographic appearance of healing bacterial endocarditis. *Am J Cardiol* 1979;44:754–60.
245. Stratton JR, Werner JA, Pearlman AS, et al. Bacteremia and the heart: serial echocardiographic findings in 80 patients with documented or suspected bacteremia. *Am J Med* 1982;73:851–8.
246. Tak T, Rahimtoola SH, Kumar A, et al. Value of digital image processing of two-dimensional echocardiograms in differentiating active from chronic vegetations of infective endocarditis. *Circulation* 1988;78:116–23.
247. Stewart JA, Silimperi D, Harris P, et al. Echocardiographic documentation of vegetative lesions in infective endocarditis: clinical implications. *Circulation* 1980;61:374–80.
248. Buchbinder NA, Roberts WC. Left-sided valvular active infective endocarditis: a study of forty-five necropsy patients. *Am J Med* 1972;53:20–35.
249. Arnett EN, Roberts WC. Valve ring abscess in active infective endocarditis: frequency, location, and clues to clinical diagnosis from the study of 95 necropsy patients. *Circulation* 1976;54:140–5.
250. Nomeir A-M, Downes TR, Cordell AR. Perforation of the anterior mitral leaflet caused by aortic valve endocarditis: diagnosis by two-dimensional, transesophageal echocardiography and color flow Doppler. *J Am Soc Echocardiogr* 1992;5:195–8.
251. Ballal RS, Mahan EF III, Nanda NC, Sanyal R. Aortic and mitral valve perforation: diagnosis by transesophageal echocardiography and Doppler color flow imaging. *Am Heart J* 1991;121:214–17.
252. Daniel WG, Mugge A, Martin RP, et al. Improvement in the diagnosis of abscesses associated with endocarditis by transesophageal echocardiography. *N Engl J Med* 1991;324:795–800.
253. Massey WM, Samdarshi TE, Nanda NC, et al. Serial documentation of changes in a mitral valve vegetation progressing to abscess rupture and fistula formation by transesophageal echocardiography. *Am Heart J* 1992;124:241–8.
254. Afridi I, Apostolidou MA, Saad RM, Zoghbi WA. Pseudoaneurysms of the mitral-aortic intervalvular fibrosa: dynamic characterization using transesophageal echocardiographic and Doppler techniques. *J Am Coll Cardiol* 1995;25:137–45.
255. Bansal RC, Graham BM, Jutzy KR, et al. Left ventricular outflow tract to left atrial communication secondary to rupture of mitral-aortic intervalvular fibrosa in infective endocarditis: diagnosis by transesophageal echocardiography and color flow imaging. *J Am Coll Cardiol* 1990;15:449–504.
256. Rohmann S, Erbel R, Darius H, et al. Prediction of rapid versus prolonged healing of infective endocarditis by monitoring vegetation size. *J Am Soc Echocardiogr* 1991;4:465–74.

257. Vuille C, Nidorf M, Weyman AE, Picard MH. Natural history of vegetations in successfully treated endocarditis (abstr). *J Am Coll Cardiol* 1993;21:200A.

258. Rohmann S, Erbel R, Darius H, et al. Influence of antibiotics on vegetation size in infective endocarditis: a comparative study (abstr). *J Am Coll Cardiol* 1993;21:391A.

259. Meric M, Castello R, Ofili EO, et al. Transesophageal echocardiography in infective endocarditis: prognostic implications of vegetation size and mobility (abstr). *J Am Coll Cardiol* 1993;21:391A.

260. Hojnik M, George J, Ziporen L, Shoenfeld Y. Heart valve involvement (Libman-Sacks endocarditis) in the antiphospholipid syndrome. *Circulation* 1996;93:1579–87.

261. Blanchard DG, Ross RS, Dittrich HC. Nonbacterial thrombotic endocarditis: assessment by transesophageal echocardiography. *Chest* 1992;102:954–6.

262. Lopez JA, Ross RS, Fishbein MC, Siegel RJ. Nonbacterial thrombotic endocarditis: a review. *Am Heart J* 1987;113:773–84.

263. Nihoyannopoulos P, Gomez PM, Joshi J, et al. Cardiac abnormalities in systemic lupus erythematosus: association with raised anticardiolipin antibodies. *Circulation* 1990;82:369–75.

264. Roldan CA, Shively BK, Crawford MH. An echocardiographic study of valvular heart disease associated with systemic lupus erythematosus. *N Engl J Med* 1996;335:1424–30.

265. Barbut D, Borer JS, Wallerson D, et al. Anticardiolipin antibody and stroke: possible relation of valvular heart disease and embolic events. *Cardiology* 1991;79:99–109.

266. Grenadier E, Sahn DJ, Valdes-Cruz LM, et al. Two-dimensional echocardiography Doppler study of congenital disorders of the mitral valve. *Am Heart J* 1984;107:319.

267. Smallhorn J, Tommasini G, Deanfield J, et al. Congenital mitral stenosis. Anatomical and functional assessment by echocardiography. *Br Heart J* 1981;45:527.

268. Vitarelli A, Landolina G, Gentile R, et al. Echocardiographic assessment of congenital mitral stenosis. *Am Heart J* 1984;108:523.

269. Chauvaud S, Perier P, Touati G, et al. Long-term results of valve repair in children with acquired mitral valve incompetence. *Circulation* 1986;74:1104–9.

270. Coles JG, Williams WG, Watanabe T, et al. Surgical experience with reparative techniques in patients with congenital mitral valvular anomalies. *Circulation* 1987;76(suppl 111):111–17.

271. Stellin G, Bortolotti U, Mazzucco A, et al. Repair of congenitally malformed mitral valve in children. *J Thorac Cardiovasc Surg* 1988;95:480–5.

272. Curcio CA, Cronje SL. Partial atrioventricular canal in an adult: mitral valve repair by reverse implantation of a Carpentier ring. *J Thorac Cardiovasc Surg* 1987;94:444–5.

273. Levy MJ, Varco RL, Lillehei CW, Edwards JE. Mitral insufficiency in infants, children and adolescents. *J Thorac Cardiovasc Surg* 1963;45:434.

274. Shone JD, Sellers RD, Anderson RC, et al. The developmental complex of "parachute mitral valve", supravalvular ring of left atrium, subaortic stenosis, and coarctation of aorta. *Am J Cardiol* 1963;11:714.

275. Macartney FJ, Scott O, Ionescu MI, Deverall PB. Diagnosis and management of parachute mitral valve and supravalvar mitral ring. *Br Heart J* 1974;36:641.

276. Glancy DL, Chang MY, Dorney ER, Roberts WC. Parachute mitral valve. Further observations and associated lesions. *Am J Cardiol* 1971;27:309.

277. Layman TE, Edwards JE Anomalous mitral arcade. A type of congenital mitral insufficiency. *Circulation* 1967;35:389.

278. Carpentier A, Branchini B, Cour JC, et al. Congenital malformations of the mitral valve in children. Pathology and surgical treatment. *J Thorac Cardiovasc Surg* 1976;72:854–66.

279. Castaneda AR, Anderson RC, Edwards JE. Congenital mitral stenosis resulting from anomalous arcade and obstructing papillary muscles. Report of correction by use of ball valve prosthesis. *Am J Cardiol* 1969;24:237.

280. Ruckman RN, Van Praagh R. Anatomic types of congenital mitral stenosis: report of 49 autopsy cases with consideration of diagnosis and surgical implications. *Am J Cardiol* 1978;42:592–601.

281. Wenink ACG, Gittenberger-de Groot AC, Brom AG. Developmental considerations of mitral valve anomalies. *Int J Cardiol* 1986;11:85.
282. Berghuis J, Kirklin JW, Edwards JE, Titus JL. The surgical anatomy of isolated congenital mitral insufficiency. *J Thorac Cardiovasc Surg* 1964;47:791.
283. Collins-Nakai RL, Rosenthal A, Castaneda AR, et al. Congenital mitral stenosis. A review of 20 years' experience. *Circulation* 1977;56:1039.
284. Anabtawi IN, Ellison RG. Congenital stenosing ring of the left atrioventricular canal (supravalvular mitral stenosis). *J Thorac Cardiovasc Surg* 1965;49:994.
285. Snider AR, Roge CL, Schiller NB, Silverman NH. Congenital left ventricular inflow obstruction evaluated by two-dimensional echocardiography. *Circulation* 1980;61:848–55.
286. Kay JH, Zubiate P, Mendez MA, et al. Mitral valve repair for significant mitral insufficiency. *Am Heart J* 1978;96:253.
287. Cohn LH. Surgery for mitral regurgitation. *JAMA* 1988;260:2883.
288. Cooley DA. Technical problems in mitral valve repair and replacement. *Ann Thorac Surg* 1989;48:S91–2 .
289. Lessana A, Carbone C, Romano M, et al. Mitral valve repair: results and the decision-making process in reconstruction. Report of 275 cases. *J Thorac Cardiovasc Surg* 1990;99:622.
290. Cooper GJ, Wright EM, Smith GH. Mitral valve repair: a valuable procedure with good long-term results even when performed infrequently. *Br Heart J* 1991;66:156–60.
291. Krause AH, Okies JE, Bigelow JC, et al. Early experience with mitral valve reconstruction for mitral insufficiency. *Am J Surg* 1991;161:563–6.
292. Loop FD, Cosgrove DM, Stewart WJ. Mitral valve repair for mitral insufficiency. *Eur Heart J* 1991;12 (suppl B):30–3.
293. Cohn LH. Reparative mitral valve surgery. *Choices in Cardiology* 1992;7:7–9.
294. Odell JA, Hartzell VS, Orszulak TA. Early results of a simplified method of mitral valve annuloplasty. *Circulation* 1995;92:II-150.
295. Rao V, Christakis GT, Weisel RD, et al. Changing pattern of valve surgery. *Circulation* 1996;94:II113–19.
296. Michel PL, Lung B, Blanchard B, et al. Long-term results of mitral valve repair for non-ischaemic mitral regurgitation. *Eur Heart J* 1991;12(suppl B):39–43.
297. Grossi EA, Galloway AC, LeBoutillier M, et al. Anterior leaflet procedures during mitral valve repair do not adversely influence long-term outcome. *J Am Coll Cardiol* 1995;25:134–6.
298. Cohn LH, DiSesa VJ, Couper GS, et al. Mitral valve repair for myxomatous degeneration and prolapse of the mitral valve. *J Thorac Cardiovasc Surg* 1989;98:987–93.
299. Cosgrove DM. Surgery for degenerative mitral valve disease. *Sem Thorac Cardiovasc Surg* 1989;1:183–93.
300. Loop FD. Long-term results of mitral valve repair. *Sem Thorac Cardiovasc Surg* 1989;1:203–10.
301. Hendren WG, Nemec JJ, Lytle BW, et al. Mitral valve repair for ischemic mitral insufficiency. *Ann Thorac Surg* 1991;52:1246–52.
302. Kay GL, Kay JH, Zubiate P, et al. Mitral valve repair for mitral regurgitation secondary to coronary artery disease. *Circulation* 1986;74:I-88.
303. Rankin JS, Feneley MP,St. J. Hickey M, et al. A clinical comparison of mitral valve repair versus valve replacement in ischemic mitral regurgitation. *J Thorac Cardiovasc Surg* 1988;95:165–77.
304. Craver JM, Cohen C, Weintraub WS. Case-matched comparison of mitral valve replacement and repair. *Ann Thorac Surg* 1990;49:964.
305. Yun KL, Miller DC. Mitral valve repair versus replacement. *Cardiology Clinics* 1991;9:315.
306. Cohn LH, Kowalker W, Bhatia S, et al. Comparative morbidity of mitral valve repair versus replacement for mitral regurgitation with and without coronary artery disease. *Ann Thorac Surg* 1988;45:284.

307. Rankin JS, Livesey SA, Smith LR, et al. Trends in the surgical treatment of ischemic mitral regurgitation: effects of mitral valve repair on hospital mortality. *Sem Thorac Cardiovasc Surg* 1989;1:149–63.
308. Acar J, Michel PL, Luxereau P, Vahanian A, Cormier B. Indications for surgery in mitral regurgitation. *Eur Heart J* 1991;12(suppl B):52–4.
309. Lessana AL, Romano M, Lutfalla G, et al. Treatment of ruptured or elongated anterior mitral valve chordae by partial transposition of the posterior leaflet: experience with 29 patients. *Ann Thorac Surg* 1988;45:404.
310. Antunes MJ, Magalhaes MP, Colsen PR, et al. Valvuloplasty for rheumatic mitral valve disease. A surgical challenge. *J Thorac Cardiovasc Surg* 1987;94:44–56.
311. Antunes MJ. Mitral valvuloplasty for rheumatic heart disease. *Sem Thorac Cardiovasc Surg* 1989;1:164.
312. Duran CMG, Gometza B, DeVol EB. Valve repair in rheumatic mitral disease. *Circulation* 1991;84:III-125.
313. Frater RWM, Vetter HO, Zussa C, Dahm M. Chordal replacement in mitral valve repair. *Circulation* 1990;82:IV-125.
314. Kobayashi Y, Seiki N, Ohmori F, Eishi K, Miyatake K. Mitral valve dysfunction resulting from thickening and stiffening of artificial mitral valve chordae. *Circulation* 1996;94:II129–32.
315. David TE, Bos J, Rakowski H. Mitral valve repair by replacement of chordae tendineae with polytetrafluoroethylene sutures. *J Thorac Cardiovasc Surg* 1991;101:495–501.
316. Chauvaud S, Jebara V, Chachques J-C, et al. Valve extension with glutaraldehyde-preserved autologous pericardium. Results in mitral valve repair. *J Thorac Cardiovasc Surg* 1991;102:171–8.
317. Hendren WG, Morris AS, Rosenkranz ER, et al. Mitral valve repair for bacterial endocarditis. *J Thorac Cardiovasc Surg* 1992;103:124–9.
318. Aranki SF, Adams DH, Rizzo RJ, et al. Determinants of early mortality and late survival in mitral valve endocarditis. *Circulation* 1995;92:II143–9.
319. Pagani FD, Monaghan HL, Deeb GM, Bolling SF. Mitral valve reconstruction for active and healed endocarditis. *Circulation* 1996;94:II-133.
320. d'Udekem Y, David TE, Feinder CM et al. Long term results of surgery for active infective endocarditis. *Euro J Cardiothorac S* 1997;11(1):46–52.
321. David TE, Komeda M, Pollick C, Burns RJ. Mitral valve annuloplasty: the effect of the type on left ventricular function. *Ann Thorac Surg* 1989;47:524–8.
322. Unger-Graeber B, Lee RT, St. John Sutton M, et al. Doppler echocardiographic comparison of the Carpentier and Duran annuloplasty rings versus no ring after mitral valve repair for mitral regurgitation. *Am J Cardiol* 1991;67:517–19.
323. Galler M, Kronzon I, Slater J, et al. Long-term follow-up after mitral valve reconstruction: incidence of postoperative left ventricular outflow obstruction. *Circulation* 1986;74:I99–103.
324. Kronzon I, Cohen ML, Winer HE, Colvin SB. Left ventricular outflow obstruction: a complication of mitral valvuloplasty. *J Am Coll Cardiol* 1984;4:825–8.
325. Freeman WK, Schaff HV, Khandheria BK, et al. Intraoperative evaluation of mitral valve regurgitation and repair by transesophageal echocardiography: incidence and significance of systolic anterior motion. *J Am Coll Cardiol* 1992;20:599–609.
326. Kreindel MS, Schiavone WA, Lever HM, Cosgrove D. Systolic anterior motion of the mitral valve after Carpentier ring valvuloplasty for mitral valve prolapse. *Am J Cardiol* 1986;57:408–412.

3
Aortic valvular disease

Multiplane transesophageal echocardiography provides precise imaging planes, which offer improved detail and visualization of aortic valve anatomy for defining aortic pathology. Multiplane transesophageal echocardiography has significantly improved the diagnosis of aortic valvular disease in selected cases, although transthoracic echocardiography still remains a very useful technique for evaluating the structure and function of the aortic valve.

Multiplane transesophageal echocardiography has become instrumental in the diagnosis of aortic pathology, especially when questions arise resulting from transthoracic echocardiography or cardiac catheterization. In cases of aortic stenosis, multiplane transesophageal echocardiography reveals the number of cusps, the degree of valve restriction or valve area, the extent of leaflet calcification, and establishes the presence of secondary subvalvular obstruction. With aortic regurgitation, multiplane transesophageal echocardiography often defines the anatomical deformity of the aortic complex, illustrating the mechanism for regurgitation, which, when incorporated with the natural history of the disease process, greatly assists in clinical management. In addition, transesophageal echocardiography provides precise measurements of the aortic valve annulus, aortic root and other dimensions of the aorta. Most importantly, transesophageal echocardiography has become an integral part of aortic valve surgery. During surgery, transesophageal echocardiography is useful for assessing the need for reparative surgery versus valve replacement. In cases of valve replacement, transesophageal echocardiography assists in determining the type of aortic prosthesis used, as well as in evaluating the prosthesis after implant.

Normal anatomy

The normal aortic valve consists of three semilunar cusps, however to accurately describe normal aortic valve anatomy the aortic root and left ventricular outflow tract must be included (figure 3.1).[1–3] These structures constitute the "aortic valve complex" which in unison play an integral role in providing the normal structure and function of the aortic valve.

The aortic root, or proximal portion of the ascending thoracic aorta, encloses the aortic valve annulus and leaflets. The aortic annulus forms the origin of the aortic root and is located in the relative center of the fibromuscular skeleton of the heart (figure 3.2). The

central position in the fibromuscular skeleton provides the stability necessary for supporting the aortic valve and aorta. The aortic valve annulus is not as well defined anatomically as the mitral valve annulus, given that it is largely composed of muscle fibers and not fibrous connective tissue as in the latter. The muscular annulus allows the base of the leaflets to expand in diastole and to contract in systole, which promotes the unimpeded flow of blood from the left ventricular outflow tract to the aorta.
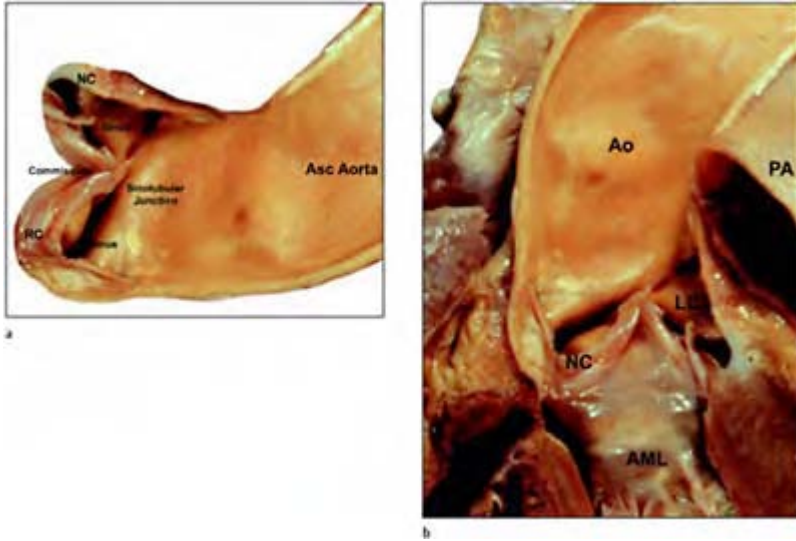
Figure 3.1 Aortic root anatomy. Aortic root anatomic preparations (a) dissection and (b) in situ preparation with the anterior aortic wall and right coronary cusp removed. To properly describe the aortic valve anatomy and function, the whole aortic valve complex must be considered (b). The aortic valve complex comprises the left ventricular outflow tract, aortic annulus, and sinuses of Valsalva, sinotubular junction and the ascending aorta. The borders of the left ventricular outflow tract are formed medially by the proximal or basal portion of the left ventricular septum and laterally by the anterior leaflet of

the mitral valve when open during diastole. This anatomic configuration produces a functional outflow tract rather than a true anatomical or morphological outflow tract, when compared with the well-delineated infundibulum of the right ventricular outflow tract. NC, non-coronary cusp; RC, right coronary cusp; LC, left coronary cusp; AML, anterior mitral leaflet; Ao, ascending aorta; PA, pulmonary artery.

The area inferior to the aortic annulus represents the subvalvular region or the left ventricular outflow tract. The borders of the left ventricular outflow tract are formed medially by the proximal or basal portion of the left ventricular septum and laterally by the anterior leaflet of the mitral valve when open during diastole. This anatomic configuration produces a functional outflow tract rather than a true anatomical or morphological outflow tract, when compared with the well-delineated infundibulum of the right ventricular outflow tract. This is especially important when considering certain developmental abnormalities that cause the anatomical configurations of specific congenital malformations. Also, since the left ventricular outflow tract is composed of a muscular portion (ventricular septum) and a fibrous portion (anterior mitral leaflet); normal function of the aortic valve is dependent on the function of both the mitral apparatus and ventricular myocardium.

The aortic valve is composed of three leaflets or cusps (figure 3.3a). Each leaflet of the aortic valve has a semilunar or crescent-shaped free margin and a rounded or semicircular-shaped base (figure 3.3c). This configuration produces a base leaflet length that is one and a half times larger than the free leaflet margin and a central leaflet height that is larger than its lateral height. The central portion of the base of the leaflets is attached to the inferior portion of the aortic annulus, blending into the proximal aortic wall and ending as the sinotubular junction before the true ascending aorta. Each aortic leaflet is connected to the other at their lateral most margins by inserting into the sinus ridge or uppermost portion of the aortic root, producing triangular hinge points or commissures (figure 3.3d). The leaflets are symmetrically arranged in the circular aortic root producing three aortic cusps and three sinuses of Valsalva. In cross-section, the commissures are attached in a triangular arrangement within the barrel of the aorta so that the leaflets with their curved free margins have a configuration that allows for a circular leaflet opening during systole. Thus, the maximum valve area during systole is normally 3–4 cm^2 produced by leaflet separation of about 2 cm.

The cusps are delineated with respect to their orientation in the annulus and by the origin of the coronary arteries (figure 3.3a). The right aortic cusp is situated
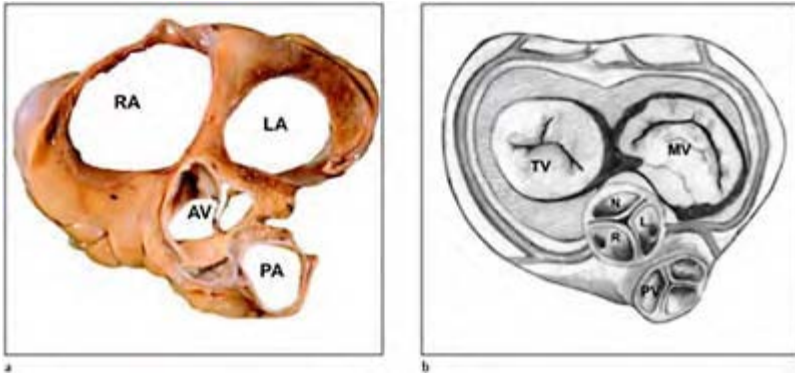
Figure 3.2 Cross-sectional anatomy of the aortic valve
and surrounding structure of the fibrous skeleton as
seen in standard horizontal transesophageal
echocardiographic views. The aortic valve is centrally
located in the fibrous skeleton and is surrounded by all
three of the other cardiac valves in various planes
depicted in (a) anatomical dissection and (b) drawing
of the fibrous skeleton. The aortic annulus is defined by
the area of attachment of the aortic cusps to the aortic
wall, and therefore is frequently described as not being
a true anatomical annulus. Due to the scalloped
attachment of the aortic cusps, the aortic annulus has a
larger vertical height corresponding to the dimension of
the whole sinus of Valsalva, in contrast to the height of
the mitral annulus with the leaflets attached in a
circular orientation in smaller vertical plane roughly
corresponding to the depth of the fibrous skeleton. In
this regard, the aortic annulus protrudes above and
below the horizontal plane or depth of the fibrous
skeleton. The aortic annulus is divided into
subcommissural and supracommissural (supra-aortic
crest) areas to define the full extent of the annulus. RA,
right atrium; LA, left atrium; AV, aortic valve; PA,
pulmonary artery; TV, tricuspid valve; MV, mitral
valve; N, non-coronary cusp; R, right coronary cusp; L,
left coronary cusp; PV, pulmonary valve.

anteriorly and to the right, the left aortic cusp is posterior and to the left, and the non-coronary cusp is posterior and to the right and is directly opposite the atrial septum. The coronary arteries originate from the respective sinuses produced by the right and left cusps, with ostia positioned centrally below the sinus ridge. The central position of the aortic annulus brings each aortic cusp into close proximity to other cardiac structures as well. The non-coronary cusp sits opposite the atrial septum and portions correspond to both atria. The left coronary cusp sits opposite the left atrium, in between the pulmonary trunk and the left atrial appendage. Both the left coronary and non-coronary cusps are attached to the fibrous portion of the anterior mitral leaflet. The right coronary cusp sits opposite the right ventricular outflow tract with a base of attachment to the muscular septum.

There is a prominent thickening or nodule in the center of the free margin of each cusp known as the node of Arantus (figure 3.3c). Two curved linear ridges of thickened leaflet tissue emanate from either side of the node, roughly 2–3 mm from the free margin border of each leaflet, and project laterally to each commissure. This ridge of tissue marks the line of approximation for each cusp during diastolic closure and the lunula provides for cuspal apposition, permitting a good seal for closure. A thin rim of leaflet tissue extends above the thickened ridge or lunula, and together comprises the free leaflet margin and provides the necessary surface of contact for the cusps during apposition. The surface area of each cusp is nearly identical, and the total surface area of all three cusps is roughly 40% greater than the cross-sectional area of the aortic root at the annular level. Therefore there is adequate leaflet tissue surface area to allow each cusp to protrude or bow slightly towards the left ventricular outflow tract during closure, thus dampening the pressure transmitted in the aorta during diastole, and ultimately preventing the cusp from eversion.

Figure 3.3 Aortic valve anatomical preparation as seen from the aorta (a) and from the ventricle (b) illustrating the relative position of the closed cusps in diastole. Dissection of a single aortic valve cusp (c) illustrating and highlighting the node of Arantus (green) and the lunula surface area (blue). Cuspal configuration of the aortic valve cusps showing the commissural attachment and alignment of the cusps. Note the right and left coronary artery ostia position relative to the cusps. The aortic valve cusps are attached to the aortic wall in a semicircular fashion with the commissures producing the apex of a tall narrow triangle between the union of

the cusps. This orientation of each cusp produces the load-bearing architecture necessary for withstanding the diastolic pressure. The broader vertical height and narrow width of the interleaflet triangle promotes the necessary leaflet surface area necessary for complete cuspal coaptation. The intercuspal triangles are highlighted in blue. R, right coronary cusp; N, non-coronary cusp; L, left coronary cusp.
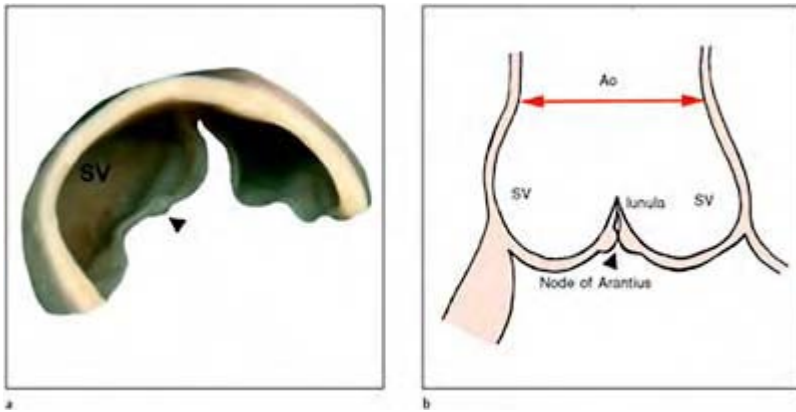
Figure 3.4 Anatomical (a) and artists rendition (b) of the aortic valve cusps showing the cuspal margins and the node of Arantus (closed arrows). The lunula provides even greater surface area and serves to reinforce the free margin of the edge of the cusps. The maximum load point at the center of each cusp is further reinforced by the nodule of Arantus represented as a further thickening of the central portion of the leaflet lunula. Working in unison, the valve cusps and commissures support the physiologic diastolic pressure load during closure. The sinotubular junction is illustrated in b, which is usually narrower by 10 to 15% in comparison with the aortic annulus diameter. Ao, aorta.

The sinotubular junction or superior margin of the sinus of Valsalva is well delineated horizontally. The sinotabular junction is composed of collagen and elastin connective tissue and is 10 to 15% smaller in diameter than the aortic annulus.[3] This allows the aortic wall to protrude or balloon slightly above the annulus when the leaflets are opposed, forming the sinuses of Valsalva. This anatomical configuration of the sinuses allows for a pocket of blood to form above each cusp, which promotes diastolic filling of the coronary artery (figure 3.4). This allows the stress developed in diastole to be equally distributed

by the leaflet tissue as well as the aortic wall. It also prevents the cusps from collapsing or becoming trapped against the aortic wall with the high pressures generated during systole when the valve is open, and overall decreases leaflet degeneration and/or wear.

Echocardiographic visualization of the normal aortic valve

Multiplane transesophageal echocardiography provides excellent anatomical images of the aortic valve for assessment of the number of cusps, cuspal motion and structure as well as for defining pathology of the aortic valve and root. Multiplane transesophageal echocardiography permits the aortic valve to be visualized enface in the short axis planes and in long axis projections with only minor manipulation of the probe, in comparison with either monoplane or biplane probes.
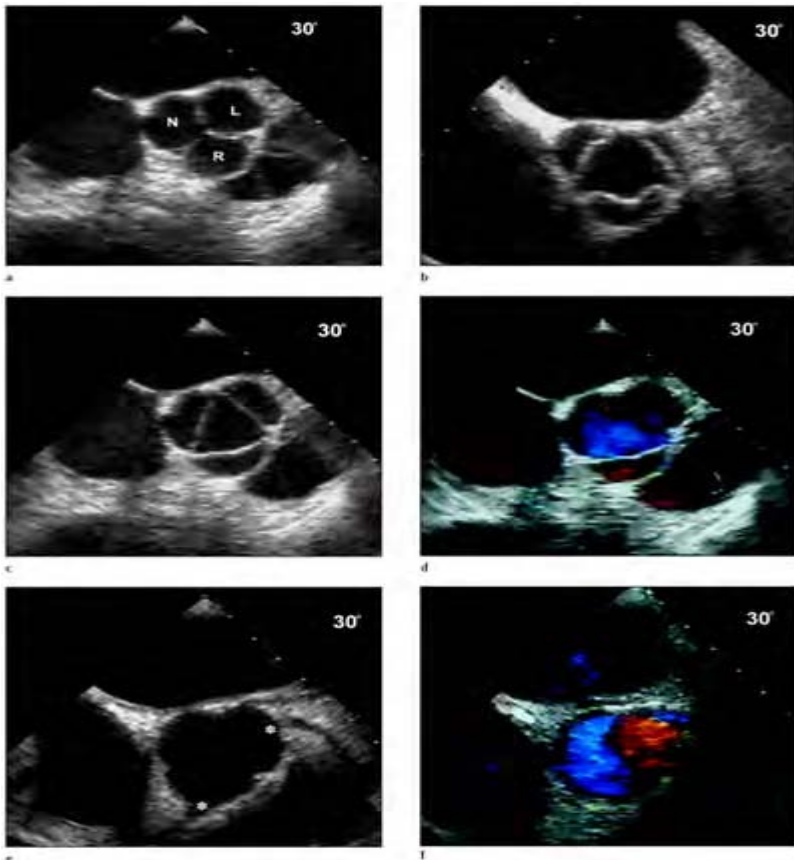
Figure 3.5 Normal horizontal, short axis aortic valve complex transesophageal anatomy as viewed from the mid to upper esophageal windows at 15–60 degrees. All three

cusps are visualized in a short axis projection during systole and diastole (a–d). The left coronary cusp is to the right of the image sector; the right coronary cusp is anterior and to the left of the image sector and the non-coronary cusp sits to the right opposite the atrial septum (a). In the normal aortic valve the leaflets gradually assume a triangular opening (c) and the leaflet margins may appear slightly redundant (b). With the valve leaflets fully open during systole the margins assume a circular opening blending into the aortic wall and are usually not visible, but slight indentions may be seen projecting from the aortic wall representing the commissures (d). With minor withdrawal of the probe and antegrade flexion the coronary artery ostia are visible (e–f). N, non-coronary cusp; L, left coronary cusp; R, right coronary cusp; star, coronary ostia.

The three cusps of the aortic valve are best visualized enface in the short axis plane, with the probe in the mid to upper esophageal position at a depth of 10–12 cm. The aorta is initially identified and centered with rotation of the probe in the echo sector with conventional image display (transducer artifact at the top of the display and the patient's right side on the left of the display). The transesophageal echocardiography probe is advanced or withdrawn occasionally with mild anteflexion until the aortic valve leaflets are visualized and the transducer is then rotated to approximately 15–45 degrees, until all three cusps are visualized enface in the center of the echocardiography sector (figure 3.5). The most anterior cusp in the bottom portion of the image sector is the right coronary cusp; the non-coronary cusp lies adjacent to the atrial septum, with the left coronary cusp posterior and to the right closer to the top of the image sector. All three cusps should appear symmetrical in size and shape. The commissures are always visualized in contrast to transthoracic studies, which only visualize the commissures in about 73% of cases.[4] Motion of the valve cusps is readily assessed with multiplane transesophageal echocardiography. With normal tricuspid aortic valve motion during early and late systole, the partially open valve resembles a three-arm star shape. Just before midsystole the open valve assumes a triangular shape, with nearly straight cuspal margins, and during midsystole the orifice assumes a circular shape.[5] The normal aortic valve orifice area is in the range of 2.5 to 3.5 cm^2.[5] During diastole the cusps should appear well apposed, producing a configuration that resembles the Mercedes-Benz emblem. When lack of closure of the leaflets is suspected, color flow Doppler is often useful in the short axis view for identifying the location of aortic regurgitation jet (and/or jets) and the size of the regurgitant orifice area. Diffuse or focal thickening of the leaflets and restriction of leaflet motion and/or commissures is readily apparent. Planimetry of the aortic valve systolic orifice area, measurement of the length of the free cuspal margin and leaflet separation may easily be performed in this view. With further anteflexion at this level, the sinuses of Valsalva are visualized with the orifice of both coronary arteries visualized

adjacent to their respective cusps, slightly superior to the valve but below the sinotubular junction (figure 3.5).

The long axis view of the aortic valve is obtained by centering the aortic valve in the short axis image sector and by rotating the transducer to between 120 to 145 degrees (approximately 90° past the true short axis, figure 3.6). Minimal manipulation of the probe may be necessary to maximize the internal diameter of the aortic root. The left ventricular outflow tract should appear to the left of the sector and the proximal ascending aorta to the right of the image sector in a horizontal plane perpendicular to the transducer. The aortic valve should appear in the mid portion of the aortic root and the full extent of two cusps should appear as thin linear echoes. The most anterior cusp toward the bottom of the image sector is the right coronary cusp, and the most posterior cusp toward the top of the display may be either the non-coronary or left coronary cusp depending upon the image beam orientation to the aortic valve. The aortic valve annulus is readily identified by the points of attachment of the valve cusps to the aortic root walls originating from the left ventricular outflow tract. During systole, the leaflets appear as thin linear echoes originating from the annulus, which move parallel to and almost approximate the aortic root walls when they frequently disappear from view. During diastole the leaflets move toward the center of the aortic root, producing a central line of closure with the body of the leaflets bowing slightly towards the outflow tract with symmetrical protrusion to the annulus.

The size of the aortic root may be assessed by measuring each segment. The diameter is measured at the aortic annulus, sinuses of Valsalva, sinotubular junction and proximal ascending aorta (figure 3.7). The normal aortic systolic annular diameter is about 1.8–2.5 cm.[6] The normal sinotubular junction should be approximately 10 to 15% smaller in diameter than the aortic annulus.[7,8] Color flow Doppler is useful in the long axis view for identifying increased flow velocities and/or turbulent flow when restricted motion is suspected during systole, or for detecting and quantifying aortic regurgitant jets. The supravalvular and subvalvular structures are also best assessed in the long axis views.

Hemodynamic assessment of the aortic valve with conventional Doppler is usually more easily accomplished with transthoracic echocardiography than with the transesophageal approach, owing to the inability to obtain parallel imaging planes with transesophageal echocardiography. Continuous and pulsed-wave Doppler may be successfully performed in around 80% of patients, with multiplane transesophageal echocardiography in the deep transgastric view or the transgastric long axis views.
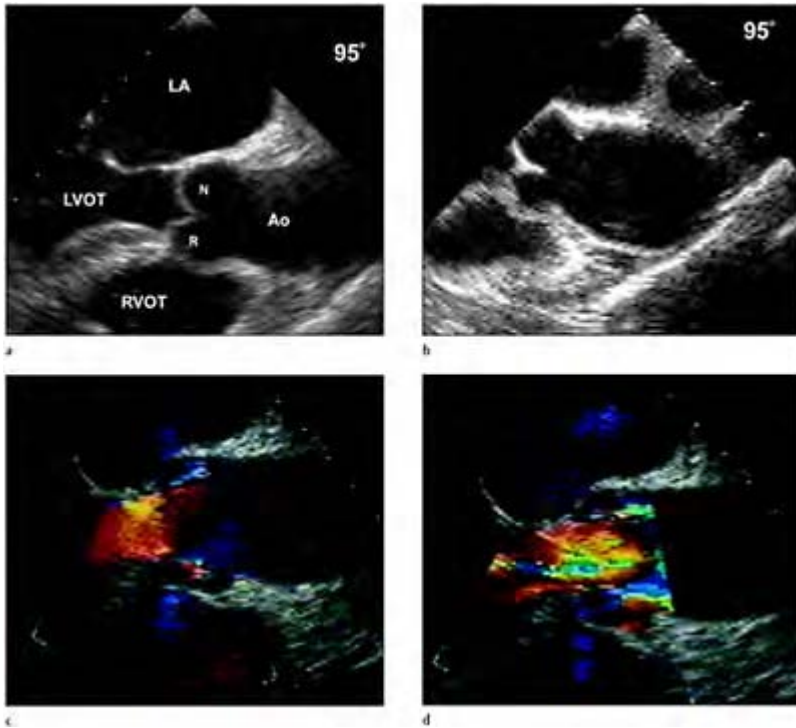
Figure 3.6 Normal longitudinal, long axis aortic valve complex transesophageal anatomy. Long axis views are obtained of the aortic root with rotation of the transducer about 90 degrees from the short axis (enface) aortic valve views (a–d). The most superior cusp represents the left or non-coronary cusp depending on the interrogating plane, with the right coronary cusp appearing in the inferior portion of the image sector. With a normal aortic valve the aortic annulus is fully appreciated, with bulging of the sinus of Valsalva and narrow neck of the sinotubular junction. With valve opening during systole, the aortic valve leaflets blend into the aortic walls and are usually not visible. LA, left atrium; LVOT, left ventricular outflow tract; RVOT, right ventricular outflow tract; Ao, aorta; N, non-coronary cusp; R, right coronary cusp.
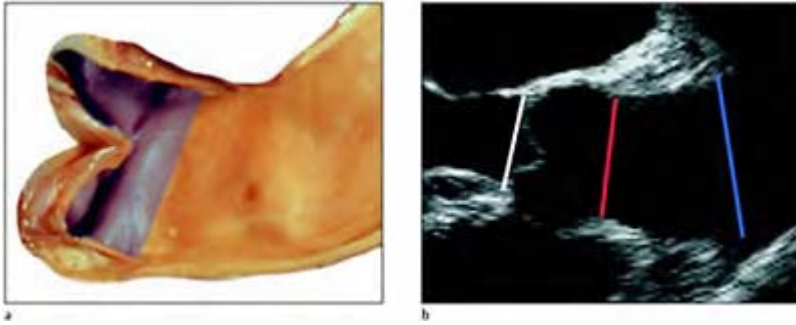
Figure 3.7 Normal echocardiographic measurements of the aortic valve complex in the longitudinal imaging planes. Anatomical preparation (a) and corresponding echocardiographic image (b) of the aortic valve complex to show the usual points of measurement for the aortic valve annulus, sinotubular junction and ascending aorta. White, annular diameter; red, sinotubular junction diameter; blue, ascending aorta diameter.

The deep transgastric view is obtained by advancing the probe deep into the stomach approximating the level of the left ventricular apex. The probe is then slowly withdrawn with maximum anteflexion until an image is produced similar to the apical five view obtained with transthoracic echocardiography. To obtain the deep transgastric view it is often helpful to start with the short axis gastric view with the left ventricle centered in the image sector. The probe is then advanced into the stomach while maintaining maximum anteflexion of the probe almost as to produce buckling of the probe on itself to open the deep transgastric window of the heart. The echocardiographic depth sector is changed to approximately 20 to 22 cm, to accommodate the whole heart image. The ventricular apex is directed obliquely towards the top of the display, with the left ventricle to the right and the right ventricle to the left of the display (figure 3.8). The aortic valve is displayed in the center of the display in the far field with the left ventricular outflow tract roughly parallel to the image plane. Adequate assessment of the aortic valve apparatus is usually not possible in this view, with the exception of occasional pathology of the ventricular surface of the valve and subvalvular pathology. Pulsed-wave Doppler can be performed in the left ventricular outflow tract with the sample volume positioned proximal to the aortic valve. Continuous-wave Doppler can be used to interrogate flow across the aortic

valve with the mapping assistance of color flow Doppler. In our experience, adequate continuous-wave Doppler signals are obtained in around 80% of cases.

The transgastric long axis view is obtained by rotating the transducer from 90 to 120 degrees from the mid short axis transgastric view of the left ventricle (figure 3.9). The ventricular apex is directed towards the left of the image and the base of the heart to the right of the image display. The left ventricular outflow tract and the aortic valve appear obliquely projected in the far field to the right lower quadrant of the display. Slight probe manipulation with rightward flexion may be helpful in visualizing the aortic valve, and as with the deep transgastric view the echocardiographic depth may need to be increased to greater than 16 cm to accommodate the whole image. Color flow Doppler may be helpful to direct both pulsed and continuous-wave Doppler for interrogation of the left ventricular outflow tract and aortic valve flows. As with the deep transgastric views, adequate Doppler signals for velocity measurements may not be obtained in all patients. When adequate Doppler signals are obtained with the transesophageal approach, the velocities measured are identical to and as accurate as those obtained with transthoracic echocardiographic measurements.

Bicuspid aortic valve

The bicuspid aortic valve is one of the most common congenital abnormalities, occurring in about 1% of the general population.[9] The congenitally bicuspid valve is identified by two cusps of unequal size, the conjoined cusp is the larger, and contains a raphe that represents the site of fusion of the conjoined cusps. This configuration produces a narrowed elliptical orifice rather than a circular orifice, which occurs with a tricuspid valve. Bicuspid aortic valves may function normally throughout life, but because of their opening and closing configuration, most become stenotic, regurgitant, or both stenotic and regurgitant. In 85 patients with bicuspid aortic valves studied by Roberts[9] 15% had a normally functioning aortic valve. In 72%, there was aortic stenosis with or without regurgitation, with only 13% having pure aortic regurgitation. Additionally, 9% of bicuspid aortic valves that were purely regurgitant were associated with infective endocarditis.

The mechanism responsible for stenosis or regurgitation of a bicuspid aortic valve originates from the differences in cuspal configuration and arrangement or

orientation in comparison with tricuspid valves (figure 3.10).

The most obvious anatomical differences in cuspal configuration between tricuspid and bicuspid aortic valves are commissure positioning and in cuspal length. These differences cause inadequate opening or closure of the valve.[10] The cuspal configuration of a tricuspid aortic valve produces a line of cuspal closure, which assumes the shape of a curve. This curvature in tricuspid aortic valves allows for the extra length necessary for the cusps to move maximally during opening and provide adequate leaflet tissue length for approximation with closure. With a bicuspid leaflet configuration, the line of cuspal closure between the commissures approaches a straight line instead of a curve, in effect shortening the cuspal margin length. In addition minor differences in cuspal length produces abnormal cuspal contact. When each cusp of a bicuspid valve is approximately
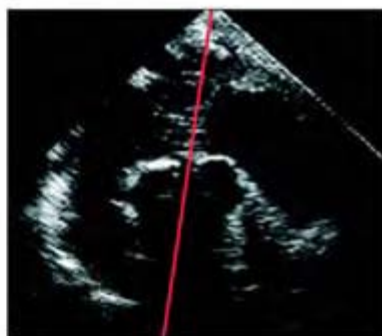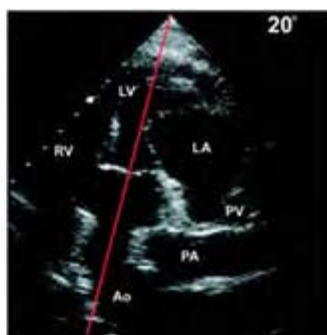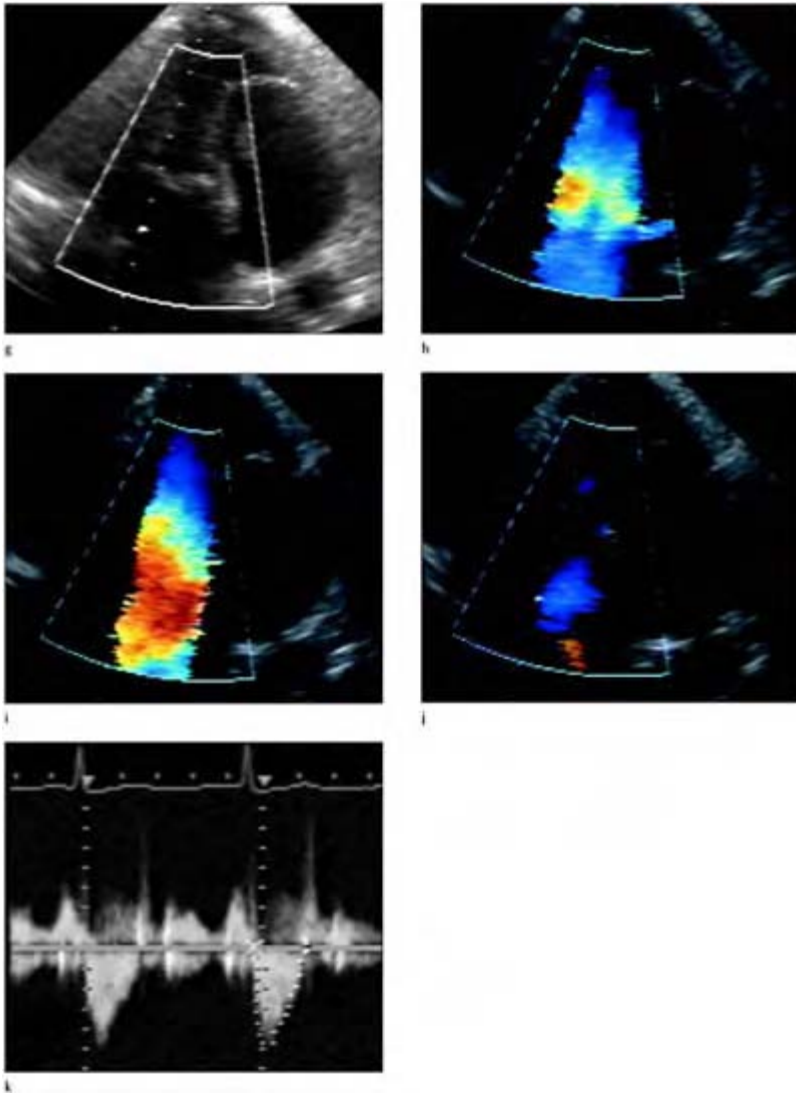
Figure 3.8 Normal deep transgastric
views of the aortic valve complex. In
most patients the aortic valve complex
may be visualized and assessed from
the deep transgastric views, which
allows an almost parallel orientation of
the aortic root to the imaging beam.
The entire aortic root in three-

dimensions may be visualized in a circumferential fashion with rotation of the transducer from 0 to 120 degrees (g–k). In zoom mode the aortic valve leaflets are readily visible to assess opening and closing motion. Conventional and color flow Doppler may be used in these views to assess valve function. LV, left ventricle; Ao, aorta; RV, right ventricle; PA, pulmonary artery; PV, pulmonary vein; LA, left atrium; RA, right atrium; AV, aortic valve; MV, mitral valve.
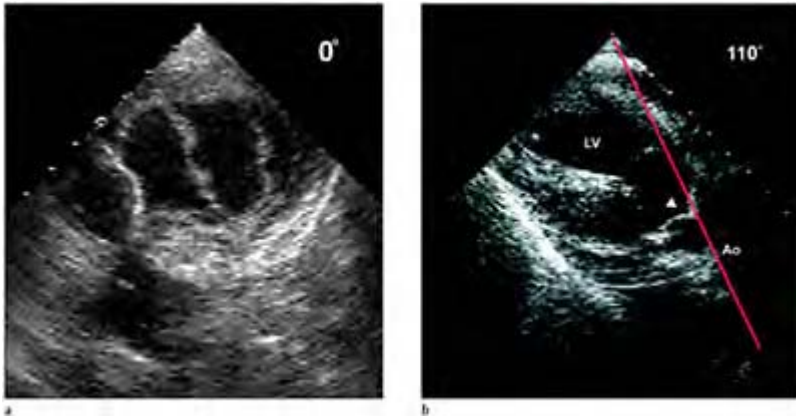
Figure 3.9 Normal transgastric views of the aortic valve complex. From the transgastric views with the probe in the stomach close to the gastroesophageal junction, the aortic valve is usually seen in an oblique orientation. At 0 degrees the aortic valve relationship to the mitral valve is well appreciated, and with rotation of the transducer to 90 to 110 degrees the aortic root is visualized obliquely and to the right of the imaging sector and may be assessed with Doppler echocardiography. LV, left ventricle; Ao, aorta.
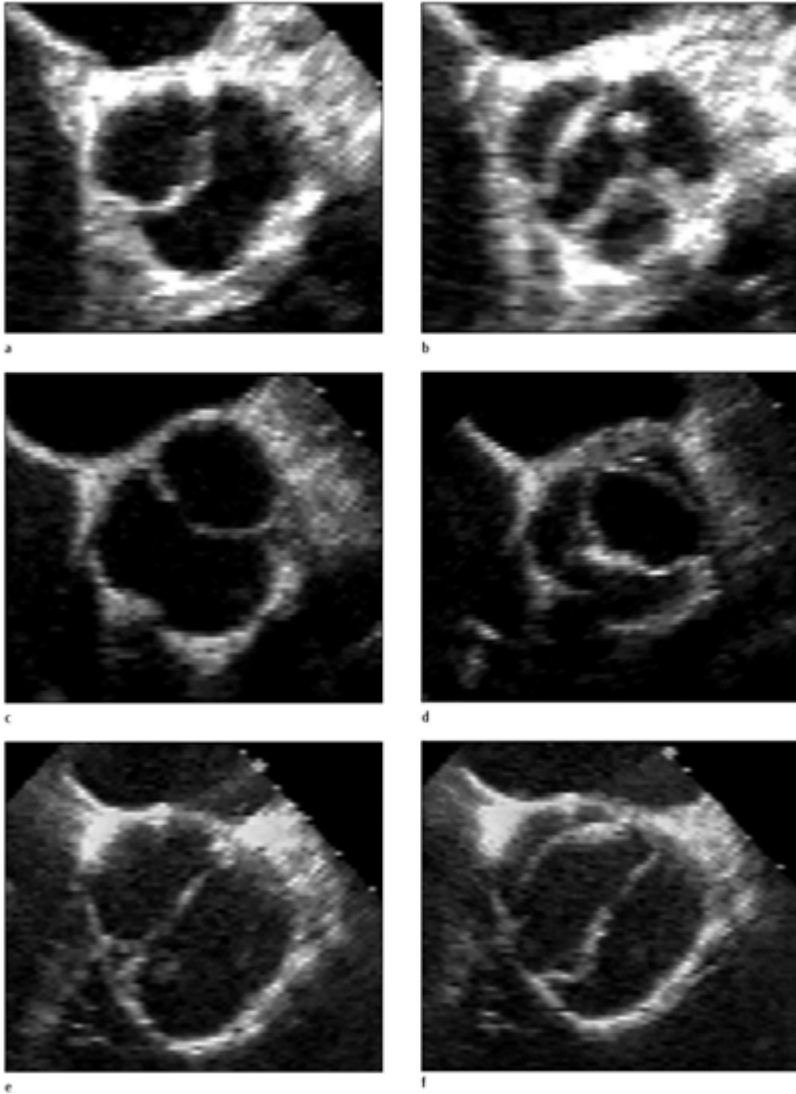
Figure 3.10 (right) Bicuspid aortic
valves. The size of the bicuspid aortic
valve leaflets is easily assessed with
transesophageal echocardiography in
the short axis planes during systole and
diastole. The proportional size of each
aortic valve leaflet determines the
hemodynamic consequences produced

by the bicuspid aortic valve. In stenotic bicuspid valves (a, diastole; b, systole) the two valve leaflets are near identical in size. When one cusp is slightly larger than the other (c, diastole; d, systole), the valve functions normally, no hemodynamic stenosis or regurgitation is produced, and the valve frequently goes unrecognized for the life of the patient. In regurgitant bicuspid aortic valves (e, diastole; f, systole) one cusp is significantly larger than the other and the valve leaks due to prolapsing of one leaflet during closure. All types of bicuspid valves are subject, however, to the normal degenerative (wear and tear) changes of older age.

equal in size, stenosis is produced, due to the restricted and elliptical opening configuration produced by the cusps, rather than a circular opening normally produced with tricuspid aortic valves. Regurgitation however is usually prevented in these valves, since cusp closure is not affected, even though there is abnormal cuspal contract during apposition. If one cusp is slightly larger than the other, the cusps still have abnormal contact during apposition, however the extra cuspal length preserves a near normal circular opening, which permits normal function, without stenosis or regurgitation. Excessive length of one cusp, however, produces abnormal closure from prolapse of one cusp past the other, resulting in pure aortic regurgitation.

There are two basic types of cusp orientation in congenitally bicuspid aortic valves.[10] In 53% of bicuspid aortic valves, the commissures are vertically situated with the cusps oriented rightward and leftward with the respective coronary artery originating from the respective sinuses of Valsalva. In the other 47%, the commissures are horizontally placed with the cusps oriented in an anterior and posterior position, and with both coronary arteries arising from the anterior sinus of Valsalva. The anterior-posterior type is more likely to calcify.

A raphe or false commissure is found in one of the two cusps in about 50% of the valves, irrespective of valve type. When present, the raphe is always found in the right cusp of the right-left or vertical orientation and in the anterior cusp of the anterior-posterior or horizontal type.

Minor rotations of the commissures of the two basic types of bicuspid aortic valves result in the various configurations in bicuspid aortic valves and may account for the variable sensitivity and specificity in detection of bicuspid valves with M-mode and two-dimensional echocardiography. With M-mode echo, eccentric cusp closure appears better

detected with the A-P types of bicuspid valve; false-negative detection with the appearance of midline closure appears with the R-L types. The short axis view obtained with two-dimensional echocardiography has the highest sensitivity and specificity in detecting either type of bicuspid valve.[11]

Bicuspid aortic valves are usually mildly regurgitant. In younger patients, significant aortic regurgitation is more prevalent than significant stenosis, despite an elliptical aortic orifice. As patients mature with bicuspid valves, calcification of the raphe, annulus and valve cusps further narrow the orifice, producing symptomatic aortic stenosis, and this is the most common cause of aortic stenosis in patients between 15 and 65 years of age.[12] Bicuspid aortic stenotic valves calcify early and are significantly stenotic by the 5th to 6th decade. Calcification tends to be the heaviest in bicuspid aortic stenosis, in comparison with the other causes of aortic stenosis. Calcification tends to be greatest along the raphe and at the base of the anterior or right cusp.[13] In contrast to stenotic bicuspid aortic valves, regurgitant or normally functioning bicuspid valves have minimal calcification. Isolated aortic valve calcification without mitral disease is a sign of congenital stenosis.[14] Diffuse calcification of the aortic valve, with calcium limited to focal areas of the anterior mitral leaflet and/or mitral annulus, is more likely to be the result of a calcified bicuspid aortic valve with extension of calcium to the fibrous skeleton and mitral valve.

Bicuspid aortic valves are frequently associated with dilatation of the aortic root and ascending aorta, irrespective of the hemodynamics produced by the anatomical configuration of the valve.[15] Post-stenotic dilatation of the aorta is common with stenotic bicuspid valves. In bicuspid aortic valves that are not stenotic, the aorta is still frequently enlarged because of the associated weakening of the aortic medial layer that is associated with the developmental abnormality that produces the abnormal leaflet configuration. Due to the association of bicuspid aortic valve and coarctation of the aorta, coarctation should also be excluded.[16]

An acquired bicuspid aortic valve, in contrast to a congenital valve, is produced when there is acquired inflammatory fusion of one of the three commissures of a tricuspid aortic valve (acquired bicuspid structure).[17] On inspection, this pathology produces the anatomical appearance of a raphe (false commissure) where a "true commissure" would be. This frequently becomes calcified, which makes it more confusing. There are a few characteristics that help to distinguish congenital valves from acquired valves. Raphes are only present in 50% of congenital bicuspid valves, whereas acquired valves always contain a false raphe at the site of fusion of the true commissure. When present, the raphe of the bicuspid valve inserts toward the base of the sinus, below the sinotubular junction, unlike the acquired valve which originates at the sinotubular junction. With congenital bicuspid valves, the cuspal free margin lengths during closure of the two cusps are similar, with the cusp containing raphe being slightly shorter than the non-raphe cusp. The annular circumferential length of the two cusps in congenital valves will be similar, whereas in acquired bicuspid valve the length of the fused two cusps will be twice as large as the other cusp, coinciding with the fusion of two separate cusps. The corpus Arantus is usually absent on the free edge of the conjoined cusp in congenitally bicuspid valves.

Quadricuspid aortic valve

Quadricuspid aortic valves are extremely rare (figure 3.11).[18] Quadricuspid valves possess four cusps that may be either equal or unequal in size.[19] Quadricuspid valves may function normally, they are almost never stenotic and about 50% are regurgitant. Similarly to bicuspid valves, a proposed mechanism for regurgitation is suggested by unequal cuspal margin length. In short axis echocardiographic views the four cusps produce a characteristic x-shaped configuration during valve closure.[20] In contrast to bicuspid valves, quadricuspid aortic valves are rarely associated with other congenital abnormalities, with the exception of truncus arteriosus.[21]
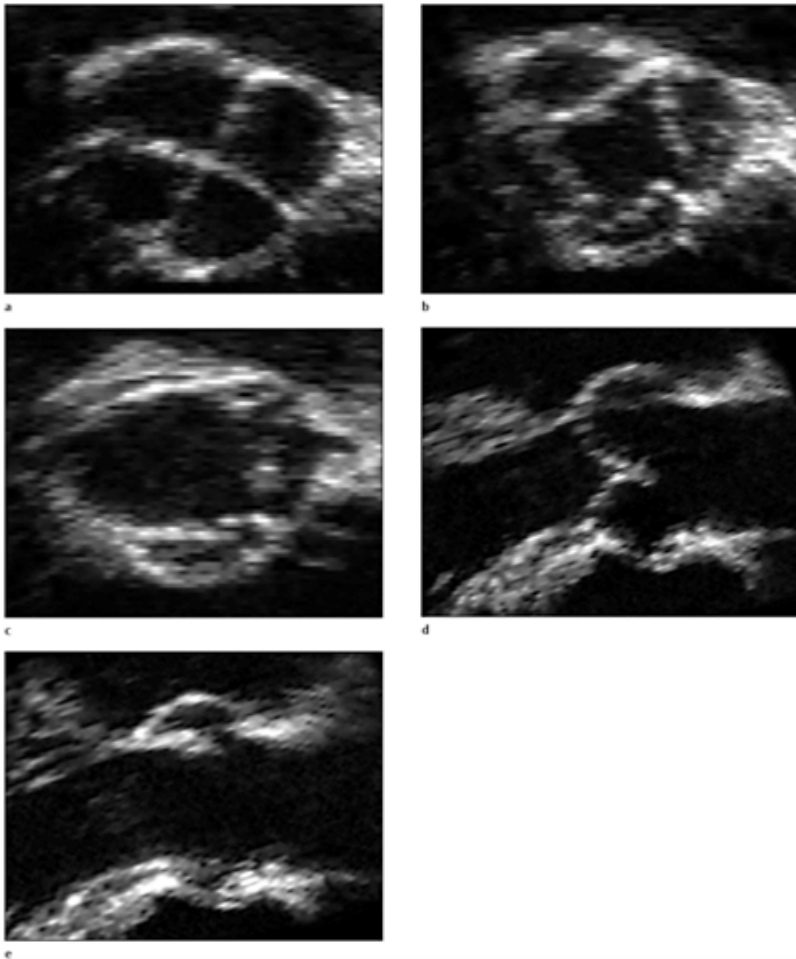
Figure 3.11 Quadricuspid aortic valve. The quadricuspid aortic valve has four nearly identical valve leaflets. During

diastole the valve leaflet margins produce an "X" configuration when closed (a). In early systole (b) the valve opens with a diamond shape and nearly assumes a circular configuration when fully open (c) in systole. In the longitudinal views the valve appears normal and is indistinguishable from a tricuspid aortic valve, except that the valve leaflets are usually visible during opening since they do not fully approximate to the aortic root walls. Despite this appearance, significant stenosis is not produced and quadricuspid valves usually produce regurgitation clinically.

Aortic stenosis

Hemodynamically, aortic stenosis produces obstruction to the left ventricular outflow tract. In classic aortic stenosis, the obstruction is produced as a result of reduction of the aortic valve orifice area. However, the obstruction may also occur at the subvalvular or supravalvular level, or with various combinations of the three levels. Valvular aortic stenosis is the predominate lesion in all age groups, since discrete sub-aortic stenosis and supravalvular aortic stenosis are rarely discovered after the age of 15 years.[22,23] Multiplane transesophageal echocardiography is extremely advantageous in demonstrating subvalvular and supravalvular stenosis in the adult when present as solitary or combined lesions.

Valvular aortic stenosis is either congenital or acquired in origin. The most common causes of acquired valvular aortic stenosis include rheumatic (post-inflammatory) and degenerative causes. Roberts[24] reported that aortic stenosis was found as an isolated non-rheumatic lesion in 25 and as a rheumatic lesion with an associated abnormal mitral valve in 40 of 1000 necropsy patients he studied. Rare causes include infectious endocarditis producing large vegetations, Fabry's disease, ochronosis, hyperlipidemic states (homozygous type II), hypercalcific syndromes, lupus erythematosus associated with antiphospholipid syndrome or anticardiolipin antibody, and Paget's disease.[25-31] The cause of aortic stenosis can usually be predicted by the age of the patient upon presentation for surgery. Congenital stenosis (unicuspid or bicuspid valves) presents in the pediatric or younger age groups, rheumatic stenosis in the mid age group, and degenerative stenosis in the elderly.

Degenerative aortic stenosis

Degenerative or senile aortic stenosis most commonly occurs in elderly patients with tricuspid aortic valves, and presents with calcific (nodular) deposits within the body of the valve cusps, without significant commissural fusion. Since fusion of the commissures is usually absent, aortic regurgitation is rarely associated with degenerative aortic stenosis. Degenerative aortic stenosis typically occurs in the 7th and 8th decade, with equal sex distribution in most studies. Degenerative aortic stenosis is frequently associated with other degenerative types of lesions such as a calcified mitral annulus, calcification of the conduction system, calcified proximal coronary arteries, or degenerative lesions in the other valves, suggesting a wear and tear mechanism, or an exaggerated aging process at work. Degenerative aortic stenosis is thought to occur predominately with previously normal tricuspid aortic valves, although some authors have suggested that minor abnormalities such as asymmetry in leaflet size, small aortic annular size and dystrophic valve leaflets give rise to premature senile calcification.[32–34]

Calcification of the valve cusps usually occurs within the cusp body as nodular calcifications, originating at the base of the cusp or annular attachment or hinge point extending towards the free cusp margin, thereby limiting its range of motion. In comparison with congenital aortic valves, calcification tends to be less heavy in degenerative disease. In a few cases of degenerative disease, calcification has been described as diffuse, with an eggshell-type fragility.[35] Although commissural fusion is rare when compared with rheumatic disease, it tends to occur in the commissure between the right and non-coronary cusps. Calcification of the cusps renders them rigid and immobile, producing progressive reduction in the aortic valve area as the calcium accumulation increases. The echocardiographic appearance of degenerative aortic stenosis includes highly reflective valve cusps, thickened leaflets with obvious restriction of motion, and a reduced and often distorted orifice geometry. Multiplane transesophageal echocardiography frequently identifies nodular calcifications within the cusp body with freely mobile cuspal margins. Transesophageal echocardiography readily shows and distinguishes aortic sclerosis, or diffusely thickened aortic valves without a reduced orifice area or significant stenosis from calcific aortic stenosis.

Rheumatic or post-inflammatory disease

With the decline of rheumatic fever in western countries, rheumatic heart disease is no longer the most common cause of aortic stenosis. Post-inflammatory fibrocalcific diseases including rheumatic disease now accounts for only 18 to 35% of all cases of aortic stenosis in patients presenting for aortic valve replacement.[36,37] The hallmark of rheumatic aortic stenosis is commissural fusion with cuspal thickening secondary to fibrosis, with or without calcification. Rheumatic aortic stenosis is almost always associated with commissural thickening and fusion of the mitral valve leaflets, producing some degree of mitral or tricuspid stenosis and/or regurgitation. Typically, all three aortic commissures are involved along with thickening and retraction of the valve cusps. Thickening of the valve cusps occurs predominately at the cuspal free margins. All of these findings produce a central, triangular appearance or dome-shape valve with a reduced aortic valve orifice. With multiplane transesophageal echocardiography a central,

triangular orifice is easily shown in the short axis views, with systolic doming apparent in the long axis. In the later stages of the disease process, the fibrotic cusps

Discrete fibrous band or membrane

Fibrous plaque
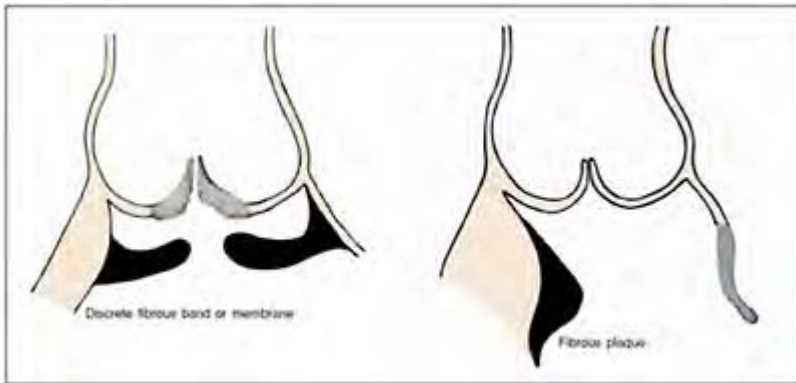
Figure 3.12 Artist's rendition of the types of subaortic stenosis. Subaortic stenosis may be produced by a discrete fibrous band or membrane just proximal to the aortic valve annulus. In the adult, this congenital abnormality may be detected with transesophageal echocardiography by demonstrating a narrow and abnormal appearing outflow tract, but the membrane must be widely patent (Swiss cheesy) in order for this entity to go undetected until adulthood. The aortic valve undergoes early degeneration with resultant regurgitation due to stenotic jets produced from the subvalvular obstruction. Subaortic membranes may be distinguished from left ventricular outflow tract obstruction such as in hypertrophic obstruction, which usually yields a fibrous plaque near the site of obstruction on the ventricular septal endocardium and degenerative changes of the anterior mitral leaflet.

become calcified and with further restriction the orifice appears circular and fixed, often with no apparent opening or closing motion. At this point, systolic doming is less apparent. Occasionally, commissural fusion occurs in only one or two commissures and when calcified may be indistinguishable from a bicuspid valve or degenerative aortic stenosis. Generally as the number of fused commissures increases, the valve orifice area decreases with a resultant increase in the severity of stenosis.

Post-inflammatory disease is usually designated as a chronic, fibrosing process that results in valvular pathology virtually identical to chronic rheumatic disease, without a documented history of rheumatic fever. Although the incidence of rheumatic aortic stenosis appears to be declining in the western world, the relative incidence of post-inflammatory disease appears to be stable. Therefore, post-inflammatory disease may occur as either a result of sub-clinical rheumatic fever or non-rheumatic aortic valvulitis. Coxsackieviruses and other viruses have been implicated in producing similar findings to rheumatic disease.[38–40] Post-inflammatory disease appears to be twice as common in men than women.[36]

Subvalvular aortic stenosis

The site of obstruction in subvalvular aortic stenosis typically occurs in the basal half of the left ventricular outflow tract.[41–44] Two types of subvalvular aortic stenosis occur: discrete sub-aortic stenosis and muscular obstruction as seen in hypertrophic cardiomyopathy (figure 3.12). Although both types may mimic valvular aortic stenosis clinically, they are quite different anatomically. Additionally, subvalvular stenosis may accompany valvular aortic stenosis. Acquired subvalvular aortic stenosis may also occur secondarily to mitral valve replacement or mitral valve repair and again mimic valvular aortic stenosis, although the cause should be clear with its development following those procedures.

In discrete sub-aortic stenosis, obstruction to flow occurs inferior to or below the aortic valve and is the cause of stenosis in about 10 to 12% of pediatric cases.[22,23] In 90 patients described by Oztunc et al, sub-aortic stenosis was caused by a subvalvular membrane in 67%, by a fibromuscular ridge opposite the level of the mitral annulus in 22%, by a combination of a membrane and fibrous ridge in 4% and by a subvalvular fibromuscular collar or tunnel in 7%.[41] Subvalvular membranes usually occur just below the aortic valve as a thin fibrous membrane within a normal outflow tract. Subvalvular fibrous rings or ridges occur about 1–2 cm beneath the aortic valve and may extend into the left ventricular outflow tract for another 1 to 2 cm. The obstructing tissue is comprised of white fibroelastic tissue and may form a discrete band, an accumulation of tissue bands, or a diffuse ridge that may extend across the outflow tract onto the base of the anterior mitral leaflet. Subvalvular fibromuscular tunnels produce the most extensive pathology and the most notable narrowing of the outflow tract, especially during systole. The area of outflow tract narrowing may extend for several centimeters affecting all borders of the outflow tract.

Despite the frequent involvement of the mitral valve in sub-aortic stenosis, the ventricular surface of mitral leaflets remain normal with discrete stenosis, in contrast to the thickened mitral valve in hypertrophic cardiomyopathy.[23] Turbulent, high velocity jets produced by the sub-aortic obstruction produce thickened aortic valve cusps often

distorting the cusps to produce aortic regurgitation with a propensity for endocarditis.[23] Sub-aortic stenosis is frequently associated with other congenital abnormalities. In the patients studied by Oztunc, 42% were associated with patent ductus arteriosus, ventricular septal defect or valvular aortic stenosis.[43]

Multiplane transesophageal echocardiography has greatly improved the detection of sub-aortic stenosis in the adult patient.[44,45] Using views obtained from the deep transgastric, long axis transgastric and long axis mid esophageal, the left ventricular outflow tract is very well visualized with excellent resolution for detecting the narrowing produced as well as the sub-aortic membranes, ridges and tunnels. Color flow Doppler routinely detects and locates the turbulence produced by the sub-aortic obstruction separating it from the aortic valve. This is especially helpful for diagnosis when conventional Doppler is not helpful from either the transesophageal or transthoracic methods, owing to associated lesions such as a ventricular septal defect or concomitant valvular stenosis.

Assessment of aortic stenosis

In classic aortic valvular stenosis there is a reduction of the aortic valve orifice area secondary to pathology limiting aortic cusp motion. Typically, the aortic valve orifice area must be reduced to about 25% of its normal size before there is significant effect on circulatory hemodynamics. The normal aortic valve orifice area of 3–4 cm^2 must be reduced to $\geq$ 1.0–0.75 cm^2 before critical aortic stenosis is achieved.[46] This is somewhat arbitrary, however, since critical aortic stenosis may occur at 1.0 cm^2 in larger patients and be an adequate valve area in smaller patients with critical stenosis occurring with an area of 0.7 cm^2.[46–48] The degree of severity of aortic stenosis is usually graded as mild (> 1.5 cm^2), moderate (1.0 to 1.5 cm^2) or severe ($\leq$ 1.0 cm$^{2)}$.

The need for valve replacement is not determined solely by the absolute valve area or transvalvular pressure gradient.[49,50] Aortic valve replacement in aortic stenosis is based largely on the presence or absence of symptoms, since it is not unusual to have normal cardiac outputs with severe stenosis with mean transvalvular gradients > 50 mmHg.[47–54] When Doppler aortic velocities of greater than 4 m/s are reached, patients generally are or will soon become symptomatic.[54] Angina, dyspnea or syncope usually occurs in 38% of patients within 2 years and in 79% within 3 years.[47–54]

Echocardiography is useful to follow the progression of aortic stenosis over time, but it may be difficult to individualize these data for specific patients.[55–63] After moderate aortic stenosis develops, the valve area has been shown to decrease with Doppler/echo studies from 0.1 to 0.3 cm^2/yr (average 0.12 cm^2/yr), with pressure gradients increasing from 10 to 15 mmHg/yr. These studies have also shown that the progression of aortic stenosis is more rapid in degenerative senile disease than with congenital bicuspid or rheumatic disease. In patients with severe aortic stenosis, echocardiography may be appropriate on a yearly basis to assess the progression of left ventricular hypertrophy and to detect the onset of left ventricular dysfunction.[56]

When cardiac catheterization data is inconclusive for determining the degree of aortic stenosis due to low cardiac output and left ventricular dysfunction, echocardiography may be particularly useful in diagnosing the degree of aortic stenosis.[64] In the presence of left ventricular dysfunction and low cardiac output, transvalvular gradients of < 30

mmHg may be obtained, even with severe or critical aortic stenosis. To distinguish critical aortic stenosis from less severe cases in this scenario, dobutamine echocardiography may be useful. With dobutamine echocardiography in cases of low gradient stenosis due to low cardiac output, the aortic valve area increases with increases in cardiac output in cases of mild to moderate aortic stenosis, and no change is detected in critical stenosis.[64] Conversely, in clinically high-flow rate states, the systolic gradient may be high when only mild or moderate aortic stenosis is identified with echocardiography.

The role of transesophageal echocardiography for the assessment of aortic stenosis is limited, since most patients are adequately diagnosed by transthoracic echocardiography. A major limitation of transesophageal echocardiography is the inability to obtain parallel imaging planes for Doppler interrogation of the proximal aorta and left ventricular outflow tract. Occasionally, parallel views are obtained from the deep transgastric view or gastric views, but the aortic flow depth is too far into the far-field to yield diagnostic results. Irrespective of these limitations, multiplane transesophageal echocardiography is ordinarily used when discrepancies occur between the clinical scenario and/or the transthoracic echocardiography study or cardiac catheterization data. This frequently occurs when cusp motion or opening is not discernible by transthoracic echocardiography due to a heavily calcified aortic valve, when there is significant left ventricular dysfunction limiting cusp excursion, or occasionally in the assessment of a bicuspid valve, especially with coexistent aortic disease or congenital abnormalities. Multiplane transesophageal echocardiography is particularly advantageous in diagnosing these cases of aortic stenosis by direct visualization of the valve opening and in evaluating the subvalvular or supravalvular anatomy.

Many studies[65–75] have shown excellent correlations between aortic valve areas measured with valve orifice planimetry performed with transesophageal echocardiography and aortic valve areas obtained with cardiac catheterization, irrespective of normal or impaired left ventricular function. The analysis of agreement of aortic valve areas by transesophageal aortic planimetry, continuity equation by transthoracic echocardiography and the Gorlin formula with cardiac catheterization was reported by Kim et al,[69] and showed that the "limits of agreement" between the three groups did not differ significantly and may be used interchangeably. Transesophageal echocardiography is significantly most accurate in comparison to the Gorlin formula in mildly or moderately calcified valves and may overestimate the area of severely calcified aortic valves.[70]

Multiplane transesophageal echocardiography provides high-resolution, detailed images, due to the close proximity of the aortic valve to the transducer in the mid esophageal position. The aortic valve opening is easily viewed enface in a near perfect transverse plane, with slight rotation of the transducer from 0 to 90 degrees (average 15–30 degrees) with multiplane probes.

Numerous studies[71–75] have shown the clear superiority of multiplane transesophageal echocardiography to monoplane or biplane transesophageal echocardiography for planimetry of the aortic valve orifice and calculation of aortic valve areas. Short axis images of the aortic valve are usually obtained in 88% of patients with biplane transesophageal echocardiography, and in every patient with multiplane transesophageal echocardiography. Hoffmann et al[71] have shown an excellent correlation of r = 0.95

between multiplane transesophageal aortic valve planimetry and areas derived from the Gorlin formula in the catheterization laboratory. Severe aortic stenosis with valve areas of less than 0.75 cm^2 was predicted with a high sensitivity of 96% and a specificity of 88%. In addition, when there is no apparent visible orifice or when transesophageal echocardiography fails to demonstrate leaflet motion, severe aortic stenosis is present with Gorlin derived valve areas of less than 0.3 cm.

In addition, identification of aortic valve morphology is improved with multiplane transesophageal echocardiography. Espinal et al[76] reported the sensitivity and specificity of multiplane transesophageal echocardiography versus biplane transesophageal echocardiography in 710 patients undergoing aortic valve replacement for the detection of bicuspid versus tricuspid aortic valve morphology. The sensitivity for multiplane transesophageal echocardiography was 87% with a specificity of 91%, and for biplane transesophageal echocardiography the sensitivity was 66% with a specificity of 56%.

The planimetered aortic valve area correlates well with the continuity equation and the Gorlin formula derived from catheterization data.[77,78] Unlike the Gorlin formula, however, transesophageal echocardiographic aortic valve areas are not substantially altered by changes in transvalvular volume flow. With the addition of color flow Doppler, the flow orifice is readily identified along with any aortic insufficiency that may be present. Morelli and colleagues have shown that planimetery of the aortic valve area with multiplane transesophageal echocardiography is reliable even in the presence of significant aortic regurgitation.[79]

Conventional Doppler assessment of aortic stenosis is a little more difficult with transesophageal echocardiography, since most views do not allow for the proper parallel alignment of the Doppler ultrasound beam to the left ventricular outflow tract or aortic transvalvular flow.[80–83] The most appropriate views for Doppler assessment are the transgastric longitudinal long-axis view or the frontal deep transgastric view. Unfortunately, these views may be difficult to obtain, especially in patients with aortic stenosis due to the horizontal heart position produced by left ventricular hypertrophy, marked left atrial enlargement or with coexisting extensive mitral annular calcification. When these views are obtainable, however, accurate pressure gradient estimation can be achieved with pulsed and continuous wave Doppler, which correlate nicely with those obtained with transthoracic echocardiography and cardiac catheterization. In the transgastric probe position, the left ventricular outflow tract with the aortic valve may be obtained by obtaining the short-axis mid-papillary muscle view at 0 degrees and then rotating the transducer from 90 to 135 degrees until the left ventricular outflow tract comes into view, with the aortic valve plane appearing roughly in the middle of the image sector. In this view, the left ventricular outflow tract diameter can be measured and continuous and pulsed wave Doppler interrogation can be done in an almost parallel path. Continuous-wave Doppler enables estimation of maximum instantaneous and mean transvalvular pressure gradients by application of the modified Bernoulli formula. With the addition of pulse-wave Doppler of the left ventricular outflow tract, the continuity formula may be used to calculate aortic valve area.

The feasibility and learning curve for doing Doppler transesophageal echocardiography for aortic valve area determination was reported by Stoddard et al.[80] Aortic valve areas were initially successful in only 56% of patients studied with Doppler transesophageal echocardiography, compared with 88% after the technique was

established. After becoming comfortable with the technique, mild, moderate and severe aortic stenosis was correctly identified in 93%, 79% and 77% of patients respectively, in comparison with aortic valve planimetry by transesophageal echocardiography. Blumberg et al,[81] studied 39 patients with multiplane transesophageal echocardiography, and transthoracic echocardiography, and found good correlation in 90% of the patients in whom transesophageal echocardiography measurements could be obtained, with good intra- and interobserver variability. Correlations between maximal pressure gradients ($r = 0.95$, $p < 0.0001$), mean pressure gradient ($r = 0.93$, $p < 0.0001$) and aortic valve area ($r = 0.97$, $p < 0.0001$) were excellent. In 22 patients who underwent cardiac catheterization, the maximal versus peak-to-peak pressure gradient ($r = 0.85$, $p < 0.0001$), mean pressure gradient ($r = 0.82$, $p < 0.0001$) and aortic valve area ($r = 0.88$, $p < 0.0001$) were highly significant.

Multiplane transesophageal Doppler echocardiographic assessment of aortic valve stenosis is also feasible in the critical care setting in mechanically ventilated patients, which specifically hampers the transthoracic approach. Blumberg et al[83] reported that multiplane transesophageal Doppler/echocardiography was feasible in 89% of patients during mechanical ventilation, and good correlations were obtained with transthoracic echocardiography (maximal pressure gradient $r = 0.93$, mean pressure gradient $r = 0.91$, aortic valve area $r = 0.97$) and cardiac catheterization (maximal pressure gradient $r = 0.84$, mean pressure gradient $r = 0.80$, aortic valve area $r = 0.84$).

Although flow dependence does not affect aortic valve planimetry for aortic stenosis, flow dependence does affect valve area determination by the continuity equation and the Gorlin formula according to the morphological characteristics that cause the stenosis. Shively et al[83] have shown that the slope of flow dependence for valve area in patients with aortic stenosis is different for calcific tricuspid aortic stenotic valves compared to bicuspid or rheumatic aortic stenosis, in which the valve orifice is usually off-center or ovoid in shape.

Tribouilloy et al[85] reported the usefulness of transesophageal echocardiography to predict significant coronary artery disease, in aortic stenosis with the demonstration of thoracic aortic plaque. The severity of thoracic aortic plaque was the most significant independent predictor of coronary artery disease, along with angina and age. In 63 patients with significant coronary artery disease, plaque was shown in 57 patients, but was only present in 19 of 69 patients with normal or mild coronary artery disease. Transesophageal echocardiography identified coronary artery disease with a sensitivity of 91%, a specificity of 73% and a positive predictive value of 75% and a negative predictive value of 89% in patients with aortic stenosis.

Aortic valvuloplasty

Although aortic valvuloplasty has a limited role in the treatment of aortic stenosis in the adult patient, multiplane transesophageal echocardiography serves as a useful adjunct to the procedure. Since Cribier[86] first reported the dramatic relief of symptoms in three adult patients with critical aortic stenosis and balloon aortic valvuloplasty who were not surgical candidates, numerous subsequent reports have substantiated incomplete relief of aortic valve obstruction with a high rate of restenosis in older patients undergoing aortic

valvuloplasty.[87–89] Results have shown only modest reductions in aortic valve gradients, with small improvements in aortic valve area and restenosis, occuring in more than half of the patients within 6 months.[87,88]

The lack of reduction in aortic valve gradients and increase in valve area in patients with degenerative aortic stenosis should probably be expected, since direct visualization of the valve after valvuloplasty does not show any change in the appearance of the valve.[90] The proposed mechanism of improving valve area lies in the fracture of calcific deposits in the valve cusps, which only permits increased mobility of the valve. Nevertheless since the relationship of outflow tract obstruction to the increase in after-loading conditions of the heart follows a curvilinear rather than linear trend, a small increase in valve area, albeit still in the severe range (0.7 to $\leq$ 1.0 cm$^{2)}$, may result in a dramatic improvement in symptoms.[91] In addition, even though there is a high restenosis rate, some individuals may not reach the critical level of obstruction with restenosis, and may remain free of symptoms for 1 year. This is most common in younger patients with less calcified valvular pathology.[87–89]

Since the natural history of critical aortic stenosis shows dismal 1 to 3 year survival rates in elderly patients when valve replacement is not done, valvuloplasty may be the only alternative treatment for these patients.[92] The current recommendations for aortic balloon valvuloplasty have largely evolved as a bridge to another procedure.[87–89,93] In older patients who require non-cardiac surgery and are at high risk of mortality or morbidity, successful valvuloplasty may allow the patient to undergo non-cardiac surgery with a reduced risk.[94] In patients with cardiogenic shock and critical aortic stenosis, aortic valvuloplasty may help to stabilize hemodynamics substantially and allow further cardiac intervention.[91] Patients in whom the severity of aortic stenosis is difficult to determine, due to low cardiac outputs and low gradients coexisting with left ventricular dysfunction, may be unmasked with aortic valvuloplasty. The decision to undergo valve replacement may be entertained if the left ventricular function improves after valvuloplasty. Aortic valvuloplasty may also be considered for adolescent and young adults to prolong the time to aortic valve replacement, especially if significant valvular calcification is not present.

The role of transesophageal echocardiography in aortic balloon valvuloplasty is considerable. It may assist in obtaining successful results and serve as an early indicator of procedure complication. In the pre-evaluation of aortic valvuloplasty the transesophageal procedure for valvuloplasty is identical to that done to assess aortic stenosis, with visualization in the same views and using the same techniques in the Doppler examination. The left ventricular outflow tract and aortic root should be visualized in numerous planes to exclude the presence of sub-or supra-annular stenosis. The aortic valve annular dimension is determined from the longitudinal view obtained between 100 to 135 degrees from the gastric window. The annular dimension dictates the balloon size used, and balloons larger than 120% of the annular dimension should be avoided as to not overdilate the valve.[95] The presence or absence of aortic regurgitation should be documented to serve as a baseline for post-valvuloplasty comparison. If technically feasible, Doppler gradients and valve area may be obtained by the continuity equation and valve motion may be assessed again, to serve as baseline variables as to the severity of aortic stenosis.

The catheter position and relative balloon position are observed. The inflation and deflation visualized and optimal balloon position noted. Visually the balloon should

appear to inflate initially with a "waist" centered within the valve plane, and it ultimately assumes a sausage or oval shape when fully inflated, to give the impression that the balloon occupies the total area of the aortic root. During the procedure there is generally not enough time to calculate aortic valve areas with the continuity equation etc, therefore improvement is assessed usually just by observing valve motion.

The post-procedure echocardiogram should rule out complications, notably development or worsening aortic regurgitation, development of dissection or pericardial effusion. Aortic regurgitation after aortic valvuloplasty plays a smaller role than with mitral valvuloplasty since it usually occurs in only 10 to 15% of cases and is a significant problem in less than 2% of patients.[87–89,96] This probably coincides with the observations that visually the aortic valve does not change much after dilation, and in most cases splitting of the leaflets does not occur as splitting of the commissures does in most cases of mitral stenosis. Rarely, attributable to using an excessively large balloon(s) in reference to the annular dimension, rupture of the aortic annulus, aortic wall tears or leaflet disruption may occur. If aortic regurgitation occurs due to leaflet disruption, flail or prolapsed leaflets may be seen.[97] In extensive aortic wall tear, aortic dissection may be seen.[98,99] Due to the stiffness of the catheters used, cardiac chamber perforation may occur, with resultant pericardial effusion and possibly pericardial tamponade. Doppler determinants of gradient and aortic valve area should coincide with a reduction in gradient of 50% and an improvement in valve area, which rarely exceeds 1.0 cm^2.

Aortic regurgitation

The four most common causes of pure aortic regurgitation include post-inflammatory or rheumatic disease, congenital aortic valvular disease, aortic root dilatation (Marfan's disease) and infectious endocarditis.[99–102] In contrast to aortic stenosis, there are numerous pathologies that cause aortic regurgitation, which produce structural changes readily shown with multiplane transesophageal echocardiography (figure 3.13). In addition, unlike aortic stenosis, which is usually associated with some degree of regurgitation, "pure" aortic regurgitation may be present as an isolated finding without an obstructive aortic component or associated mitral valve dysfunction. Through echocardiography, the etiology of aortic regurgitation can be defined by describing the primary structural abnormalities produced by the disease process according to involvement of the valve and/or the aorta. Specifically, primary pathologies of aortic regurgitation can be further elucidated by describing the effect produced on the motion of the aortic valve leaflets; ie, normal leaflet motion, excessive or prolapsing leaflet motion, or restricted leaflet motion.[103] In over 75% of cases the pathology primarily affects the valve, and in most of the other cases the aortic root is the primary site of involvement. In aortic regurgitation associated with systemic hypertension, neither the valve nor the aorta illustrates the primary site of involvement.[104] Ankylosing spondylitis is the only disorder in which the valve and aorta are both primarily involved.[104] The disease process of ankylosing spondylitis involves the wall of the aorta behind the sinuses of Valsalva and extends to involve the basal portion of the aortic valve cusps, portions of membranous septum and the anterior mitral leaflet.[105] Congenitally malformed aortic valves are least likely to be purely regurgitant unless associated with infective endocarditis, and then they

account for the largest percentage of purely regurgitant valves that are not rheumatic.[101] It has also been suggested that patients with bicuspid valves have a higher prevalence of severe aortic regurgitation than patients with tricuspid aortic valves.[104]
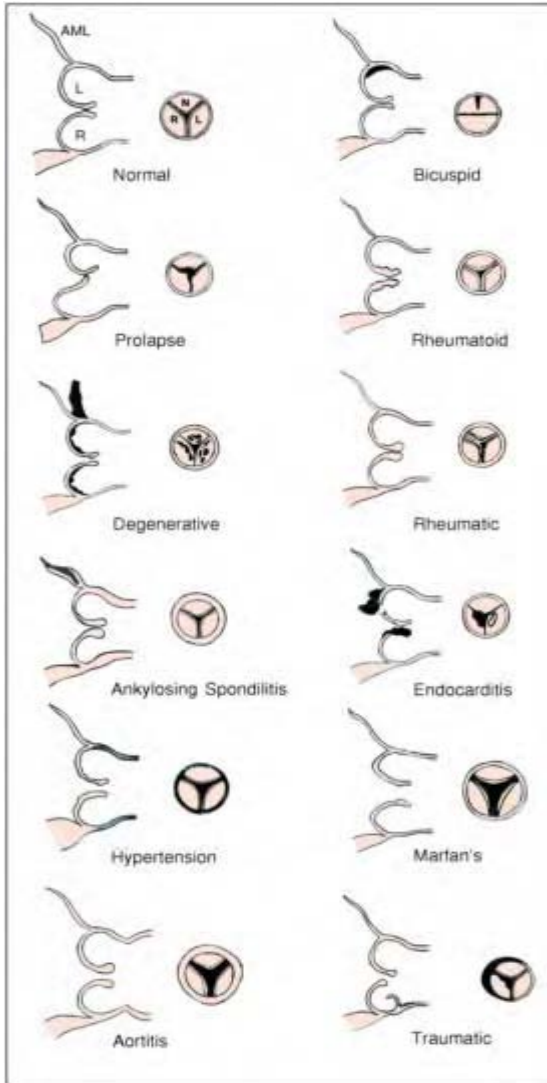
Figure 3.13 Unlike aortic stenosis, there are numerous pathologies associated with aortic regurgitation.

With multiplane transesophageal echocardiography the etiology of aortic valve regurgitant pathology may be determined by noting specific structural changes found in the aortic valve complex. Pathology may produce modifications in structure or function of the aortic valve cusps, the annulus, or aorta individually or in various combinations. Artist's rendition of the typical diastolic longitudinal view of the aortic root at 100 degrees and the short axis view of the aortic valve at 45 degrees. Normal tricuspid aortic valve. Bicuspid valve, two cusps with or without raphe. Prolapsing right coronary cusp. Rheumatoid arthritis, cuspal nodules. Degenerative, slightly dilated aorta, focal cuspal fibrous thickening and calcification, mitral annular calcification. Rheumatic fever, commissural fusion, extensive fibrous thickening, diffusely thickened anterior mitral leaflet, mild calcification. Ankylosing spondylitis slightly thickened aortic wall, thickened cuspal margins, fibrous thickening of the anterior mitral leaflet. Endocarditis, vegetation, loss of cuspal tissue or focal thickening, perforation. Hypertension, dilated ascending aorta, focal fibrous thickening, central leak secondary to taut margins of closure. Marfan's dilated aorta, taut margin or closure, redundant cusp, weakened aortic wall with focal aneurysm, loss of sinotubular junction narrowing. Aortitis, aortic root dilatation, large

central leak. Traumatic, tear or laceration, disruption of aortic wall, flail leaflet. (Modified from Waller B.F. Rheumatic and non-rheumatic conditions producing valvular heart disease. In Frankl, WS and Breast, AN (eds). *Cardiovascular clinics. Valvular Heart Disease: Comprehensive Evaluation and Management.* Philadelphia; F.A. Davis, 1986:30–31).

Other causes of purely regurgitant valves include floppy valves secondary to myxomatous degeneration, traumatic cusp tears (usually associated with an aortic disruption from trauma or dissection), discrete sub-aortic stenosis, systemic lupus erythematosus, rheumatoid arthritis nodules or granuloma, mediastinal irradiation, metastatic sarcoma, tricuspid aortic valves associated with ventricular septal defects and surgical trauma.[100] Although the aortic valve may be intrinsically normal, pure aortic regurgitation may result from primary disease of the ascending aorta including syphilis, non-inflammatory disease (Marfan's or Marfan-like disease; ie, Ehler–Danlos syndrome, homocystinuria and osteogenesis imperfecta), aortitis (non-specific or inflammatory), rheumatoid arthritis, laceration of the aorta (dissection, trauma, ruptured sinus of Valsalva aneurysm) which all involve the aortic root, and specifically the aortic annulus.[100] The hallmark of most of these subgroups is the demonstration of varying degrees of focal or diffuse elastic and/or smooth muscle destruction and absence of an active inflammatory process.[104]

Eloquent descriptions of the mechanisms that cause AR as it relates to aortic valve and root anatomy have been provided by Thubrikar and others.[106–109] The main purpose of the aortic valve complex is to provide the structural integrity necessary to allow the aortic valve cusps or leaflets to interact properly during systole and diastole; ie, full opening of the valve during systole with minimal gradient and complete closure of the leaflets during diastole, and minimal valve leaking.

Specifically with regard to aortic regurgitation, the architecture of the valve and root must be able to withstand the high diastolic pressure transmitted to the closed valve from within the aorta. The aortic annulus is defined by the area of attachment of the aortic cusps to the aortic wall, and is frequently described as not a true anatomical annulus. Due to the scalloped attachment of the aortic cusps, the aortic annulus has a larger vertical height corresponding to the dimension of the whole sinus of Valsalva, in contrast to the height of the mitral annulus with the leaflets attached in a circular orientation in a smaller vertical plane roughly corresponding to the depth of the fibrous skeleton. In this regard the aortic annulus protrudes above and below the horizontal plane or depth of the fibrous skeleton. The aortic annulus is divided into subcommissural and supracommissural (supra-aortic crest) areas to define the full extent of the annulus. This orientation of annular leaflet attachment frequently leads to confusion when conceptualizing the aortic annulus, and often only the subcommissural area or the inferior vertical plane produced by cusp closure is referred to as the aortic annulus. The aortic valve cusps are attached to

the aortic wall in a semicircular fashion, with the commissures producing the apex of a tall narrow triangle between the union of the cusps. This orientation of each cusp produces the load-bearing architecture necessary for withstanding the diastolic pressure. The broader vertical height and narrow width of the interleaflet triangle promotes the leaflet surface area necessary for complete cuspal coaptation. In addition the lunula provides even greater surface area and serves to reinforce the free margin of the edge of the cusps. The maximum load point at the center of each cusp is further reinforced by the nodule of Arantus. A further thickening of the central position leaflet lunula. Working in unison, the valve cusps and commissures support the load during closure.

Cases of aortic regurgitation without significant annular dilatation and normal leaflet motion may be illustrated in occasional cases of rheumatic pathology, with similar findings occurring with systemic hypertension. Fibrous thickening of one or more cusps occurs without significant cuspal retraction or commissural fusion. Absent or only small amounts of calcific deposits produce cuspal margins that become shorter than normal, resulting in abnormal coaptation of the three cusps and usually producing a mild (or, less commonly, moderate) central leak.

Isolated annular dilatation with normal or slightly restricted leaflet motion is associated with a central leak roughly in the middle of the valve plane. The most frequent abnormality is widening of the narrow interleaflet triangle, which prevents leaflet apposition at the central load-bearing point. With aortic regurgitation resulting from annular dilatation and excessive leaflet tissue, such as with aortic valve prolapse or bicuspid valves, the annular architecture is further disrupted. The annular dilatation results in widening of the interleaflet triangle. In addition, the excessive tissue or leaflet size mismatch results in regurgitation as the load-bearing point changes along the valve coaptation plane and/or the excessive tissue protrudes past the line of closure as dictated by the other leaflets, producing an eccentric regurgitant jet. Specifically with bicuspid valves the maximum load point is further disrupted by the lack of a well-formed lunula and nodule of Arantus in the conjoined aortic cusp, and by the position of the raphe if present which has its insertion point below the sinotubular junction toward the base of the sinus of Valsalva.

Restricted aortic valve motion may be associated with normal or, occasionally, with a mildly dilated annulus. The load-bearing point will be related to the area where the leaflet is restricted, causing the normal leaflet to move past the restricted and shortened cuspal margin in the normal valve coaptation plane. In all types, when leaflet fibrosis or calcification occurs, primarily or secondarily, due to the progression of the pathology, leaflet motion is altered and the maximum load-bearing point may change.

The mechanism and pathological cause of valve dysfunction may also be determined by describing the character of the color flow jet of aortic regurgitation.[110] With transesophageal echocardiography the valve mobility, jet direction and jet origin between the cusps is eccentric, central or diffuse. Bicuspid and tricuspid aortic valve prolapse is associated with excessive valve mobility (69%) and eccentric jet direction and origin. In patients with annular dilation, rheumatic disease, sclerosis and perforation the AR is associated with normal or reduced cusp mobility (71%) and a central jet direction and origin is seen.

Aortic valvular disease has also been reported after exposure to fenfluramine, dexfenfluramine and phentermine, serotonin-like drugs similar to ergotamine induced

valvular disease or carcinoid disease. Connolly et al characterized the changes produced in the aortic valve as thickened (focal or diffuse) and mildly retracted valve leaflets, resembling rheumatic disease without stenosis.[111] The aortic valve is the most commonly affected valve, which usually results in mild to moderate degrees of aortic regurgitation. The development of significant aortic regurgitation does not correlate with the dose or duration of phen-fen therapy.[112] It does appear that the prevalence of significant valvular regurgitation is related to the duration of exposure to the anorectic agents (fenfluramine and dexfenfluramine) and occurs in around 30% of patients who take the drugs, although many dispute this finding.[113] The natural history of the valvular disease is unknown at the present time, but the valvular disease may resolve after withdrawal of the anorectic drugs.[114] The phen-fen aortic valvular disease controversy has prompted the premise that aortic regurgitation is related to obesity and age-related changes, but this has largely been refuted by the Strong Heart Study.[115] Aortic regurgitation occurred in 10% of middle-aged to older adults and was related to increased age, larger aortic root diameter, aortic and mitral stenosis and albuminuria, and not to being overweight. There was a negative association with diabetes. In addition, the frequency of aortic regurgitation in anorectic drug use does appear to be higher than that expected in the general population.

Aortic regurgitation is classified as acute or chronic. In the acute type, significant aortic regurgitation is produced in a short amount of time. Hemodynamically, the normal left ventricle suddenly experiences a large regurgitant volume, which rapidly increases end-diastolic pressure and left atrial pressure. Despite the development of tachycardia, the Frank-Starling mechanism for increasing ventricular performance is overwhelmed, which results in a decrease in forward stroke volume. The end result of acute aortic regurgitation is rapid equilibration of aortic and left ventricular diastolic pressure, which results in a short regurgitant diastolic half time (< 300 ms), a short mitral deceleration time (< 150 ms) and premature closure of the mitral valve. In addition to identifying these findings with Doppler, visualizing the aortic valve and aorta with multiplane transesophageal echocardiography usually identifies the cause of acute aortic regurgitation. Since acute aortic regurgitation is not tolerated well hemodynamically, emergency surgery is usually necessary and transesophageal echocardiography is an excellent test for a rapid diagnosis.

Chronic aortic regurgitation produces a combined volume and pressure overload to the left ventricle, due to its slow progression. Left ventricular function is preserved despite the increase in afterload produced by the regurgitation, owing to recruitment of preload reserve and the compensatory LV hypertrophy that occurs. Initially the ejection fraction is normal or increased, but as aortic regurgitation worsens, the ejection fraction slowly falls below normal with progressive chamber enlargement producing a spherical left ventricular geometry. Often a fall in ejection fraction occurs with exercise, despite remaining normal at rest. Dyspnea occurs with declining systolic function and elevated filling pressures although this may not be noticeable until severe left ventricular dysfunction has developed. Initially, left ventricular dysfunction is reversible; therefore timing of aortic valve surgery is crucial. Various reports have shown that left ventricular systolic function and end-systolic size are the most important determinants of survival and improvement in postoperative left ventricular function in patients undergoing aortic valve replacement.[116–118] With this in mind, patients are being taken to surgery, especially if repair is feasible, when they show left ventricular dysfunction even if they are

symptom-free. Transesophageal echocardiography is very good in confirming the diagnosis of aortic regurgitation and often elucidates the cause through defining the valve morphology. It is also useful for assessing left ventricular dimension, mass and systolic function as well as aortic root size. Doppler provides a semiquantitative estimate of the severity of regurgitation.

Aortic regurgitation may also occur as a result of spontaneous laceration of the aorta producing a flail aortic valve.[119] In addition, aortic regurgitation may be found after mitral valve repair when the annuloplasty ring interferes with the aorto-mitral intervalvular fibrosa.[120]

Assessment of aortic regurgitation

The transesophageal echocardiographic assessment of aortic regurgitation includes color-flow Doppler imaging, continuous-wave and pulsed-wave Doppler. Most of the echocardiographic/Doppler data on the quantification of aortic regurgitation for multiplane transesophageal echocardiography is extrapolated from the transthoracic literature. In the few reports available that compare transesophageal with transthoracic quantification of aortic regurgitation severity, there is good correlation as long as the imaging planes obtained provide parallel interrogation of the left ventricular outflow tract.[121] The same physiological and technical factors that affect the dimensions of the regurgitant jet, that pertain to transthoracic imaging apply to transesophageal echocardiography. The size of the regurgitant jet area, particularly the length of the jet will be determined by the compliance of the left ventricle, duration of diastole and the left ventricular end diastolic pressure. Technically the regurgitant jet should be maximized and assessed in multiple planes with attention to the gain setting, angle dependence and transducer frequency. As with transthoracic studies, most methods for assessing aortic regurgitation are most valid when the jet is central rather than eccentric in orientation to the valve plane.

When echocardiography shows severe left ventricular dysfunction with only mild aortic regurgitation, other causes of left ventricular dysfunction should be excluded such as cardiomyopathy, coronary artery disease or hypertension. With severe aortic regurgitation and left ventricular dysfunction, aortic valve replacement should be considered in symptomatic patients with ejection fractions of 25 to 49%, in patients without left ventricular dysfunction who show NYHA class III/IV symptoms, and in symptom-free patients with end-diastolic dimensions > 75 mm or end-diastolic dimensions > 55 mm and normal ejection fractions.[122] It is important to remember that women tend to develop symptoms and/or left ventricular dysfunction with less left ventricular dilation than men, shown by an excess late mortality in aortic valve replacement.[116] Therefore, surgical correction of aortic regurgitation should be considered when the left ventricular end-systolic dimension is 25 mm or greater when corrected for body surface area. In aortic regurgitation in the setting of aortic root dilation, aortic valve replacement may be considered when the root diameter is ≥ 50 mm.

Color-flow imaging and conventional continuous and pulsed wave Doppler of the aortic regurgitation jet is best accomplished in the deep transgastric views at 0 to 15 degrees or the longitudinal gastric view at 125 to 135 degrees, which best show the left

ventricular outflow tract. The size of the color flow regurgitant jet, including length or maximal extent, correlates poorly with the angiographic grade obtained from any view. Good correlation has been shown however, with determining the ratio of the regurgitant jet area to the annulus area obtained in the short axis plane with color-flow imaging.[123,124] The width of the proximal regurgitant jet relative to the left ventricular outflow tract dimension in the longitudinal plane is also a good predictor of the severity of aortic regurgitation when compared with angiographic grade with central regurgitant jets but falls short with eccentric jets.[123] Aortic regurgitation is graded as I to IV to correlate with angiographic grade, corresponding to the ratio obtained of the proximal jet area or width to the left ventricular outflow area or width.[124] Mild or Grade I aortic regurgitation corresponds to a ratio of less than 0.25, moderate or Grade II to a ratio of 0.25–0.46, moderate-severe or Grade III to a ratio of 0.47–0.64, severe or Grade IV to a ratio equal to or greater than 0.65.

Willems et al have shown that the reproducibility of jet-left ventricular outflow tract diameter is better than the jet-left ventricular outflow tract area measurement, and is more accurate in assessing the severity of aortic regurgitation from color Doppler images.[125]

The effective regurgitant orifice area (EROA) is a basic determinant of the regurgitant volume (RV) and therefore a good determinant for the severity in aortic regurgitation.[126] Reimold et al demonstrated that with chronic aortic regurgitation both the jet width and Doppler-derived regurgitant orifice area increased over time, suggesting that one factor in the progression of aortic regurgitation is enlargement of the orifice.[127] The RV can be calculated from the difference between the left ventricular ejection flow volume and either the transmitral inflow volume or the pulmonary outflow volume.

$$\text{Aortic regurgitant volume} = (D^2 \times 0.785 \times \text{TVI}_{\text{LVOT}}) - (D^2 \times 0.785 \times \text{TVI}_{\text{MV}})$$

The regurgitant fraction is represented by the percentage of regurgitant volume compared with the total flow across the regurgitant aortic valve.

$$\text{Regurgitant fraction} = (\text{Aortic regurgitant volume/LVOT stroke volume}) \times 100\%$$

Regurgitant orifice area can be estimated with the PISA method or vena contracta methods.

$$\text{Flow rate} = 2\pi r^2 \times \text{aliasing velocity}$$
$$\text{ERO} = \text{Flow rate/peak AR velocity} = 6.28 \times r^2 \times \text{aliasing velocity/peak AR velocity}$$

Measuring the width of the vena contracta, the smallest area of regurgitant flow jet at its origin, provides a good method for assessing the severity of aortic regurgitation, irrespective of whether the jet is central or eccentric.[128] Tribouilloy et al studied 79 patients with aortic regurgitation with the vena contracta method and obtained good correlations with quantitative Doppler and two-dimensional transthoracic

echocardiography.[129] A vena contracta width of $\geq$ 6 mm and a calculated EROA $\geq$ 30 mm^2 predicted severe aortic regurgitation with a sensitivity of 95% and specificity of 90%.

The proximal isovelocity surface area (PISA) method is also useful for determining the severity of aortic regurgitation with both transthoracic and multiplane transesophageal echocardiography.[130] Sato et al determined that PISA is also accurate for eccentric aortic jets.[131,132] Values of PISA radius $\geq$ 0.70 cm and EROA $\geq$ 0.25 cm^2 were always associated with a regurgitant fraction 40%, while PISA radius < 0.70 cm and EROA < 0.25 cm^2 were always associated with a regurgitant fraction < 0.40. Underestimation of the EROA by PISA may occur in patients with an obtuse flow convergence angle (> 220°), but otherwise it is excellent.[130]

Other signs of severe aortic regurgitation include holodiastolic flow reversal shown in the descending thoracic aorta, and a shortened deceleration time of the mitral early diastolic E wave flow and shortened pressure halftime and deceleration time of the aortic regurgitant jet determined with continuous wave Doppler. The slope and pressure half-time of the aortic regurgitation velocity curve are rate-dependent; the relative-pressure half-time appeared to limit the influence of the heart rate on pressure half-time.[133]

In patients without parallel imaging planes of the left ventricular outflow tract, diastolic flow reversal in the descending aorta may be used to assess aortic regurgitation. Sutton et al studied 45 patients with aortic regurgitation during surgery and found that identifying aortic flow reversal in the descending aorta confirmed the presence of severe aortic regurgitation.[134] Aortic valve replacement successfully eliminated the flow reversal.

Regurgitant volume and fraction can be measured by the volumetric method, using the continuity formula. Total forward volume or flow across a valve is the sum of systemic stroke volume and regurgitant volume. The regurgitant volume is calculated by determining the difference between the total forward stroke volume and the systemic stroke volume. As long as there is no concomitant significant mitral regurgitation the volumetric method for aortic regurgitation may be calculated from the difference between the stroke volume across the left ventricular outflow tract and mitral inflow. In clinical practice, numerous methods are used in combination to estimate the severity of aortic regurgitation.

Vilacosta et al studied the pulmonary and mitral inflow patterns in aortic regurgitation.[135] Patients with severe acute aortic regurgitation showed an absence of the transmitral A wave with prominent pulmonary venous AR wave (retrograde atrial kick). These patients had a systolic/diastolic ratio < 1 (restrictive Doppler pattern). Patients with chronic aortic regurgitation had a Doppler pattern of abnormal left ventricular relaxation E/A ratio < 1, systolic/diastolic pulmonary venous flow ratio > 1.

There is progressive dilation of the aortic root at all levels, even in patients with mild AR. More rapid progression in aortic size is associated with more rapid progression of the underlying aortic insufficiency, as well as more rapid increases in left ventricular volume and mass.[136]

Aortic valve repair

In contrast to the success and acceptance of mitral valve repair, aortic valve repair is not as well accepted or supported by the medical literature.[137–139] In many studies, aortic valve repair in the setting of aortic stenosis and aortic regurgitation has shown a wide variety of results, with certain institutions demonstrating better results than others. Good results with aortic valve repair seem to be highly dependent on the surgical expertise and patient selection in either aortic stenosis or aortic regurgitation. The specific pathology and its affect on the valve also appear to influence postoperative results. In addition, there have been many new alternatives for replacement of the aortic valve such as allografts, stentless bioprostheses and pulmonary autografts that have also limited the surgical enthusiasm for aortic valve repair. In any event, aortic valve repair remains a good alternative to prosthetic valve replacement with its inherent drawbacks and complications, in selected cases. In mild and moderate aortic regurgitation, aortic valve repair with cusp resuspension for prolapse or when associated with dissection, and aortic root remodeling with annuloplasty techniques provide good long and short-term results. Although there appears to be less experience with aortic stenosis, commissurotomy and debridement and decalcification of the valve cusps have had reported success in a few cases. As with mitral valve repair, multiplane transesophageal echocardiography plays an essential role and successfully defines the pathology and valvular structure, which greatly assists in identifying patients appropriate for repair, as well as assessing the results of the techniques used for surgical aortic repair. The specifics of performing a transesophageal echocardiogram are similar to that for assessing aortic regurgitation and are summarized in table 3.2.

Whereas repair of congenital aortic disease is an attractive option, avoiding replacement with a prosthetic valve, repair of rheumatic and degenerative aortic valves has largely been abandoned because of poor results. In senile or degenerative calcification, the aortic cusps are usually more affected than the commissures. There is preservation of the gross anatomical structure of the aortic valve, with bar calcification present on the surface of the cuspal body and the bottom of the sinuses, which restrict leaflet motion and produce stenosis. Mechanical decalcification of the leaflet cusps and surgical commissurotomy has mixed results. The groups with the best results, usually dealing with focal calcific pathology, report about 50% survival after 12–20 years, with 75–100% free from reoperation or valve related symptoms at 8–12 years with mechanical debridement.[140,141] In rheumatic stenosis, repair is generally unsuccessful due to cusps that are usually very retracted and distorted where calcification is usually diffuse, resulting in calcification of the full thickness of the leaflet and/or fusion of the commissures. Only 20% of patients are free from re-operation after 12 years. Generally, aortic valve repair may be attempted in rheumatic disease, if the pathological process is not diffuse and the cusps can be easily shaved or simple commissurotomy may be done with good results common.
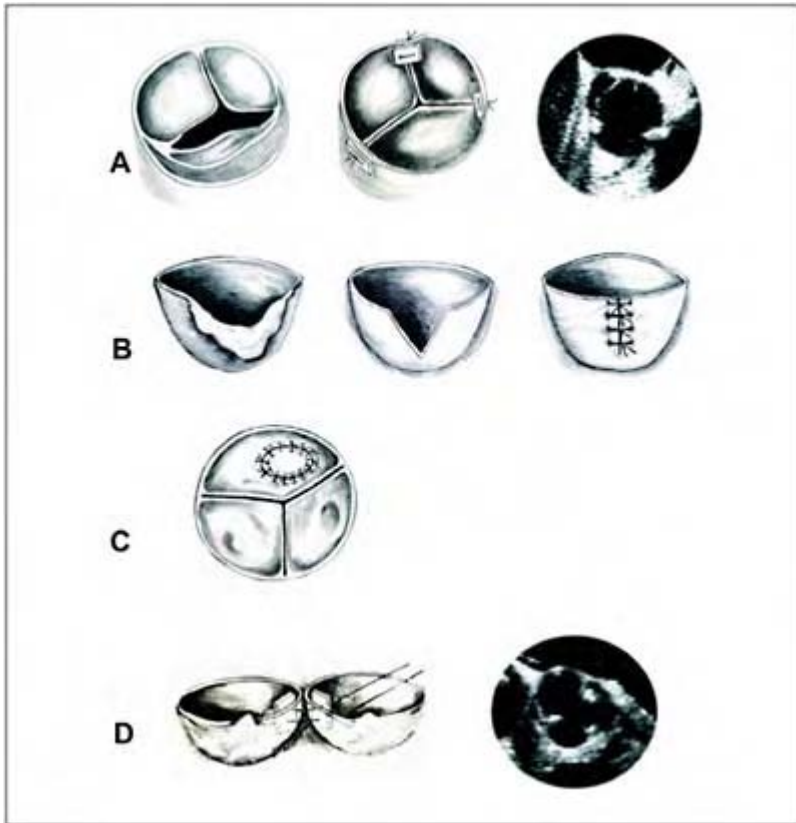
Figure 3.14 Artist's rendition of aortic
valve reparative techniques. A. Aortic
dissection. Aortic valve repair with
resuspension of the native valve
provides competence to the valve
cusps eliminating aortic regurgitation.
Surgical resuspension of the aortic
valve in these cases significantly
decreased the root size and restored
structural integrity to the aortic
annulus, significantly decreasing
postoperative aortic regurgitation to
trace to mild degrees. After repair the
pledgets are often visible along with
the cuspal margins. B. Aortic valve

prolapse. In repairing a bicuspid aortic valve a triangular resection is done, removing the prolapsing segment including the raphe if present to achieve leaflet symmetry. After resection, the triangular defect is closed with a continuous suture line. In addition, focal areas of fibrous thickening or calcification may be trimmed or shaved to promote good cuspal mobility. C. Aortic valve perforation. Perforations or fenestrated valve cusps may be repaired with resection or patching with pericardium when large. D. Annular plication. Annular plication is done at all commissures. This technique uses a pledgeted horizontal mattress suture through each commissure of two leaflets. The height of the interleaflet triangle produced is determined by the depth in the sinus of the suture, which dictates the resultant degree of leaflet coaptation. After repair, echocardiographically the valve should appear normal with the exception of the commissural pledgets, which are usually visible and very echogenic in diastole.

In contrast to aortic stenosis, rheumatic and congenital aortic regurgitation may be more amenable to reparative surgical techniques. In rheumatic aortic regurgitation Duran has described several techniques for aortic repair, including cusp augmentation or replacement, cusp edge unfolding, and supra-aortic crest enhancement. Good results were reported in patients for whom prosthetic valve replacement was not ideal, or avoided placing a homograft or autograft in a root with rheumatic pathology.[142] Patients were free from valve-related events in 77% of cases over a 2.5–year follow-up, even when the surgical results were not perfect and aortic regurgitation was not totally eradicated.

Repair of congenital bicuspid valves, aortic valve prolapse and annular dilatation to date have yielded the best results.[143,144] As with mitral regurgitation, aortic regurgitation can be grouped and described with echocardiography as Type I, normal cusp motion;

Type II, excessive (prolapse) cusp motion; or Type III, restricted cusp motion. Reparative surgical techniques may then be directed towards the cause of the regurgitation. Aortic regurgitation may be corrected through reducing the diameter of the aortic annulus, which approximates the commissures by reducing the area in between the commissures, which improves the geometry and shape of the aortic root—specifically the sinuses—and which allows improved leaflet apposition with minimal leaflet stretching, effectively promoting full leaflet closure and a competent valve. This may be accomplished with reshaping or remodeling the subcommissural area and the supracommissural (supra-aortic crest) level. In bicuspid and prolapsing aortic valves, Cosgrove et al have obtained the best results thus far with wedge resection of the leaflet tissue (involving the raphe when present) and sub-commissural annuloplasty, and have recently reported their long-term results (figure 3.14).[143] In a follow-up report on the intermediate results (mean follow-up 5.5 yrs [0.2 to 9 years]), freedom from re-operation was 95%, 87% and 84% at 1, 5, and 7 years respectively, with no deaths.[145] 12 patients out of 94 required an aortic valve replacement or re-repair. The highest risk for re-operation occurred early after surgery and fell to about 2% per year and less after 2 years. The presence of residual trace to mild aortic regurgitation on immediate intraoperative post-repair transesophageal echocardiographic examination was the only risk factor. Late occurring aortic regurgitation did not progress over time. In patients with dilated and poorly functioning left ventricles, valve repair was more difficult.

There may be several mechanisms for producing regurgitation in bicuspid aortic valves. If present in the conjoined cusp, the raphe (whether it is calcified or not) may cause some degree of restricted cusp motion. The free edge of the conjoined cusp is longer and somewhat thickened than the other cusp, which produces prolapse and renders the valve incompetent during diastole. In addition, the cuspal attachment of the bicuspid valve is more shallow, rather than a semicircular attachment, effectively shortening the commissure and widening the intercommissural area, stretching the unaffected cusp and decreasing the load-bearing capability of the cusps. Jet lesions are produced on the cuspal surface owing to regurgitation that promotes fibrosis, thickening and further restriction of the cusp motion, in addition to providing a nidus for bacterial endocarditis that frequently results in cuspal perforation.

In repairing a bicuspid aortic valve, a triangular resection is done, removing the prolapsing segment, including the raphe if present, to achieve leaflet symmetry. After resection, the triangular defect is closed with a continuous suture line. Annular plication is performed at both commissures. This technique uses a pledgeted horizontal mattress suture through each commissure of both leaflets. The height of the interleaflet triangle produced is determined by the depth in the sinus of the suture, which dictates the resultant degree of leaflet coaptation. In addition, focal areas of fibrous thickening or calcification may be trimmed or shaved to promote good cuspal mobility.

In tricuspid aortic valve prolapse, repair has been performed when there is only one prolapsing cusp with triangular resection in the prolapsing cusp to equalize the symmetry of all three cusps, followed by commissural plication. Perforations or fenestrated valve cusps may be repaired with resection or patching with pericardium when large.

Disruption of the aortic root with Type A dissection often produces significant aortic regurgitation. Aortic valve repair with resuspension of the native valve provides competence to the valve cusps, eliminating aortic regurgitation. Multiplane

transesophageal echocardiography readily shows the severity of aortic regurgitation, aortic root diameter, circumference of the aortic annulus, percentage of the annulus dissected and the presence of leaflet prolapse. Keane et al described operative findings in 34 patients with proximal dissections and found the degree of dissection of the valve annulus is the most significant determinant of leaflet prolapse and aortic regurgitation severity.[146] Overall size of the aortic root also contributed to the degree of aortic regurgitation. Surgical resuspension of the aortic valve in these cases significantly decreased the root size and restored structural integrity to the aortic annulus, and significantly decreased postoperative aortic regurgitation to trace to mild degrees.

In the report by Movosowitz et al, 50 patients with type A dissection were studied with multiplane transesophageal echocardiography and over half of the patients exhibited moderate or severe aortic regurgitation.[147] With transesophageal echocardiographic examination the aortic valve leaflets were described as intrinsically normal, with one or more surgically correctable lesions. Specifically, these aortic valves showed incomplete leaflet closure due to leaflet tethering in a dilated aortic root, leaflet prolapse due to disrupted leaflet attachments, and dissection flap prolapse through the aortic valve orifice. Repair can be considered in such patients unless Marfan's syndrome, bicuspid aortic valve and aortitis may indicate aortic valve replacement.

Aortic valve endocarditis

Multiplane transesophageal echocardiography is excellent to detect aortic valve vegetations and to detect the complication of infectious endocarditis. In studies comparing transesophageal echocardiography with transthoracic echocardiography, multiplane transesophageal echocardiography reliably detects vegetations between 2 and 5 mm, with a sensitivity between 90 and 100%.[148–157]

Vegetations usually occur on the ventricular surface of the aortic valve, and appear as discrete masses with distinct echogenicity, with a distinct propensity for forming on bicuspid valves. Aortic vegetations may be sessile or mobile, appearing as large localized thickening of the aortic cusps or as mobile masses, which exhibit chaotic motion and frequently prolapse between the left ventricular outflow tract and the aorta during the cardiac cycle.[158] Multiplane transesophageal echocardiography readily shows large vegetations that affect the opening and closing of the aortic valve cusps by identifying abnormal Doppler flows during systole and diastole. With the multiple planes, increased resolution, and regional expansion (zoom) mode of multiplane transesophageal echocardiography, vegetations may be distinguished from fibrous or filamentous mobile strands such as Lambl's excrescence or papillary fibroelastomas.

The complications of aortic valve endocarditis include local valvular cusp destruction or extension of the infection into the periannular space. Perforations of an aortic cusp associated with endocarditis may be seen in the short axis views depicting the abnormal origin of regurgitant jets with color Doppler, which are not associated with the valvular line of closure and may frequently be demonstrated as originating from the body of the cusp. Flail aortic cusps are usually readily identified in longitudinal views, as shown by prolapse of the cuspal body past the annular plane or as a deformed, disrupted cusp, which exhibits chaotic or vibratory motion.[158]

Perivalvular spread of infection may occur with extension into the valve annulus or adjacent myocardium (ventricular septum and rarely interatrial septum), and has been shown in around 30% of postmortem and surgical cases of aortic valve endocarditis.[159,160] Annular abscess is usually an ominous sign, as denoted by a high incidence of severe heart failure, heart block and fistula/pseudoaneurysm formation. Annular abscesses are most frequently associated with aortic valve endocarditis (52 to 75%) in comparison with the other valves, and when present are usually identified with multiplane transesophageal echocardiography.[161] Annular abscesses are generally limited to the area of the perimeter of the aortic valve dictated by the composition of the perivalvular tissue of the fibrous skeleton, and are associated with the cusp showing a vegetation. In the report of Baumgartner et al, the abscess was less than 1cm in 67%, larger but confined to the perimeter of one cusp in 22%, large and associated with two cusps in 9%, and circumferential in only one case (2%).[162] Occasionally, abscess is also noted without a visible vegetation. Transesophageal echocardiography accurately shows periannular abscess in 87 to 99% of cases when present and in 100% of cases when the ventricular septum is involved.[161–163] Aortic annular abscesses are identified as localized confluent areas of echogenicity confined to the sub-commissure or subaortic perivalvular area along the plane of the fibrous skeleton. Annular abscesses may appear as echodense or echolucent regions distinct from the normal annulus or perivalvular tissue, which usually distorts the normal appearance of the proximal aortic root. Initially, abscesses appear more confluent, echodense and homogenous and as the abscess matures with pus it takes on a heterogeneous or echolucent appearance and may appear multi-cystic. Rupture of the abscess produces an echolucent free space or cavity, often with necrotic debris or residue within the cavity and a large or a small fistulous communication with an adjacent cardiac chamber. Blood flow entering the abscess cavity is frequently detected with color Doppler during the cardiac cycle, identified with systolic expansion and diastolic collapse of the cavity. In addition, abscess rupture may provide an abnormal communication between cardiac chambers, producing significant turbulent shunt flow which is also readily identified with color flow Doppler. Fistulous flow may commonly shown between the aortic root and the left atrium or the aortic root and the left ventricular outflow tract (ventriculoaortic discontinuity), in a single direction or a "to and fro" pattern. Rarely, a communication is produced with the pericardial cavity, which produces pericardial effusion and subsequent pericardial tamponade.

Table 3.1 Severity of AI with TEE

Degree of AI	Ratio (%) regurgitant $JW/LVOT_D$	Ratio (%) regurgitant $JA/LVOT_{area}$	AR PHT (msec)	RF (%)	RV (mL)	ERO (cm^2)
Mild	≤ 30	≤ 30	≥ 400	< 30	< 25	< 0.10
Severe	≥ 60	≥ 60	≤ 250	≥ 55	≥ 60	≥ 0.30

AI, aortic insufficiency; JW, regurgitant jet width; $LVOT_D$, left ventricular outflow tract diameter; JA, regurgitant jet area; $LVOT_{area}$, left ventricular outflow tract area; ARPHT, aortic regurgitant pressure half-time; RF, regurgitant fraction; RV, regurgitant volume; ERO, effective regurgitant orifice area.

Abscesses associated with the right coronary cusp may invade the proximal ventricular septum and appear in longitudinal planes as echogenic spaces within the ventricular myocardium. When ruptured, the ventricular abscess appears as a ragged defect distorting the endocardial margin. Abscesses of the left coronary cusp, and occasionally the non-coronary cusp, are often associated with extension to the aorto-mitral intervalvular fibrosa and produce a fungal aneurysm. Meticulous examination in multiple planes must be done to exclude direct sub-aortic extension of vegetation to the anterior mitral leaflet, before diagnosing an aorto-mitral intervalvular fibrosa fungal aneurysm. Vegetations occuring on both the aortic and mitral valve have higher complication rates for embolic potential and surgery, than isolated infection of either valve alone. Implications for surgical intervention are obvious in that vegetations of both valves would require replacement of each valve.

Aorto-mitral intervalvular fibrosa fungal pseudoaneurysm, as also discussed in chapter 2, present as deformities to the annular attachment of the anterior mitral leaflet and usually extend above and below the sub-commissural annular plane.[164–172] The aortic abscess appears to protrude to a greater extent into the left atrium towards the mitral leaflet than does a typical periannular abscess, which conforms to the aortic cusp perimeter. The deformity produced in the intervalvular fibrosa appears to originate in the basal portion of the mitral leaflet and may resemble the leaflet folding on itself in that area. This appearance must be distinguished from isolated mitral vegetation. With examination in the zoom mode in multiple planes, vegetation may be excluded with confidence. With rupture of the mycotic aneurysm, shunts may be produced and are usually detected from the left ventricular outflow tract to the left atrium.

Care must be taken to differentiate annular abscess and its variants from sinus of Valsalva aneurysm with or without rupture (figure 3.15). Congenital forms of sinus of Valsalva aneurysm display a typical echocardiographic appearance of a diverticular shaped deformity to the sinus protruding into the adjacent chamber in a two-dimensional plane, and are easily distinguished from an annular abscess. Acquired sinus of Valsalva aneurysm may be more difficult to distinguish from an annular abscess. As discussed in chapter 5, acquired sinus of Valsalva aneurysm produces a dilatation-type deformity to the sinus or proximal segment of the aorta in the fashion of a saccular aneurysm. When related to inflammation or infection, acquired sinus of Valsalva aneurysm is probably related to aortitis, producing weakening of the aortic wall allowing a dilatation-type expansion and not abscess formation. When rupture of a sinus of Valsalva aneurysm occurs and produces a communication between cardiac chambers, the flow originates with the aortic root and communicates between the adjacent cardiac chambers with a smaller communication.

Table 3.2 TEE in aortic valve repair

Grade AI*
Determine the location of the AI jet (central or eccentric)
Describe leaflet motion
Normal motion
Excessive or prolapse
Restriction

Measure annular size+

Determine number of leaflets

Bicuspid or tricuspid

Presence of calcification

Presence of leaflet perforation

Co-existing valvular disease

Describe left ventricular function

Determine presence of pulmonary hypertension

*Moderate to severe AI needed preoperatively, only accept trivial (1+) AI postoperatively; +Small annular size results in postoperative stenosis

Non-bacterial endocarditis associated with either primary or secondary antiphospholipid syndrome may cause aortic valve dysfunction and result in aortic regurgitation (25 to 28% of patients) and rarely stenosis (3 to 4% of patients).[173,174] Echocardiographic studies have disclosed heart valve abnormalities in about 32 to 38% of primary antiphospholipid cases, with higher prevalence noted in secondary cases associated with systemic lupus erythematosus (35% to 65%). Valvular lesions consist of valve masses (non-bacterial vegetations as described in Libman–Sacks endocarditis), 43% or leaflet thickening or both. Antibodies have also been implicated in promoting valve thrombi. The mitral valve is most frequently affected, followed by the aortic valve. Roldan et al described aortic cusp thickening in one or more cusps greater than 2 mm in 30% of patients, or discrete aortic vegetation in 19% of patients with systemic lupus erythematosus, with approximately two-thirds having both thickening and vegetation.[174] Vegetations were located on the basal, middle or tip portions of the leaflets on the vessel side of the valve. Vegetations were of variable size (0.06 to 1.25 cm^2) and shape, frequently associated with irregular borders and heterogeneous echogenicity. Mild or moderate valvular regurgitation did not become severe. Leaflet thickening was associated with decreased mobility in two-thirds of patients and less than 10% had leaflet calcification or involvement of the annulus. In the Antiphospholipid Antibodies in Stroke Study Group, which was a retrospective echocardiographic analysis of cerebral ischemic events in patients with antiphospholid antibodies, 2.8% of the aortic valves showed abnormalities implicating a cardiac source of embolus.[175] Fibrous plaques were noted in the healed form of non-bacterial endocarditis, occasionally with focal calcification, which may further lead to valve deformity.
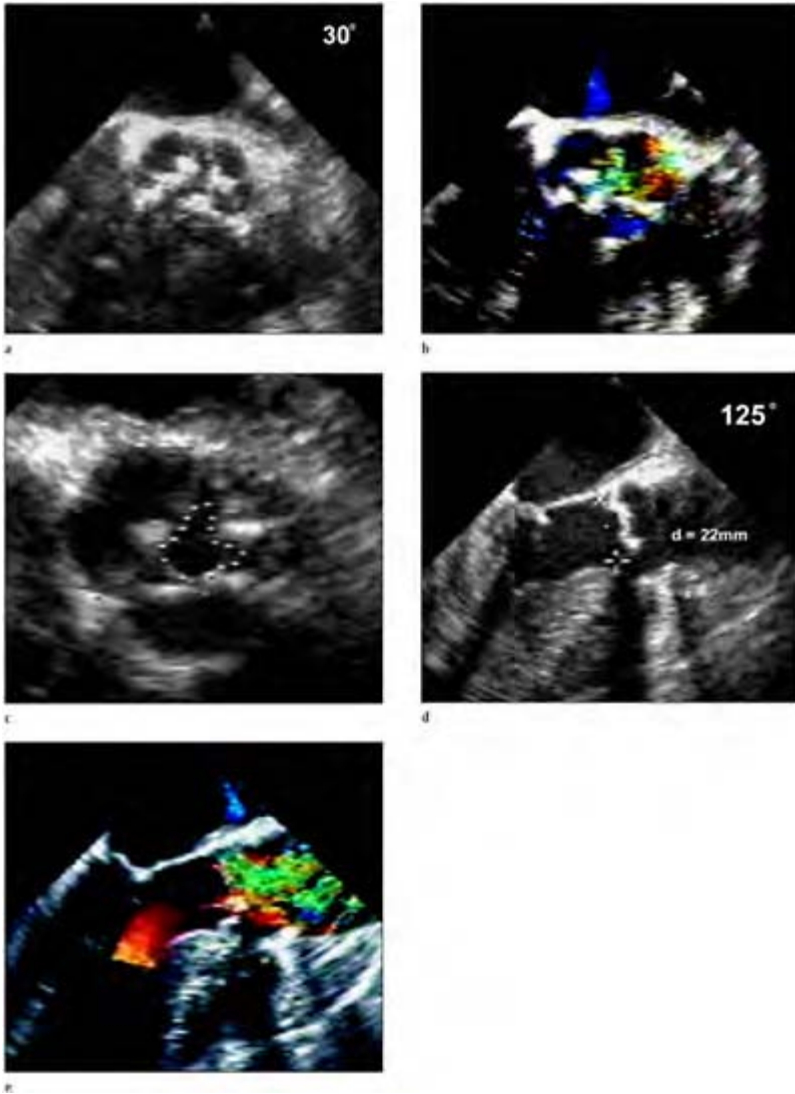
Case 3.1 Degenerative aortic stenosis produces marked thickening of the valve cusps producing retraction of the leaflet tissue. Short axis transesophageal views of degenerative aortic stenosis demonstrate marked calcification of the closed valve during diastole (a–b) producing shadowing

and ghosting of the surrounding cardiac structures. With careful visualization the valve can be captured in the maximal open position for planimetry of the valve orifice during systole (c). Many studies have shown excellent correlations between aortic valve areas measured with valve orifice planimetry done with transesophageal echocardiography and aortic valve areas obtained with cardiac catheterization, irrespective of normal or impaired left ventricular function. Longitudinal views of the degenerative stenotic valve showing measurement of the left ventricular outflow tract diameter (d) and color flow Doppler during systole (e) showing mosaic turbulence and high velocity flow produced by obstruction to flow from the stenotic leaflets.
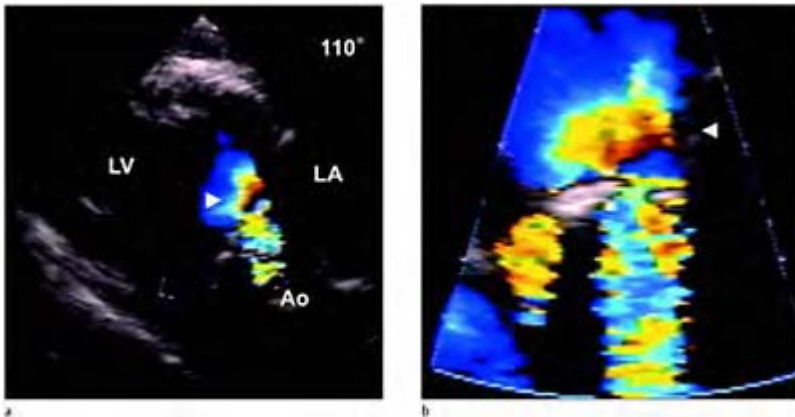
Case 3.2 Transgastric views obtained in the longitudinal axis demonstrating a typical stenotic flow jet through the aortic valve orifice. In zoom mode, the components of the color flow jet may

be delineated and measured for computations for PISA and or the vena contracta method. Flow convergence, vena contracta, stenotic jet.
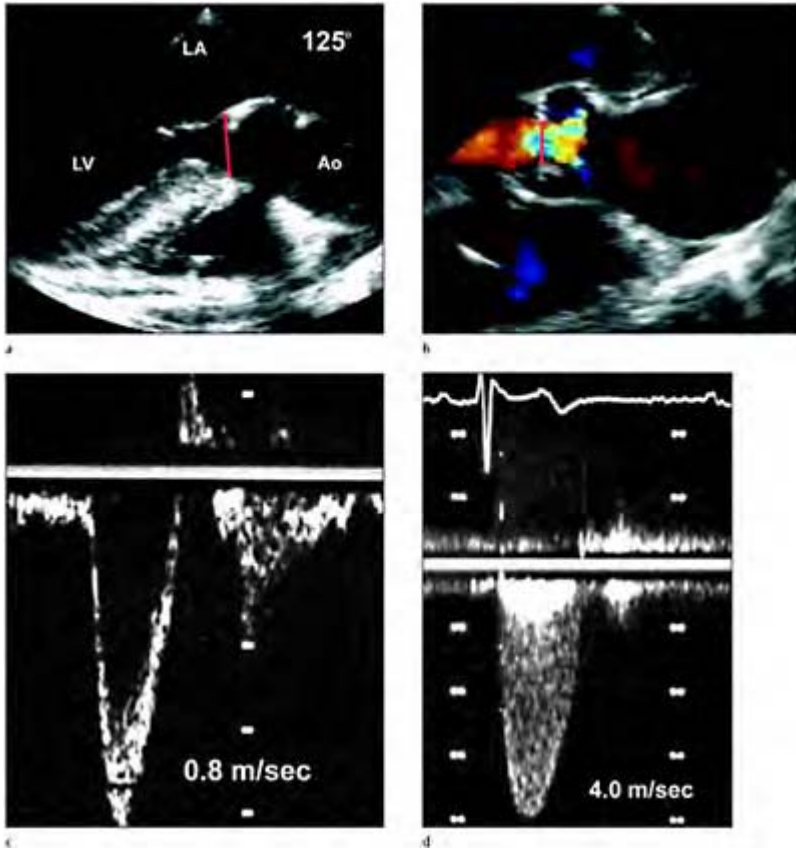
Case 3.3 Transesophageal assessment of aortic stenosis using the continuity equation. With the probe in the lower to mid esophageal position and the transducer rotated to approximately 100–125 degrees the left ventricular outflow tract diameter can be measured (a) and the diameter of the vena contracta of the color flow jet may be measured (b). In the transgastric probe

position, the left ventricular outflow tract with the aortic valve may be obtained by obtaining the short-axis mid-papillary muscle view at 0 degrees and then rotating the transducer from 90 to 135 degrees until the left ventricular outflow tract comes into view with the aortic valve plane appearing roughly in the middle of the image sector. In this view, continuous and pulsed wave Doppler interrogation (c, d) can be done in an almost parallel path. Continuous-wave Doppler enables estimation of maximal instantaneous and mean transvalvular pressure gradients by application of the modified Bernoulli formula. With the addition of pulse-wave Doppler of the left ventricular outflow tract, the continuity formula may be used to calculate aortic valve area. LA, left atrium; LV, left ventricle; Ao, aorta.
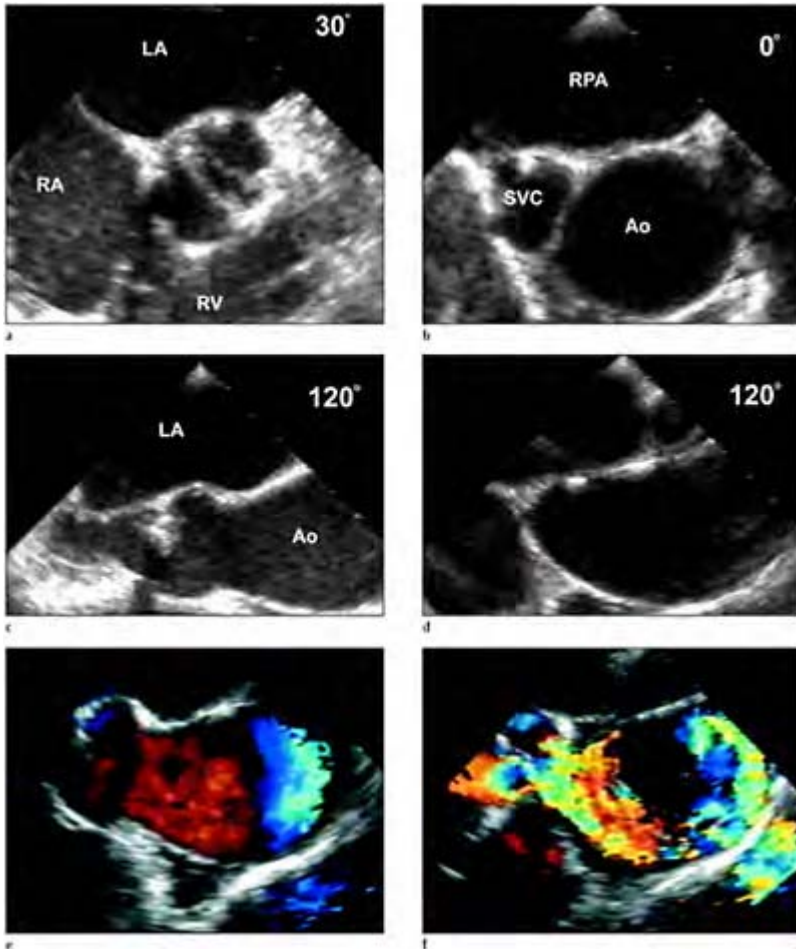
Case 3.4 Bicuspid aortic stenosis with post-stenotic dilatation of the ascending aorta. Bicuspid aortic valve exhibiting equal leaflet size with a right–left configuration of the cusps. Short axis view of the ascending aorta demonstrating dilation of the aorta. In the longitudinal projections the post-stenotic dilatation is most prominent along the greater curvature of the aorta, which is highlighted by color flow Doppler that shows the eccentric

nature of the aortic flow directed toward the greater curvature, produced by the orientation of cuspal opening. RA, right atrium; LA, left atrium; RV, right ventricle; SVC, superior vena cava; RPA, right pulmonary artery; Ao, aorta.
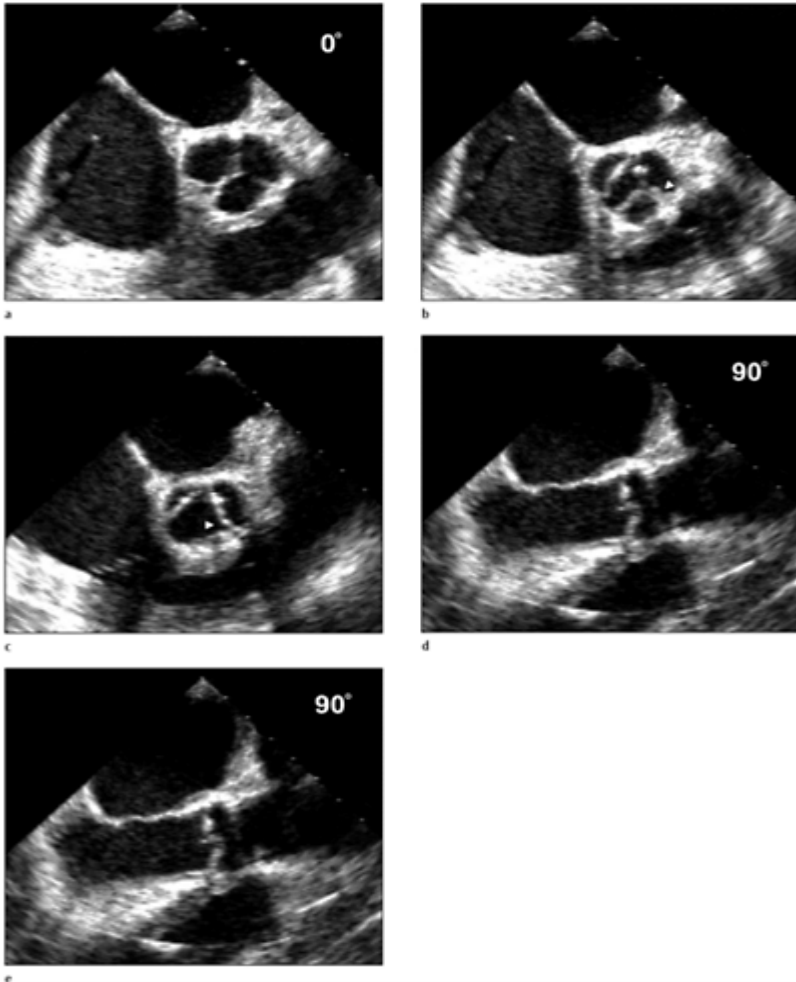
Case 3.5 Acquired bicuspid aortic stenosis produced by fusion of the commissure of the right and left aortic

cusps. Commissural fusion is typical of rheumatic pathology and may involve all three commissures, or occasionally only one or two commissures. Note the lack of cuspal calcification as shown in case 1, more typical with degenerative aortic stenosis, which usually spares the commissures.
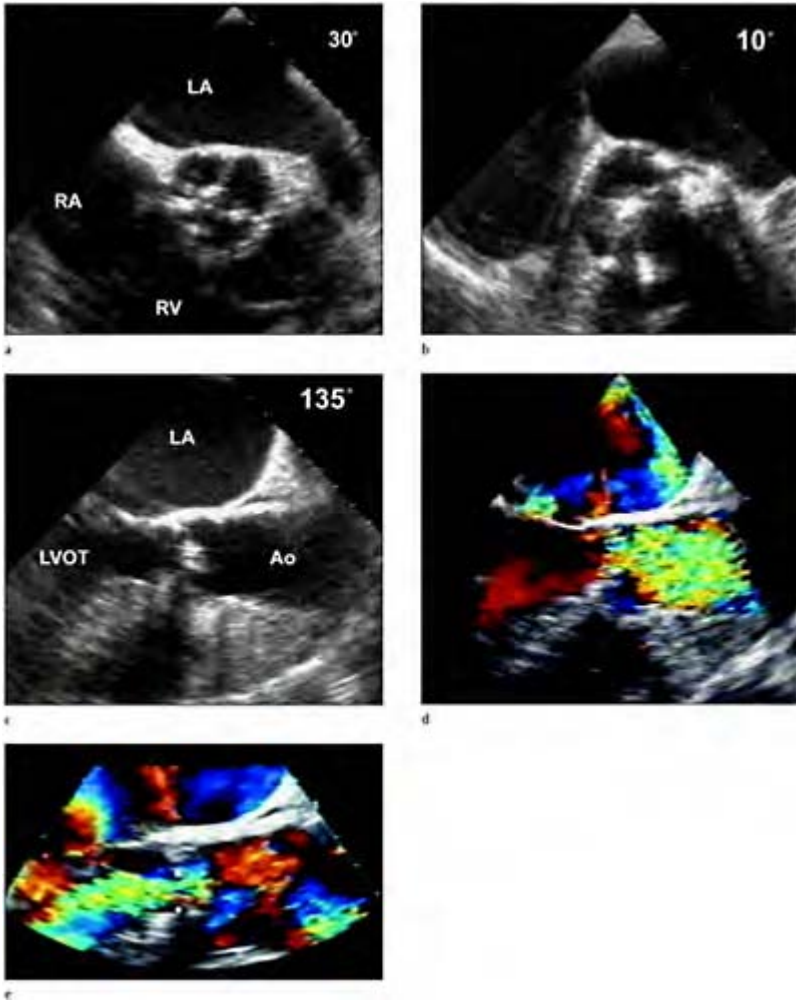
Case 3.6 Degenerative tricuspid aortic stenosis and regurgitation. With severe

aortic stenosis the aortic valve frequently does not open or close fully due to a fixed orifice (a–e). Multiplane demonstration of severe aortic stenosis with a fixed orifice (a–c). Color flow Doppler shows the stenotic jet (d) and the regurgitant jet (e). RA, right atrium; LA, left atrium; RV, right ventricle; LVOT, left ventricular outflow tract; Ao, aorta.
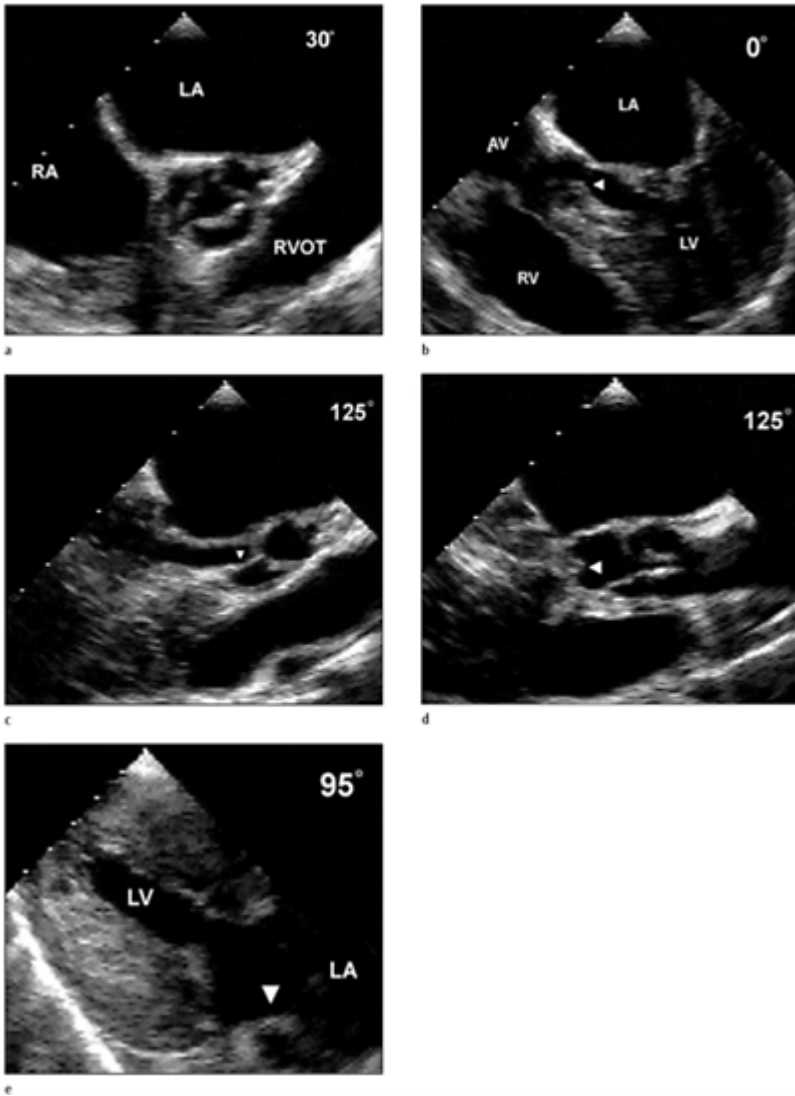
Case 3.7 Subaortic stenosis caused by a congenital membrane proximal to the aortic valve producing significant obstruction in a patient with a history of valvular aortic stenosis. The aortic valve appeared normal (a) on examination. A fibromuscular ring was present (arrows) which was visible in

multiple planes with transesophageal echocardiography producing distortion of the left ventricular outflow tract (b–e).
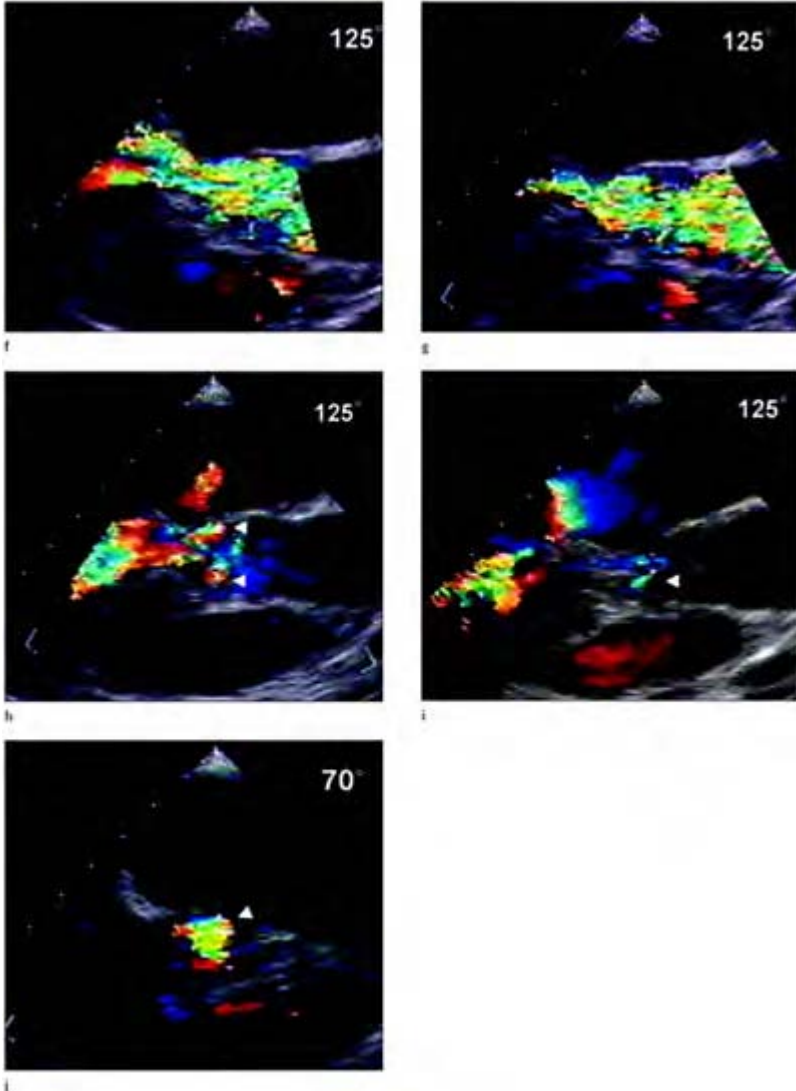
Color flow Doppler, in longitudinal views (f–i), shows the discreet site of obstruction, of the left ventricular

outflow tract, proximal and inferior to the valvular plane. High velocity mosaic flow is noted in the outflow tract and aorta. At about 70 degrees in a low esophageal window (j) the site of obstruction is viewed almost enface (arrow). RA, right atrium, LA, left atrium; RVOT, right ventricular outflow tract; RV, right ventricle; AV, aortic valve; LV, left ventricle; Ao, aorta.
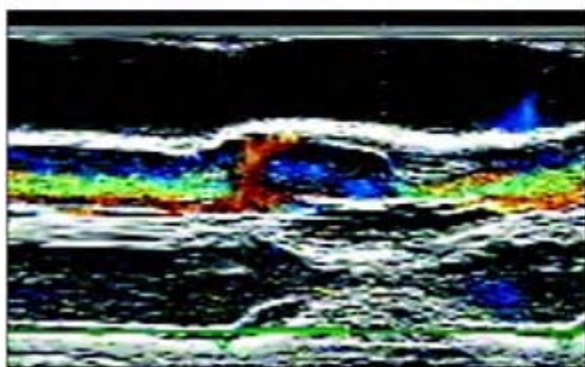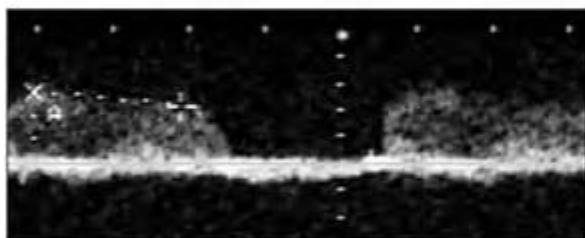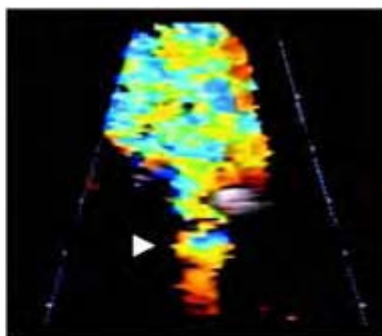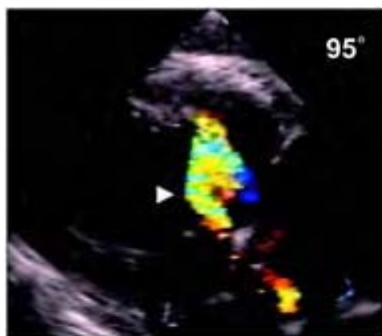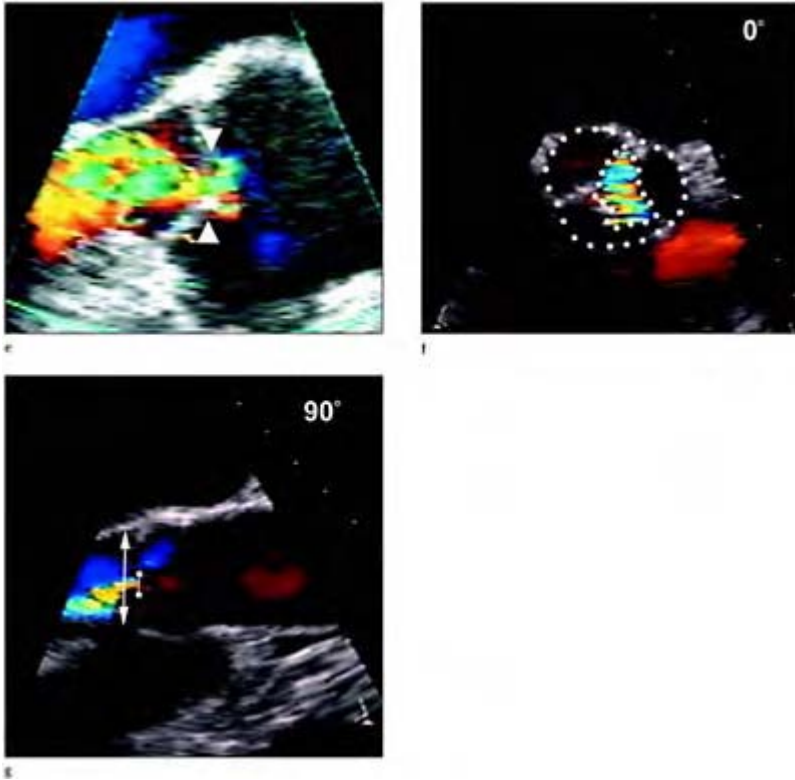
Case 3.8 Measurement of aortic
regurgitation. In the transgastric probe
position, the left ventricular outflow
tract with the aortic valve may be
obtained by obtaining the short-axis
mid-papillary muscle view at 0 degrees
and then rotating the transducer from
90 to 135 degrees until the left
ventricular outflow tract comes into
view, with the aortic valve plane
appearing roughly in the middle of the
image sector. Color flow Doppler of a
typical aortic regurgitant flow jet (a)
and zoom mode (b). In this view
continuous wave Doppler assessment
can also be done in an almost parallel
path. Continuous-wave Doppler

enables estimation of the pressure half-time or deceleration of the aortic regurgitant jet (c). Color flow m-mode Doppler can also be used to assess aortic regurgitation. (e) Visualizing and measuring the vena contracta (arrows) of an aortic regurgitant jet at 110 degrees in zoom mode from the mid esophageal position. Good correlation has been shown by determining the regurgitant jet area to the annulus area in the short axis plane with color-flow imaging (f). The width of the proximal regurgitant jet relative to the left ventricular outflow tract dimension in the longitudinal plane is also a good predictor of the severity of aortic regurgitation compared with angiographic grade with central regurgitant jets and falls short with eccentric jets (g). Aortic regurgitation is graded as I to IV to correlate with angiographic grade, corresponding to the ratio obtained of the proximal jet area or width to the left ventricular outflow area or width. The reproducibility of jet-left ventricular outflow tract diameter is better than the jet-left ventricular outflow tract area measurement and is more accurate to assess the severity of aortic regurgitation from color Doppler images.
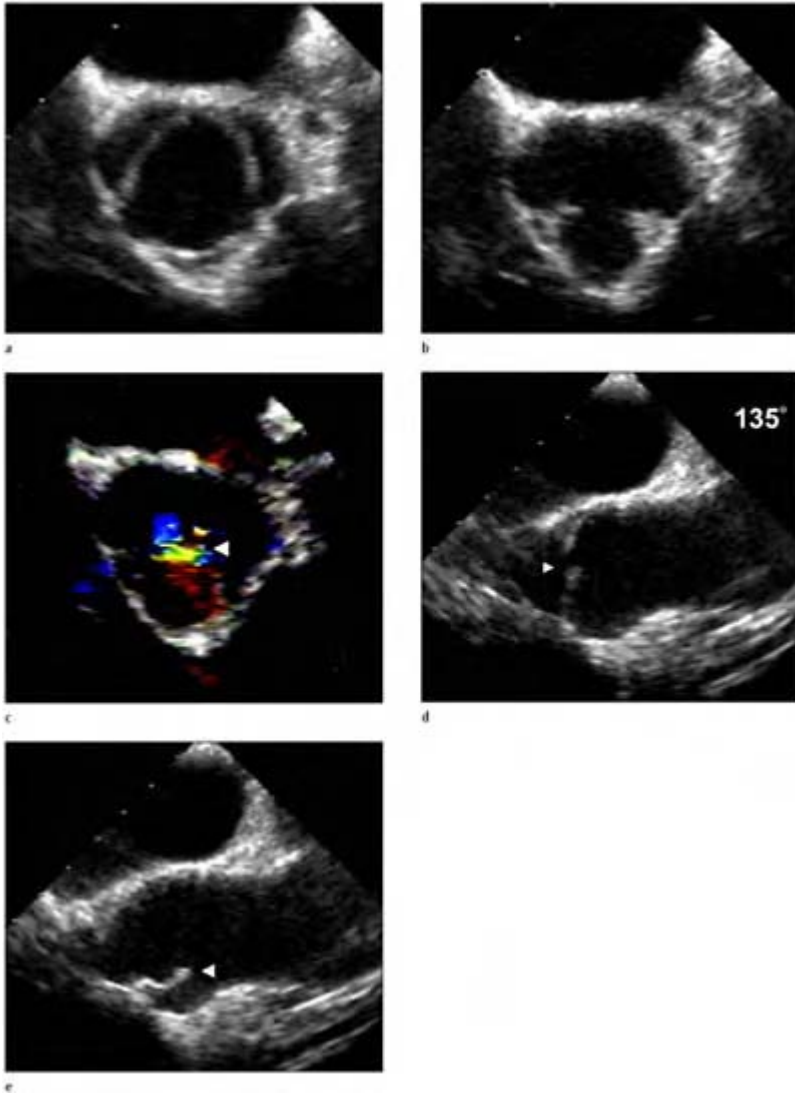
Case 3.9 Multiplane transesophageal demonstration of aortic regurgitation in a tricuspid aortic valve with prolapse of the right coronary cusp. Short axis views of the aortic valve shows distortion and asymmetry of right cusp compared with the non and left coronary cusps (a, b). Color flow

Doppler shows an almost central jet
more toward the right cusp margin (c).
Longitudinal views demonstrating
redundancy and abnormal motion
(arrow) of the right coronary cusp
during diastole (d) and systole (e).
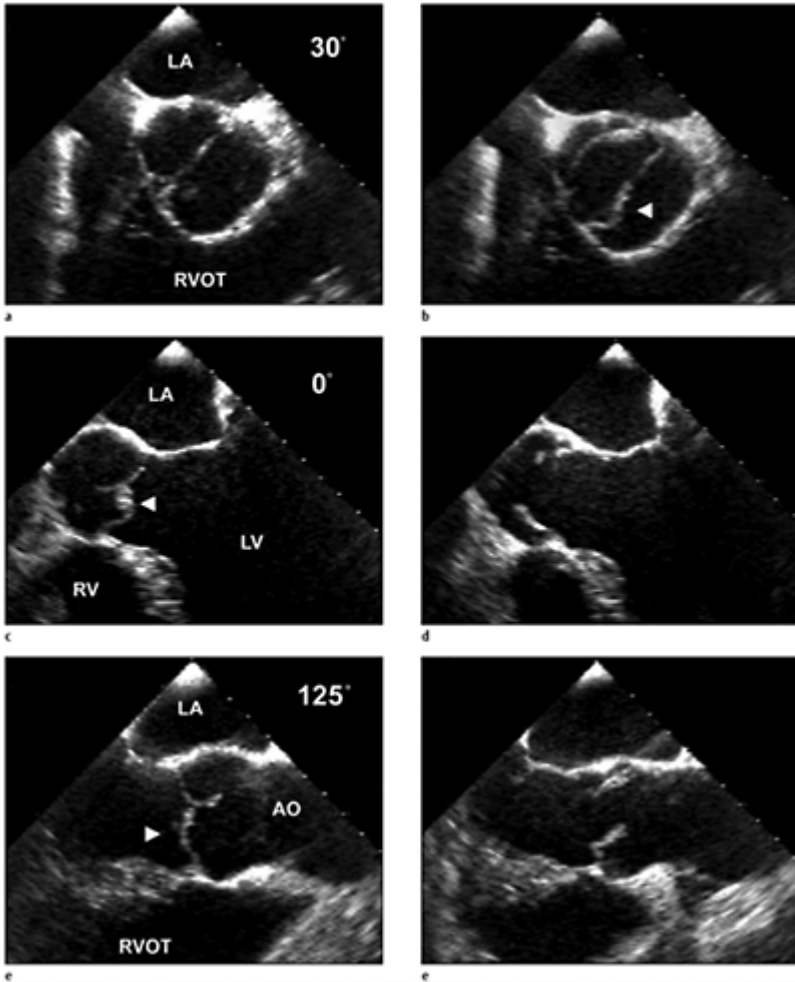
Case 3.10 Aortic regurgitation
associated with prolapse of the
conjoined leaflet of a bicuspid aortic
valve. Anterior–posterior configuration

with a larger anterior conjoined leaflet and a smaller posterior leaflet (a–f). The larger conjoined leaflet allows prolapse (arrow) of the cusp during diastole past the smaller cusp. LA, left atrium; RVOT, right ventricular outflow tract; LV, left ventricle; RV, right ventricle; Ao, aorta.
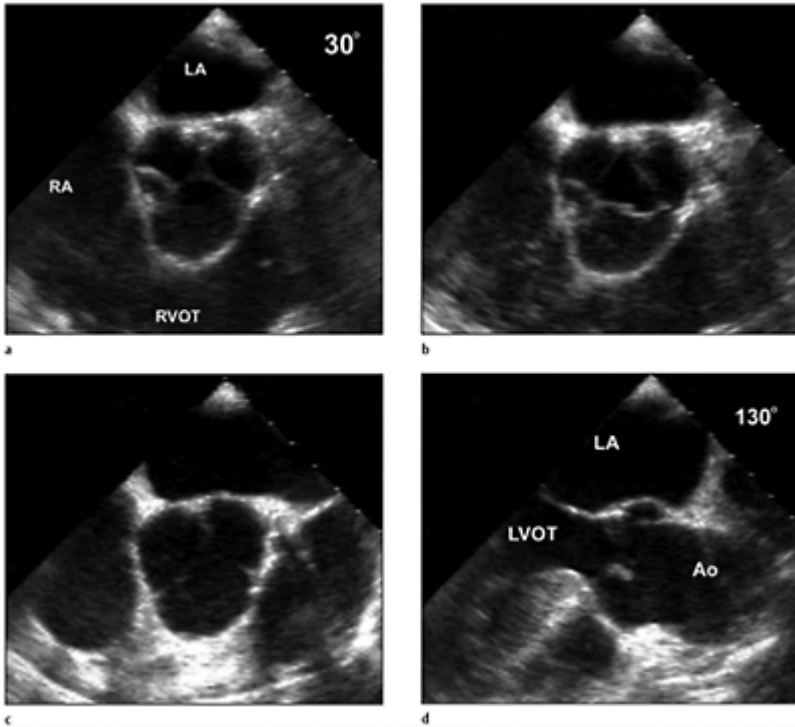
Case 3.11 Tricuspid aortic valve prolapse. Severely enlarged aortic valve leaflets associated with an enlarged aortic root and aorta, secondary to myxomatous degeneration. Short and long axis views show redundant leaflets with floppy leaflet margins (a–d).
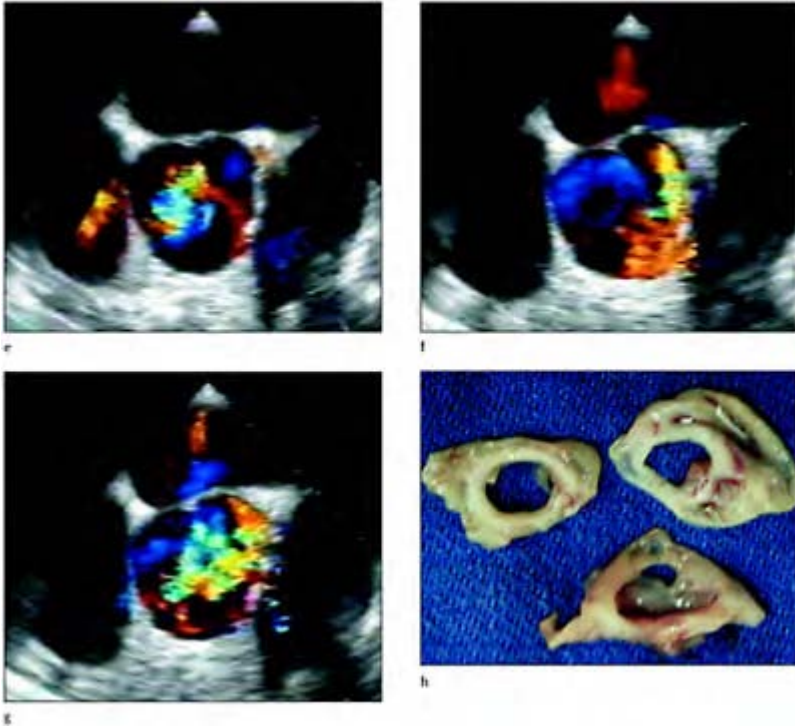
Color flow Doppler shows multiple regurgitant jets (e–g) in short axis planes. Surgical pathology (h) shows large boggy cusps with multiple exaggerated fenestrations, which caused severe aortic regurgitation. LA, left atrium; RA, right atrium; RVOT, right ventricular outflow tract, LVOT, left ventricular outflow tract, Ao, aorta.
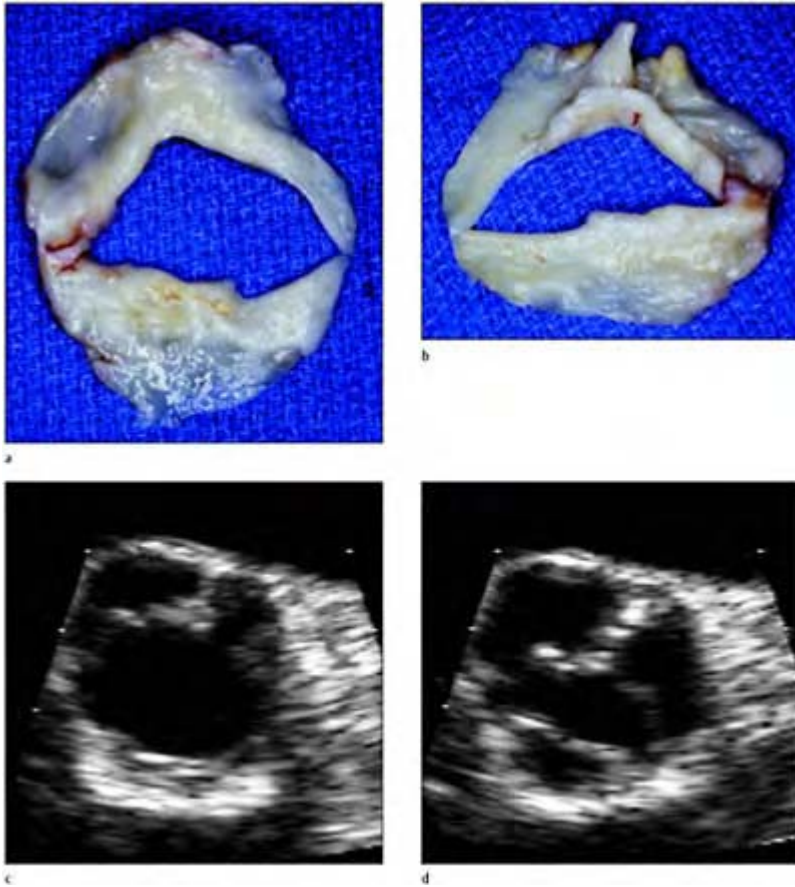
Case 3.12 Severe bicuspid aortic regurgitation. Bicuspid aortic valve with an anterior–posterior leaflet orientation. Anatomical preparation of the valve from the aortic side (a) and the ventricular side (b). Note the raphe and the curled leaflet margin secondary to redundancy of the leaflet located in the posterior cusp, which is rarely seen. Short axis views of the bicuspid valve in systole (c) and diastole (d).
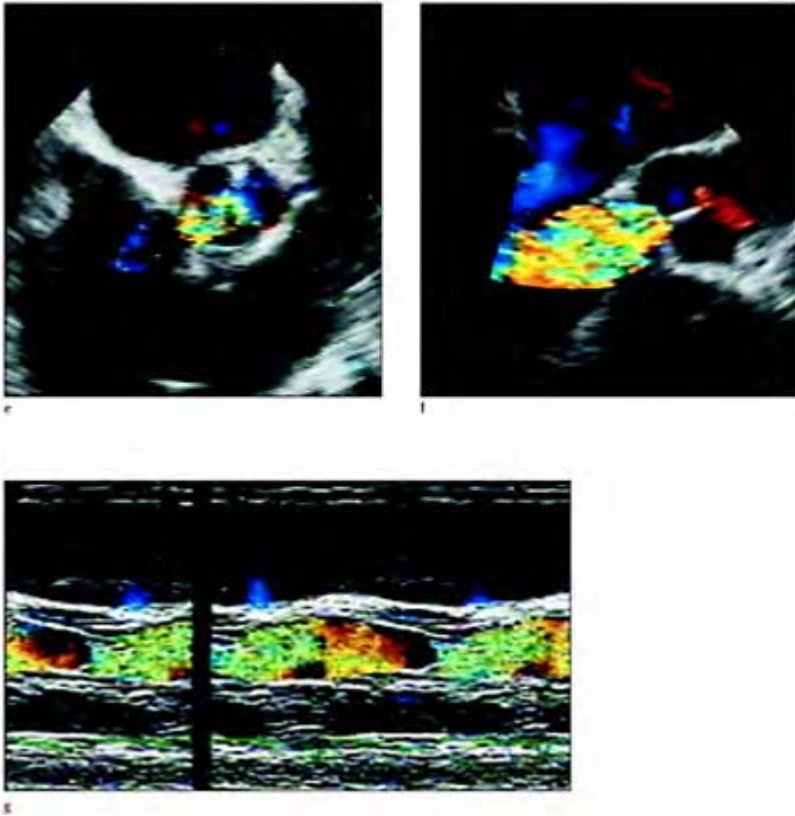
Color flow Doppler shows severe
aortic regurgitation filling the left
ventricular outflow tract in the short
axis (e), long axis plane (f) and color
m-mode Doppler (g).
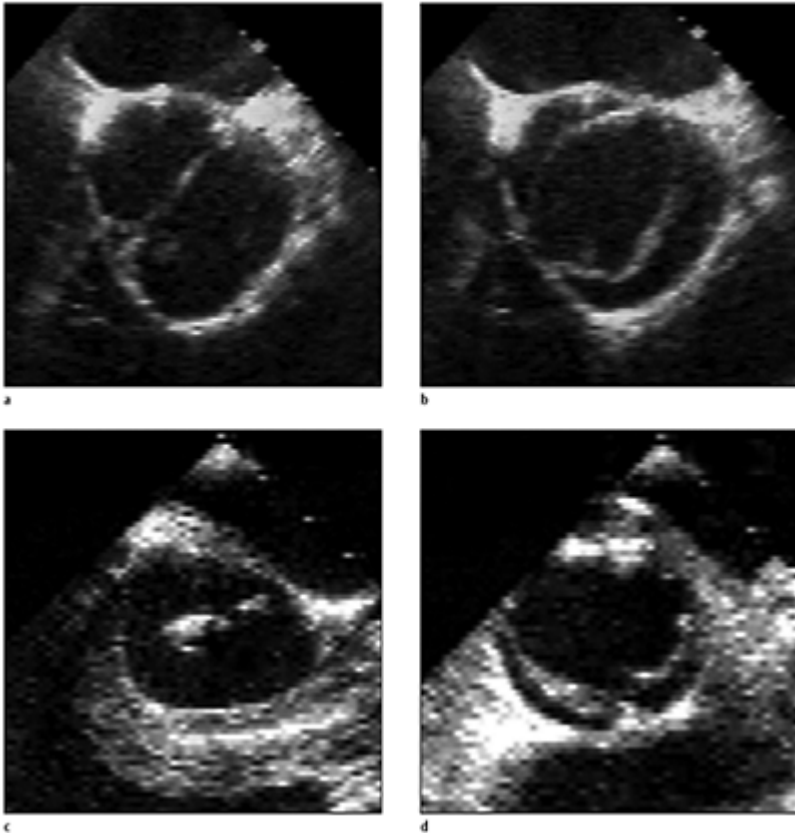
Case 3.13 Common cuspal orientations in bicuspid aortic valves. In 53% of bicuspid aortic valves the commissures are vertically situated, with the cusps oriented rightward and leftward, with the respective coronary artery originating from the respective sinuses of Valsalva. In the other 47% the commissures are horizontally placed with the cusps oriented in an anterior and posterior position, with both coronary arteries arising from the anterior sinus of Valsalva. The anterior-posterior type has been noted to be more likely to calcify.
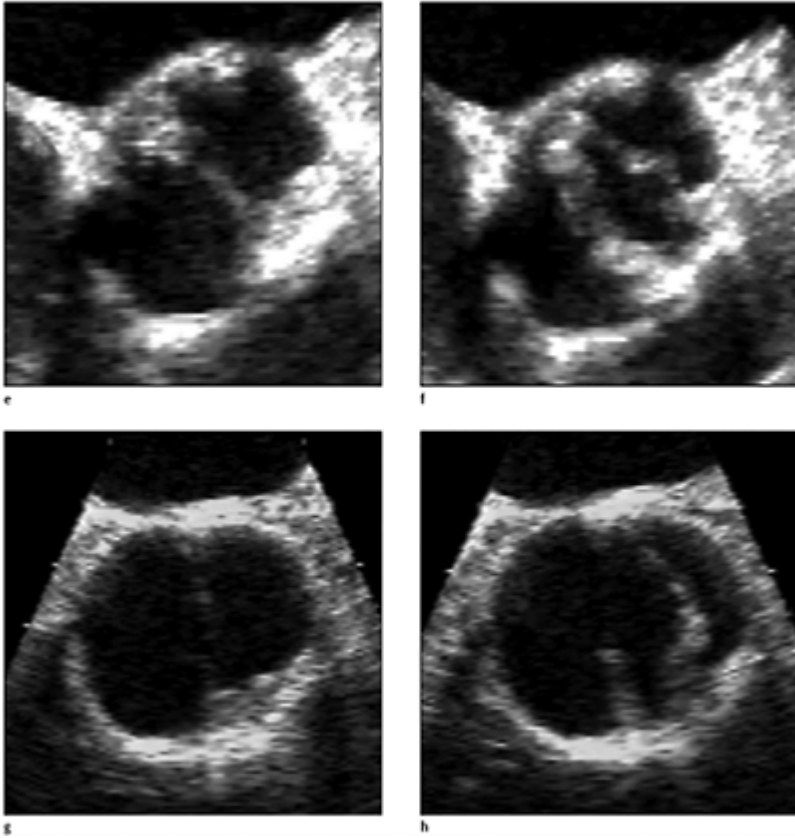
Minor rotations of the commissures of the two basic types of bicuspid aortic valves result in the various configurations in bicuspid aortic valves and may account for the variable sensitivity and specificity in detection of bicuspid valves with M-mode and two-dimensional echocardiography. With M-mode echo, eccentric cusp closure appears better detected with the A-P types of bicuspid valve; false-negative detection with the appearance of midline closure appears with the R–L types. The short axis view obtained with two-dimensional

echocardiography has the highest sensitivity and specificity in detecting either type of bicuspid valve.[11] Top views diastolic frames and bottom frames corresponding systolic frames.
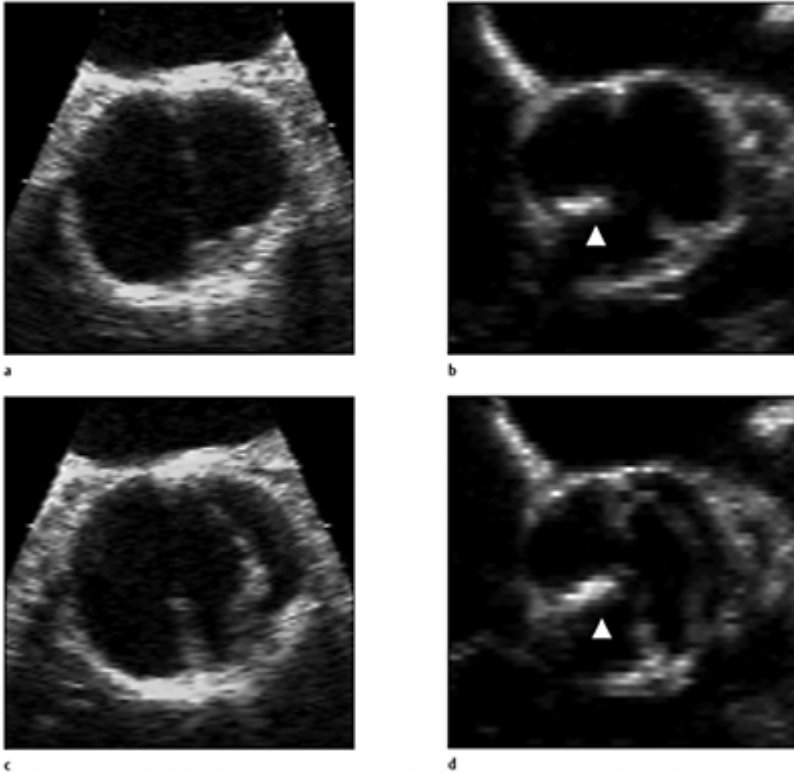
Case 3.14 Right–left bicuspid aortic valves with and without a prominent raphe. Bicuspid valve without a raphe (a, systolic frame; c, diastolic frame). Right–left bicuspid valve with raphe denoted with the arrow (b, systolic frame; d, diastolic frame). A raphe or false commissure is found in one of the two cusps in about 50% of the valves, irrespective of valve type. When present, the raphe is always found in

the right cusp of the right–left or
vertical orientation as seen in band d,
and usually in the anterior cusp of the
anterior–posterior or horizontal type.
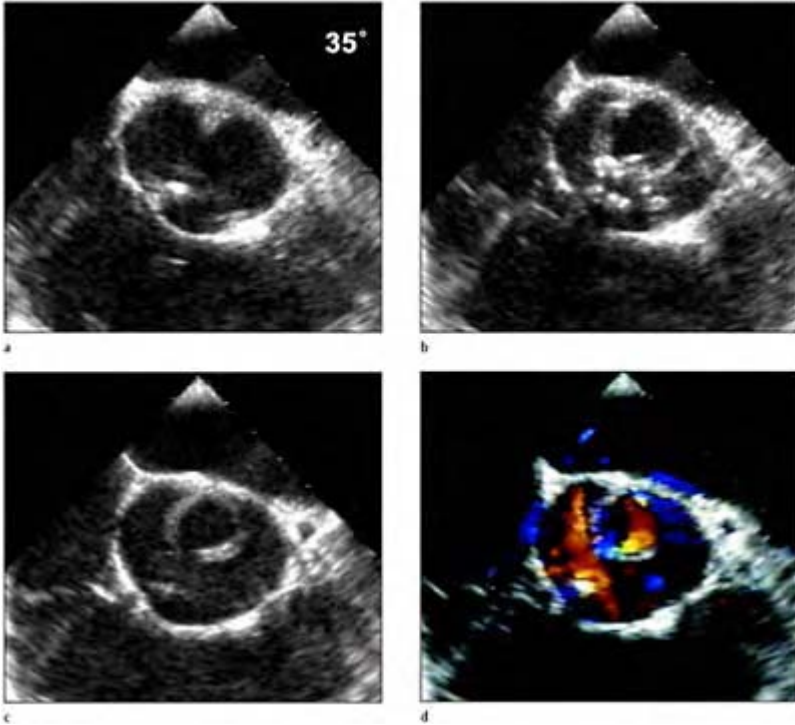
Case 3.15 Bicuspid aortic stenosis
producing an acquired monocuspid
appearance due to fusion of one
commissure from rheumatic disease.
Short axis frames from diastole to
systole show the eccentric circular
valve opening (a–d).
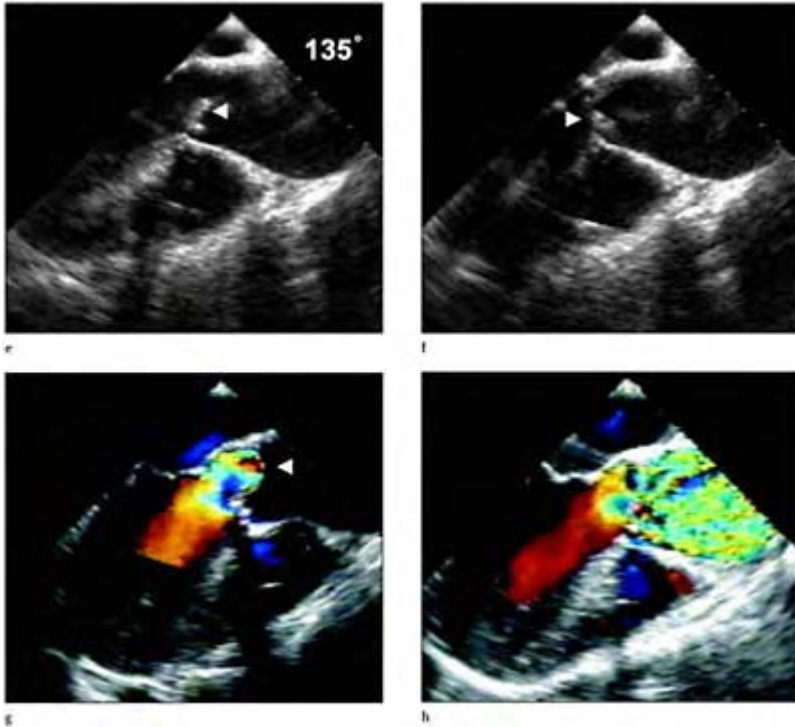
Longitudinal frames (e–h) show systolic doming (arrows) highlighted with color flow Doppler which also elicits high velocity turbulent flow across the aortic valve.
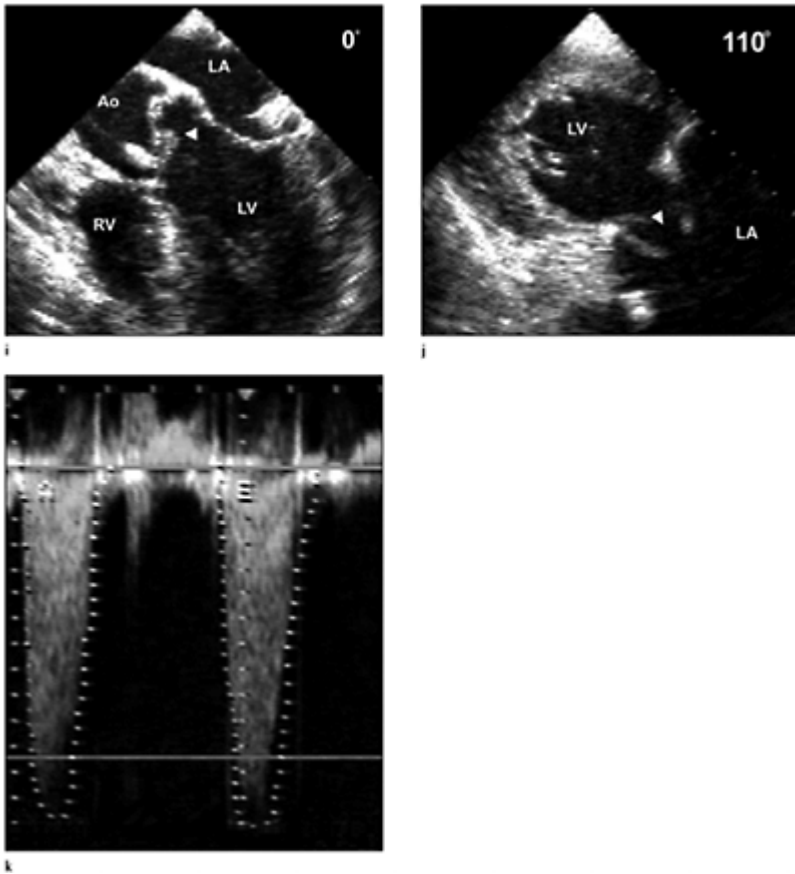
Five chamber lower esophageal view at 0 degrees (i) shows the abnormal configuration of the valve leaflets (arrow). Gastric view at 110 degrees (j) nicely shows the doming of the valve and opening orifice. Corresponding continuous wave Doppler of flow across the aortic valve (k) obtained from the gastric view, with high velocity flow and a significant gradient. LA, left atrium; RV, right ventricle; LV, left ventricle; Ao, aorta.
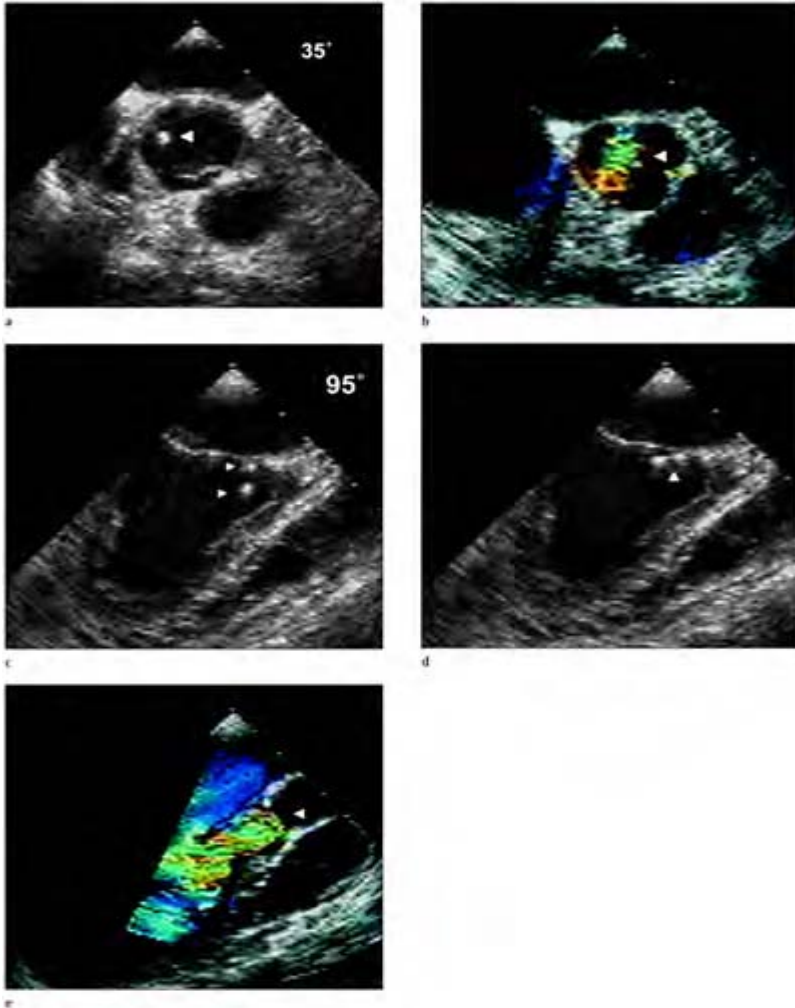
Case 3.16 Bicuspid aortic valve endocarditis. Two small peduncular vegetations are noted in the short axis projections in the valve plane (a, b) which prolapse into the left ventricular outflow tract and produce severe aortic regurgitation in longitudinal views (c–e). Roberts[9] found that 9% of bicuspid aortic valves that were purely regurgitant were associated with infective endocarditis.
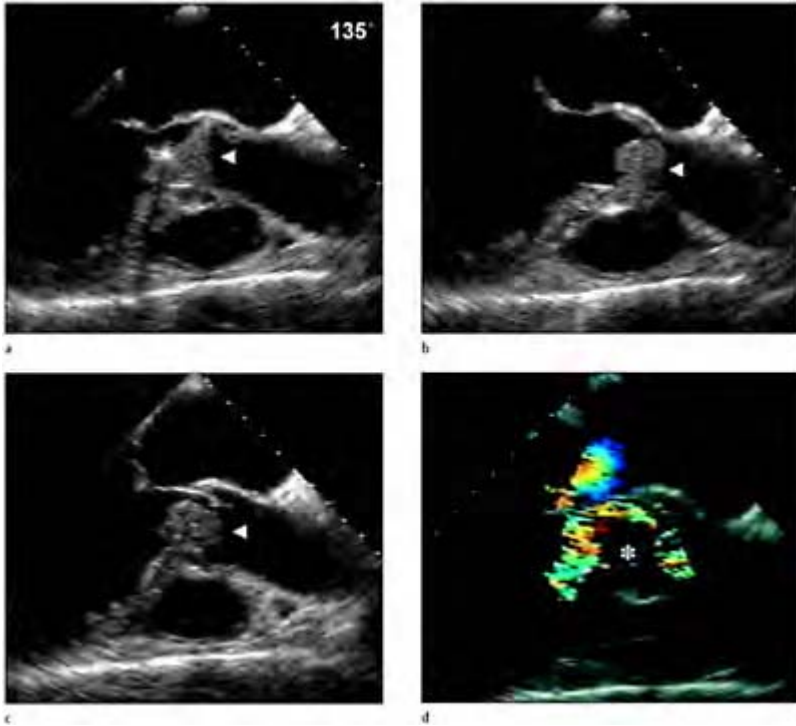
Case 3.17 Large aortic valve
vegetation in staphylococcus
endocarditis. The aortic valve is
tricuspid and there is a large
vegetation, which freely prolapses
through the valve plane between the
left ventricular outflow tract and aorta
in longitudinal views (a–d).
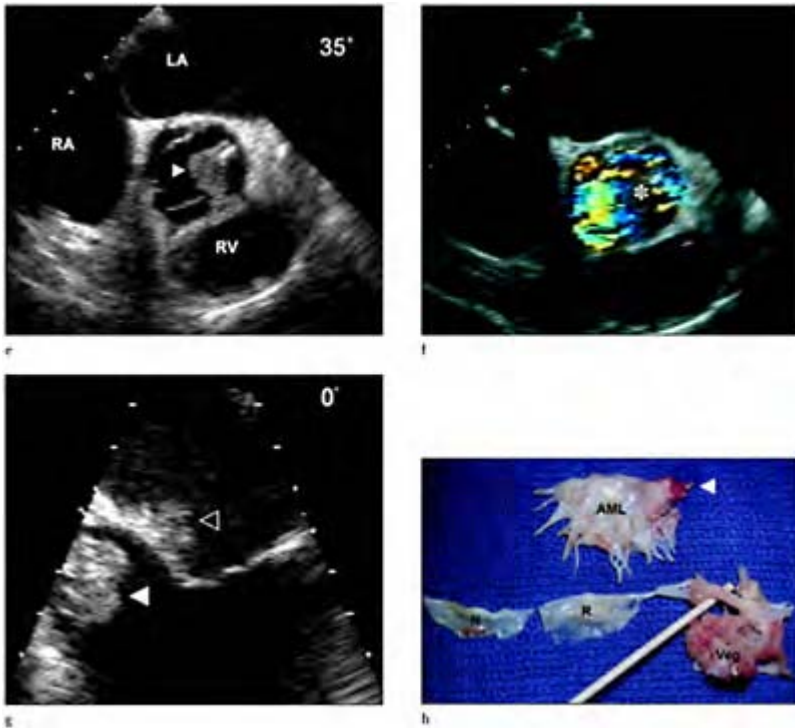
In short axis planes (e, f) the vegetation (arrow) is seen preventing cusp closure and producing slight obstruction to forward flow and regurgitation (star). In zoom mode (g) the vegetation appears in the left ventricular outflow tract (closed arrow) and extends to the anterior mitral leaflet directly (open arrow). A post-surgical specimen (h) shows the vegetation with perforation in the left coronary cusp of the aortic valve (probe) and destruction of the anterior mitral leaflet (arrow). LA, left atrium; RA, right atrium; RV, right ventricle; AML, anterior mitral leaflet; N, non-coronary cusp; R, right coronary cusp; Veg, vegetation.
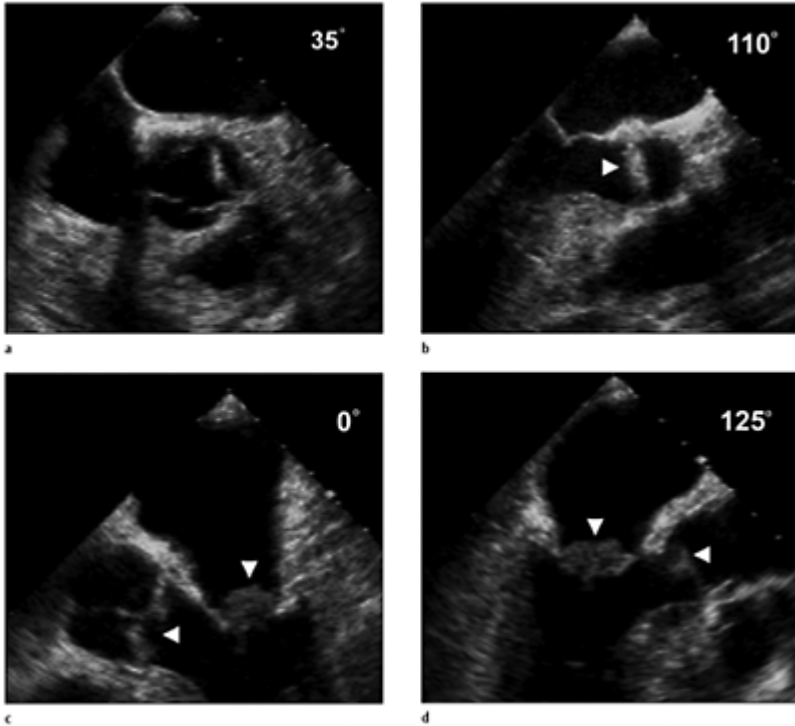
Case 3.18 Non-bacterial aortic valve endocarditis. A 56-year-old woman presented with a cerebrovascular accident. The workup revealed the presence of antiphospholipid antibodies. A transesophageal echocardiogram revealed vegetations on both the aortic and mitral valves. In the Antiphospholipid Antibodies in Stroke Study Group, which was a retrospective echocardiographic analysis of cerebral ischemic events in patients with antiphospholid antibodies, 2.8% of the aortic valves demonstrated abnormalities implicating a cardiac source of embolus.[175] In the short axis view (a) the aortic valve leaflet margins appear thickened, but in longitudinal views (b, c) there is a discrete mass noted (arrow). The vegetations (arrow) of the mitral valve appear as discreet large masses (c, d) associated with the leaflet tips.
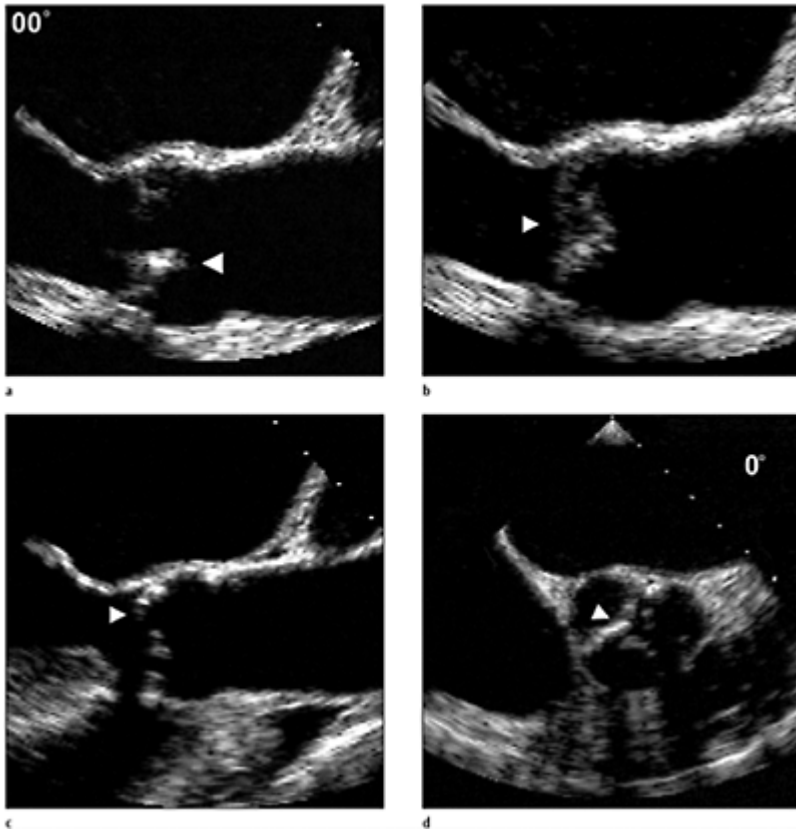
Case 3.19 Aortic valve thickening associated with anorectic drug use. The aortic valve is the most commonly affected valve, which usually results in mild to moderate degrees of aortic regurgitation. Connolly et al characterized the changes produced in the aortic valve as thickened (focal or diffuse) and mildly retracted valve leaflets, resembling rheumatic disease without stenosis.[111] Note the thickening (arrow) of the aortic valve leaflets (a–d). Lack of closure is suggested in the short axis view (d) in diastolic frames.
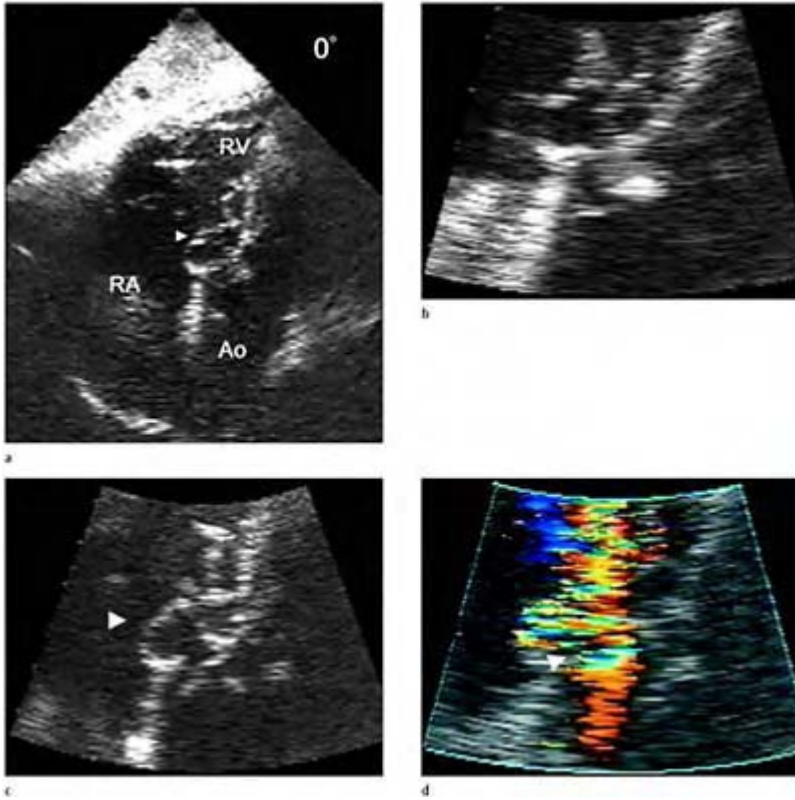
Case 3.20 Congenital sinus of Valsalva aneurysm with rupture. Congenital sinus of Valsalva aneurysm usually appear as long narrow diverticular deformities of the sinus, which distinguishes them from acquired aneurysms that appear as bulging, out pouching deformities to the sinus. Congenital sinuses of Valsalva aneurysms are usually detected in adulthood as coincidental findings or after they have ruptured and produced clinical findings. Congenital aneurysms usually occur with the right coronary cusp and much less frequently with the non-coronary cusp as illustrated in this case. The sinus of Valsalva aneurysm is best-appreciated and shown in deep transgastric views (a–d).
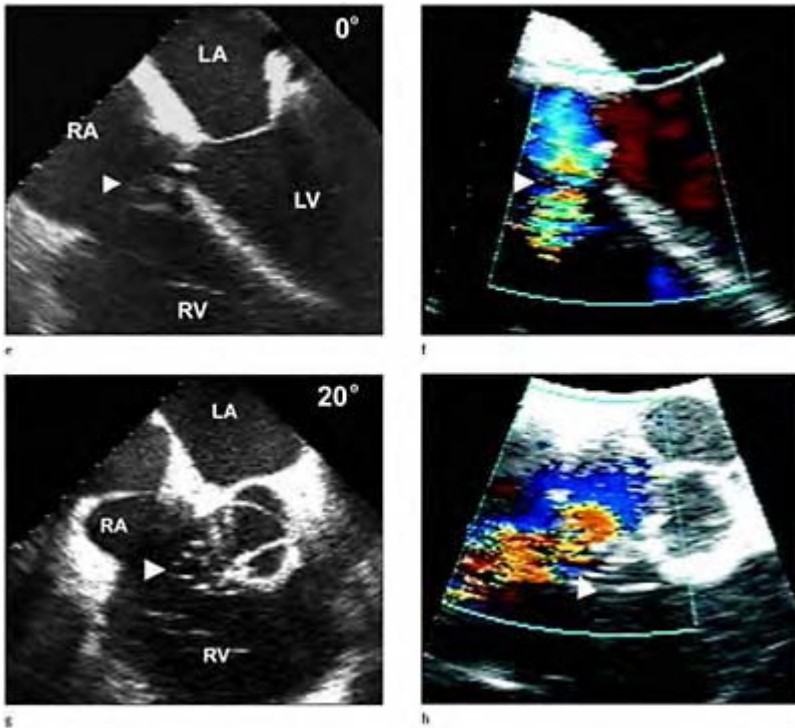
The aneurysm is seen originating from the annular plane and coursing parallel to the ventricular septum ending proximal to the tricuspid valve annulus. In zoom mode there is better appreciation of the neck and long diverticular shape of the aneurysm. With color flow Doppler, a flow jet is detected from the aorta and emanating through a jagged rupture into the right atrium (d). Lower esophageal four chamber view (e) and corresponding zoom mode with color flow Doppler shows the rupture flow jet. Horizontal short axis view of the aortic valve shows the aneurysm (g) and corresponding zoom mode with color flow Doppler. In both the four chamber and short axis views, the shape and the size of the aneurysm are not fully appreciated due to oblique imaging, compared to the deep transgastric views. RA, right atrium; LA, left atrium; RV, right ventricle; LV, left ventricle; Ao, aorta.
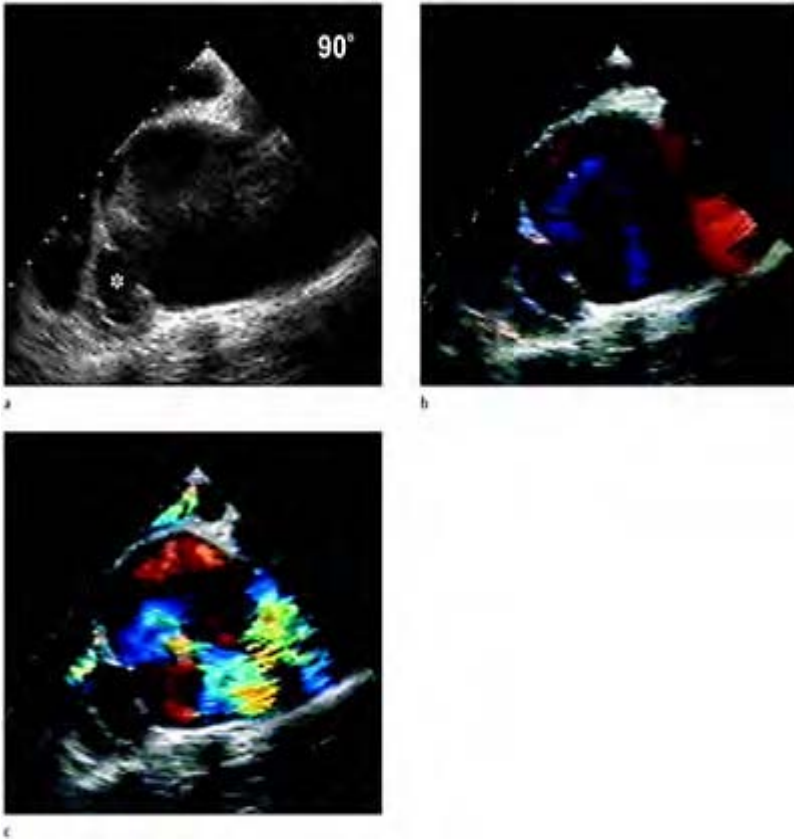
Case 3.21 Acquired sinus of Valsalva aneurysm
without rupture. Acquired aneurysms appear similar to
saccular aneurysms of the aorta. The aneurysm appears
as a bulging, out pouching from the sinus, which
distinguishes it from congenital aneurysms. Both
congenital and acquired aneurysms have a propensity
for rupture, but acquired aneurysms may be associated
with all three coronary cusps. Longitudinal views (a, b)
of the aortic root show an acquired sinus of Valsalva
aneurysm associated with the right coronary cusp
(star). Note the narrow neck and well-formed, round
out-pouching of the sinus. Flow is detected in the sinus
with color flow Doppler (c) throughout the cardiac
cycle, predominately during diastole.
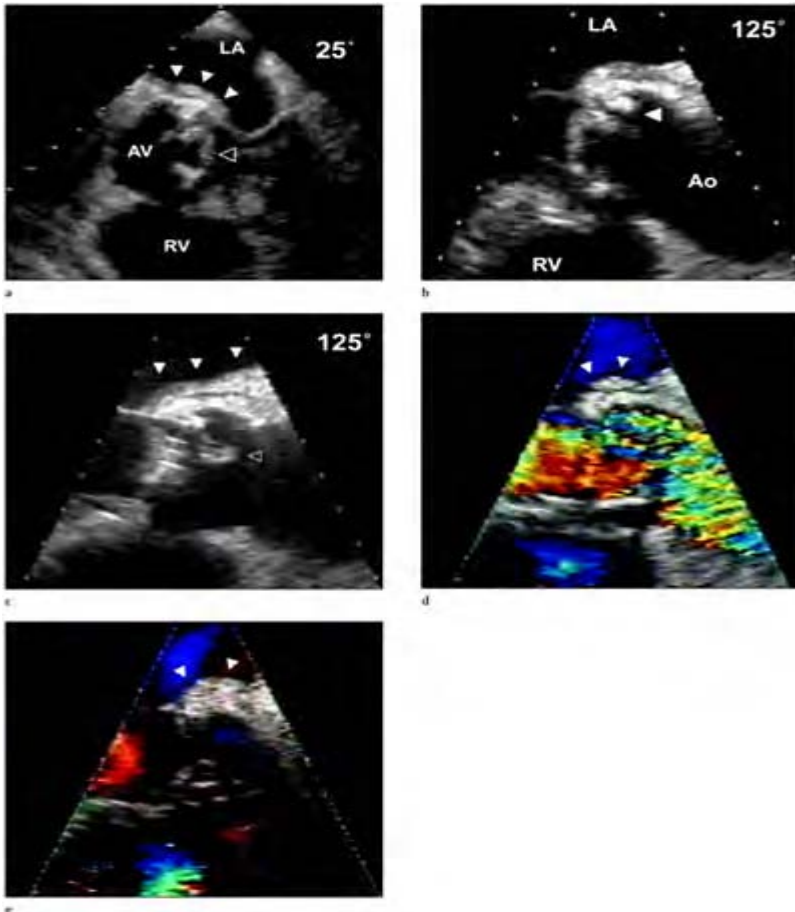
Case 3.22 Annular abscesses are generally limited to the area of the perimeter of the aortic valve dictated by the composition of the perivalvular tissue of the fibrous skeleton, and are associated with the cusp showing a vegetation. Annular abscess may appear as echodense or echolucent regions distinct from the normal annulus or perivalvular tissue, which usually distorts the normal appearance of the proximal aortic root anatomy. Blood flow entering the abscess cavity is frequently detected with color Doppler during the cardiac cycle, identified with systolic expansion and diastolic collapse of the cavity. LA, left atrium; AV, aortic valve; RV, right ventricle; Ao, aorta.
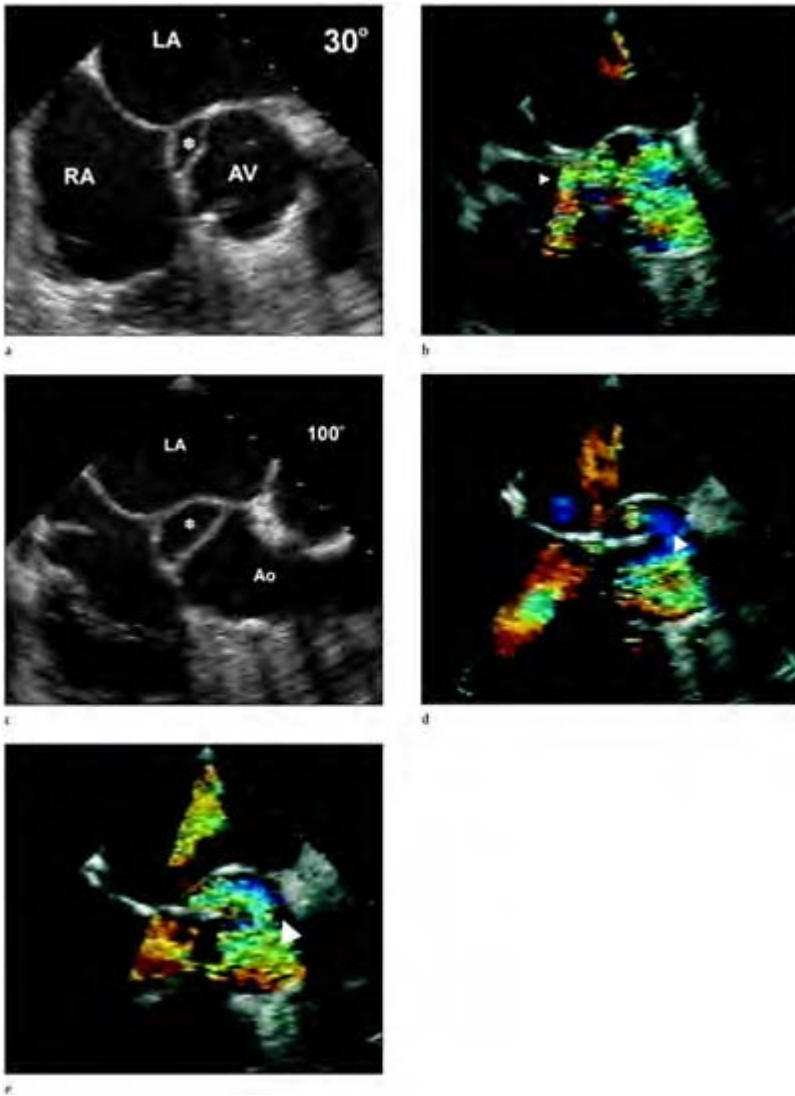
Case 3.23 Rupture of the abscess produces an echolucent free space or cavity, often with necrotic debris or residue within the cavity and a large or a small fistulous communication emptying into the left ventricular outflow tract. LA, left atrium; AV, aortic valve; RA, right atrium; Ao, aorta.
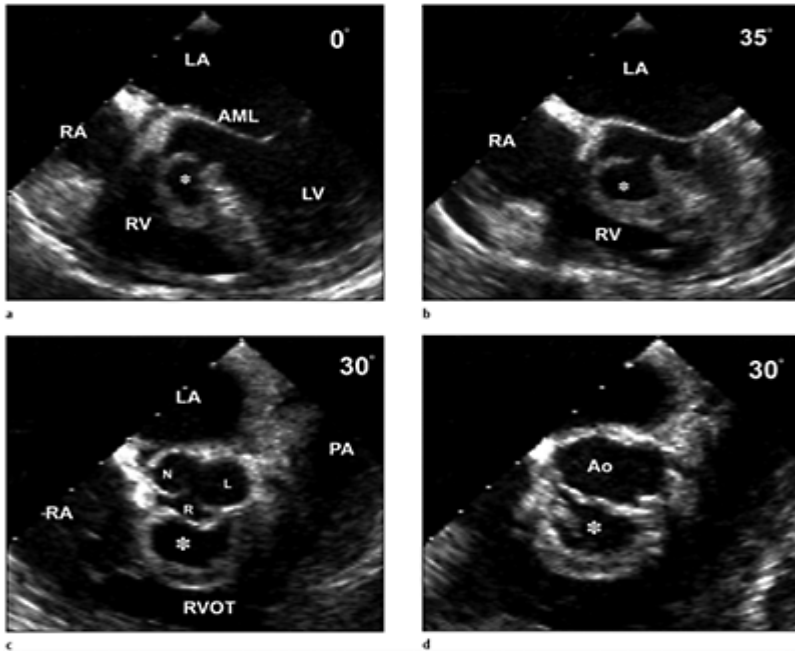
Case 3.24 Perivalvular extension of aortic valve
endocarditis with spread to the ventricular septum.
Perivalvular spread of infection may occur with
extension into the valve annulus or adjacent
myocardium (ventricular septum and rarely interatrial
septum), and has been shown in around 30% of
postmortem and surgical cases of aortic valve
endocarditis. Multiplane transesophageal
demonstration of an aortic valve annular abscess with
extension to the ventricular septum with rupture into
the left ventricular outflow tract. The abscess (star) is
noted in close proximity to the right coronary cusp in
the proximal ventricular septum. The abscess causes
distortion of the right coronary cusp and the left
ventricular outflow tract, and is ruptured as illustrated
by jagged discontinuous margin. Flow is detected in
the abscess and empties into the left ventricular outflow
tract, with color flow Doppler. RA, right atrium; LA,
left atrium; AML, anterior mitral leaflet; RV, right
ventricle; LV, left ventricle; Ao, aorta; N, non-coronary

cusp; L, left coronary cusp; R, right coronary cusp;
RVOT, right ventricular outflow tract; LVOT, left
ventricular outflow tract; PA, pulmonary artery.
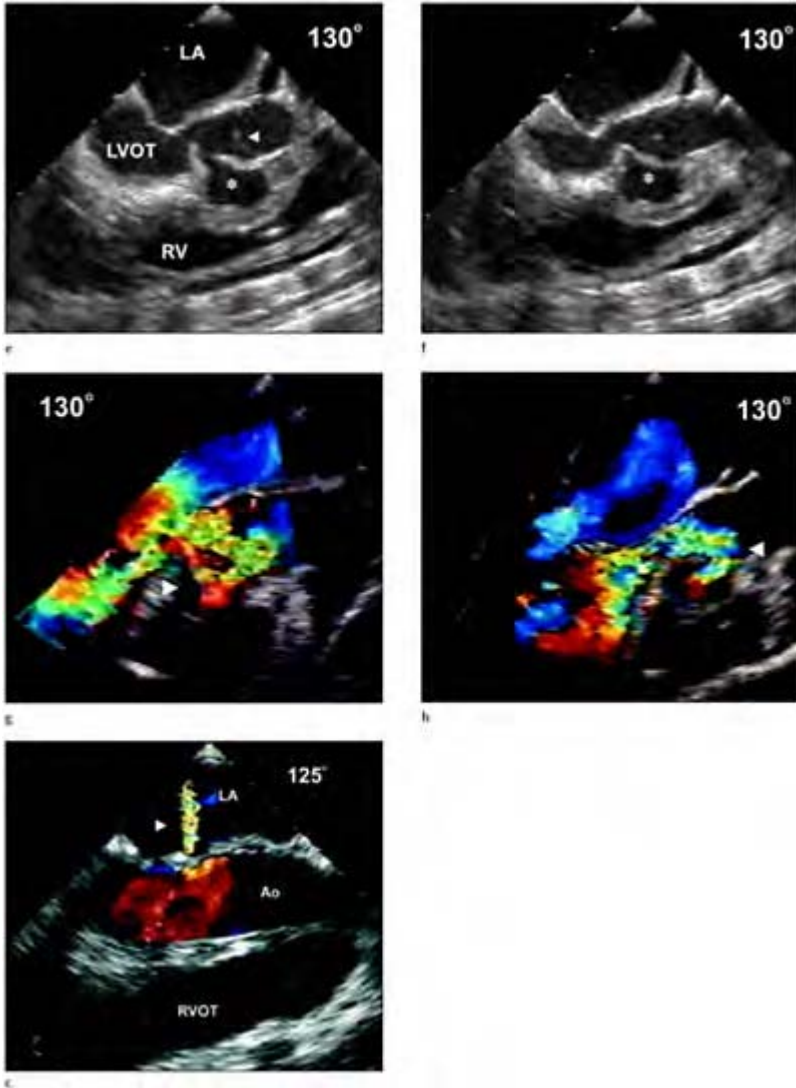
Case 3.25 Abscess rupture may provide an abnormal
communication between cardiac chambers producing
significant turbulent shunt flow, which is also readily
identified with color flow Doppler. Fistulous flow may

be commonly shown between the aortic root and the left atrium or the aortic root and the left ventricular outflow tract (ventriculoaortic discontinuity), in a single direction or a "to and fro" pattern. Longitudinal view of the aortic root at 125 degrees shows fistulous flow with color flow Doppler from the aortic annulus to the left atrium. LA, left atrium; Ao, aorta; RVOT, right ventricular outflow tract; LVOT, left ventricular outflow tract.
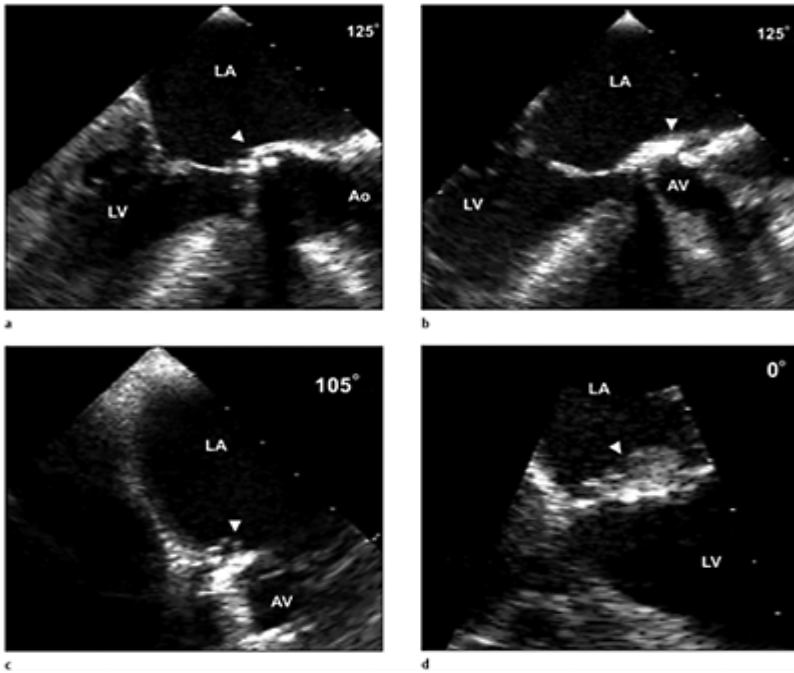
Case 3.26 Aorto-mitral intervalvular fibrosa fungal or pseudoaneurysms appear as a deformity to the annular attachment of the anterior mitral leaflet and usually extend above and below the sub-commissural annular plane. The aortic abscess (arrow) appears to protrude to a greater extent into the left atrium towards the mitral leaflet, in comparison with a typical periannular abscess, which conforms to the aortic cusp perimeter (a–d).
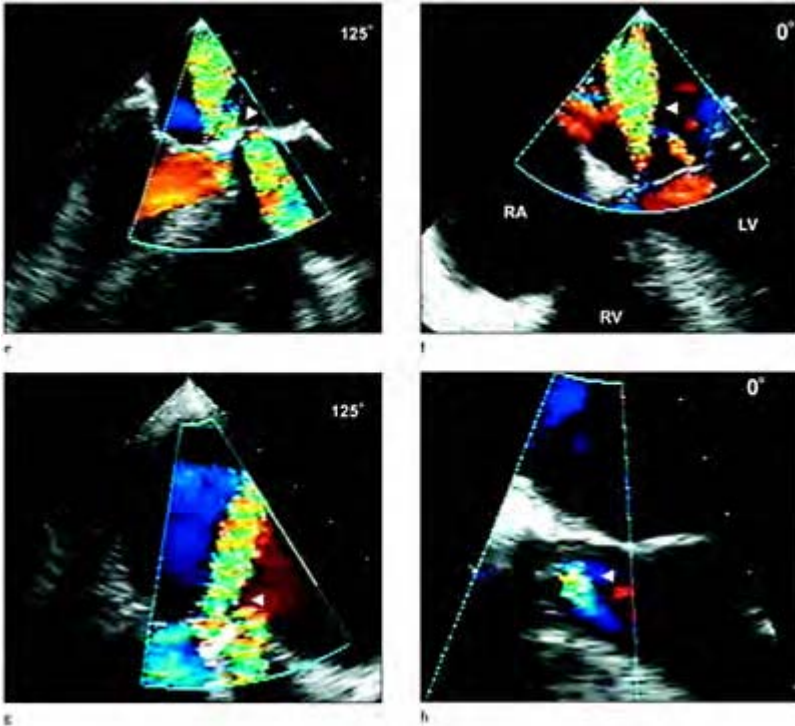
The deformity produced in the intervalvular fibrosa (arrow) appears to originate in the basal portion of the mitral leaflet and may resemble the leaflet folding on itself in that area. This appearance must be distinguished from isolated mitral vegetation (d). With examination in the zoom mode in multiple planes, vegetation may be excluded with confidence. With rupture of the fungal aneurysm, shunts may be produced and are usually detected (arrow) with color flow Doppler in the left atrium (e–g) and left ventricular outflow tract (h). LA, left atrium; LV, left ventricle; Ao, aorta; RA, right atrium; RV, right ventricle; AV, aortic valve.
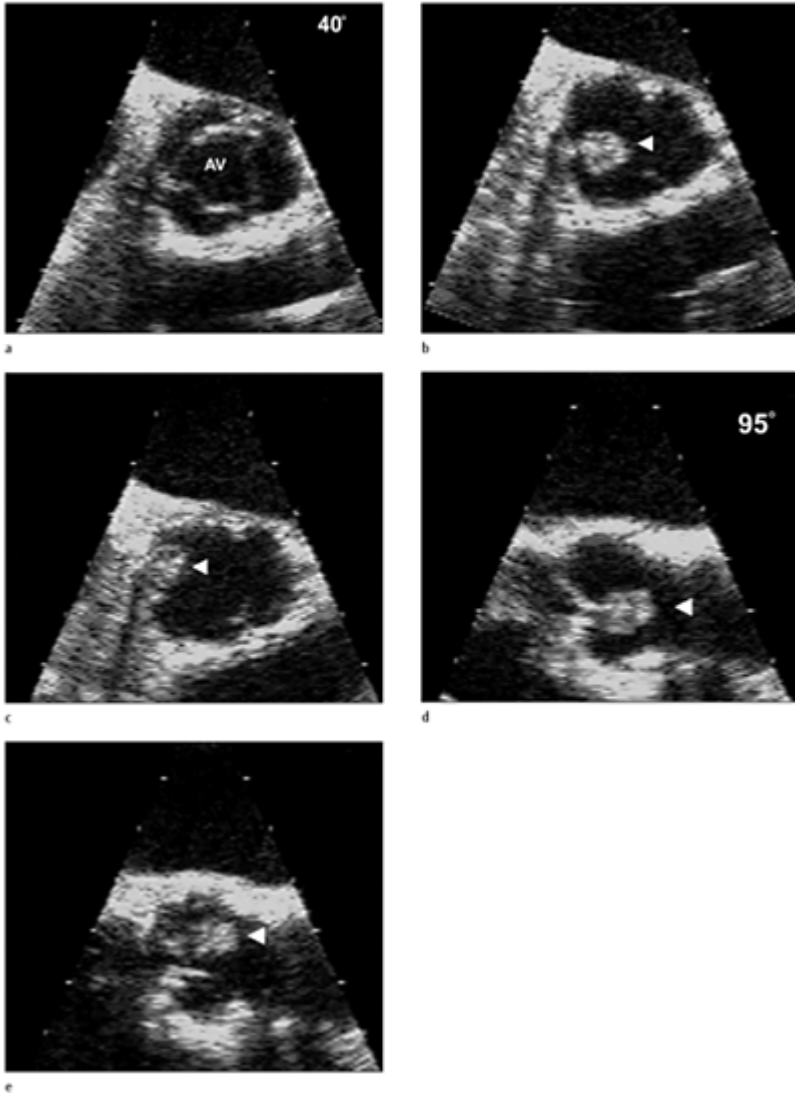
Case 3.27 Papillary fibroelastoma of the aortic valve. Papillary fibroelastomas are small tumor projections usually 2–3 mm in size, attached to valve leaflet margins. Multiplane transesophageal echocardiography is especially useful in detecting papillary fibroelastomas,

since tumors are small and may only appear as linear thin projections. When viewed in multiple planes these tumors may appear as small polyps. Horizontal short axis (a–c) and longitudinal views (d, e) of the aortic valve with a polypoid papillary fibroelastoma (arrow) attached near the commissure of the non-coronary and right coronary cusp. The benign tumor is highly mobile and moves freely in and out of the echocardiographic plane during the cardiac cycle. These entities have been associated as a cardiac source of embolus, owing to their mobility and thrombus formation. AV, aortic valve.

95°
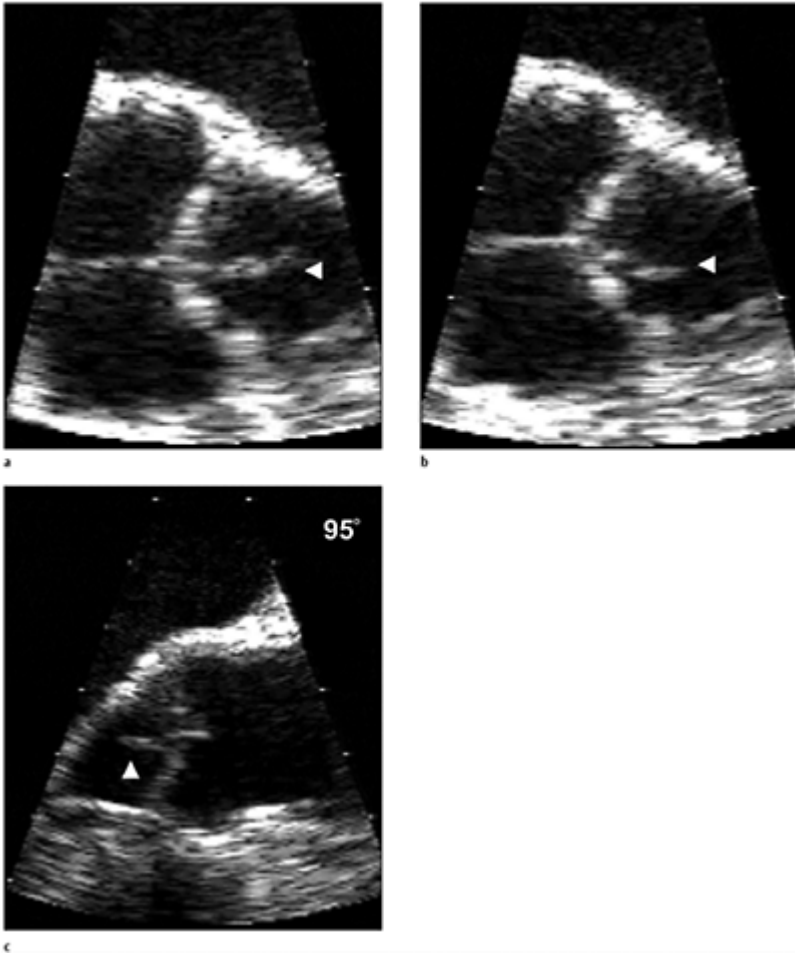
Case 3.28 Papillary fibroelastoma of the aortic valve versus Lambl's excrescence. Papillary fibroelastomas must be differentiated from normal anatomic variants such as Lambl's excrescences of the heart valves. Lamellar and sublunar excrescences may form owing to the shear stress caused by the blood flow or to friction of the valve surfaces during valve closure. Two types of Lambl's excrescences are associated with

normal aortic valve echocardiographically. In patients under 30 years of age, lamellar excrescences are found along the lower border of the lunulas, often with thickening of the body of the cusp. In older patients, filiform excrescences emanate from the nodules of Arantus and along the free margin of the cusps. A patient with an extensive workup for cardiac source of embolus had a small linear echogenicity associated with the aortic valve margin (a–c) which was freely mobile in serial frames protruding into the left ventricular outflow tract.
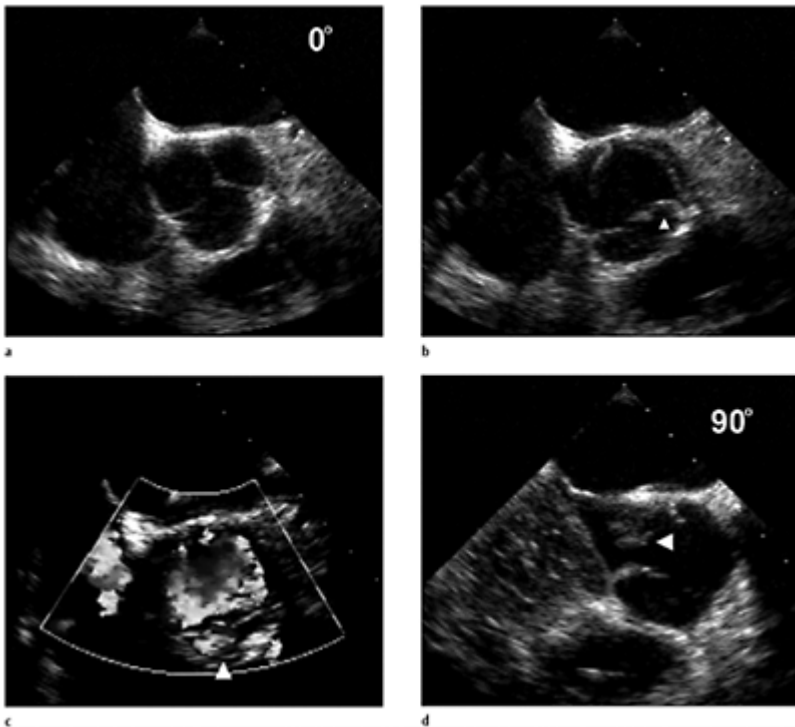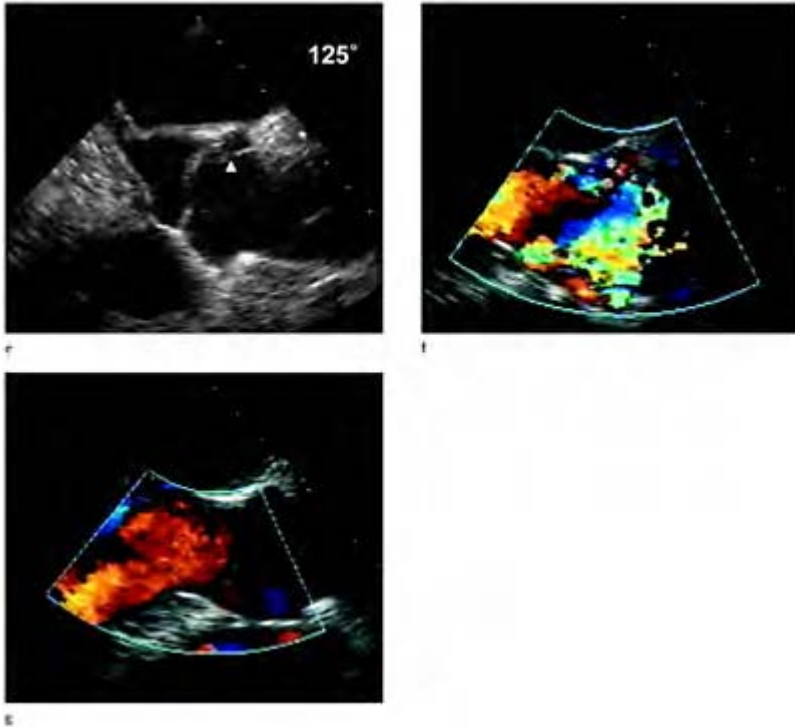
Case 3.29 Traumatic rupture of the aortic valve. Abrupt deceleration-type injuries that result from falls of significant height or motor vehicle accidents produce traction and torsion forces that generate excessive high shear stress together with sudden increases in the intraluminal pressure, which lead to traumatic disruption of the thoracic aorta in its less mobile segments. In addition, avulsion of the aortic valve is noted, probably due to the increase in intraluminal pressure generated in these types of trauma, especially with the use of seat belts. Although rare, transesophageal echocardiography demonstrates that aortic valve rupture either associated or

unassociated with transection of the aorta occurs more often than thought previously. Multiplane transesophageal demonstration of a traumatic aortic valve rupture (a–g) producing significant acute aortic regurgitation. The deformity produced to the aortic valve cusps (a–b) and also the exact site of the rupture (e) may be easily shown in multiple planes. Color flow Doppler shows an abnormal chaotic flow pattern at the rupture site as well as a significant aortic regurgitant flow jet (c, d, f, g).

References

1. Gray H. Gray's Anatomy, 29th edn. Goss CM (ed) Philadelphia: Lea & Febiger, 1973.
2. Angelini A, Ho SY, Anderson RH, et al. The morphology of the normal aortic valve as compared with aortic valve having two leaflets. *J Thorac Cardiovasc Surg* 1989;98:362–7.
3. Gould SE (ed). Pathology of the Heart, 2nd ed. Springfield, Illinois: Charles C Thomas.
4. Bansal RC, Tajik AJ, Seward JB, Offord RP. Feasibility of detailed two-dimensional echocardiographic examination in adults: prospective study of 200 patients. *Mayo Clin Proc* 1980;55:291–308.
5 Darmon PL. Hillel Z. Mogtader A. Thys DM. A study of the human aortic valve orifice by transesophageal echocardiography. *J Am Soc Echocardiogr* 1996;9:668–74.
6. Vasan RS, Larson MG, Benjamin EJ, Levy D. Echocardiographic reference values for aortic root size: the Framingham Heart Study. *J Am Soc Echocardiogr* 1995;8:793–800.
7. Reid K. The anatomy of the sinus of Valsalva. *Thorax* 1970;25:79–85.
8. Kunzelman KS, Grande KJ, David TE, et al. Aortic root and valve relationships: impact on surgical repair. *J Thorac Cardiovasc Surg* 1994;107:162–70.
9. Roberts WC. The congenitally bicuspid aortic valve. A study of 85 autopsy patients .*Am J Cardiol* 1970:26:72–83.
10. Edwards JE. The congenital bicuspid aortic valve. *Circulation* 1961:23:485.
11. Brandenburg RO, Tajik AS, Edwards ED, et al. Bicuspid aortic valve. *Am J Cardiol* 1983;51;1469–73.
12. Roberts WC. The structural basis of abnormal cardiac function: a look at coronary, hypertensive, valvular, idiopathic myocardial, and pericardial heart disease. In: Levine, JJ (ed). Clinical Cardiovascular Physiology. New York: Grune & Stratton, 1976.
13. Subramanian R, Olson LJ, Edwards WD. Surgical pathology of pure aortic stenosis: a study of 374 cases. *Mayo Clin Proc* 1984;59:683–90.
14. Roberts WC, Elliott LP. Lesions complicating the congenitally bicuspid aortic valve. *Radiol Clin North Am* 1968;6:409.
15. Hahn R, Roman M, Mogtader A, Devereux R. Association of aortic dilatation with regurgitant, stenotic and functionally normal bicuspid aortic valves. *J Am Coll Cardiol* 1992;19:283–8.

16. Shone JD, Sellers RD, Anderson RD, et al. The development complex of "parachute mitral valve", supravalvular ring of the left atrium and coarctation of the aorta. *Am J Cardiol* 1963;11:714–25.
17. Waller BF, Carter JV, Williams HJ, et al. Bicuspid aortic valve. Comparison of congenital and acquired types. *Circulation* 1973;48:1140–50.
18. Hurwitz LE, Roberts WC. Quadricuspid semilunar valves. *Am J Cardiol* 1973;31:623–6.
19. Davia JE, et al. Quadricuspid aortic valves. *J Cardiovasc Surg* 1984;25:252.
20. Barbosa M, Motta M. Quadricuspid aortic valve and aortic regurgitation diagnosed by Doppler echocardiography. Report of two cases and review of the literature. *J Am Soc Echocardiogr* 1991;4;69–74.
21. Roberts WC. Valvular, subvalvular and supravalvular aortic stenosis. *Cardiovasc Clin* 1973;5:104.
22. Davies, JJ. Pathology of cardiac valves. London: Butterworth, 1980.
23. Roberts, WC. Valvular, subvalvular and supravalvular aortic stenosis: Morphologic features. *Cardiovasc Clin* 1973;5:97–126.
24. Roberts WC. Morphologic features of the normal and abnormal mitral valve. *Am J Cardiol* 1983;51:1005–28.
25. Roberts WC, Dangel JC, Bulkley BH. Nonrheumatic valvular cardiac disease: A clinicopathologic survey of 27 different conditions causing valvular dysfunction. *Cardiovasc Clin* 1973;5:333–446.
26. Roberts WC, Ewy GA, Glancy DL, et al. Valvular stenosis produced by active infective endocarditis. *Circulation* 1976;36:449–51.
27. Roberts WC, Ferrans VJ, Levy RI, et al. Cardiovascular pathology in hyperlipoproteinemia: Anatomic observations in 42 necropsy patients with normal or abnormal lipoprotein patterns. *Am J Cardiol* 1973;31:557–70.
28. Silver MD. Obstruction to blood flow related to the aortic valve. In Silver MD (ed). Cardiovascular Pathology. New York: Churchill Livingstone, 1983.
29. Gould L, Reddy CVR, DePalma D, et al. Cardiac manifestations of ochronoses. *J Thorac Cardiovasc Surg* 1976;72:788.
30. Helou J. Masters RG. Keon WJ. Veinot JP. Ochronosis: an unusual finding at aortic valve replacement. *Can J Cardiol* 1999;15:1013–15.
31. Pritzker MR, Ernst JD, Caudill C, et al. Acquired aortic stenoses in systemic lupus erythematosus. *Ann Intern Med* 1980;93:434–6.
32. Vollebergh FE, Becker AE. Minor congenital variations of cusp size in aortic valves. Possible link with isolated aortic stenosis. *Br Heart J* 1977; 39:1006–11.
33. Davis GL, McAlister WH, Friedenberg MM. Congenital aortic stenosis due to failure of histogensesis of the aortic valve (Myxoid dysplasia). *Am J Roentgenol Radium Ther Nucl Med* 1965;95:621–8.
34. Reeve R Jr, Robinson SJ. Hypoplastic annulus—an unusual type of aortic stenosis: a report of three cases in children. *Dis Chest* 1964;45:99.
35. Wong M, Tei C, Sadler N, Wittig JH, Drinkwater D, Shah PM. Echocardiographic observations of calcium in operatively excised stenotic aortic valves. *Am J Cardiol* 1987;59:324–9.
36. Subramanian R, Olson LJ, Edwards WD. Surgical pathology of pure aortic stenosis: a study of 374 cases. *Mayo Clin Proc* 1984;59:683–90.
37. Passik CS, Ackermann DM, Pluth JR, Edwards WD. Temporal changes in the causes of aortic stenosis: a surgical pathologic study of 646 cases. *Mayo Clin Proc* 1987;62:119–23.
38. Pomerance A. Pathogenesis of aortic stenosis and its relation to age. *Circulation* 1970;34:569–74.
39. Pomerance A. Acquired nonrheumatic valvular and endocardial pathology. *Pathol Annul* 1977;12:151–87.
40. Chandy KG, John TJ, Cherian G. Coxsackieviruses and chronic valvular heart disease. *Am Heart J* 1980;100:578–80.

41. Reis RL, Peterson LM, Mason DT, et al. Congenital fixed subvalvular aortic stenosis. An anatomic classification and correlations with operative results. *Circulation* 1971;43(suppl I):11.

42. Sung CS, Price EC, Cooley DA. Discrete subaortic stenosis in adults. *Am J Cardiol* 1978;42:283–90.

43. Oztunc F, Ozme S, Ozkutlu S, Saraclar M, Bilgic A, Ozer S. Fixed subaortic stenosis in childhood. Medical and surgical course in 90 patients. *Jpn Heart J* 1992;33:327–35.

44. Schwinger ME, Kronzon I. Improved evaluation of left ventricular outflow tract obstruction by transesophageal echocardiography. *J Am Soc Echocardiogr* 1989;2:191–4.

45. Mügge A, Daniel WG, Wolpers HG, et al. Improved visualization of discrete subvalvular aortic stenosis by transesophageal color-coded Doppler echocardiography. *Am Heart J* 1989;117:474–5.

46. Grossman W. Profiles in valvular heart disease. In Grossman W, Baim D (eds). Cardiac catheterization and angiography, 4th ed. Philadelphia: Lea and Febiger, 1991.

47. Ross J, Braunwald E. Aortic stenosis. *Circulation* 1968;38(suppl 5):V61–7.

48. Bruanwald E. On the natural history of severe aortic stenosis. *J Am Coll Cardiol* 1990;15:1018–20.

49. Carabello BA. Indications for valve surgery in asymptomatic patients with aortic and mitral stenosis. *Chest* 1995;108:1678–82.

50. Kennedy K, Nishimura R, Holmes D, et al. Natural history of moderate aortic stenosis. *J Am Coll Cardiol* 1991;17:313–19.

51. Bergon J, Abelmann WH, Vazquez-Milan H, et al. Aortic stenosis: clinical manifestations and course of disease. *Arch Intern Med* 1954;94:911–24.

52. Chizner MA, Pearle DL, DeLeon AC Jr. The natural history of aortic stenosis in adults. *Am Heart J* 1980;99:419–24.

53. Pellikka P, Nishimura, Bailey K, et al. The natural history of adults with asymptomatic, hemodynamically significant aortic stenosis. *J Am Coll Cardiol* 1990;15:1012–17.

54. Currie PJ, Seward JB, Reder GS, et al. Continuous vs Doppler echocardiographic assessment of severity of calcific aortic stenosis: a simultaneous Doppler-catheter correlative study in 100 adult patients. *Circulation* 1985;71:1162–9.

55. Otto C, Pearlman A, Gardner C. Hemodynamic progression of aortic stenosis in adults assessed by Doppler echocardiography. *J Am Coll Cardiol* 1989;13:545–50.

56. Roger V, Tajik J, Bailey K, et al. Progression of aortic stenosis in adults: new appraisal using Doppler echocardiography. *Am Heart J* 1990; 2:331–8.

57. Faggiano P, Ghizzoni G, Sorgato A, et al. Rate of progression of valvular aortic stenosis in adults. *Am J Cardiol* 1992;70:229–33.

58. Peter M, Hoffmann A, Parker C, et al. Progression of aortic stenosis: role of age and concomitant coronary artery disease. *Chest* 1993;103:1715–19.

59. Wagner S, Selzer P. Patterns of progression of aortic stenosis: a longitudinal hemodynamic study. *Circulation* 1982;65:709–12.

60. Nitta M, Nakamura T, Hultgren HN, et al. Progression of aortic stenosis in adult men: detection by noninvasive methods. *Chest* 1987;92:40–3.

61. Davies SW, Gershnick AH, Balcon R. Progression of valvular aortic stenosis: a long-term retrospective study. *Eur Heart J* 1991;12:10–14.

62. Nestico PF, DePace NL, Kimbiris D, et al. Progression of isolated aortic stenosis: analysis of 29 patients having more than one cardiac catheterization. *Am J Cardiol* 1983;52:1054–8.

63. Jonasson R, Jonsson B, Nordlander R, et al. Rate of progression of severity of valvular aortic stenosis. *Acta Med Scand* 1983;213:51–4.

64. deFilippi CR, Willett DL, Brickner ME, et al. Usefulness of dobutamine echocardiography in distinguishing severe from nonsevere valvular aortic stenosis in patients with depressed left ventricular function and low transvalvular gradients. *Am J Cardiol* 1995;75:191–4.

65. Hofmann T, Kasper W, Meinertz T, et al. Determination of aortic valve orifice area in aortic valve stenosis by two-dimensional transesophageal echocardiography. *Am J Cardiol* 1987;59:330–5.

66. Stoddard MR, Arce J, Liddell NE, Peters G, Kupersmith J. Two-dimensional transesophageal echocardiographic determination of aortic valve area in adults with aortic stenosis. *Am Heart J* 1991; 122:1415–22.

67. Chandrasekaran K, Foley R, Weintraub A, et al. Evidence that transesophageal echocardiography can reliably and directly measure the aortic valve area in patients with aortic stenosis – a new application that is independent of LV function and does not require Doppler data (abstr). *J Am Coll Cardiol* 1991;17:20A.

68. Okura H, Yoshida K, Hozumi T, Akasaka T, Yoshikawa J. Planimetry and transthoracic two-dimensional echocardiography in noninvasive assessment of aortic valve area in patients with valvular aortic stenosis. *J Am Coll Cardiol* 1997;30:753–9.

69. Kim CJ, Berglund H, Nishioka T, Luo H, Siegel RJ. Correspondence of aortic valve area determination from transesophageal echocardiography, transthoracic echocardiography and cardiac catheterization. *Am Heart J* 1996;132;1163–72.

70. de la Fuente Galan L, San Roman Calvar JA, Munoz San Jose JC, et al. Influence of the degree of aortic valve calcification on the estimate of valvular area using planimetry with transesophageal echocardiography. *Rev Esp Cardiol* 1996;49:663–8.

71. Hoffmann R, Flachskampf FA, Hanrath P. Planimetry of orifice area in aortic stenosis using multiplane transesophageal echocardiography. *J Am Coll Cardiol* 1993;22:529–34.

72. Tribouilloy C, Shen WF, Peltier M, Mirode A, Rey JL, Lesbre JP. Quantitation of aortic valve area in aortic stenosis with multiplane transesophageal echocardiography: comparison with monoplane transesophageal approach. *Am Heart J* 1994;128:526–32.

73. Cormier B, Iung B, Porte JM, Barbant S, Vahanian A. Value of multiplane transesophageal echocardiography in determining aortic valve area in aortic stenosis. *Am J Cardiol* 1996;77:882–5.

74. Tardif JC, Schneider A, Schwartz S, Vannan M, Pandian NG. Clinical utility of multiplane transesophageal echocardiography: comparison to biplanar imaging. *Am Heart J* 1994;128:156–66.

75. Kim KS, Maxted W, Nanda NC, et al. Comparison of multiplane and biplane transesophageal echocardiography in the assessment of aortic stenosis. *Am J Cardiol* 1997;79:436–41.

76. Espinal M, Fuisz AR, Nanda NC, Aaluri SR, Mukhtar O, Sekar PC. Sensitivity and specificity of transesophageal echocardiography for determination of aortic valve morphology. *Am Heart J* 2000;139:1071–6.

77. Tardif JC, Miller DS, Pandian NG, et al. Effects of variations in flow on aortic valve area in aortic stenosis based on in vivo planimetry of aortic valve area by multiplane transesophageal echocardiography. *Am J Cardiol* 1995;76:193–8.

78. Tardif JC, Rodriques AG, Hardy JF, et al. Simultaneous determination of aortic valve area by the Gorlin formula and by transesophageal echocardiography under different transvalvular flow conditions. *J Am Coll Cardiol* 1997;29:1296–302.

79. Morelli S, De Castro S, Cartoni D, et al. Planar determination of the aortic valve area with tee with mutiplanar probe in patients with aortic stenosis and insufficiency. Comparison with transthoracic Doppler echocardiography. *G Ital Cardiol* 1995;25:851–7.

80. Stoddard MF, Hammons RT, Longaker RA. Doppler transesophageal echocardiographic determination of aortic valve area in adults with aortic stenosis. *Am Heart J* 1996;132(2 Pt 1):337–42.

81. Blumberg FC, Pfeifer M, Holmer SR, Kromer EP, Riegger GA, Elsner D. Transgastric Doppler echocardiographic assessment of the severity of aortic stenosis using multiplane transesophageal echocardiography. *Am J Cardiol* 1997;79:1273–5.

82. Cormier B, Iung B, Porte JM, Barbant S, Vahanian A. Value of multiplane transesophageal echocardiography in determining aortic valve area in aortic stenosis. *Am J Cardiol* 1996;77:882–5.

83. Blumberg FC, Pfeifer M, Holmer SR, Kromer EP, Riegger GA, Elsner D. Quantification of aortic stenosis in mechanically ventilated patients using multiplane transesophageal Doppler echocardiography. *Chest* 1998;114:94–7.

84. Shively BK, Charlton GA, Crawford MH, Chaney RK. Flow dependence of valve area in aortic stenosis: relation to valve morphology. *J Am Coll Cardiol* 1998;31:654–60.

85. Tribouilloy C, Peltier M, Rey JL, Ruiz V, Lesbre JP. Use of transesophageal echocardiography to predict significant coronary artery disease in aortic stenosis. *Chest* 1998;113:671–5.

86. Cribier A, Savin T, Saoudi N, Rocha P, Berland J, Letac B. Percutaneous transluminal valvuloplasty of acquired aortic stenosis in elderly patients: an alternative to valve replacement? *Lancet* 1986;1:63–7.

87. Nishimura RA, Holmes DR Jr, Reeder GS, et al. Doppler evaluation of the results of percutaneous aortic balloon valvuloplasty in calcific aortic stenosis. *Circulation* 1988;78:791–9.

88. Safian RD, Berman AD, Diver DJ, et al. Balloon aortic valvuloplasty in 170 consecutive patients. *N Engl J Med* 1988;319:125–30.

89. Litvack F, Jakubowski AT, Buchbinder NA, Eigler N. Lack of sustained clinical improvement in an elderly population after percutaneous aortic valvuloplasty. *Am J Cardiol* 1988;62:270–5.

90. Safian RD, Mandell VS, Thurer RE, et al. Postmortem and intra-operative balloon valvuloplasty of calcific aortic stenosis in elderly patients: mechanisms of successful dilation. *J Am Coll Cardiol* 1987;9:655–60.

91. Desnoyers MR, Salem DN, Rosenfield K, Mackey W, O'Donnell T, Isner JM. Treatment of cardiogenic shock by emergency aortic balloon valvuloplasty. *Ann Intern Med* 1988;108:833–5.

92. O'Keefe JH Jr, Vlietstra RE, Bailey KR, Holmes DR Jr. Natural history of candidates for balloon aortic valvuloplasty. *Mayo Clin Proc* 1987;62:986–91.

93. Rahimtoola SH. Catheter balloon valvuloplasty of aortic and mitral stenosis in adults: 1987. *Circulation* 1987;75:895–901.

94. Hayes SH, Holmes DR Jr, Nishimura RA, Reeder GS. Palliative percutaneous aortic balloon valvuloplasty before noncardiac operations and invasive diagnostic procedures. *Mayo Clin Proc* 1989;64:753–7.

95. Helgason H, Keane JF, Fellows KE, Kulik TJ, Lock JE. Balloon dilation of the aortic valve: studies in normal lambs and in children with aortic stenosis. *J Am Coll Cardiol* 1987;9:816–22.

96. Cribier A, Savin T, Berland J, et al. Percutaneous transluminal balloon valvuloplasty of adult aortic stenosis: report of 92 cases. *J Am Coll Cardiol* 1987;9:381–6.

97. Phillips RR, Gerlis LM, Wilson N, Walker DR. Aortic valve damage caused by operative balloon dilatation of critical aortic valve stenosis. *Br Heart J* 1987;57:168–70.

98. Waller BF, Girod DA, Dillon JC. Transverse aortic wall tears in infants after balloon angioplasty for aortic valve stenosis. Retional of aortic wall damage to diameter of inflated angioplasty balloon and aortic lumen in seven necropsy cases. *J Am Coll Cardiol* 1984;4:1235–41.

99. Lembo NJ, King SB III, Roubin GS, Hammami A, Niederman AL. Fatal aortic rupture during percutaneous balloon valvuloplasty for valvular aortic stenosis. *Am J Cardiol* 1987;60:733–6.

100. Davies JJ. Pathology of Cardiac Valves. London: Butterworth, 1980.

101. Roberts WC, Morrow AG, McIntosh CL, et al. Congenitally bicuspid aortic valve causing severe, pure aortic regurgitation without superimposed infective endocarditis. *Am J Cardiol* 1981;47:206.

102. Olson LJ, Subramanian R, Edwards WD. Surgical pathology of pure aortic insufficiency: a study of 225 cases. *Mayo Clin Proc* 1984;59:835–41.

103. Cosgrove DM, Fraser CD. Aortic valve repair. *Operat Tech Card Thorac Surg* 1996:1;30–37.

104. Waller BF. Rheumatic and nonrheumatic conditions producing valvular heart disease. Cardiovascular Clinics. Valvular Heart Disease: Comprehensive evaluation and Management. F.A. Davis Co. 1986.

105. Bulkley, BH, Roberts, WC: Ankylosing spondylitis and aortic regurgitation. Description of the characteristic cardiovascular lesion from study of 8 necropsy patients. *Circulation* 1973;48:1014–27.

106. Thubrikar M. The Aortic Valve. Boca Raton, Fla: CRC Press, 1990.

107. Thubrikar MJ, Aouad J, Nolan SP. Comparison of the in vivo and in vitro mechanical properties of the aortic valve leaflets. *J Thorac Cardiovasc Surg* 1986;92:29–36.

108. Thubrikar MJ, Bosher LP, Nolan SP. The mechanism of opening of the aortic valve. *J Thorac Cardiovasc Surg* 1979;77:863–70.

109. Wilcox BR, Anderson RH. Surgical Anatomy of the Heart. New York: Raven Press, 1985.

110. Cohen GI, Duffy CI, Klein AL, et al. Color Doppler and two-dimensional echocardiographic determination of the mechanism of aortic regurgitation with surgical correlation. *J Am Soc Echocardiogr* 1996;9:508–15.

111. Connolly HM, Cary JL, McGoon MD, et al. Valvular heart disease associated with fenfluramine-phentermine. *N Engl J Med* 1997;337:581–8.

112. Lepor NE, Gross SB, Daley WL, et al. Dose and duration of fenfluramine-phentermine therapy impacts the risk of significant valvular heart disease. *Am J Cardiol* 2000;86:107–10.

113. Kimmel SE, Keane MG, Cary JL, et al. Detailed examination of Fenfluramine-phentermine users with valve abnormalities identified in Fargo, North Dakota. *Am J Cardiol* 1999;84;304–8.

114. Hensrud DD, Connolly HM, Grogan M, et al. Echocardiographic improvement over time after cessation of use of fenfluramine and phentermine. *Mayo Clin Proc* 1999;74:1191–7.

115. Lebowitz NE, Bella JN, Roman MJ, et al. Prevalence and correlates of aortic regurgitaion in American Indians: the Strong Heart Study. *J Am Coll Cardiol* 2000,36:461–7.

116. Klodas E, Enriquez-Sarano M, Tajik AJ, et al. Surgery for aortic regurgitation in women . Contrasting indications and outcomes compared with men.*Circulation* 1996;94:2472–8.

117. Klodas E, Enriquez-Sarano M, Tajik AJ, et al. Optimizing timing of surgical correction in patients with severe aortic regurgitation: role of symptoms. *J Am Coll Cardiol* 1997;30:746–52.

118. Dujardin KS, Enriquez-Sarano M, Schaff HV, et al. Mortality and morbidity of aortic regurgitation in clinical practice. A long term . A long term follow-up study. *Circulation* 1999;99:1851–7.

119. Yeo TC, Ling LH, Ng WL, Chia BL. Spontaneous aortic laceration causing flail aortic valve and acute regurgitation. *J Am Soc Echocardiogr* 1999;12:76–8.

120. Ducharme A, Courval JF, Dore A, et al. Severe aortic regurgitation immediately after mitral valve annuloplasty. *Ann Thoracic Surg* 1999;67:1487–9.

121. Castello R, Fagan L Jr, Lenzen P, Pearson AC, Labovitz AJ. Comparison of transthoracic and transesophageal echocardiography for assessment of left-sided valvular regurgitation. *Am J Cardiol* 1991;68:1677–80.

122. Bonow RO, Carabello B, de Leon AC, et al. Guidelines for the management of patients with valvular heart disease: Executive Summary: A report of the American College of Cardiology/American Heart Association task force on practice guidelines (Committee on management of patients with valvular heart disease). *Circulation* 1998;98:1949–84.

123. Dittrich HC, McCann HA, Walsh TP, et al. Transesophageal echocardiography in the evaluation of prosthetic and native aortic valves. *Am J Cardiol* 1990;66:758–61.

124. Perry GJ, Helmcke F, Nanda NC, et al. Evaluation of aortic insufficiency by Doppler color flow mapping. *J Am Coll Cardiol* 1987;9:952–9.

125. Willems TP, Steyerberg EW, van Herwerden LA, et al. Reproducibility of color Doppler flow quantification of aortic regurgitation. *J Am Soc Echocardiogr*1997;10:899–903.

126. Mizushige K, Nozaki S, Ohmori K, Matsuo H. Evaluation of effective aortic regurgitant orifice area and its effect on aortic regurgitant volume with Doppler echocardiography. *Angiology* 2000;51:241–6.

127. Reimold SC, Orav EJ, Come PC, Caquioa ES, Lee RT. Progressive enlargement of the regurgitant orifice in patients with chronic aortic regurgitation. *J Am Soc Echocardiogr* 1998;11:259–65.
128. Ishii M, Jones M, Shiota T, et al. Quantifying aortic regurgitation by using the color Doppler-imaged vena contracta: a chronic animal model study. *Circulation* 1997;96:2009–15.
129. Tribouilloy CM, Enriquez-Sarano M, Bailey KR, Seward JB, Tajik AJ. Assessment of severity of aortic regurgitation using the width of the vena contracta: A clinical color Doppler imaging study. *Circulation* 2000;102:558–64.
130. Tribouilloy CM, Enriquez-Sarano M, Fett SL, Bailey KR, Seward JB, Tajik AJ. Application of the proximal flow convergence method to calculate the effective regurgitant orifice area in aortic regurgitation. *J Am Coll Cardiol* 1998;32:1032–9.
131. Sato Y, Kawazoe K, Nasu M, Kiramori K. Clinical usefulness of the proximal isovelocity surface area method using echocardiography in patients with eccentric aortic regurgitation. *J Heart Valve Dis* 1999;8:104–11.
132. Sato Y, Kawazoe K, Kamata J, et al. Clinical usefulness of the effective regurgitant orifice area determined by transesophageal echocardiography in patients with eccentric aortic regurgitation. *J Heart Valve Dis* 1997;6:580–6.
133. Gozzelino G, Aletto C, Curti MT, et al. The effect of heart rate on the slope and pressure half-time of the Doppler regurgitant velocity curve in aortic insufficiency. *J Am Soc Echocardiogr* 1996;9:516–26.
134. Sutton DC, Kluger R, Ahmed SU, Reimold SC, Mark JB. Flow reversal in the descending aorta: a guide to intraoperative assessment of aortic regurgitation with transesophageal echocardiography. *J Thoracic Cardiovasc Surg* 1994;108:576–82.
135. Vilacosta I, San Roman JA, Castillo JA, et al. Retrograde atrial kick in acute aortic regurgitation. Study of mitral and pulmonary venous flow velocities by transthoracic and transesophageal echocardiography. *Clin Cardiol* 1997;20:35–40.
136. Padial LR, Oliver A, Vivaldi M, et al. Doppler echocardiographic assessment of progression of aortic regurgitation. *Am J Cardiol* 1997;80:306–14.
137. Antunes MJ. Repair for acquired aortic valve disease. *Isr J Med Sci* 1996;32:817–20.
138. Haydar HS, He G-W, Hovaguimian H, et al. Valve repair for aortic insufficiency: surgical classification and techniques. *Eur J Cardiothoracic Surg* 1997;11:258–65.
139. Antunes MJ, Franco CG. Advances in surgical treatment of acquired valve disease. *Curr Opin Cardiol* 1996;11:139–54.
140. King RM, Pluth JR, Giuliani ER, et al. Mechanical decalcification of the aortic valve. *Ann Thorac Surg* 1986;42:269–72.
141. Shapira N, Lemole GM, Fernandez J, et al. Aortic valve repair for aortic stenosis in adults. *Ann Thorac Surg* 1990;50:110–20.
142. Duran C, Kumar N, Gometza B, Halees ZA. Indications and limitations of aortic valve reconstruction. *Ann Thorac Surg* 1991;52:447–54.
143. Cosgrove DM, Rosenkranz ER, Hendren WG, et al. Valvuloplasty for aortic insufficiency. *J Thorac Cardiovasc Surg* 1991;102:571–7.
144. Fraser CD Jr, Wang N, Mee RBB, et al. Repair of insufficient bicuspid aortic valve. *Ann Thorac Surg* 1994;58:386–90.
145. Casselman FP, Gillinov AM, Akhrass R, et al. Intermediate-term durability of bicuspid aortic valve repair for prolapsing leaflet. *Eur J Cardiothoracic Surg* 1999;15:302–8.
146. Keane MG, Wiegers SE, Yang E, Ferrair VA, Sutton MG, Bavaria JE. Structural determinants of aortic regurgitation in type A dissection and the role of valvular resuspension as determined by intraoperative transesophageal echocardiography. *Am J Cardiol* 2000;85:604–10.
147. Movsowitz HD, Levine RA, Hilgenberg AD, Isselbacher EM. Transesophageal echocardiographic description of the mechanisms of aortic regurgitation in acute type A aortic dissection: implications for aortic valve repair. *J Am Coll Cardiol* 2000;36:884–90.

148. Erbel R, Rohmann S, Drexler M, et al. Improved diagnostic value of echocardiography in patients with infective endocarditis by transesophageal approach. A prospective study. *Eur Heart J* 1988;9:43–53.
149. Gilbert BW, Haney RS, Crawford R, et al. Two-dimensional echocardiographic assessment of vegetative endocarditis. *Circulation* 1977;55:346–53.
150. ügge A, Daniel WG, Frank G, Lichtlen PR. Echocardiography in infective endocarditis: reassessment of prognostic implications of vegetation size determined by the transthoracic and the transesophageal approach. *J Am Coll Cardiol* 1989;14:631–8.
151. Scanlon JG, Seward JB, Tajik AJ. Valve ring abscess in infective endocarditis: visualization with wide-angle two-dimensional echocardiography. *Am J Cardiol* 1982;49:1794–800.
152. Daniel WG, Schroder E, Nonnast-Daniel B, Lichtlen PR. Conventional and transesophageal echocardiography in the diagnosis of infective endocarditis. *Eur Heart J* 1987;8 (suppl J):287–92.
153. Daniel WG, Schroder E, ügge A, Lichtlen PR. Transesophageal echocardiography in infective endocarditis. *Am J Card Imaging* 1988;2:78–85.
154. Taams MA, Gusenhoven EJ, Bos E, et al. Enhanced morphological diagnosis in infective endocarditis by transesophageal echocardiography. *Br Heart J* 1990;63:109–13.
155. Shively BK, Gurule FT, Roldan CA, et al. Diagnostic value of transesophageal compared with transthoracic echocardiography in infective endocarditis. *J Am Coll Cardiol* 1991;18:391–7.
156. Birmingham GD, Rahko PS, Ballantyne F III. Improved detection of infective endocarditis with transesophageal echocardiography. *Am Heart J* 1992;123:774–81.
157. Klodas E, Edwards WD, Khandheria BK. Use of transesophageal echocardiography for improving detection of valvular vegetations in subacute bacterial endocarditis. *J Am Soc Echocardiogr* 1989;2:386–9.
158. Berger M, Gallerstein PE, Benhuri P, et al. Evaluation of aortic valve endocarditis by two-dimensional echocardiography. *Chest* 1981;80:61–7.
159. Arnett EN, Roberts WC. Valve ring abscess in active infective endocarditis: frequency, location and clues to clinical diagnosis from the study of 95 necropsy patients. *Circulation* 1976;54:140–5.
160. Buchbinder NA, Roberts WC. Left-sided valvular active infective endocarditis: a study of forty-five necropsy patients. *Am J Med* 1972;53:20–35
161. Daniel WG, Mügge A, Martin RP, et al. Improvement in the diagnosis of abscesses associated with endocarditis by transesophageal echocardiography. *N Engl J Med* 1991;324:795–800.
162. Baumgartner FJ, Omari BO, Robertson JM, et al. Annular abscesses in surgical endocarditis: anatomic, clinical and operative features. *Ann Thorac Surg* 2000;70:442–7.
163. David TE, Bos J, Christakis GT, et al. Heart valve operations in patients with active infective endocarditis. *Ann Thorac Surg* 1990;49:701–5.
164. Saner HE, Asinger RW, Homans DC, Helseth HK, Elsperger KJ. Two-dimensional echocardiographic identification of complicated aortic root endocarditis: implications for surgery. *J Am Coll Cardiol* 1987;10:859–68.
165. Marcos-Alberca P, Rey M, Serrano JM, et al. Aneurysm of the anterior leaflet of the mitral valve secondary to aortic valve endocarditis. *J Am Soc Echocardiogr* 2000:13:1050–2.
166. Espinosa-Caliani JS, Montijano A, Melero JM, Montiel A. Pseudoaneurysm in the mitral-aortic intervalvular fibrosa. A cause of mitral regurgitation. *Eur J Cardiothoracic Surg* 2000;17:757–9.
167. Hwang SW, Yucel EK, Bernard S. Aortic root abscess with fistula formation. *Chest* 1997;111:1436–8.
168. Nomeir A-M, Downes TR, Cordell AR. Perforation of the anterior mitral leaflet caused by aortic valve endocarditis: Diagnosis by two-dimensional, transesophageal echocardiography and color flow Doppler. *J Am Soc Echocardiogr* 1992;5:195–8.

169. Ballal RS, Mahan EF III, Nanda NC, Sanyal R. Aortic and mitral valve perforation: diagnosis by transesophageal echocardiography and Doppler color flow imaging. *Am Heart J* 1991;121:214–17.
170. Massey WM, Samdarshi TE, Nanda NC, et al. Serial documentation of changes in a mitral valve vegetation progressing to abscess rupture and fistula formation by transesophageal echocardiography. *Am Heart J* 1992;124:241–8.
171. Afridi I, Apostolidou MA, Saad RM, Zoghbi WA. Pseudoaneurysms of the mitral-aortic intervalvular fibrosa: dynamic characterization using transesophageal echocardiographic and Doppler techniques. *J Am Coll Cardiol* 1995;25:137–45.
172. Bansal RC, Graham BM, Jutzy KR, et al. Left ventricular outflow tract to left atrial communication secondary to rupture of mitralaortic intervalvular fibrosa in infective endocarditis: diagnosis by transesophageal echocardiography and color flow imaging. *J Am Coll Cardiol* 1990;15:449–504.
173. Hojnik M, Jacob G, Ziporen L, Shoenfeld Y. Heart valve involvement (Libman–Sacks endocarditis) in the antiphospholipid syndrome. *Circulation* 1996;93:1579–87.
174. Roldan CA, Shively BK, Crawford MH. An echocardiographic study of valvular heart disease associated with systemic lupus erythematosus. *N Engl J Med* 1996;335:1424–30.
175. The Antiphospholipid Antibodies in Stroke Group. Clinical and laboratory findings in patients with antiphospholipid antibodies and cerebral ischemia. *Stroke* 1990;21:1268–73.

4
Tricuspid valve, pulmonary valve and pulmonary artery

Tricuspid valve

The tricuspid valve is similar to and possesses the same physical and functional characteristics as the mitral valve. The tricuspid valve is one of the most anterior structures in the heart and is almost completely retrosternal, which may make it difficult to examine by transthoracic echocardiography. Transesophageal echocardiography (TEE) has an advantage of visualizing the tricuspid valve from the esophagus, which allows imaging the tricuspid valve in detail, from many views. Transesophageal color Doppler examination allows assessment of tricuspid regurgitation, but it is difficult to obtain the parallel imaging planes necessary for conventional Doppler measurements of peak tricuspid regurgitant jet velocity.

It is important to regard the tricuspid valve apparatus as an integrated unit when assessing valvular function. The major differences between the two atrioventricular valves are that the tricuspid valve has three leaflets and a larger diameter with a different annular shape compared with the mitral valve. Anatomically the tricuspid subvalvular apparatus is more extensive than the mitral valve. The physiological function of the tricuspid valve is to allow the uninterrupted flow of blood from the right atrium to the right ventricle in diastole, and to prevent blood flow reversal during right ventricular contraction. In many cardiac disorders the pressure in the right heart is increased, which produces functional incompetence of the tricuspid valve unit, and thus evaluation of the tricuspid valve apparatus is important.

Anatomy

The tricuspid valve unit has three leaflets, three commissures, chordae tendineae, an annulus, and papillary muscles integrated with the right atrial and ventricular endocardium[1] (figure 4.1). The tricuspid valve leaflets are demarcated by scallops (indentations) rather than well-formed leaflets. The anterior, posterior, and septal leaflets are unequal in size and project from the tricuspid valve annulus like an apron. The tricuspid leaflets are triangular in shape with broad bases of annular attachment and apices projecting toward the centre of the valve line of closure. This architecture produces a funnel shape when the valve is open, with the largest enface diameter at the

annular plane and a smaller diameter in the ventricle. This arrangement produces a normal tricuspid valve area of about 7.0 cm^2.[2]

The anterior (infundibular) leaflet is the largest leaflet, approximately 22 mm wide from base to free margin, and is attached to the anterior wall in the region of the infundibulum and to the inferolateral wall for a circumference of 38.7 mm.[3,4] The posterior leaflet, or marginal leaflet, is approximately 20 mm wide and curves around the diaphragmatic surface of the heart from the inferolateral wall to the septum. It has a circumference of 37.8 mm, and is divided into one to three scallops.[3,4] The septal or medial leaflet is the smallest leaflet, approximately 15 mm wide. It has a circumference of 35.9 mm and a characteristic indentation or fold at the junction of the leaflet at the posterior ventricular wall and membranous septum.[3,4] The septal leaflet is attached to both the membranous and
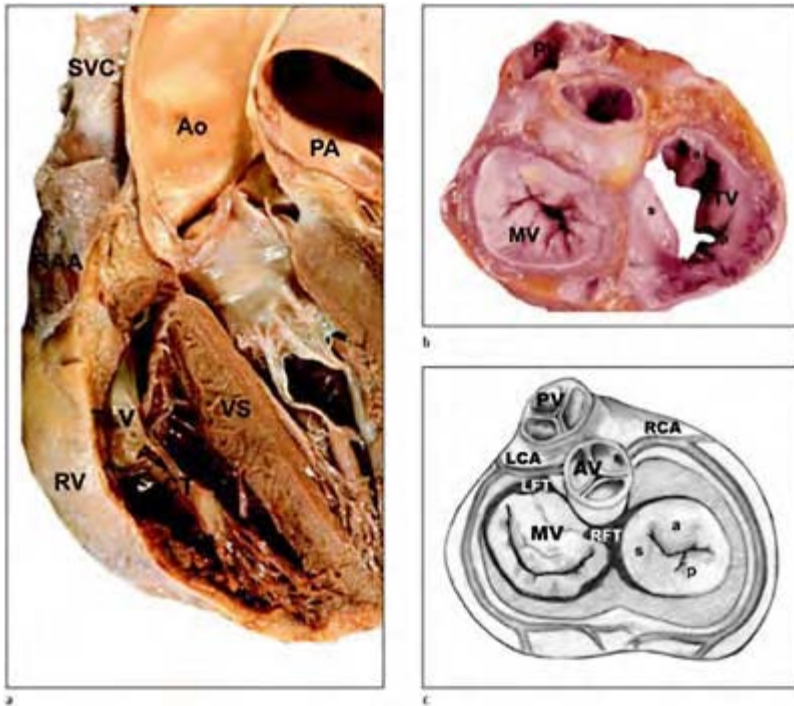
Figure 4.1 Anatomically the tricuspid subvalvular apparatus is more extensive than the mitral valve. The tricuspid valve leaflets are demarcated by scallops (indentations) rather than well-formed leaflets. The anterior, posterior, and septal leaflets are unequal in size and project from the

tricuspid valve annulus like an apron. The tricuspid leaflets are triangular in shape with broad bases of annular attachment and apices projecting toward the centre of the valve closure line. This architecture produces a funnel shape when the valve is open, with the largest enface diameter at the annular plane and a smaller diameter in the ventricle and produces a normal tricuspid valve area of about 7.0 cm^2. The tricuspid annulus originates as a fibrous thickening of the superior border of the right ventricular myocardium, and is not as well defined anatomically as the mitral annulus. The tricuspid annulus is larger than the mitral annulus and is approximately 8.5–12 cm (average 11 cm) in circumference. The posterior leaflet comprises approximately 50% of the annulus. The septal portion of the annulus is an integral part of the fibrous skeleton of the heart. The annulus does not lie in a single plane relative to the fibrous skeleton with the anteroseptal commissure tilting superior or higher than the rest of the valve plane. In the normal heart, the transverse annular diameter is greater than the anteroposterior diameter, and the length of the annulus along the septal portion is about one-third of the total circumference of the annulus. The portion of the fibrous skeleton along the septal wall of the annulus consists of strong connective tissue preventing dilatation of that portion of the annulus. Dilatation only occurs along

the base of the anterior and posterior leaflets of the valve. Anatomic preparation of the tricuspid valve unit (a), and the fibrous skeleton (b) with corresponding artists rendition of the fibrous skeleton. PV, pulmonary valve; AV, aortic valve; LCA, left coronary artery; RCA, right coronary artery; LFT, left fibrous trigone; RFT, right fibrous trigone; MV, mitral valve; a, anterior tricuspid leaflet; s, septal tricuspid leaflet; p, posterior tricuspid leaflet; SVC, superior vena cava; RV, right ventricle; TLV, tricuspid valve leaflet; CT, chordae tendinae; VS, ventricular septum; Ao, aorta; PA, pulmonary artery; RAA, right atrial appendage; TV, triscuspid valve.

muscular ventricular septa between the anterior and posterior leaflets. The atrioventricular node is located very close to the insertion of the anterior portion of the septal leaflet, as the leaflet runs parallel to the conduction system. The tricuspid valve leaflets, similar to the mitral valve, are made of strong fibrous connective tissue, thicker in the central portion and thinner at the leaflet edges.

The tricuspid annulus originates as a fibrous thickening of the superior border of the right ventricular myocardium, and is not as well defined anatomically as the mitral annulus. The tricuspid annulus is larger than the mitral annulus and is approximately 8.5–12 cm (average 11 cm) in circumference.[5] The posterior leaflet makes up about 50% of the annulus. The septal portion of the annulus is an integral part of the fibrous skeleton of the heart. The annulus is not in a single plane, because the anteroseptal commissural is in a superior plane. In the normal heart, the transverse annular diameter is greater than the anteroposterior diameter, and the length of the annulus along the septal portion is roughly one-third of the total circumference of the annulus. The portion of the tricuspid annulus along the septal wall that forms part of the fibrous skeleton of the heart does not dilate. Dilatation only occurs along the base of the anterior and posterior leaflets of the valve.

Commissures are formed by the infolding of the leaflets to produce indentations, with a corresponding papillary muscle inserted into the right ventricular myocardium just below each commissure point. The commissures are distinguished from the numerous indentations of the leaflets by the insertion of fan-like chordae. The anteroseptal commissure is approximately 7.7 mm, the septalposterior commissure is 17.3 mm and the anteroposterior commissure is 16.3 mm.[4]

The anterior papillary muscle is the most prominent, arising from the moderator band and the anterior septal wall of the right ventricle. The posterior papillary muscle, which

usually has multiple heads, emanates from the posterior wall of the right ventricle. The septal papillary muscle is usually rudimentary, originating from the septal wall. Additional multiple small papillary muscles may also be present echocardiographically as prominent trabecula-tions of the right ventricular endocardium.[1–4]

The papillary muscles are attached to the ventricular surface of the leaflet margins by chordae tendineae. The chordae tendineae of the tricuspid valve are made up of five types: fan-shaped, rough zone, basal, free-edge, and deep.[5] Chordal insertion to the tricuspid leaflet margins produces a well-delineated rough zone at the surface of the leaflet, which provides for increased surface area for leaflet approximation. Free-edge and deep chordae are unique to the tricuspid valve apparatus. In contrast to mitral chordae tendineae, there are around 20 tricuspid chordae tendineae, which vary greatly in length and thickness.[3,5]

Echocardiographic visualization

The tricuspid valve can be visualized in the longitudinal projection of the right ventricular inflow from the mid and lower esophageal views at 0 degrees, with the transducer in the neutral or minimally retroflexed position (figure 4.2). The transducer transects the tricuspid valve through the anterior and septal leaflets. Further retroflexion brings the coronary sinus and the posterior leaflet into view. Motion of the tricuspid valve leaflets resembles that of the mitral valve, with rapid diastolic filling followed by a slow descent of the leaflets toward the annulus, followed promptly by reopening with atrial contraction. During systole, the leaflets close with approximation of the leaflet free margins, which should not protrude beyond the annular plane into the right atrium. When the transducer beam orientation is directed to the right, the chordae tendineae and papillary muscle insertions may be assessed. This imaging plane provides adequate orientation for color flow mapping and conventional Doppler interrogation of the right ventricular inflow tract for the evaluation of tricuspid stenosis and regurgitation.

The short-axis views from the transgastric transducer positions provide multiple cross-sectional cuts through the tricuspid valve annulus (figure 4.3). Careful angling of the transducer enables imaging of the total circumference of the annulus and all three leaflets. The normal tricuspid annulus is usually less than 11 cm in circumference. The posterior leaflet is closest to the transducer, the anterior leaflet is anterior and lateral, and the septal leaflet projects medially from the right ventricular septum. The tricuspid valve is in a different plane than the mitral valve, prohibiting simultaneous visualization of both valves in the same orientation. The short axis views allow the shape of the annulus to be appreciated, and the antero-posterior transverse diameter of the annulus to be measured. The tricuspid valve orifice area can be planimetered in this view at the point of maximal valve opening, close to the base of the right ventricle.

Rotating the transducer to 90 to 110 degrees in the transgastric view and directing the echocardiographic beam towards the right heart provides a longitudinal view of the right ventricular inflow tract, with the tricuspid valve to the right of the echocardiographic sector and the right ventricular apex towards the right (figure 4.4). The transducer transects the tricuspid valve, providing an antero-posterior diameter of the tricuspid valve annulus. The right ventricular apex is usually foreshortened in this view and the right ventricular outflow is visualized coursing obliquely toward the inferior aspect of the

sector in the centre of the echocardiographic image. This view images the whole right heart with both the inflow and outflow tracts.

The deep transgastric views produce images similar to that of the transthoracic echocardiographic subxyphoid
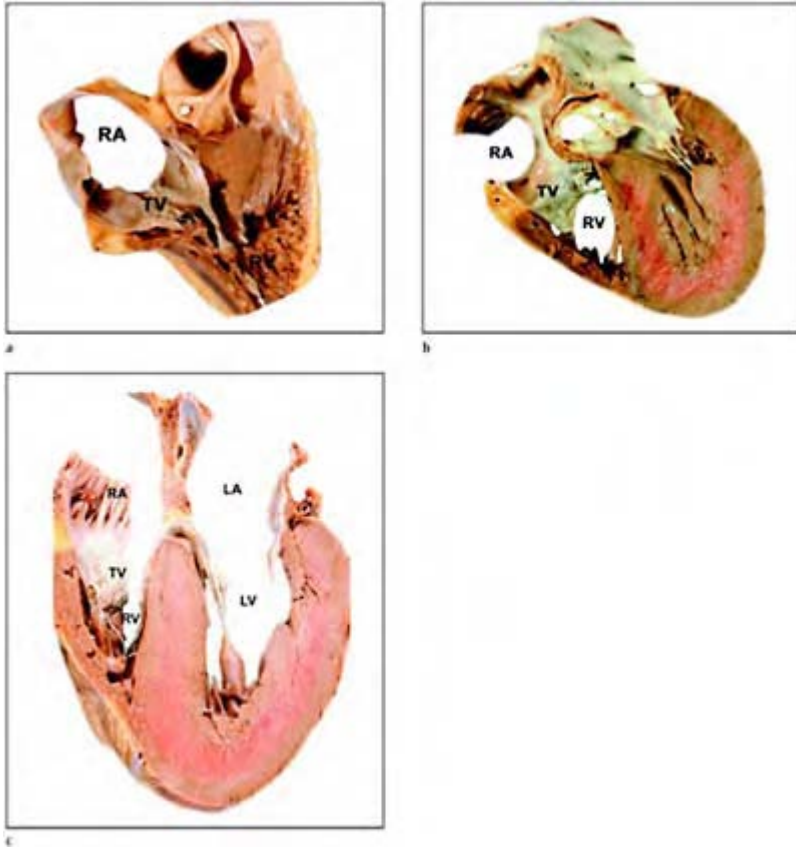
Figure 4.2 Anatomical preparation representing typical multiplane transesophageal echocardiographic imaging planes for the tricuspid valve unit. The tricuspid valve can be visualized in the longitudinal projection of the right ventricular inflow from the mid and lower esophageal views at 0 degrees, with the transducer in the neutral or minimally retroflexed position (a). The

transducer transects the tricuspid valve through the anterior and septal leaflets. Further retroflexion brings the coronary sinus and the posterior leaflet into view (b). In the four-chamber view, the motion of the tricuspid valve leaflets resembles that of the mitral valve, with rapid diastolic filling followed by a slow descent of the leaflets toward the annulus, followed promptly by reopening with atrial contraction. During systole, the leaflets close with approximation of the leaflet free margins that should not protrude beyond the annular plane into the right atrium. When the transducer beam orientation is directed to the right, the chordae tendineae and papillary muscle insertions may be assessed. This imaging plane provides adequate orientation for color flow mapping and conventional Doppler interrogation of the right ventricular inflow tract for the assessment of tricuspid stenosis and regurgitation (c). RA, right atrium; LA, left atrium; TV, tricuspid valve; RV, right ventricle; LV, left ventricle.

four-chamber view. The transducer beam transects the tricuspid valve leaflets obliquely, with the anterior leaflet the most lateral, and the septal leaflet most medial. The insertion of the tricuspid valve septal leaflet is more apically oriented in the four-chamber view than the insertion of the anterior leaflet of the mitral valve. Leaflet thickness is easily assessed and motion can be evaluated for restriction and prolapse as well as for vegetation or masses. These are ideal views for color Doppler analysis of the right ventricular inflow tract.
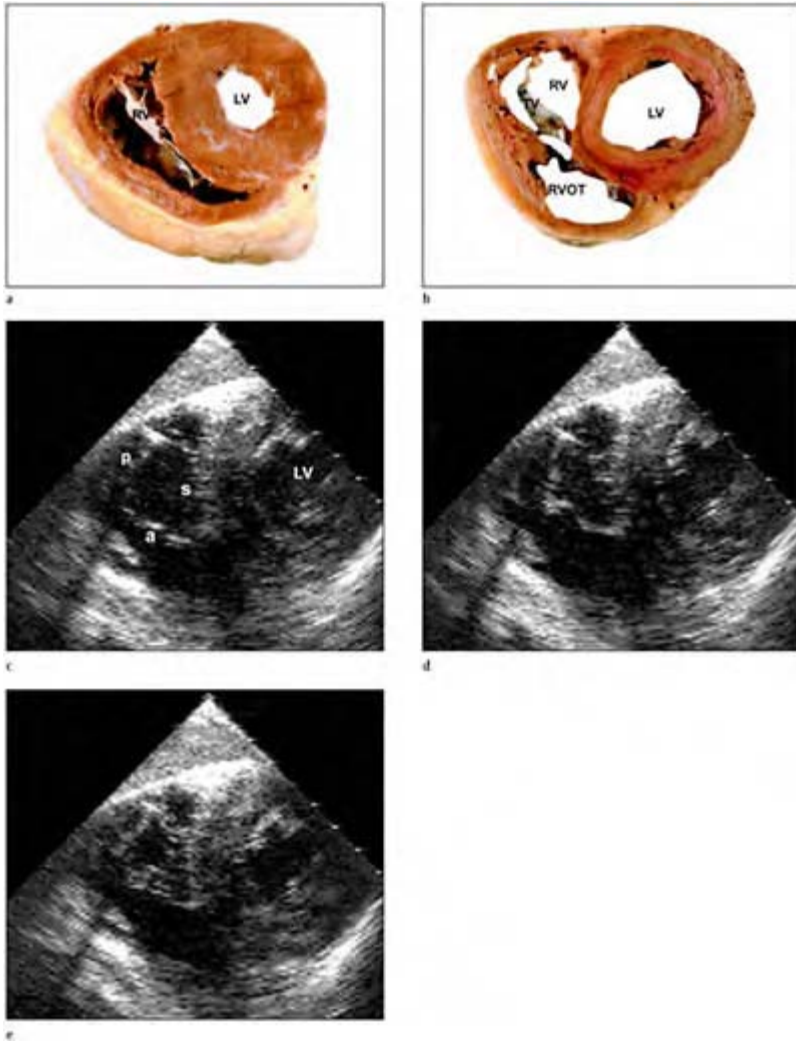
Figure 4.3 Anatomical preparation and corresponding echocardiographic short axis images of the tricuspid valve plane (a–e). The shortaxis views from the transgastric transducer positions provide multiple cross-sectional cuts through the tricuspid valve annulus. Careful angling of the transducer enables imaging of the total circumference of the annulus and all

three leaflets. The normal tricuspid annulus is usually less than 11 cm in circumference. The posterior leaflet is closest to the transducer; the anterior leaflet is anterior and lateral, and the septal leaflet projects medially from the right ventricular septum. The tricuspid valve is in a different plane than the mitral valve, prohibiting simultaneous visualization of both valves in the same orientation. The short axis views allow the shape of the annulus to be appreciated, and the anteroposterior transverse diameter of the annulus to be measured. The tricuspid valve orifice area can be planimetered in this view at the point of maximal valve opening close to the base of the right ventricle. RV, right ventricle; LV, left ventricle; TV, tricuspid valve; RVOT, right ventricular outflow tract; a, anterior tricuspid leaflet; s, septal tricuspid leaflet; p, posterior tricuspid leaflet.
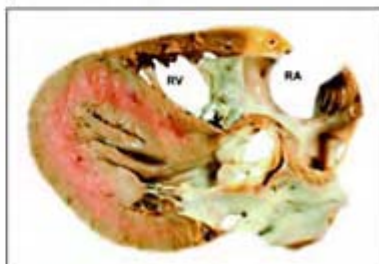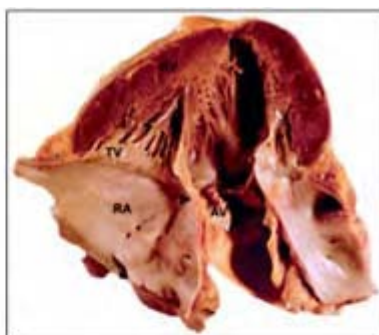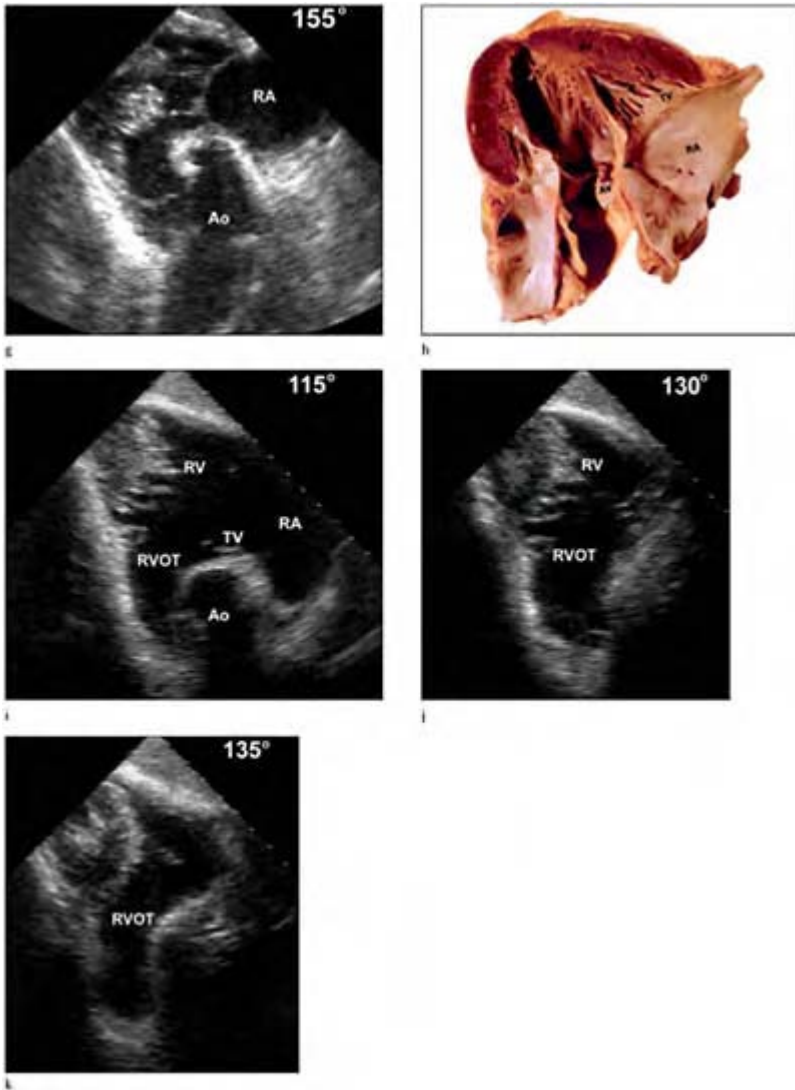
Figure 4.4 Rotating the transducer
from 0 to 180 degrees in the deep
transgastric view and directing the
echocardiographic beam towards the
right heart provides a longitudinal
view of the right heart (a–k). Typical
echocardiographic short axis view of
the tricuspid valve from the

transgastric position at 0 degrees. Longitudinal views of the right heart produced by slightly advancing the transducer and rotating toward the right heart. At 0 degrees the right ventricular inflow is imaged with the tricuspid valve to the left of the echocardiographic sector and the right ventricular apex left and superior to the left ventricle towards the top of the image, representative anatomical preparation (b) and corresponding echocardiographic images from 0 to 10 degrees (c–e). Switching from the right ventricular inflow (d) and outflow (e) views is performed with lateral flexion of the transducer. In this view the transducer transects the tricuspid valve providing an antero-posterior diameter of the tricuspid valve annulus. The right ventricular apex is usually foreshortened in this view and the right ventricular outflow is visualized coursing obliquely toward the inferior aspect of the sector in the center of the echocardiographic image. With further rotation of the transducer to 155 degrees the entire right heart may be visualized along its longitudinal axis (f–k). RA, right atrium; TV, tricuspid valve; RV, right ventricle; AV, aortic valve; Ao, aorta; LV, left ventricle; PA, pulmonary artery; SVC, superior vena cava; RVOT, right ventricular outflow tract.

Tricuspid stenosis

Tricuspid stenosis is usually a result of rheumatic disease, and invariably coexists with mitral stenosis, and not infrequently with aortic valve involvement.[6] The valve leaflets are diffusely thickened and fibrotic, which results in restricted leaflet motion[7–10] (figure 4.5). In contrast to mitral stenosis, tricuspid stenotic leaflets rarely become calcified.[6,11] There is commissural fusion of two or usually three commissures, which produces diastolic doming most marked with the anterior leaflet right ventricular outflow tract. Fibrosis and shortening of the chordal structures further reduces valve motion during diastole, but usually not to the degree that occurs in mitral stenosis. Invariably there is associated tricuspid regurgitation. Obstruction to the right ventricular inflow produces right atrial enlargement.[12]

Occasionally, carcinoid produces tricuspid stenosis, from deposits of mucopolysaccharide material and fibrous
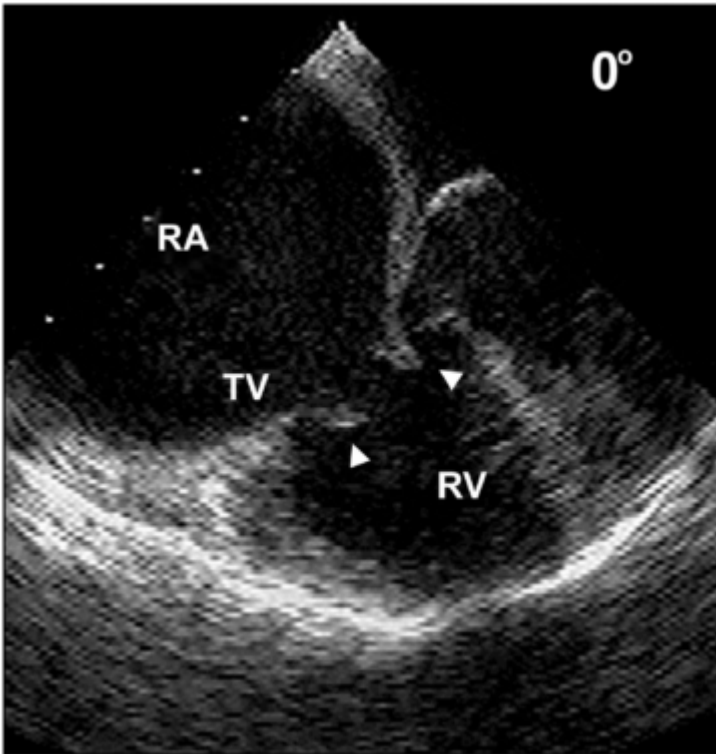
Figure 4.5 In tricuspid stenosis, the valve leaflets are diffusely thickened and fibrotic which results in restricted leaflet motion. In contrast to mitral

stenosis, tricuspid stenotic leaflets rarely become calcified. There is commissural fusion of two and usually three commissures that produces diastolic doming, most noticeable with the anterior leaflet. Fibrosis and shortening of the chordal structures further reduces valve motion during diastole, but usually not to the degree that occurs in mitral stenosis. Invariably there is associated tricuspid regurgitation. Obstruction to the right ventricular inflow produces right atrial enlargement. RV, right ventricle; RA, right atrium; TV, tricuspid valve.

tissue on the surface of the tricuspid leaflets and the right atrial and ventricular endocardium.[13] The carcinoid plaque is a white, fibrous lesion that coats the valve without causing destruction of the underlying valve structure. Carcinoid plaques usually occur on the ventricular surface of the tricuspid leaflets and may extend to the chordae tendineae. These deposits severely restrict leaflet motion, usually fixing the leaflets in an open position, which causes combined obstruction and regurgitation of flow.

Isolated tricuspid stenosis is usually congenital in origin but may result from active infective endocarditis. In rare cases of Ebstein's anomaly the valve leaflets do not separate, producing a stenotic diaphragm. Large infected vegetations, although rare, may produce obstruction of the tricuspid valve orifice.[14] Other rare causes of non-rheumatic tricuspid stenosis include Fabry's disease, Whipple's disease, methysergide therapy, and giant blood cysts.[15,16] Supravalvular or subvalvular stenosis is usually the result of primary or secondary tumors of the right heart that may produce obstruction of the tricuspid apparatus.

Transthoracic and transesophageal Doppler echocardiographic estimation of the transvalvular gradient is extremely useful in determining the severity of tricuspid valve stenosis, and correlates well with gradients measured at cardiac catheterization.[8] Care must be taken to align the ultrasound beam parallel to the direction of blood flow through the right ventricular inflow tract, to obtain accurate valve gradients.[9,17–19] Since transtricuspid valve gradients are small, it is easy to underestimate valve gradients, leading to the overall underestimation of tricuspid stenosis especially by transesophageal echocardiography. We have measured the tricuspid valve areas by PISA from the deep transgastric views with good correlation with catheterization data in our laboratories. It is usually not helpful to grade the severity of tricuspid valve stenosis. Significant hemodynamic stenosis is present with bicuspid valve areas of $\geq 1.5 cm^2$.

Tricuspid regurgitation

Tricuspid regurgitation may be produced by primary disease of the tricuspid valve apparatus or secondarily due to changes in the right ventricular configuration.[20-34] Primary valvular disease may result from rheumatic disease, carcinoid syndrome, myxomatous disease with chordal rupture (prolapse syndrome), bacterial endocarditis and papillary muscle dysfunction coexistent with ischemic heart disease. Right ventricular enlargement producing annular dilatation (with anatomically normal leaflets) and tricuspid regurgitation frequently accompanies idiopathic dilated cardiomyopathy and left heart failure associated with secondary pulmonary hypertension. The most common cause of organic tricuspid regurgitation is rheumatic disease. Rare causes of tricuspid regurgitation include congenital leaflet clefts, endomyocardial fibrosis, radiation therapy, rheumatoid arthritis, hypereosinophilic syndrome, constrictive pericarditis, and thyrotoxicosis. Physiological or mild tricuspid regurgitation is usually detected in most normal tricuspid valves by color Doppler and transesophageal echocardiography.

Tricuspid regurgitation often results from increased pulmonary blood flow states such as occur with intracardiac shunts and associated with other forms of congenital heart disease. When pulmonary arterial systolic pressure exceeds 40 mmHg, the incidence of tricuspid regurgitation approaches 90%, and in cases of severe pulmonary hypertension, the incidence of tricuspid regurgitation is present in nearly 100% of cases.[35-41] Acute tricuspid regurgitation develops after pulmonary embolism due to the abrupt increase in pulmonary arterial pressure, especially in patients with concomitant cardiopulmonary disease.

Etiology based on morphology

The etiology of tricuspid regurgitation may be ascertained from the alterations in the tricuspid valve apparatus[5,42] (table 4.1). In rheumatic tricuspid regurgitation there is diffuse fibrous thickening of the leaflet free margins, with variable degrees of focal fibrous thickening of the remaining leaflet tissue. The commissures are not fused, the valve leaflets are free of calcific deposits and the annular circumference is normal, less than 12 cm.

In tricuspid valve prolapse, there is increased leaflet area, due to leaflet redundancy, hooding or excessive leaflet motion beyond the annular plane in systole, with lack of apposition of the leaflet free margins. Floppy tricuspid valves show the greatest degree of annular dilatation, usually greater than 14 cm.

The tricuspid valve in Ebstein's anomaly resembles the floppy tricuspid valve in appearance.[43] The hallmark of Ebstein's anomaly is the apically displaced annular insertion of the tricuspid valve leaflets, which produces a large right atrium and a dilated annulus. Apical displacement of the tricuspid valve results in a septal leaflet displacement of > 8 mm from the mitral valve insertion.

Functional tricuspid regurgitation occurs with normal leaflets and chordae tendineae with moderate annular dilatation of between 12–14 cm, and pulmonary systolic pressures ≥ 55 mmHg.

In infective endocarditis there is usually focal thickening with or without vegetation and frequently ruptured chordae tendineae. The tricuspid annulus is usually normal.

Tricuspid regurgitation due to carcinoid is associated with thickened leaflets and chordae tendineae from deposition of fibrous plaque, which appears echo bright

Table 4.1 Tricuspid apparatus morphology in pure regurgitation

Etiology of TR	Leaflet area	Annulus dimension
Rheumatic	Normal	Normal
Carcinoid	Normal	Normal
Tricuspid prolapse	Increased	Increased
Ebstein's anomaly	Increased	Increased
Endocarditis	Normal	Normal
Papillary muscle dysfunction	Normal	Normal
Cor pulmonale	Normal	Increased
Functional TR	Normal	Increased
Dilated cardiomyopathy	Normal	Increased
Trauma	Normal	Normal

while the annulus is usually normal. Plaques may extend on to the ventricular myocardium, causing the leaflets to adhere to the right ventricular wall and preventing coaptation during systole.

Papillary muscle dysfunction may produce pure tricuspid regurgitation due to fibrosis, necrosis and atrophy of the papillary muscle from coronary artery disease. The tricuspid valve apparatus usually appears normal in the setting of papillary muscle dysfunction.

Doppler and tricuspid regurgitation

Color flow Doppler is most useful for the detection of tricuspid regurgitation.[44–46] The regurgitant jet is represented as a blue, flame-shaped jet in the right atrium whose length, width and jet area can be measured. This provides a semiquantitative estimate of the severity of tricuspid regurgitation (figure 4.6). Color flow Doppler is extremely useful for the detection of mild tricuspid regurgitation, and in allowing the proper determination of alignment of the conventional (pulsed or continuous wave) Doppler beam for the calculation of the right atrial–right ventricular systolic pressure difference using the peak velocity of the regurgitant signal and the modified Bernoulli equation $(P_1-P_2) = 4[V_{max}]^2$,[35,45,47] (figure 4.7). Pulmonary arterial systolic pressure can be obtained by the addition of the clinical estimate of the height of the jugular venous pressure or by adding 14 mmHg[35] derived from the regression equation in which simultaneous Doppler recording and direct measurements of pulmonary arterial pressure are compared.[45,47] Continuous wave Doppler velocity signals in tricuspid regurgitation show holosystolic flow with peaking in mid-systole.
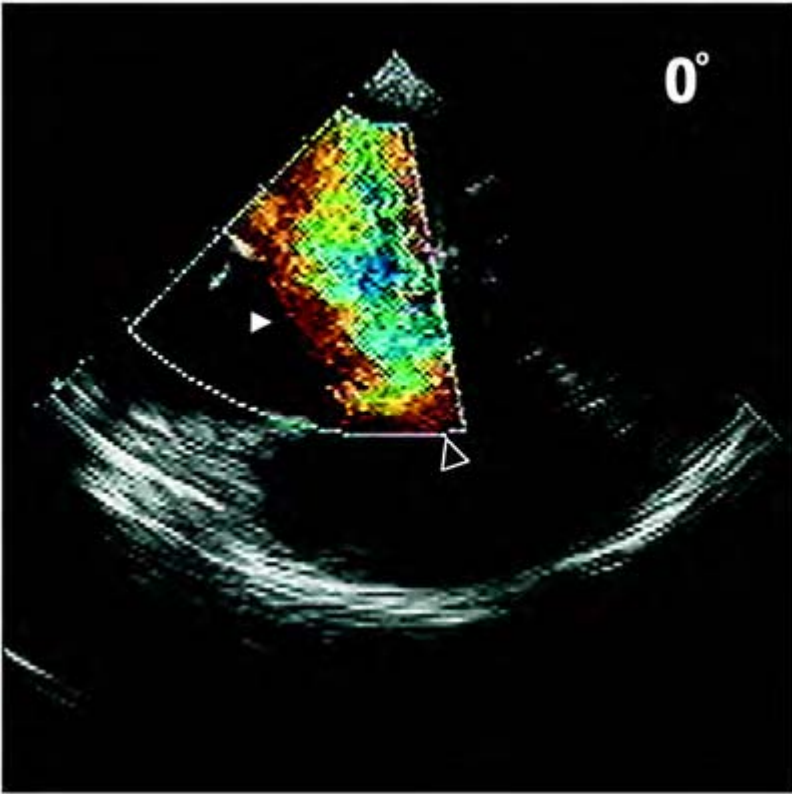
Figure 4.6 Color flow Doppler is most useful for the detection of tricuspid regurgitation. The regurgitant jet (arrow) is represented as a blue, flame-shaped jet in the right atrium whose length, width and jet area can be measured, to provide a semiquantitative estimate of the severity of tricuspid regurgitation. RA, right atrium; RV, right ventricle; TV, tricuspid valve.
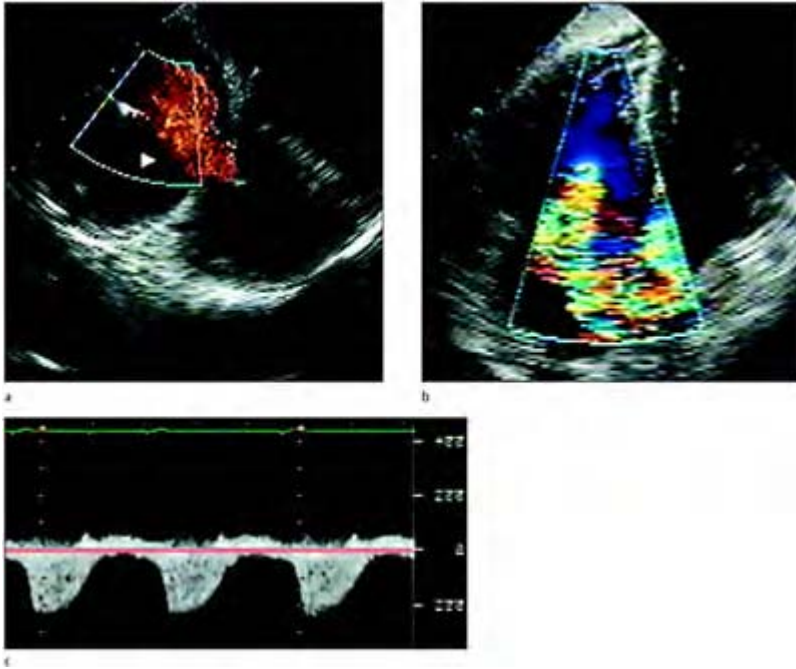
Figure 4.7 Color flow Doppler is extremely useful for the detection of tricuspid regurgitation (arrows), and in allowing the proper determination of alignment of the conventional (pulsed or continuous wave) Doppler beam for the calculation of the right atrial–right ventricular systolic pressure difference using the peak velocity of the regurgitant signal and the modified Bernoulli equation.

When severe tricuspid regurgitation develops because of high right-sided filling pressures and right ventricular failure, the tricuspid regurgitation signal peaks earlier and develops a late systolic shoulder signifying secondary right ventricular failure[48] (figure 4.8).

Estimating the regurgitant fraction, which is the difference between volumes across the tricuspid and pulmonary valves, enables a quantitative estimate of the severity of tricuspid regurgitation. Volume flow across the tricuspid and pulmonary valves is calculated as the product of the respective flow velocity integrals and cross-sectional areas of the flow streams expressed as a percentage of the total flow across the tricuspid

valve. Calculation of the regurgitant fraction for tricuspid insufficiency is best calculated by transthoracic echocardiography.
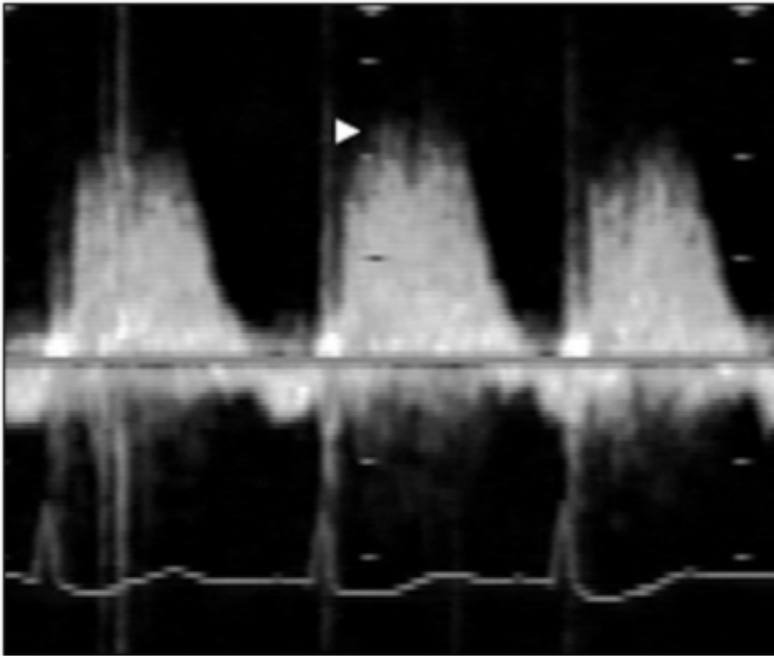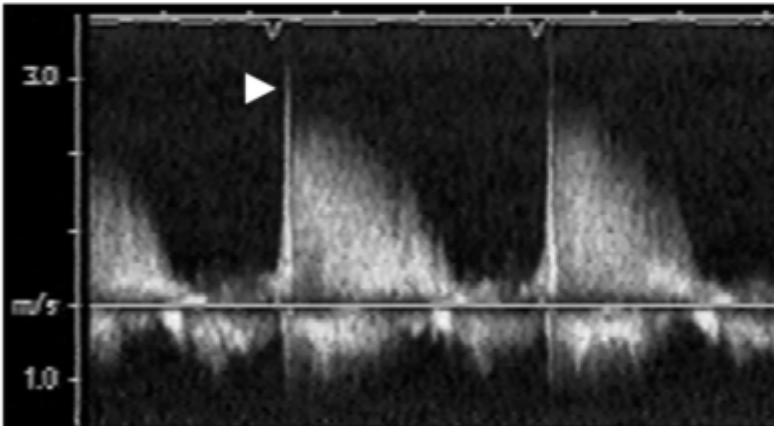
Figure 4.8 Continuous wave Doppler velocity signals in tricuspid

regurgitation show holosystolic flow
with peaking in mid-systole (a). When
severe tricuspid regurgitation develops
due to high right sided filling pressures
and right ventricular failure, the
tricuspid regurgitation (arrow) signal
peaks earlier and develops a late
systolic shoulder signifying secondary
right ventricular failure (b).

+1 Tricuspid regurgitation	2 cm^2
+2	2–4
+3	4–10
+4	10+

In patients with severe tricuspid regurgitation systolic flow reversal is recorded in the hepatic veins.[49] In moderate regurgitation, normal forward flow is typically absent or diminished.

The prevalence of physiological tricuspid regurgitation increases with age and physical conditioning.[50,51] Physiological regurgitation is present in 8% of patients less than 20 years of age and in 30% of patients over than 60 years of age. Physiological regurgitation occurred in 93% of athletes studied but only in 24% of patients labeled as sedentary. Physiological regurgitation is visualized as small flow jets projecting less than 2.5 cm into right atrium or as flow jets with a jet area/right atrial area ratio of less than 18%.

Tricuspid annular calcification

Calcification of the tricuspid annulus occurs much less frequently than calcification of the mitral annulus; however, the two commonly occur together, especially in the elderly and in association with aortic sclerosis. Mattelman et al[52] studied 80 patients retrospectively with a two-dimensional echocardiographic diagnosis of mitral annular calcification, and detected only one patient with tricuspid annular calcification. Isolated, tricuspid annular calcification may also occur secondarily to long-standing pressure or volume overload of the right ventricle and has been described with pulmonic stenosis, atrial septal defect or with cor pulmonale.[53,54] Tricuspid annular calcification is readily distinguished as increased reflectiveness of the posterior tricuspid annulus in the four chamber lower esophageal views at 0 degrees and in the two chamber transgastric views at 90 degrees (figure 4.9).

Endocarditis

In patients with suspected right-sided infective endocarditis, transesophageal echocardiography is mandatory when the right heart valves are not well visualized by transthoracic echocardiography. Right-sided infective endocarditis occurs less commonly than left-sided endocarditis. In a study of 137 hearts with infective endocarditis the right heart was affected in 23 or 17% of cases.[14] In that study
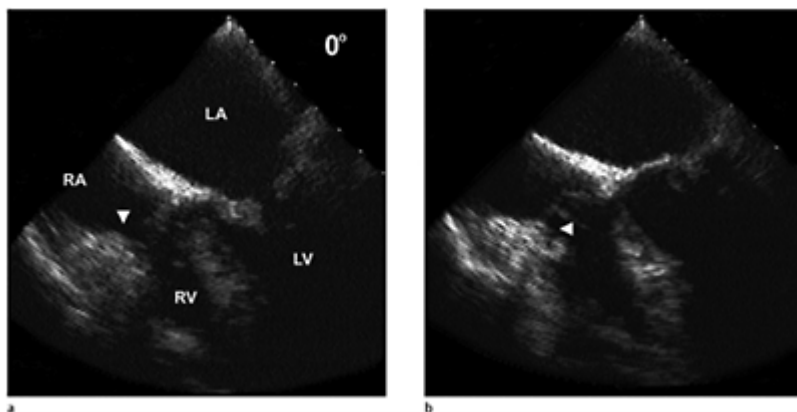
Figure 4.9 Tricuspid annular calcification (arrow) is readily distinguished as increased reflectiveness of the posterior tricuspid annulus in the four chamber lower esophageal views at 0 degrees (a, b) and the two chamber transgastric views at 90 degrees. RA, right atrium; LA, left atrium; TAC, arrow; RV, right ventricle; LV left ventricle.

Arnett reported that infective endocarditis of the right side usually involves the tricuspid valve (9% of cases) with or without pulmonary valve vegetation. Intravenous drug abuse is the most common cause of isolated right-sided infective endocarditis. Other factors associated with right-sided infective endocarditis include alcoholism, neoplasms, infected indwelling catheters, multiple pacemaker leads, extensive skin burns, and immune deficiency disorders. Frequently patients with right-sided infective endocarditis present with the signs and symptoms of pneumonia or lung abscess secondary to septic emboli.

Bacterial vegetations associated with tricuspid valve endocarditis vary greatly in size, but are usually larger than aortic or mitral valve vegetations and commonly occur on previously normal valve leaflets. Vegetations appear as sessile or pedunculated irregular

masses attached to one or more valve leaflets, or chordae tendineae.[34,58–60] Ginzton et al[35] followed eight patients with tricuspid valve vegetations for a mean of 11 months. In four patients the vegetation disappeared, in three it was found to be smaller, and in one it remained the same size. The presence of a vegetation at follow-up study and rate of regression do not correlate with clinical outcome during the acute illness or with functional class at late follow-up. Valve ring abscess was present in 17% of cases, and of all myocardial abscesses 57% accompanied tricuspid valve vegetation.[14] Valve ring abscess may occasionally burrow into and through the membranous ventricular septum.

Many reports have addressed the sensitivity and specificity of transthoracic and transesophageal echocardiography for the diagnosis of right-sided endocarditis.[56,57] Although vegetations are more precisely characterized by transesophageal echocardiography, both techniques are reliable for the diagnosis of bacterial endocarditis and one should not expect to diagnose a vegetation on transesophageal echocardiography when the transthoracic study is negative. Chirillo et al[56] used discriminate analysis of transesophageal echocardiography characteristics of vegetations to show that chaotic motion was most consistently associated with infective lesions.

In addition to bacterial endocarditis, non-bacterial endocarditis associated with lupus erythematosus and antiphospholid syndrome are rare causes of vegetations in the right heart, typically involving the tricuspid valve.[58–60]

Tricuspid valve prolapse

The true incidence of tricuspid valve prolapse in unknown, and there are no generally accepted criteria for its diagnosis, but it has been reported in association with mitral valve prolapse more frequently than as an isolated finding. The reported incidence of tricuspid valve prolapse has emanated from necropsy studies, but these studies have varied markedly. In a series of 3083 necropsies,[26] myxomatous degeneration of the mitral valve occurred in 30 (1%); in nine (0.3%) of these, the tricuspid valve leaflets were myxomatous and voluminous, consistent with prolapse. Davies et al[27] detected mitral valve prolapse in 102 (7.4%) of 1367 necropsies, of which 41 (3.0%) also had tricuspid valve prolapse. On two-dimensional echocardiography, prolapse of the septal, anterior and posterior leaflets, individually or together, superior to the tricuspid annulus have been described in 19% to 50% of patients with mitral valve prolapse.[61–63] Tricuspid valve prolapse primarily involves the anterior and septal leaflets, and is a common finding in Marfan syndrome.

Ruptured chordae tendineae of the tricuspid valve have been described on echocardiographic studies.[22–25,63] Irregular low-frequency diastolic fluttering, wide excursion of the anterior leaflet and chaotic paradoxical motion of the tricuspid leaflets have been described in association with ruptured tricuspid chordae. In addition, marked prolapse of the tricuspid valve leaflets into the right atrium beyond the valve annular plane occurs with loss of the normal leaflet coaptation. Tricuspid regurgitation invariably results from ruptured chordae with right ventricular dilatation, vigorous contractile function, and a dilated, pulsatile right atrium, with incomplete closure of the tricuspid valve leaflets. Incomplete closure is defined as failure of the tricuspid leaflet tips to reach within 1cm of the plane of the tricuspid annulus in systole.[20]

Tricuspid repair

Various techniques have been used for repair of the tricuspid valve[4,64–77](figure 4.10). Kay and DeVega have used suture techniques for remodeling the tricuspid valve annulus in tricuspid regurgitation. Carpentier and Duran have developed annuloplasty rings that remodel the annulus and have also described techniques for total repair of the tricuspid apparatus. Despite controversy over when to repair, replace or do nothing to the tricuspid valve, various reports have shown promising results in the setting of tricuspid valvular disease.

Carpentier and Duran techniques

The principles of tricuspid valve repair for tricuspid regurgitation are the same as for repair of mitral regurgitation.[4,64–68] The right atrial incision is started close to the atrial appendage and directed obliquely downward towards the posterior aspect of the right atrium, between the inferior right pulmonary vein and the inferior vena cava. When a mitral valve repair is also being done, the right atrium is opened parallel to the atrioventricular groove, medial to the cannulation sites. Tricuspid repair is done without aortic cross clamping. The surgeon inspects the valve after opening the right atrium, cognizant of the echocardiographic findings. Functional tricuspid valve regurgitation results when there is more than a 10% increase in annular size and is easily corrected with tricuspid annuloplasty. The annulus is measured with obturators to assess the degree of distention or deformation. Indications for valve repair are based on an annular size greater than a No. 33 obturator in women and a No. 35 obturator in men, with or without organic lesions of the tricuspid valve apparatus.
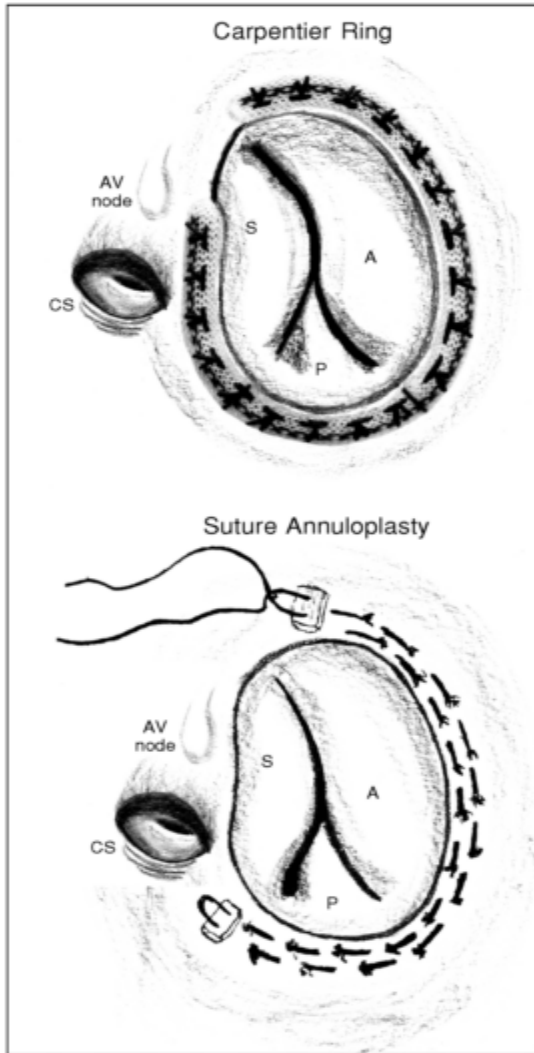
Figure 4.10 Artist's rendition of tricuspid valve reparative techniques. S, septal tricuspid leaflet; A, anterior tricuspid leaflet; P, posterior tricuspid leaflet; CS, coronary sinus; AV node, atrioventricular node.

Figure 4.11 Tricuspid annuloplasty rings. A, Carpentier ring; B, Carpentier ring sizers; C, St. Jude ring.

Annular repair is accomplished by prosthetic annular rings. Deloche and colleagues, have shown that annular dilatation is associated with deformation of the tricuspid orifice.[4] The anteroposterior diameter enlarges to a greater degree than the transverse diameter. Normally the transverse annular diameter is greater than the anteroposterior diameter. Individual regions of the annulus are affected to varying degrees; the posteroseptal and anteroposterior commissures, the posterior and the anterior leaflets and, to a lesser degree, the anteroseptal commissure and the septal leaflet. Tricuspid rings remodel the shape of the annulus as well as reducing the annular size, by selectively reducing the annulus at the commissures rather than the leaflets. Ring sizing is done by measuring the anterior leaflet area with the sizing obturator.

Tricuspid annuloplasty rings. D, Duran ring; E, Duran ring on mounting ring; F, Duran ring sizers.

The Carpentier ring is a fixed ring that conforms to the normal configuration of the tricuspid annulus (figure 4.11). The ring has demarcations that allow the ring to be positioned along the curve of the anterior and posterior leaflets, and one curvilinear segment for positioning along the septal leaflet. The ring is open at the position of the anteroseptal commissure. The Duran ring is a flexible ring, and is the same ring used for the mitral ring (figure 4.11). Both rings are placed on the atrial surface and sutured to the tricuspid annulus.

A previous technique for restoring valve competence was use of a semicircular suture of DeVega or annular plication to reduce the orifice of the tricuspid annulus without restoring the proper annular shape. This procedure may result in annular stenosis.

Commissural fusion is treated by incising and splitting the commissures and placement of an annuloplasty ring. Occasionally it is necessary to resect secondary

chordae to mobilize the leaflet, and occasionally splitting the papillary muscle by at least 1 cm may be indicated to increase leaflet mobility.

Endocarditis vegetations may be resected after adequate (about 15 days) antibiotic therapy, provided that sufficient leaflet tissue remains after resection. Leaflets can be resected or a pericardial patch may be used to repair the leaflets.[77]

Carpentier[67] reported on 1,345 tricuspid valve repairs, of which 1,210 were achieved with ring annuloplasty with a re-operation rate of 0.6%. Organic lesions were present in 30% of patients. Follow-up catheterization in 30 patients demonstrated good results, with significant tricuspid valve stenosis in only one patient with preoperative severe organic disease. A benefit for placement of a tricuspid annular ring is that it does not require long-term anticoagulation.

Transesophageal echocardiography after tricuspid valve repair almost always shows a reduction in the amount of tricuspid regurgitation. The tricuspid valve should be assessed for stenosis, and normally there should be no obstruction to flow. The tricuspid annular ring appears as an area of increased echogenicity on either side of the annulus, with normally moving leaflets and trace to mild residual regurgitation.

Kay technique

Zubiate and Kay first reported the technique of tricuspid annuloplasty in 1964 for the treatment of tricuspid regurgitation and tricuspid stenosis.[69] This technique consists of narrowing the tricuspid annulus by eliminating the posterior leaflet and creating a competent bileaflet tricuspid valve. Two (or at most three) figure-of-eight silk or mattress sutures with Teflon felt are placed in the annulus of the posterior leaflet, until there is a two-finger-breadth opening in the tricuspid valve orifice. When first introduced the competence of the valve was determined by saline injection, but intraoperative transesophageal echocardiography provides a more accurate assessment of tricuspid valve competence.

Kay et al reported on 156 patients with both mitral and tricuspid valve disease, who underwent mitral or tricuspid replacement or repair.[69] Tricuspid repair was accomplished with this method in 127 or 81% of patients. Of the patients who underwent tricuspid annuloplasty, 91% were free from re-operation at 10 years, which was similar to patients with tricuspid valve replacement.

DeVega technique

DeVega described an adjustable tricuspid annuloplasty technique in 1972. This technique consisted of placing double purse-string sutures in the tricuspid annulus encompassing the anterior and posterior leaflets, which were anchored with Teflon felt and passed through the atrial wall. Immediately after cardiopulmonary bypass and after stabilization of hemodynamics, the annular sutures were adjusted to constrict the tricuspid annulus in the beating heart.

Intraoperative transesophageal echocardiography has been advocated to visualize the tricuspid regurgitant jet to assist in adjusting the annular suture.[73–76] The tricuspid regurgitation jet size and severity is estimated semi-quantitatively and tension is placed on the sutures until tricuspid regurgitation is eliminated but before stenosis of the valve is

produced on color flow Doppler mapping in the right ventricular inflow tract. A few reports have described the utility of the DeVega technique as guided by transesophageal echocardiography with good results.[73–76]

Pulmonary valve

Normal anatomy

The pulmonary valve is a semilunar valve composed of three crescent shaped cusps similar to the aortic valve[3,5,78,79] (figure 4.12). The major differences between the pulmonary valve and the aortic valve are (1) the pulmonary valve tissue is noticeably thinner, (2) it has a slightly larger valve orifice area, (3) there is no continuity between the pulmonary and tricuspid valve leaflets, because the right heart valves are separated by the infundibulum and lie in different planes within the fibrous skeleton, and (4) neither cusp normally gives off coronary arteries (5). The pulmonary valve is seated, posterior and slightly cephalad and to the left of the aortic valve within the fibrous skeleton.[3] The valve cusps are thin and translucent in the body of the leaflets. In the centre of the valve cusp near the margin is the node of Arantus. Lunula are formed from fibrous thickening extending in an arc-like fashion from each side of the node along the inferior border of the free margin of the leaflet, with convexity toward the pulmonary artery, ending at the commissures. The free edge superior to this zone of thickening is thin and often fenestrated. The lunula provides a zone for apposition of the cusps during systole. A rim of fibrous tissue or the annulus attaches the cusps to the right ventricular outflow tract. The wall of the pulmonary artery and the juncture of the hingepoints or commissures produce the sinuses of Valsalva, by duplication of the endocardial lining and reinforcement by fibrous tissue. The length of the free edge of each pulmonic valve cusp equals the diameter of the pulmonary artery at the sinus rim, and the combined length of the free edges of the pulmonic cusps equal the circumference of the pulmonary artery at the sinus rim.
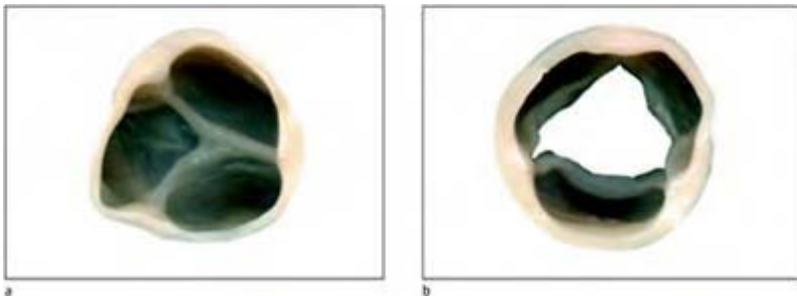
Figure 4.12 Anatomic preparation of the pulmonary valve. The pulmonary valve is seated, posterior and slightly

cephalad and to the left of the aortic valve within the fibrous skeleton. The valve cusps are thin and translucent in the body of the leaflets. In the centre of the valve cusp near the margin is the node of Arantus. Lunula are formed from fibrous thickening extending in an arc-like fashion from each side of the node along the inferior border of the free margin of the leaflet, with convexity toward the pulmonary artery, ending at the commissures. A, Pulmonary valve closed (diastole); B, Pulmonary valve open (systole).

The terminology used to label the pulmonary cusps has varied in the literature. Since in most cases a pulmonary commissure is almost always adjacent to an aortic commissure, Kerr and Goss have suggested that the pulmonary valve cusps be labeled as right adjacent, left adjacent and opposite cusps in reference to the aortic valve cusps.[80]

Similar to the aortic valve, the pulmonary valve may be quadricuspid, bicuspid or unicuspid. The quadricuspid pulmonary valve is the most common variant, which functions normally in 94–96% of cases.[81,82] Unicuspid pulmonary valves comprising acommissural and unicommissural valves are generally stenotic or insufficient, and occasionally both.[83]

Echocardiographic visualization

The pulmonary valve is not easily examined by transesophageal echocardiography, since the pulmonary valve is usually the furthest cardiac structure from the esophageal window. The normal pulmonary valve leaflets are faintly visualized longitudinally, and a short axis projection of the valve is not easily obtained even with multiplane transesophageal echocardiography (figure 4.13). In addition, Doppler techniques are extremely difficult to perform from transesophageal windows since the pulmonary outflow tract is usually orthogonal to the Doppler beam.

The right ventricular outflow tract can be visualized from the deep transgastric view, with the transducer maximally anteflexed with rightward rotation of the probe. The ventricular apex is at the top of the echocardiographic sector, with the right ventricular outflow tract coursing obliquely in the centre of the inferior portion of the sector. This view provides the best opportunity for Doppler interrogation, presenting the right ventricular outflow tract as close to parallel to the ultrasound beam as possible.

A similar view of the right ventricular outflow tract is obtained from the transgastric transducer position with rightward rotation of the probe, with its imaging plane from 90–115 degrees. In this view the right ventricular inflow and outflow tracts may be

visualized in the same echocardiographic sector with foreshortening of the right ventricular apex.
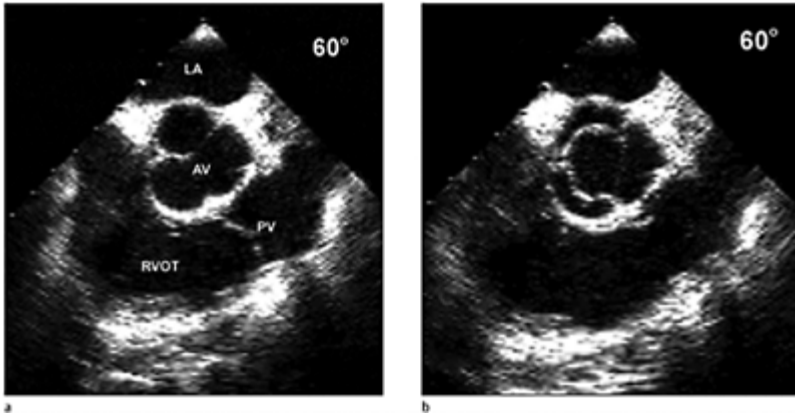
Figure 4.13 The pulmonary valve is not easily examined by transesophageal echocardiography, since the pulmonary valve is usually the furthest cardiac structure from the esophageal window. The normal pulmonary valve leaflets are faintly visualized longitudinally, and a short axis projection of the valve is not easily obtained even with multiplane transesophageal echocardiography. A, Pulmonary valve closed (diastole); B, Pulmonary valve open (systole); LA, left atrium; AV, aortic valve; PV, pulmonary valve; RVOT, right ventricular outflow tract.

A longitudinal view of the right ventricular outflow tract may be obtained from the lower esophageal position with rightward rotation of the probe by steering the transducer to approximately 110–135 degrees. The infundibulum, pulmonary valve and main pulmonary artery are visualized in a longitudinal plane coursing obliquely in the image sector.

The mid to upper esophageal position at 0 degrees produces a horizontal plane of the base of the heart, with the right ventricular inflow tract cut obliquely and the right ventricular outflow tract wrapping around the aortic valve. A small portion of the main

pulmonary artery is seen before it is obscured by the left atrial appendage. With rotation of the transducer from 75 to 90 degrees, the pulmonary valve may be occasionally visualized in its true short axis.

Doppler interrogation of blood flow in the right ventricular outflow tract across the pulmonary valve normally shows laminar flow that peaks in midsystole.

Normal right ventricular outflow velocities in the adult are between 0.6 and 0.9 m/sec with a mean of 0.75 m/sec, which is less than that across the aortic valve owing to the larger valve area of the pulmonic valve.[84]

Pulmonary stenosis

Congenitally malformed valves, rheumatic disease and carcinoid disease may produce pulmonary valve stenosis.[85–90] Pulmonary valve stenosis is rare in patients over the age of 20 years, and survival beyond the sixth decade has been documented only in a few individual reports.[90–93] Calcification of the valve cusps has rarely been reported in congenital pulmonic valve stenosis.[85,94,95] Congenital pulmonic stenosis is often associated with an interatrial communication of the patent foramen ovale or ostium secundum type, with an intact ventricular septum and post-stenotic dilatation of the pulmonary artery.[96]

Large deposits of calcium in the pulmonic valve are exceptional and encountered only in patients older than 40 years with severe stenosis.[85,94,95] Calcific deposits occur
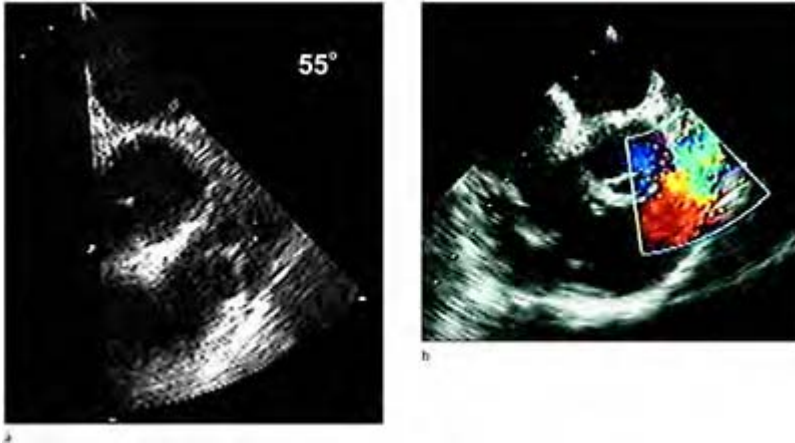
Figure 4.14 Echocardiographic demonstration of pulmonary stenosis. (a) The pulmonic valve is heavily thickened, with calcification and is restricted. Systolic doming is easily seen. With color flow Doppler (b) disturbed and turbulent, high velocity

flow is detected across the pulmonic
valve orifice.

on the ventricular surface of the valve cusps, whereas calcific deposits on the stenotic aortic valves are located predominantly on the aortic surface of the cusps. It is uncertain whether healed infective endocarditis plays an additional part in the formation of calcific deposits. Life expectancy is generally dependent upon the interaction of three main variables: the severity of obstruction, the rate of its progression and the functional adequacy of the pressure-overloaded right ventricle.[97] The severity of the obstruction is the major variable in determining longevity. Severe pulmonary stenosis should be relieved before fibrotic changes develop in the right ventricular muscle.[98–100]

Balloon valvuloplasty for the relief of congenital pulmonic valve stenosis has had a rapid growth in use since its introduction in 1981.[101] Although predominantly used in the pediatric age group,[102] occasionally older patients have benefited from this procedure when oversized[103] or double balloon techniques have been used.[104,105] The recently published VACA study indicates that the greatest use of this procedure has been in the age group of 5–9 years old with a dramatic decline thereafter.[106] Immediately after the valvuloplasty the valve gradient may be estimated using Doppler techniques; however, due to the fluctuation in gradients obtained immediately after the dilatation, final gradients should be measured at least one to two days after valvuloplasty for determining the true residual gradient and estimating long-term results.[107]

Echocardiographic visualization

Pulmonary stenosis is usually diagnosed by imaging techniques and color flow Doppler (figure 4.14). Color Doppler shows flow convergence before the valve orifice, with a decrease in flow area at the valve level, and with flow turbulence distal to the valve in the main pulmonary artery. The severity of the stenosis and degree of post-stenotic dilatation of the pulmonary artery determine the size, shape, direction and length of the turbulent jet distal to the stenotic valve. In more severe cases of pulmonic stenosis the post-stenotic jet increases in velocity and turbulence and decreases in diameter as it is directed towards the left pulmonary artery. Preferential flow to the left pulmonary artery is due to the architecture of the main pulmonary artery and its direct continuity with the left pulmonary artery, which may increase the ratio of left and right pulmonary artery flow to values of 70:30.[108,109]

Grading the severity of stenosis by conventional Doppler techniques is difficult with transesophageal echocardiography since it is almost impossible to direct the Doppler beam parallel to blood flow in the right ventricular outflow tract, even with a multiplane transducer. The best views for orienting the Doppler beam parallel to the right ventricular outflow tract is the deep transgastric view, imaging the right ventricular outflow tract and the pulmonary valve in long axis. In this view, the pulmonary valve area may be measured by the vena contracta method assuming a circular stenotic pulmonary valve orifice. Peak gradients may be estimated in this view, with slight underestimation of the gradient compared with catheterization measurements.[110–114]

Pulmonary regurgitation

Pulmonic valve regurgitation may result from anatomically normal or abnormal valve cusps. The most common cause of pulmonic valve regurgitation is dilatation of the pulmonary trunk and pulmonic valve annulus associated with pulmonary arterial hypertension.[5,87] Pulmonic valve regurgitation also results from congenital or acquired disease such as rheumatic disease, carcinoid, infective endocarditis and trauma. In most patients physiological or trace pulmonic regurgitation is seen with color flow Doppler techniques[115,116] (figure 4.15). Pulmonary valve regurgitation, despite its cause, rarely necessitates valve replacement and follows a benign course.

Color Doppler identifies pulmonary regurgitation as a retrograde, turbulent flow jet originating at the valve plane and directed into the right ventricular outflow tract. The pulmonary artery/right ventricular gradient and regurgitant volume dictates the size and the extent of the color jet. The planimetered jet area indexed for body surface area has also been used as a measure of severity.[84] When compared with angiographic grade, a pulmonary regurgitant area index of 0.64 ± 0.60 cm^2/m^2 is seen with mild regurgitation, 1.07 ± 0.63 with moderate, and 2.2 ± 1.67 with severe regurgitation. The regurgitant index also shows a strong correlation with pulmonary regurgitant fraction by videodensitometric techniques ($r = 0.84$).

Physiological pulmonary regurgitation has been reported in 40–78% of normal valves, without evidence of structural heart disease or pulmonary hypertension.[115,116] Physiological regurgitation is identified with color flow Doppler as small, thin, central jets that extend less than 1 cm into the right ventricle.[115,116]

Endocarditis

Pulmonic valve endocarditis is rare, despite an increase in frequency of right-sided endocarditis. Shapiro et al have suggested that the true incidence of pulmonic valve endocarditis may be higher than previously reported, due to the under detection of pulmonary valve vegetation with transthoracic echocardiography.[117] They reported three cases of pulmonary valve endocarditis diagnosed with transesophageal echocardiography that had negative transthoracic echocardiographic studies. Careful examination of the pulmonary valve should be performed when patients present with clinical evidence of right-sided endocarditis.

Pulmonary artery

Acquired disease of the pulmonary arteries is similar to that affecting the aorta, but its frequency is considerably lower than that of the aorta. Disease of the pulmonary arteries can be categorized according to the pathology, as aneurysmal dilatation or luminal narrowing by obstruction. Diseases of the pulmonary trunk and pulmonary arteries include medial degeneration, atherosclerosis, arteritis, and trauma. Congenital diseases may produce stenosis, atresia, and aneurysm. The most common condition affecting the pulmonary arteries, however, is not in situ disease but pulmonary embolism, from thrombi formed elsewhere in the systemic venous system.

Normal anatomy

The pulmonary trunk originates from the right ventricular outflow tract and branches into the right and left main pulmonary arteries (figure 4.16). The length of the pulmonary trunk averages 4 to 5 cm, with an internal diameter of 2 to 3 cm. The internal diameter of the pulmonary artery is usually smaller compared with the adjacent segment of the aorta.[118] The diameter and thickness of the intima and media increase in size with advancing age.[119] The right pulmonary artery forms an acute angle, usually around 90 degrees as it branches from the pulmonary trunk, following a horizontal course almost parallel to the roof of the atria. The left pulmonary artery projects as an extension of the pulmonary trunk in an antero-posterior direction into the chest. The ductus arteriosum comes off the superior portion of the bifurcation of the main pulmonary artery, towards the left chest and joins the inferior surface of the junction of the distal aortic arch and descending thoracic aorta. The aorta and the pulmonary trunk share adventitia with the aorta on its right antero-lateral surface.[120]
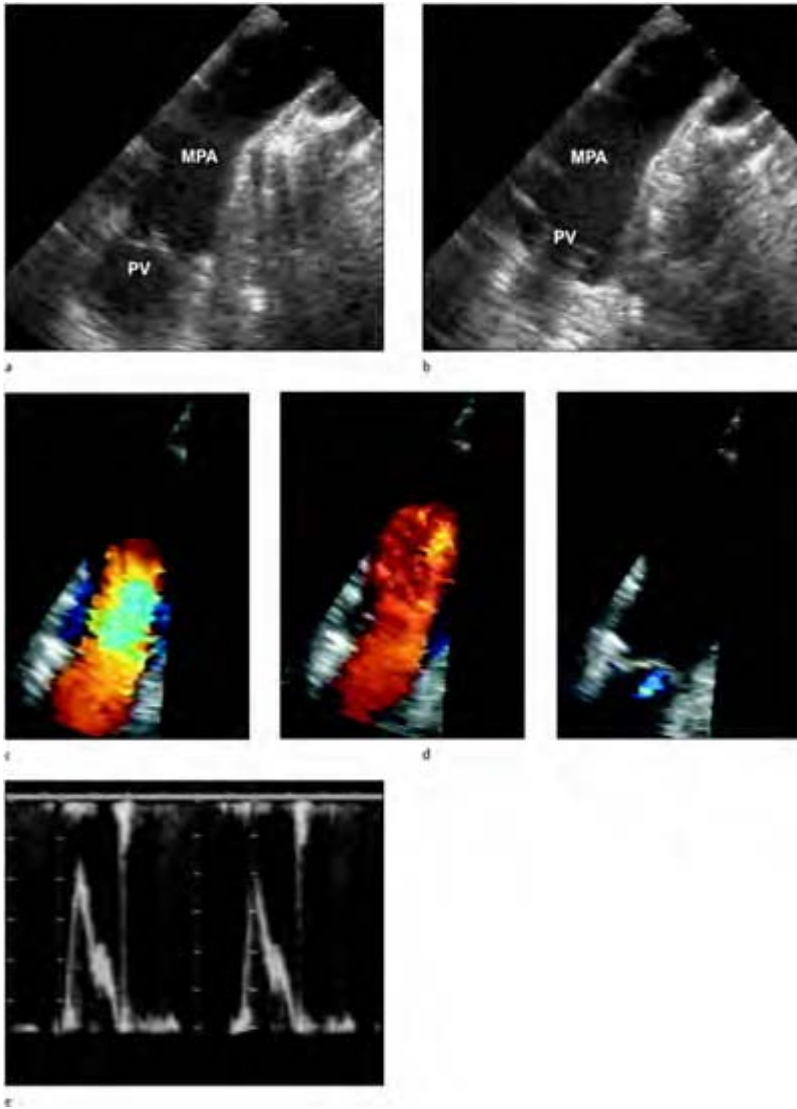
Figure 4.15 Pulmonary regurgitation. In most patients physiological or trace pulmonic regurgitation is seen with color flow Doppler techniques. Pulmonary valve regurgitation, despite the cause, rarely necessitates valve replacement and follows a benign course. Color flow Doppler identifies pulmonary regurgitation as a retrograde, turbulent flow jet originating at the valve plane and directed into the right ventricular outflow

tract. The pulmonary artery/right ventricular gradient and regurgitant volume dictates the size and the extent of the color jet. MPA, main pulmonary artery; PV, pulmonary valve.
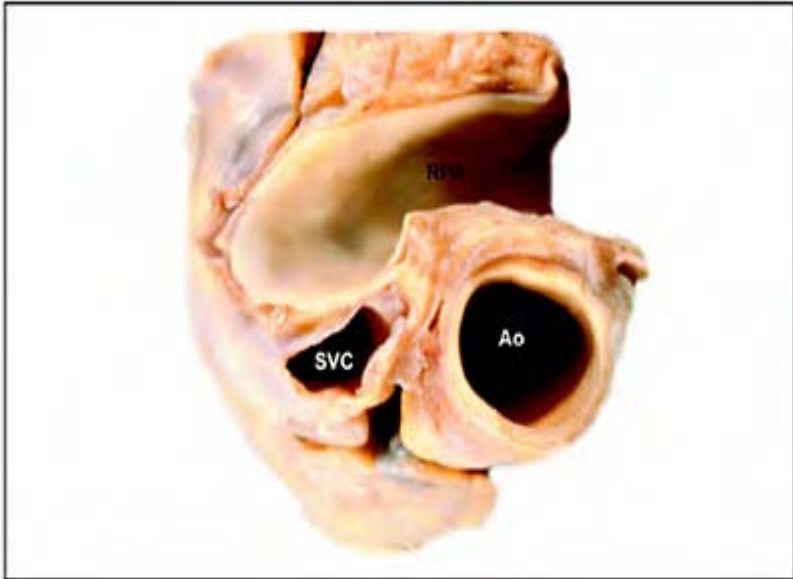
Figure 4.16 Anatomical preparation of the great arteries as visualized from the upper esophageal windows. The pulmonary trunk originates from the right ventricular outflow tract and branches into the right and left main pulmonary arteries. The length of the pulmonary trunk averages 4 to 5 cm, with an internal diameter of 2 to 3 cm. The internal diameter of the pulmonary artery is usually smaller in comparison to the adjacent segment of the aorta. Ao, aorta; SVC, superior vena cava; RPA, right pulmonary artery; MPA, main pulmonary artery.
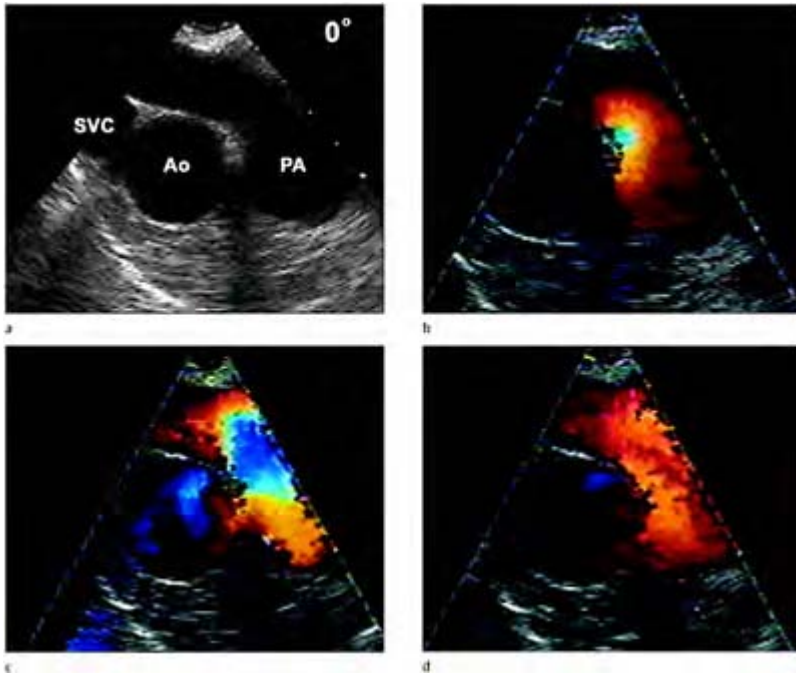
Figure 4.17 The pulmonary artery is visualized in the upper esophageal position with the transducer in the neutral or anteflexed position at 0 degrees. The main pulmonary artery and the proximal bifurcation of the right and left pulmonary arteries are visualized (a). Rotating the probe slightly to the right visualizes the right pulmonary artery coursing horizontally in a longitudinal projection and can often be followed out to the first branches. Rotating the probe slightly to the left visualizes a short segment of the left pulmonary artery in short axis. Normal systolic color flow pattern of the pulmonary artery (b–d). Ao, aorta; SVC, superior vena cava; PA, pulmonary artery.

Echocardiographic evaluation

The pulmonary artery is visualized in the upper esophageal position with the transducer in the neutral or anteflexed position at 0 degrees (figure 4.17). The main pulmonary artery and the proximal bifurcation of the right and left pulmonary arteries are visualized. Rotating the probe slightly to the right visualizes the right pulmonary artery coursing horizontally in a longitudinal projection and can visually be followed out to the first branches. Rotating the probe slightly to the left visualizes a short segment of the left pulmonary artery in short axis.

Idiopathic dilation

Although rarely encountered, the most common reason for pulmonary artery enlargement is idiopathic dilation.[118,121] Idiopathic dilation of the pulmonary trunk is poorly understood as it has been labeled as a forme fruste of Marfan syndrome, since histology of the artery wall reveals focal disruption of the elastica, not dissimilar to cystic medial necrosis.[122,123]

Aneurysms

Aneurysm of the pulmonary trunk and the main pulmonary artery are extremely rare, with an incidence of 0.04% in a necropsy study by the National Heart, Lung and Blood Institute.[124] Most aneurysms of the pulmonary artery are associated with left-to-right shunts, and have also been described with Marfan syndrome, primary pulmonary hypertension,[125] mitral stenosis,[126] mycotic aneurysm,[118] tuberculosis and syphilis.[126–130] Pulmonary artery aneurysms that have been described without pulmonary hypertension are post-stenotic dilation, trauma and Marfan syndrome. Despite these reports, most cases of pulmonary artery aneurysm are judged congenital.[126] Pulmonary artery aneurysm typically involves the pulmonary trunk with or without its branches in 80–90% of cases.[130] The right pulmonary artery is involved more frequently than the left pulmonary artery, in 8% of cases compared with 3%.[126] Rupture of pulmonary artery aneurysms has been reported in 11% of cases.[130]

    Medial degeneration of the pulmonary arteries occurs in Marfan syndrome with histological changes similar to that found in the aorta.[121] The media of the pulmonary trunk and main pulmonary arteries may contain an increased amount of mucopolysaccharides with pools of mucoid material.[121]

    Case reports of arteritis have been reported with tuberculosis and syphilis.[89] Most vasculitides, Wegener's granulomatosis, lymphomatoid granulomatosis, and necrotizing sarcoid angiitis involve the intrapulmonary pulmonary arteries and spare the main pulmonary arteries.[131]

Atherosclerosis

With advancing age, the intima of the pulmonary artery thickens from its single layer of endothelial cells in youth. Thickening and focal patches of atherosclerotic plaque occur predominately at bifurcation points in patients with pulmonary hypertension and/or hyperlipidemia.[132,133]

Atherosclerosis of the pulmonary arteries is a rather common finding at necropsy. Moore et al described necropsy findings in 337 consecutive adults older than 15 years.[133] Pulmonary artery atherosclerosis correlated significantly with age, right ventricular dilatation and hypertrophy, pulmonary emphysema, pulmonary embolization and aortic atherosclerosis.

Dissection

Dissection of the main pulmonary arteries is a rare complication of dilated pulmonary artery secondary to chronic pulmonary arterial hypertension.[134–138] Pulmonary dissection may also occur with normal pulmonary pressures as in idiopathic dilatation, chronic arteritis (syphilis and tuberculosis), right heart endocarditis, amyloidosis and bronchogenic carcinoma. In most published case reports, the diagnosis was made at necropsy; however, recent reports have described diagnosis of dissection with echocardiography, and cine-magnetic resonance imaging.[138] In many cases, death is caused by pulmonary artery dissection with pericardial tamponade produced by bleeding into the mediastinum.

Steurer et al reviewed 28 cases of pulmonary artery dissection that preceded their cases in the literature.[134] Clinical symptomatology with pulmonary artery dissection was non-specific, 82% of patients experienced dyspnea, 67% had retrosternal chest pain that resembled the pain of aortic dissection or myocardial ischemia, and 52% had central cyanosis. In seven patients with dissection, right heart catheterization showed raised pulmonary artery pressures equal to systemic pressure.

In review of necropsy findings in patients with pulmonary artery dissection, the dissection was located in the first 2 or 3 cm of the main pulmonary artery. In five patients there was more than one intimal dissection and in four patients the dissection was associated with a true aneurysm. Two patients had chronic dissection that did not result in pulmonary artery rupture. Most patients had atherosclerosis and/or cystic medial necrosis.

Transesophageal echocardiography is extremely helpful in diagnosing pulmonary artery dissection and compliments transthoracic echocardiography in making the diagnosis.

Pulmonary embolism

The most frequent disease of the pulmonary arteries is pulmonary artery embolism. The diagnosis of pulmonary embolism can be difficult to establish since the clinical manifestations are similar to those of other cardiopulmonary disorders.[139,140] The characteristic symptoms and signs, which include dyspnea, chest pain, tachypnea, and hypotension, are not specific for definitive diagnosis of pulmonary embolism. Accurate diagnosis is important since untreated in-hospital mortality is up to 30%, whereas it is only 8% if diagnosed and treated appropriately.[140] When transesophageal echocardiography is performed in critically ill patients, unsuspected pulmonary embolism is frequently observed.[141–145]
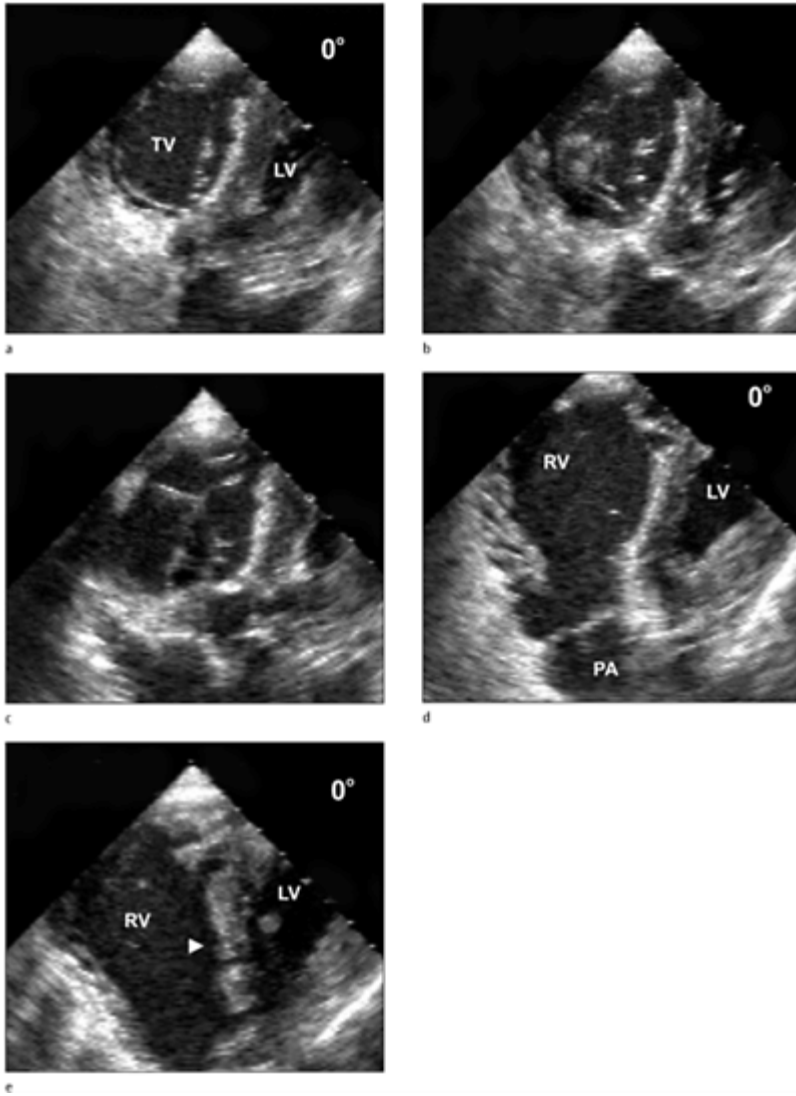
Case 4.1 Pressure/volume overload of the right heart. Short axis (enface) views of the tricuspid valve are obtained with clockwise rotation (towards the patient's right) of the probe in the gastric position at 0 degrees. All three tricuspid valve leaflets are visible and their motion can

be assessed throughout the cardiac cycle (a–c). Best images are usually obtained when the right heart is dilated, as in this study. With mild advancement of the probe past the tricuspid annular plane the right ventricular cavity is visualized in short axis (e) and with mild counterclockwise rotation the right ventricular outflow tract is brought into view (d). Note the flattening of the ventricular septum towards the left ventricle and right ventricular hypertrophy, consistent with pressure/volume overload. TV, tricuspid valve; LV, left ventricle; RV, right ventricle, PA, pulmonary artery.

Wittlich et al assessed the role of transesophageal echocardiography in patients proved to have pulmonary embolism, and detected central pulmonary artery thromboemboli in 35 of 60 patients with pulmonary embolism.[143] Transesophageal echocardiography is a sensitive, specific, and safe technique for diagnosing pulmonary embolus in critically ill patients.[143–145] Transthoracic echocardiography may also show right heart strain, or right ventricular dilatation and increased right ventricular systolic pressures. Kasper et al studied 105 patients with pulmonary embolus by transthoracic echocardiography and found that 75% had right heart dilatation.[146] Transthoracic echocardiography has demonstrated pulmonary embolus passing through the right heart chambers.[147] Thromboemboli in the main pulmonary artery and its bifurcation have rarely been detected by transthoracic echocardiography due to poor visualization of the pulmonary arteries beyond the main pulmonary artery. Establishing a prompt diagnosis of pulmonary embolus favorably affects the short-term outcome in critically ill patients with cardiopulmonary disease. In a study by Patel et al the diagnosis of pulmonary embolus by transesophageal echocardiography altered treatment in 14 patients with clinically unsuspected pulmonary embolus.[141] Ten of 14 patients recovered clinically and were discharged from the hospital while four patients died despite appropriate treatment.
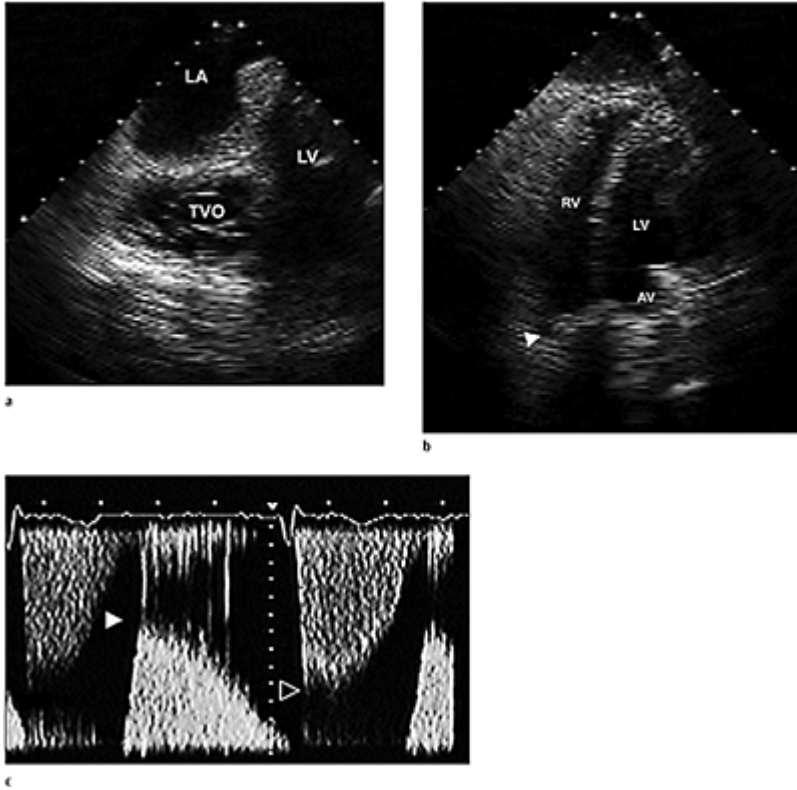
Case 4.2 Tricuspid stenosis. The tricuspid valve may be visualized in short axis from the lower esophageal and transgastric position which is useful for planimetery of the valve orifice when restricted (a). In the deep transgastric view the tricuspid valve is visualized in a longitudinal plane (b) along the annulus (arrow) similar to a four chamber transthoracic image, which shows a small, narrow right ventricular cavity. This view allows an almost parallel orientation for pulsed and continuous wave interrogation (c) of the right ventricular inflow tract for demonstrating tricuspid stenosis

(closed arrow) and regurgitation (open arrow). Although the tricuspid valve is thickened with restricted opening, the valve is rarely heavily calcified as with mitral stenosis, which explains why tricuspid stenosis is frequently overlooked. RV, right ventricle; LV, left ventricle, AV, aortic valve; TVO, tricuspid valve orifice; LA, left atrium.
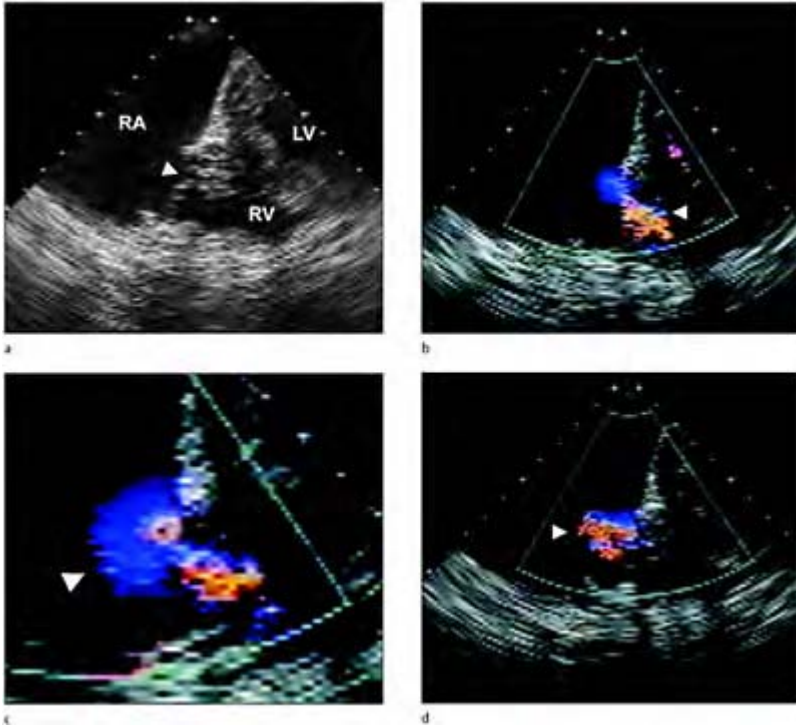
Case 4.3 Tricuspid stenosis and tricuspid regurgitation. In the lower esophageal view the probe is rotated towards the patient's right in a clockwise fashion to assess the tricuspid valve in a longitudinal plane. In a patient with tricuspid stenosis (a) the tricuspid valve apparatus and

leaflets are markedly thickened with restricted amplitude of opening (arrow). The tricuspid annulus is mildly calcified. With color flow Doppler a stenotic flow jet (arrow) is demonstrated in the right ventricular inflow tract (b) and flow convergence (arrow) is seen in zoom mode. During systole a small tricuspid regurgitant jet (arrow) is detected (d). RA, right atrium; RV, right ventricle; LV, left ventricle.
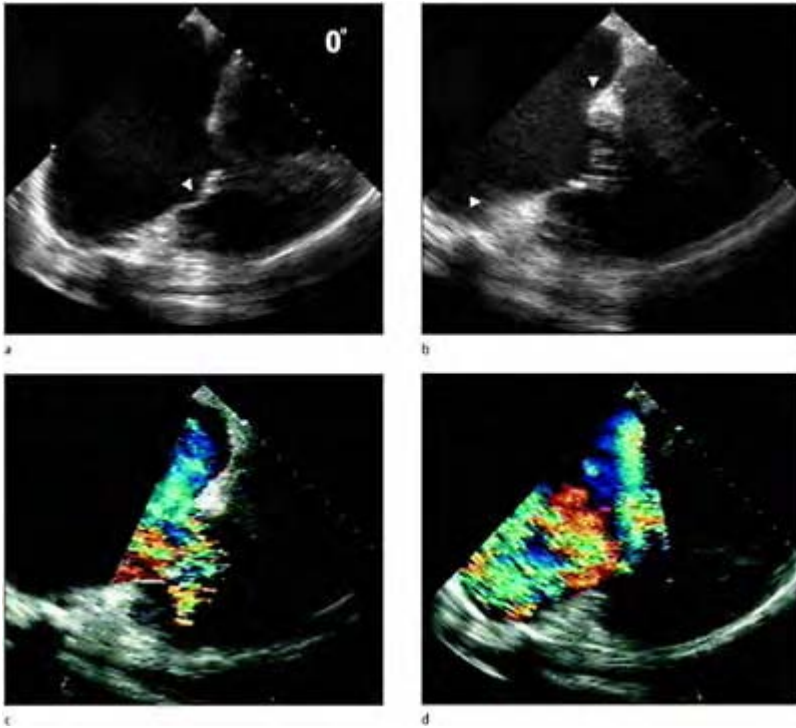
Case 4.4 Tricuspid stenosis and severe tricuspid regurgitation in a patient with rheumatic disease. The tricuspid valve is thickened with decreased mobility and demonstrates diastolic doming (a).

The right atrium is markedly enlarged with severe calcification of the tricuspid annulus (b). Color flow Doppler shows a stenotic jet across the valve (c) with a large regurgitant jet filling almost the entire right atrium (d).
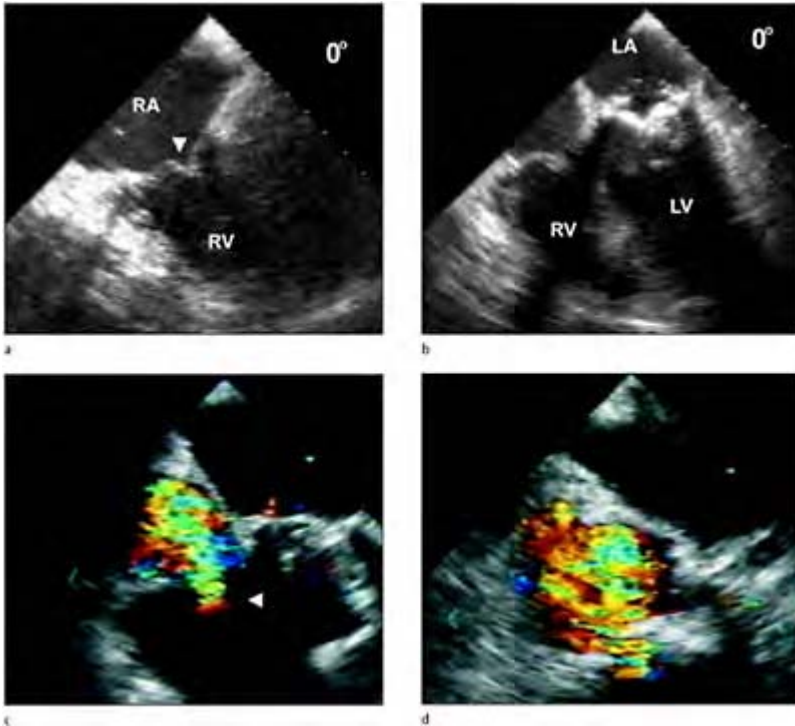
Case 4.5 Rheumatic mitral stenosis and severe tricuspid regurgitation. The tricuspid valve shows annular calcification with leaflet thickening and prolapse (arrow) during systole (a) in a two-chamber view. In a four-chamber view marked mitral stenosis is noted with biatrial enlargement. With color flow Doppler, severe tricuspid regurgitation (c, d) is noted

filling the right atrium. Flow convergence of the regurgitant jet (arrow) is demonstrated.
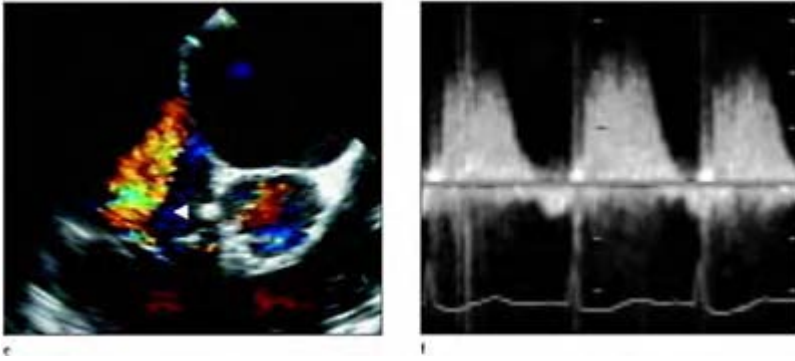
Short axis views of the base of the heart in the upper esophageal position (e) demonstrate the tricuspid regurgitant jet and allow parallel orientation of the jet to permit continuous wave Doppler interrogation of the regurgitant jet (f). LA, left atrium; RV, right ventricle; LV, left ventricle.
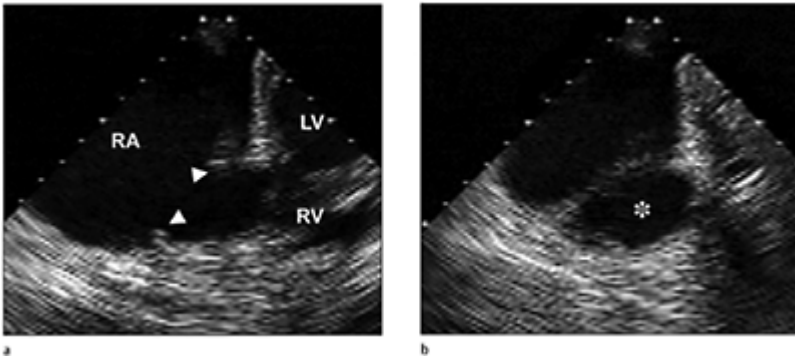
Case 4.6 Tricuspid valve annuloplasty ring. Following surgical implantation of a Carpentier annuloplasty ring, the annular orifice (star) and the ring

(arrows) is shown from manipulation
of the probe between the lower
esophageal and transgastric windows
at 0 degrees. RA, right atrium; RV,
right ventricle; LV, left ventricle.
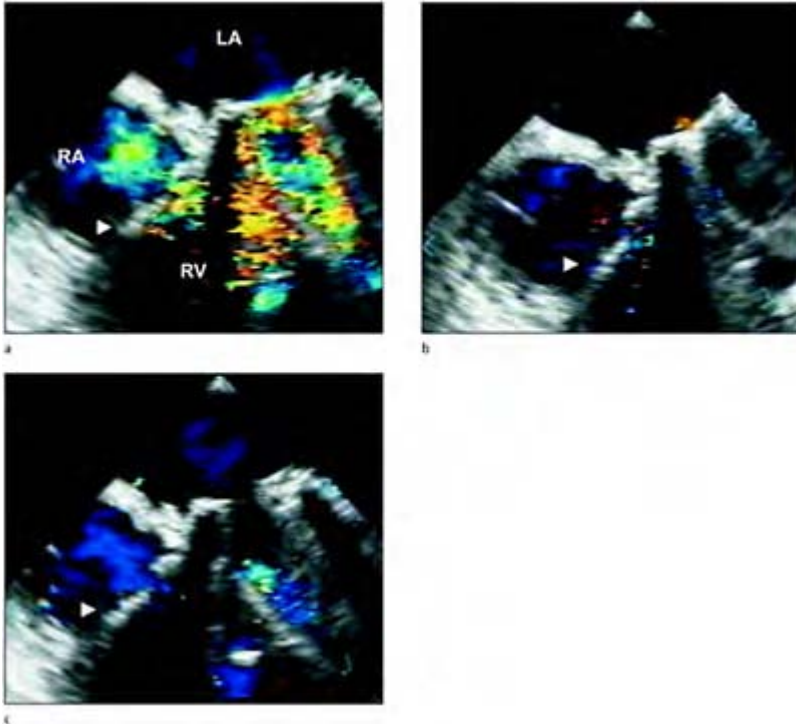
Case 4.7 Color flow Doppler after
surgical implantation of a Carpentier
annuloplasty ring in the tricuspid
position (arrow) and a mitral valve
prosthesis (a). Disturbed flow is
depicted across the tricuspid valve
during diastole. There was no
detectable tricuspid regurgitation
during systole (c, d) with physiological
regurgitation from the mitral prosthesis
(b). RA, right atrium; LA, left atrium;
LV, left ventricle.
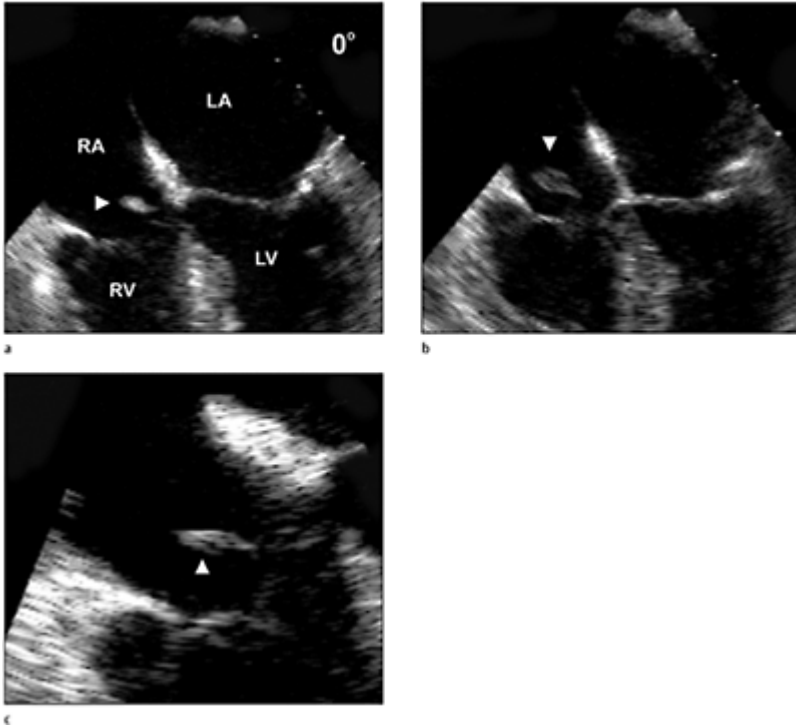
Case 4.8 Tricuspid valve mobile, pedunculated vegetation (arrow) attached to the atrial surface of the septal leaflet as visualized from the mid-lower esophageal window at 0 degrees (a–c). Small tricuspid valve vegetations may require the zoom mode for better appreciation (c). RA, right atrium; RV, right ventricle; LA, left atrium; LV, left ventricle.
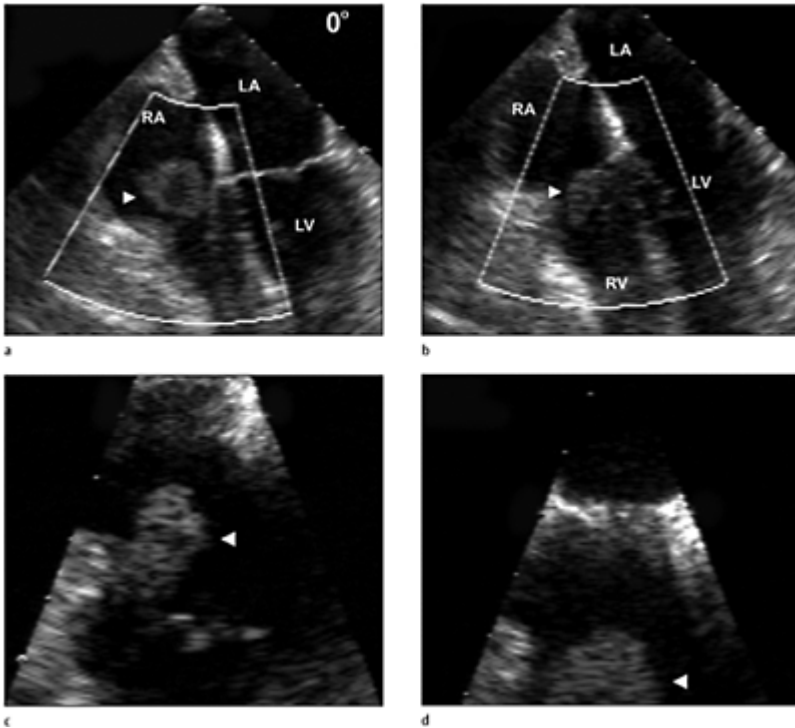
Case 4.9 Fungal endocarditis in an intravenous drug abuser, with a large globular tricuspid vegetation (arrow) producing partial obstruction of the right ventricular inflow tract (a–d). The vegetation is freely prolapsing through the tricuspid valve plane from the right atrium to the right ventricle during the cardiac cycle. RA, right atrium; RV, right ventricle; LA, left atrium; LV, left ventricle.
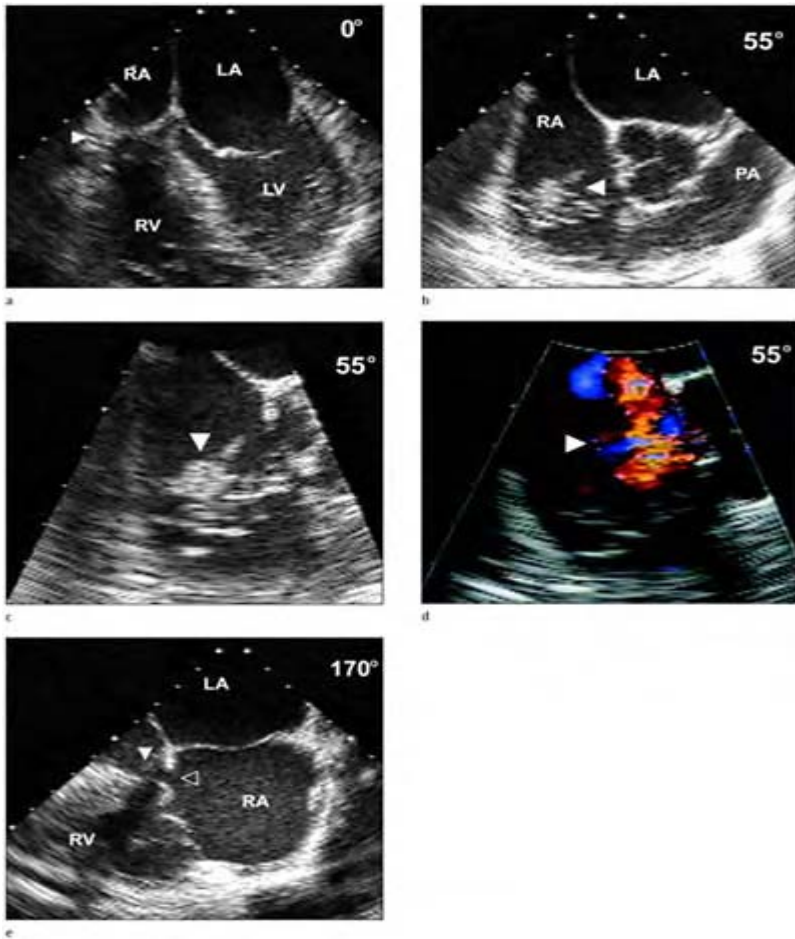
Case 4.10 Tricuspid valve vegetation with an annular abscess and rupture into the right atrium. A shaggy large vegetation (arrow) with finger like projections is demonstrated in multiple views (a–c). Color flow Doppler shows tricuspid regurgitation (arrow) during systole (d). With rotation of the transducer from 90 through 170 degrees the abscess cavity and rupture are demonstrated. Although 0 and 180 degrees are roughly mirror-image echo planes, in this case better posterior cardiac views are obtained of the right heart. An abscess in the tricuspid annulus is suggested at 170 degrees (e) near the membranous portion of the

ventricular septum (closed arrow) with discontinuity of the tricuspid leaflet at the site of attachment (open arrow).
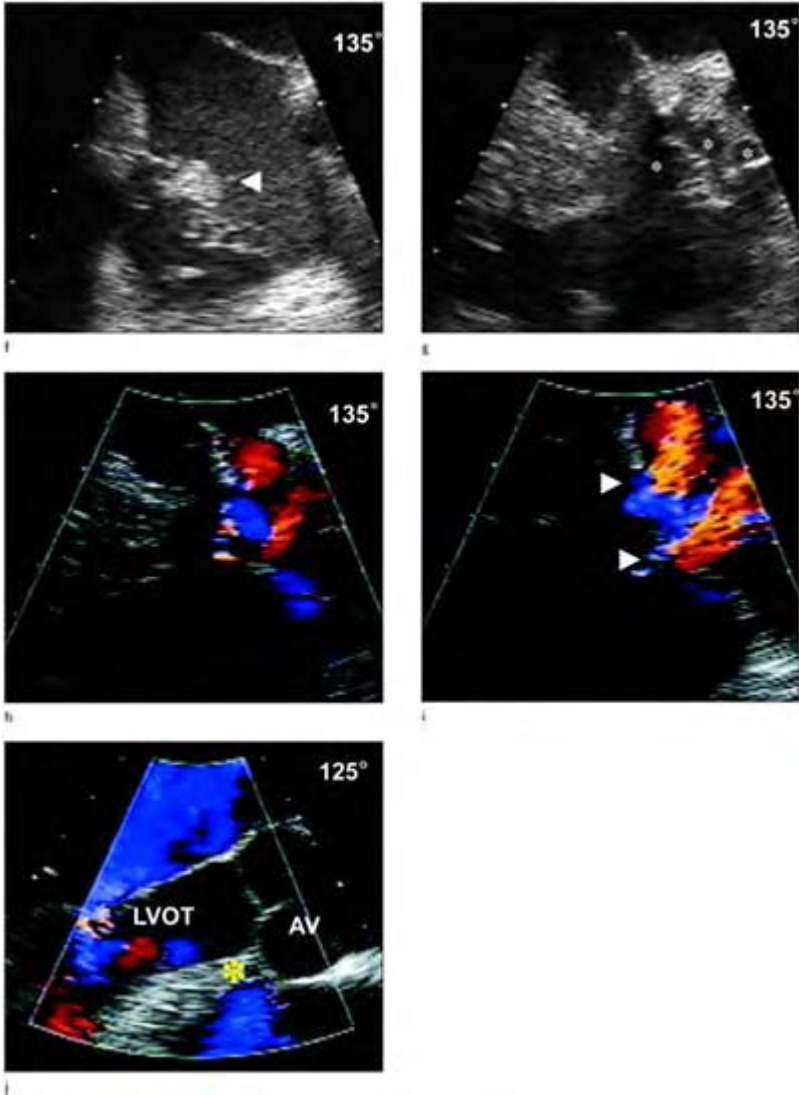
In zoom mode at 135 degrees, the vegetation is noted associated with friable tissue (arrow), which shows chaotic motion (f). With minor

manipulation of the probe the most posterior aspect of the annulus is inspected, which shows the abscess as multiple cystic echolucencies (star) that fill with color Doppler (h). Further manipulation of the probe (i) yields two systolic jets (arrows), which emanate from the tricuspid orifice and near the area of discontinuity of the tricuspid leaflet. Rotating the transducer to 125 degrees (j) to the anterior aspect of the right heart shows normal anatomy of the left ventricular outflow tract and the ventricular septum. RA, right atrium; RV, right ventricle; LA, left atrium; LV left ventricle; PA, pulmonary artery; LVOT, left ventricular outflow tract; AV, aortic valve.
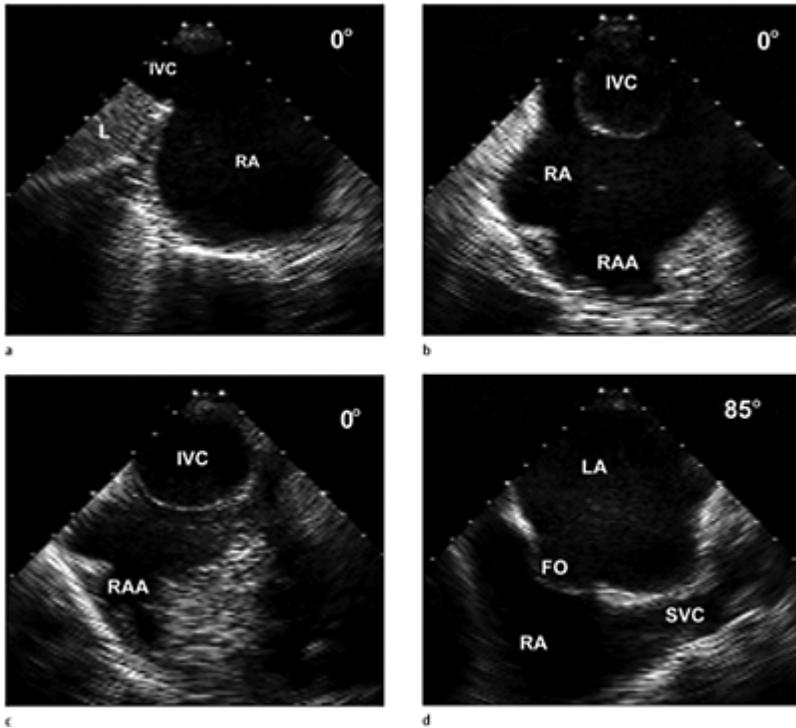
Case 4.11 Multiplane transesophageal echocardiographic demonstration of idiopathic pulmonary artery dilatation. In the transgastric position at 0 degrees with the probe rotated clockwise the inferior vena cava is shown entering the right atrium, which is enlarged (a). Withdrawal of the probe to mid esophageal position with anteflexion visualizes a dilated inferior vena cava in short axis with a full view of the right atrial appendage (b, c). Rotating the transducer to 85 degrees visualizes the bi-caval view of the right atrium (d).
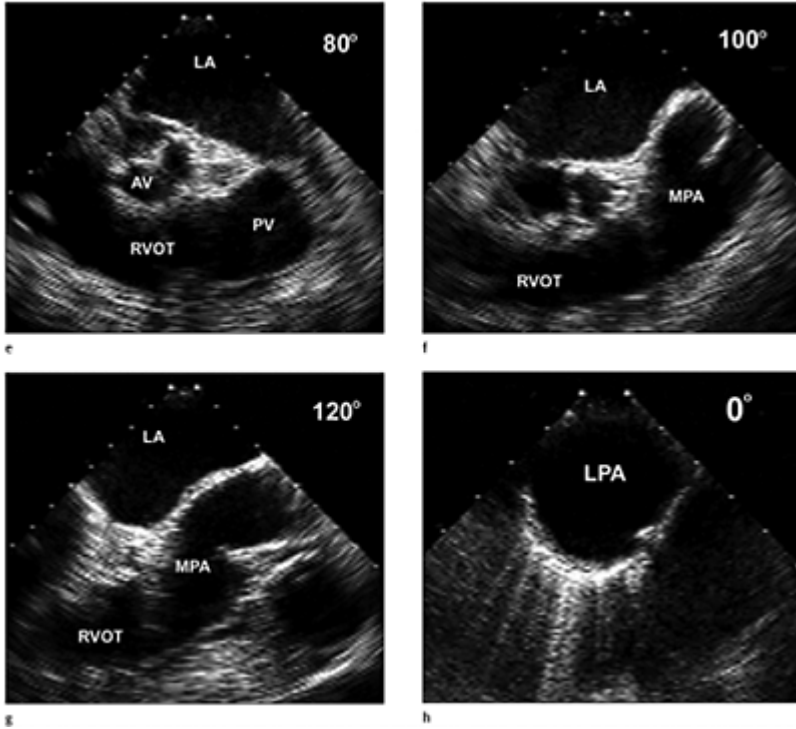
Counterclockwise rotation of the probe and further rotation of the transducer from 80 to 120 degrees visualizes the right ventricular outflow tract and proximal branching of the main pulmonary artery (e–g).
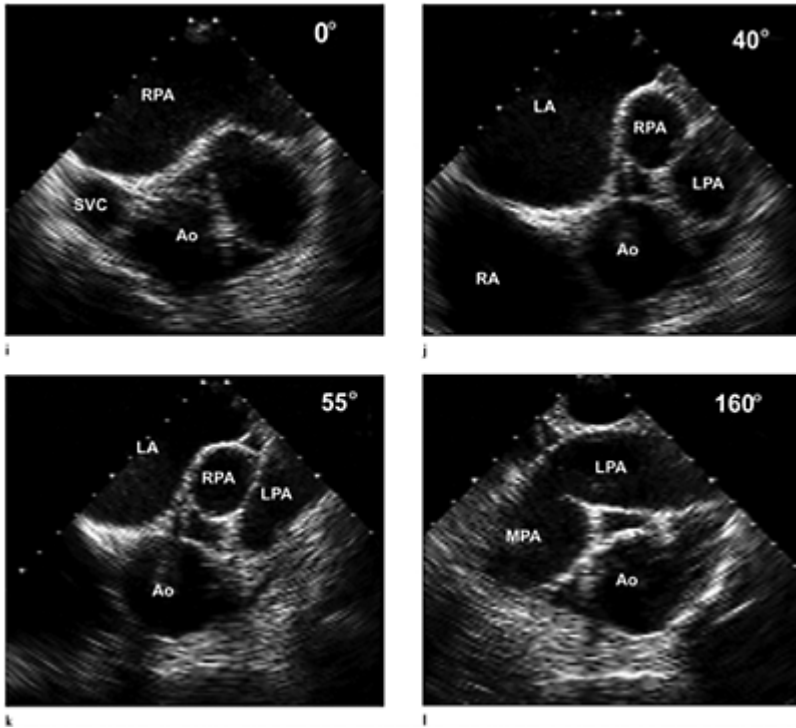
Withdrawal of the probe to the upper esophageal window from 0 to 160 degrees, with mild anteflexion demonstrates dilatation of the main pulmonary artery and the right and left pulmonary arteries (h-l) when compared with the aorta and the surrounding anatomic structures. Normally, the pulmonary arteries are not as well demarcated as they are when dilated.
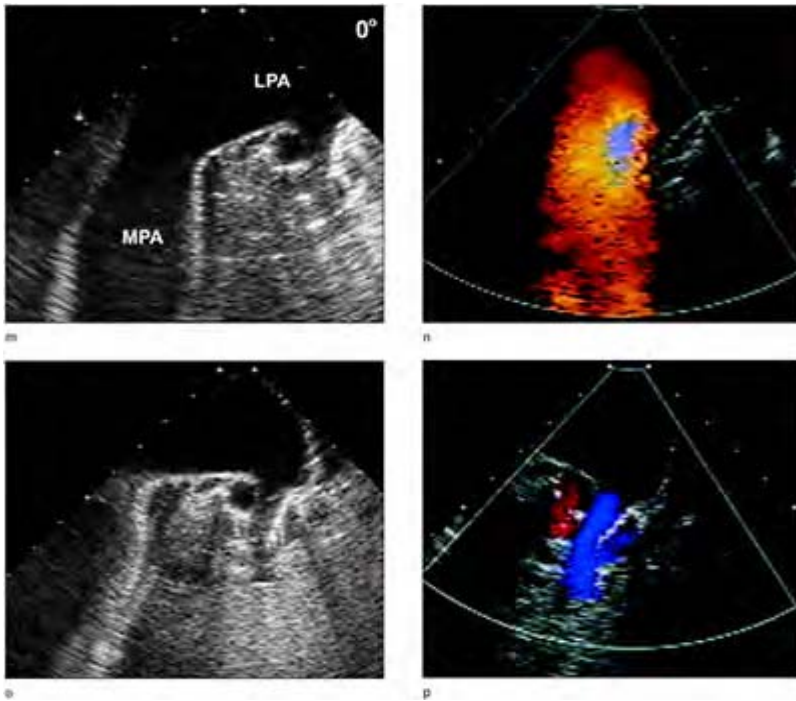
Further withdrawal of the probe in the neutral position allows visualization of the main pulmonary artery with branches in longitudinal projection (m–p). Color flow Doppler shows flow in the pulmonary artery (n) and branches (p), which also allows for parallel orientation of pulmonary flow for interrogation with conventional Doppler. IVC, inferior vena cava; RA, right atrium; RAA, right atrial appendage; LA, left atrium; SVC, superior vena cava; FO, foramen ovale; AV, aortic valve; RVOT, right ventricular outflow tract; PV, pulmonary valve; MPA, main pulmonary artery; LPA, left pulmonary artery; RPA, right pulmonary artery; Ao, aorta.
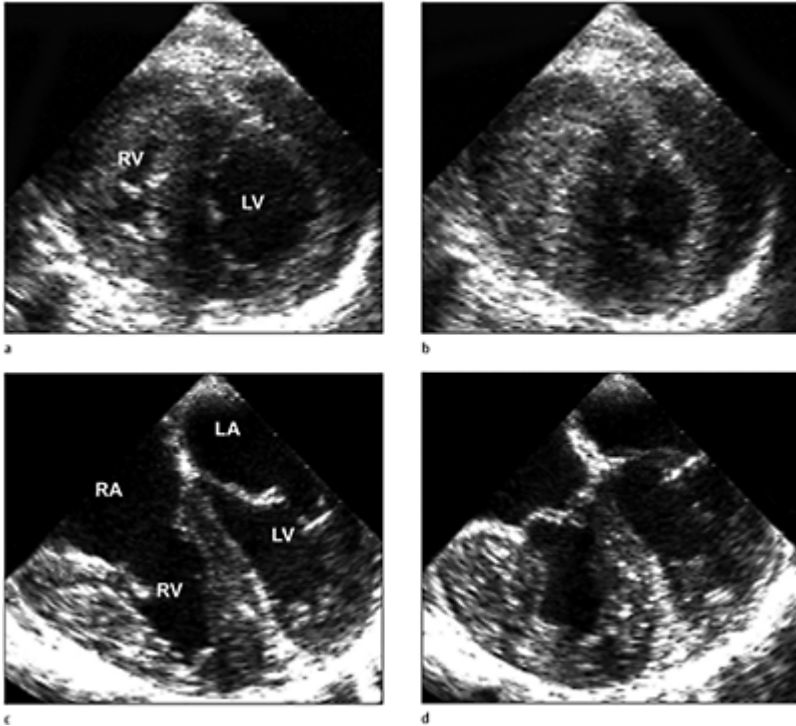
Case 4.12 Right ventricular hypertrophy. Short axis transgastric views of the right and left ventricle obtained at 0 degrees. Diastolic frame (a) and systolic frame (b) show markedly thickened right ventricular walls and near cavity obliteration during systole. Four-chamber view from the lower esophageal view with mild retroflexion at 0 degrees shows right ventricular wall thickening during diastole (c) and systole (d). RA, right atrium; LA, left atrium; RV, right ventricle; LV, left ventricle.
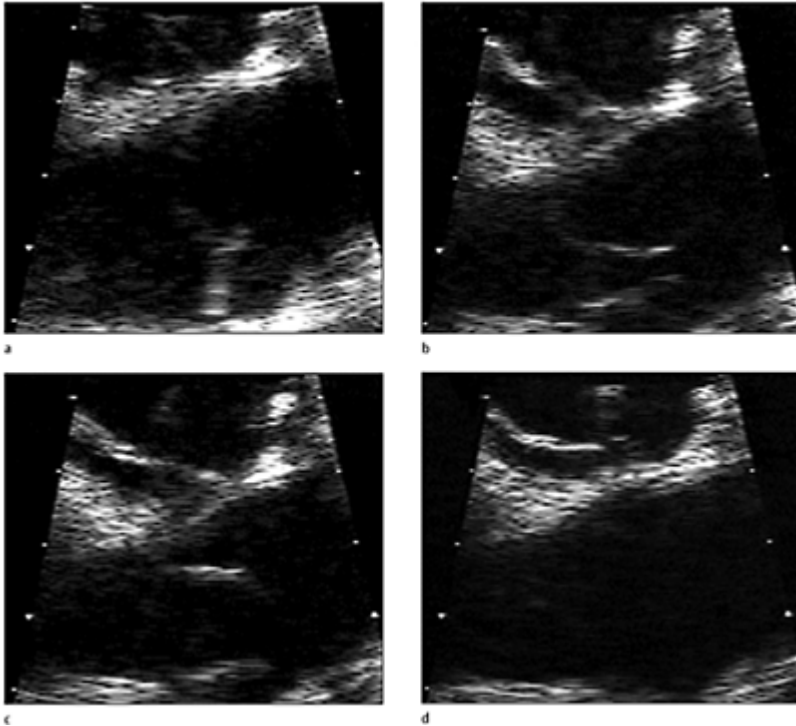
Case 4.13 Normal pulmonary valve. The pulmonary valve is not as well visualized as the other cardiac valves, even with transesophageal echocardiography, largely due to its thin leaflets and the valve's distance from the esophagus. Longitudinal (a–d) and short axis (e–g) views of the normal pulmonary valve in zoom mode throughout the cardiac cycle from diastole to systole, obtained from the mid to upper esophageal window at 60 degrees. The leaflets are not fully visualized, as they move out of plane especially in the short axis views.

e

f

g
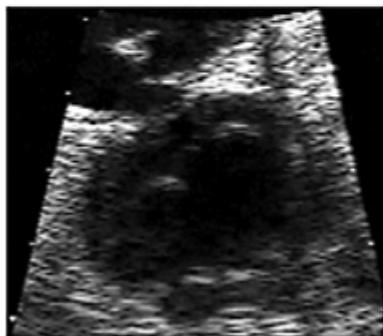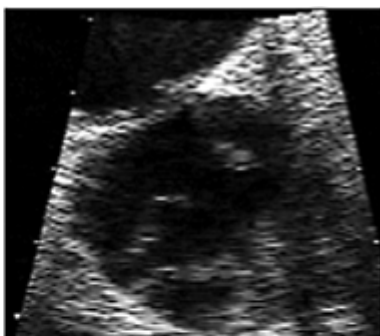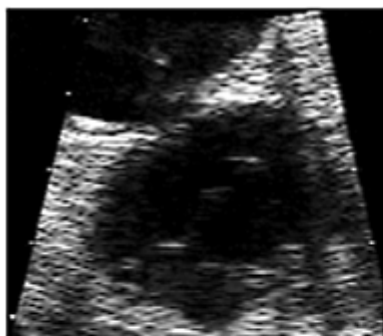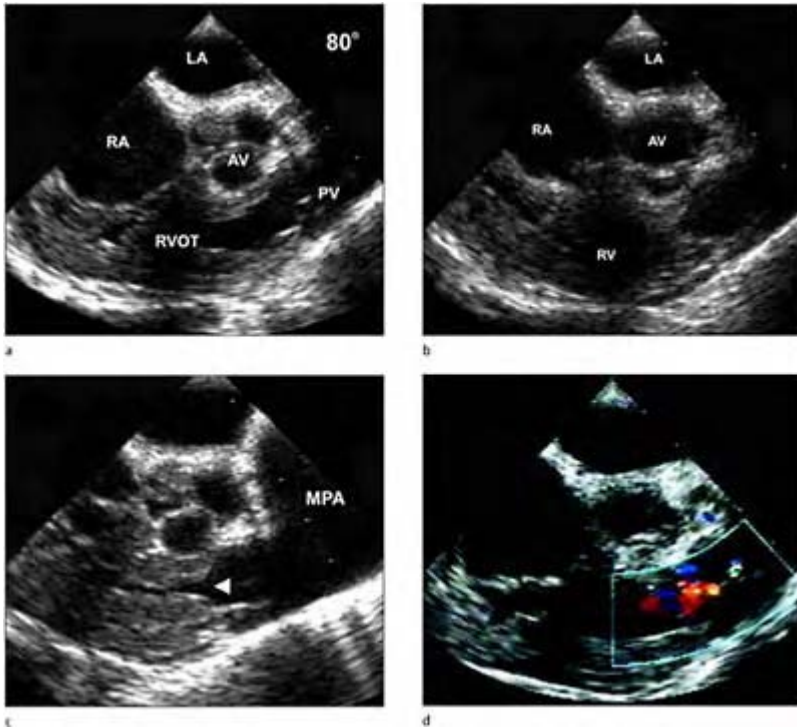
Case 4.14 Pulmonary stenosis. Right ventricular outflow tract views obtained from the mid to upper esophageal window demonstrate thickening of the pulmonary valve during diastole (a) and systole (b). Note that the right ventricle shows hypertrophy. With fine manipulation of the probe centering on the infundibular region subvalvular stenosis is demonstrated (arrow) (c).
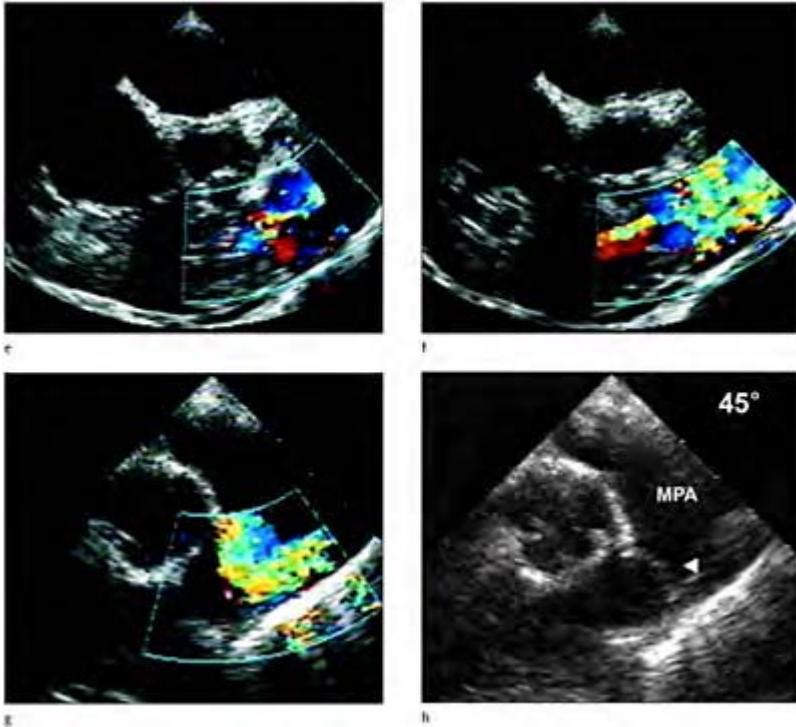
With color flow Doppler, disturbed and high velocity flow is detected during systole in the subvalvular and valvular region consistent with pulmonic stenosis (d–f). Withdrawal of the probe to the upper esophageal position with anteflexion (g–h) demonstrate the stenotic pulmonary valve (arrow) with thickened, restricted leaflets and systolic doming (h) with a stenotic flow jet.
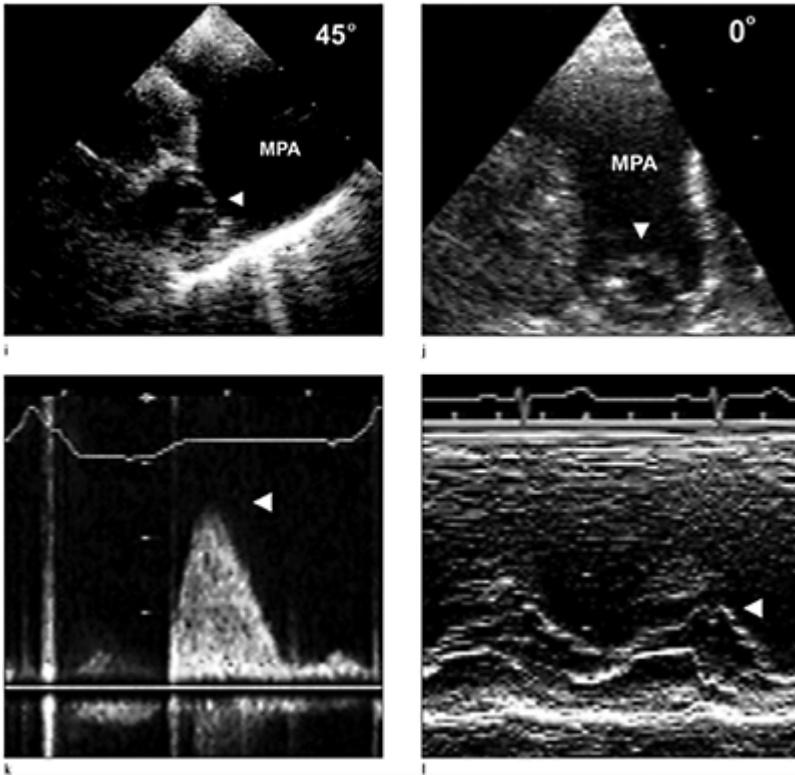
Longitudinal views of the main pulmonary artery from the upper esophageal view demonstrate the stenotic valve (j) enface and also allow continuous wave Doppler interrogation (k) as well as m-mode of valve leaflet motion (l). RA, right atrium; LA, atrium; RVOT, right ventricular outflow tract; AV, aortic valve; PV, pulmonary valve; MPA, main pulmonary artery.
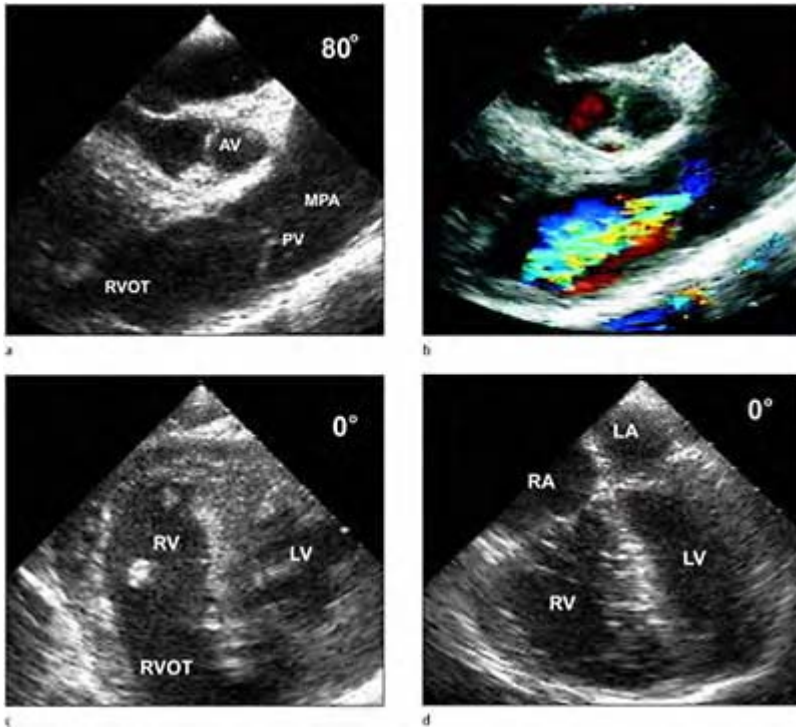
Case 4.15 Pulmonic regurgitation. The pulmonary valve is mildly thickened during diastole with dilatation of the main pulmonary artery. With color flow Doppler a large diastolic regurgitant jet is visualized. The right ventricle is dilated and hypertrophied in short axis (c) and four-chamber longitudinal views (d). AV, aortic valve; RVOT, right ventricular outflow tract; PV, pulmonary valve; MPA, main pulmonary valve; RV, right ventricle; LV, left ventricle.
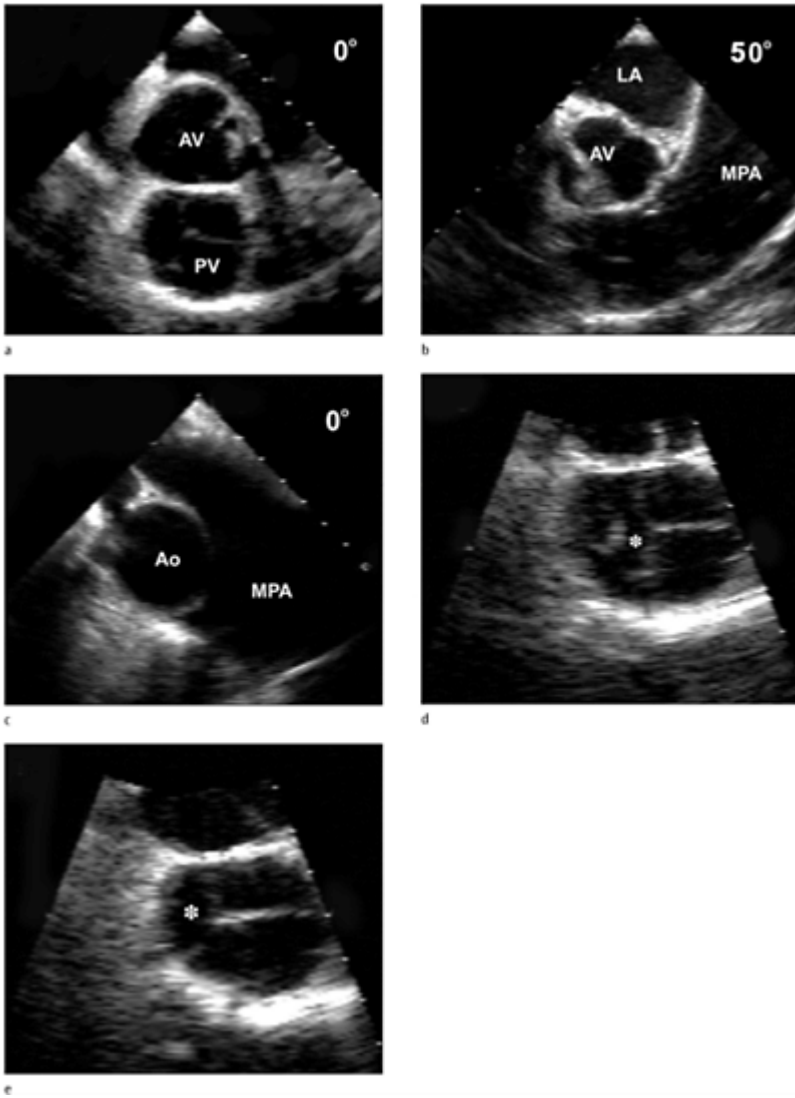
Case 4.16 Bicuspid pulmonary valve
with a dilated pulmonary artery. The
patient underwent a multiplane
transesophageal examination for chest
pain two years after aortic root and
valve replacement for aortic dissection.
The patient had a bicuspid aortic valve
at the time of surgery. Short axis view

of the base of the heart showed the pulmonary valve enface during diastole (a) and systole (b). With anteflexion of the probe, dilatation of the main pulmonary artery was noted in reference to the aortic graft (c) at 0 degrees. Dilatation of the pulmonary artery and the aortic graft allowed visualizing the valve plane enface, during early systole (d, e) the eccentric valve orifice (star) was visualized and with full valve opening (f) the commissures were clearly shown (arrow). LA, left atrium; AV, aortic valve; PV, pulmonary valve; MPA, main pulmonary artery; Ao, aorta.
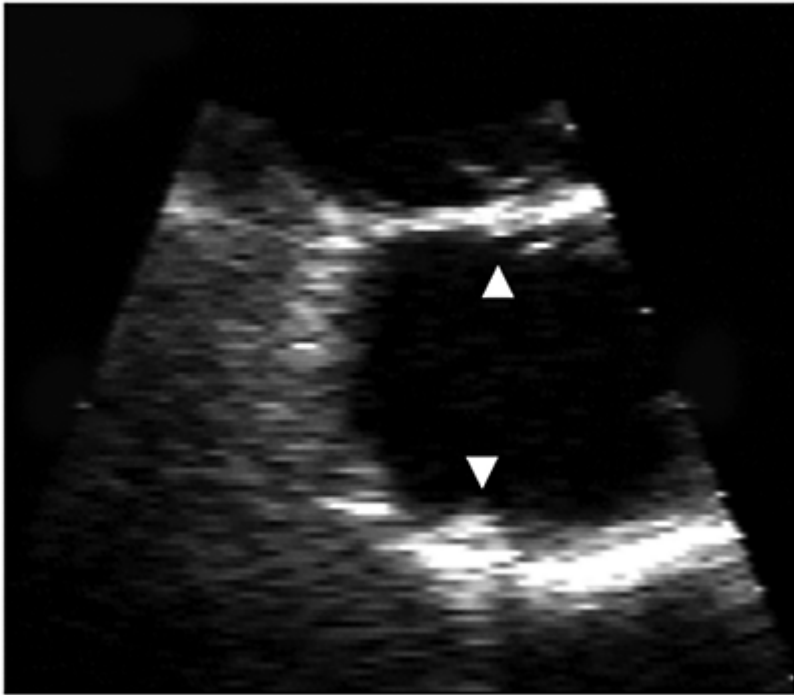
f
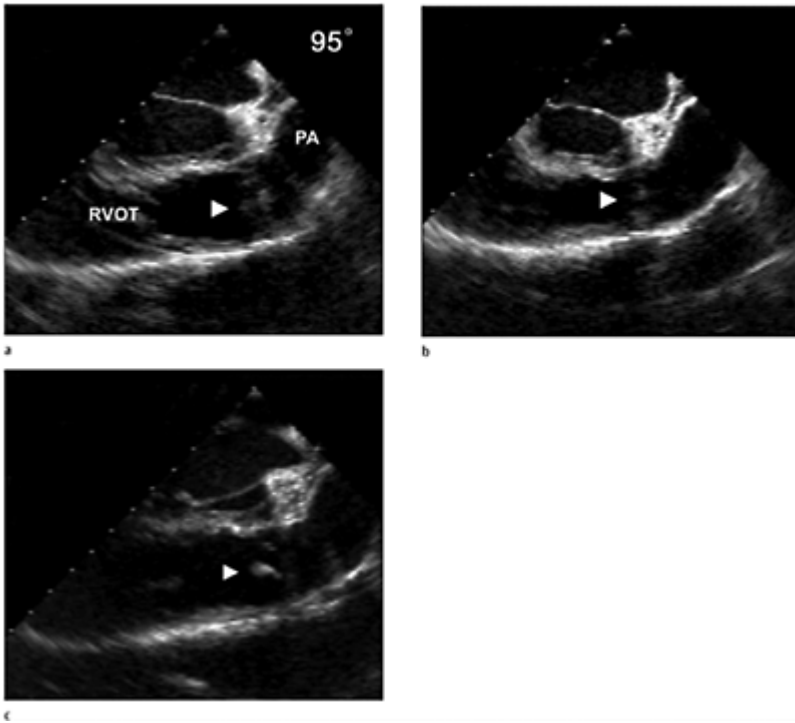
Case 4.17 Pulmonary valve vegetation (arrow) visualized on the ventricular surface of the pulmonary valve. Pulmonary valve vegetations are more frequently shown with multiplane transesophageal echocardiography (TEE) although the resolution of TEE is not always ideal for detailed analysis (a, b). Pulmonary valve vegetations appear as shaggy masses of increased echogenicity in the area of the valve plane. PA, pulmonary artery; RVOT, right ventricular outflow tract.
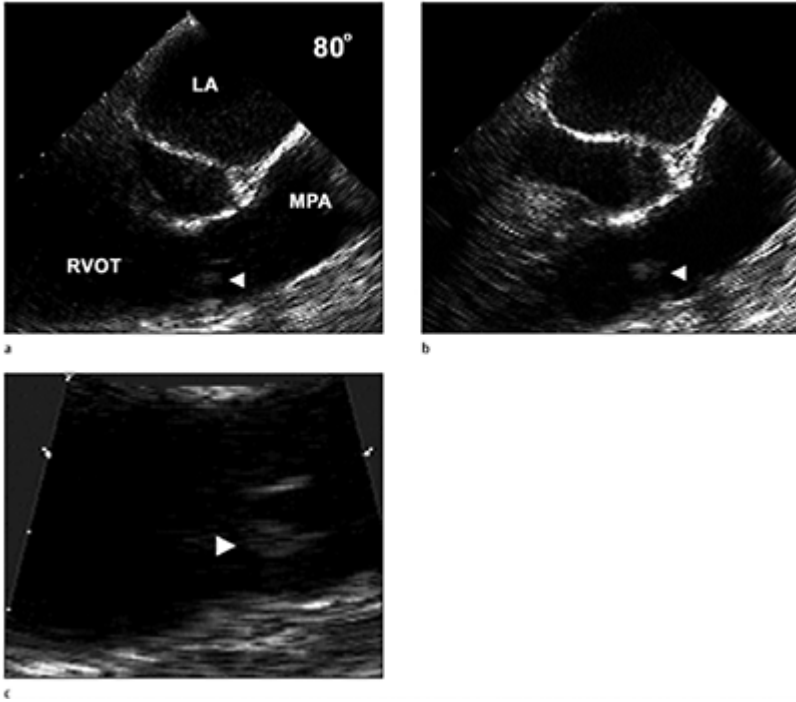
Case 4.18 Pulmonary valve vegetation. Horizontal views obtained from the mid-esophageal window at 80 degrees show increased echogenicity (arrow) in the pulmonary valve plane suggesting a mass or vegetation during systole (a) and diastole (b). A discreet, fixed but shaggy mass is attached to the anterior cusp of the pulmonary valve in zoom mode (c). RVOT, right ventricular outflow tract; MPA, main pulmonary artery; LA, left atrium.
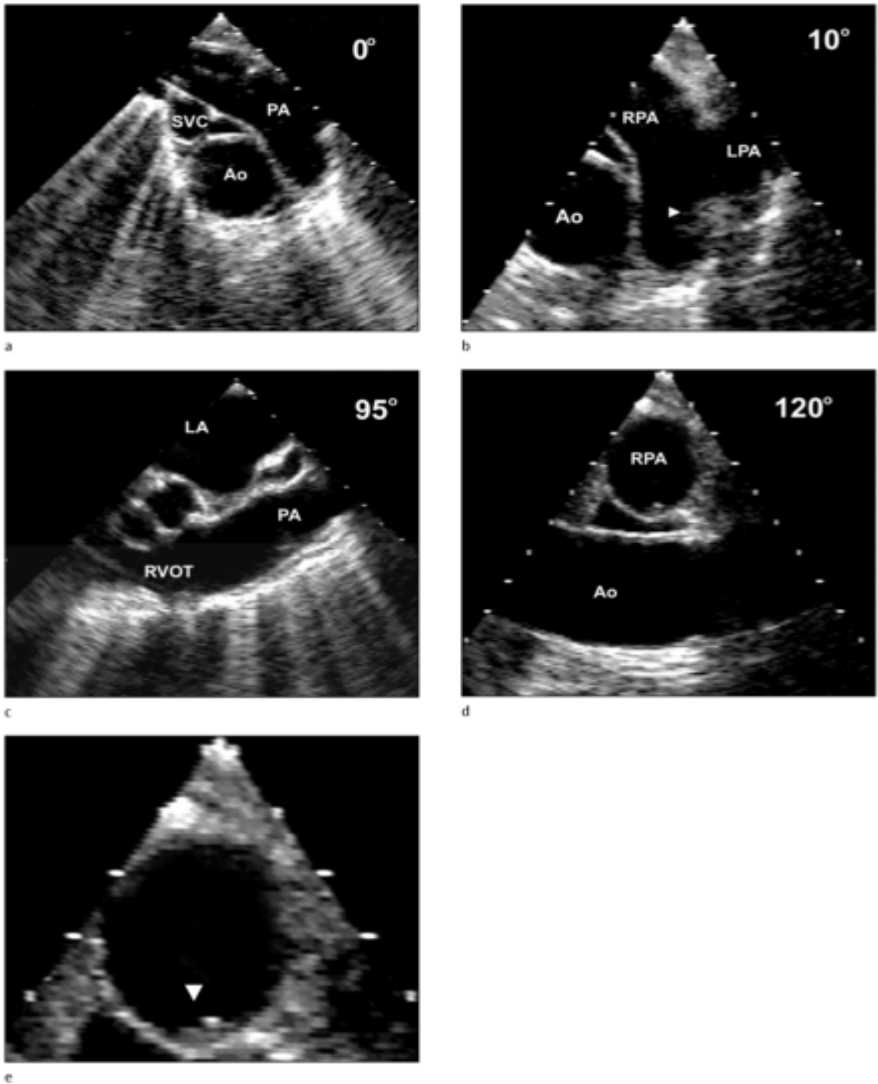
Case 4.19 Pulmonary artery plaqueing
and debris. Atherosclerotic disease of
the pulmonary artery is often
overlooked, but is common in
association with significant aortic
atherosclerosis. Horizontal views
obtained from the upper esophageal
window show the main pulmonary

artery and branches (a–c) at 0 to 95 degrees. The pulmonary artery walls appear thickened and calcified, as exhibited by ghosting and shadowing with small intraluminal echogenic masses (arrows). Longitudinal views of the right pulmonary artery cross-section (d) show debris (arrow), as does the corresponding zoom mode (e). SVC, superior vena cava; Ao, aorta; RPA, right pulmonary artery; LPA, left pulmonary artery; LA, left atrium; PA, pulmonary artery; RVOT, right ventricular outflow tract. a b
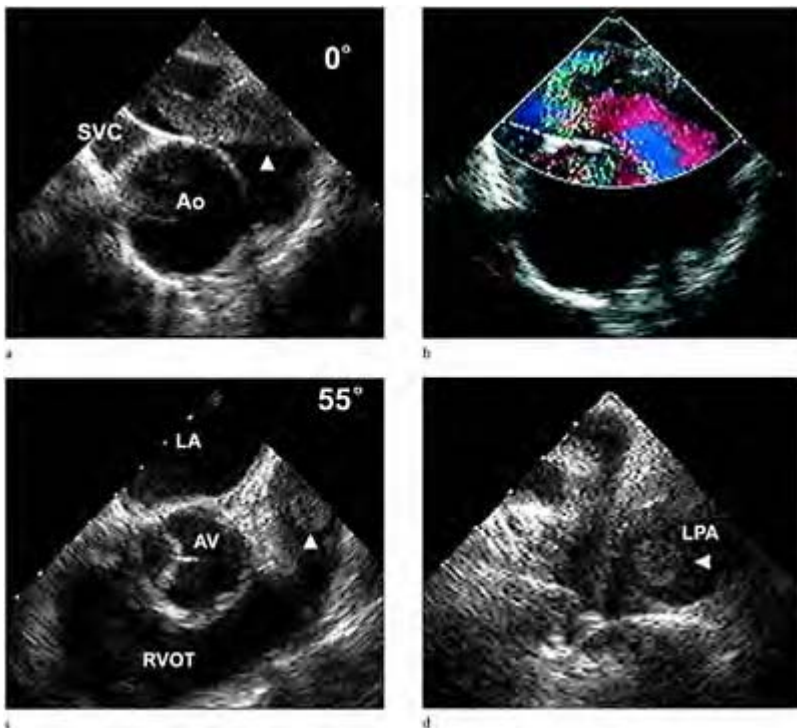
Case 4.20 Pulmonary embolus. Saddle pulmonary embolus (arrows) nearly obstructing the main, right and left

pulmonary arteries (a–d) as visualized in multiple views with transesophageal echocardiography. Color flow Doppler shows pulmonary artery flow outlining the pulmonary embolus occupying the right pulmonary artery. SVC, superior vena cava; Ao, aorta; LA, left atrium; AV, aortic valve; RVOT, right ventricular outflow tract; LPA, left pulmonary artery.
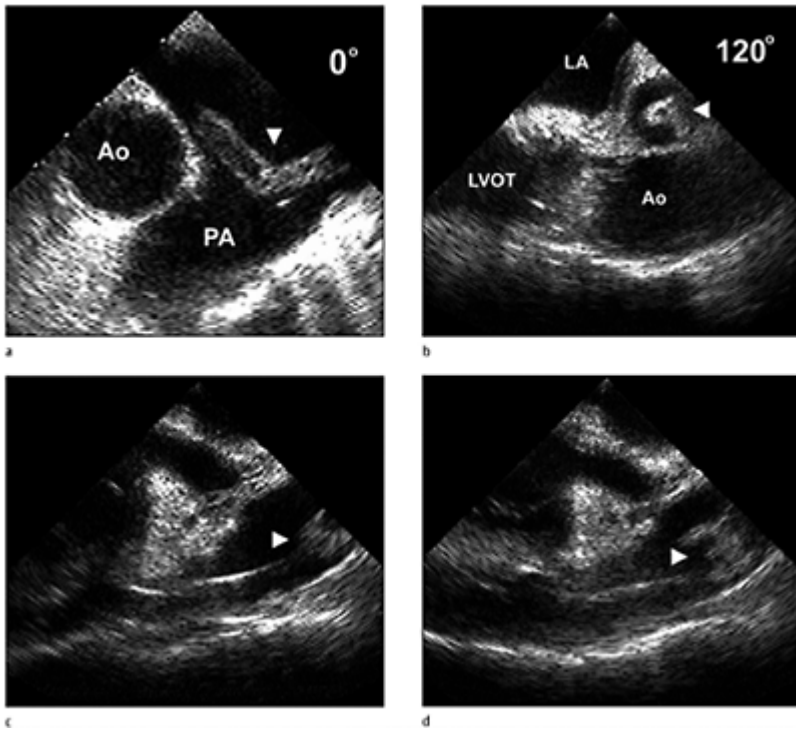
Case 4.21 Pulmonary embolus. A venous cast that migrated to the pulmonary artery producing a pulmonary embolus, horizontal view (a) and longitudinal view demonstrating the tip of the cast in the right pulmonary artery (b). Pulmonary

embolus associated with right heart catheter in a patient that developed signs and symptoms of a pulmonary embolus after Swan–Ganz placement. The thrombus producing the embolus was thought to be dragged to the pulmonary artery from the neck veins. Longitudinal views of the right ventricular outflow tract demonstrate a large thrombus in close proximity and attached to a right heart catheter during diastole (c) and systole (d). Ao, aorta; PA, pulmonary artery; LA, left atrium; LVOT, left ventricular outflow tract;
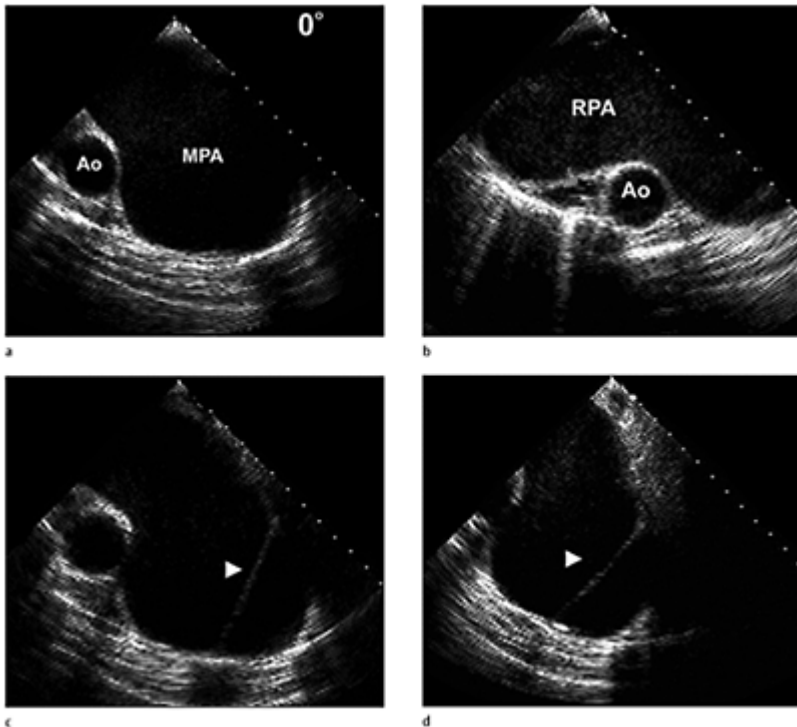
Case 4.22 Pulmonary artery dissection. Horizontal views of the main (a) and right pulmonary artery (b) obtained

from the upper esophageal window with anteflexion at 0 degrees demonstrating marked dilatation in reference to the aorta.
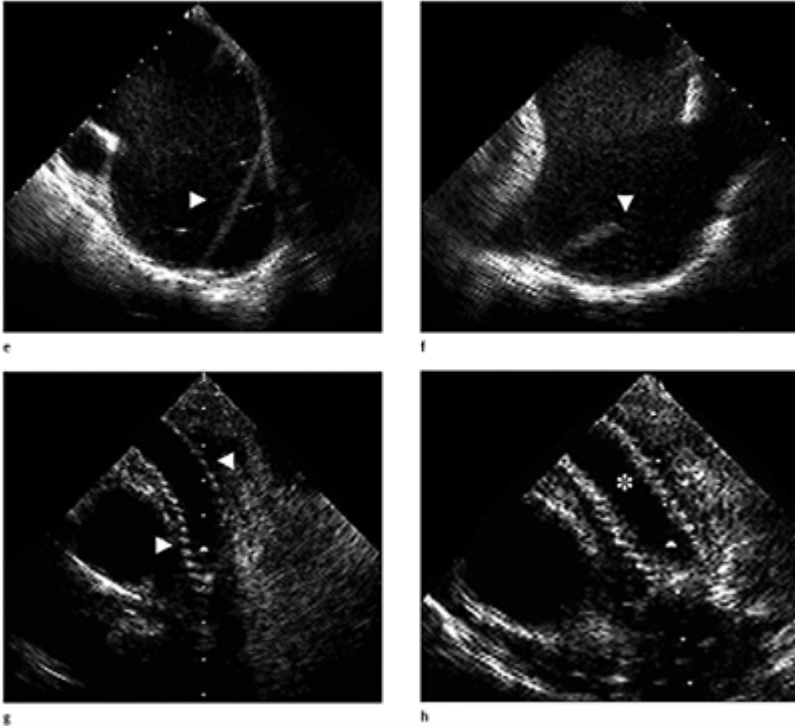
Spontaneous contrast is noted predominately in the right pulmonary artery. With minor clockwise and counterclockwise manipulation of the probe (c–e) an intimal flap (arrow) is confirmed in the main pulmonary artery extending to the left pulmonary with the entry tear (arrow) located in the proximal main pulmonary artery just distal to the pulmonary valvular plane (f). Postoperative views (g, h) show a surgical graft (star) in the pulmonary artery position. The

corrugated appearance of the graft
(arrows) is well defined by
transesophageal echocardiography (g).
Ao, aorta; MPA, main pulmonary
artery; RPA, right pulmonary artery.

References

1. Silver, MD, Lam JHC, Ranganathan N, et al. Morphology of the human tricuspid valve. *Circulation* 1971;49:333–48.
2. Perloff JK, Harvey WP. Clinical recognition of tricuspid stenosis. *Circulation* 1960;22:346.
3. Gray H. *Anatomy of the Human Body*. Philadelphia:Lea & Febiger, 1973;543.
4. Carpentier A. Cardiac valve surgery – The "French Correction". *J Thorac Cardiovasc Surg* 1983;86:323–37.
5. Waller BF, Bloch T, Eble JN, et al. Etiology of tricuspid stenosis and pure tricuspid regurgitation. In: *Pathology of the Heart and Great Vessels*. Waller BF (ed.) New York: Churchill Livingstone, 1988.
6. Waller BF. Morphological aspects of valvular heart disease: part II. *Curr Probl Cardiol* 1984;9:1–74.
7. Nanna M, Chandraratna PA, Reid C, et al. Value of two-dimensional echocardiography in detecting tricuspid stenosis. *Circulation* 1983;67:221–4.
8. Guyer DE, Gillam LD, Foale RA, et al. Comparison of echocardiographic and hemodynamic diagnosis of rheumatic tricuspid stenosis. *J Am Coll Cardiol* 1984;3:1135–44.
9. Daniels SJ, Mintz GS, Kotler MN. Rheumatic tricuspid valve disease: two-dimensional diagnosis of rheumatic tricuspid stenosis. *Am J Cardiol* 1983;51:492–6.
10. Shimada R, Takeshita A, Nakamura M, et al. Diagnosis of tricuspid stenosis by M-mode and two-dimensional echocardiography. *Am J Cardiol* 1984;53:164.
11. Datta BN, Nagrani B, Khatti HN, et al. Rheumatic heart disease at autopsy: an analysis of 260 cases in Chandigark, India. *Indian Heart J* 1978;30:39–46.
12. Joyner CR, Hey BE Jr, Johnson J, Reid JM. Reflected ultrasound in the diagnosis of tricuspid stenosis. *Am J Cardiol* 1967;19:66–73.
13. Ross EM, Roberts WC. The carcinoid syndrome: comparison of 21 necropsy subjects with carcinoid heart disease to 15 necrospy subjects without carcinoid heart disease. *Am J Med* 1985;79:339–54.
14. Arnett EN, Roberts WC. Active infective endocarditis: a clinicopathologic analysis of 137 necropsy patients. *Curr Prob Cardiol* 1976;1:2–76.
15. Silver MD. Obstruction to blood flow related to tricuspid, pulmonary and mitral valve. In Silver MD (ed): Cardiovascular Pathology, Vol 1. New York: Churchill Livingstone, 1883;551.
16. Gallucci V, Stritoni P, Fasoli G, Thiene G. Giant blood cyst of tricuspid valve: successful excision in an infant. *Br Heart J* 1976;38:990–2.
17. Veyrat C, Kalmanson D, Farjon M, et al. Noninvasive diagnosis and assessment of tricuspid regurgitation and stenosis using one and two-dimensional echo pulsed Doppler. *Br Heart J* 1982;47:596–605.
18. Dennig GK, Henneke KH, Rudolph W. Assessment of tricuspid stenosis by Doppler echocardiography. *J Am Coll Cardiol* 1987;9:237A.
19. Parris TM, Panidis IP, Ross J, Mintz GS. Doppler echocardiographic findings in rheumatic tricuspid stenosis. *Am J Cardiol* 1987;60:1414–16.

20. Gibson TC, Roale RA, Guyer DE, Weyman AE. Clinical significance of incomplete tricuspid valve closure seen on two-dimensional echocardiography. *J Am Coll Cardiol* 1984;4:1052–7.

21. Howard RJ, Drobac M, Rider WD, et al. Carcinoid heart disease: diagnosis by two-dimensional echocardiography. *Circulation* 1982;66:1059–65.

22. Watanabe T, Katsume H, Matsukubo H, et al. Ruptured chordae tendineae of the tricuspid valve due to nonpenetrating trauma. *Chest* 1981;80:751–3.

23. Donaldson RM, Ballester M, Richards AF. Rupture of a papillary muscle of the tricuspid valve. *Br Heart J* 1982;48:291–3.

24. Oliver J, Benito F, Gallego FG, Sotillo J. Echocardiographic findings in ruptured chordae tendineae of the tricuspid valve. *Am Heart J* 1983;105:1033–5.

25. Bates ER, Sorkin RP. Echocardiographic diagnosis of flail anterior leaflet in tricuspid endocarditis. *Am Heart J* 1983;106:161–3.

26. Pomerance A. Ballooning deformity of atrioventricular valves. *Br Heart J* 1969;31:343–51.

27. Davies MJ, Moore BP, Braimbridge MV. The floppy mitral valve: study of incidence, pathology and complication in surgical necropsy and forensic material. *Br Heart J* 1978;40:468–81.

28. Rippe JM, Angoff G, Sloss LJ, et al. Multiple floppy valves: an echocardiographic syndrome. *Am J Med* 1979;66:817–24.

29. Chandraratna PSN, Lopez JM, Fernandex JJ, Cohen LS. Echocardiographic detection of tricuspid valve prolapse. *Circulation* 1975;51:823–6.

30. Schlamowitz RA, Gross S, Keating E, et al. Tricuspid valve prolapse: a common occurrence in the click murmur syndrome. *J Clin Ultrasound* 1982;10:435–9.

31. Brown GK, Anderson V. Two-dimensional echocardiography and the tricuspid valve. *Br Heart J* 1983;49:495–500.

32. Lee CC, Ganguly SN, Magnisalis K, Robin E. Illustrative echocardiogram: detection of tricuspid valve vegetations by echocardiography. *Chest* 1974;66:432–3.

33. Crawford FA Jr, Wechsler AS, Kisslo JA. Tricuspid endocarditis in a drug addict: detection of tricuspid vegetations by two-dimensional echocardiography. *Chest* 1978;74:473–5.

34. Ginzton LE, Siegel RJ, Criley JM. Natural history of tricuspid valve endocarditis: a two-dimensional echocardiographic study. *Am J Cardiol* 1982;49:1853–9.

35. Yock BP, Popp RL. Non-invasive estimation of right ventricular systolic pressure by Doppler ultrasound in patients with tricuspid regurgitation. *Circulation* 1984;70:657–62.

36. Wooley CF. The spectrum of tricuspid regurgitation. *Am Heart Monograph* 1975;46:139.

37. Cha SD, Gooch AS. Diagnosis of tricuspid regurgitation. *Arch Intern Med* 1983;143:1763.

38. Sepulveda G, Kukas DS. The diagnosis of tricuspid insufficiency. Clinical features in 60 cases with associated mitral valve disease. *Circulation* 1972;45:793.

39. Hansing CE, Rowe GG. Tricuspid insufficiency. A study of hemodynamics and pathogenesis. *Circulation* 1972;45:793–9.

40. Schwartz F, Manthey J, Schuler G, Mauer W, Mehmel A, Kubler W. The effect of tricuspid insufficiency on right ventricular performance in patients with valvular heart disease. *Z Kardiol* 1981;70:466.

41. Lichtlen PR, Simon R. Incidence, severity and mechanisms of tricuspid regurgitation in patients with rheumatic mitral valve disease analyzed by right ventricular angiography. *Circulation* (Suppl. II), 1976;II–104.

42. Waller BF, Moriarty AT, Eble JN, et al. Etiology of pure tricuspid regurgitation based on annular circumference and leaflet area: analysis of 45 necropsy patients with clinical and morphologic evidence of pure tricuspid regurgitation. *J Am Coll Cardiol* 1986;7:1063–74.

43. Shiina A, Seward JB, Edwards WD, et al. Two-dimensional echocardiographic spectrum of Ebstein's anomaly: detailed anatomic assessment. *J Am Coll Cardiol* 1984;3:356–70.

44. Suzuki Y, Kambara H, Kadota K, et al. Detection and evaluation of tricuspid regurgitation using a real time, two-dimensional, color-encoded, Doppler flow imaging system: comparison

with contrast two-dimensional echocardiography and right ventriculography. *Am J Cardiol* 1986;57:811–15.

45. Chan KL, Currie PJ, Seward JB, et al. Comparison of three Doppler ultrasound methods in the prediction of pulmonary artery pressure. *J Am Coll Cardiol* 1987;9:549–54.

46. Nishimura RA, Miller FA Jr, Callahan MJ, et al. Doppler echocardiographic: instrumentation, technique and application. *Mayo Clin Proc* 1985;60:321–43.

47. Currie PJ, Seward JB, Chan KL, et al. Continuous wave Doppler determination of right ventricular pressure: a simultaneous Doppler-catheterization study in 127 patients. *J Am Coll Cardiol* 1985;6:750–6.

48. Come PC, Kim D, Parker JA, et al. Early reversal of right ventricular dysfunction in patients with acute pulmonary embolism after treatment with intravenous tissue plasminogen activator. *J Am Coll Cardiol* 1987;10:971–8.

49. Miyatake K, Okamoto M, Kinoshita N, et al. Evaluation of tricuspid regurgitation by pulsed Doppler and two-dimensional echocardiography. *Circulation* 1982;66:777–89.

50. Akasaka T. Age-related valvular regurgitation: a study by pulsed Doppler echocardiography. *Circulation* 1987;76:262–5.

51. Kral J, Hradec J, Petrasek J. Valvular regurgitations in healthy young people. Cor-Vasa 1989;31:485–94.

52. Mattleman S, Panidis I, Kotler MN, et al. Calcification of the tricuspid annulus diagnosed by two-dimensional echocardiography. *Am Heart J* 1984;107:986–8.

53. Rogers JV Jr, Chandler NW, Franch RH. Calcification of the tricuspid annulus. *Am J Roentgenol Radium Ther Nucl Med* 1969;106:550.

54. Bonchek LI. Calcification of the annulus of the tricuspid valve. *Chest* 1972;61:307.

55. Panidis IP, Kotler MN, Mintz GS, et al. Right heart endocarditis: a two-dimensional study. *Am J Cardiol* 1976;38:302.

56. Chirillo F, Bruni A, Giujusa T, Cavarzerani A, Stritoni P. Echocardiography in infective endocarditis: reassessment of the diagnostic criteria of vegetation as evaluated from the transthoracic and transesophageal approach. *Am J Card Imaging* 1995;9:174–9.

57. San Roman JA, Vilacosta I, Zamorano JL, Almeria C, Sanchez-Harguindey L. Transesophageal echocardiography in right-sided endocarditis. *J Am Coll Cardiol* 1993;21:1226–30.

58. St John Sutton M, Lie JT. Clinical importance and recognition of non-bacterial thrombotic endocarditis. *Practical Cardiol* 1985;2:45–57.

59. Roldan CA, Shively BK, Crawford MH. An echocardiographic study of valvular heart disease associated with systemic lupus erythematosus. *N Engl J Med* 1996;335;1424–30.

60. Roldan CA. Shively BK, Lau CC, et al. Systemic lupus erythematosus valve disease by transesophageal echocardiography and the role of antiphospholipid antibodies. *J Am Coll Cardiol* 1992;20:1127–34.

61. De Maria AN, Evaluation of tricuspid valve prolapse by two-dimensional echocardiography (abstr.) *Am J Cardiol* 1979;43:385.

62. Mardelli RJ, Morganroth J, Meixell LL, Vergel J. Enhanced diagnosis of tricuspid valve prolapse by cross-sectional echocardiography (abstr.) *Am J Cardiol* 1979;43:385.

63. Marks AR, Choong CY, San Filippo AJ, et al. Identification of high-risk subgroups of patients with mitral valve prolapse. *N Engl J Med* 1989;320:1031–6.

64. Carpentier A. Valve Repair with Carpentier Techniques – The Second Decade. *J Thorac Cardiovasc Surg* 1990;99:990–1002.

65. Carpentier A, Relland J. Carpentier Ring and tricuspid insufficiency. *Ann Thorac Surg* 1979;27:95–6.

66. Carpentier A, et al. A new reconstructive operation for correction of mitral and tricuspid insufficiency. *J Thorac Cardiovasc Surg* 1971;6:1–13.

67. Carpentier A, Deloche A, Hanania G, et al. Surgical management of acquired tricuspid valve disease. *J Thorac Cardiovasc Surg* 1974;67:53–65.

68. Czer LSC, Maurer G, Bolger A, et al. Tricuspid valve repair: operative and follow-up evaluation by Doppler color flow mapping. *J Thorac Cardiovasc Surg* 1989;98:101–11.
69. Kay GL, Morita S, Mendez M, et al. Tricuspid regurgitation associated with mitral valve disease: repair and replacement. *Ann Thorac Surg* 1989;48:S93–5.
70. Grondin P, Meere C, Limet R et al. Carpentier's annulus and DeVega's annuloplasty – the end of the tricuspid challenge. *J Thorac Cardiovasc Surg* 1975;70:852–61.
71. Konishi Y, Tatsuta N, Minami K et al. Comparative study of Kay-Boyd's, DeVega's and Carpentier's annuloplasty in the management of functional tricuspid regurgitation. *Jpn Circ J* 1983;47:1167–72.
72. Rivera R, Duran E, Ajuria M, et al. Carpentier's flexible ring versus DeVega's annuloplasty. A prospective randomized study. *J Thorac Cardiovasc Surg* 1985;89:196–203.
73. DeSimone R, Lange R, Saggau W. Tanzeem A, Hagl S. Intraoperative evaluation of tricuspid valve annuloplasty with transesophageal echocardiography. *Cardiologia* 1992;37:195–201.
74. Karatasakis G, Karamintziou R, Taylor KM, Cokkinos DV. Transthoracic and transesophageal echocardiographic diagnosis of a DeVega tricuspid annuloplasty rupture. *J Am Soc Echocardiography* 1994;7:321–3.
75. De Simone R, Lange R, Tanzeem A, Gams E, Hagl S. Adjustable tricuspid valve annuloplasty assisted by intraoperative transesophageal color Doppler echocardiography. *Am J Cardiol* 1993;71:926–31.
76. Cook JW. Accurate adjustment of DeVega tricuspid annuloplasty using transesophageal echocardiography. *Ann Thorac Surg* 1994;58:570–2.
77. Allen MD, Slachman F, Eddy AC, et al. Tricuspid valve repair for tricuspid valve endocarditis: tricuspid valve "recycling". *Ann Thorac Surg* 1991;51:593–8.
78. Gross L, Kugel MA. Topographic anatomy and histology of the valves in the human heart. *Am J Pathol* 1931;7:445.
79. Barry A, Patten BM. The structure of the adult heart. In Gould SE (ed): Pathology of the Heart and Blood Vessels (3rd edn). Springfield, IL: Charles C. Thomas, 1968:91.
80. Kerr A Jr, Goss CM. Retention of embryonic relationship of aortic and pulmonary valve cusps and a suggested nomenclature. *Anat Rec* 1956;125:777.
81. Hurwitz LE, Roberts WC. Quadricuspid semilunar valves. *Am J Cardiol* 1973;31:623.
82. Cavia JE, DeCastro CM, McAllister HA Jr. Quadricuspid semilunar valves. *Chest* 1977;72:186.
83. Gikonyo BM, Lucas RV, Edwards JE. Anatomic features of congenital pulmonary valvular stenosis. *Pediatr Cardiol* 1987;8:109.
84. Weyman AE. Right ventricular outflow tract. In: Principles and Practice of Echocardiography (2nd edn).Philadelphia: Lea & Febiger, 1994:875.
85. Roberts WC, Mason DT, Morrow AG, Braunwald E. Calcific pulmonic stenosis. *Circulation* 1968;37:973.
86. Covarrubias EA, Sheikh MU, Isner JI, et al. Calcific pulmonic stenosis in adulthood. Treament by valve replacement. *Chest* 1979;75:399.
87. Waller BF. Morphologic aspects of valvular heart disease. Part I. *Curr Probl Cardiol* 1984;9:1–74.
88. Taussig HB. Congenital malformations of the heart. New York: The Commonwealth Fund, 1947:169.
89. Greene DG, Baldwin ED, Baldwin JS, Himmelstein A, Roh CE, Cournand A. Pure congenital pulmonary stenosis and idiopathic congenital dilatation of the pulmonary artery. *Am J Med* 1949;6:24–40.
90. White PD, Hurst JW, Fennel RH. Survival to the age of seventy-five years with congenital pulmonary stenosis and patent foramen ovale. *Circulation* 1950;2:558–64.
91. Genovese PD, Rosenbaum D. Pulmonary stenosis to the age of 78 years. *Am Heart J* 1951;41:755–61.
92. Eklund B, Freyschuss U. Congenital pulmonary stenosis at the age of 76. *Acta Med Scand* 1968;183:455–6.

93. Voci G, Maniet AR, Diego JN, et al. Severe calcific pulmonic valve stenosis and restrictive ventricular septal defect in a 64–year-old man. Results of percutaneous double balloon valvuloplasty. *Cardiologia* 1994;39;863–8.
94. Dinsmore RE, Sanders CA, Hathorne JW, Austen WG. Calcification of the congenitally stenotic pulmonary valve. *N Engl J Med* 1966;275:99–100.
95. Rodriguez GR, Bennet KR, Lehan PH. Calcification of the pulmonary valve. *Chest* 1971;59:160–4.
96. Engle MA, Taussig HB. Valvular pulmonic stenosis with intact ventricular septum and patent foramen ovale. Report of illustrative cases and analysis of clinical syndrome. *Circulation* 1950;43:687–95.
97. Lababidi Z, Wu JR. Percutaneous balloon pulmonary valvuloplasty. *Am J Cardiol* 1983;52:560–2.
98. Perloff JK, Child JS. Congenital heart disease in adults. Philadelphia: WB Saunders Company, 1991:24.
99. Johnson LW, Grossman W, Dalem J, Dexter L. Pulmonic stenosis in the adult long-term follow-up study. *N Engl J Med* 1972;287:1159–63.
100. Rao PS, Fawzy ME, Solymar L, Mardini MK. Long-term results of pulmonary valvuloplasty of valvar pulmonic stenosis. *Am Heart J* 1988;115:1291–6.
101. Kan JS, White RI, Mitchell SE, Gardner TJ. Percutaneous balloon valvuloplasty; a new method for treating congenital pulmonary valve stenosis. *N Engl J Med* 1982;307:540–2.
102. Pepine CJ, Gessner IH, Feldman RL. Percutaneous balloon valvuloplasty for pulmonic valve stenosis in the adult. *Am J Cardiol* 1982;50:1442–5.
103. Radtke W, Keane JL, Fellows KE, et al. Percutaneous balloon valvotomy of congenital pulmonary stenosis using oversized balloons. *J Am Coll Cardiol* 1986;8:909–15.
104. Al Kasab S, Ribeiro P, Al Zaibag M. Use of a double balloon technique for percutaneous balloon pulmonary valvotomy in adults. *Br Heart J* 1987;58:136–41.
105. Ali Khan MA, Youself SA, Mullius CE. Percutaneous transluminal balloon valvuloplasty for the relief of pulmonary stenosis with special reference to double-balloon technique. *Am Heart J* 1986;112:158–66.
106. Stanger P, Cassidy SC, Girod DA, et al. Balloon pulmonary valvuloplasty: results of the valvuloplasty and angioplasty of congenital anomalies registry. *Am J Cardiol* 1990;65:775–83.
107. Lim MK, Houston AB, Doig WB et al. Variabilty of the Doppler gradient in pulmonary valve stenosis before and after balloon dilatation. *Br Heart J* 1989;62:212–16.
108. Philpot E, Yoganathan AP, Sung HW, et al. In-vitro pulsatile flow visualization studies in a pulmonary artery model. *J Biomed Eng* 1985;107:368–75.
109. Chen JTT, Robinson AE, Goodrich JK, Lester RG. Uneven distribution of pulmonary blood flow between the left and right lungs in isolated valvular pulmonary stenosis. *Am J Roentgenol Radium Ther Nucl Med* 1969;107:343–50.
110. Lima C, Sahn D, Valdes-Cruz L, et al. Noninvasive prediction of transvalvular pressure gradients in patients with pulmonary stenosis by quantitative two-dimensional echocardiographic Doppler studies. *Circulation* 1983;67:866–71.
111. Johnson G, Kwan O, Handshoe S, et al. Accuracy of combined two-dimensional echocardiography and continuous wave Doppler recordings in the estimation of pressure gradient in right ventricular outlet obstruction. *J Am Coll Cardiol.* 1984;3:1013–18.
112. Stevenson J, Kawabori I. Noninvasive determination of pressure gradients in children: two methods employing pulsed Doppler echocardiography. *J Am Coll Cardiol* 1984;3:179–92.
113. Goldberg S, Allen SV, Marx G. Can the technique for Doppler estimate of pulmonary stenosis gradient be simplified? *Am Heart J* 1986;111:709–13.
114. Riggs T, Weinhouse E. Respiratory influence on Doppler estimation of valvular gradients in congenital pulmonic stenosis. *Am J Cardiol* 1992;70:956–8.
115. Takao S, et al. Clinical implications of pulmonary regurgitation in healthy individuals: detection by cross sectional pulsed Doppler echocardiography. *Br Heart J* 1988;59:542–50.

116. Choong CY. Prevalence of valvular regurgitation by Doppler echocardiography in patients with structurally normal hearts by two-dimensional echocardiography. *Am Heart J*1989;117:636–42.

117. Shapiro SM, Young E, Ginzton LE, Bayer AS. Pulmonic valve endocarditis as an underdiagnosed disease: role of transesophageal echocardiography. *J Am Soc Echocardiogr*1992;5:48–51.

118. Wagenvoort CA, Wagenvoort N. Disease of the pulmonary circulation. In: Silver MD (ed). Cardiovascular Pathology. New York: Churchill Livingstone, 1983:683.

119. Plank L, James J, Wagenvoort CA. Caliber and elastin content of the pulmonary trunk. *Arch Pathol Exp Med*1979;104:238.

120. Roberts WC. Aortic dissection: anatomy, consequences, and causes. *Am Heart J*1981;101:195–214.

121. Deshmukh M, Gavenc S, Bentivoglio S, Goldberg H.Idiopathic dilatation of the pulmonary artery. *Circulation*1960;21:710.

122. Gasul BM, Arcilla RA, Lev M. Heart Disease in Children: diagnosis and treatment (1st edn). Philadelphia: JB Lippincott, 1966:807.

123. Edwards JE. Congenital malformations of the heart and great vessels. I. Malformations of the pulmonary arteries, In: Gould SE (ed). Pathology of the Heart and Great Vessels (3rd edn). Springfield, IL: Charles C. Thomas,1968.

124. Barbour DJ, Roberts WC. Aneurysm of the pulmonary trunk unassociated with intracardiac or great vessel left-to-right shunting. *Am J Cardiol* 1987;59:192–4.

125. Luchtrath H. Dissecting aneurysm of the pulmonary artery. *Virchows Arch Pathol Anat Histol* 1981;391:241–7.

126. Deterling RA, Clagett OT. Aneurysm of the pulmonary artery: review of the literature and report of a case. *Am Heart J* 1947;34:471.

127. Tung HL, Liebow AA. Marfan's syndrome. Observations at necropsy: with special reference to medionecrosis of the great vessels. *Lab Invest*1952;1:382.

128. Headley RN, Carpenter HM, Sawyer CG. Unusual features of Marfan's syndrome including two postmortem studies. *Am J Cardiol* 1963;11:259.

129. Roberts WC, Honig HS. The spectrum of cardiovascular disease in the Marfan syndrome: a clinicomorphologic study of 18 necropsy patients and comparison to 151 previously reported necropsy patients. *Am Heart J*1982;104:115–35.

130. Boyd LJ, McGavack TH. Aneurysm of the pulmonary artery. A review of the literature and report of two new cases. *Am Heart J* 1939;18:1952.

131. Spittell JA Jr, Wallace RB. Aneurysms. In: Juergens JL, Spittell JA Jr, Fairbairn II JF (eds): Peripheral Vascular Disease. Philadelphia: WB Saunders, 1980:415.

132. Tejada E, Waller BF. Non-neoplastic diseases of the aorta and pulmonary trunk. In: Pathology of the Heart and Great Vessels. Waller BF (ed). New York: Churchill Livingstone, 1988:367.

133. Moore GW, Smith RR, Hutchins GM. Pulmonary artery atherosclerosis: correlation with systemic atherosclerosis and hypertensive pulmonary vascular disease. *Arch Path Lab Med* 1982;106:378–80.

134. Steurer J, Jenni R, Medici TC, et al. Dissecting aneurysm of the pulmonary artery with pulmonary hypertension. *Am Rev Respir Dis* 1990;142:1219–21.

135. Shilkin KB, Low LP, Chen BTM. Dissecting aneurysm of the pulmonary artery. *J Pathol* 1969;98:25–9.

136. Chiu B, Magil A. Idiopathic pulmonary arterial trunk aneurysm presenting as cor pulmonale: report of a case. *Hum Pathol* 1985;16:947–9.

137. Foord AG, Lewis RD. Primary dissecting aneurysms of the peripheral and pulmonary arteries. *Arch Pathol* 1959;673:553.

138. Stern EJ, Sourtney G, Gordon G, Golden JA, Higgins CB. Pulmonary artery dissection: MR findings. *J Comp Ass Tomogr* 1992;16:481–3.

139. Modan B, Sharon E, Jelin N. Factors contributing to the incorrect diagnosis of pulmonary embolic disease. *Chest* 1972;62:388–93.
140. Dalen JE, Alpert JS. Natural history of pulmonary embolism. *Prog Cardiovasc Dis* 1975;17:259–70.
141. Patel JJ, Chandrasekaran K, Maniet AR, et al. Impact of the incidental diagnosis of clinically unsuspected central pulmonary artery thromboembolism in treatment of critically ill patients. *Chest* 1994;105:986–90.
142. Nixdorff U, Erbel R, Drexler M, Meyer J. Detection of thromboembolus of the right pulmonary artery by transesophageal two-dimensional echocardiography. *Am J Cardiol* 1988;61:488–9.
143. Wittlich N, Erbel R, Eichler A, et al. Detection of central pulmonary artery thromboemboli by transesophageal echocardiography in patients with severe pulmonary embolism. *J Am Soc Echocardiogr* 1992;5:515–24.
144. Rittoo D, Sutherland GR, Samuel L, Flapan A, Shaw TRD. Role of transesophageal echocardiography in diagnosis and management of central pulmonary artery thromboembolus. *Am J Cardiol* 1993;71:1115–18.
145. Klein AL, Stewart WC, Cosgrove DM, et al. Visualization of acute pulmonary emboli by transesophageal echocardiography. *J Am Soc Echocardiogr* 1990;3:412–15.
146. Kasper W, Meinertz T, Henkel B, et al. Echocardiographic findings in patients with proved pulmonary embolis. *Am Heart J* 1986;112:1248–91.
147. Farfel Z, Shechter M, Vered Z, et al. Review of echocardiographically diagnosed right heart entrapment of pulmonary emboli-in-transit with emphasis on management. *Am Heart J* 1987;113:171–8.

5
Diseases of the thoracic aorta

Historical perspective

Although diseases of the aorta have been known to plague man for centuries, diagnosing and treating aortic disease has slowly progressed through the years. In 1557, Vesalius[1] described the first traumatic aortic rupture in a patient who suffered a serious fall from a horse, and it was realized that the aorta was vulnerable to injury from traumatic accidents. Although dissection of the aorta was first described in the 16th century, it was not until 1819 that Laennec coined the term "dissecting aneurysm",[2] proving that the aorta was subject to destructive pathological processes. The first modern report of the clinical and pathologic findings of aortic dissection was described by Shennan[3] in 1934. However, aortic disease remained largely an elusive disorder for physicians, since the aorta could only be studied at necropsy. The first successful surgical repair of a dissecting descending aneurysm of the thoracic aorta in 1953 by DeBakey and colleagues[4] enhanced our understanding of aortic pathology, and along with it the hope that aortic disease could be treated before a catastrophic event occurs. In 1959, Passaro and Pace[5] spurred the interest in aorta surgery when they performed the first surgical repair of a traumatic aortic transection. Much of the knowledge about aortic disease was still left to the pathologists, since a good imaging technique for examining the aorta was not available. Edwards et al.[6] subsequently described variations in the patterns of aortic dissection, and Stanson et al.[7] described the variant of penetrating atherosclerotic ulcers in 1974. These reports both improved the understanding of the dissection process and created controversy as to the initiating cause and progression of aortic disease. It was not until the mid-1980s that atherosclerotic plaques of the aorta were visualized by ultrasound techniques[8] to illustrate their role in obstructive aortic disease.

Since that time, efforts have focused on improving diagnostic and surgical techniques using non-invasive techniques. Diagnostic imaging methods in the 1990s, including computed axial tomographic (CAT) scanning, magnetic resonance imaging (MRI) and transesophageal echocardiography (TEE), have expanded our knowledge of aortic disease beyond atherosclerosis, aneurysm, and dissection. They have characterized the natural history of aortic disease, affording the potential for aortic surgical repair with optimum timing earlier in the course of the disease.

Transthoracic echocardiography, although used routinely to evaluate the thoracic aorta, is difficult and time consuming, and is often unrevealing. Multiple views and

imaging planes are required to image the aorta in its entirety from the chest wall owing to the ultrasound impedance induced by the chest wall and lungs. In older patients and in patients with significant atherosclerotic disease, the aorta becomes increasingly tortuous, displacing the aorta deeper into the chest cavity to prevent optimal imaging from the anterior chest wall. Thus, the complete diagnosis of aortic disease is not often made with certainty by use of transthoracic echocardiography alone.
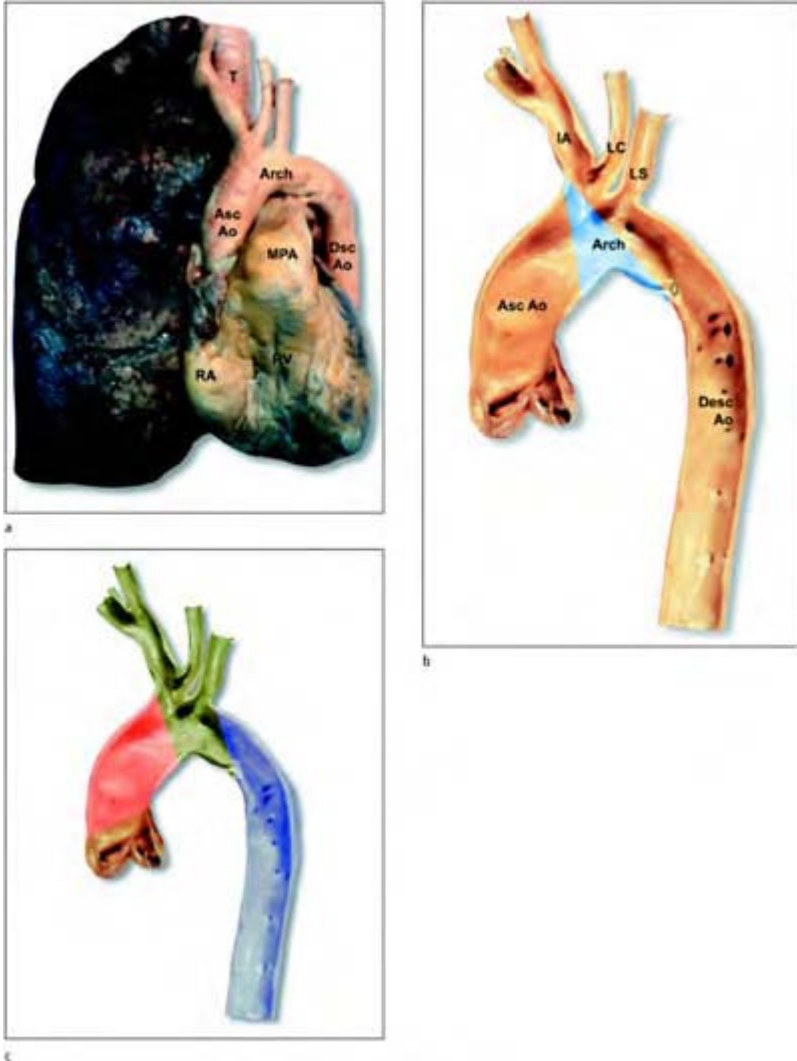
Figure 5.1 Normal thoracic aorta anatomy. Heart and lung post-mortem specimen (a) with left lung removed

demonstrating the anatomical relationships of the thoracic aorta, heart, trachea and right lung. The ascending aorta lies anterior to the right bronchus and the crossover represents the transverse aortic arch. The esophagus (not shown) is posterior to the trachea and one may gain an appreciation of the anatomical layers the ultrasound beam travels in order to visualize the thoracic aorta. Longitudinal cross-sectional preparation of the thoracic aorta (b, c) demonstrating the ascending, arch, descending aorta and great vessels, ligamentum arteriosum (open arrow), thoracic arteries (closed arrow). The area of the so-called aortic blind spot that occurs with monoplane and biplane transesophageal echocardiography (TEE) imaging is highlighted in blue. With multiplane TEE full visualization of the aorta and great vessels are readily identified in most cases. In (c), the aortic segments are color-coded, ascending, arch, and descending to demonstrate the boundaries of each segment. Asc Ao, ascending thoracic aorta; Arch, aortic arch; D Ao, descending aorta; IA, innominate artery; LC, left carotid; LS, left subclavian.

Owing to the close proximity of the esophagus to the aorta, TEE has had a tremendous impact in the examination of the aorta because it provides imaging planes with spectacular detail of the aortic wall. One limitation of biplane and monoplane TEE has been in imaging the entire aorta. Aortic transesophageal imaging is obscured where the trachea and right bronchus traverse and pass between the esophagus and the aorta (figure 5.1). An echocardiographic blindspot thus occurs at the level of the distal ascending aorta where it blends into the aortic arch. By contrast to the limited number of imaging planes obtained with monoplane or biplane TEE probes, multiplane TEE has virtually eliminated

the blindspot and allows adequate visualization of the whole aorta. Multiplane TEE also allows for better visualization of the continuity of the aortic arch and great vessels over that provided by biplane or monoplane scopes.

Multiplane TEE is arguably the method of choice for diagnosing aortic dissection and other forms of aortic disease in most clinical circumstances. Patients can be evaluated safely at the bedside and an immediate diagnosis can be obtained, with little patient discomfort. In addition, the presence of intra-aortic atheromatous debris can be identified, which is a source of systemic embolus and a precursor of other forms of aortic disease.

Normal thoracic aorta

The normal aorta is a tubular structure, which twists and turns in the thoracic cavity beginning at the aortic valve, extending longitudinally into the lower abdomen and ending in the pelvis by dividing into two common iliac arteries. The aortic diameter is largest at its origin in the thorax and slowly tapers in size prior to bifurcation in the abdomen. The overall dimensions, length and diameter of the aorta, are dependent on the body habitus (table 5.1).[9–13] The aorta is anatomically denoted as the thoracic aorta and abdominal aorta. Dividing the aorta into segments is useful for anatomic notation as well as for classifying aortic diseases.

Table 5.1 Normal diameters ofthe aorta according to body habitus[115]

Aortic segment	Average diameter (mm)		
	Body habitus		
	Small	*Medium*	*Large*
Aortic root	27	31	37
Ascending	28	32	39
Aortic arch	28	32	39
Descending thoracic	21	27	33
Diaphragmatic	20	26	33
Suprarenal	16	22	29
Infrarenal	13	19	26
Bifurcation	11	17	24
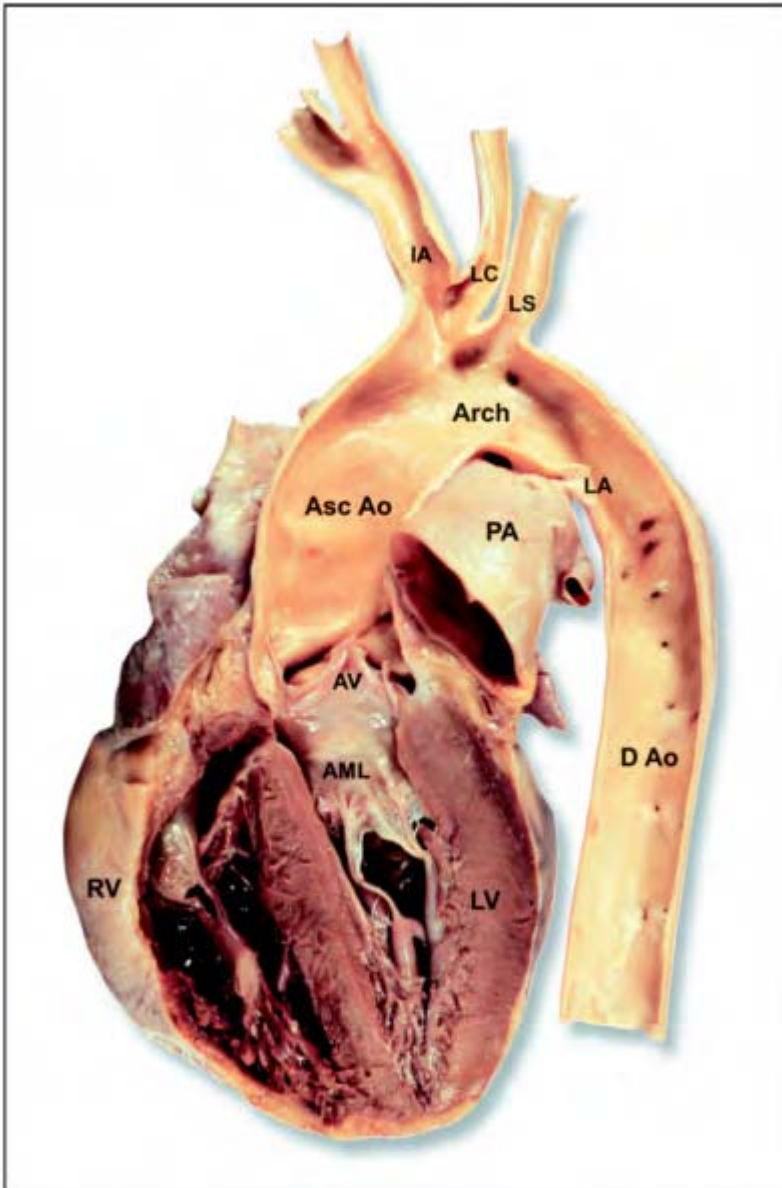
Figure 5.2 Longitudinal heart, pulmonary artery and thoracic aorta cross-sectional anatomical preparation. Appreciation for the anatomical relationships of the aorta is

demonstrated, as they would be seen on a multiplane TEE examination. A full appreciation of these relationships is necessary to interpret accurately the information obtained with multiplane examinations. RV, right ventricle; LV, left ventricle; AML, anterior mitral leaflet; AV, aortic valve (left and non-coronary cusps); Asc Ao, ascending aorta; IA, innominate artery; LC, left carotid; LS, left subclavian artery; PA, pulmonary artery; LA, ligamentum arteriosum; D Ao, descending aorta.

The thoracic aorta is divided into the ascending aorta, aortic arch, and descending thoracic aortic segments by specific anatomic landmarks in the chest (figures 5.2 and 5.3). The ascending aorta originates with the aortic valve and ends at the origin of the innominate artery. The aorta is further subdivided into the aortic root and the tubular ascending aorta. The aortic root is composed of the aortic annulus, aortic valve leaflets, and sinuses of Valsalva, and is referred to as the aortic valve complex (figure 5.4). The aortic leaflets are attached to the aortic wall above which are sinuses of Valsalva. The aortic root ends where the sinuses of Valsalva join the ascending aorta with a discrete area of narrowing designated as the sinotubular junction. In the normal aorta the sinotubular junction is approximately 10–15% smaller in diameter than the aortic annulus (table 5.2, figure 5.4).[12,13] The sinotubular junction enlarges with age and this waisted appearance is lost. The tubular ascending aorta is usually divided into proximal and distal segments using as a reference the crossover of the right pulmonary artery.
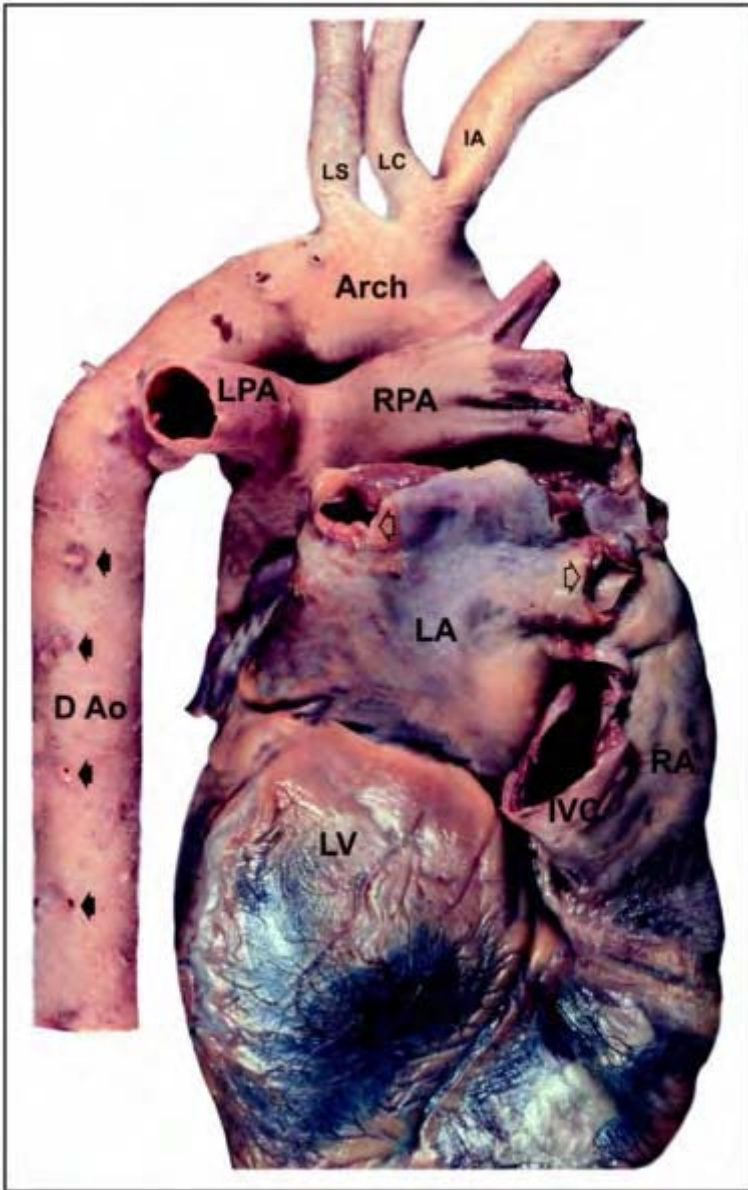
Figure 5.3 Normal heart and thoracic aorta anatomical specimen demonstrating the posterior relationship of these structures as would be encountered and visualized

from the esophagus with TEE. LV, left ventricle; IVC, inferior vena cava; RA, right atrium; LA, left atrium; RPA, right pulmonary artery; LPA, left pulmonary artery; D Ao, descending aorta; LS, left subclavian; LC, left carotid; IA, innominate artery.
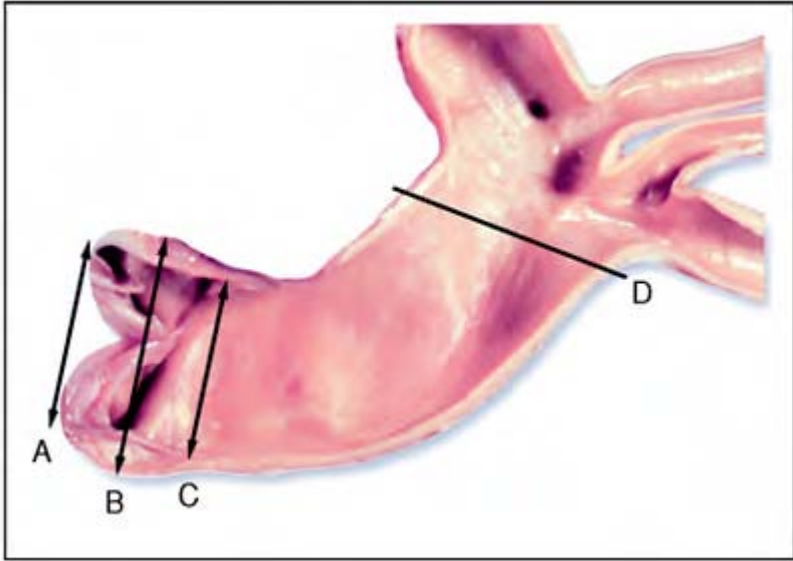
Figure 5.4 Anatomical preparation of the aortic root demonstrating normal dimensions. Progressing from left to right, aortic annulus, sinuses, sinotubular junction and junction between the ascending aorta and arch. Echocardiographic measurements may be made in each section where arrows represent where to measure. Table 2 lists the normal dimensions for each area of the aortic root and thoracic aorta.[199]

Table 5.2 Normal adult cross-sectional echocardiographic values

Parasternal long axis	N	Mean ± SD* (cm)	Range (cm)
Aorta (end-diastole)			
Aortic annulus	68	1.9 ± 0.2	1.4–2.6
Sinus of Valsalva	68	2.8 ± 0.3	2.1–3.5
Sinotubular junction*	64	2.4 ± 0.4	1.7–3.4
Ascending aorta	44	2.6 ± 0.3	2.1–3.4
Triulzi M, Gilliam LD, Gentile F, et al. Normal adult cross-sectional echocardiographic values: linear dimensions and chamber areas. *Echocardiography* 1984;1:403–26.			

The aortic arch begins at the origin of the innominate artery as a continuation of the curved distal ascending tubular aorta, and ends at the aortic isthmus directly opposite the origin of the left subclavian artery. This area gives rise to the ligamentum arteriosum on the lesser or minor curvature of the arch, producing the most acute angle of the aorta. The aortic arch gives rise to the great vessels on the superior margin.

The thoracic descending aorta begins at the level of the ligamentum arteriosum and ends where the aorta penetrates the diaphragm and becomes the abdominal aorta (figures 5.2 and 5.3). The thoracic descending aorta changes its position in relation to the esophagus as it extends longitudinally. The descending thoracic subdivisions are loosely defined by this relationship. The proximal descending aorta begins with the aortic isthmus where the aorta is anterior to the esophagus in the chest. The mid-descending aorta occurs at the mid-chest level with the aorta almost directly lateral to the esophagus. The distal descending aorta ends at the level of the diaphragm, at which point it is directly posterior to the esophagus.

Echocardiographic assessment of the aorta

The resolution of current TEE transducers depicts the thoracic aortic wall in two layers. When examining the aorta it is often helpful to increase the frequency of the TEE probe, if this option is available, to allow the best near field resolution. The intima and media are combined as the inner layer and the adventia as the outer layer, represented as two rings when visualized in short axis. The intima and media are smooth and are moderately echogenic with the same echo consistency around the entire circumference of the aorta. The adventia is the thickest, most echogenic layer and is less homogeneous. It often blends into the adjacent chest structures. The size of the aorta may be determined by measuring the intraluminal diameter in the horizontal planes in the anterior–posterior or right–left direction and in the longitudinal planes in the anterior–posterior or a superior–inferior direction (figures 5.5–5.8). The aorta should be circular in the horizontal planes and there is a tapering in diameter in the longitudinal planes from the ascending to the descending aorta. When the aorta dilates, it becomes more tortuous.

The largest portion of the thoracic aorta lies posterior to the heart and can only be assessed by rotating the transesophageal probe within the esophagus a full 180 degrees in

a clockwise or counterclockwise maneuver (the transducer facing directly posterior towards the spine). It may be better to examine the aorta in two stages. First, the heart and the ascending aorta are assessed with one pass of the probe and then the descending aorta, aortic arch and great vessels are assessed in the second pass of the probe. We prefer to assess the aorta in its entirety following the full examination of the heart, which enables a systematic study of the heart and great vessels.
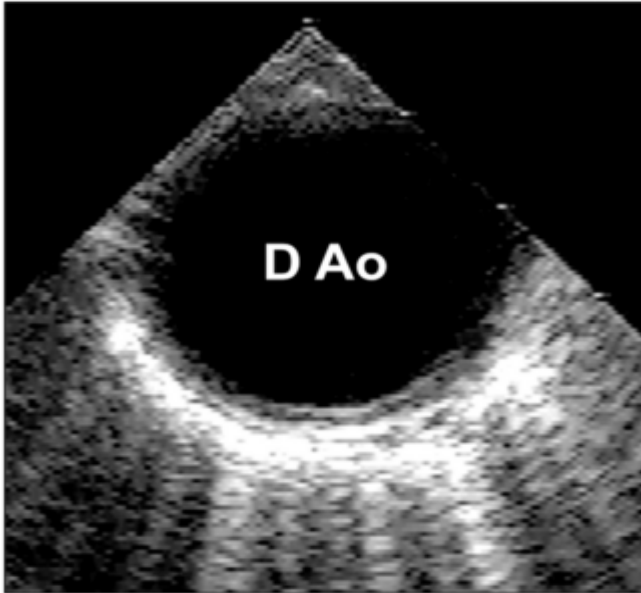
a
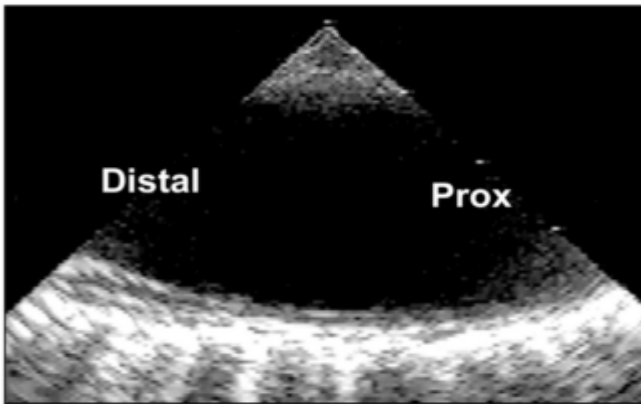
b

Figure 5.5 TEE normal cross-sectional (a) and longitudinal views (b) of the

descending aorta as would be obtained at 0° and 90°, respectively. TEE echocardiography allows good visualization of the aortic walls with the currently available technology. Typically with 5–7 mHz transducers two layers of the aorta are visualized. The near field or anterior half of the aorta is not as well visualized as the posterior half of the aorta visualized in the far field. Careful attention to the transducer focal point may help decrease this phenomenon. With multiplane TEE the so-called blind spot of the junction of the ascending aorta and the arch is virtually eliminated by providing more imaging planes, however, pathology may be missed in the near field. With standardized imaging protocols, the longitudinal views (b) exhibit the distal portion of the aorta on the left of the imaging display and the proximal portion of the aorta on the right of the image sector. This standard is important when determining the level of aortic pathology during examination.
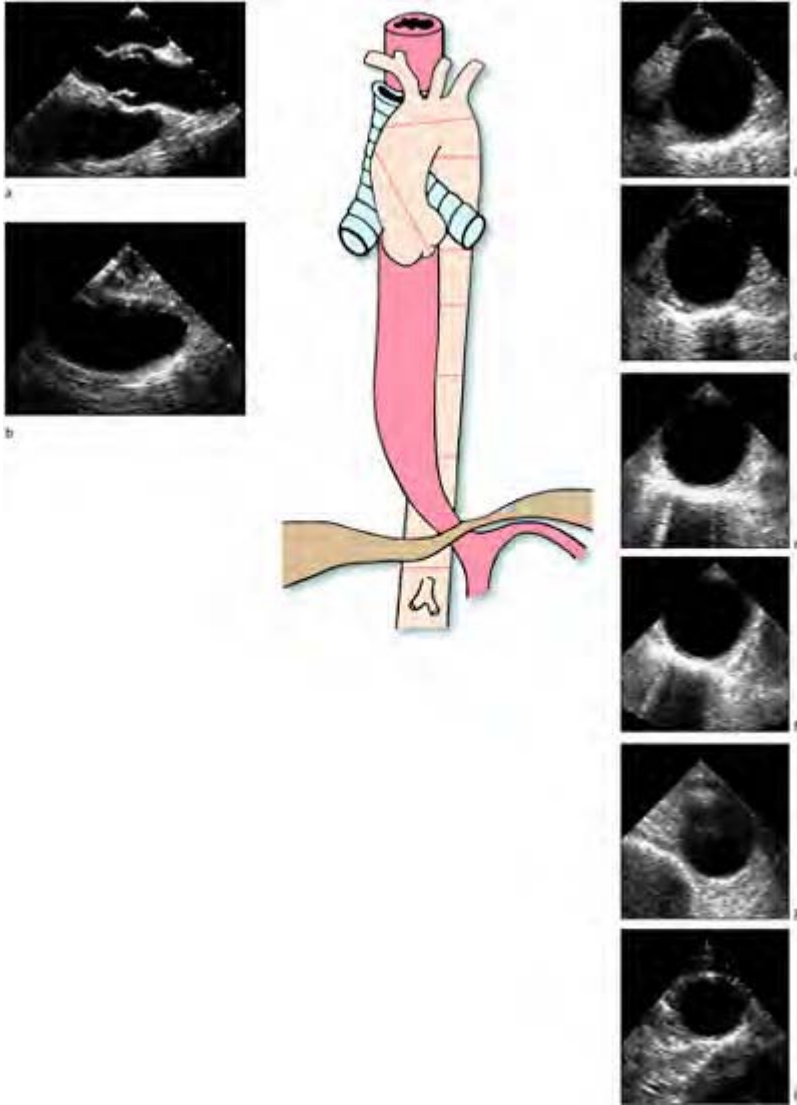
Figure 5.6 Normal echocardiographic anatomy of the aorta. This diagram illustrates the normal relationship of the aorta to the bronchus and esophagus and demonstrates typical echocardiographic images obtained during routine imaging. It is often helpful to construct a mental image of

the echocardiographic images in this fashion in order to describe best the exact position and extent of aortic pathology. Normal longitudinal images of the aortic root (a) and arch (b). Normal short-axis slices along the entire descending aorta (c–h). Care must be taken in defining the level of the images obtained during the study in order to describe the exact location of the descending aorta, since the aorta and esophagus shift in anatomical position from the diaphragm to the neck. Near the diaphragm the transducer faces posterior directly towards the spine, at the mid-chest level the transducer the aorta and esophagus lie side by side and with the esophagus to the right of the aorta. In the upper chest the esophagus is directly posterior and to the right of the descending aorta and the aortic arch. Typically the aortic images are labeled in reference to the probe depth markings. In addition, note the position of the aorta in reference to the spinal and lung interface artifact. With slow withdrawal of the probe the spine is located to the left of the image sector near the diaphragm and assumes a central position in the mid-descending aorta and moves to the right of the image sector and is replaced by the lung interface in the mid to upper portion of the descending aorta. In the horizontal planes the aorta should be circular and tapers in diameter as demonstrated from the ascending to the descending aorta.
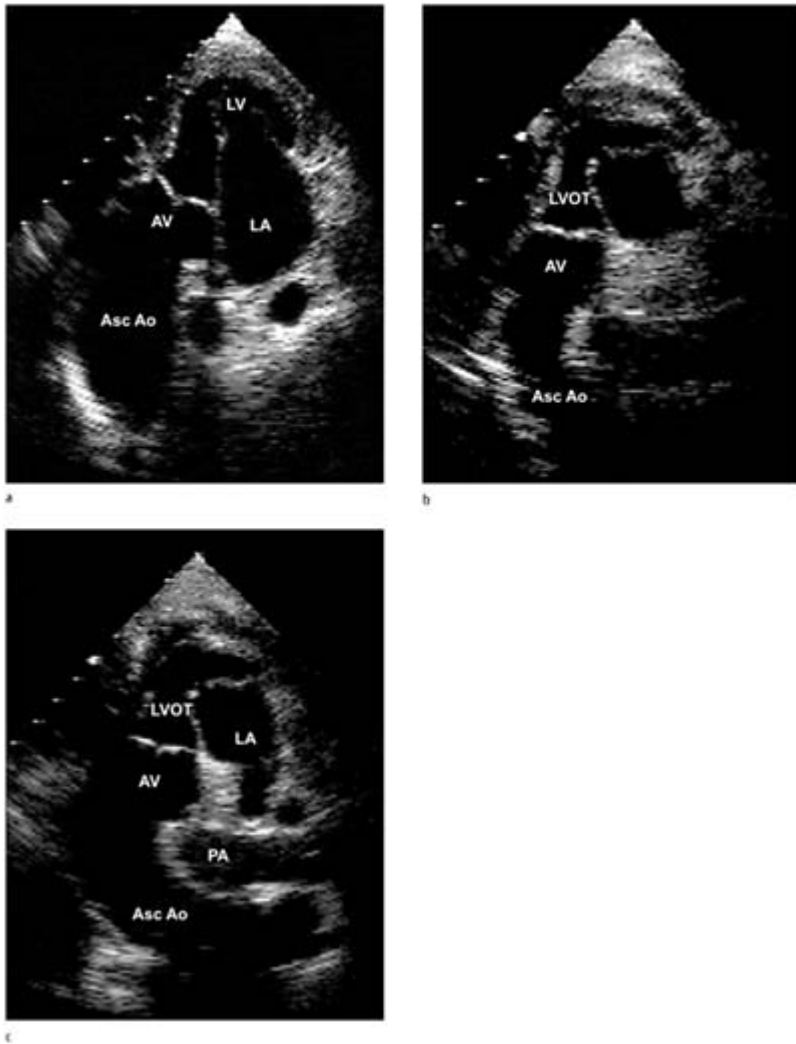
Figure 5.7 Normal tomographic echocardiographic longitudinal axis projections of the ascending aorta obtained from the deep transgastric window. In addition to the conventional upper esophageal views for visualizing the ascending aorta and arch, diagnostic, contiguous longitudinal views (a–c) of the ascending aorta and arch may be

frequently obtained from the deep transgastric views. With minor rotation and manipulations of the probe longitudinal sections of the aorta may be demonstrated in multiple planes depending on the tortuosity and dimensions of the aorta. In addition the origin of the great vessels may be seen.

Full assessment of the aorta requires technical skill in obtaining all the necessary views of a TEE examination, especially in evaluating the distal ascending aorta and take-off of the brachio-cephalic vessels.[14–16] In the awake or sedated patient, the TEE probe is often not well tolerated in the upper esophageal position, which is necessary to evaluate the arch and great vessels. The echocardiographer must be careful not to allow the probe to buckle at this level of the esophagus, which stimulates the gag reflex and provokes coughing. For this reason it is best to perform this part of the examination last, and with the least amount of manipulation of the probe to avoid termination of the study before all necessary information is obtained. It may be necessary to administer more sedation to patients in whom there is a high likelihood of pathology involving the aortic arch.

The esophagus and the descending aorta change positions in the chest in a twisting and turning fashion which influences optimal imaging of the aorta (figure 5.6).
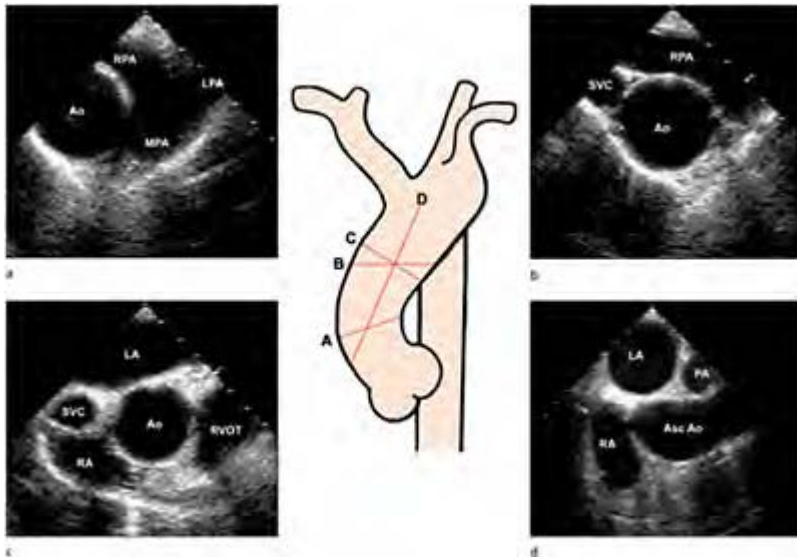
Figure 5.8 Normal tomographic echocardiographic projections of the ascending aorta. The ascending aorta

may be imaged in entirety from 0° to 90° with multiplane TEE. The level of the ascending aorta may be determined according to the corresponding structures in the imaging plane. At the most superior position with the transducer directed anteriorly in the horizontal plane at 0° (a) the aorta is visualized to the left of the image sector with the main pulmonary artery bifurcation to the right. The probe is rotated counterclockwise to orient the ascending aorta to the middle of the sector (b). The aorta is draped in a longitudinal section in the near field by the right pulmonary artery with the superior vena cava visualized in short axis to the left and superior to the aorta (c). Advancing the probe in the esophagus further visualizes the sinotubular junction (d) of the aorta alongside of the superior vena cava with the pulmonary artery being replaced by superior cuts through the left atrium at the top of the image sector and right atrium to the left and below the superior vena cava. The right ventricular outflow tract is to the right of the image. Rotating the transducer to 90° provides a longitudinal plane of the same level of the aorta superior to the aortic valve level. The left atrium is superior in the image sector, with the right atrium below and to the left and the right pulmonary artery is visualized in cross-section to the right of the left atrium and superior to the aorta.

In the lower esophageal view at approximately 45 cm from the incisors, the esophagus is anterior to the descending aorta. At the mid-chest level, 30–35 cm from the incisors, the aorta and esophagus lie side by side, with the esophagus to the right of the aorta. In the upper chest at the level of the origin of the left subclavian artery, 15–20 cm from the incisors, the esophagus is directly posterior and to the right of the descending aorta and aortic arch. The echocardiographer must pay particular attention to this fact when designating the aortic wall as anterior, posterior, medial, or lateral to identify the orientation of aortic pathology, since the aortic wall segments change in position in the ultrasound image when recorded from different levels. In the lower esophageal views the anterior wall segment of the aorta will be shown in the superior aspect of the ultrasound image closest to the transducer
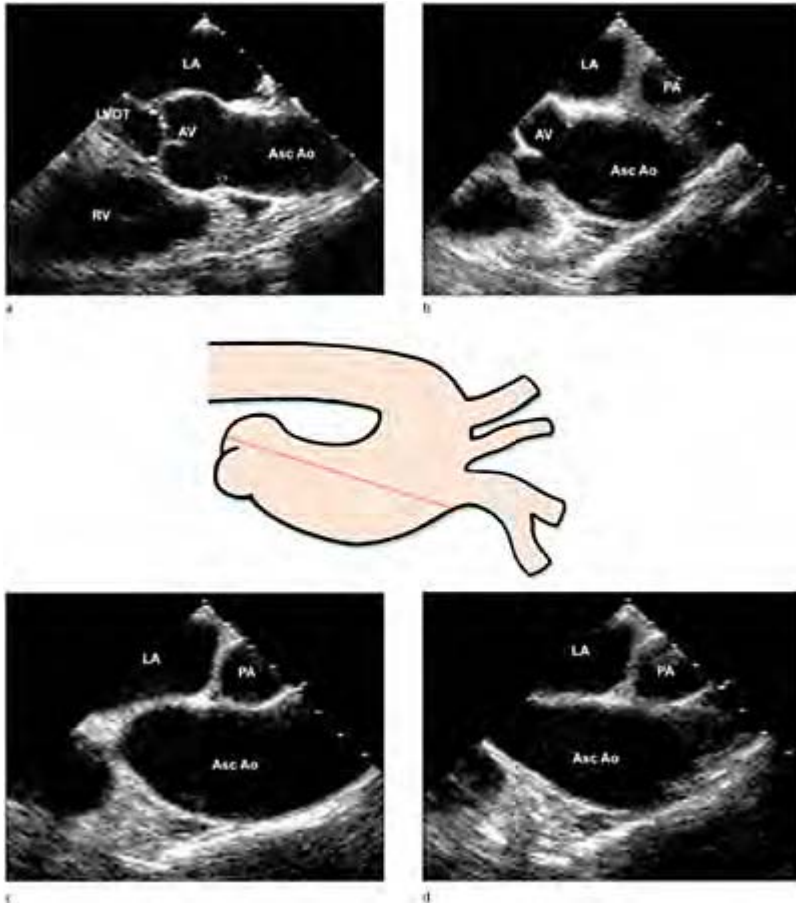
Figure 5.9 Normal tomographic echocardiographic longitudinal axis projections of the ascending aortic

root. Following horizontal imaging of the ascending aorta and establishing circumferential pathology, the transducer can be rotated to 90° to visualize representative longitudinal cuts of the entire aortic root (a, b). With further withdrawal of the probe views of the superior portion of the aorta towards the distal ascending and proximal arch are visualized. One must remember since a limited section is provided with longitudinal cuts, fine manipulation of the probe is necessary to provide a full circumferential evaluation of the aorta to visualize pathology. It is therefore important to evaluate fully with both horizontal and longitudinal planes with multiplane TEE to eliminate the so-called "blind spot of the aorta".
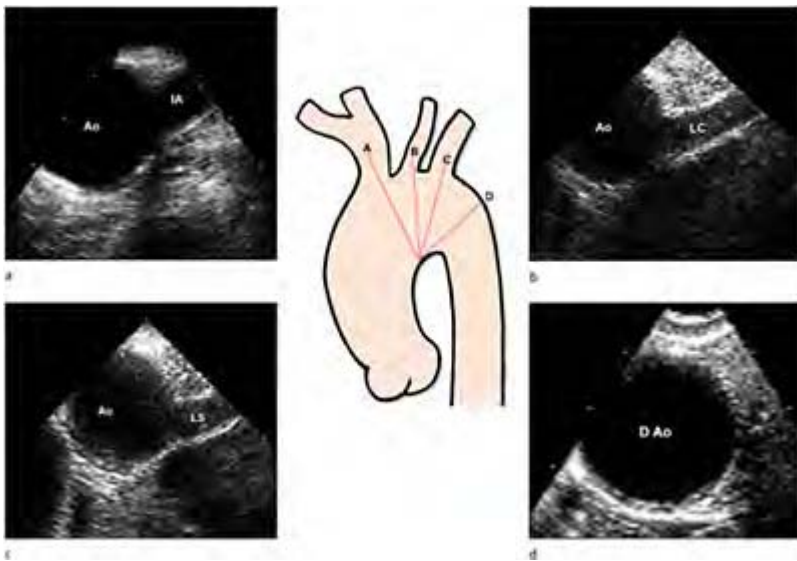
Figure 5.10 Normal tomographic echocardiographic short axis

projections of the aortic arch vessels. Multiplane TEE is extremely advantageous when evaluating the great vessels and their origin from the aortic arch. With fine manipulation of the probe and rotation of the transducer, the great vessels are frequently demonstrated in the horizontal images of the aortic arch. Multiplane TEE is much better tolerated by the patient in awake studies than monoplane or biplane examinations. (a) Innominate artery. (b) Left carotid artery. (c) Subclavian artery. (d) Descending aorta distal to the ligamentum arteriosum. The technique of visualizing the great vessels starts as the probe is withdrawn with a clockwise rotation until the level of the left subclavian artery is visualized to the left of the image sector or the distal aortic arch disappears from view. At this level a greater portion of the subclavian artery may be visualized by slight rotation of the probe counterclockwise and rotating the transducer from 0° to 45°. With further rotation of the transducer the carotid and innominate may also be visualized.

artifact. In the upper esophageal views the aortic wall segments are reversed, with the posterior wall segment of the aorta closest to the transducer artifact at the top of the ultrasound image. When doing the examination it is therefore important to label the aortic images with careful reference to the depth of the scope in the esophagus.

To begin the examination of the aorta, the TEE probe is inserted into the stomach. In the deep transgastric view the whole ascending aorta and arch coursing around the pulmonary artery may be visualized at a depth of field of 24 cm. With minor manipulation (extreme anteflexion of the probe tip and rotating the transducer between 0 and 15 degrees) of the probe, the take-off of the innominate artery can be visualized

(figure 5.7). To improve image quality it may be necessary to decrease the transducer frequency and increase overall gains.

After obtaining the deep transgastric views of the aorta, a routine examination of the heart is performed. With the TEE probe in the mid to upper esophageal position the aorta is visualized near the base of the heart at approximately 0 degrees (figure 5.8). Slowly withdrawing the probe provides horizontal short-axis planes through the
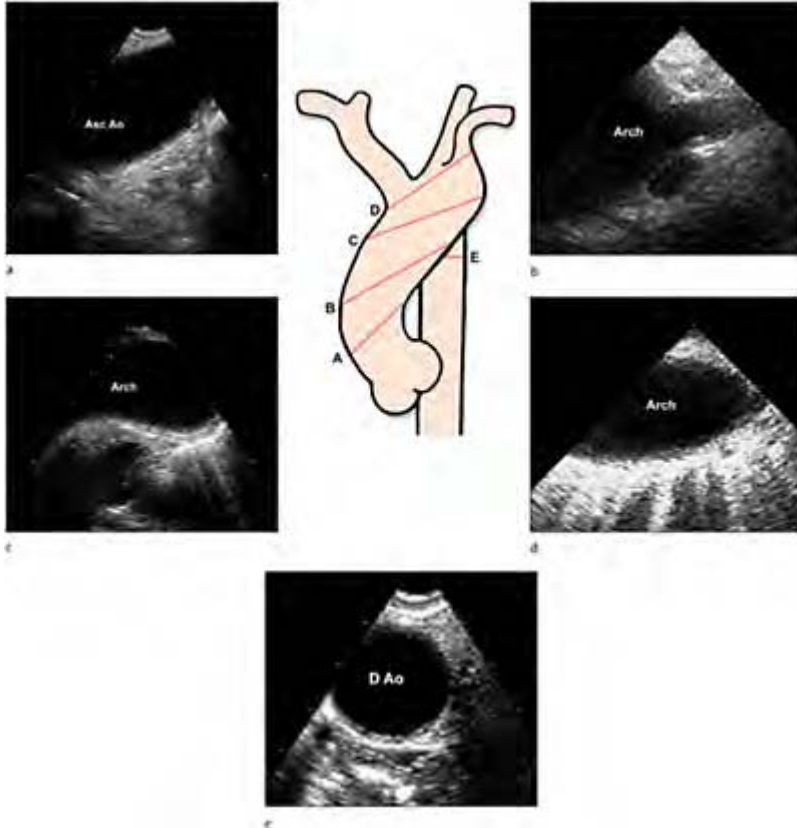
Figure 5.11 Normal tomographic echocardiographic projection of the aortic arch. The aortic arch may be best visualized in representative sections in longitudinal planes from 45° to 90° as the probe is withdrawn and rotated after initially imaging the ascending aorta or descending aorta. (a) Distal ascending aorta. (b)

Proximal arch and origin of the innominate artery. (c) Proximal aortic arch. (d) Distal arch. (e). Proximal descending aorta. The technique for visualizing the arch after initially visualizing the descending aorta in horizontal planes involves further slow withdrawal and anterior rotation of the probe with a slight degree of anteflexion. As the transducer is rotated to 90°, the aortic arch is represented as an oval structure running in a tangential fashion in the image sector, with the distal arch to the right and the proximal arch to the left of the image. Further anterior rotation of the probe visualizes the distal ascending aorta and proximal arch running in a more superior to inferior orientation in the image. Frequently the innominate artery is better visualized (b) during withdrawal of the probe facing directly anterior, visualizing the ascending aorta in the same manner the subclavian artery is found by initially visualizing the descending aorta with withdrawal of the probe.

ascending aorta until the level of the right bronchus is reached. Depending on the position and size of the aorta, anteflexion of the probe may be necessary to obtain true short axis images. After obtaining the short axis images, the TEE probe is advanced back to the level of the aortic valve plane and the TEE transducer is rotated through 90 to 120 degrees to obtain a longitudinal projection of the entire aortic root (figure 5.9). Minor adjustment of the probe with right to left flexion may be required to provide the best images, so as not to provide an oblique plane. In the longitudinal plane the whole ascending aorta is usually visualized up to the level of the aortic arch.

Rotation of the TEE probe through 180 degrees, so that the transducer faces the posterior aspect of the esophagus at a depth of field between 4–6 cm, enables visualization of the descending thoracic aorta. At this depth, a detailed examination of the aorta is obtained especially when there is aortic dilatation or aneurysm formation. The

aorta is centered in the field of view and the probe is manipulated until the celiac aortic is in view, emanating from the aorta to the right of the ultrasound image. The aorta appears deeper in the image sector and is usually visualized 2cm from the apex of the echo sector. The TEE probe is slowly withdrawn into the lower esophagus (45 cm) with the probe at 0 degrees. Imaging of the aorta is best at the higher frequency with decreased near-gain setting to prevent artifactual shadowing. The aorta may be visualized with slight manipulation of the controls in cross-section at 0 degrees and longitudinally by steering the transducer to 90 degrees (figure 5.5). In the horizontal planes the aorta appears circular, and in longitudinal planes, the aorta appears as a parallel-sided tube with the proximal segment to the right and the distal segment to the left. There is usually no advantage to visualizing the descending aorta in additional planes, except when attempting to identify the site of re-entry intimal tears that occur in dissection, atheromatous ulcers, and debris. The probe is continuously withdrawn in the esophagus in 3–5 cm increments, with slight rotation of the probe in a clockwise manner to keep the aorta central in the ultrasound image (figure 5.6). The spinal column artefact often helps to determine the level of the aortic segment since it is only visible in the distal thoracic aorta and is lost when the aorta lies alongside the esophagus. In the mid segment of the aorta the spinal column artefact appears in the distal field of view by lung. It is useful to annotate the ultrasound screen with the probe depth or to use the equipment microphone to record the probe depth. The probe is withdrawn with a clockwise rotation until the level of the left subclavian take-off is visualized to the left of the ultrasound image, or the distal aortic arch disappears from view. At this level, a greater portion of the subclavian artery may be visualized by slight rotation of the probe counterclockwise and rotating the transducer from 0 to 45 degrees (figure 5.10). With slightly further rotation of the transducer probe the other two brachiocephalic vessels are usually visualized. The left common carotid artery can be imaged taking origin proximal to the subclavian, by rotating the transducer by 10–30 degrees further than required to visualize the subclavian artery. The innominate artery may be visualized proximal to the origin of the left carotid artery by clockwise rotation beyond the neutral position. The innominate artery is the most difficult artery to visualize, since it lies in the plane in which the right bronchus crosses in between the esophagus and aorta—the so-called blindspot—and is usually only visualized in 40% of all cases, even in the most experienced hands. The aortic arch is seen when the transducer is rotated a full 90 degrees, as an oval structure running in a tangential fashion in the ultrasound image, with the distal arch to the right and the proximal arch to the left of the image (figure 5.11). Further anterior rotation of the probe visualizes the distal ascending aorta and proximal arch running in a more superior to inferior orientation in the ultrasound image.

Aortic disease

It is extremely important when describing aortic disease to have a clear understanding of the accepted terms used in describing aortic pathology. This is important for three reasons; first, TEE has become the procedure of choice and frequently the only method used for diagnosing aortic disease emergently to direct treatment in many institutions. Second, TEE images of the aorta are frequently compared with CT scans, MRI, contrast

aortograms, or direct surgical visualization, so that a consistent set of terms are necessary for accurate understanding and communication of pathological findings obtained by these different diagnostic imaging methods. Third, different aortic pathologies may be visually similar or indistinguishable by cursory examination of TEE images, which may give an inaccurate diagnosis.

Aortic diseases may be attributable to congenital disease, genetic connective tissue disorders, arteriosclerotic disease, and inflammatory processes involving the aorta. Frequently the type of aortic disease has a predilection for a particular aortic segment, as described in table 5.3. Diseases of the aorta may result in complete occlusion or compromise of the aortic lumen or aneurysmal dilatation. Whether there is occlusive or aneurysmal aortic disease, distal embolization of atherosclerotic debris or thrombus frequently occurs. The most devastating consequences of occlusive aortic disease and aortic aneurysm are complete occlusion of the aorta and rupture of the diseased aortic segment, respectively.

Aortic aneurysm

Aneurysms of the aorta may exist as an isolated entity or occur in association with other aortic pathologies.[17–22] An aneurysm of the aorta is present when there is an increase in the intraluminal diameter of the aorta above the normal 95% confidence limits, after correction for patient age and body habitus (figure 5.12).[9,10] "Aortic aneurysm" is defined pathologically as a twofold increase of the transverse diameter of the aorta compared with the normal aortic segment. In addition to an enlarged diameter, the aorta also increases in length in the diseased segment producing distortion, unfolding, and tortuosity of the affected and distal segments. Before imaging methods were available, thoracic aortic aneurysms usually remained undiagnosed until presenting with significant enlargement. With the advent of better imaging methods such as TEE, aortic aneurysmal disease is better appreciated and is more frequently diagnosed earlier in its course. As discussed above, the normal aorta is tubular and gradually tapers as it progresses distally, away from the sinotubular junction. The normal dimensions of the aorta have been described pathologically and differ according to body size, age, and sex. Subtle dilatations of the aorta are easily recognized with TEE, in sharp contrast to normal aortic segments, because serial tomographic slices of the entire thoracic aorta can be obtained. In patients with diffuse aortic dilatation, the aortic dimensions should be compared with the size of the pulmonary artery or dimensions of the cardiac chambers, which together with body habitus serve as a reference for appropriate aortic sizing.

Figure 5.12 Photograph taken during surgical exposure demonstrating an ascending aortic aneurysm. Typical appearance of annuloaortic ectasia in a patient with Marfan's syndrome usually associated with significant

aortic regurgitation secondary to annular dilatation of the aortic valve. Ascending aortic aneurysm is one of the most frequent manifestations with Marfan's syndrome and leads to progressive dilatation with eventual rupture or dissection. An aortic aneurysm is defined pathologically as a two-fold increase of the transverse diameter of the aorta compared to the normal aortic segment producing distortion, unfolding and tortuosity of the affected and distal segments.

Aortic aneurysms are classified according to their location, etiology, and gross appearance. Aortic aneurysms may occur in any segment of the thoracic aorta. Location of aortic aneurysms is by the segment of aortic involvement; annulus, sinus, ascending, arch, and/or descending thoracic aorta. The etiology of the aneurysm is based on the specific nature of vascular damage that leads to the aneurysmal dilatation. Arteriosclerotic, inflammatory (aortitis), dissecting (cystic medial necrosis), and traumatic processes are the most common causes. The etiology of aortic aneurysm may frequently be deduced from the pathology detected by TEE. Irrespective of the cause of an aneurysm, damage occurs in the aortic tunica media layer, which results in weakening and dilatation of the aortic wall. The shape and size of the aneurysmal segment describe the gross appearance of aortic aneurysms. Thoracic aortic aneurysms may be saccular, fusiform, or cylindroid in shape and appearance.

Saccular aneurysms are spherical protrusions or out-pouching of the aorta, which narrow to varying degrees to connect to the true lumen of the tubular aorta. Saccular aneurysms are often partially or completely filled with laminated thrombus. If a saccular aneurysm is filled with thrombus, contrast aortography may not fill the aneurysmal sac and therefore it will not be diagnosed. With transesophageal echocardiography and careful inspection of the aorta, saccular aneurysms may be identified with two-dimensional imaging and color flow Doppler. Usually, a spherical protrusion is identified in close proximity to the aorta, and with minor manipulations of the probe the neck of the aneurysmal sac may be identified and color flow Doppler may show low velocity flow within the aneurysm. If the aneurysm has contained thrombus, this is easily identified by the difference in echocardiographic texture between the thrombus and the aortic wall. Additionally, color flow Doppler usually delineates the interface between blood and thrombus.

Table 5.3 Aortic syndromes – site of involvement (%)

Aortic syndrome	Ascending	Arch	Descending
Classic dissection	75	10–19	25
Intramural hematoma	48	8	44
Penetrating aortic ulcer	5		95
Atherosclerosis	10–30	70	30
Aortic aneurysm	51	11	38
Aortitis	15		15
Transection	23	8	13
Isthmus	45		

Fusiform aneurysms of the thoracic aorta are illustrated by a gradual, progressive symmetric dilatation of the aortic lumen. The lumen of the aneurysmal segment is in direct continuity with the true lumen of the normal aortic segments. In longitudinal visualization of the aorta a fusiform aneurysm will give a spindle appearance to the aortic lumen. Dilatations of the aortic lumen in fusiform aneurysms are frequently eccentric, involving one wall of the aorta more than the other. In short-axis imaging of the aorta, the circular shape of the aorta will be distorted. Fusiform aneurysms of the thoracic aorta vary in size and length and may involve the entire thoracic aorta. When fusiform aneurysms extend over a considerable length they may lose their tapered appearance and appear more cylindrical. These have been termed cylindroid aneurysms concordant with the pathological descriptions. Fusiform aneurysms, which are similar to saccular aortic aneurysms, are frequently lined with mural thrombus.

The incidence of thoracic aortic aneurysms is 5.9 per 100,000 population per year as reported by Bickerstaff in Rochester, Minnesota.[19] In that study, aneurysms occurred in the ascending aorta in 51%, the aortic arch in 11% and the descending aorta in 38% of patients. By contrast to the incidence of abdominal aortic aneurysms, thoracic aneurysms have not shown a decline in incidence. The growth rate of thoracic aneurysms appears to be faster than that of abdominal aneurysms, with an overall rate of 0.42 cm/year for the entire thoracic aorta and up to 0.56 cm/year in aneurysms involving the aortic arch (table 5.4). This explains in part why thoracic aneurysms have a greater rate of rupture than abdominal aortic aneurysms. Bickerstaff reported that rupture occurred in 74% of patients with thoracic aortic aneurysms. Current recom mendations for prophylactic aortic surgery of the thoracic aorta irrespective of signs include aortic dilatation exceeding twice the size of the normal aorta, aortic diameter greater than 5 cm, and rapidly dilating aneurysms on serial follow-up studies.[23–25] Since the highest rate of rupture is shown in Marfan syndrome, many surgeons advocate surgical repair/replacement when the aortic dimension reaches 4.7–5 cm in diameter.[26]

Table 5.4 Aortic measurements and definitions

Average rate of growth of the aorta (diameter) = 2 mm per year
Adults Aortic root diameter/height = –45.9 + 0.493 height (cm) – 0.001 × 2 Aortic root diameter/BSA = –1.915 + 3.826 BSA –0.704 × 2
Growing children Aortic root diameter = 24 $(BSA\ m^2)^{1/3}$ + 0.1 (age) – 4.3 *or* = 11.8 $(weight\ kg)^{0.213}$ + 0.1 (age) – 4.3
Diagnosis of aortic aneurysm Aneurysm of the aorta is present when there is an increase in the intraluminal diameter of the aorta above the normal 95% confidence limits, after correction for patient age and body habitus
Indications for aneurysm resection Aortic growth rate greater than 5–7 mm Asymptomatic aneurysms 2 × the normal aortic diameter *or* aneurysms exceeding 4.7–5 cm

Marfan syndrome

Marfan syndrome is an inherited, autosomal dominant disorder of connective tissues, with a predilection for the heart and blood vessels, particularly the aorta. The eyes, bones, and joints are also affected and account for the musculoskeletal and ophthamalogicalfindings that comprise the full syndrome. Cardiovascular abnormalities are the most frequent cause of death in Marfan syndrome, which usually occurs prematurely. In a study by Murdoch et al.[27] on Marfan syndrome, the cause of death was cardiovascular in 93% of cases with an average age at death of 32 years. Ascending aortic aneurysm is one of the most frequent manifestations and leads to progressive dilatation with eventual rupture or dissection. The prevalence of Marfan syndrome is 4 to 6 per 100,000 people, with a higher prevalence in the Chinese population of 17 per 100,000.[28–30]

Table 5.5 Diagnosis of Marfan syndrome: Berlin Nosology,1986

Diagnostic manifestations	Abdominal aortic aneurysm
Skeletal	Dysrhythmia
Anterior chest deformity, especially asymmetric pectus excavatum/carinatum	Endocarditis
Dolichostenomelia not due to scoliosis	**Pulmonary**
Arachnodactyly	Spontaneous pneumothorax
Vertebral column deformity	Apical bleb

Scoliosis	
Thoracic lordosis or reduced thoracic kyphosis	**Skin and integument**
Tall stature, especially compared to unaffected 1° relatives	Striae distensae
High, narrowly arched palate and dental crowding	Inguinal hernia
Protrusio acetabulae	Other hernia (umbilical, diaphragmatic, incisional)
Abnormal appendicular joint mobility	**Central nervous system**
Congenital flexion contractures	Dural ectasia*
Hypermobility	Lumbosacral meningocele
Ocular	Dilated cisterna magna
Ectopia lentis*	Learning disability (verbal-performance discrepancy)
Flat cornea	Hyperactivity with or without attention-deficit disorder
Elongated globe	**Requirements for diagnosis**
Retinal detachment	In the absence of an unequivocally affected 1° relative: Involvement of the skeleton and at least two other systems; at least one major manifestation
Myopia	
Cardiovascular	In the presence of at least one unequivocally affected 1° relative: Involvement of at least two systems; at least one major manifestation preferred, but this will depend somewhat on the family's phenotype
Dilatation of the ascending aorta*	
Aortic dissection*	
Aortic regurgitation	
Mitral regurgitation due to mitral valve prolapse	
Calcification of the mitral annulus	Urine aminoacid analysis in the absence of pyridoxine supplementation confirms absence of homocystinuria
Mitral valve prolapse	
*denotes major criteria	
Beighton P, de Paepe A, Danks D, et al. International nosology of heritable disorders of connective tissue, Berlin, 1986. Am J Med Gen 1988;29:581–94.	

Histology of the aorta in Marfan syndrome usually illustrates marked medial degeneration of elastic tissue with some degree of medial necrosis of the smooth muscle cells, often referred to as cystic medial necrosis. The replacement of elastic fibers with mucoid material in the aortic wall predisposes the aorta to stiffness or a loss of the normal distensibility, leading to a weakened aortic wall that dilates in response to sheer hemodynamic forces. The ascending aorta is most affected owing to its higher content of elastic tissue in comparison to more distal segments of the aorta.

The diagnosis of Marfan syndrome is based on clinical findings, classified into major and minor manifestations, by McKusick and Pyeritz[28,32] (table 5.5). The four major criteria are ocular, musculoskeletal deformities, a family history of Marfan syndrome, and cardiovascular abnormalities. In patients with a family history of at least one primary relative with Marfan syndrome, diagnosis requires two body systems to be affected with at least one major manifestation. In about 25% of patients who are without a first degree relative with the syndrome, musculoskeletal system involvement with at least two other systems involved (at least one major manifestation) is required to establish the clinical diagnosis of Marfan syndrome. Recently haplotype-segregation analysis has become available, which may be helpful to diagnose clinically challenging patients and to screen first-degree relatives of probands.

The spectrum of cardiovascular manifestations in Marfan syndrome was summarized by Roberts and Honig,[33] who studied 18 necropsy patients from the National Heart, Lung and Blood Institute (NHLBI) and 151 necropsy cases previously reported. In necropsy studies they were able to classify the cardiovascular manifestations into three predominate groups based on their findings: (1) fusiform ascending aneurysm, (2) aortic dissection, and (3) isolated mitral regurgitation. In our experience, use of this classification has greatly assisted in the interpretation of transthoracic and transesophageal echocardiograms in Marfan syndrome by presenting the many manifestations of this complex disease in a logical order.

Group I: Fusiform ascending aneurysm

In patients with fusiform ascending aneurysm roughly 95% showed aortic valve incompetence caused by annular dilatation.[35] The aneurysm showed annuloaortic ectasia or involvement of the sinus and proximal tubular aorta, with progression to the aortic arch in a few cases. Mitral regurgitation and/or chest pain was present in roughly 50% of patients by clinical history. Five of 13 cases from the NHLBI group had small healed tears of the intimal lining of the aorta, probably representing healed dissection or partial rupture. The principal causes of death were congestive heart failure, aortic rupture, or death following cardiovascular surgery. Two patients also had descending thoracic fusiform aneurysms. Aortic valves were all tricuspid with mild marginal rolling of the cusps and stretching at the commissures due to annular dilatation. Histologically the aortic cusps had increased amounts of acid mucopolysaccharide material. The mitral valves in this group showed varying degrees of mitral valve prolapse, annular dilatation and mitral annular calcification. Histologically, the mitral leaflets were similar to the aortic valves.

These findings are consistent with those reported by Roman et al.[34] who showed generalized ascending aortic dilatation in 58% of male patients. Ascending aortic aneurysm favored male patients and grew more rapidly (0.11 mm/year) than in females, with 19% of all aortic complications occurring within 49 months of initial diagnosis or follow-up.

Of note, in the NHLBI group these patients did not develop dissection, rather they experienced aortic rupture. The authors postulated that the deposition of collagen and mucoid material, replacing the elastic fibers of the media, prevents longitudinal aortic dissection.

Group II: Aortic dissection

One of the most striking features of the NHLBI cases of aortic dissection was that dissection occurred in apparently normal and nondilated aortas, and the dilatation of the aorta that was observed at necropsy was attributable to the dissection pathology. To corroborate these findings, there was no prior clinical history of aneurysm, aortic or mitral insufficiency, or congestive heart failure, and patients were reported free of symptoms until the appearance of chest pain heralding the aortic dissection. A few cases did have a history of systemic hypertension. At necropsy, the dissection process frequently affected the entire aorta and extended to the iliac arteries. Histological examination of the aorta failed to show the typical findings of cystic medial necrosis that accompanies normal aortic dimensions. Severe aortic insufficiency was due to dissection, and the mitral and tricuspid valves were normal except for annular dilatation. Svennson et al.[35] have also reported that aortic dissection in these patients may be painless and without hemodynamic compromise. In addition, there appears to be a sub-group of families with Marfan syndrome who express a predilection for dissection.

By contrast to other reports, aortic dissection in the NHLBI study occurred in undilated aortas. In review of many of these studies, if aortic dilatation is present it does not appear to be as significant as that found with fusiform ascending aortas—as in group I patients—and many reports describe normal aortas histologically. Svennson et al.[35] have also suggested that patients with sinus of Valsalva dilatation only appear to be less prone to dissection and the rate of further dilatation is less than in fusiform aneurysms.

Group III: Isolated mitral regurgitation

Cases with isolated mitral regurgitation showed severe mitral regurgitation secondary to marked mitral valve prolapse with floppy leaflets, elongated chordae tendinae, ruptured chords, and annular calcification. Annular dilatation was more marked than those in the aortic dissection group. In all patients the aorta and aortic valves were normal. Clinical findings before death were consistent with chronic congestive heart failure, and a few patients showed findings of previous endocarditis.

These findings are further substantiated by echocardiography studies of Marfan syndrome by Spangler et al.[36] who found mitral valve abnormalities in 62% of patients, and by Pyeritz and McKusick,[28] who found mitral valve prolapse in 58% as an isolated incident or in combination with the other manifestations of Marfan syndrome. In addition mitral valve abnormalities have been described in Marfan patients before 1 year of age,[37] whereas aortic aneurysm and dissection are usually described initially later in life. Edwards and others[38–42] have suggested that patients with mitral valve prolapse are prone to sudden death, which may be related to malignant arrhythmias.

Management

The successful management of the cardiovascular manifestations of Marfan syndrome remains surgical correction.[42] Medical therapy with beta-blockers has been shown to slow the rate of aneurysmal dilatation, probably as a result of decreasing the dP/dt in the aorta, producing a negative inotropic effect and controlling blood pressure in certain individuals. However, these results are self-limited.[35,43,44]

Indications for surgery in Marfan syndrome patients vary according to the aggressiveness of the institution, and in our experience are usually directly proportional to the overall experience and the comfort level of the institution for patients with Marfan syndrome. Dissection and aneurysmal rupture of the aorta require immediate surgical repair. With the advent of mitral and aortic reparative procedures, surgery is generally performed when symptoms dictate or at the first signs of left ventricular dysfunction. Most reports suggest reparative aortic surgery with aortic dilatation greater than 5 cm in diameter.[42,45] Other factors may also be considered, however, especially since excellent surgical survival rates have been reported with aortic valve conduit grafts. Rapidly expanding aortic aneurysms greater than 5–7 mm or more per year, or aortic aneurysm dilatation greater than 4.5 cm in childbearing females, should be considered for early surgery due to the higher rupture and dissection rate in these individuals.[42]

Patients with Marfan syndrome in our institution are followed with echocardiography 6 months after initial presentation or diagnosis, and then every 6 months to 1 year or as dictated by clinical findings or symptoms.

Bicuspid aortic valve and aneurysm

Bicuspid aortic valves are frequently associated with proximal aortic aneurysms and with an increased incidence of fatal aortic dissection in younger and middle-aged patients. The true incidence of aortic aneurysm in patients with bicuspid valve is unknown, since the presence of aortic aneurysm may be independent of the severity of valvular hemodynamics of stenosis or regurgitation. Aortic aneurysm has frequently been diagnosed as post-stenotic dilatation, especially when the proximal aorta has not been adequately visualized. In a necropsy review of aortic dissection by Larsen and Edwards,[46] bicuspid aortic valve was seen more frequently (6%) in aortic dissection than in the general population, and was associated more frequently with dissection than tricuspid aortic valves (0.7%).

Patients with both bicuspid aortic valve and coarctation of the aorta may be at added risk for aortic dissection. Abbot et al.[47] reported a 23% incidence of bicuspid aortic valve at necropsy in 200 cases of aortic coarctation. Aortic dissection occurred in 37% of cases with bicuspid aortic valve. Bicuspid aortic valve appears to be an independent risk factor for dissection; however, aortic dissection has been observed after surgical repair of aortic coarctation, with or without valve replacement.

A few studies[47,48] have suggested that there is a primary abnormality of the aortic root in patients with bicuspid aortic valves. In patients with tricuspid and bicuspid valves studied with echocardiography, Hahn et al.[49] showed that aortic root dimensions were larger in patients with bicuspid valves irrespective of the presence of stenosis or regurgitation. Histological sections of aortic tissue after dissection have illustrated cystic medial necrosis, similar to that in Marfan syndrome. It has also been noted that progression of aortic root dilatation and dissection may still occur after valve replacement. This is in contradistinction to the post-stenotic dilatation that occurs with tricuspid aortic stenosis, and supports a primary pathology of the aortic root.

Despite the similarities between aortic aneurysm associated with bicuspid aortic valve and Marfan syndrome, the natural history of aneurysm in the setting of bicuspid aortic

valve has not been well studied. Despite the prevalence of bicuspid valve in post-mortem studies of dissection, the incidence of dissection is low in a condition with a 1% incidence in the general population.[50] Until further studies are done, patients that have known aortic root enlargement and a bicuspid aortic valve should be followed closely with echocardiographic surveillance before and after valve replacement, and patients at greatest risk may warrant consideration for a combined valveroot replacement.[51] Additionally, patients with bicuspid aortic valve and aortic root enlargement should be carefully assessed for bicuspid pulmonary valve and dilation of the main pulmonary artery.

Pregnancy

The diagnosis of aortic aneurysm is extremely important in women of childbearing age, in whom aneurysms or aortic root dilatation are frequently overlooked on echocardiography because aortic dimensions are often not corrected for body habitus. Pregnancy in patients with aortic aneurysm, especially those with Marfan or Ehlers—Danlos syndrome, poses a significant risk of aortic rupture and as such is an important management problem. These patients require close echocardiographic surveillance and may necessitate early intervention due to the high rate of dissection and spontaneous rupture that occurs during pregnancy. In women under 40 years old, 50% of all aortic dissection or rupture occurs during pregnancy.[52–54] The abrupt changes in hemodynamics associated with shifts in hormones during pregnancy, as well as the direct weakening affect on the aortic wall of increased relaxin levels, may lead to aortic complications, irrespective of the presence of aortic valvular disease. Patients are predominately susceptible to aortic complications during the third trimester of pregnancy, during labor and delivery,[55–59] and for 6–8 weeks after delivery. Dissection of the proximal aorta occurs most frequently and is usually associated with some degree of aortic insufficiency.[60–62] Without adequate prenatal follow-up, dissection during pregnancy carries a poor prognosis, with rupture of the diseased aortic segment occurring in about 71% of patients, producing significant maternal mortality.[63]

Most recently, reports in the literature have described the clinical management and the surgical repair of the dissected aorta in pregnancy.[59,64–66] Successful management in patients that dissect or rupture late in pregnancy requires immediate cesaren section followed by aortic repair. Rapid diagnosis and accurate assessments of the degree of aortic involvement are extremely important and frequently depend on TEE imaging. TEE imaging is usually the diagnostic method of choice since it may be done at the bedside, and it avoids delay caused by transfer of unstable patients to other areas of the hospital. TEE imaging is also essential for patient monitoring during the surgery and helps in optimal anesthetic management especially with the use of uterotonic drugs. Surgical techniques for repair of dissection or rupture during pregnancy do not differ from those for dissection in non-pregnant patients, and the precise identification of the site of intimal tear is extremely important. A proximal dissection, with aortic insufficiency, pericardial or pleural effusion, mediastinal hematoma or great vessel compromise, as identified by TEE, poses the most immediate risk to the patient. Patients that present with distal thoracic dissections may be treated conservatively unless signs and symptoms of

imminent rupture or vital organ compromise are evident, or as long as hypertension can be adequately controlled.

The management of pregnancy in patients with preexistent aortic disease poses another problem, especially if the mother wishes to maintain the pregnancy. In patients with Marfan syndrome, counseling is usually advisable prior to pregnancy. Patients should be informed of the increased risk of aortic rupture or dissection, especially when there is aortic dilatation greater than 4 cm, as well as the possibility of passing on the dominant gene to 50% of their offspring.[61] Previous reports suggesting excessive morbidity and mortality during pregnancy in Marfan syndrome have been refuted by Rossiter et al,[67] who reported that pregnancy is not prohibitive in patients who show minor cardiovascular involvement. Pyeritz[61] has proposed that women with minor cardiovascular involvement and aortic root diameter of less than 4 cm should be advised of the relatively small risk of dissection in comparison to normal women without Marfan syndrome, after retrospective observations in patients who completed pregnancy. Further larger prospective studies need to be done in childbearing females with Marfan syndrome before definitive recommendations are adopted.

Elective surgical repair of aortic disease including aortic-root replacement should be avoided whenever possible during pregnancy, due to placental dysfunction and fetal compromise precipitated by cardiopulmonary bypass. Becker[68] has described a 27% abortion rate in pregnant patients undergoing cardiac surgical procedures. In patients with aortic aneurysms, especially those with Marfan syndrome, serial echocardiography should be done throughout pregnancy to afford the greatest opportunity for a successful and uncomplicated delivery. In our institution, transthoracic echocardiograms are done every 4–6 weeks or as dictated by clinical signs and symptoms to observe aortic luminal and wall dimensions, corrected for body surface area. TEE is often done initially to serve as a baseline, especially if transthoracic images are not adequate. Pregnant patients who show worsening of any cardiac valvular and/or aortic lesions that are life-threatening should have them repaired before the third trimester.[64,69]

Sinus of Valsalva aneurysm

Aneurysm of the sinuses of Valsalva may occur on a congenital or acquired basis. Congenital sinus of Valsalva aneurysm is discussed in the chapter on congenital heart disease. Acquired aneurysms of the aortic sinus of Valsalva are caused by cystic medial necrosis similar to Marfan syndrome, endocarditis, atherosclerosis, aortitis, and trauma.[70–73] Acquired aneurysms of the sinuses of Valsalva differ from congenital aneurysms in that they are often associated with dilatation of the ascending aorta, involve more than one sinus, and may protrude or rupture outside the heart into the pericardium. Sinus of Valsalva aneurysms are best appreciated echocardiographically in horizontal or short-axis views of the aortic valve plane, using the other cusps as reference points against enlargement and protrusion. TEE is especially useful when transthoracic images are not diagnostic. Color Doppler findings are optimal with multiplane TEE, which allows for better identification of rupture sites into the cardiac chambers—a frequent complication of endocarditis. Surgical intervention is usually dictated by associated aortic

abnormalities, aortic valve endocarditis, or when rupture causes significant hemodynamic compromise.[74–76]

Atherosclerotic aneurysms

Aneurysm formation in the aorta resulting from athero-sclerosis is a degenerative disease process, which occurs in part with increasing age. Atherosclerotic aneurysms most commonly occur in the abdominal aorta; however, they also occur in the thoracic aorta and are usually fusiform. Atherosclerotic aneurysms typically occur in the presence of severe atherosclerotic disease, although the involvement of the aorta may be localized. Atherosclerotic lesions may not be detected in direct proximity to the aneurysm; however, histologically atheroma extends into the media to cause destruction of the fibromuscular and elastic support layer of the aorta. Atheromatous ulcers are often observed within the aneurysm and may be covered by mural thrombus. The natural history of atherosclerotic aneurysms is that they continue to enlarge until they rupture and distal thromboembolic events are common.

Dissecting aneurysms

Acute aortic dissection is a life-threatening emergency that requires a rapid clinical assessment and an immediate diagnosis to enable timely and appropriate medical and surgical treatments. Classical aortic dissection shares many similarities and may easily be confused clinically and diagnostically with the variants of aortic dissection, which include intramural hematoma, penetrating atherosclerotic (ulcerative) plaques, and contained aortic rupture. Therefore, it is extremely important that the echocardiographer has a clear and thorough understanding of the pathology of aortic dissection in order to make an accurate diagnosis and convey complete information to the clinician or surgeon involved in the patient's treatment.

In classical aortic dissection there are two parallel flow channels.[79] The dissection of the aortic wall begins when a tear occurs in the intimal layer and extends into the middle layer of the media (figure 5.13).[80,81] The second channel or false lumen is formed from the cleavage of the medial muscle layers splitting the media in a longitudinal fashion by the flow of blood entering into the intimal tear. The location of the false channel is situated towards the outer half of the aortic media, leaving a thinner aortic wall of the false channel in comparison with the inner wall. The intimal flap is usually thicker and stronger than the outer wall, and the subsequent necrosis of the thinner outer wall may provide an explanation for aortic rupture in the setting of dissection.[79,82] The false lumen migrates distally (antegrade dissection) and re-emerges in the true lumen through one or several re-entry sites or tears. Re-entry usually occurs at the sites of arteriosclerotic plaques or major arterial side branches as they are split from the true
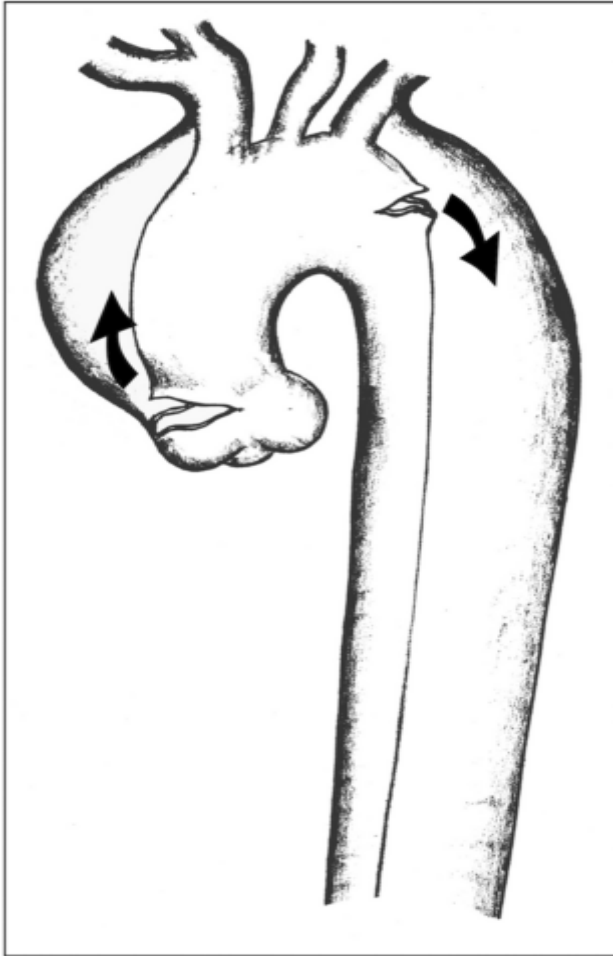
Figure 5.13 Artist's rendition of a typical aortic dissection. Entry and re-entry defects of an intimal medial flap associated with a type A aortic dissection producing two parallel communicating flow channels or a "double barrel aorta". The dissection of the aortic wall begins when a tear (entry site) occurs in the intimal layer and extends into the middle layer of the media. The second channel or false lumen is formed from the cleavage of the medial muscle layers splitting the media in a longitudinal fashion by the flow of blood entering via the entry site. The location of the false channel is situated towards the outer half of the aortic

media. The false lumen migrates distally and re-emerges in the true lumen during the dissection process. The false lumen may end abruptly at the last re-entry site or may extend distally to end in a blind pouch.
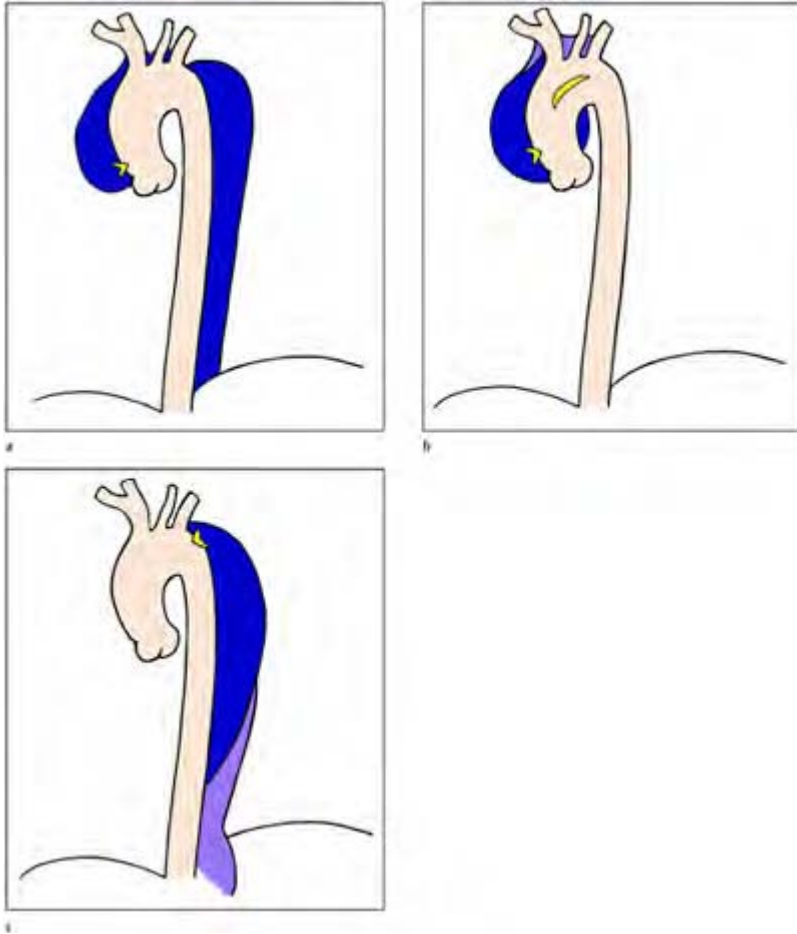
Figure 5.14 Classifications of aortic dissection. Aortic dissection may be classified according to the DeBakey or the Stanford classifications. DeBakey type I (a) involves dissection originating in the proximal aorta, which usually extends throughout the

entire aorta. DeBakey type II (b) aortic dissections involve, and are limited to, the ascending aorta only. DeBakey type IIIa dissections (c) are limited to the descending aorta with type IIIb dissections involving the descending aorta extending beyond the diaphragm into the abdominal aorta.

The Stanford Type A dissection (a, b) involves the ascending aorta, regardless of the entry site, and the extent of the distal aortic involvement. Type B dissections (c) usually involve only the distal or descending thoracic aorta.

DeBakey classification is based on the operative difficulty and the rates of risk for perioperative complications that occur in different contiguous aortic segments. The Stanford classification is more useful for emphasizing the prognosis of the location of the dissection.

lumen during the process of dissection. Thus, the hallmark of aortic dissection that distinguishes it from the variants of dissection is the presence of two parallel communicating flow channels. The false lumen may end abruptly at the last re-entry site or may extend a short distance to end in a blind pouch.[79,83] The extent of the dissection varies and it is not uncommon that the entire aorta is involved. Dissection is rarely limited to the ascending aorta and has only been observed in our experience in the earliest stages of the dissection process when initially assessed. By the time the patient is in surgery the dissection has extended. Dissections may stop anywhere along the aorta due to fibrotic areas in the media, aneurysms, or significant arteriosclerotic plaques.[84] There is frequently retrograde dissection from the origin of the intimal tear, which usually extends in a blind pouch or may extend further by traversing the full extent of the ascending aorta to end at the sinotubular junction or in the pericardium. The segment of the aortic wall that has been separated by the dissection process, and hence separates the true from false lumen, is referred to as an intimal flap. The term "intimal flap" has led to much confusion in the understanding of aortic dissection pathology, since the predominate layer of the aorta involved and destroyed with dissection is the media and not the intima. Because the aortic media and the outer layers—rather than the intima—split, the aortic wall weakens

and expands due to the transmural pressure necrosis to the point where it may rupture. Rupture accounts for the major mortality associated with dissection.[79] When rupture does not ensue, flow usually continues in the false lumen, and eventually some degree of endothelialization and fibrosis occurs in the false lumen to produce a double-barrel aorta. It is rare that the false channel thromboses and completely obliterates. The weakening of the outer aortic walls, even without frank rupture, allows the diapedesis of blood through the aortic wall and results in bloody pericardial or pleural effusions and adventitial hematomas, sometimes referred to as a leaking aneurysm.

Several reports[85–87] have described aortic dissection in stages, alluding to the prognosis and the pathological processes involved in the dissection process when the patient survives the acute event. The acute stage of dissection occurs between day 1 and day 14, and is the time period when aortic tissue is most friable. The subacute stage occurs between 14–60 days. The chronic stage occurs after the first two months and firm scarring of the outer aortic wall develops during this stage. Theoretically, fibrosis of the outer aortic wall occurs after the 6th week, which is the best time for surgical intervention when this is not done during the acute stage.

Aortic dissection may be classified according to the DeBakey[86,87] or the Stanford (Dailey)[88] classifications (figure 5.14). The DeBakey classification of aortic dissection is based on the operative difficulty and on the rates of risk for perioperative neurological and other complications that occur in different segments of the aorta. DeBakey type I involves dissection originating in the proximal aorta, which usually extends throughout the entire aorta. Type II aortic dissections involve, and are limited to, the ascending aorta only. Type IIIa dissections are limited to the descending aorta, with type IIIb dissections involving the descending aorta extending beyond the diaphragm into the abdominal aorta (thoracoabdominal dissections).

The Stanford classification[88] was developed to emphasize the prognosis of the location of dissection. Type A dissection involves the ascending aorta, regardless of the entry site, and the extent of distal aortic involvement. Type B dissections usually involve only the distal or descending thoracic aorta. With this classification all type A dissections require emergent diagnosis and surgical intervention since ascending aortic dissections carry the highest mortality, whereas type B dissections can usually be managed by either medical or surgical treatment since they may not be as life-threatening.
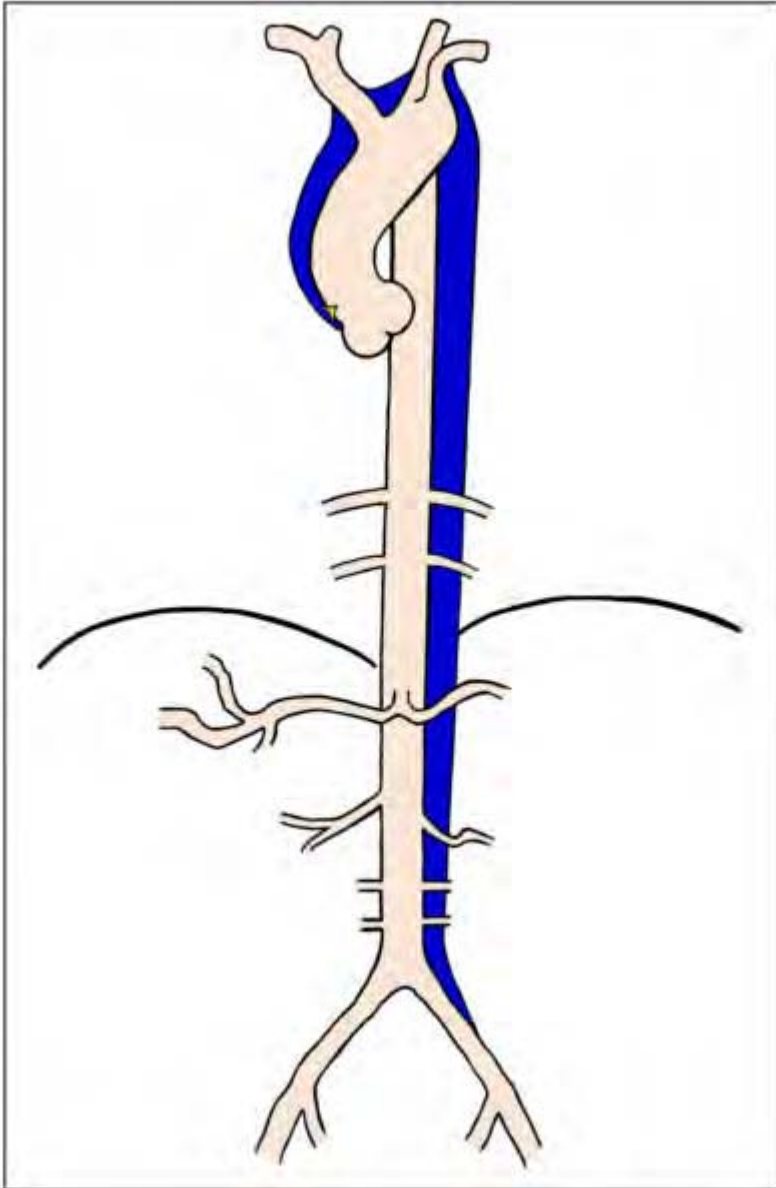
Figure 5.15 Typical example of the course of an aortic dissection. The normal aorta is a tubular structure, which twists and turns in the thoracic cavity during development. Therefore

it may be difficult to identify properly the true and false lumens in dissection, which has led to the idea that dissections tend to occur in random patterns. With most aortic dissections the false lumen tends to follow a typical coarse from origin to ending. The location of the false channel is situated towards the outer half of the aortic media with the origin close to the right coronary artery. As the false lumen extends around the aortic arch it usually involves the great vessels, followed by the left intercostal arteries as it extends through the descending aorta and continues on a leftward path through the left renal artery. To label correctly the true and false lumen it is extremely important to have a full appreciation for the level the aortic images were obtained which may be aided by reconstructing the echocardiographic images as in Figure 5.6.[115]
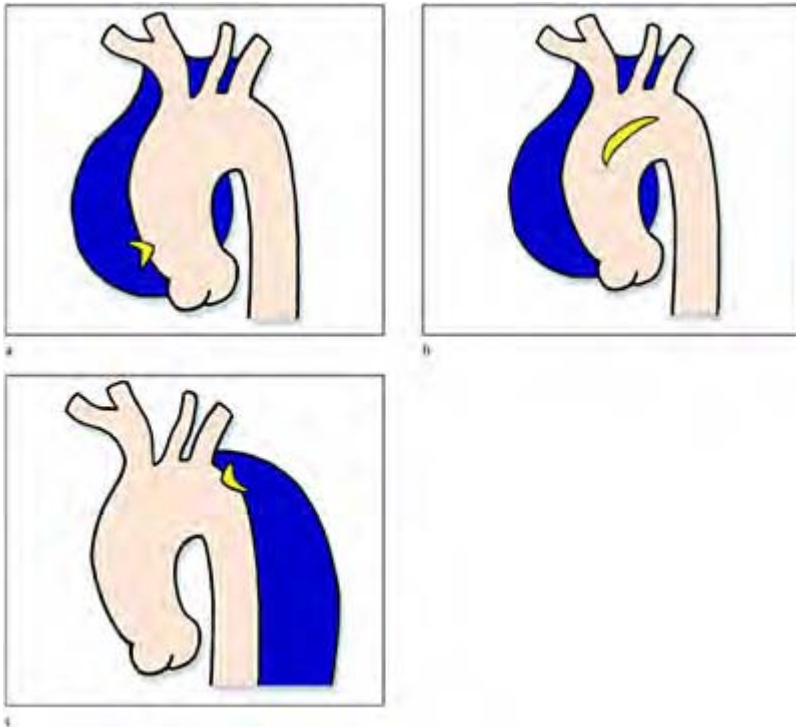
Figure 5.16 Typical entry sites of aortic dissection. Intimal entry sites that occur with aortic dissection typically occur near the aortic "stress points" which are probably caused by the natural twisting and turning of the aortic tube during development and aging. Therefore entry sites usually occur in certain aortic positions depending on the location of the aortic dissection rather than in random patterns. Knowledge of the location of entry sites greatly enhances the ability to demonstrate them with multiplane TEE, in the shortest amount of time. In dissection of the ascending aorta (a) the primary intimal tear occurs in a transverse direction approximately 2–5

mm above the sinotubular junction in the right anterolateral wall above the non-coronary cusp. With dissections of the aortic arch (b) the inferior concave surface of the arch is spared and the intimal tear is usually located near and opposite the innominate artery. Descending aortic dissections (c) usually originate with an entry site at the junction of the aortic arch and descending thoracic aorta immediately distal to the origin of the left subclavian artery.

Most series[53,89–94] report a predominance of dissections occurring in the ascending aorta in roughly 75% of cases. Dissections originating in the ascending aorta frequently extend to the abdominal aorta, and have been reported in 40–100% of cases. Isolated descending thoracic aortic dissection occurs in the remaining 25% of cases and extends to the abdominal aorta in most cases.[79,80] Dissection originating in the aortic arch is less common and occurs with a frequency of 10–19%.[79,95,96]

In extensive dissection involving the entire aorta, the false lumen usually follows an identical or similar course (figure 5.15), which is why particular arterial branches of the aorta are typically involved in dissections.[52,84] Knowledge of the typical patterns of dissection helps to distinguish the true from the false lumen by TEE. Dissection in the proximal ascending aorta occurs anteriorly and to the right aortic wall, often involving the right coronary artery ostia and, less frequently, the left coronary artery ostia.[79] The dissection travels from the ascending aorta to the superior portion of the aortic arch, involving the origin of the great vessels. Distal from the arch, the dissection usually extends laterally to the left of the descending aorta interrupting the left intercostal arterial branches. When dissection extends past the diaphragm it courses in the same orientation to the left and frequently involves the left renal artery, sparing the anterior placed visceral artery branches. When the aortic dissection extends further, the left iliac artery is frequently involved.
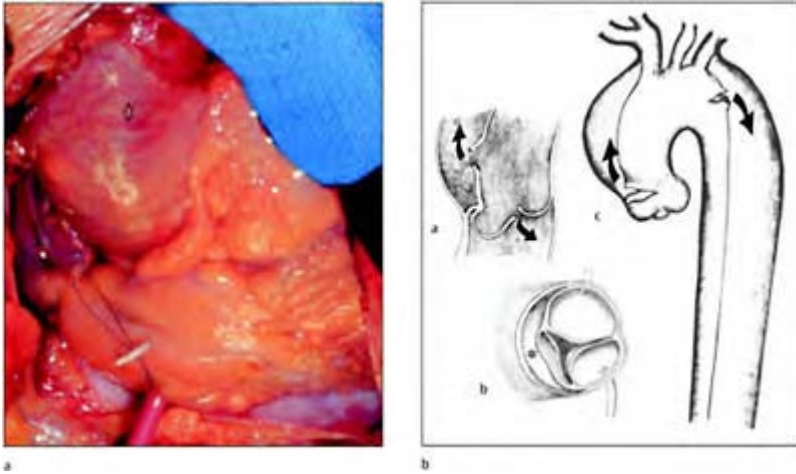
Figure 5.17 Typical ascending aortic dissection. Surgical photograph (a) of an acute ascending aortic dissection. A large blue, subadvential hematoma is noted along an ectatic, dilated aortic wall typical of an ascending dissection. Surgical suture denotes the area of the right coronary origin. Artist's rendition in multiple planes of an acute ascending aortic dissection (b) illustrating the entry and re-entry sites, intimal tear, true and false lumen. Arrows demonstrate the path of typical blood flow in aortic dissection, including disruption of the aortic cusp producing aortic insufficiency. The relationship of the intimal tear and false lumen to the aortic valve and right coronary artery is depicted.

In ascending aortic dissections the aorta is initially either normal in size or there is mild dilatation of the aortic root. The primary intimal tear occurs in a transverse direction about 2–5 mm above the sinotubular junction in the right anterolateral wall above the noncoronary cusp[96] (figures 5.16, 5.17). Dissections predominantly produce disruption longitudinally along the length of the ascending aorta, and usually do not result in complete circumferential involvement. TEE visualization of the dissected ascending aorta demonstrates a strip of aorta parallel and in close proximity to the pulmonary artery,

which is left unaffected by the dissection. Rarely, a circular disruption of the intima and media occurs, producing intimointimal intussusception.[97,99] The true lumen encompassing the intima becomes completely invaginated in the false lumen and may produce total occlusion of the aorta or the great vessels. Blood-flow through the false lumen travels either anterior, posterior, or completely surrounding the great vessels, usually on the superior surface or greater curvature of the aortic arch. Aortic insufficiency is produced by retrograde dissection and associated with detachment of the aortic commissures and prolapse of the aortic cusps and resultant enlargement of the sinuses and annulus.[80,99,100] Aneurysmal dilatation accompanying ascending dissection may cause compression of the superior vena cava and proximal pulmonary vessels. Bloody pericardial effusions are usually found at the time of surgery or by imaging techniques. Retrograde dissection may also involve the right coronary ostia producing myocardial ischemia or infarction.[57] With extensive retrograde dissection the left main coronary artery may also be compromised, with a grave outcome.

When dissections of the aortic arch occur, the inferior concave surface of the arch is spared. The intimal tear is usually located near the innominate artery (figure 5.16). The great vessels usually arise from the true lumen and, rarely, the origins of the great vessels are torn with intimal insussusception causing occlusion of these vessels and stroke from cerebral ischemia or infarction. If the ascending aorta is involved and the intimal tear is not readily identified in the ascending aorta, then the intimal tear probably originates in the arch and has resulted in a retrograde dissection of the ascending aorta.

Descending aortic aneurysms usually originate at the junction of the aortic arch and descending thoracic aorta immediately distal to the origin of the left subclavian artery (figure 5.16). Descending aortic dissections frequently progress beyond the diaphragm and extend to the abdominal aorta. Because of the longitudinal orientation of the aorta, expansion of the false lumen occurs at the expense of the true lumen. Rupture or diapedesis of blood through the aortic wall tracks into the left pleural cavity. Circular dissections visualized near the junction of the aortic arch and proximal descending aorta suggest retrograde extension of the dissection.[100]

TEE evaluation in aortic dissection

When TEE is done on a patient with suspected aortic dissection it is important to obtain a full study to identify the presence of dissection, any coexisting complications, and to assess cardiac chamber function. If a false lumen (double lumen aorta) is identified, the extent of dissection must be classified, according to DeBakey's or Stanford's classification, and the location of the intimal entry tear identified as well as the presence or absence of flow in the false lumen. The presence of pericardial effusion and/or findings suggesting tamponade, pleural effusion, presence or severity of aortic insufficiency, and the presence of ventricular regional wall motion abnormalities, should be unequivocally established.

The hallmark of aortic dissection is the demonstration of an intimal flap, which divides the aortic lumen into true and false channels to produce a fusiform dilatation of the dissected segment of aorta.[102] Intimal flaps appear as a uniform dense, hyperrefractile linear echo, running parallel with the aortic wall within the aortic lumen to produce an

undulating or chaotic motion. Intimal flaps are readily apparent in the short-axis views of the aorta and should be confirmed in orthogonal views. When true and false lumen are identified, the flow characteristics of the aorta should be described and color Doppler used to determine the presence of flow in the false lumen. Frequently the flow in the false lumen is not readily apparent, because of its lower velocity, and the Doppler settings must be adjusted by increasing the color-flow gain and decreasing the velocity setting. Sluggish flow is noted in the false lumen by the presence of spontaneous echo contrast in about 41% of cases.[103] On close inspection, the false lumen may contain thrombus or be totally thrombosed (suggesting a chronic dissection). Totally thrombosed false lumens may be identified by displacement of intimal calcifications.[104] If no flow is detected in the false lumen it is considered thrombosed, which carries a good prognosis. If flow is detected in the false lumen survival is 43%, although survival is 90% in patients without detectable flow in the false lumen.[105,106] The true lumen is distinguished from the false lumen with color Doppler illustrating the systolic expansion of the true lumen and systolic compression of the false lumen. As previously mentioned, since dissections usually follow a typical course, the true and false lumens may be distinguished by their anatomic position in the aortic lumen. True aortic lumens tend to have higher velocity flows detected, compared with low velocity flows in the false lumen. In the descending aorta the false lumen tends to be larger than the true lumen and commonly travels down the leftward aspect of the aorta. Also the false lumen commonly shows the most spontaneous contrast or thrombus formation.

After visualization of the false lumen, it is necessary to identify the location of the entry site or intimal tear. An intimal tear is visualized as a discrete disruption in the intimal flap, producing the most chaotic motion in the flap.[107,108] Color Doppler shows a low velocity flow jet directed from the true lumen towards the false lumen.[109,110] Conventional pulsed-wave Doppler shows a low velocity biphasic or triphasic flow pattern predominately during late systole.[111] Identification of the site of the intimal tear is extremely important for classification of the aortic dissection and for the cardiac surgeon to decide the best type of aortic repair. In Stanford type A dissections, the intimal tear usually occurs just above the aortic valve, opposite the innominate artery or 2–5 cm distal to the origin of the left subclavian artery. In Stanford type B dissections, the intimal tear is always near the subclavian artery or cardiac isthmus. In addition to identifying the entry site or intimal tear it is useful to identify re-entry tears when present. Re-entry sites may be multiple, usually occurring close to the most distal site of dissection. The importance of identifying re-entry sites is to ensure that the cardiac surgeon does not neglect a re-entry site and accidentally incorporate a re-entry site in the repair to turn this site into a potential new starting point for recurrent dissection or a failed surgical repair. Flow is commonly noted in the descending aorta in the posterior aspect, which represents flow to the intercostal arteries, and it is important that these are not confused with re-entry sites.[113]

Multiplane TEE easily identifies coronary artery involvement with aortic dissection. Wall motion abnormalities are readily seen with the transesophageal approach. Dissection extending to the coronary arteries occurred in 21% of the patients studied by Ballal et al.[103] and was accurately detected in 86% of cases. Interestingly, only 29% had clinical evidence of myocardial infarction.

It is important to identify the sites of aortic involvement of the dissection, and to define whether the ascending aorta, aortic arch. Preoperative identification of the intimal tear and of whether there is a retrograde dissection is helpful in minimizing aortic cross-clamp time and hypothermic arrest. TEE allows quantification of the degree of aortic insufficiency.

Intraoperative TEE enables assessment of perfusion during bypass and detection of inadequate perfusion of vital organs.[113] When arterial cannulation is done in the femoral artery, the perfusionist can inject prime solution through the cannula to determine whether the true lumen or false lumen was cannulated by observing the appearance of contrast artefact in one or both lumens. In addition, once the patient is placed on bypass, the flow characteristics in the true and false lumens are observed with color Doppler by illustrating a non-pulsatile flow jet characteristic of pump flow in one or both lumens. Flow is usually detected throughout the aorta on cardiopulmonary bypass and, depending on the type of dissection, flow in the great vessels may be detected. TEE is helpful at the completion of surgery to assess the adequacy of the results, and to locate free debris such as thrombi in the aortic lumen that may have become dislodged during surgery. Flow characteristics of the aortic graft are assessed for increased gradient at the anastomotic sites, which may occur from a kinking of the graft that is not obvious to the surgeon after the cross-clamp is removed. In patients with elephant-trunk graft placement, the flow dynamics of the outlet are observed to ensure adequate flow in the true and false lumen, which is necessary for distal organ perfusion. The distal portion of the elephant-trunk graft expands in systole and contracts in diastole as flow enters the aortic lumen, with a tendency to show a floating motion in the aortic lumen due to mismatch between the aortic diameter and the graft dimension.[114,115] In patients who require reimplantation of the coronary arteries, flow from the graft to the coronary arteries is shown readily by color Doppler.

Many studies have described sensitivity and specificity for TEE in aortic dissection, approaching 100% for each.[103,104,107,116] In earlier studies the specificity of TEE findings were lower, ranging from 65–75%, and were largely attributed to monoplane and biplane technology missing the so-called aortic blindspot in the distal ascending aorta. The lower sensitivity and specificity has been attributed to false positive echocardiography findings, illustrating the learning curve of TEE in interpretation of ultrasound images and in technical skills involved in endoscopy. When TEE is compared with other imaging techniques, such as CT or MRI scanning, the results generally reflect the expertise of the institution in each technique.[116] In our own institution, TEE is complementary to spiral CT and MRI scanning in confirming the diagnosis of aortic dissection.

False-positive echo findings for an intimal flap may occur as a result of plaques near the aortic valve, producing lateral resolution artefact; thickening or calcification causing reverberations may be produced from other cardiac or thoracic structures; and the use of excessive gain may introduce abnormal echoes into the aortic lumen. Pulmonary artery catheters, intra-aortic balloon catheters, and pacing catheters produce side-lobe or linear echo artefacts that appear within the aorta in various views. Linear artefacts are frequently produced in the ascending aorta when the aortic diameter is greater than the left atrial diameter.[121] The echo interface between the aorta and the lung in the aortic arch and proximal descending aorta produces a typical appearance that should not be confused with the appearance of a true and false lumen, or a double-barrel aorta. Pericardial

effusion with fluid in the transverse sinus separating the proximal ascending aorta and the pulmonary artery also may be confused with true and false lumen. Pneumothorax, pulmonary blebs, and atelectasis may also produce shadowing artefacts within the thoracic aorta or obscure the aorta producing non-diagnostic images.

False-negative transesophageal echocardiograms have been observed in aortic dissection. In ascending aortic dissection of an extremely dilated aorta, small intimal tears may be overlooked when comprehensive examinations are not done or if tears are overshadowed by mural thrombus or spontaneous contrast within the aortic lumen.

Intramural hematoma

Intramural hematoma of the aorta represents one of the variants of aortic dissecting aneurysm. Intramural hematoma of the aorta is defined by the presence of the intramural accumulation of blood as a localized hematoma within the layers of the aortic wall. Intramural hematoma comprises approximately 12.8–13.2% of all aortic syndromes and has a high rate of progression to overt dissection.[122,123] Because of the frequent lack of intimal tears discovered at necropsy it was once believed that intramural hematoma were the precursor to aortic dissections. It was postulated that spontaneous rupture of the aortic vasa vasorum may initiate aortic wall degeneration, which eventually lead to hematoma formation in the aortic wall and splitting of the aortic wall layers or dissection formation without an intimal tear.[124] Comparison of histological findings with intramural hematoma and those with typical dissection showed that the medial split tended to occur in the outer third of the medial layer in a high proportion of patients with intramural hematoma. Aortic wall rupture may therefore be greater in the setting of intramural hematoma than with overt aortic dissection, but this finding needs further validation in clinical trials.

Intramural hematoma is prevalent in the setting of chronic hypertension, diabetes mellitus, pregnancy, Marfan syndrome, or in abdominal aortic aneurysms.[126–131] Peripheral vascular involvement is usually less common than in cases of classic aortic dissection, but usually more than in penetrating aortic ulcerative plaque.[132] Patients with intramural hematoma present with severe chest or back pain, and signs of fluid extravasation, pericardial and pleural effusion are typical features.

TEE findings of intramural hematoma consist of a localized thickening of the aortic wall of more than 7 mm, producing a circular or cresentric shape.[132] The hallmark of intramural hematoma is thickening of the aortic wall without evidence of an intimal tear or dissection. It is extremely important that a thorough examination by use of multiple planes (by slowly rotating the transducer through 180 degrees) is done in the segment involved with the hematoma to exclude an intimal tear and to rule out a classic dissection since it may not be readily apparent after the aorta is opened surgically.

Initially, intramural hematoma has the typical reflection pattern of sequestered blood in-between the intima-media and advential layers. This pattern changes with the formation of a homogenous echogenicity similar to that of an intramural thrombus. At this stage, it may be difficult to distinguish an intramural hematoma or aortic debris with intraluminal thrombosis from classic aortic dissection with a thrombosed false lumen, especially when the hematoma extends a considerable distance longitudinally down the aorta. The sensitivity and specificity of TEE for the diagnosis of intramural hematoma

reported by Keren et al.[125] were 90% and 99%, respectively. Intramural hematoma occurred in the ascending aorta in 48%, the aortic arch in 8% and in the descending thoracic aorta in 44% of patients.[132] In addition, intramural hematoma of the ascending aorta occurred predominantly in younger patients.

Surgical intervention for intramural hematoma is similar to that for classical aortic dissection. The 30-day mortality of ascending intramural hematoma was 80% and 50% for aortic arch intramural hematoma in patients treated without surgery.[132] The 1-year survival with surgery was 71% versus 20% with medical therapy. In patients with descending aorta intramural hematoma the 1-year survival was not significantly different between medical and surgical management; 83% and 80%, respectively.[132] Current recommendations for the surgical management of intramural hematoma are similar to those for classic aortic dissection, including ascending and aortic arch intramural hematoma.[126,132] Medical therapy with diligent follow-up is recommended for uncomplicated descending aortic intramural hematoma. Surgery should be considered in patients with recurrent or intractable pain despite aggressive medical therapy, rapid and localized aortic expansion, leakage or threatened rupture particularly in a previously aneurysmal aorta, major branch vessel compromise with vital organ ischemia, and in patients with pre-existent connective tissue abnormality.[126,132]

Penetrating aortic ulcerative plaque

Ulceration of aortic atheroma is common in patients with aortic disease. Typically, ulceration of the atheroma is confined to the intimal wall, resembling a gastric ulcer in imaging techniques. Ulceration is not associated with intramural hematoma and is generally symptom-free. In penetrating aortic ulcerative plaque, the ulcer extends beyond the intimal border, to produce a subjacent hematoma through the aortic wall with full or partial thrombosis of a pseudoaneurysm of the adjacent advential connective tissue. The long-term result of this contained rupture is not known, although ruptures with hemorrhage and exsanguination have been reported.[133]

Rarely does spontaneously contained adventitial pseudoaneurysm extend for the length of the descending thoracic aorta in a proximal and/or distal direction. In Shennan's classic series, penetrating ulcerative plaque was the cause of aortic dissection in six of 218 patients.[3] A distinguishing factor from classical dissection is that the penetrating ulcers need not occur at the aortic stress sites, but are usually located in the mid or distal descending thoracic aorta.[134,135] Typically, penetrating aortic ulcers tend to produce pathology that is more extensive than in classic dissection, due to the severe atherosclerotic changes found in ulcerative aortas. The propagation of the longitudinal plane of cleavage tends to be limited by the associated medial fibrosis and atrophy that accompanies the atherosclerotic process.[136] When surgical repair is required, the segment of diseased aorta including the ulcer is excised and replaced by a tubular graft.[136]

Patients with penetrating aortic ulcer present with similar findings as classical aortic dissection, without the propensity for pulse deficits. Chronic hypertension, history of smoking, significant atherosclerotic disease, and older patients are the norm. Patients are usually elderly and generally do not have a history of connective-tissue disease.[135]

Patients do not develop pericardial effusion, valvular regurgitation or neuromuscular compromise, but may accumulate effusions in the mediastinal or pleural space.[137]

The TEE diagnosis of penetrating aortic ulcer may be difficult to make, especially when the findings are not extensive. Since the patient's clinical findings are similar to that of classic aortic dissection, TEE is usually done to rule out both diagnoses. Usually the first indication of a penetrating aortic ulcer is the finding of an adventitial hematoma or pseudoaneurysm in a severely atherosclerotic aorta, together with mediastinal fluid or pleural fluid near the affected segment of the aorta and absence of dissection flap. Meticulous examination of the aorta may reveal an ulcerative plaque as a small protrusion at or near an atheromatous plaque that projects deep into the medial wall layer, frequently with spontaneous contrast at the site. Color-flow Doppler may show flow within the area of the aortic ulcer, tracking into the subjacent hematoma where lower velocities are recorded.

The diagnosis of penetrating aortic ulcer has only rarely been reported in the literature worldwide (less than 100 cases), due to the lack of appreciation of this disease before the development of newer imaging methods. In the past, the diagnosis could be made only by aortography, which was not an easy task. In most patients the ulcer was identified in the mid to distal descending aorta with severe atherosclerosis;[46] however, two patients with ulcers in the ascending aorta and one patient with an arch ulcer were recently identified.[133,138] 40% of patients have a prior concomitant diagnosis of abdominal aortic aneurysm.[136] Most of the patients reported have had surgical intervention, because the risk of rupture of a penetrating aortic ulcer is thought to be higher than with aortic dissection. Since the long-term results of contained rupture are not known, many investigators believe that a confined hematoma may remain stable while it is relatively protected from the hemodynamics of blood flow. Recent reports suggest that surgical therapy may not be indicated in all patients. Hussain et al.[139] reported five patients who did well with medical therapy. Surgery may be avoided in stable cases; but intervention is recommended for aortic ulcers in the ascending aorta and aortic arch, in patients with clinical and laboratory findings of ongoing hemorrhage, and in patients with recurrent symptoms and enlarging hematoma on subsequent imaging.[140]

Aortitis

Aortitis, or inflammation of the aortic wall, is a rare and infrequently recognized acquired disease of the aorta responsible for aneurysmal formation (figure 5.18). Aortitis is also referred to as infective endarteritis or fungal aneurysm, leading to much confusion regarding this disorder. Aortitis has many etiologies, and should be considered as an inflammation of the arterial wall with or without pre-existing aneurysm formation. Aortitis should include all extracardiac and intracardiac aneurysms with an inflammatory or infectious etiology.
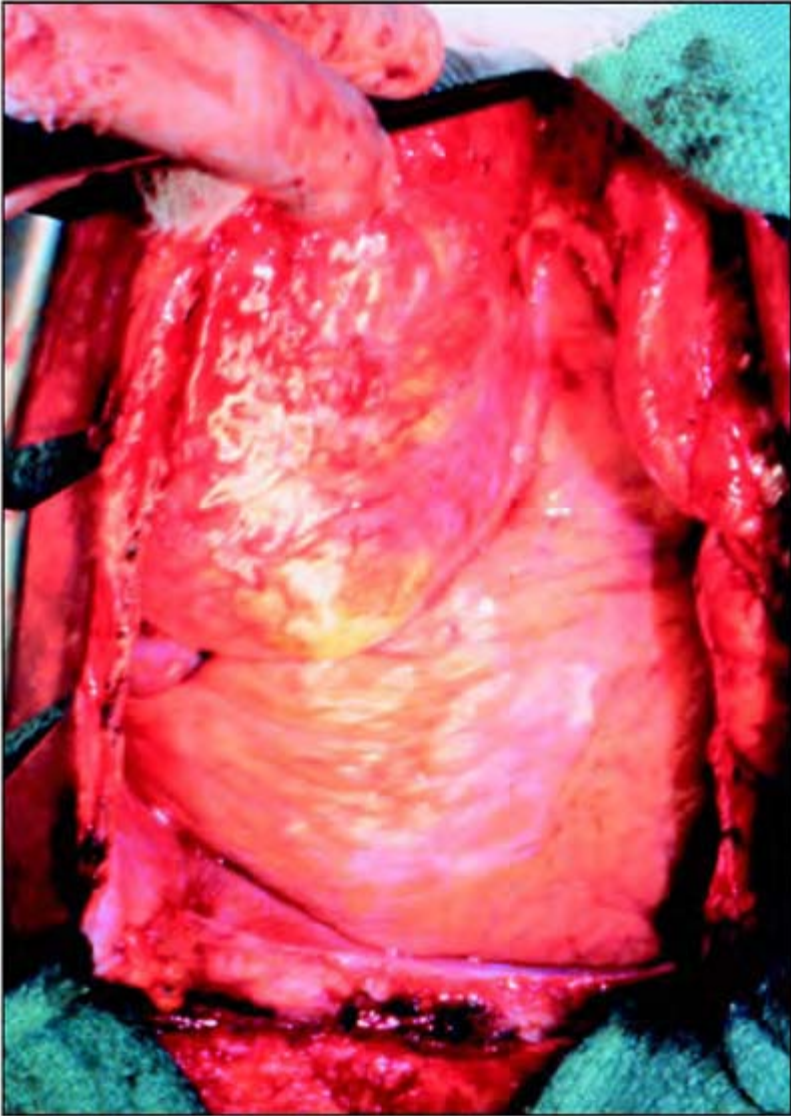
Figure 5.18 Surgical photograph of an ascending aortic aneurysm resulting from aortitis. Aortitis, or inflammation of the aortic wall, is a rare and an infrequently recognized type of acquired aortic disease responsible for aneurysmal formation. Enlargement of

the total ascending aorta is noted
which is almost as large as the cardiac
structures visualized, with chronic
inflammatory appearance to the
adventitia. When aortitis is left
undiagnosed it frequently results in
rupture of the involved aortic segment.

The incidence of aortitis is rare, as illustrated by a Mayo Clinic study of necropsy findings. Between 1925 and 1954 only six cases of aortitis were discovered in 20,000 necropsies. The rare incidence of aortitis may be attributed to difficulty in making the diagnosis as well as the changing clinical circumstances in which it occurs. Recent reports suggest that the incidence of aortitis is increasing in frequency, which may be due to improved awareness of aortitis as a clinical entity plus to the introduction of better imaging methods such as TEE.

In the pre-antibiotic era, 86% of aortitis cases occurred in conjunction with infectious endocarditis.[142,143] Aortitis was also commonly associated with syphilis (75% of all cases). Although the incidence of syphilitic aortitis has dramatically declined since the introduction of penicillin, it may still be seen in developing countries.[144,145] Syphilitic aneurysm is almost always confined to the thoracic aorta and involves the aortic arch. Aneurysms may be saccular, fusiform, or cylindrical when the whole thoracic aorta is involved. Medial destruction is produced initially by the leuetic lesion, with the subsequent development of atherosclerotic disease later in the process, which further weakens the aortic walls. Extensive atherosclerosis, which may occur in syphilitic aortitis, may occasionally result in porcelain-type aortas. Syphilitic aneurysms tend to grow extensively, are usually quite large, and may erode through the chest wall. Erosion of the chest wall has led to the misconception that aneurysms are usually very large.

The most common mechanism today for aortitis is the hematogenous seeding of preexisting atherosclerotic disease. Thrombus formation associated with intraaortic debris and aortic aneurysm serve as the nidus for aortic infection in the presence of bacteremia. Pre-existing aortic disease may become infected secondarily to distant foci of infection or contiguous spread from local infection. Traumatic or iatrogenic causes (surgery or cardiac catheterization) of aortitis and endovascular infection may result from direct bacterial contamination of the aorta from arterial injury. Aortitis is also associated with many immunological or rheumatic disorders.

Embolic seeding of bacteria may occur in the setting of bacterial endocarditis or intravenous drug abuse.[146] Aortitis may produce saccular aneurysms or, less commonly, fusiform aneurysms. In more than 70% of cases the aneurysm develops in the ascending aorta proximal to the aortic arch. Infection of the aortic wall leads to the obliteration of the elastic and muscular layers, but leaves the intima intact.[147]

Aortitis secondary to infection of a pre-existing aneurysm is most common in the abdominal aorta, since this area is most frequently damaged by atherosclerosis. Involvement may occur in the ascending and descending aorta in about 15% of cases.[143,148,149] The wall of the aneurysm is usually very thin and expands as the inflammation progresses. The bacterial species involved with endocarditis are different

from aortitis. Gram-positive cocci, predominately staphylococcus species, are present in 60% of cases, with salmonella as the gram-negative bacteria in 35% of cases.[150,151]

When aortitis is left undiagnosed, it results in rupture of the involved aortic segment in 75% of cases.[143,152] Therefore it is important to diagnose aortitis accurately. Successful treatment of aortitis includes appropriate antibiotic therapy combined with surgical resection, since the incidence of rupture does not decrease with antibiotic use alone. The mortality of aortitis is high and rupture occurs earlier when Gram-negative bacteria are the cause of infection.[143] Surgical results are usually better in Grampositive infections, and when all infected tissue can be removed.[143]

TEE may be very helpful in diagnosing and recognizing aortitis. The diagnosis of aortitis should be considered in patients presenting with non-specific chest pain, fevers and chills, increased white-blood-cell counts and positive blood cultures. Although there are no specific findings with TEE to suggest aortitis and there is considerable overlap between the findings of other types of aortic disease seen with TEE, multiplane TEE with its excellent anatomic detail should be extremely helpful in these clinical situations. Recent case-reports illustrate the potential role of TEE in the diagnosis of aortitis, including the advantages over aortography and CT scanning.[153,154] TEE findings suggestive of aortitis include aortic wall thickening and focal saccular aneurysms that occur in atypical locations of the aorta. In patients with aortitis secondary to trauma, pseudoaneurysms are commonly detected. The aorta is usually normal in adjacent areas to these findings, or there may be areas with associated intraaortic debris. Color-flow Doppler usually shows flow from the aortic lumen into the aneurysm or abscess cavity. Serial TEE examinations illustrating the rapid enlargement of a known aneurysm should suggest the diagnosis of aortitis. The aorta should also be screened for these findings in the setting of infectious endocarditis during TEE assesments to look for areas of embolic seeding.

Aortic transection

Aortic transection, or traumatic aortic rupture, is a life-threatening emergency that accounts for 20% of deaths from motor-vehicle accidents.[155] Blunt aortic trauma is infrequent but causes death in 25% of trauma patients[156] Abrupt deceleration-type injuries that result from falls of significant height or motor-vehicle accidents produce traction and torsion forces that generate very high shear stress together with sudden increases in intraluminal pressure. These lead to traumatic disruption of the thoracic aorta in its less mobile segments. Aortic transection occurs in 90% of cases at the aortic isthmus where the mobile aortic arch becomes relatively fixed in the thorax by the ligamentum arteriosum, left subclavian artery, and intercostal arteries.[157] In 80–90% of cases all three layers of the aortic wall are torn, causing immediate death from massive periaortic hemorrhage. Patients generally incur multiple injuries and survival of the transection depends on the relative strength of the pseudoaneurysm that forms.

Chest radiography typically shows a widened mediastinum of more than 8 cm in patients with aortic transection.[158] Contrast aortography has been the gold standard for diagnosis in aortic transection, but it is difficult to do on critical patients. Reports have focused on the time delay caused by aortography, which varies from 50 to 75 minutes.[159]

Parmley et al.[160] in a classic report of 275 necropsies in traumatic injury of the aorta, classified non-penetrating aortic injuries into six categories: intimal hemorrhage with or without laceration; medial laceration; complete laceration; pseudoaneurysm formation; and periaortic hemorrhage. In that series, only 14% of patients reached the hospital alive and only 20% of these patients lived longer than 1 h, with 30% dying within 6 h. The site of aortic rupture was at the isthmus in 45%, ascending in 23%, descending in 13%, arch in 8%, abdominal in 5%, and multiple sites in 6%. In addition, avulsion of the aortic valve was noted, probably due to the increased intraluminal pressure generated in these types of trauma especially with the use of seat belts.

With this information in mind, TEE is a logical choice for the emergency assessment of traumatic aortic injury.[161–176] Recently, many reports have shown the efficacy of TEE in aortic transection with sensitivities of 91–100% and specificity of 100%, especially with the use of multiplane TEE.[162,177] The only drawbacks of TEE are its use in patients with severe edema from facial or mandibular fractures and in patients with unstable neck trauma, which makes it difficult to intubate the esophagus successfully.

Findings of TEE in aortic transection include intimal tears, subadvential lacerations, pseudoaneurysms, and mediastinal hematoma (figure 5.19). Findings in aortic transection may resemble classic aortic dissection.

Traumatic aortic intimal tears appear as thin, mobile intraluminal projections emanating from the aortic wall close to the aortic isthmus.[177] Because the intimal tears are small, the aortic contour and diameter usually remain normal and pseudoaneurysms do not occur. Color-flow Doppler does not show significant turbulence at the site of the tear.

Subadventitial traumatic aortic disruption produces subtotal, complete or partial aortic disruption.[177] A subtotal subadventitial aortic disruption involves roughly two-thirds of the aortic circumference from a spiraling tear, with the aorta held together with a small residual band of the aortic wall. Echocardiography shows an abnormal thick intraluminal flap that produces a non-symmetrical aortic deformity. Since the flap includes the intima and media, the luminal flap is usually 3–5 mm in thickness, distinguishing it from the thin intimal flaps in classic dissection. The medial flap in subadventitial disruption appears in the transverse view as a linear structure completely traversing the lumen of the aortic isthmus in either a vertical, oblique, or nearly horizontal manner. In longitudinal views the medial flap is almost always nearly perpendicular to the isthmus wall, vertically traversing the entire aortic lumen. Complete subadventitial aortic disruptions involve the entire circumference of the aorta. The tear is horizontal and complete, resulting in visualization of the entire circular intimal-medial layer disrupted inside a circular adventitial layer. The medial tear oscillates with each cardiac cycle and spontaneous contrast can be shown between each layer. Flow may also be shown by color-flow Doppler on both sides of the medial layer. Partial aortic disruption shows limited discontinuity of both intimal and medial layers with or without pseudoaneurysm formation. The aortic tear appears as a discontinuity of the intimal-medial aortic layer, without evidence of an intraluminal medial flap. Color-flow Doppler shows turbulent flow entering the pseudoaneurysm.
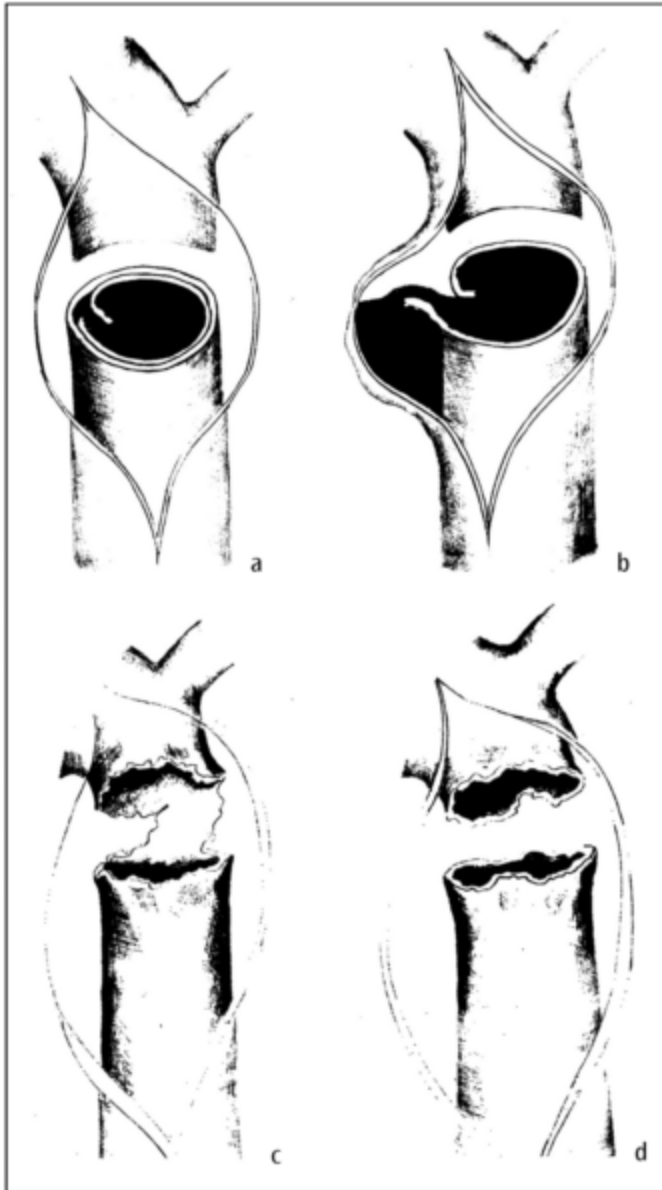
Figure 5.19 Typical types of aortic transection or tear. Artist's rendition of the four types of pathology associated with transection of the aorta. Torn aortas usually occur near the

ligamentum arteriosum and result in various degrees of intimal tear. Traumatic aortic intimal tears (a) appear as thin, mobile intraluminal projections emanating from the aortic wall close to the aortic isthmus. Because the intimal tears are small, the aortic contour and diameter usually remain normal and pseudoaneurysms do not usually occur. With larger tears (b) color flow Doppler may demonstrate significant turbulence at the tear site, which is usually associated with pseudoaneurysmal formation in the aortic wall. Subadventitial traumatic aortic disruption may also result in partial (c) or complete (d) aortic disruption. A subtotal subadventitial aortic disruption involves approximately two thirds of the aortic circumference from a spiraling tear within the aortic wall with the aorta being held together with a small residual band of aortic wall. Complete disruption produces a horizontal tear resulting in the visualization of a circumferential intimal-medial layer disrupted inside a circular adventitial layer.[177]

Mediastinal hematomas are usually present in aortic disruption. Le Bret et al.[178] have described a sensitivity for TEE of 100% and a specificity of 75% for the diagnosis of mediastinal hematoma. Mediastinal hematoma is suggested by an increased density of more than 3 mm between the TEE probe and the aortic wall, or the production of a double contour of the aortic wall. Mediastinal hematoma is also suggested when an ultrasound signal is visualized between the aortic wall and the visceral pleura.

Atherosclerotic aortic disease and debris

The most common pathology of the aorta is atherosclerotic aortic disease, present as an isolated finding or in combination with other aortic pathologies. The incidence of atherosclerotic disease increases exponentially with age in most countries. Unfortunately, patients are usually not diagnosed with severe atherosclerosis until they have a thromboembolic event or arterial occlusion with threatened limb viability (figure 5.20). TEE has contributed to early diagnosis and heightened the awareness of atherosclerotic aortic disease, especially in the thoracic aortic segments. Currently, in many echocardiography laboratories, the most common reason for doing TEE is to assess a cardiac source of thromboembolism.

Figure 5.20 The dreaded complication of diffuse severe atherosclerotic debris is the peripheral embolization of

cholesterol and thrombotic material.
The typical appearance in a photograph
highlighting peripheral thrombotic and
cholesterol emboli to both lower
extremities associated with
atherosclerotic debris of the aorta.

TEE is an excellent technique for visualizing thickening of the aortic walls, and for visualizing intraluminal plaques and thrombi, which enables assessment of the severity of aortic disease. The information obtained by TEE also gives insight into potential disease elsewhere in the circulatory system. Many recent studies have concluded that significant atherosclerotic disease of the aorta diagnosed by TEE is a powerful marker for obstructive coronary artery disease, cerebrovascular disease, peripheral vascular disease, and systemic embolization.

The resolution of TEE allows determination of the severity of aortic atherosclerotic disease. Two layers of the

Table 5.6 TEE classification ofaortic atherosclerosis

Aortic degree	Intimal thickening	Intraluminal irregularities
Normal	< 2.0 mm	None
Mild	< 3.0 mm	None
Moderate	< 5.0 mm	Raised plaques
Severe	≥ 5.0 mm	Protrusion of plaques and/or debris

aortic wall are visualized, the inner layer representing the intima and media, and the outer echogenic layer the adventia. Cross-sectional views of the normal aorta illustrate a circular aorta with a very smooth inner layer and uniform echogenicity. Atheromatous plaques are apparent as protrusions, producing abnormalities in the normally circular intraluminal contour of the aorta. The thickness of the aortic wall is assessed in these regions and compared with the corresponding normal areas. Associated intraluminal thrombus appears as a low-density mass with homogeneous echogenicity and a smooth line of interface within the aortic lumen. Intraluminal thrombus can be confused with intramural hematoma or a thrombosed false lumen in dissection. Multiplane TEE can be helpful in allowing the acquisition of many planes to illustrate a thin bright line of echogenicity on the intraluminal surface, which represents the intimal-medial layer. In addition, aortic intraluminal thrombus usually produces a convexity towards the aortic lumen whereas intramural hematoma produces a concave distortion of the aortic wall, detracting from the circular appearance of the aorta at that level. The higher the ultrasound intensity of the plaque or atheroma, the more complex the atherosclerosis.[179] Cholesterol crystals within the lesions produce the highest echogenicity, with calcification producing bright white echoes and shadowing artefact. Aortic debris is characterized by mobile protruding lesions associated with the atheromatous plaques.

Various atherosclerotic scoring systems have been advocated to grade the severity of atherosclerotic disease, the most sophisticated dealing with collaboration of other radiographic methods and histology.[179] The simplest grading score is most useful in clinical practice. We use the scoring system in table 5.6 (figure 5.21), which has been readily accepted and understood by physicians, surgeons, and radiologists alike. The aorta is normal when the intima is smooth without identifiable thickening of the wall in multiple segments of the thoracic aorta. Mild atherosclerotic disease is present when there are areas of increased thickness in the aortic wall of less than 3.0 mm and no demonstrable intraluminal irregularities. Moderate atherosclerotic disease is represented by diffuse irregularities or obvious, raised plaques of less than 5.0 mm in thickness. Severe atherosclerotic disease is present when large areas of intimal thickening of more than 5.0 mm protrude into the aortic lumen associated with atheromatous debris and adherent intraluminal thrombus. Segments of the aortic wall may have extensive areas of calcification, ulcerated plaques, or craters that appear to penetrate 5–10 mm into the aortic wall. In addition to the grade, the presence or absence of atherosclerotic disease should be noted for each segment of the thoracic aorta, and checks should be made specifically for plaques or debris close to the origin of the great vessels.

Atherosclerotic disease is commonly shown in cardiac patients studied by TEE and there is an association between significant disease and thromboembolic events. Tunick and Kronzon[180] were the first to use TEE to report the association between atherosclerotic plaque in the aortic arch and systemic thromboembolism. The relative risk of symptoms in patients with protruding atheroma shown by TEE was significantly increased. Karalis et al.[181] showed aortic debris in 7% of all the patients studied by TEE in their institution. Atheromatous disease occurred in the aortic arch and descending aorta in 70% of patients but was limited to the descending aorta alone in 30%. They concluded that atheroembolism is a well-recognized complication of aortic debris, with an embolic potential of 73% with complex plaques (moderate to severe) and only 12% with simple (mild) plaques. Davila-Roman et al.[182] reported on the prevalence of cerebrovascular events in cardiac patients with atherosclerosis of the ascending aorta. In patients less than 60 years old, atherosclerosis occurred in the ascending aorta in fewer than 10%, compared with 32% in patients 80 years old. In a more recent study from Davila-Roman et al., atherosclerosis of the ascending aorta was an independent predictor of long-term neurological events and mortality. Neurological events and mortality increased more than 1.5-fold as the severity of atherosclerosis increased from normal-mild to moderate, and there was an increase of more than 3-fold in the incidence of both as the severity of atherosclerosis increased from normal-mild to severe.[183]

Treatment of severe atherosclerosis has been largely controversial, with use of both anticoagulation and/or antiplatelet agents and no real evidence to support either. Recently Ferrari et al.[184] showed a better outcome in patients with ascending atherosclerosis treated with anticoagulants versus antiplatelet agents. Further studies are needed to validate these findings and to determine which patients do best with either therapy.

Vaduganathan and colleagues[179] described the pathological correlates of aortic debris imaged with TEE. In their study, there was agreement in 73% of patients between histology and findings of TEE. Discrepancies
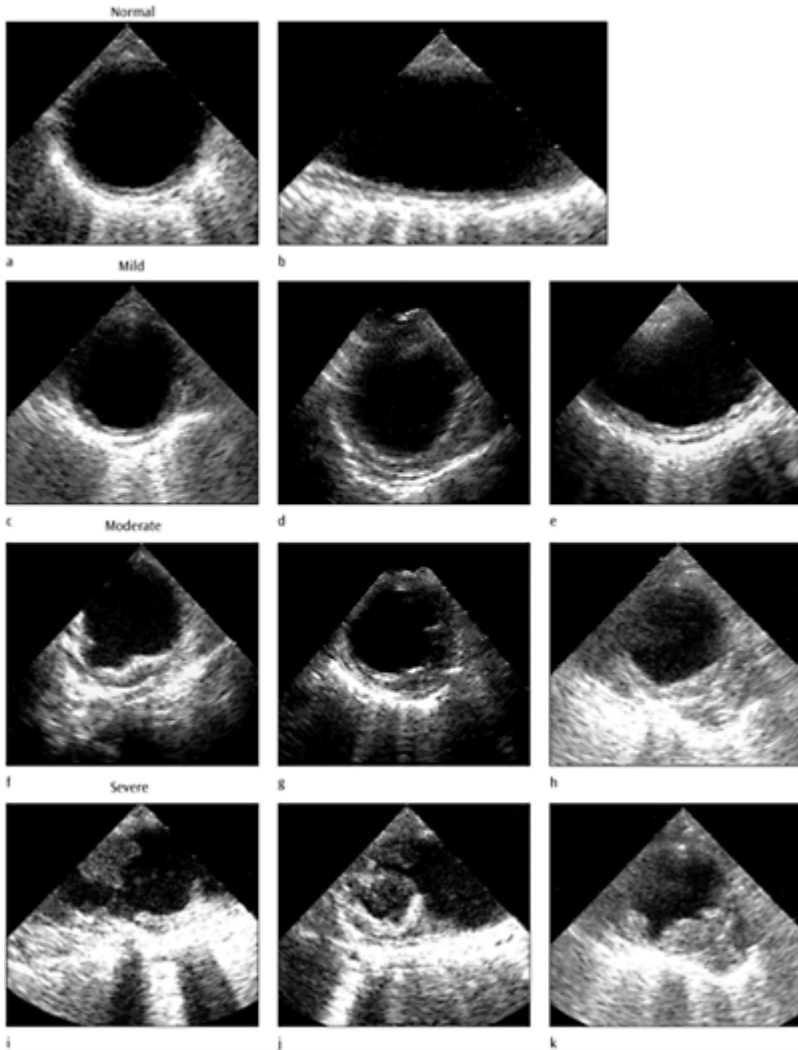
Figure 5.21 Echocardiographic demonstration of atherosclerotic aortic disease. Transesophageal echocardiography has contributed to the early diagnosis and heightened the awareness of atherosclerotic aortic disease especially in the thoracic aortic segments. The resolution of TEE permits the determination of the

severity of aortic atherosclerotic disease and the grading of the severity of disease. In the normal aorta (a, b) the intima is smooth without identifiable thickening of the wall in multiple segments. Mild atherosclerotic disease (c–e) is present when there are areas of increased thickness in the aortic wall less than 3.0 mm and no demonstrable intraluminal irregularities. Moderate atherosclerotic disease (f–h), is represented by diffuse irregularities or obvious, raised plaques less than 5.0 mm in thickness. Severe atherosclerotic disease (i–k) is present when large areas of intimal thickening greater than 5.0 mm protrude into the aortic lumen associated with atheromatous debris and adherent intraluminal thrombus. Segments of the aortic wall may have extensive areas of calcification, ulcerated plaques, or craters that penetrate 5–10 mm into the aortic wall.

occurred when TEE missed superficial ulcerations beyond the resolution of standard technology. In their patients, grade I and II (mild) atherosclerotic disease was easily distinguished from grade III and IV (moderate and severe) disease in 93% of patients. The sensitivity and specificity of TEE for identification of thrombus was 91% and 90%, respectively.

Significant aortic atherosclerotic disease detected by TEE correlates with disease elsewhere in the circulation system, especially in the coronary and cerebrovascular systems. Fazio et al.[185] showed the relation between coronary artery disease and atherosclerotic aortic disease in 61 patients who underwent TEE and cardiac catheterization. 41 patients had at least single vessel coronary obstructive disease, of whom 37 had aortic atherosclerotic plaque. Of 20 patients with normal coronary arteries only two had aortic atherosclerotic plaque. The positive predictive value of aortic plaque for obstructive coronary artery disease was 95%, with a negative predictive value of 82%. All patients with three-vessel and left main coronary artery disease had aortic atherosclerotic plaque but importantly their cardiac risk factors were weak predictors of

coronary artery disease. This finding has important implications for patients who have diagnostic TEE assessments for endocarditis, valvular disease and aortic disease before cardiac surgery. The question of whether or not to perform coronary catheterization for preoperative clearance may be settled when concomitant significant aortic atherosclerotic disease is discovered in patients with risk factors for whom obstructive coronary disease should be ruled out.

In patients with aortic debris shown by TEE, the risk of embolic complications for both cardiac catheterization and cardiac surgery are increased. Simons et al.[186] showed that the risk of systemic embolism in cardiac catheterization is approximately 0.1%, but was increased to 27% in patients with atherosclerotic plaque and debris. Perioperative stroke is a known complication of cardiac surgery, and has an increased incidence with age. Loop et al.[187] found a greater prevalence of perioperative stroke of more than 2.4% in patients older than 65 years. Gardner et al.[188] studied patients over a 10-year period and found an increased prevalence of perioperative stroke of 7.1% in patients over 75 years old. Perioperative stroke is believed to result from pre-existing cerebrovascular disease, atherosclerosis of the ascending aorta and prolonged cardiopulmonary bypass times. Kouchoukos and colleagues[187,190] have studied perioperative stroke rates and their association with atherosclerotic disease of the ascending aorta and arch extensively. Their group used epiaortic ultrasound as well as TEE for diagnosing significant atherosclerotic plaque in the ascending aorta and arch prior to cross-clamping and start of cardiopulmonary bypass. They concluded that ultrasound examination was superior to the traditional approach where the surgeon palpates the aorta to exclude aortic disease for the optimum placement of cannulas and cross-clamping. In their study, epiaortic ultrasound was more accurate than biplane TEE since the distal ascending aorta was a common site of aortic debris. Further studies need to be done with multiplane TEE. In our institutions, multiplane TEE has been sufficient for diagnosing distal ascending disease, but epiaortic examination is also done in difficult cases in whom the optimal site for cross-clamping of the aorta is found by the surgeon placing the probe directly on the aorta. In Kouchoukos' group the surgery plan was modified to accommodate atherosclerotic disease in 25% of cases.[190] Their recommendations include: alternative cannula sites, cross-clamping sites or proximal anastomotic graft sites; replacement of the severely diseased ascending aortic segment under circulatory arrest; use of the innominate or internal mammary artery to place the proximal vein anastomosis; perform endarterectomy, patch aortoplasty or graft replacement of the diseased segment; or start of hypothermic fibrillatory arrest to avoid cross-clamping; and the avoidance of intra-aortic balloon pumping. In their studies, use of these techniques produced no strokes or peripheral embolic events during the postoperative period with a 30-day mortality of 3.7%. In our own experience, TEE-guided cardiac surgery decreases the incidence of perioperative stroke as well as other postoperative complications.[191]

Porcelain aorta

An extensive manifestation of atherosclerotic aortic disease is the porcelain aorta. With a porcelain aorta, the aortic walls are lined with plates of calcium to produce an eggshell appearance on diagnostic imaging and a firm hard sensation (thus the term porcelain) on

palpation of the whole aorta. Porcelain aorta has been thought to occur as the result of inflammatory processes such as aortitis or previous radiation therapy to the chest. Fortunately, this is an uncommon finding but it does occur in the elderly presenting for valve replacement for aortic stenosis and coronary-artery bypass grafting. The ascending aorta is predominately affected, but cases have been described that included the aortic arch, great vessels and descending aorta.[192,193] With extensive involvement, one area that seems to be less affected is the area of the proximal right subclavian artery where it originates from the innominate artery.[194]

The most important ramification is that the severely calcific aortas cannot be cannulated or cross-clamped without risk of rupture, intimal laceration, dissection, or crushing of the aorta. TEE visualization of the porcelain aorta shows thickened aortic wall with bright white linear lines of echogenicity, with shadowing artefact paralleling the aortic outline—best appreciated in the longitudinal planes. The shadowing artefact often makes the aorta difficult to image or detracts from the overall cardiac imaging ability of TEE—it resembles the quality of a transthoracic imaging in technically difficult patients. In addition, aortic plaques and debris may be associated with porcelain aortas. In our experience, most postoperative dissections have occurred in patients with aortas with this manifestation of severe atherosclerotic disease. When perioperative dissection occurs, the visual appearance to the cardiac surgeon is similar to a classic aortic dissection. A deep purple hematoma appears in the wall of an enlarging aorta after the aortic cannula or cross-clamp is removed. In our experience, perioperative aortic dissection due to cardiac surgery is somewhat of a misnomer, since the injury pattern of dissection produced, as visualized by TEE, resembles the appearance of a traumatic disruption of the aortic adventitia.
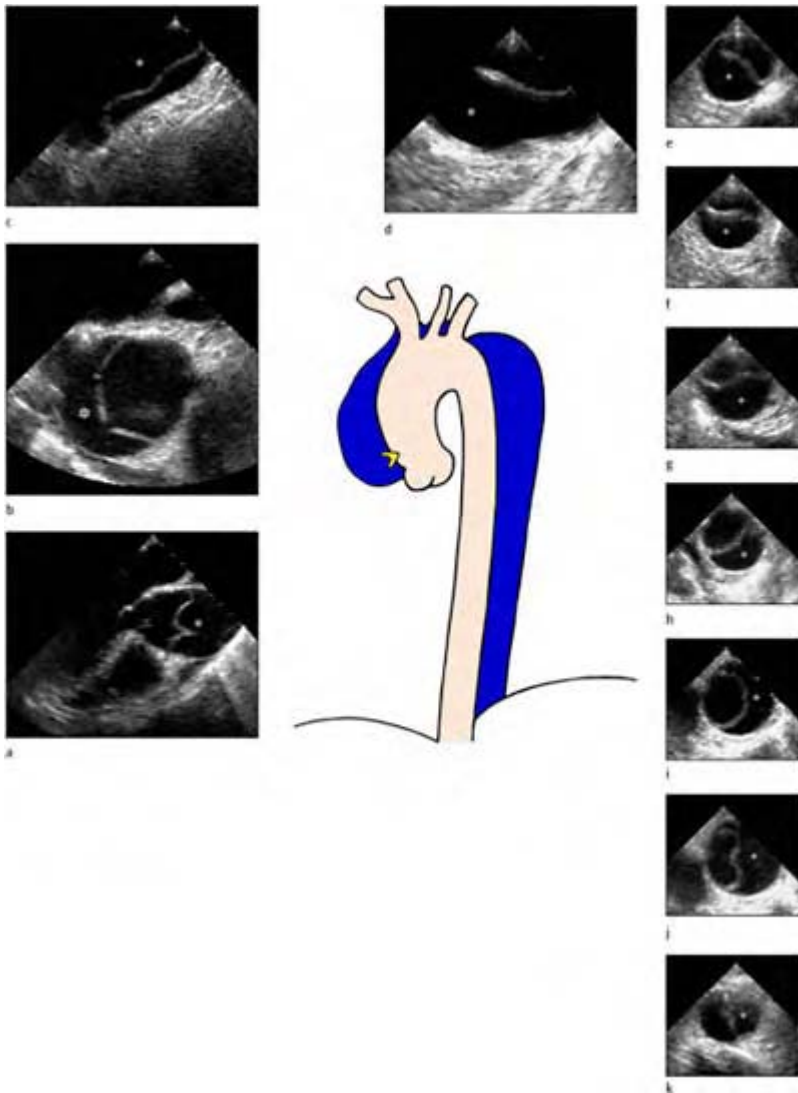
Case 5.1 Ascending aortic dissection. Multiplane TEE images of the whole aorta in a typical type I dissection. It is often helpful to display and acquire images at multiple levels in aortic dissection in order to conceptionalize the extent of aortic dissection. A true and false lumen is readily identified

and delineated by an intimal flap starting near the aortic valve extending through the entire aorta to at least the diaphragm. Note due to the normal spiraling of the aorta as well as the change in anatomical relationship of the aorta and the esophagus in the thoracic cavity the true and false lumen appear to change positions within the aortic lumen depending on the level of aorta visualized.
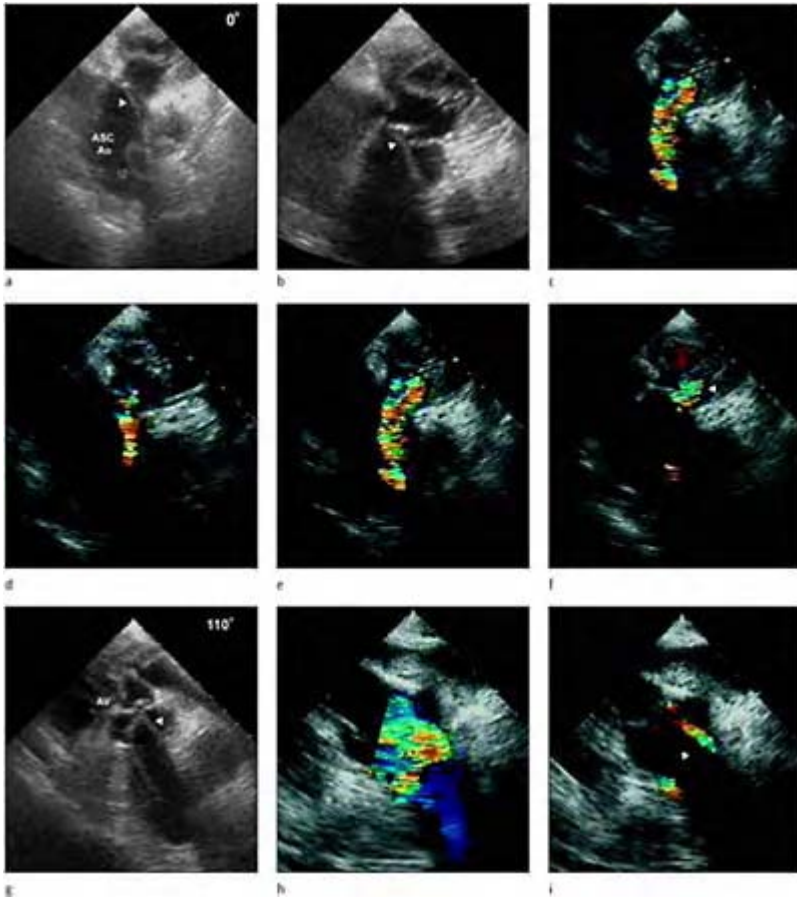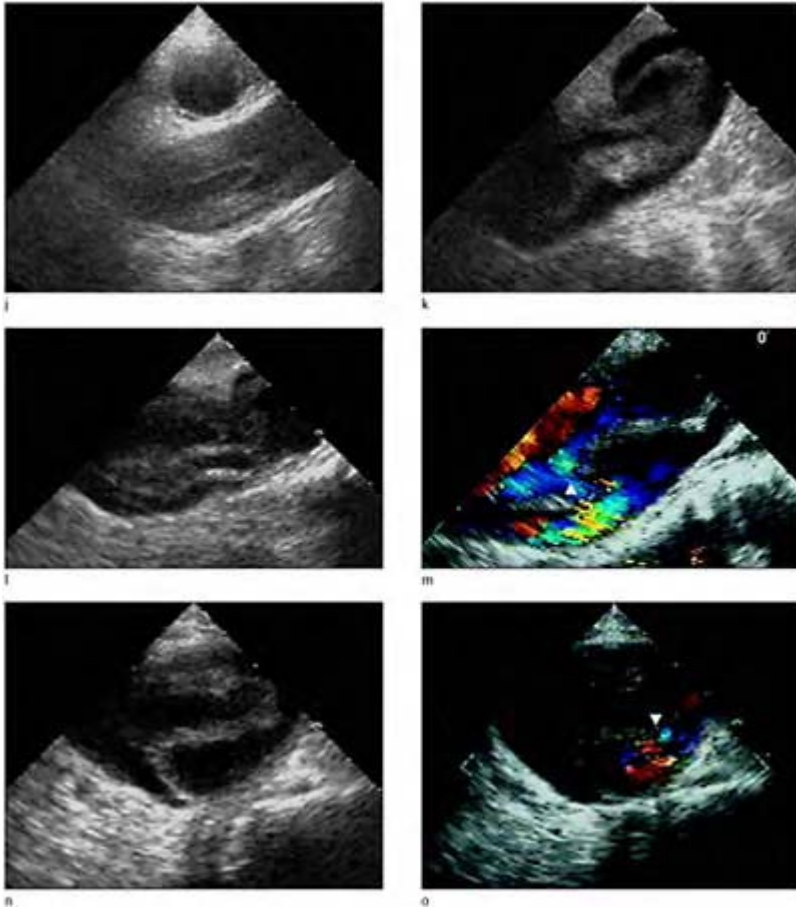
Case 5.2 Ascending aortic dissection. Multiplane TEE images of an ascending aortic dissection from the deep transgastric imaging planes. The origin of the intimal flap (arrows) near the aortic valve plane is nicely demonstrated with its extent to the aortic arch (a, b). With color flow Doppler blood flow (arrow) is delineated through out the cardiac cycle (c–f) within the true lumen. The full extent of the dissection is readily appreciated from this window in a

wider plane perspective unlike other imaging planes obtained with echocardiography. With rotation of the transducer to 90° in the gastric position, views of the aorta (g–i) similar to the deep transgastric views are seen with a shorter segment of the aorta usually to the mid-ascending aorta. The aortic valve plane is better visualized with this window in determining the extent of the dissection and involvement of the valve. Typical horizontal and longitudinal views (j–o) obtained from the upper esophageal window of the ascending aorta in the same patient. Echocardiographic imaging demonstrating the intimal flap motion (j–l), which undulates during the phases of the cardiac cycle. With color flow Doppler the intimal tear is recognized usually at the point of greatest motion with flow (arrow) entering the false lumen (m). Horizontal projections (n, o) of the distal aortic arch demonstrating the intimal flap separating the true and false lumens.
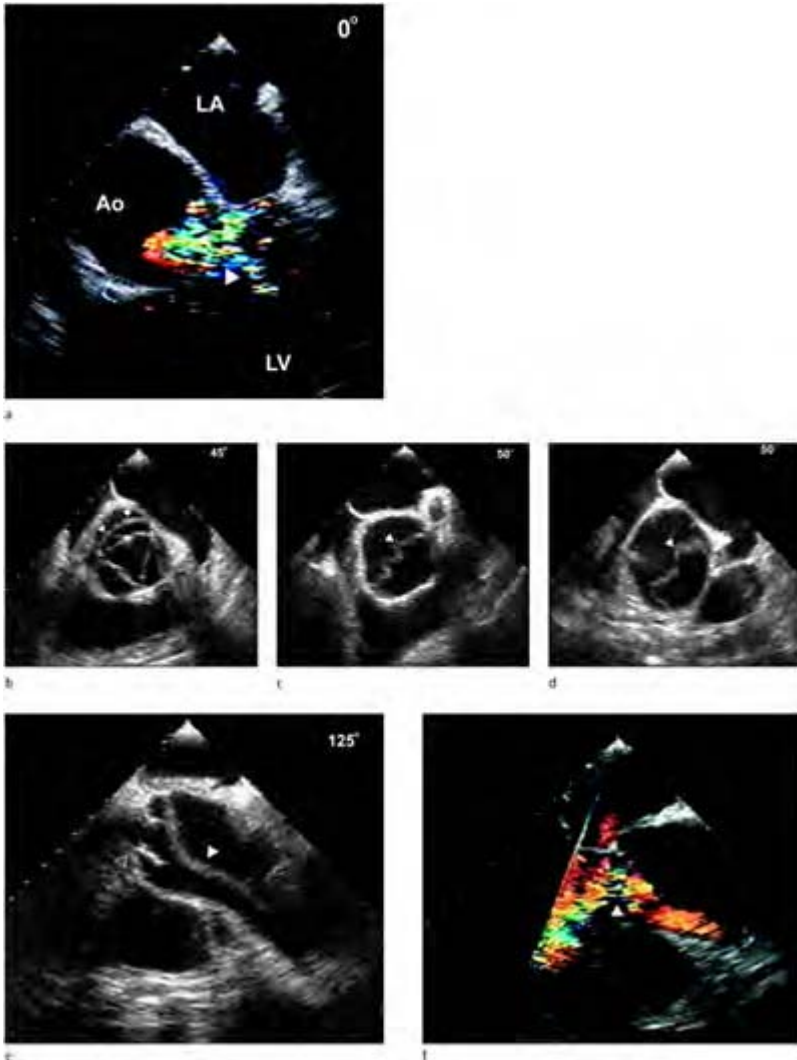
Case 5.3 Ascending aortic dissection
with aortic valve involvement. An
ascending aortic dissection with the
intimal flap involving and dissecting to
the sinus of Valsalva of the non-
coronary cusp. Four-chamber view (a)
obtained from the lower esophageal
window at 0° demonstrating an
enlarged aortic root, with aortic

insufficiency demonstrated in the left ventricular outflow tract with color flow Doppler. Horizontal view (b) obtained from the upper esophageal window at the aortic valve plane around 45° demonstrating the intimal flap (arrow) surrounding the non-coronary sinus at the valve level. Disruption of the valve is readily seen due to the extent of the dissection. With slight withdrawal of the probe and returning the transducer to 50° above the valve plane the entry site is detected. At the same imaging level and rotation of the transducer to 125° (e) the full extent of the intimal flap is demonstrated starting at the valve level, with the entry site (arrow) noted above the valve plane. With color Doppler flow (f) is demonstrated through the entry site and aortic regurgitation is detected in the left ventricular outflow tract.
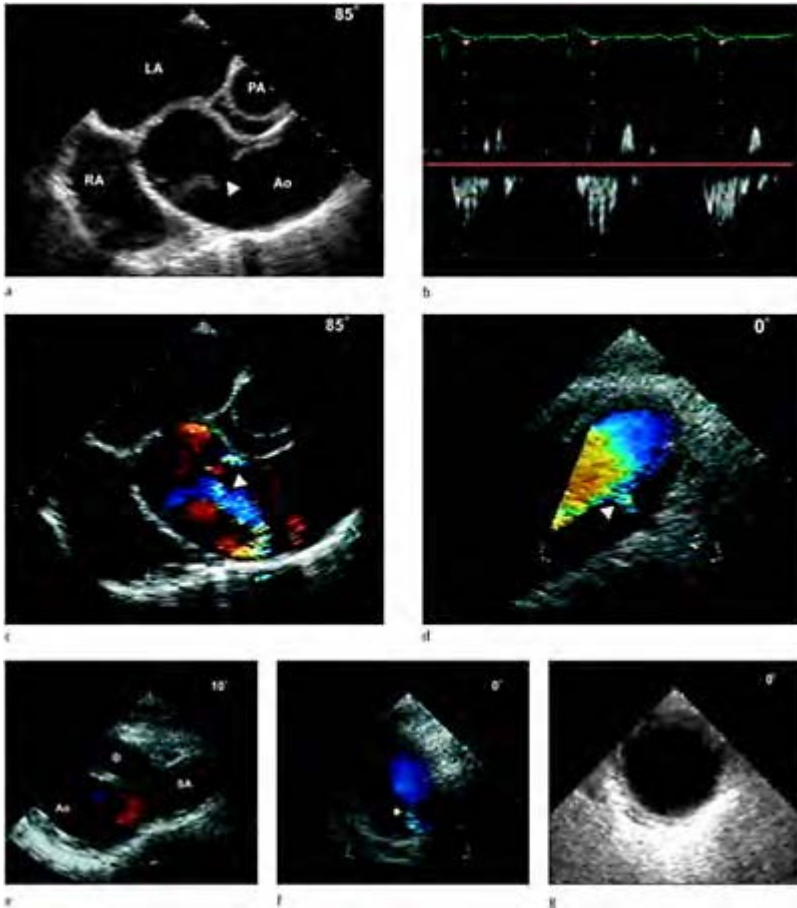
Case 5.4 Ascending and arch aortic
dissection. An intimal flap is noted in
the ascending aorta (a) with a large
entry site (arrow) above the aortic
valve plane. Pulsed Doppler of the
entry site (b) demonstrates triphasic
blood flow through the entry site.
Color flow Doppler (c) demonstrating
blood flow through the entry site from
the true to false lumen. Another entry
site is detected in the distal ascending
aorta with flow demonstrated with
color flow Doppler (d). With full

rotation of the probe to image the descending aorta the intimal flap is seen extending the origin of the left subclavian artery. An exit site (arrow) is depicted by color flow Doppler (f) just distal to the subclavian artery with the extent of the dissection ending in the normally appearing proximal descending aorta (g).
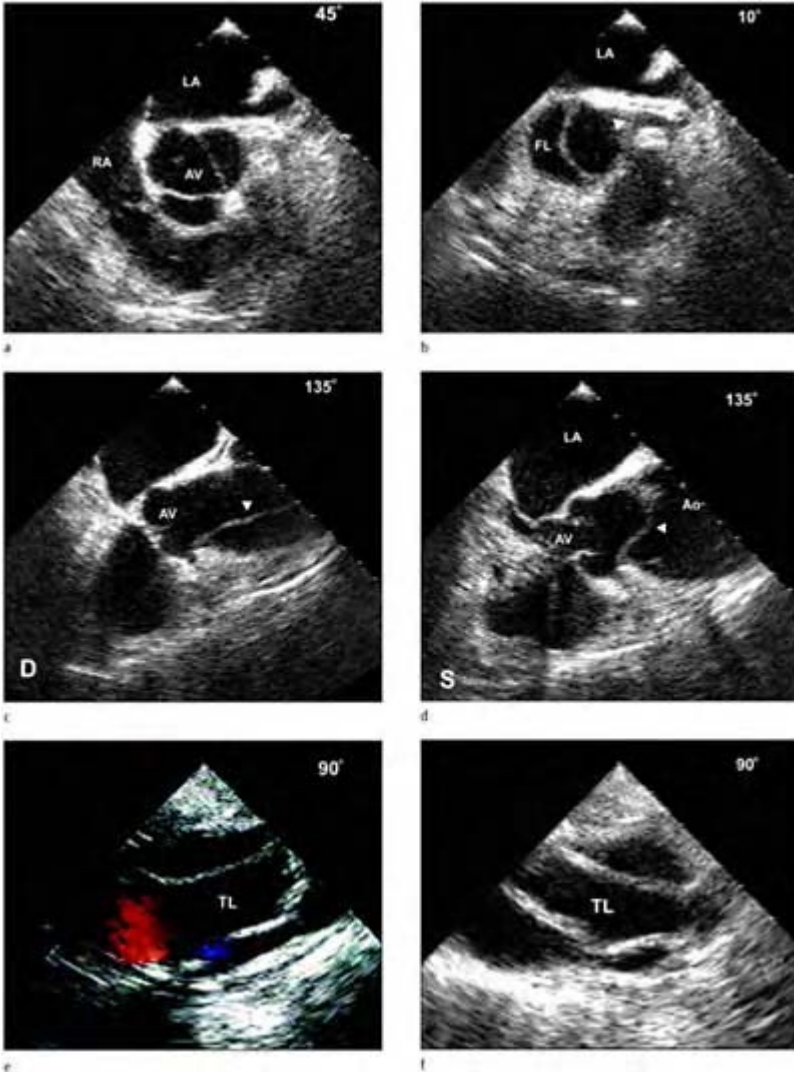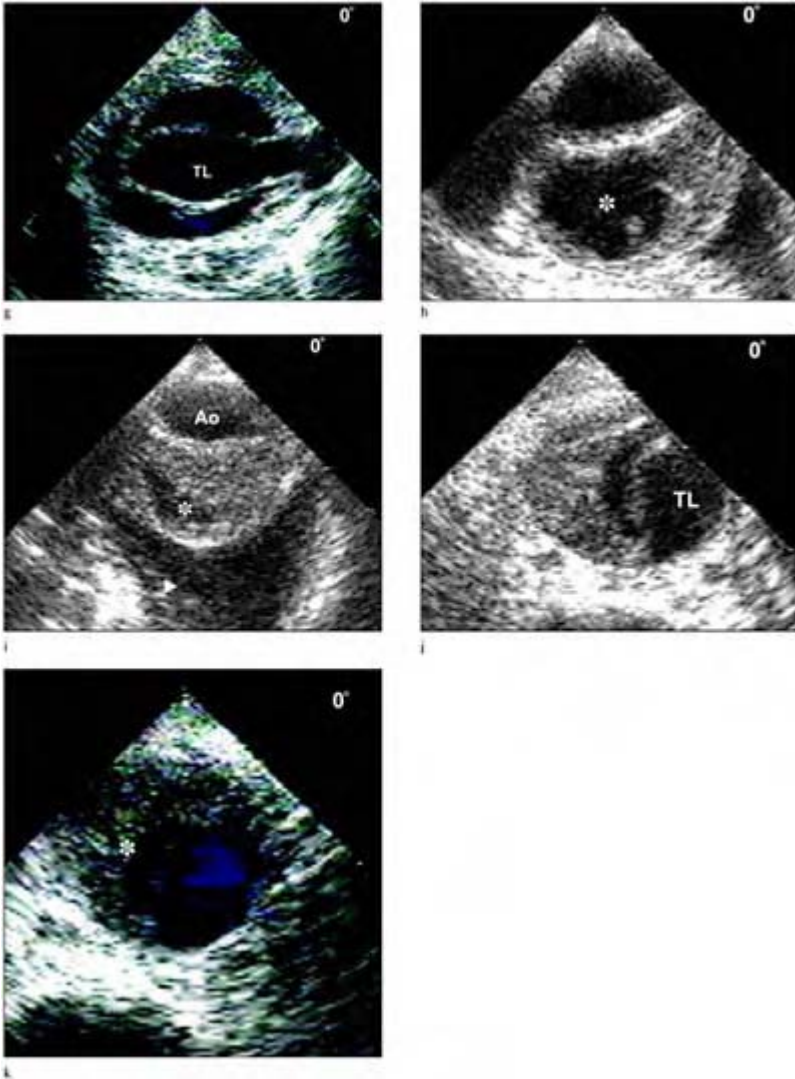
Case 5.5 Aortic arch dissection extending retrograde to the level of the coronary arteries. With dissections involving the ascending aorta it is important to visualize the origin of both coronary arteries in order to assess their involvement with the dissection process. Multiplane TEE

usually allows identification of the coronary arteries with greater frequency than other non-invasive imaging techniques, avoiding more invasive procedures. Horizontal view at the aortic valve plane (a) in a patient with dissection. The valve appeared to open and close normally. With withdrawal of the probe, the left coronary artery was visualized and it was readily apparent that it originated from the true lumen of the dissection. With rotation of the transducer to 135° the right coronary artery origin (c) was visualized with the extent of the dissection plane stopping distal to the right coronary artery ostia. With slight lateral flexion of the probe, the right coronary artery (d) is better visualized suggesting its origin from the true lumen. Demonstration of the true and false lumens in the aortic arch demonstrating intussusception at that level (e, f). The true lumen appears as the central channel and extends near the ostia of the left subclavian artery (g). The dissection extended through the entire descending thoracic aorta into the abdominal aorta and thrombus is noted (star) in the false lumen (h–k). Near the mid-thoracic level a large pleural effusion (arrow) is noted separating the aorta from the typical lung interface.
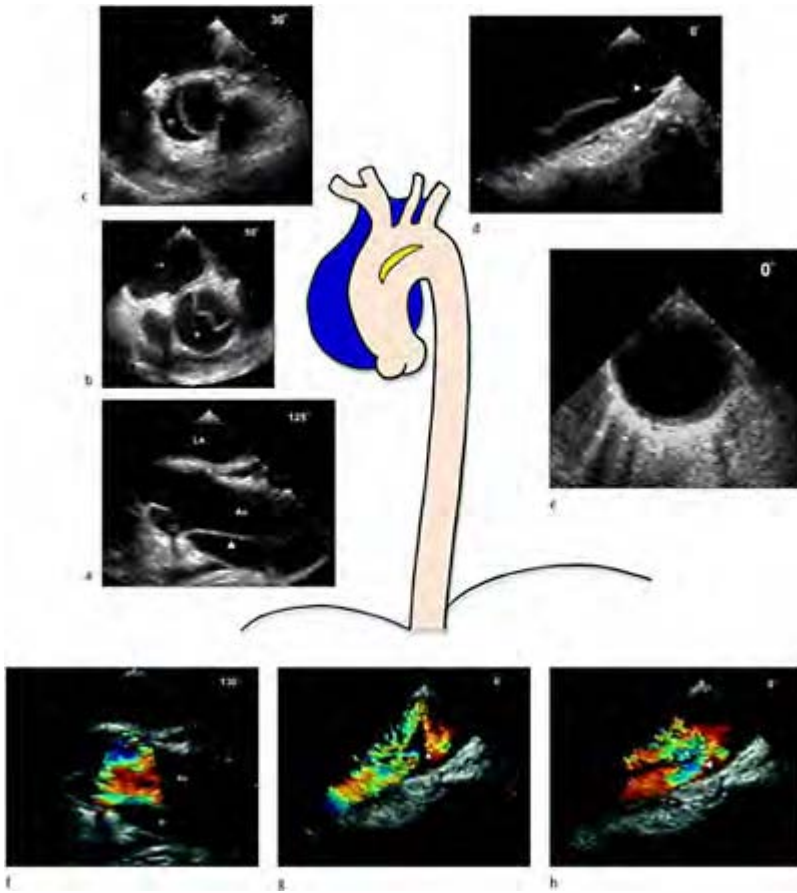
Case 5.6 Arch aortic dissection with retrograde extension. An intimal flap is noted in the ascending aorta beginning at the level of the sinotubular junction above the right coronary artery in the longitudinal plane. Horizontal views (b, c) obtained in progression of the ascending aorta demonstrate an intimal flap with no obvious entry site. Longitudinal views of the distal ascending aorta and the proximal aortic arch demonstrating a large transverse intimal tear corresponding the drawing opposite the innominate artery. The

dissection stopped in the aortic arch as demonstrated by a normal descending aorta (e). Color flow Doppler demonstrating disturbed blood flow through the true lumen produced by the dissection plane, with marked disturbance of blood flow demonstrated through the entry site (g, h) at the arch level between the true and false lumen.
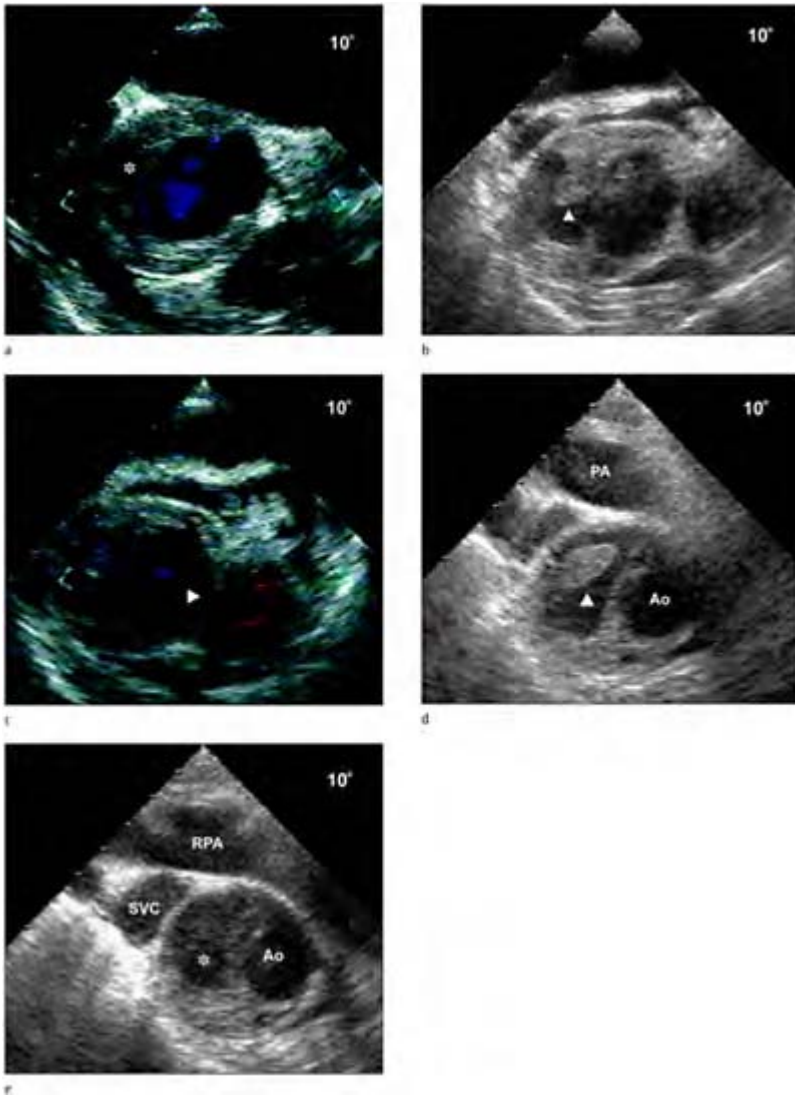
Case 5.7 Chronic ascending dissection. Chronic dissection limited to the ascending aorta and arch in an elderly hypertensive patient presented for TEE to rule out cardiac source of embolus. The patient admitted to an excruciating bout of chest pain approximately 3 months prior and was cleared by CT

scan. Symptoms of a transient ischemic attack followed 2 months later. Multiplane TEE examination revealed a partially thrombosed false lumen in the ascending aorta that extended through the aortic arch and ending in the descending aorta. Horizontal views of the ascending aorta from the upper esophageal window demonstrate thrombus (arrow) totally occluding a false lumen with partial occlusion in the distal ascending aorta. An echo free space surrounds the aorta proximally suggesting effusion in the transverse sinus, which produces an echo-free space and separation (d) between the aorta and the superior vena cava.
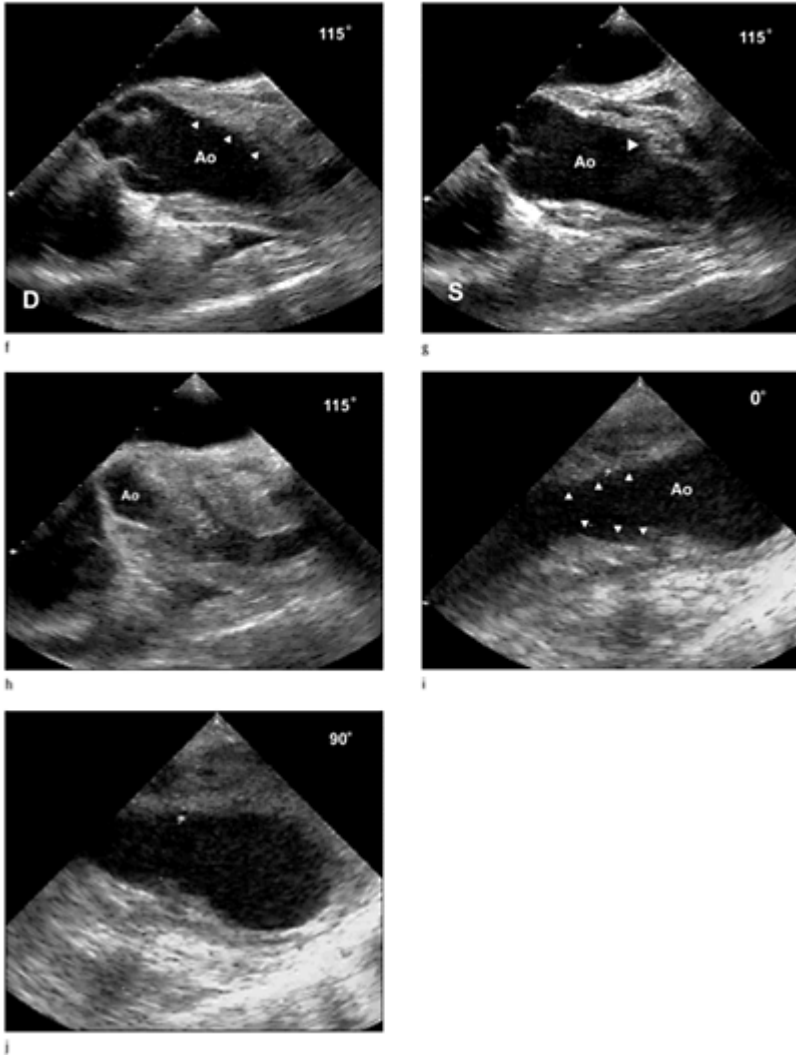
Longitudinal views at 115° (f–i) illustrate the extent of thrombosis of the false lumen adjacent to the proximal and distal walls of the aorta with a central true lumen. Horizontal view of the proximal descending aorta (j–o) demonstrating the false lumen ending in the mid descending aorta.

k

l

m

n

o
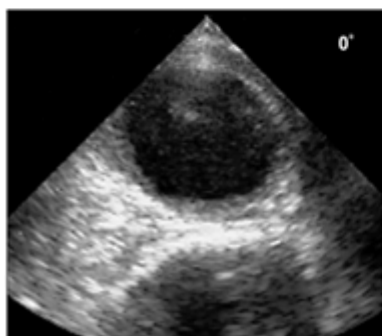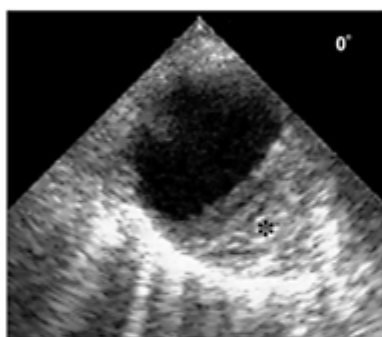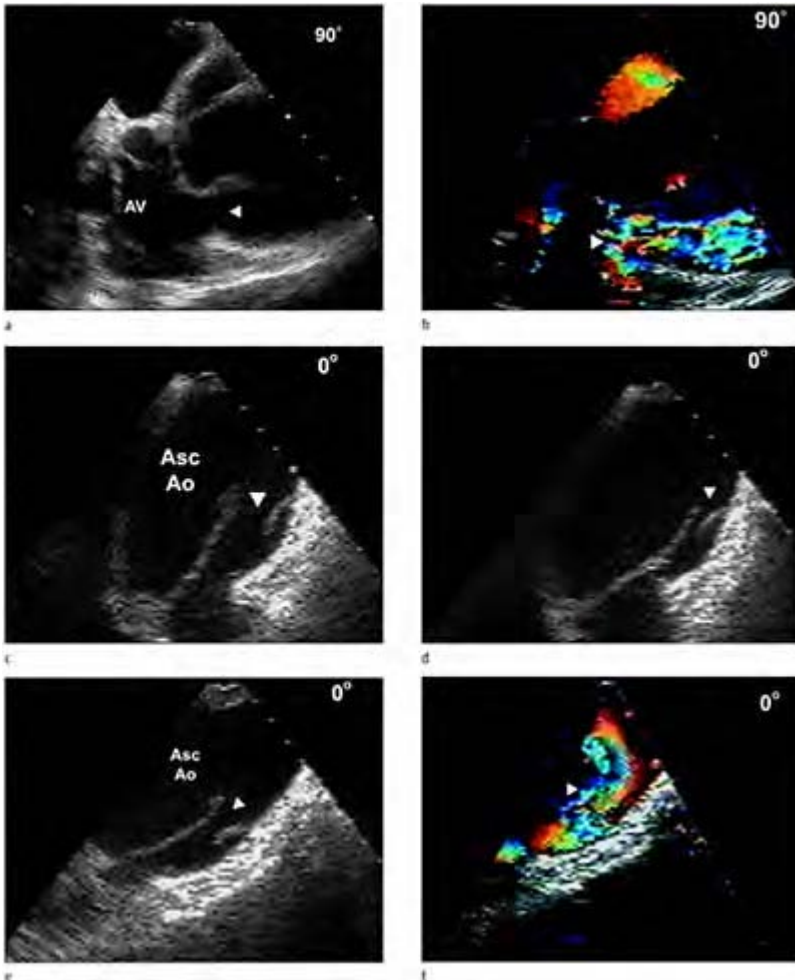
Case 5.8 Ascending aortic aneurysm and arch dissection. Longitudinal views of the aortic root (a) demonstrate aneurysmal dilatation with progressive dilatation of the ascending aorta with distortion of the sinus of Valsalva with an intimal flap noted starting near the sinotubular junction producing disturbed blood flow with color Doppler (b). A longitudinal entry site is noted proximal to the origin of the

innominate artery in the proximal aortic arch. Note the overlapping appearance of the intimal flap and separation (arrow) during the cardiac cycle (c–e). Flow between the true and false lumen produces a swirling effect with color Doppler (f).
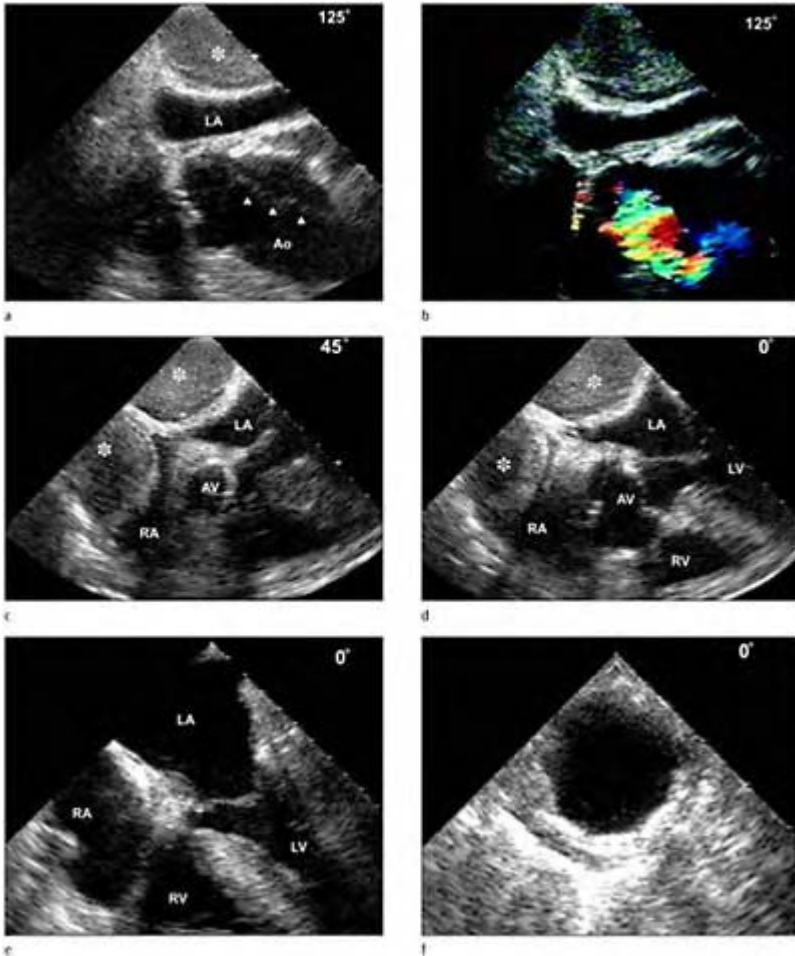
Case 5.9 Mediastinal hematoma and aortic dissection. Mediastinal hematoma as well as pericardial effusion are frequent complications

noted in patients with aortic dissection and aortic transection. Mediastinal hematoma tends to exhibit increased echogenicity rather than an echo-free space as in simple effusions due to the effects of hemorrhage. Large hematoma (a–d) producing marked external compression of the right and left atrium in views obtained from the mid-esophageal window is demonstrated in an ascending aortic dissection. In the lower esophageal window, the atria are both visualized (e) and appear normal, suggesting that the hematoma is not causing significant hemodynamic compromise due to the inability to fill the atria. Horizontal views of the proximal descending aorta exhibit moderate atherosclerotic disease without extension of the dissection.
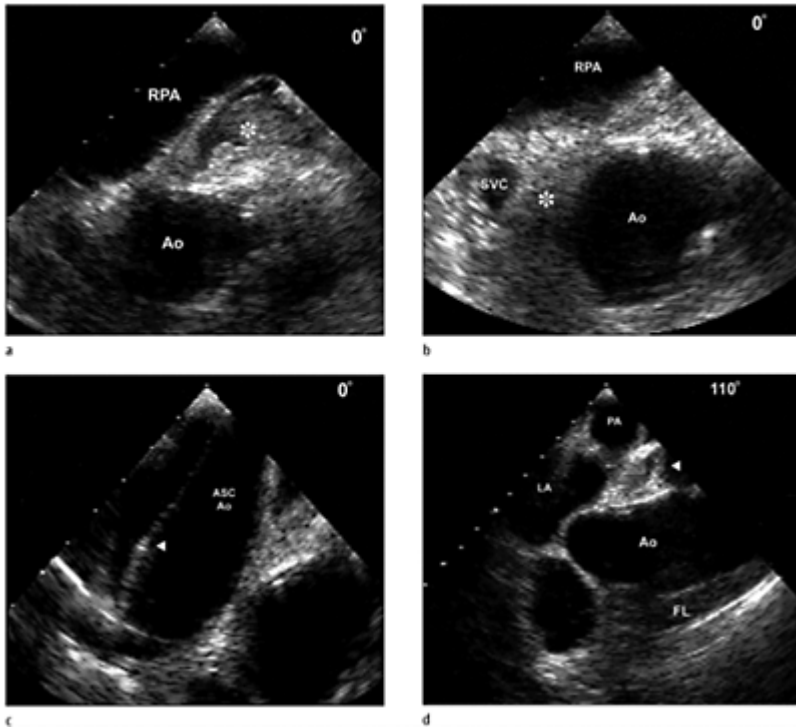
Case 5.10 Mediastinal hematoma and ascending dissection. Large mediastinal hematoma (a) associated with an ascending aortic dissection. The transverse sinus is markedly enlarged secondary to the hematoma (star) as suggested by the displacement and compression of the superior vena cava (b). Views of the ascending aorta demonstrating an intimal flap (c) at 0° from the upper esophageal window. With a longitudinal view at 110° (d) the intimal flap is demonstrated including hematoma in the transverse sinus displacing the right pulmonary artery.
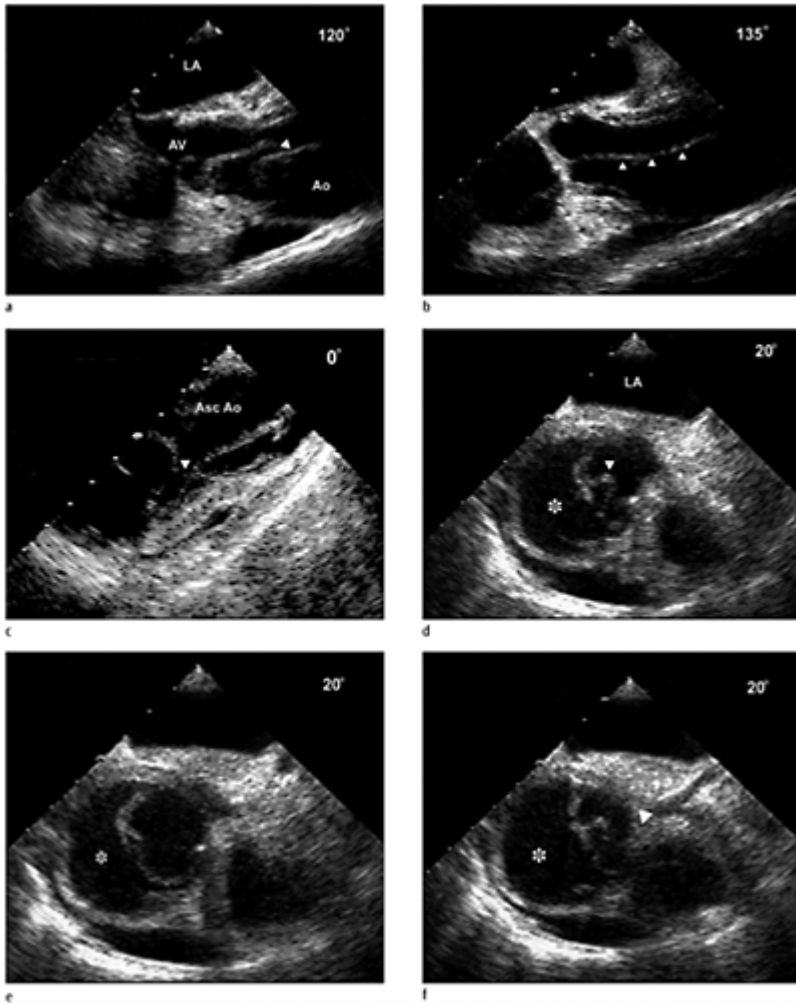
Case 5.11 Aortic arch dissection with left coronary involvement. Longitudinal views of the ascending aorta (a, b) demonstrating a retrograde extension of an aortic arch dissection, with the entry site depicted in (c). A large false lumen (star) is demonstrated in horizontal views (d–f) with a very small compromised true lumen especially at the origin of the left main coronary artery (f). EKGs

demonstrated anterior wall ischemia
and injury pattern.
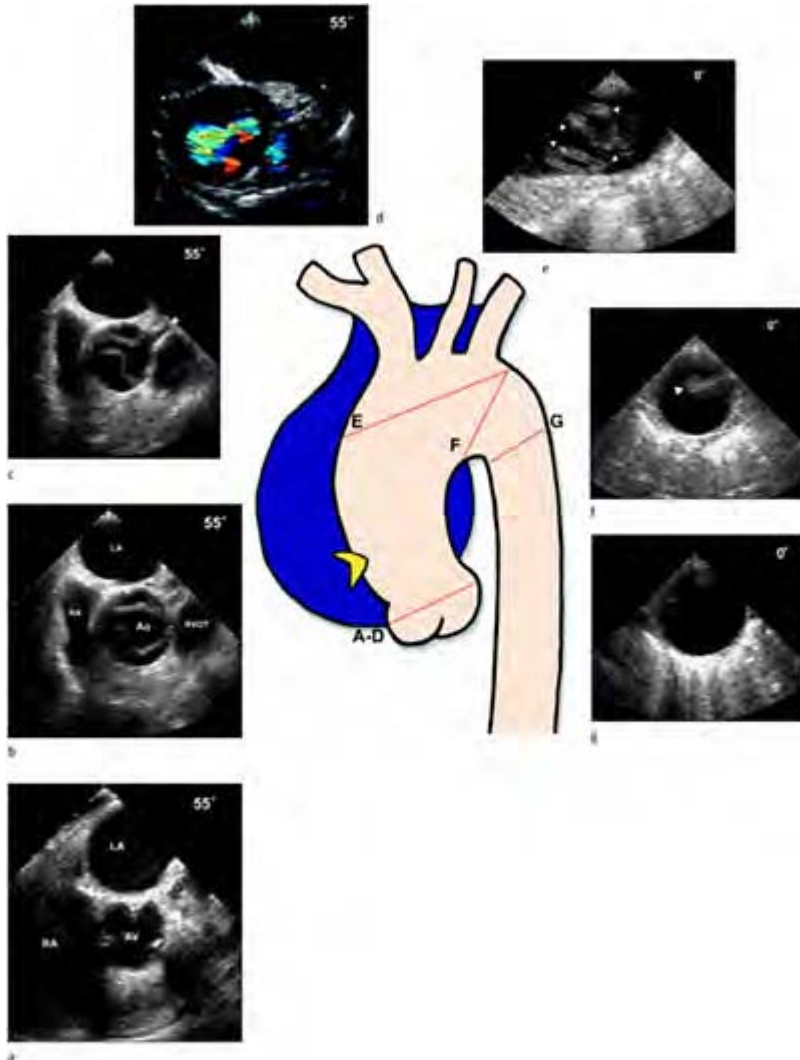
Case 5.12 Ascending dissection with
intussusception. The majority of aortic
dissections extend in a longitudinal
axis along the length of the aorta.
Rarely, there is a circular disruption of
the intima and media producing

intimointimal intussusception. The true
lumen encompassing the intima
becomes completely invaginated in the
false lumen and may produce total
occlusion of the aorta or the great
vessels. Sequential horizontal views
along the ascending aorta
demonstrating a circumferential
disruption with a central true lumen
(a–c). Views of the distal ascending
aorta at 0° (d) and 60° (e)
demonstrating near collapse due to the
dramatic in-folding of the intima lining
which may severely compromise flow
through the true lumen and eventually
the great arteries. The dissection is
seen extending to the proximal
descending aorta (f) and dramatically
stops in the mid-descending aorta (g)
with reconstitution of a normal lumen.
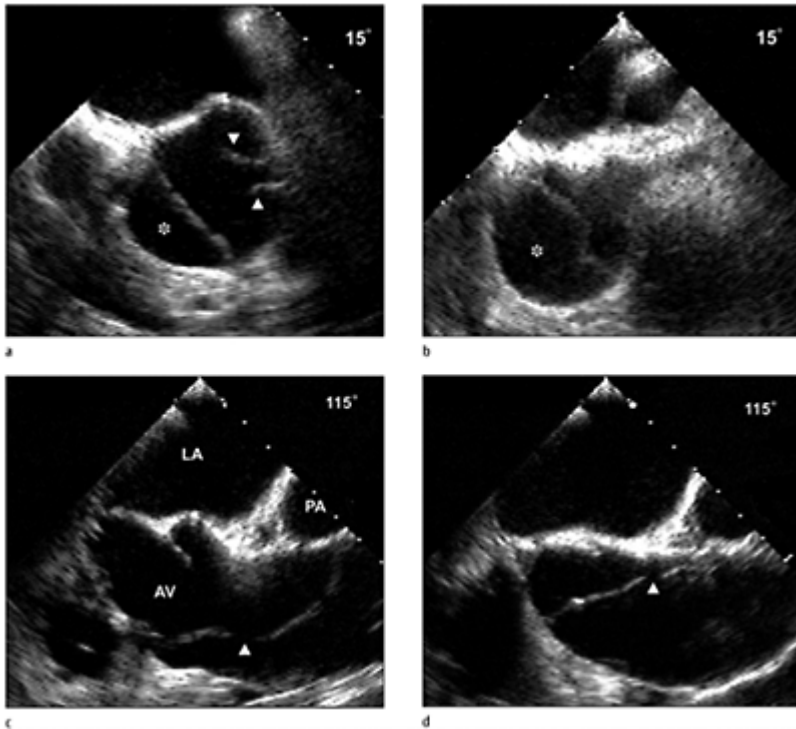
Case 5.13 Ascending dissection associated with a descending aortic aneurysm. Horizontal and longitudinal views of the ascending aorta (a–d) demonstrating a highly mobile intimal flap extending up to the right coronary cusp. The aortic valve (arrows) in (a) and the left coronary artery (b) do not appear compromised by the dissection. The false lumen (star) is demonstrated with an entry site (arrow) in the proximal aorta.
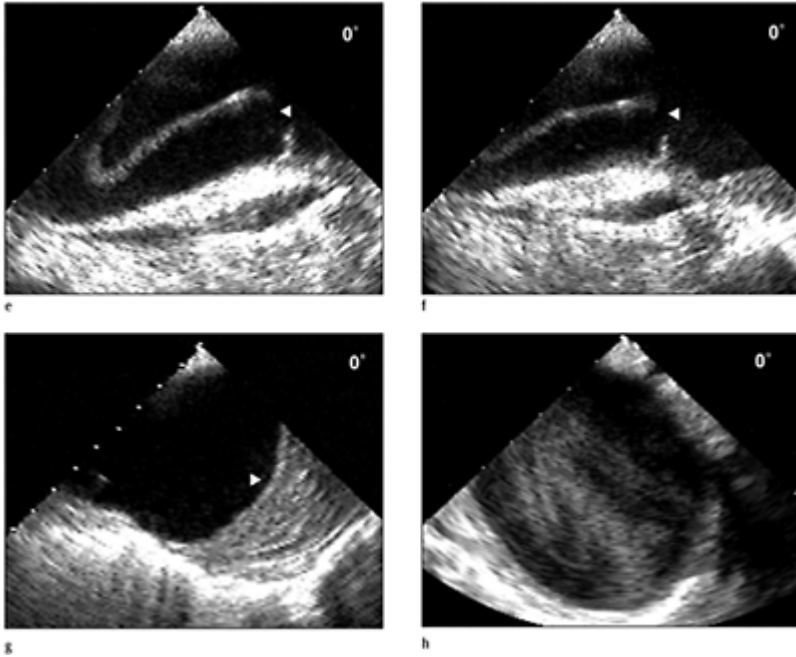
Views of the proximal aortic arch (e, f) demonstrate an exit site and extension of the dissection at the mid-arch level. The distal aortic arch (g) exhibits a thrombosed hematoma in the false lumen (star) and is enlarged. The descending aorta (h) is obviously enlarged with spontaneous echo contrast (star) swirling in the aortic lumen.
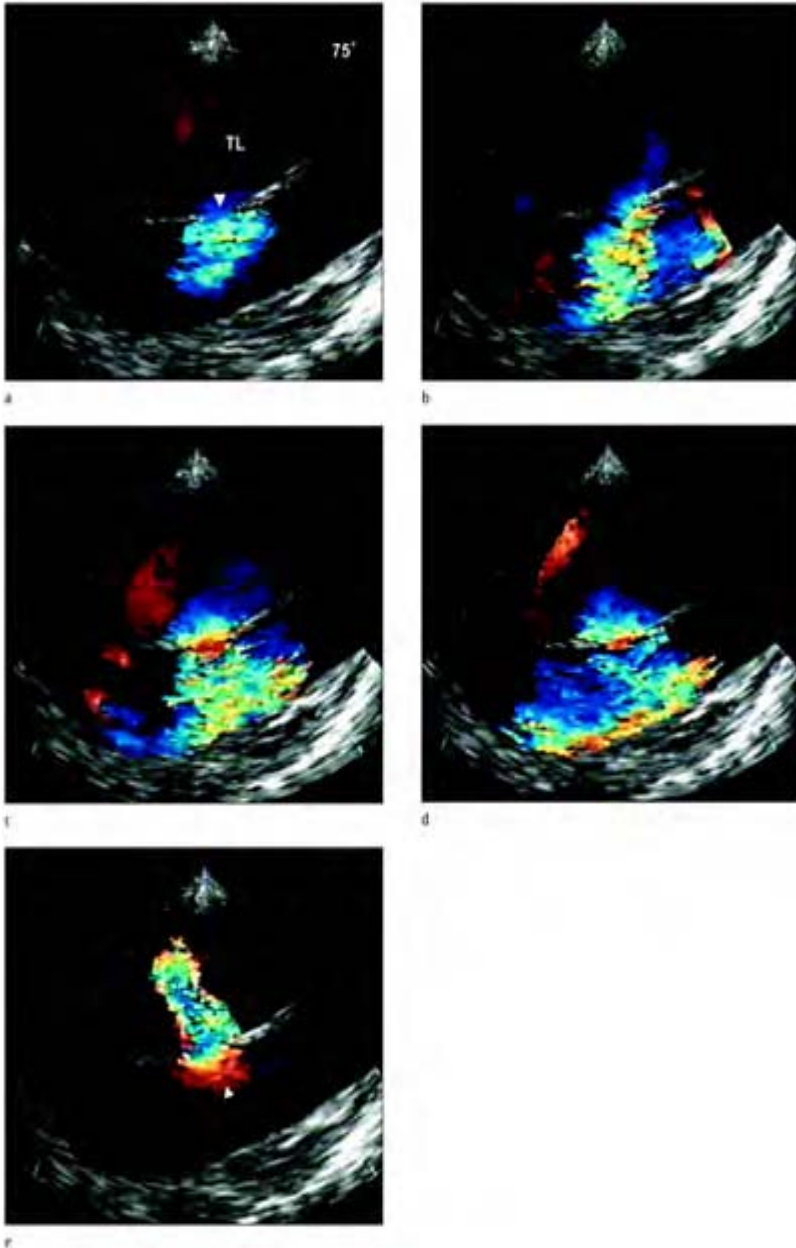
Case 5.14 Arch dissection.
Longitudinal and horizontal views (a–
e) exhibit an arch dissection with a
transverse intimal entry site with

retrograde extension to the right coronary cusp. The false lumen is partially thrombosed at its distal extent (arrow). Flow disturbance is noted in the true lumen in the proximal aortic root. Color flow Doppler exhibited phasic flow during a cardiac cycle from the true to false lumen (f–k). The dissection extended in a longitudinal fashion antegrade throughout the descending aorta (l–q), with much of the false lumen exhibiting thrombosis. TL, true lumen.

l

m

n

o

p

q
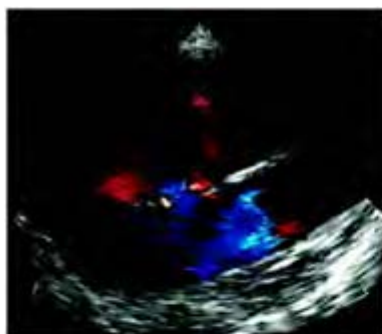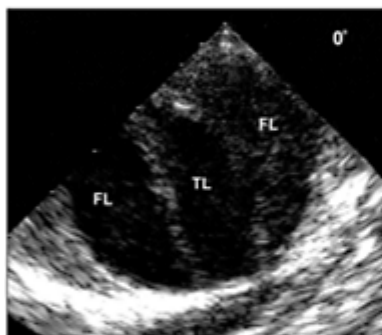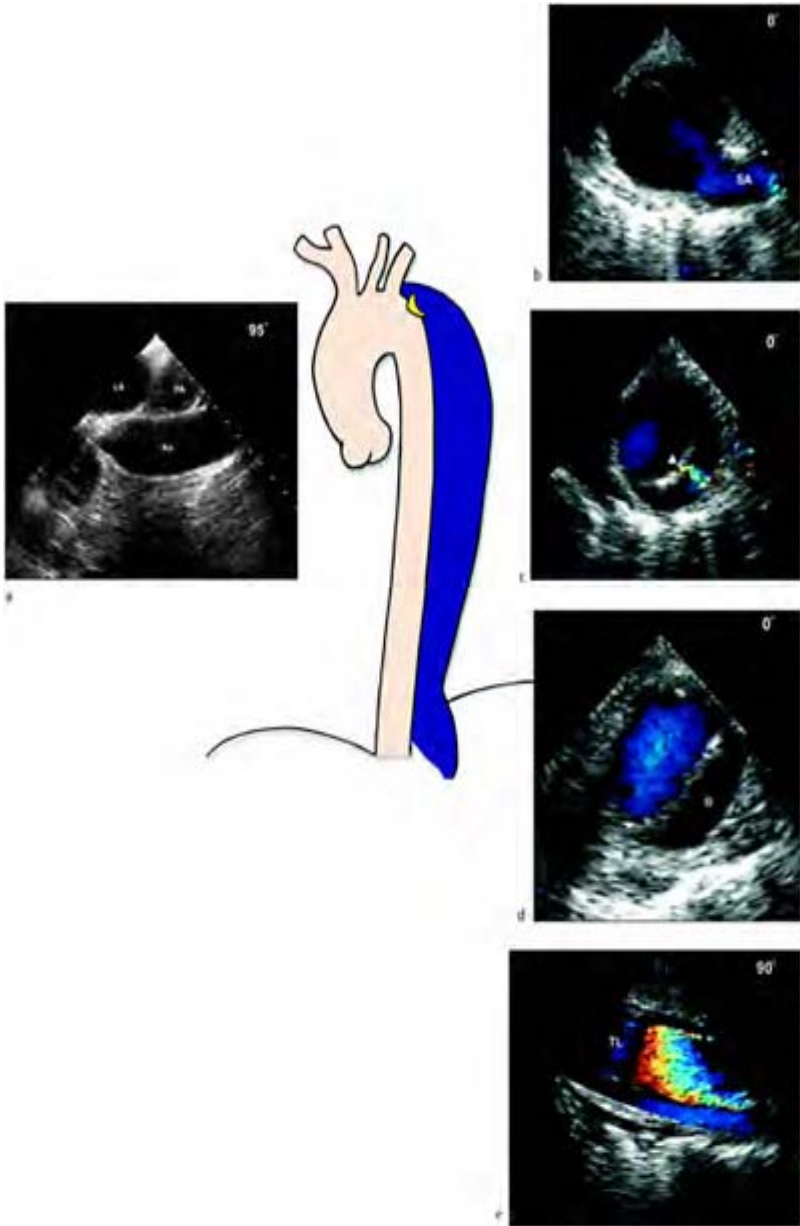
Case 5.15 Descending aortic
dissection. A DeBakey type III aortic
dissection is demonstrated with a
normal ascending aorta (a). Horizontal

view of the distal aortic arch (b) demonstrates normal origin of the left subclavian artery however it appears slightly distorted. An entry site (c) is depicted distal to the subclavian artery with color Doppler (arrow). True and false lumens are demonstrated in the descending aorta extending to at least the diaphragm at 0° (d) and 90° (e).
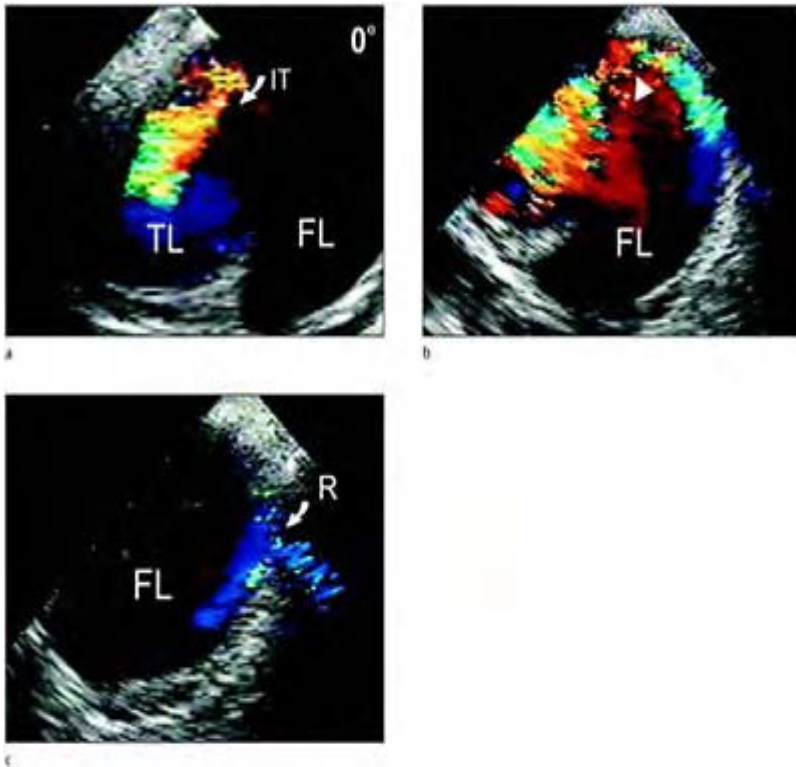
Case 5.16 Complication of aortic dissection. Aortic rupture. Rupture of the aorta is a devastating complication of aortic dissection that occasionally may be detected with multiplane TEE. Color flow Doppler in a descending thoracic aorta dissection demonstrating

an entry site and flow (a) between the true and false lumen in the proximal descending aorta distal to the origin of the left subclavian artery. Flow detected in the false lumen with flow detected outside of the adventia (arrow) denoting a rupture of the false lumen that was detected at the time of surgery. TL, true lumen; FL, false lumen; IT, intimal tear entry site; R, rupture site.
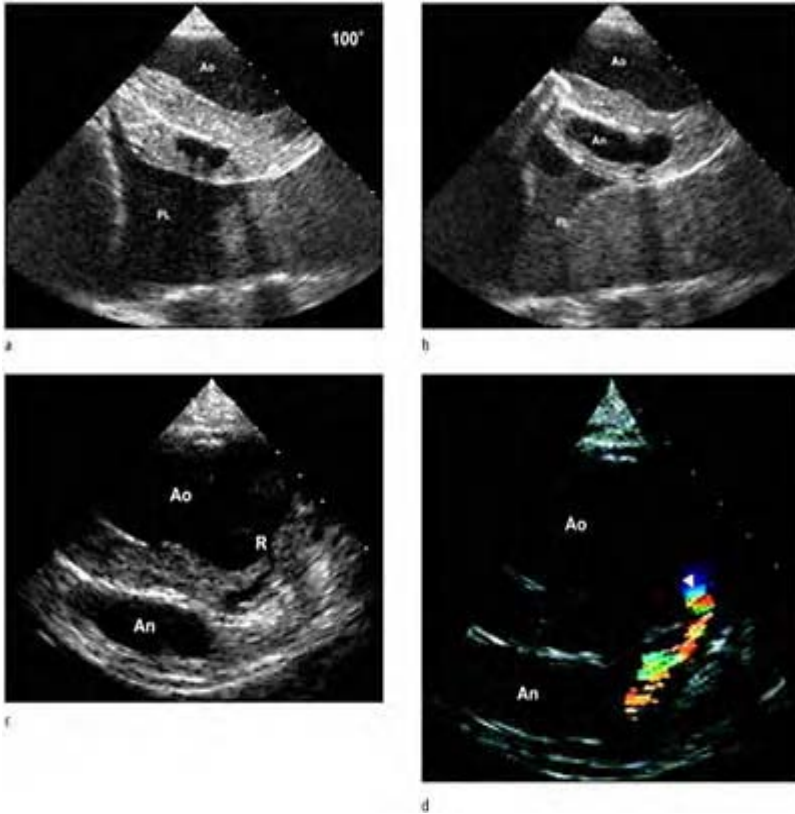
Case 5.17 Complication of aortic dissection. Aortic rupture. Longitudinal views of a descending aortic dissection (a, b) demonstrating a

partially thrombosed false lumen and a large pleural effusion as represented by an echo-free space interposed between the aorta and the lung interface in the mid-chest level. Pleural effusion may be the result of rupture or diapedisis and bleeding into the chest cavity or as a reactive process due to inflammation. Bloody pleural effusions associated with descending aortic dissection constitute a surgical emergency. On closer inspection, there appears to be spontaneous echo contrast in the pleural effusion and a tear (arrow) is visualized in the outer wall of the false lumen (c). With color flow Doppler; blood flow (d) is detected entering the tear towards the pleural effusion. Ao, true lumen of the descending aorta; PL, pleural effusion.
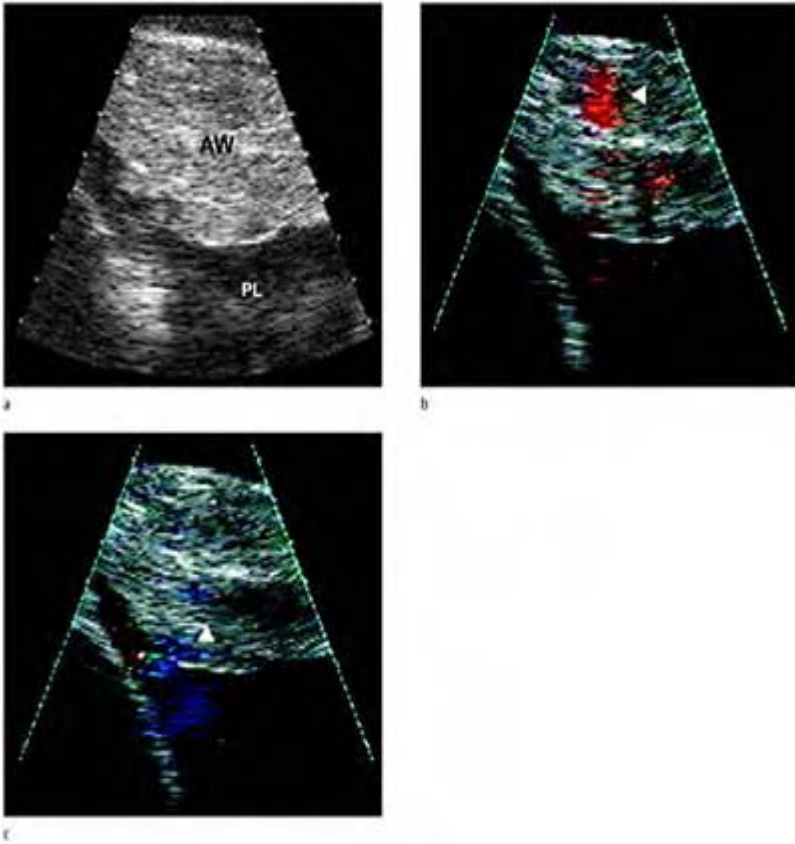
Case 5.18 Complication of aortic dissection. Aortic rupture. Horizontal views of a descending aortic dissection (a), with high resolution TEE and low aliasing velocity in the zoom mode of a thickened portion of the aortic wall adventia in a large dissection segment. Flow is detected (b, c) within and through the wall with color Doppler and presumably may represent diapedisis or an impending rupture in that segment of aortic dissection. There is an echo free space in the far field that represents a pleural effusion. AW, aortic wall; PL, pleural effusion.
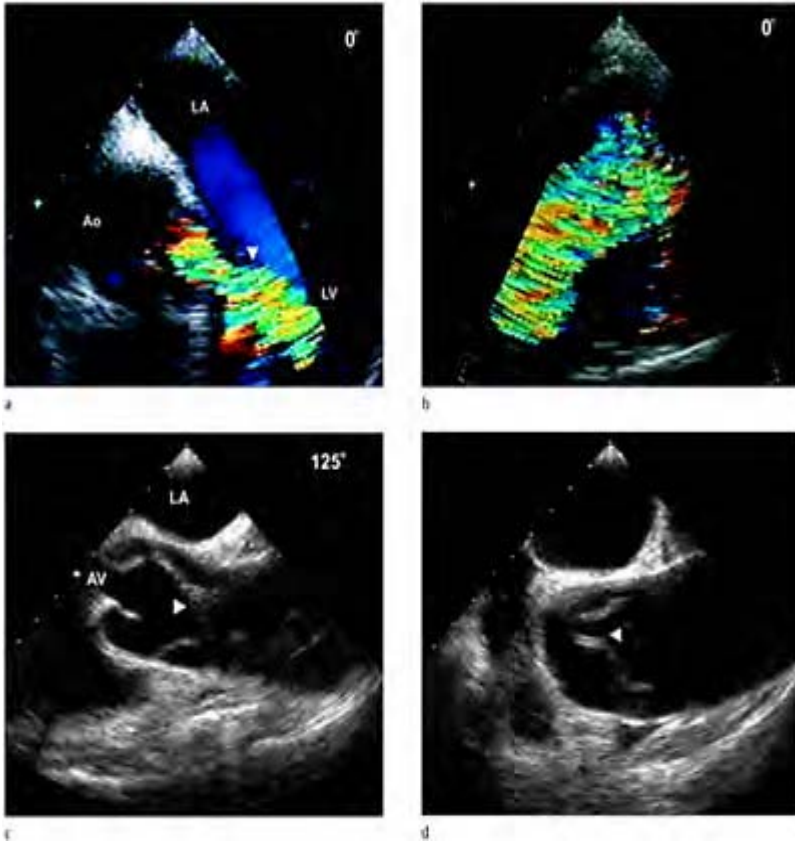
Case 5.19 Aortic dissection and severe aortic regurgitation. Aortic regurgitation is a frequent complication associated with aortic arch dissection as a result of disruption of the aortic valve cusps from a retrograde dissection plane or prolapse of the intimal flap into the aortic valve annulus interfering with valve closure. Severe aortic regurgitation demonstrated with color flow Doppler in the five-chamber view obtained from the mid-esophageal window (a). Modified views of the aorta from the lower esophageal window demonstrate

a large aorta with disturbed and high velocity flow in the true lumen. Longitudinal views of the aortic root (c) and ascending aorta (d) at 90° demonstrate disruption of the valve cusps and the intimal flap (arrow) that resulted from retrograde dissection into the ascending aorta.
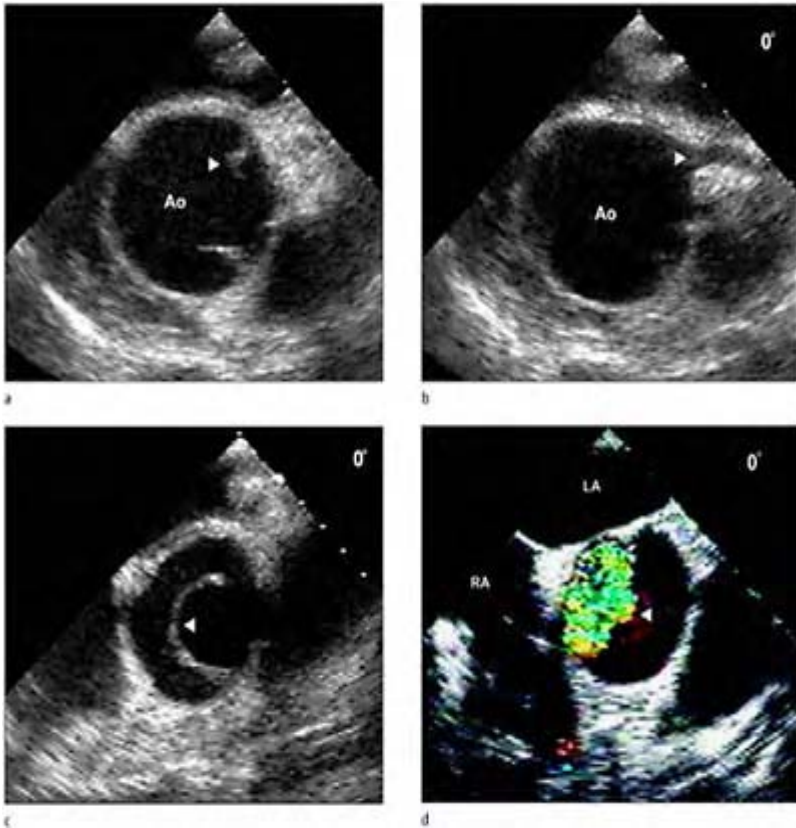
Case 5.20 Aortic dissection and severe aortic regurgitation. Aortic arch dissection with retrograde dissection to the ascending aorta and antegrade dissection to the descending aorta. Horizontal views of the proximal

ascending aorta superior to the aortic valve plane (a) and at the level of the origin of the left coronary artery do not demonstrate extension of the intimal flap. With withdrawal of the probe the dissection plane and intimal flap (arrow) appear in view with color flow Doppler demonstrating disturbed flow in the true lumen (c, d).
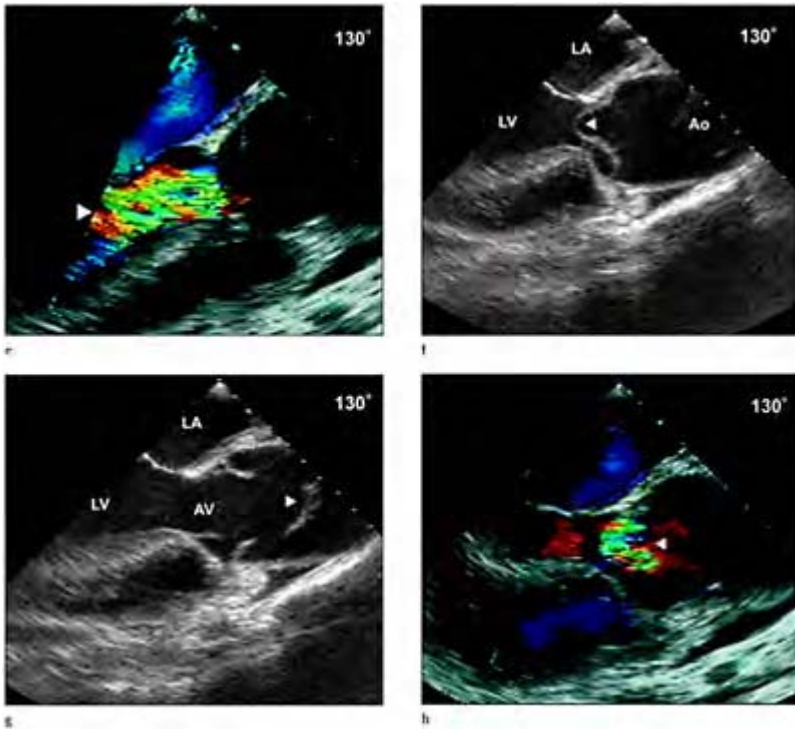
Longitudinal views demonstrating severe aortic regurgitation (e) and prolapse of the intimal flap into the aortic valve annulus during continuous phases of the cardiac cycle (f–h).
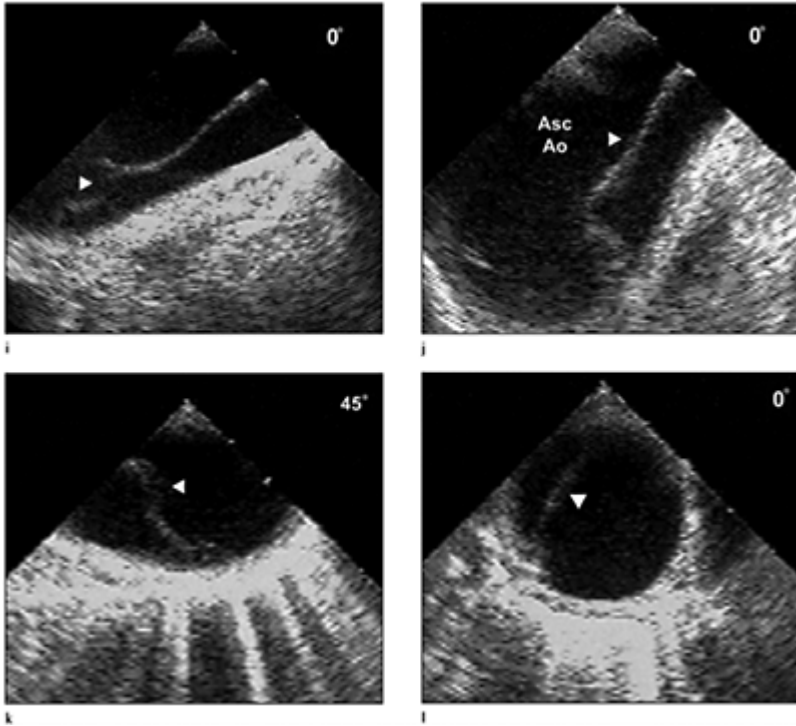
The entry site is noted in the proximal aortic arch with antegrade extension of the dissection plane longitudinally to the descending aorta (i–l).
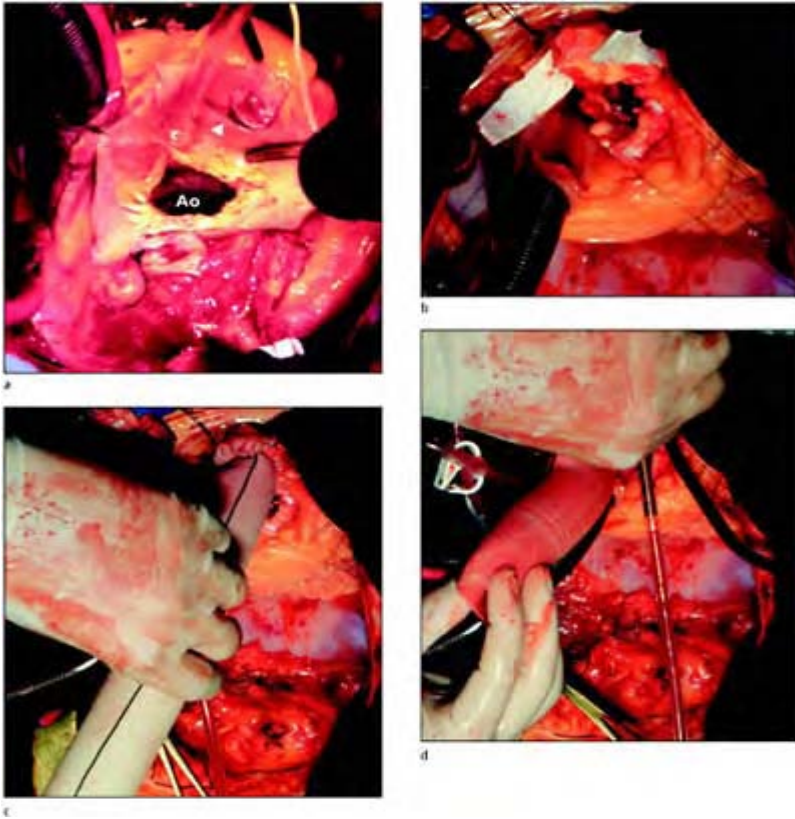
Case 5.21 Surgical photographs demonstrating supracommissural graft replacement of the ascending aorta in the setting of an ascending aortic dissection without aortic root involvement. (a) The aorta is divided and opened and demonstrates the ectatic lumen of the ascending aorta above the sinotubular junction. The intimal flap is identified above the junction of the right coronary and non-coronary cusp. (b) After excision and removal of the dissection flap pledgets are sewn to the residual remaining aorta to reconstruct and reinforce the aortic walls and allow for attachment for the tubular aortic graft.
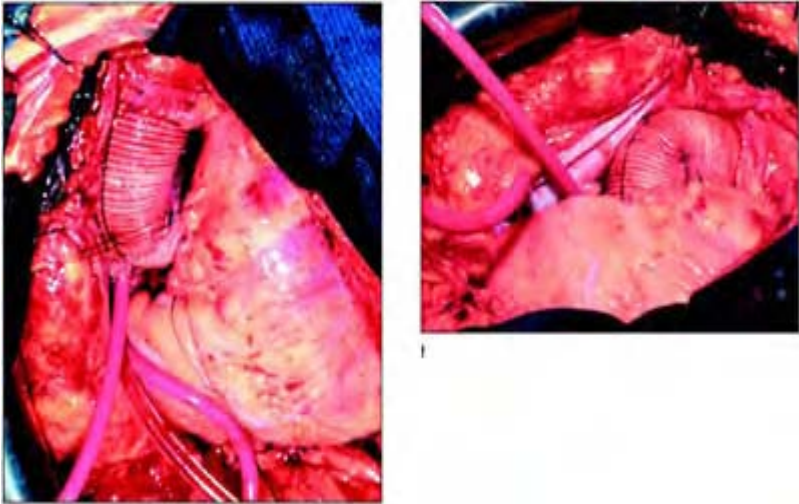
A surgical graft is first sewn to the proximal aorta followed by attachment to the proximal aortic arch (e–f). When commissural detachment is detected re-suspension of the aortic valve is performed in addition to inserting a graft. If the aortic valve is severely damaged necessitating a prosthetic evalve an aortic valve composite graft is inserted.
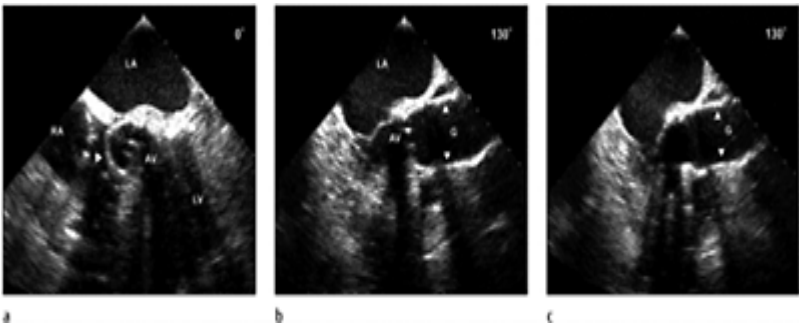
Case 5.22 Postoperative TEE following an aortic valve composite graft replacement of the ascending

aorta. Horizontal and longitudinal views of a composite bioprosthetic valve-graft. In the horizontal views the typical shadowing of the anterior circumference of the prosthetic graft is visualized with the total circumference of the graft seen with slight manipulation of the probe. The Dacron graft material is readily visualized echocardiographically as two bright parallel lines in the longitudinal planes extending through the aortic root and ascending aorta to the level of the aortic annulus. With close inspection, corrugation (zigzag of the graft material artifact) of the graft material is visualized in the lateral fields of the image sector. LA, left atrium; RA, right atrium; AV, prosthetic aortic valve; LV, left ventricle, G, surgical graft.
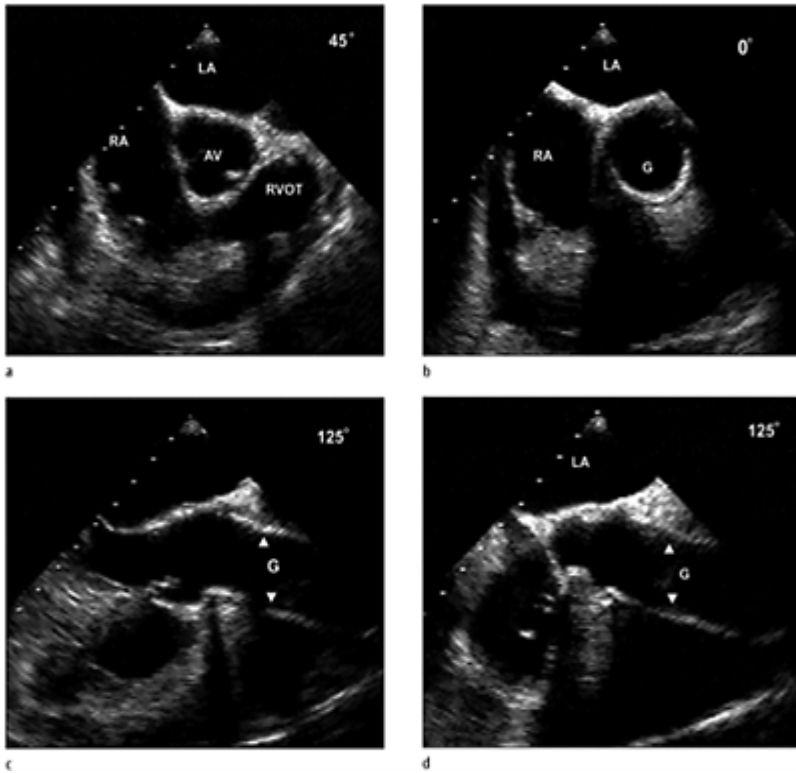
Case 5.23 Postoperative TEE following a supracommissural graft replacement of the ascending aorta. Surgical aortic graft visualized with TEE. Normal short-axis view of base of the heart (a) demonstrating a normal aortic valve and sinus of Valsalva. As the probe is withdrawn, the typical echocardiographic appearance of the graft (b) is demonstrated beginning near the sinotubular junction. Longitudinal views obtained at 100°, demonstrate the graft in the position of the ascending aorta (arrows). Note the graft rarely assumes the same contour as a normal ascending aorta and usually appears straighter and more rigid. On occasion kinking of the graft is demonstrated which must be communicated to the surgeon.
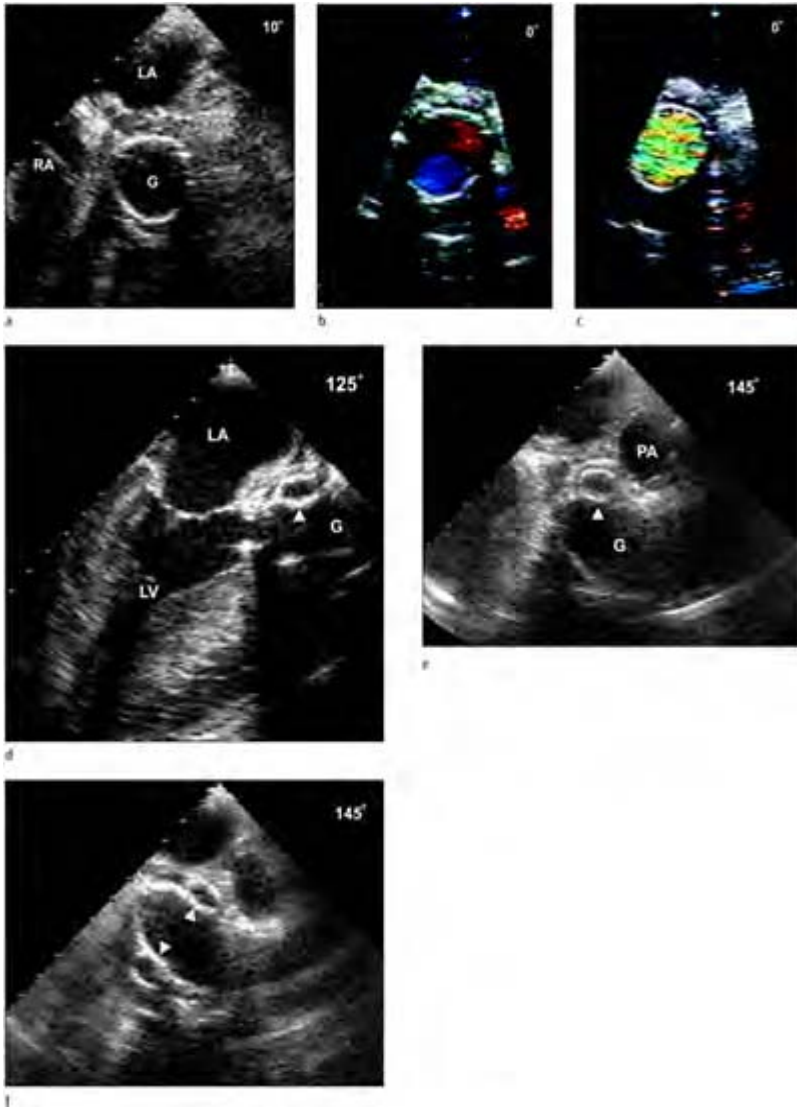
Case 5.24 Postoperative TEE following a Cabrol procedure. To surgically address coronary involvement with ascending dissections the coronary arteries need to be attached to the aortic graft. The coronary ostia may be excised in a button fashion and then anastomosed

to the ascending aorta or an interostial Cabrol-type surgical graft is created and the graft is anastomosed with the aortic prosthesis. Coronary flow should be interrogated with postoperative TEE in either procedure. Horizontal views of the ascending surgical graft in short axis (a, b), with color flow Doppler (c) blood flow should be seen filling the entire graft. Longitudinal views (d–f) demonstrate the aortic graft and the interostial surgical graft represented in cross-section by two circles (arrows) bordering the aortic graft in the vicinity of normal coronary artery anatomy. Color flow Doppler should demonstrate flow in the interostial grafts with a successful repair.
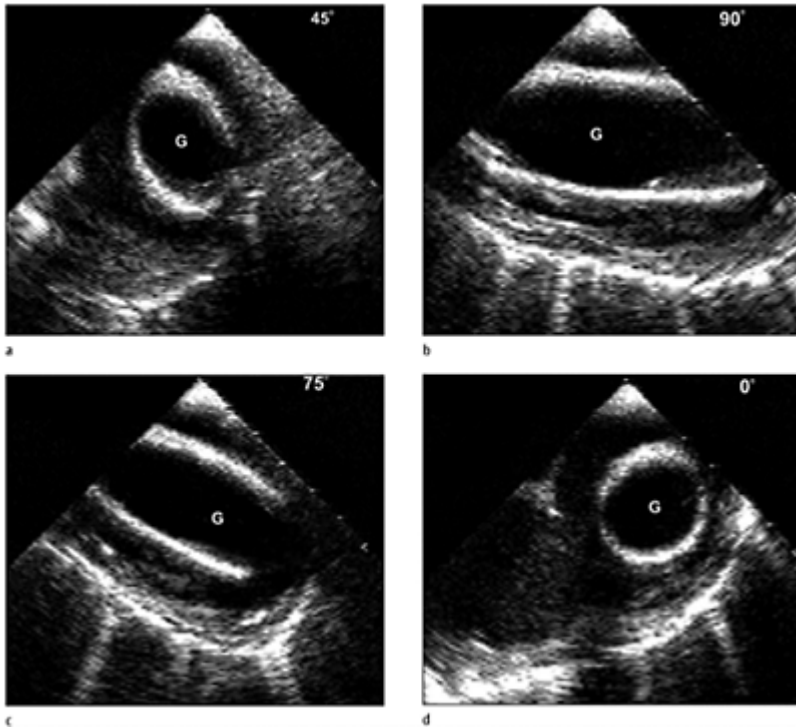
Case 5.25 Postoperative TEE following an elephant trunk procedure. In cases requiring replacement of large segments of aorta, the surgery may require two surgical incisions with a multiple stage procedure. When both the aortic arch and descending aorta need to be replaced, an elephant trunk procedure may be performed. Briefly, this technique involves replacing the proximal aorta in the usual fashion; however, the anastomosis for the distal segment of the graft is attached to allow the end of the graft to remain freely floating in the aortic lumen of the descending aorta. In the second procedure, the end of the graft may be easily obtained and anastomosed to a

second aortic surgical graft or attached to a different segment of aorta that is free of disease. With TEE an elephant trunk aortic graft (a–d) is easily visualized in horizontal or longitudinal views as a tube within a tube with its full extent visualized downstream of the aorta.
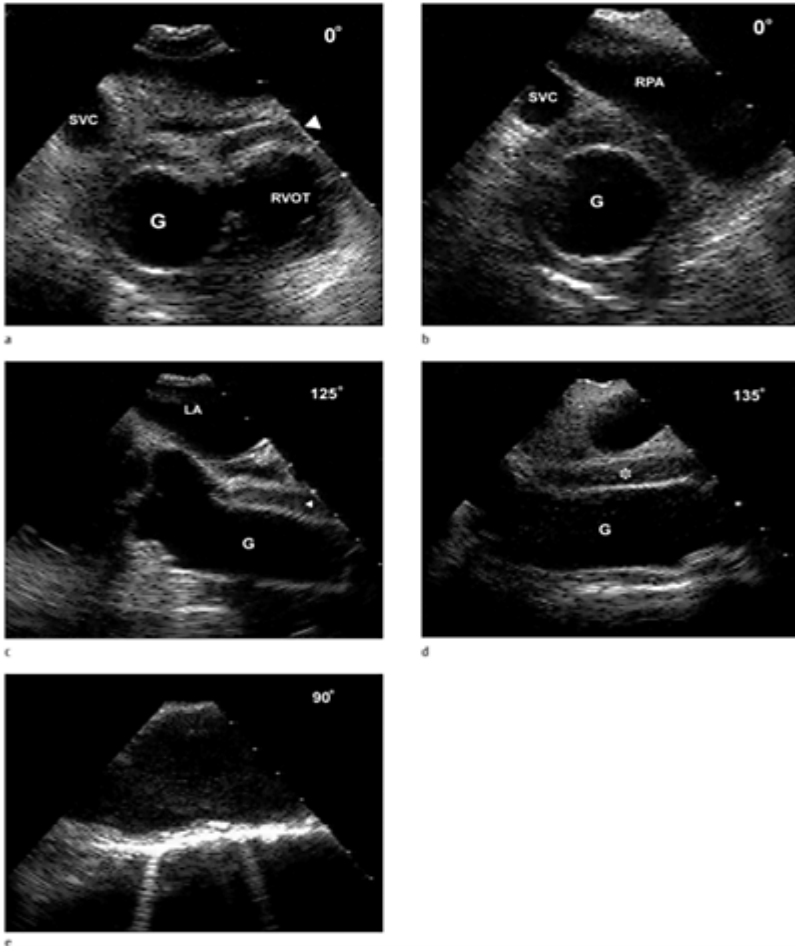
Case 5.26 Postoperative TEE following an elephant trunk procedure for total aortic replacement for an

aortic aneurysm. Horizontal and longitudinal views of a supracommissural surgical graft of the ascending aorta. The surgical graft is easily seen within an enlarged aorta with proximal anastomosis near the sinotubular junction (a–d). The surgical graft is less well seen in views of the aortic arch near the graft insertion (e, f).
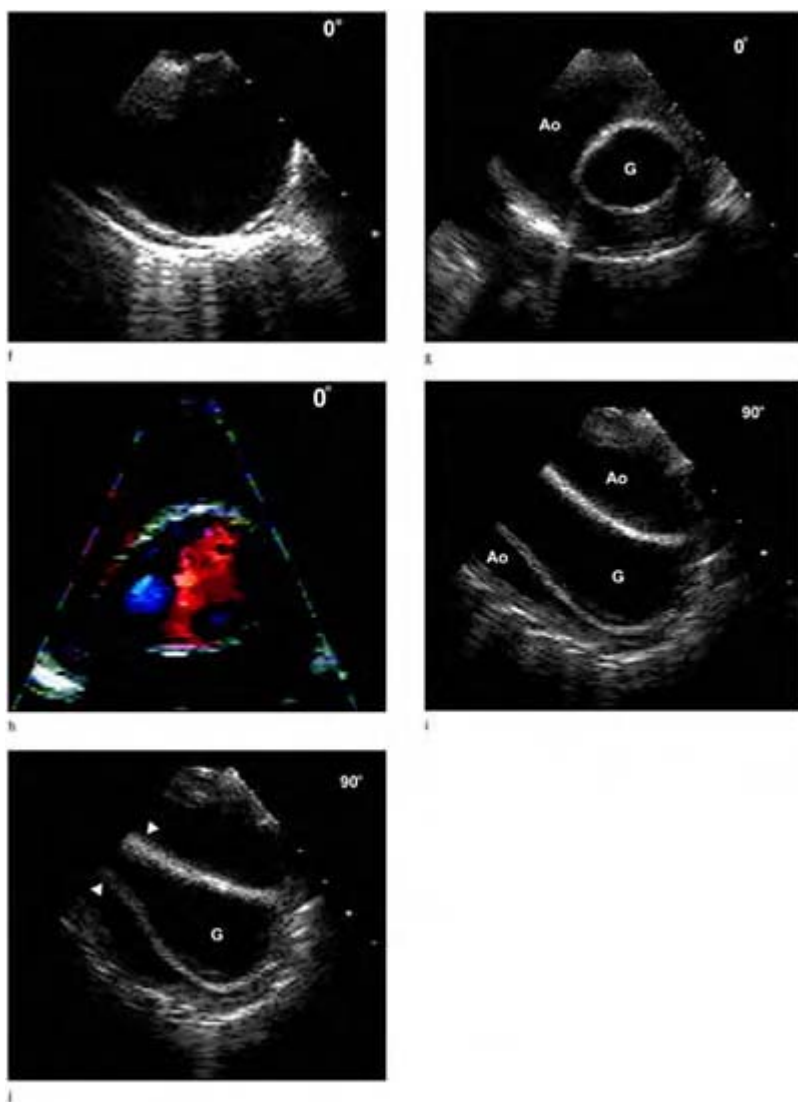
Views of the descending aorta with the
freely floating end of the graft
downstream (g–m).
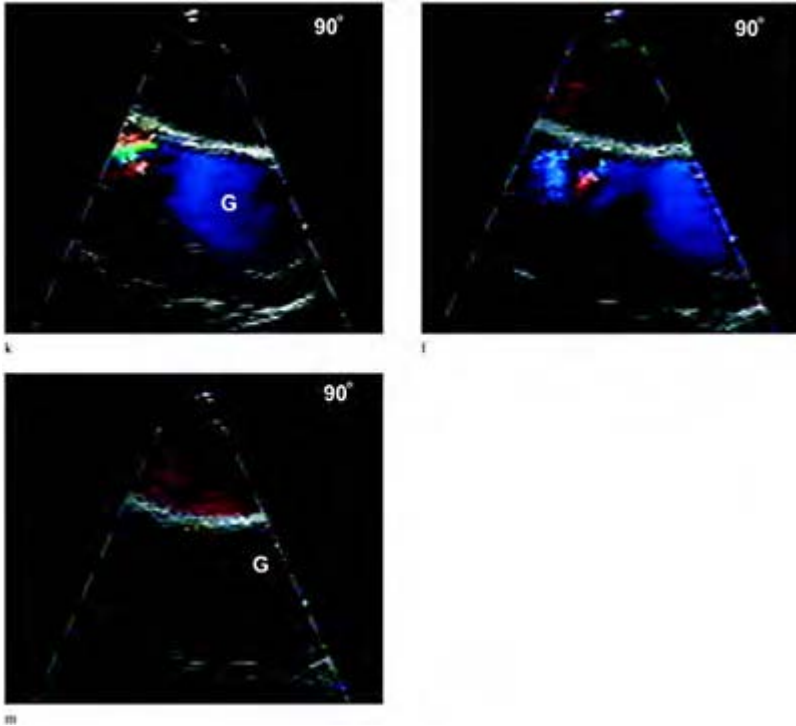
TEE imaging and color flow Doppler demonstrating normal appearance and functioning of an elephant trunk prosthesis. Note the end of the trunk expands in systole (l) and narrows progressively in diastole (j–m).
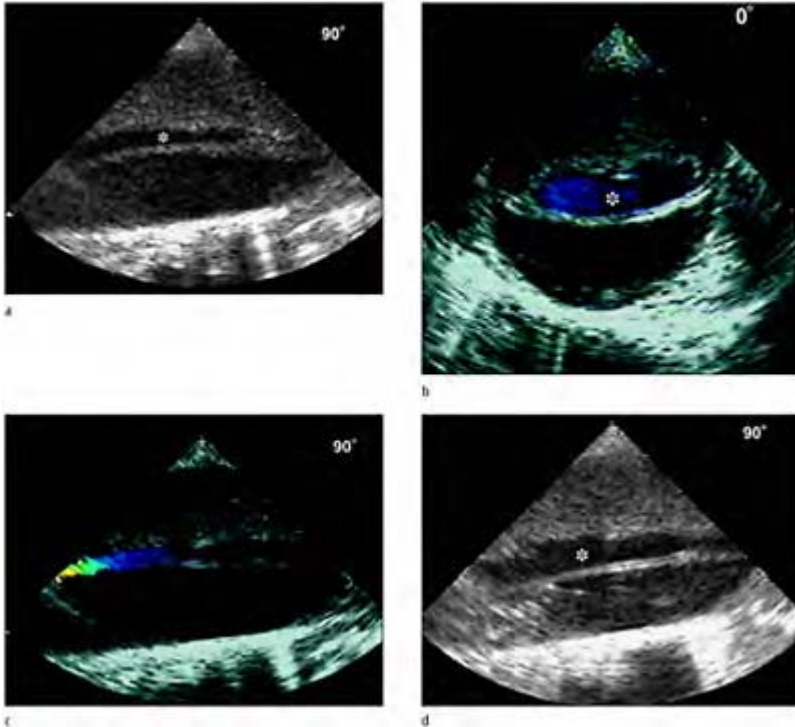
Case 5.27 During surgical repair for extensive aortic dissection TEE may be useful for determining accurate aortic cannula placement to the true lumen and not to the false lumen for performing adequate cardiopulmonary bypass. Visualization of the distal descending aorta (a–c) with extensive dissection with TEE the false lumen is partially thrombosed and the true lumen is extremely compromised as exhibited by a small slit like lumen in comparison to the normal aortic contour. An aortic cannula is placed in the left femoral artery in what is thought to be the true lumen.
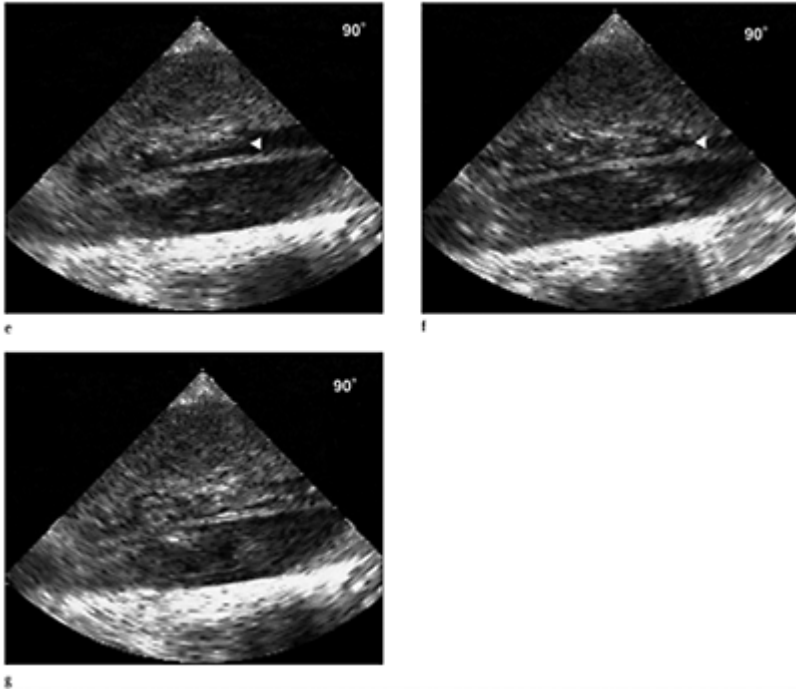
Before instituting cardiopulmonary bypass a fluid bolus is administered to the aortic cannula and echocardiographic contrast is noted (d–g) filling the small slit like true lumen. Although most of the contrast fills the true lumen a small amount appears late in the false lumen that fills under pressure retrogradely from the true lumen to the false lumen through distal exit sites.
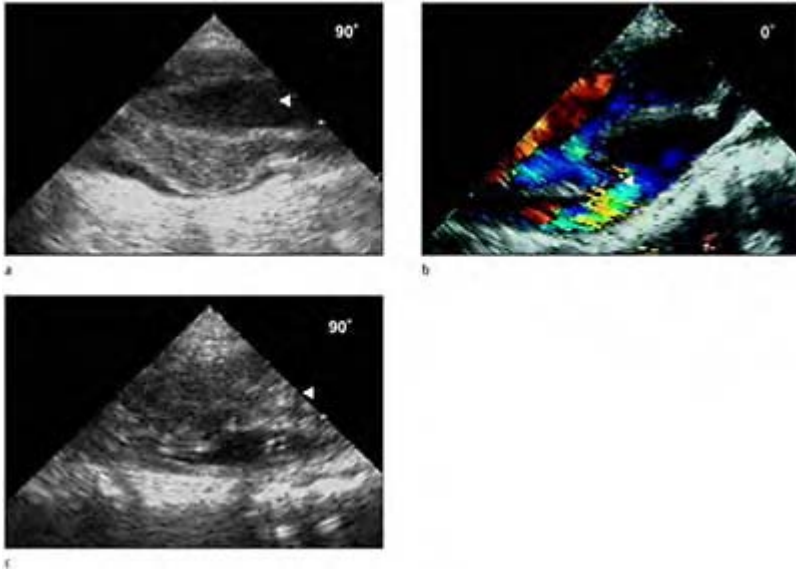
Case 5.28 Multiplane TEE and echocardiographic contrast demonstrating flow in the false lumen during cardiopulmonary bypass suggesting inadvertent placement of the aortic cannula in the false lumen instead of the true lumen of the aortic dissection.
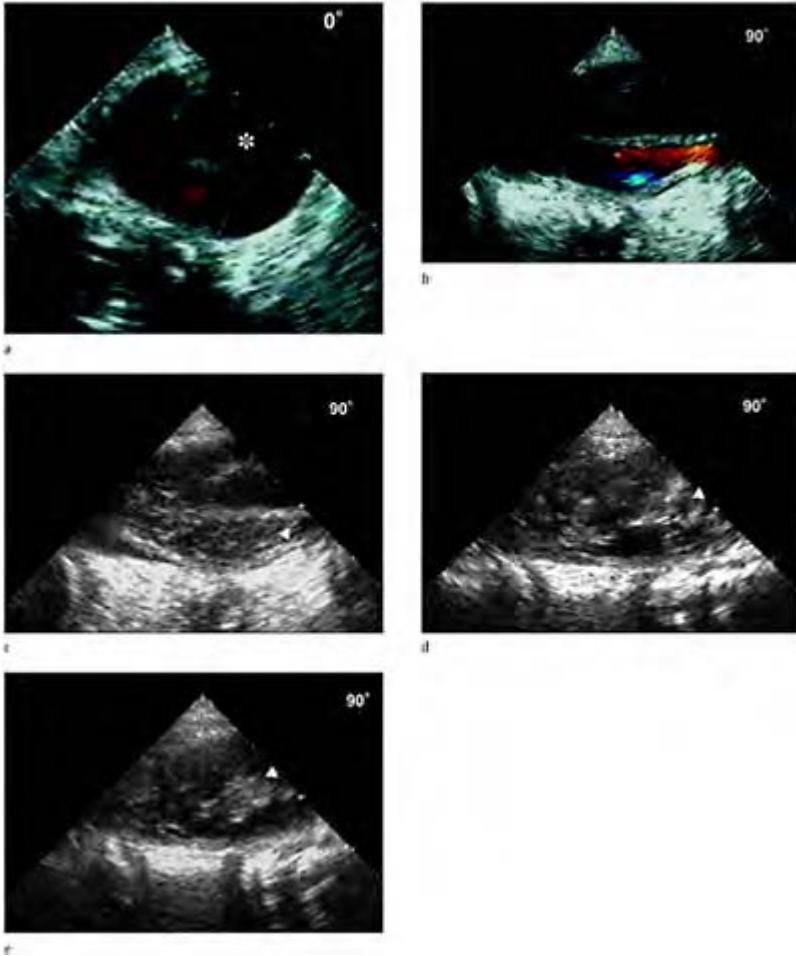
Case 5.29 Multiplane TEE and echocardiographic contrast demonstrating good flow during cardiopulmonary bypass to the proximal ascending aorta and arch with femoral cannulation, which demonstrates adequate perfusion during cardiopulmonary bypass.
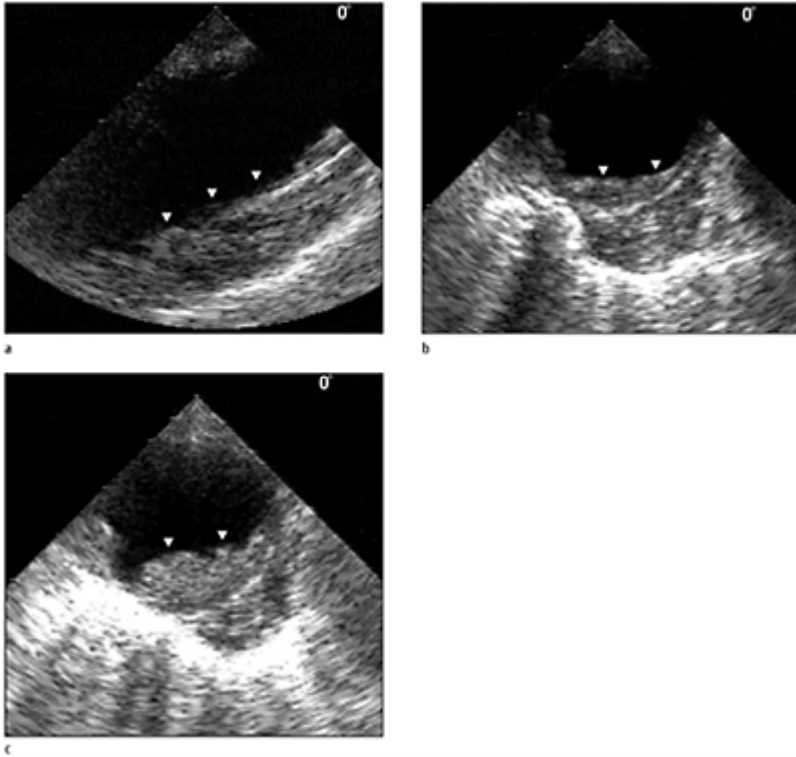
Case 5.30 Intramural hematoma. Multiplane TEE finding of intramural hematoma of the aorta consists of a localized thickening of the aortic wall greater than 7 mm producing a circular or cresentric shape to the contour of the aortic lumen, without demonstration of an intimal tear or flap. It may be difficult to distinguish an intramural hematoma or aortic debris with intraluminal thrombosis or from a classic aortic dissection with a thrombosed false lumen. Ao, aorta.
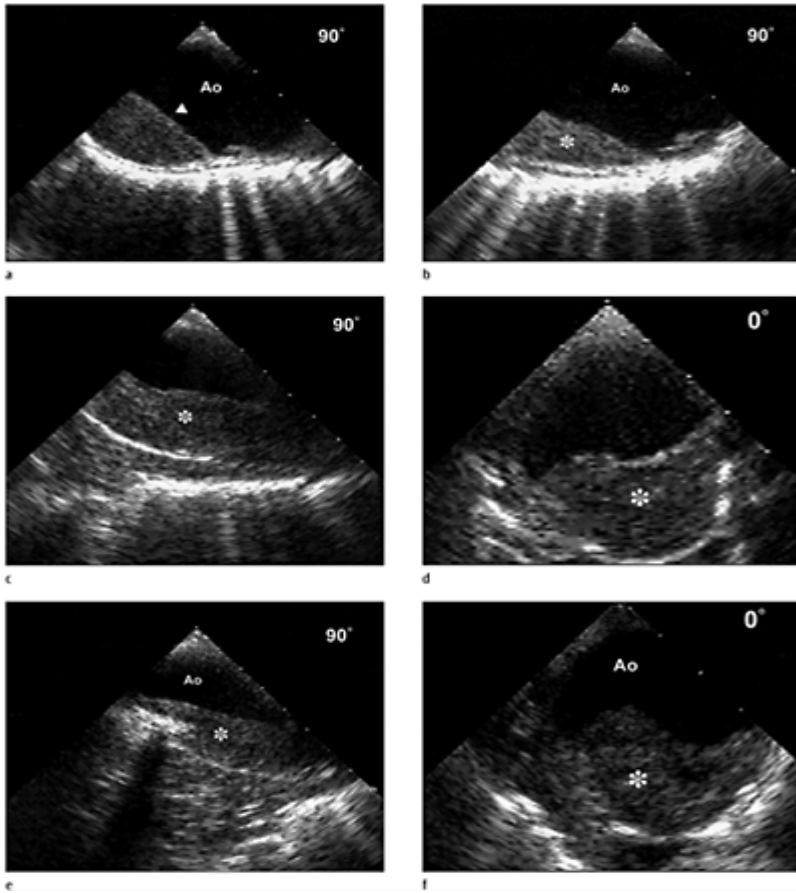
Case 5.31 Intramural hematoma (star) of the descending thoracic aorta. Thickening of the aortic wall is visualized with a distinct homogenous appearing echogenicity that appears to be within the aortic wall. In the vicinity of the intramural hematoma the aortic lumen is not significantly compromised and the hematoma is causing mild displacement of the aortic wall inward towards the lumen as well as outward from the vessel lumen towards the adventitia. Ao, aorta.
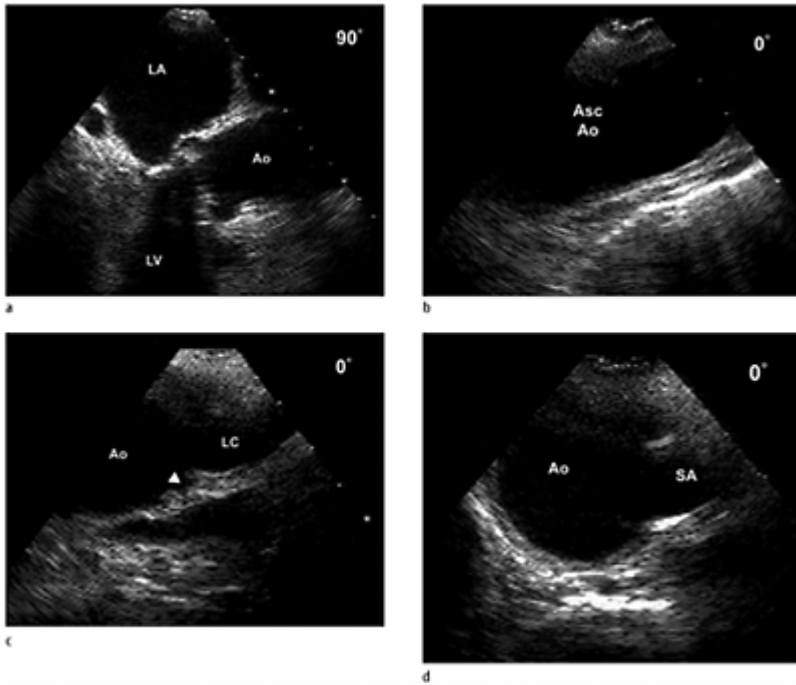
Case 5.32 Ulceration of aortic atheroma. TEE views of severe atherosclerotic pathology involving the ascending aorta and aortic arch (a–d). Intimal thickening and calcification is seen in the proximal ascending aorta near the sinotubular junction and the origin of the left subclavian artery. Intimal thickening with an ulcer crater (c) is noted in the distal ascending aorta. Ulcerative atheroma is frequently observed in the descending aorta and abdominal aorta with imaging modalities such as CT scanning with the true clinical significance being unknown. LA, left atrium; Ao, aorta; SA, subclavian artery.
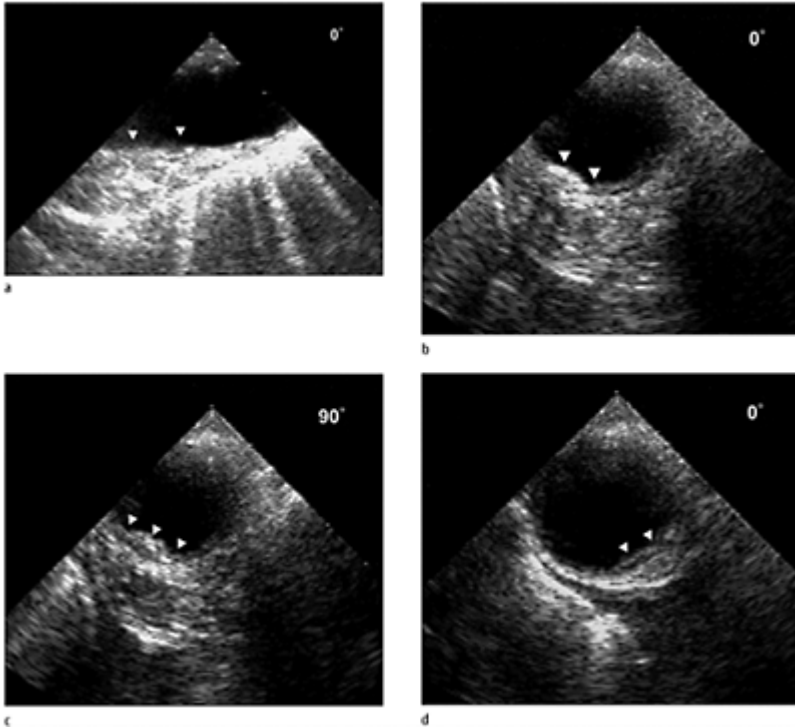
Case 5.33 Penetrating aortic ulcerative plaque. In contradistinction to simple atheroma ulceration, penetrating ulcerative plaques are more extensive presenting with similar signs and symptoms to a classic aortic dissection. With TEE aortic ulcers are associated with adventitial hematoma or pseudoaneurysm formation, with mediastinal fluid or pleural effusion near the affected aortic segment. Meticulous, multiplane TEE examination of the aorta (a–d) may reveal a small protrusion (arrow) at or near an atheromatous plaque which projects deep into the medial-advential wall layer. Ao, aorta.
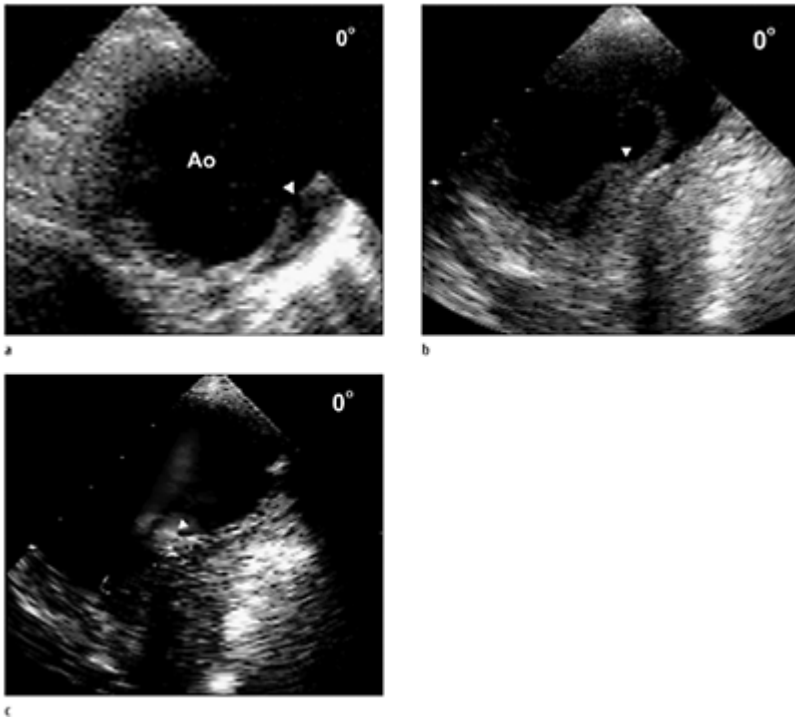
Case 5.34 Penetrating aortic ulcerative plaque. Multiplane TEE examination of the descending aorta in zoom mode demonstrates an ulcer crater or disruption of the intimal layer extending into the media. Spontaneous echocardiographic contrast (arrow) is visualized adjacent to the area of ulceration, which probably is why ulcerative plaques are frequently associated with intraluminal thrombus formation due to localized disturbed, slow blood flow. Ao, aorta.
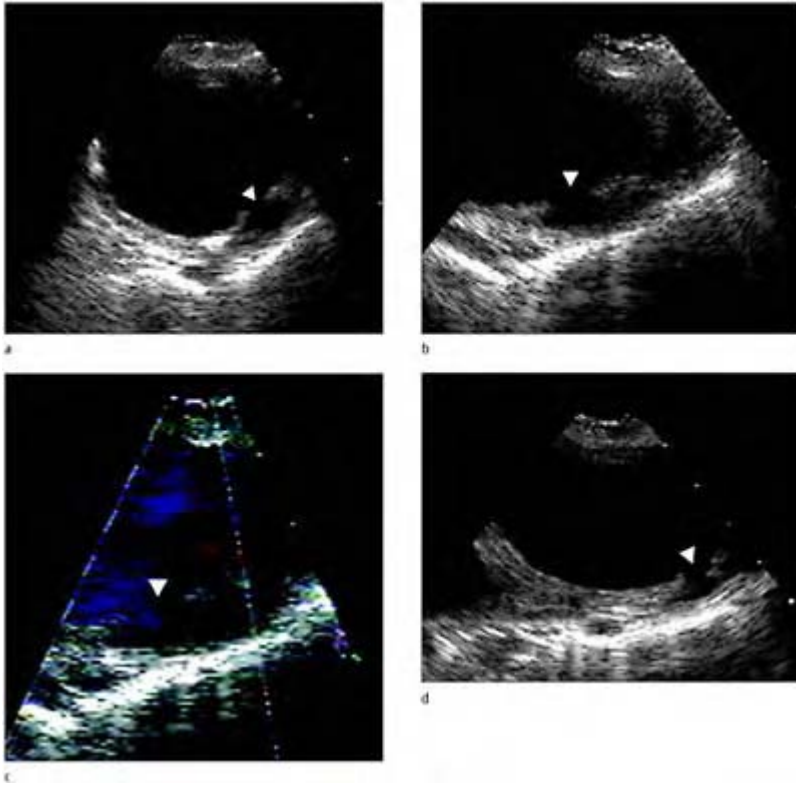
Case 5.35 Penetrating aortic ulcerative plaque. Multiplane TEE demonstrating a penetrating ulcerative plaque in the mid-descending aorta and adventitial hematoma (a–f).
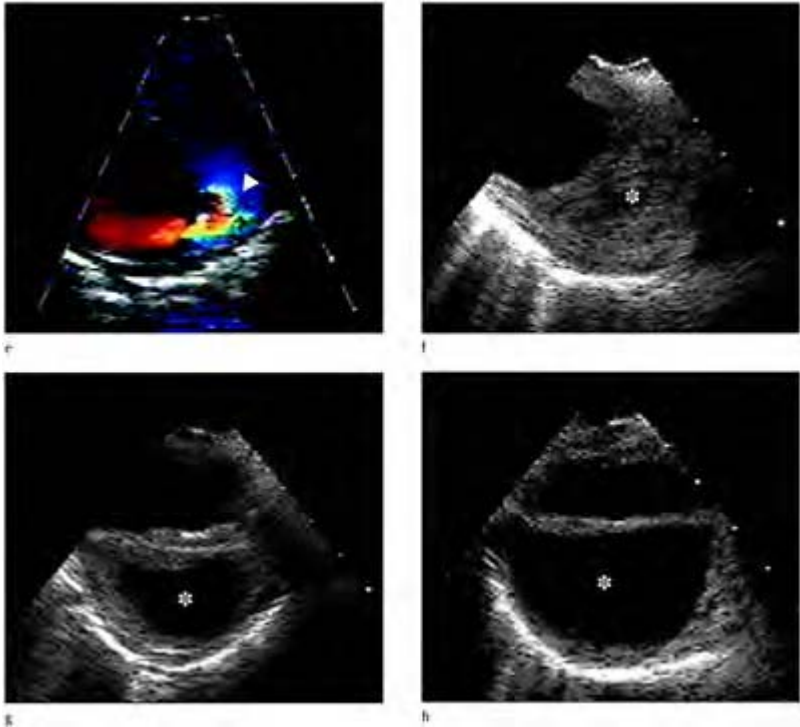
Color flow Doppler may demonstrate flow within the area of the aortic ulcer (arrow), tracking into the subjacent hematoma where lower velocities are detected (c, e). The false lumen (star) is thrombosed in various stages distal to the ulcer crater (f–h).
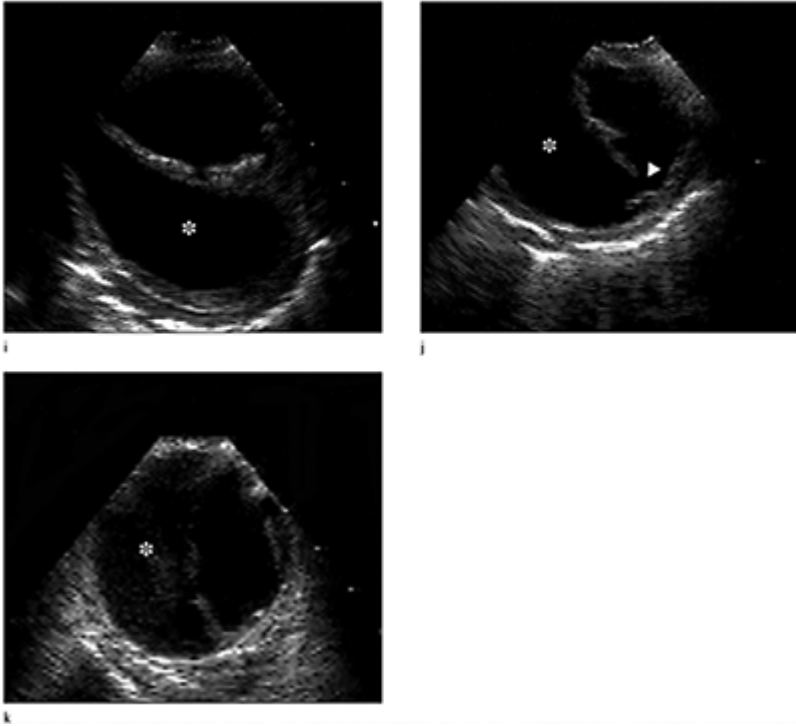
Rarely the adventitial pseudoaneurysm extends the length of the descending aorta and results in a typical distal aortic dissection (g–k).
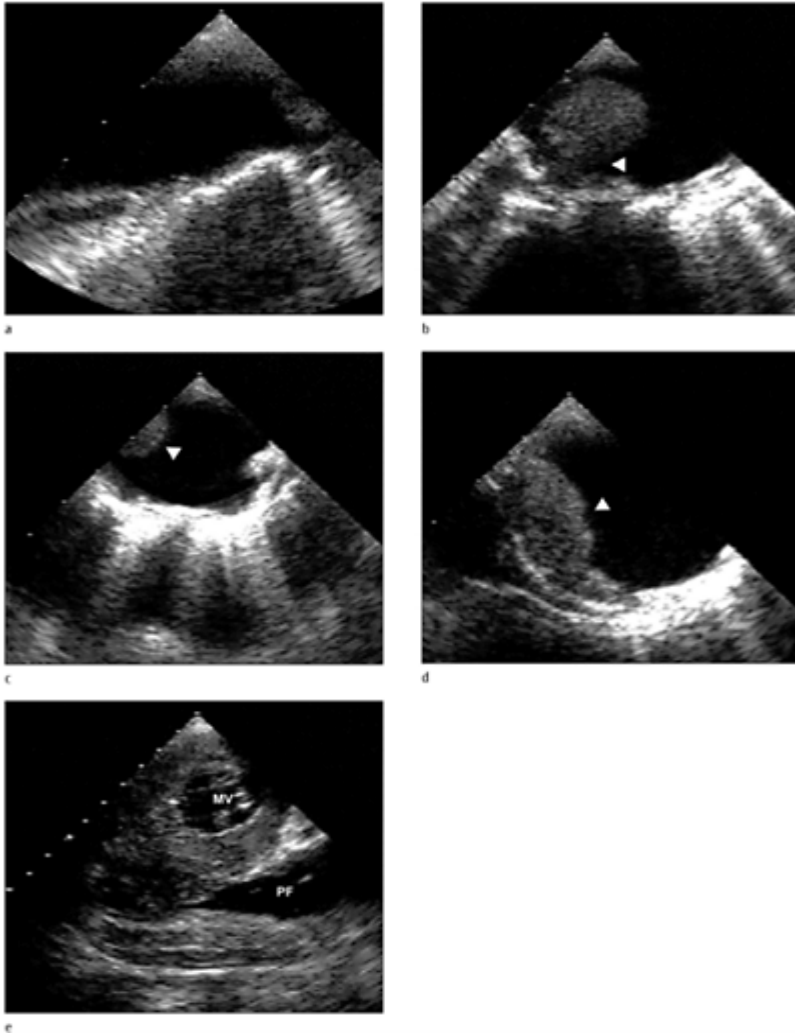
Case 5.36 Penetrating aortic ulcerative plaque. Multiplane TEE examination of a severely calcified and atherosclerotic aorta. An ulcerative aortic plaque is demonstrated with a large, nearly occlusive intraluminal thrombus (b–d). Visualization of the heart demonstrated a large pericardial effusion, which was bloody on analysis.
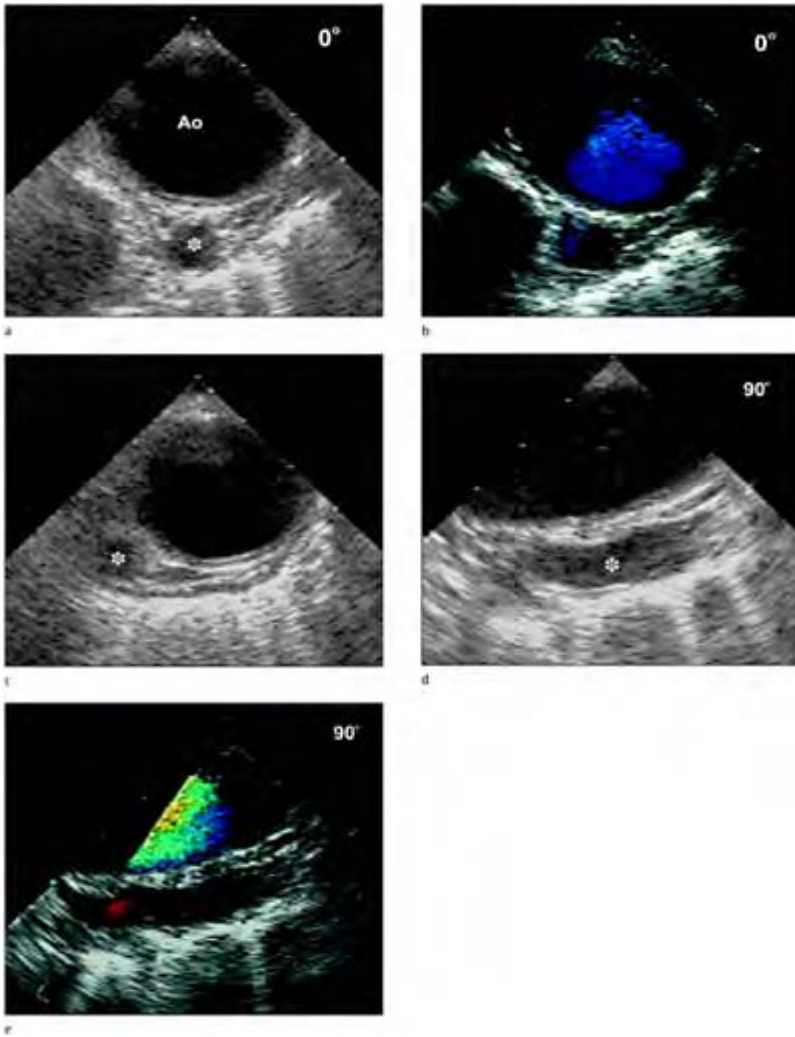
Case 5.37 False positive echocardiographic findings for an intimal flap may occur as a result of plaques near the aortic valve (a), producing lateral resolution artifact; thickening or calcification causing reverberations may be produced from other cardiac or thoracic structures; as well as the use of excessive gain may introduce abnormal echos in the aortic lumen. Linear artifacts are frequently visualized in the ascending aorta associated with severe plaque or when the aortic is larger than the left atrium (b–d).
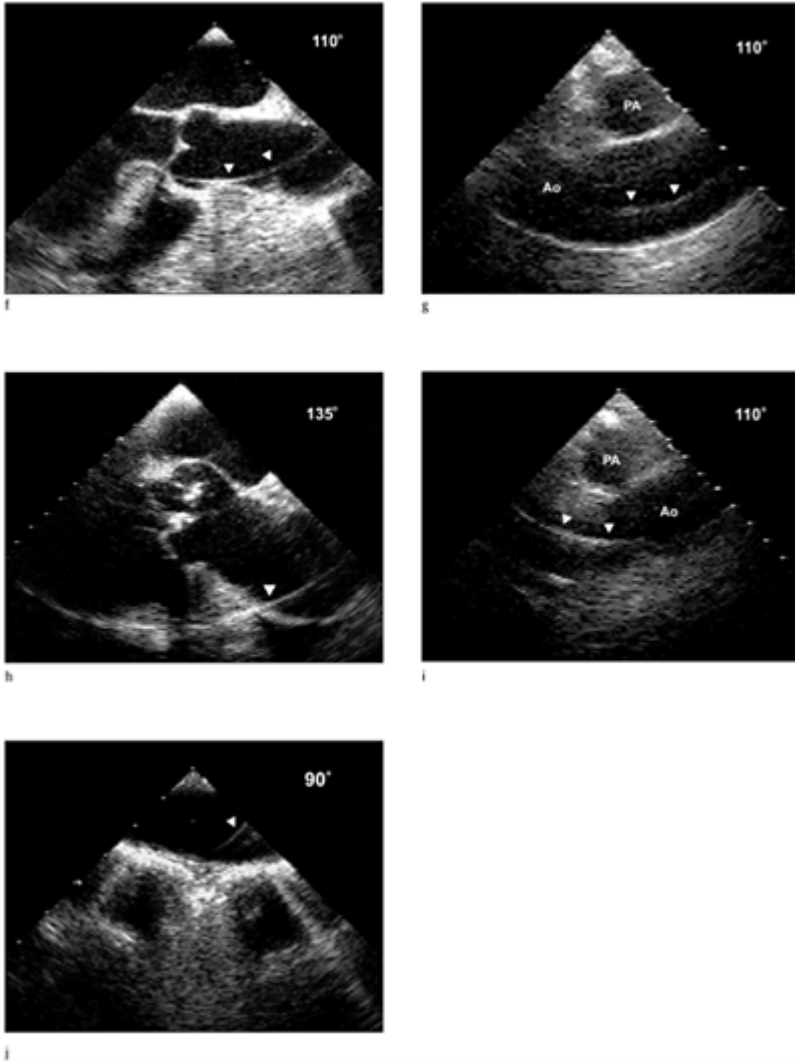
The echo interface between the aorta and the lung in the proximal descending aorta produces a typical appearance that may be confused with a false lumen or double barrel aorta (e–g). Fluid in the transverse sinus separating the proximal ascending aorta and the pulmonary artery may also be confused with a false lumen (h–j).
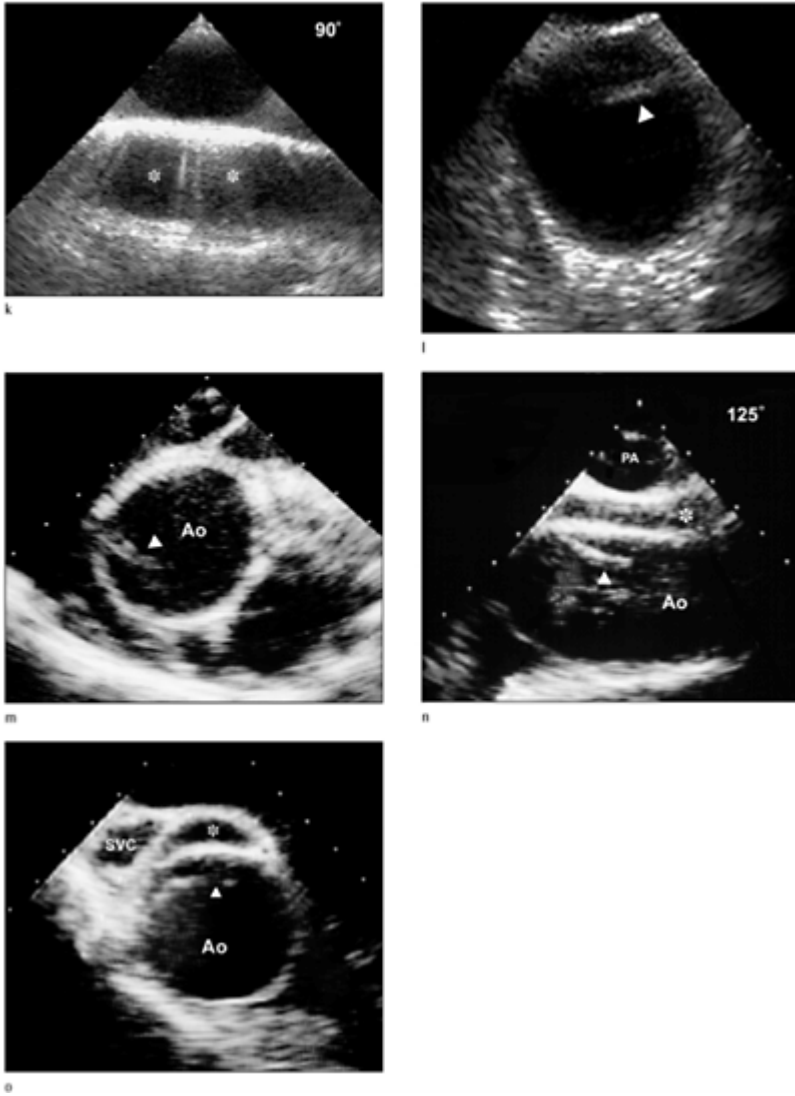
Large thoracic artery branches of the descending aorta as well as an azygous vein may produce findings that suggest an intimal flap and false lumen (k–o). Appreciation of the anatomy from multiple multiplane views readily distinguishes them from aortic dissection.
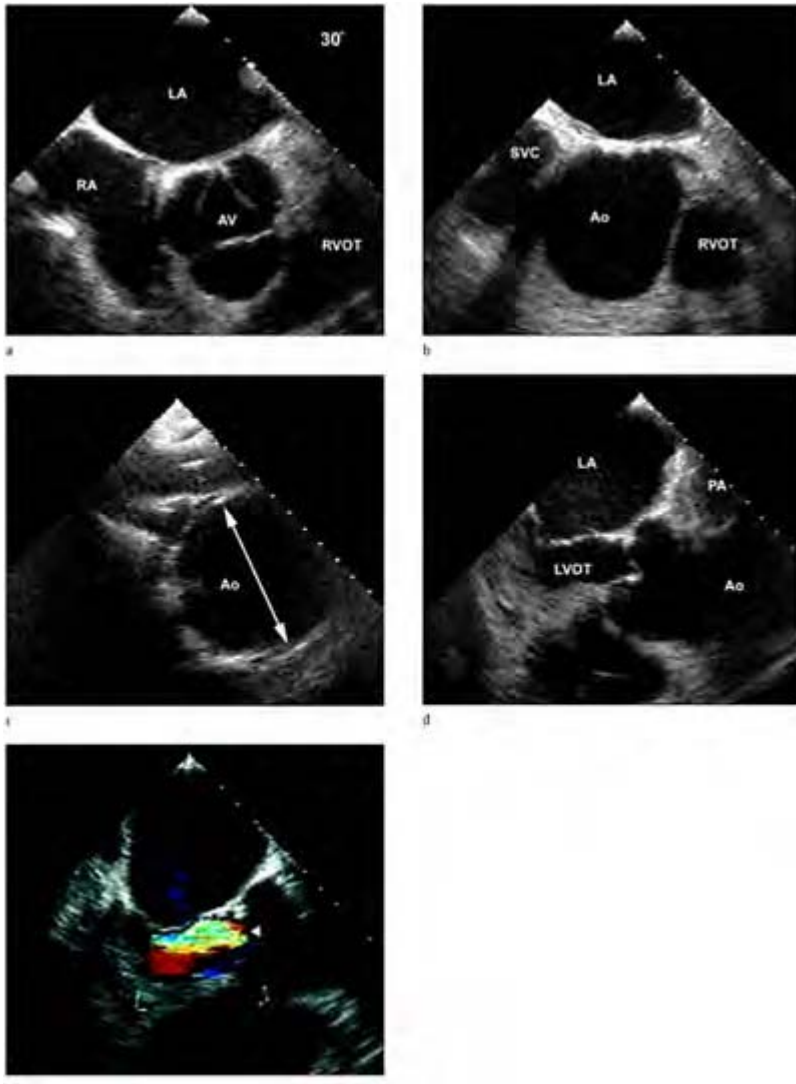
Case 5.38 Aortic aneurysm associated
with Marfan's syndrome. Sequential
horizontal images (a–c) with
corresponding longitudinal views (d–f)
from the aortic valve to the mid
ascending aorta demonstrating an
enlarged aorta with annuloaortic
ectasia.
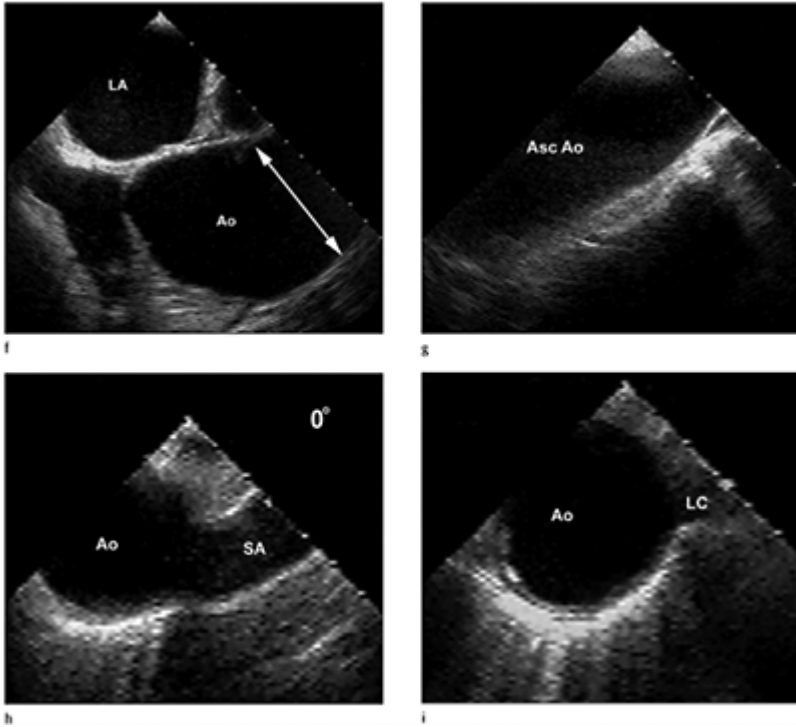
Annuloaortic ectasia is best described by the lack of the normal definition of the sinus of Valsalva and the normal narrowing at the sinotubular junction. Ascending aorta (g), descending aorta near the origin of the subclavian artery (h), mid-descending thoracic aorta.
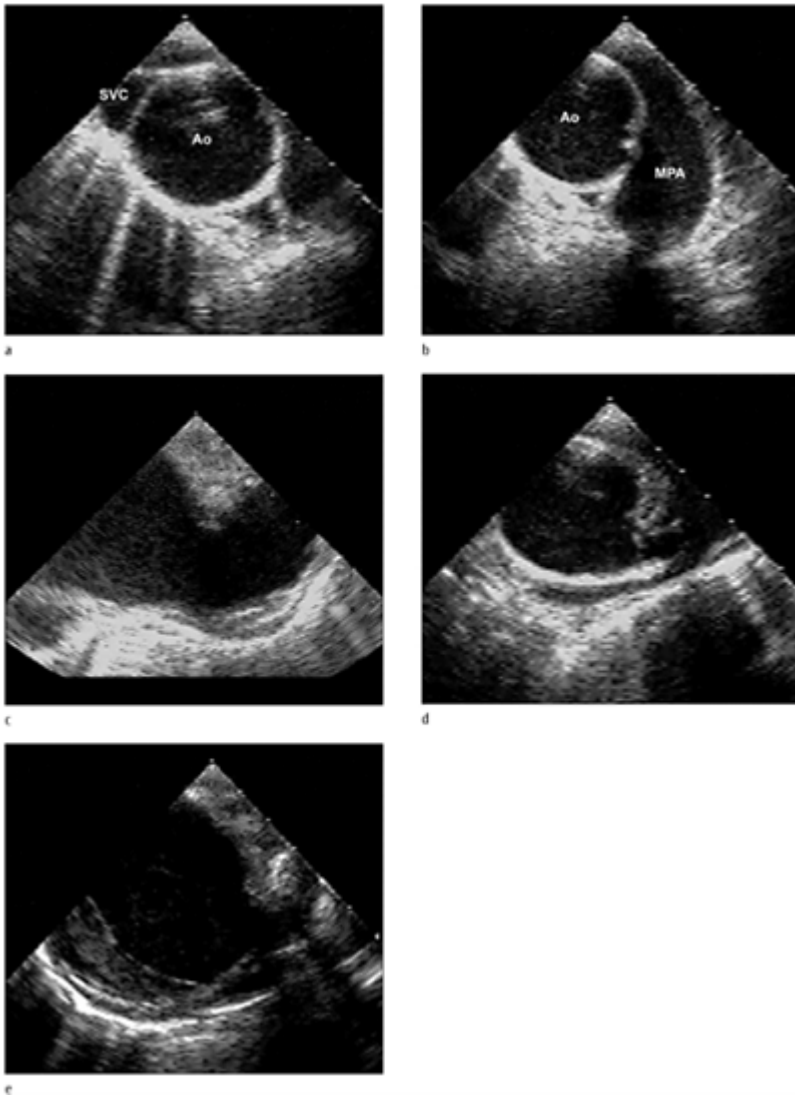
Case 5.39 Aortic aneurysm. Sequential multiplane
horizontal TEE images demonstrating a large
ascending aorta (a, b), aortic arch and markedly
enlarged descending thoracic aorta. Intraluminal
thrombus (c–i) is detected in the distal aortic arch and
extends to various degrees throughout the entire
descending aorta.
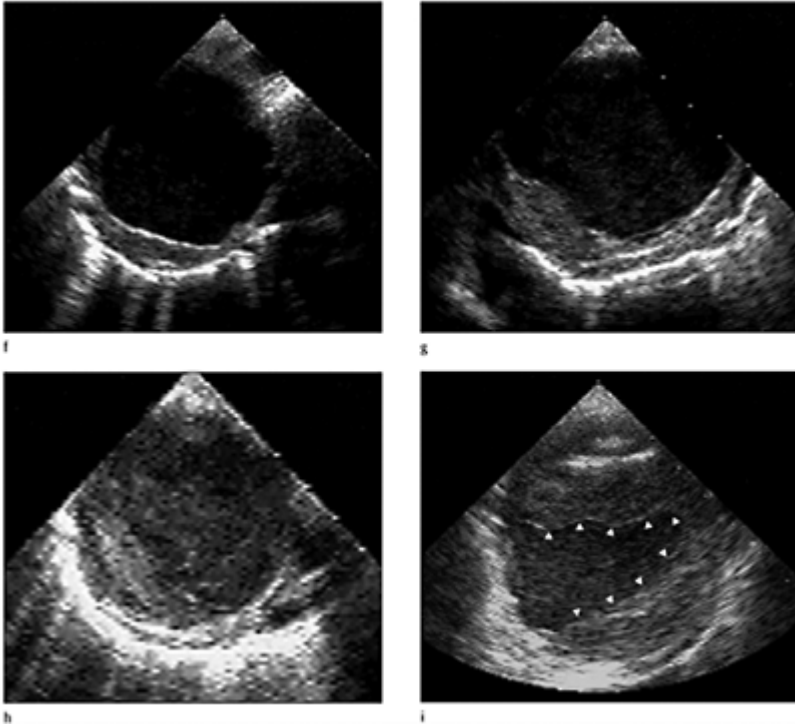
Spontaneous echocardiographic contrast (h, i) is noted in the distal most segment of the descending aorta at the level of the diaphragm.
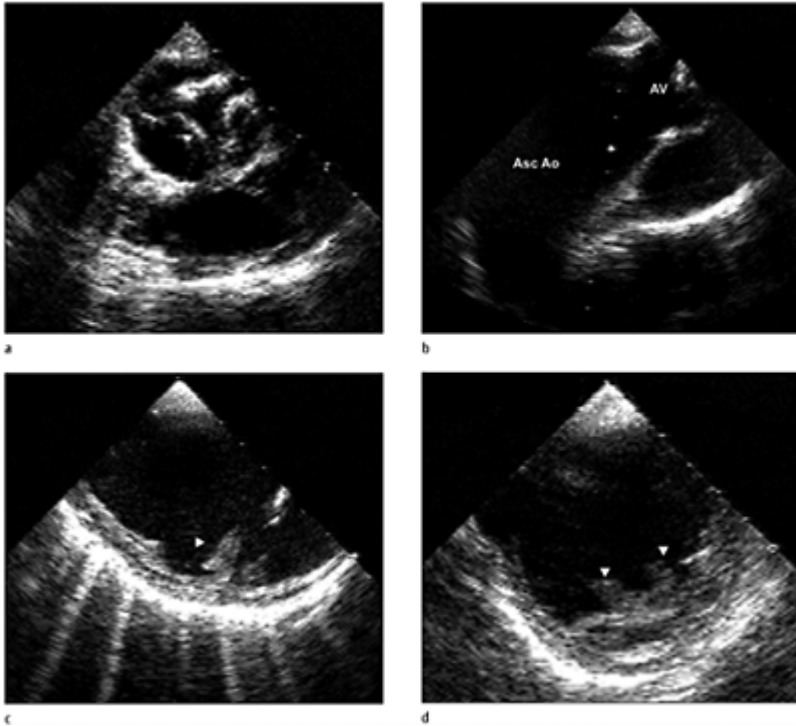
Case 5.40 Aortic stenosis, post-stenotic dilatation and a descending aortic aneurysm. Horizontal view (a) of the aortic valve suggests moderate aortic stenosis. Deep transgastric view (b) demonstrating mild post-stenotic dilatation of the ascending aorta. Horizontal views (c–g) of the distal aortic arch and descending thoracic aorta demonstrate diffuse intimal thickening with calcified plaque and spontaneous echocardiographic contrast within an increased intraluminal diameter consistent with a descending thoracic aortic aneurysm.
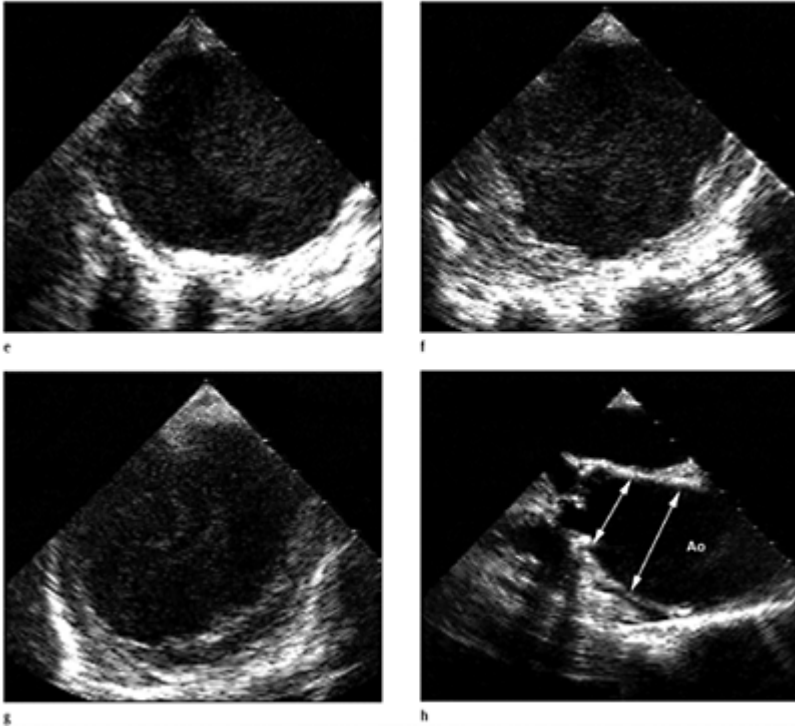
Longitudinal views (h, i) of the ascending aorta depicting post-stenotic dilatation distinct from an aneurysm located in the arch and descending aorta. Note post-stenotic dilatation usually presents as an eccentric dilatation towards and accentuating the greater curvature of the ascending aorta.
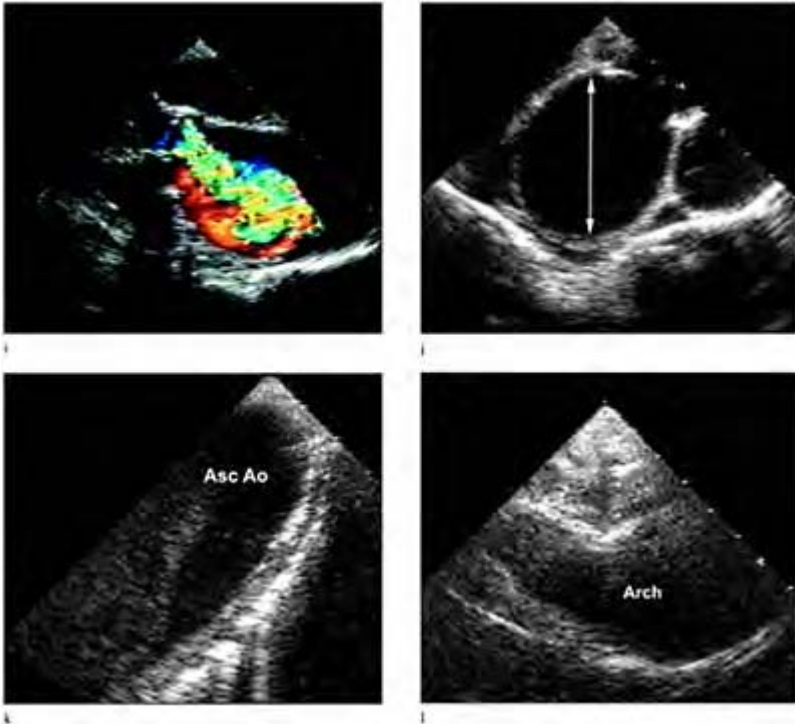
Horizontal (j) and longitudinal (k)
views of the ascending aorta obtained
from the upper esophageal window.
Longitudinal view (l) of the distal
ascending aorta at 90° demonstrating
discrete enlargement of the aortic arch.
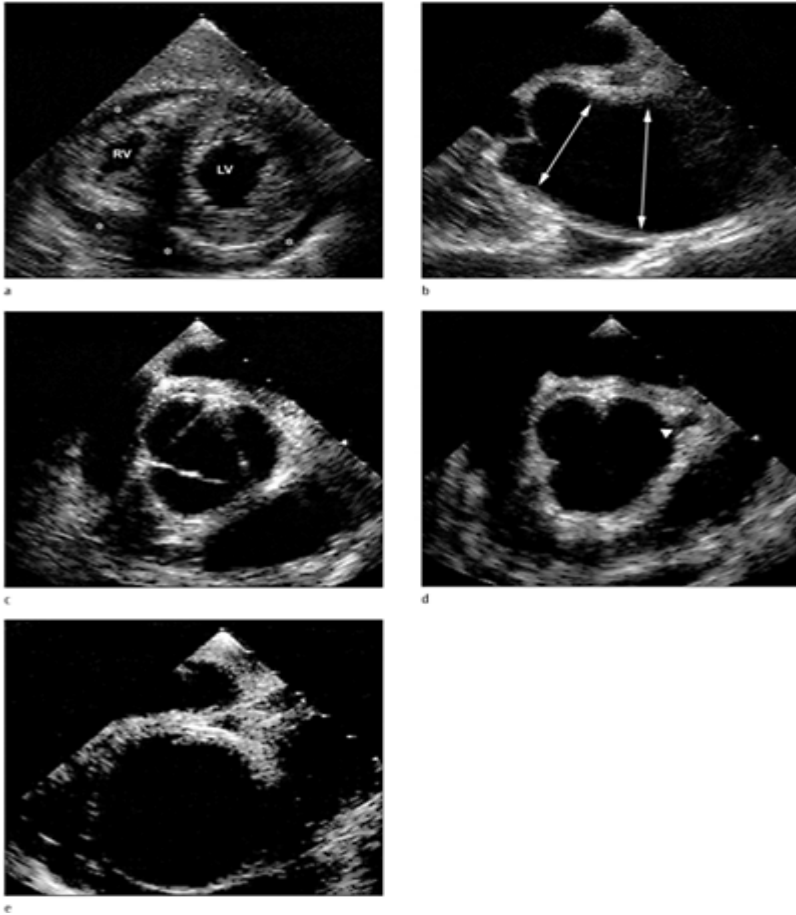
Case 5.41 Aortic rupture and aortic aneurysm.
Multiplane examination of a patient with Marfan's
syndrome presenting with 3 days of symptoms
suggesting an aortic dissection. Gastric short-axis view
(a) at the left ventricular level at 0° demonstrates left
ventricular hypertrophy and a moderate pericardial
effusion. Longitudinal view of the aortic root (b) at 90°
from the mid-esophageal level demonstrate
annuloaortic atresia. Horizontal views of the aortic
valve yield a dilated aortic annulus (c) and sinus of
Valsalva at the coronary level (d). The ascending aorta
(e) is grossly dilated with dilatation of the innominate
artery (f).
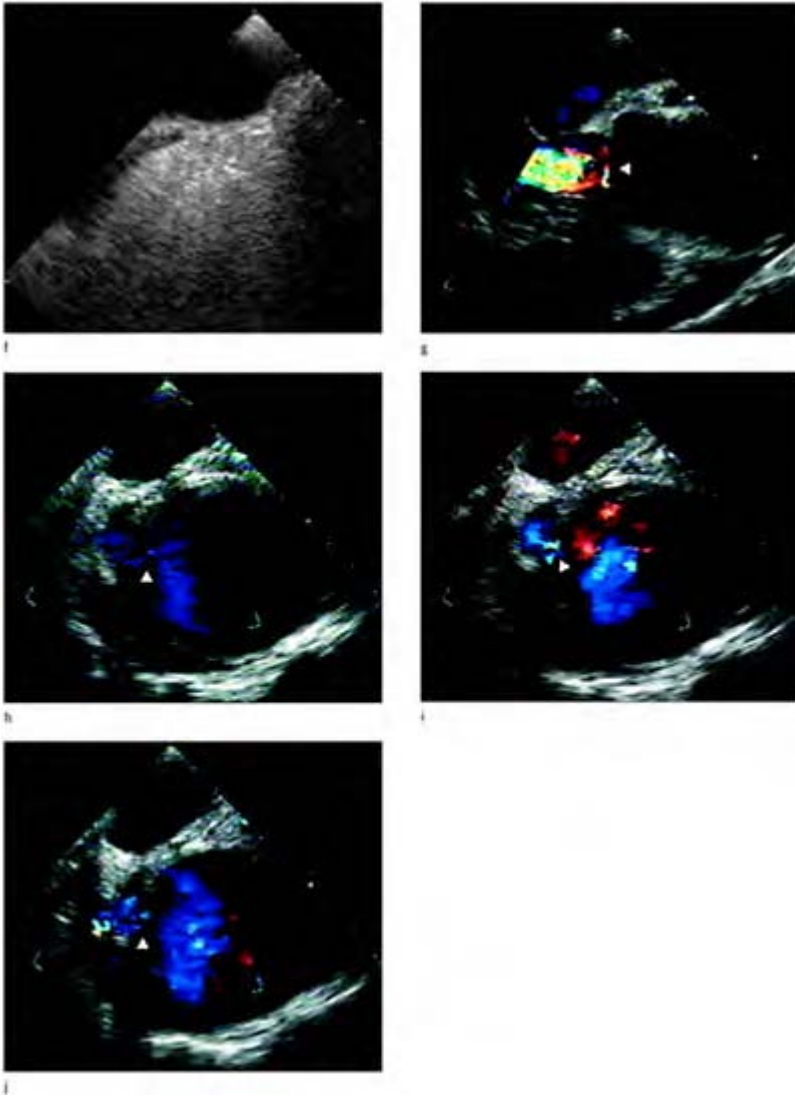
Color Doppler (g) demonstrating aortic
insufficiency in a standard longitudinal
view of the aortic root. With minor
manipulation of the probe in zoom
mode a rupture in the aorta is
demonstrated as a false pouch (h) in
the aortic wall with flow detected
through the area of the rupture (i, j).
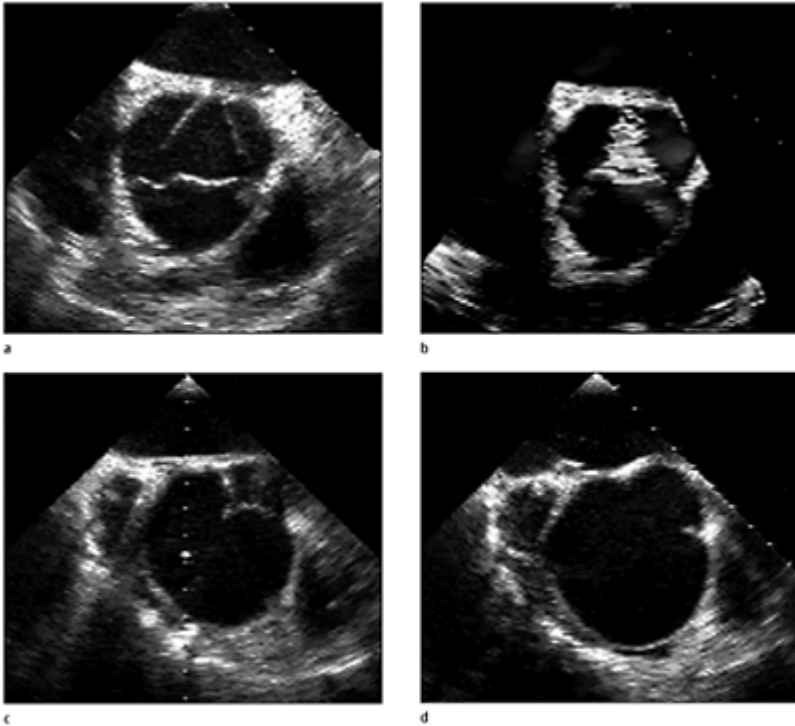
Case 5.42 Ascending aortic aneurysm. Annuloaortic ectasia of the ascending aorta in serial horizontal views (a–h) starting at the aortic annulus through the ascending aorta. The intraluminal diameter of the whole aortic root remains constant and dilated throughout.
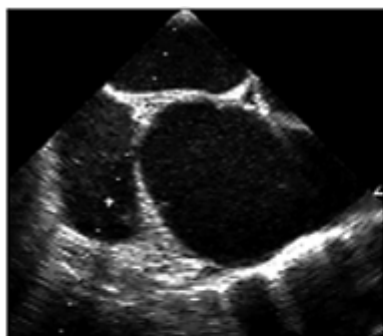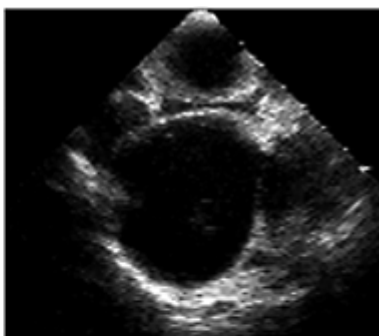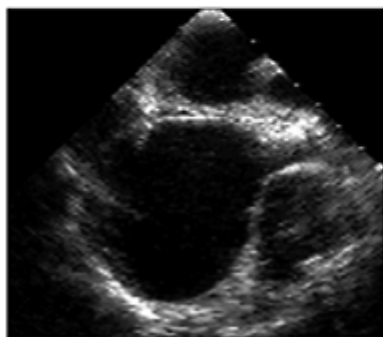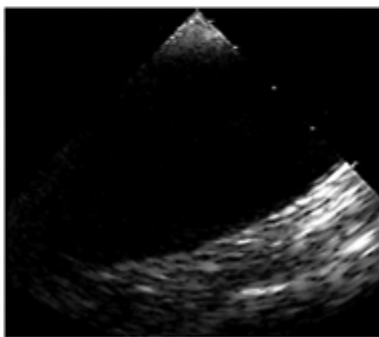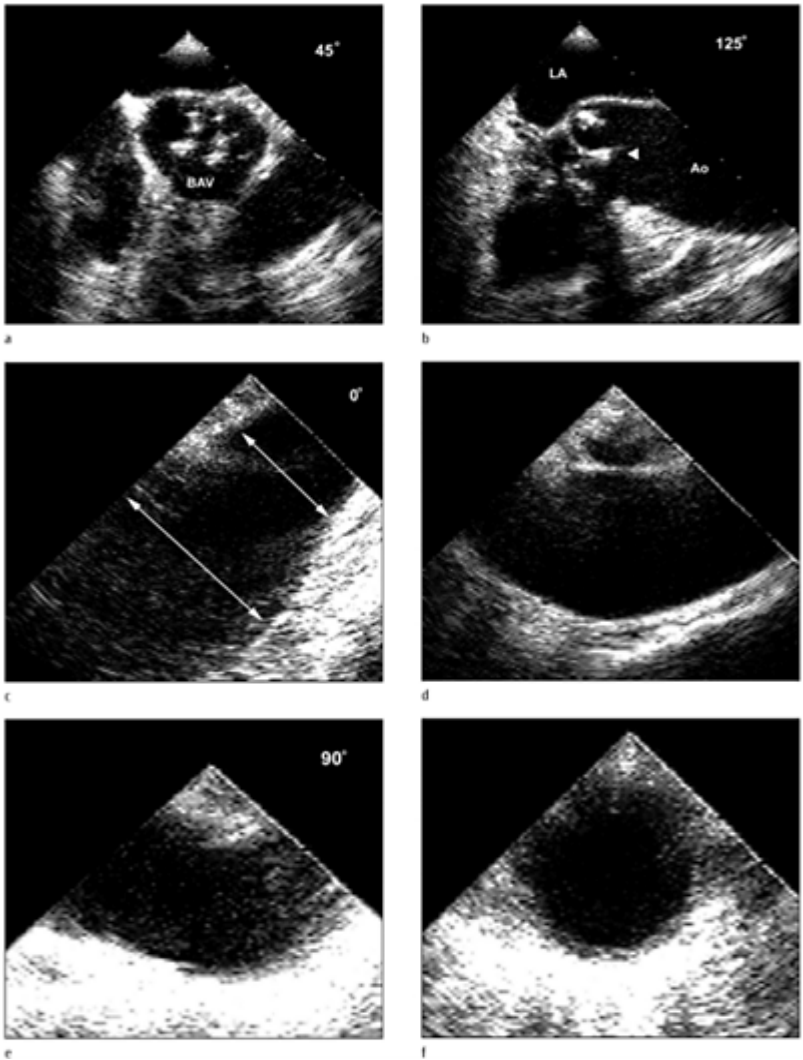
Case 5.43 (right) Stenotic bicuspid aortic valve and
post-stenotic dilatation of the ascending aorta. Stenotic
bicuspid aortic valve in the horizontal (a) and
longitudinal plane (b). Eccentric intraluminal dilatation
of the aorta is noted from the sinotubular junction to
the aortic arch (c). Note the dilatation is greater
towards the greater curvature (d) of the ascending
aorta. The distal aortic arch (e) and descending thoracic
aorta do not appear to be involved (f).
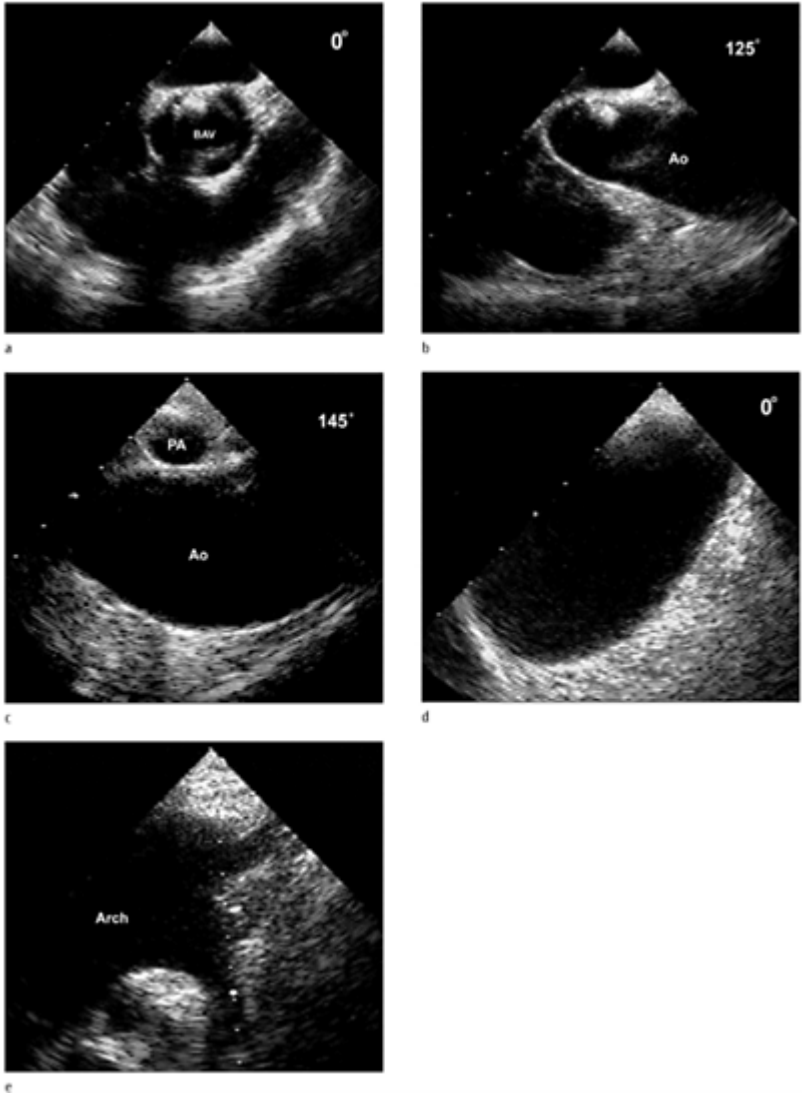
Case 5.44 Bicuspid aortic
valve and ascending aortic
aneurysm. Pre- and post-
operative multiplane TEE.
Bicuspid aortic
regurgitation is present
along with marked
aneurysmal dilatation of

the ascending aorta extending to the aortic arch (a–d). In transthoracic images (e, f) note the abrupt reduction of aortic dimension near the origin of the descending thoracic aorta (e), illustrating a coarctation. Color flow Doppler (f) illustrating increased velocity and disturbed flow through the coarctation. Normal descending thoracic aorta (g) in dimension. Postoperative demonstration of surgical aortic graft in the horizontal (h) and longitudinal (i) views. Zoom mode of the distal anastomosis graft site (j) to the aortic arch, with color flow Doppler (k) essentially normal and undisturbed flow is seen exiting the aortic graft.
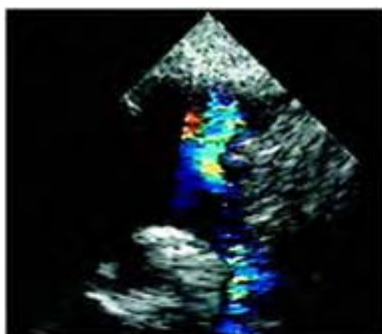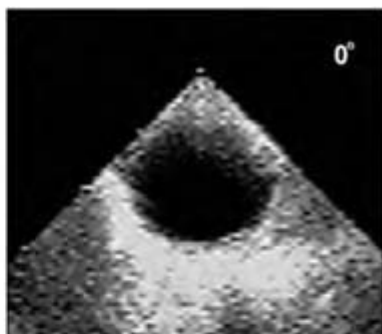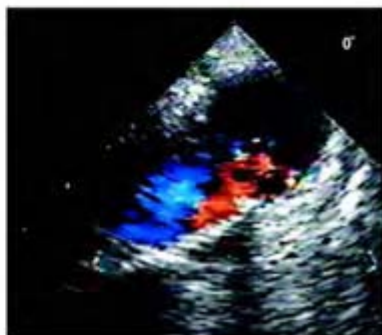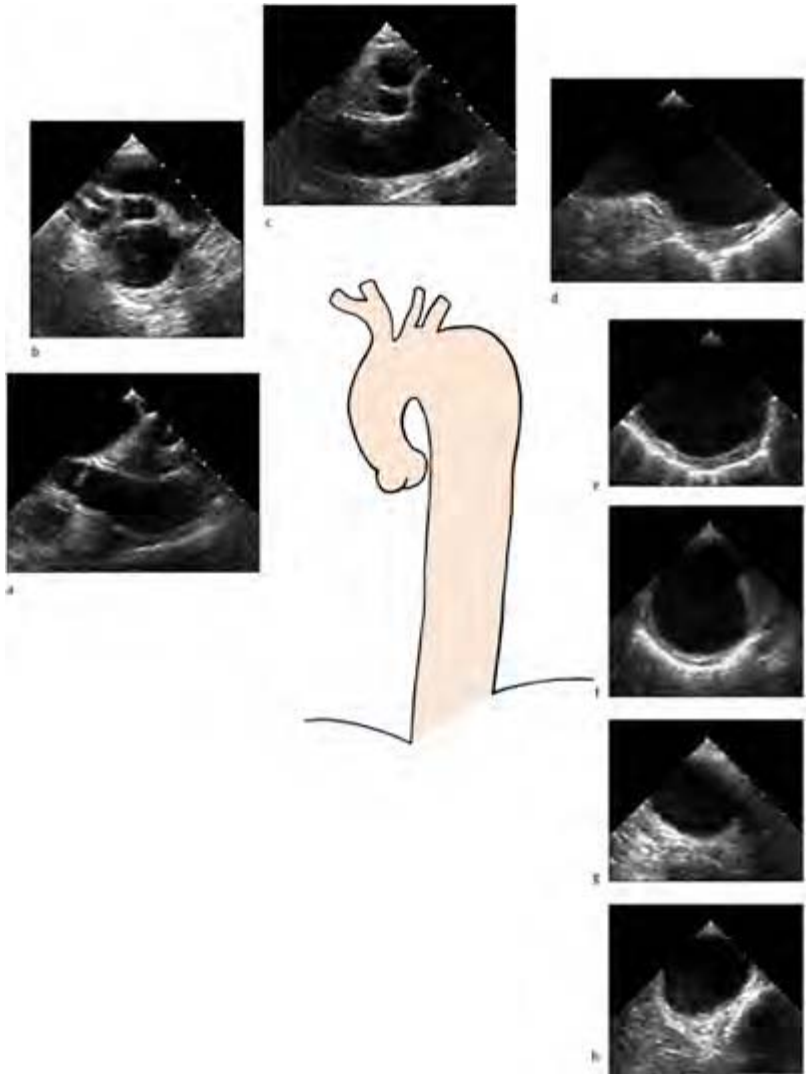
Case 5.45 Aortic arch and descending aortic aneurysm. Sequential multiplane TEE imaging of aneurysmal dilatation of the aortic arch and descending aorta. Normal aortic root and ascending aorta in longitudinal view

(a). Note the exaggeration of the transverse sinus between the ascending aorta and the right pulmonary artery. Horizontal view of the ascending aorta, demonstrating normal aortic dimension with enlargement of the transverse sinus surrounded by the right pulmonary artery, superior vena cava and aorta. Longitudinal view of the distal ascending aorta demonstrating discrete aortic luminal enlargement at the proximal aortic arch (c). Aortic enlargement of the proximal descending aorta with progressive narrowing of the aorta with normal dimensions noted in the distal descending thoracic aorta (d–h) at the diaphragm level.
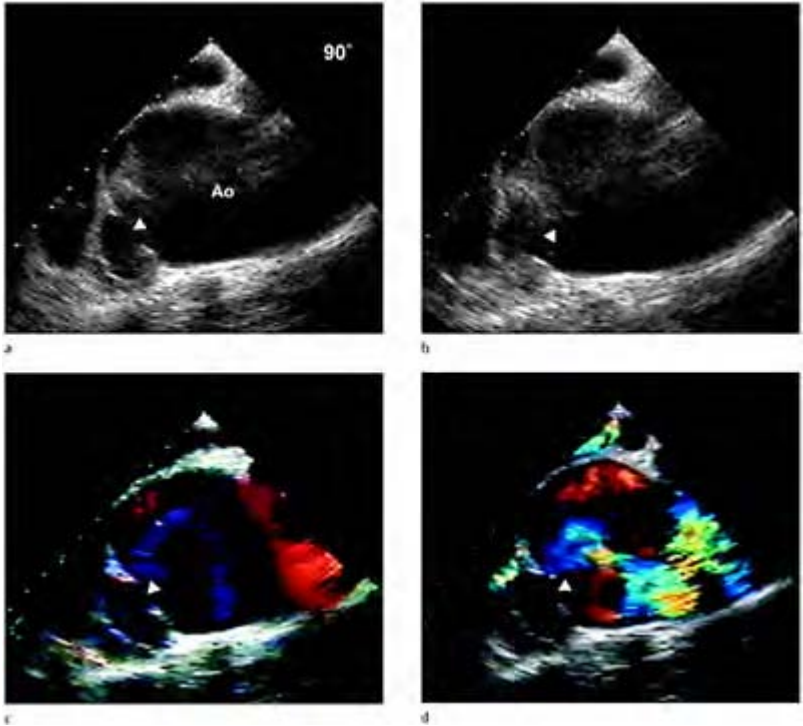
Case 5.46 Acquired sinus of valsalva aneurysm. Longitudinal view of the ascending aorta demonstrating discrete dilatation of the right sinus of Valsalva in systole (a) and diastole (b) with disturbed aortic blood flow with color flow Doppler (c, d). Deep transgastric view (e) demonstrating the typical appearance of an acquired sinus of Valsalva aneurysm in zoom mode (f).
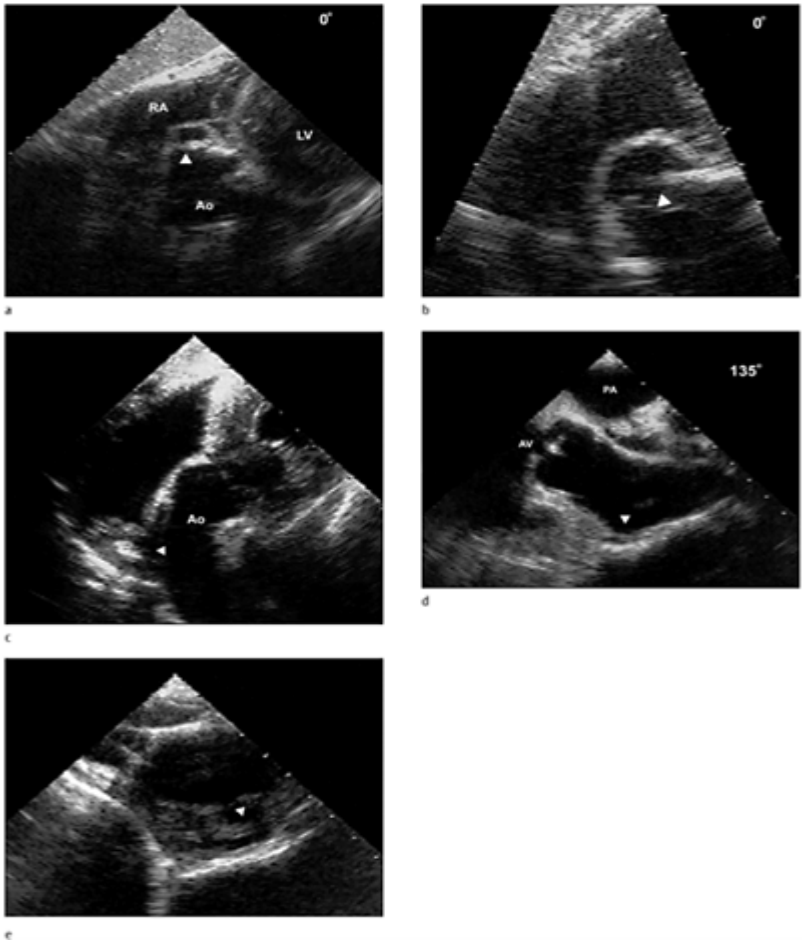
Case 5.47 Saccular aneurysm of the ascending aorta. Multiplane TEE examination demonstrating a saccular aneurysm that developed as a complication following coronary artery bypass surgery. A discrete dilatation is present of the greater curvature of the anterior surface of the ascending aorta following surgery involving the use of a partial occlusion aortic clamp. A saccular aneurysm is well-visualized from the deep transgastric (a), longitudinal aortic long axis (b), and horizontal short axis from the upper esophageal view (c).
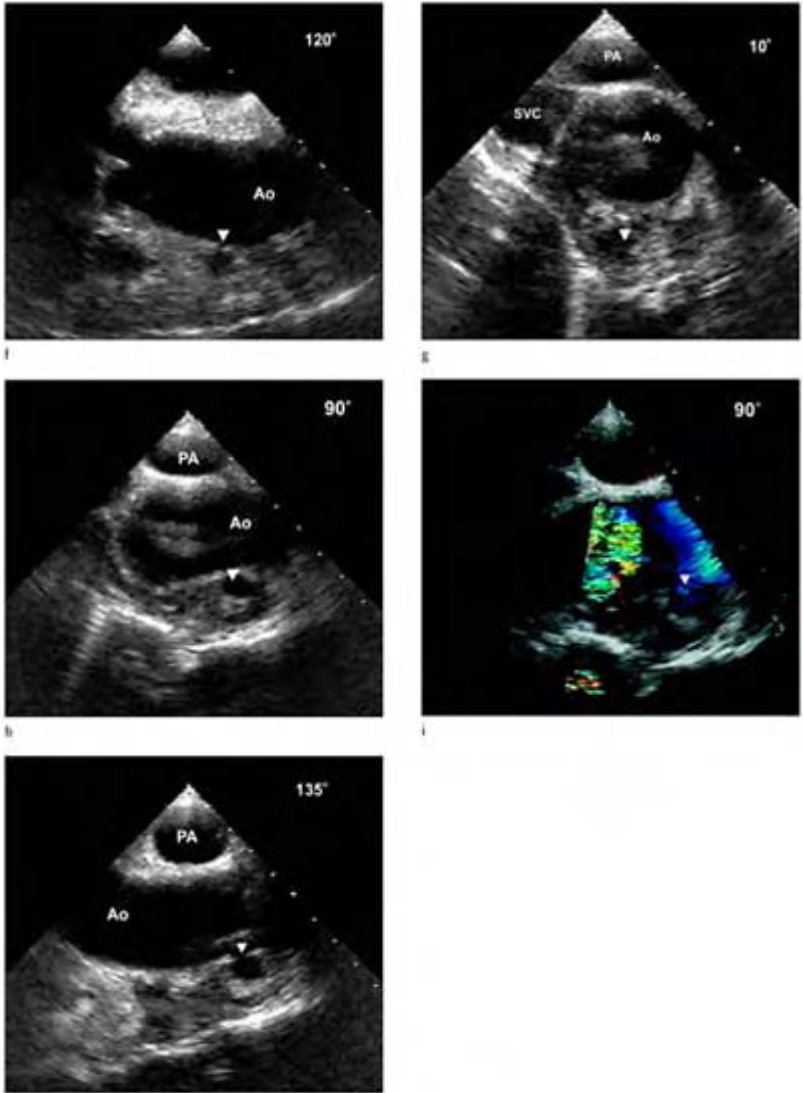
In a similar patient two small saccular aneurysms have developed at the site of proximal saphenous vein graft anastomosis, aortic long axis (d, e) and short axis (e). Color flow Doppler demonstrating flow in and about the saccular aneurysms (g, h).
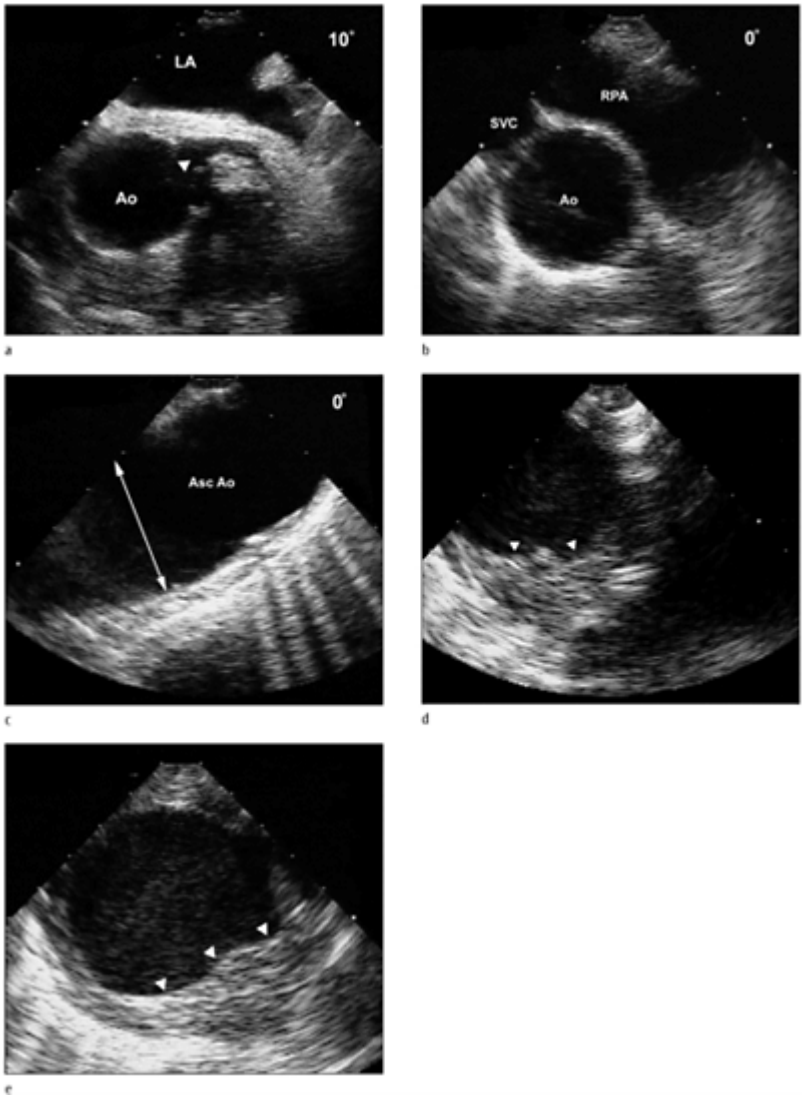
Case 5.48 Discrete aortic arch aneurysm associated with severe atherosclerotic disease. Circumferential calcification of the entire ascending aorta is demonstrated in serial horizontal views (a, b) and long axis (c). Extensive aortic wall plaque is demonstrated in the aortic arch with moderate luminal dilatation.
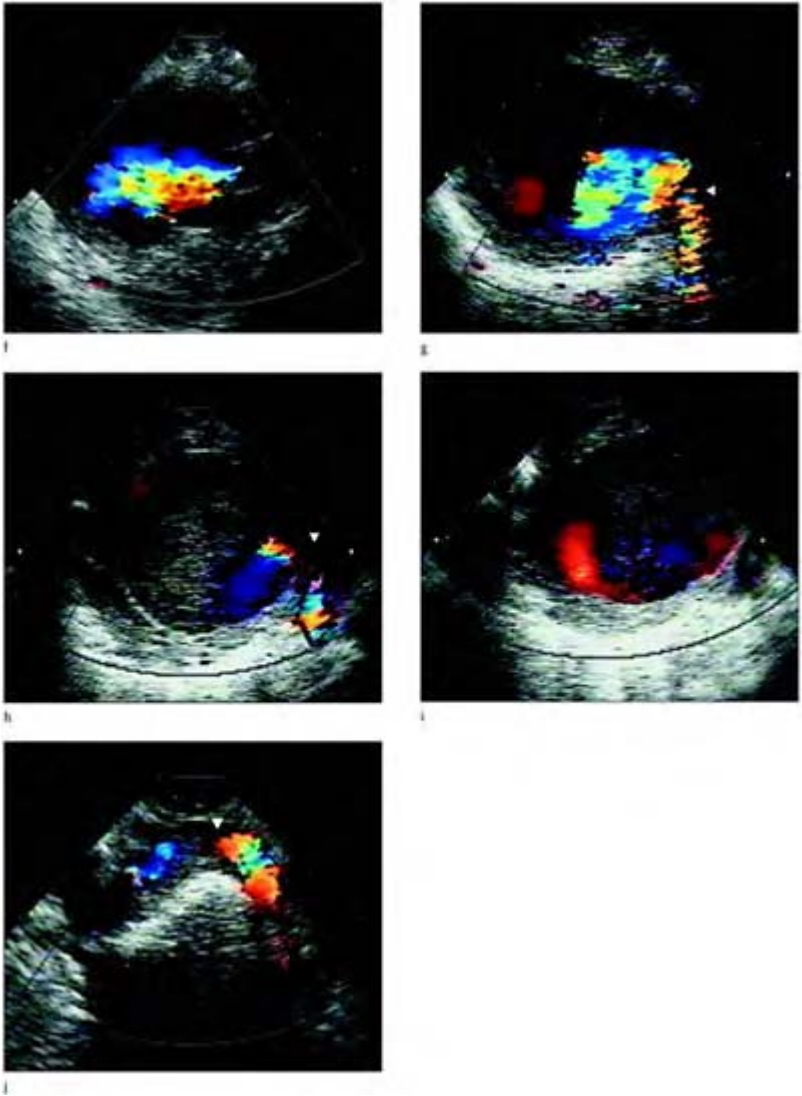
Color flow Doppler
illustrates marked
disturbed flow in the
region of the aortic debris
(f–j) with narrowing and
high velocity flow through
the origin of the left
subclavian artery
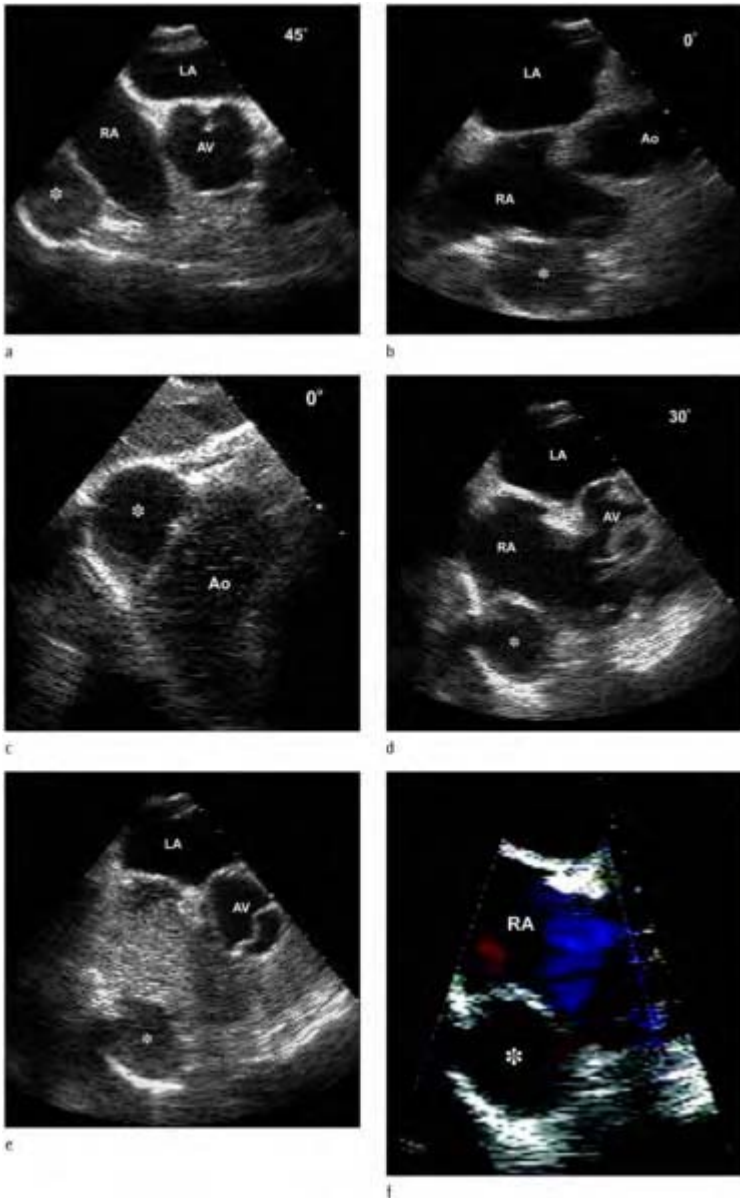
Case 5.49 Saphenous vein graft aneurysm. Multiplane TEE visualization of a diffuse aneurysm of a saphenous

vein graft, 2 years
following coronary artery
bypass surgery. A large
circular cavity with a
similar diameter to the
ascending aorta, is imaged
lateral to the right atrium
in mid-esophageal short-
axis view at 0° (a) and
longitudinal long axis at
90° (b). Deep transgastric
view of the ascending
aorta showing a large out
pouching of the area near
the saphenous vein graft
anastomosis. With saline
injection echo contrast
filling the right atrium, the
vein graft aneurysm is
delineated from the right
atrium and demonstrates
no communication with it
(d, e). Color flow Doppler
of the right atrium and
right saphenous graft
aneurysm.
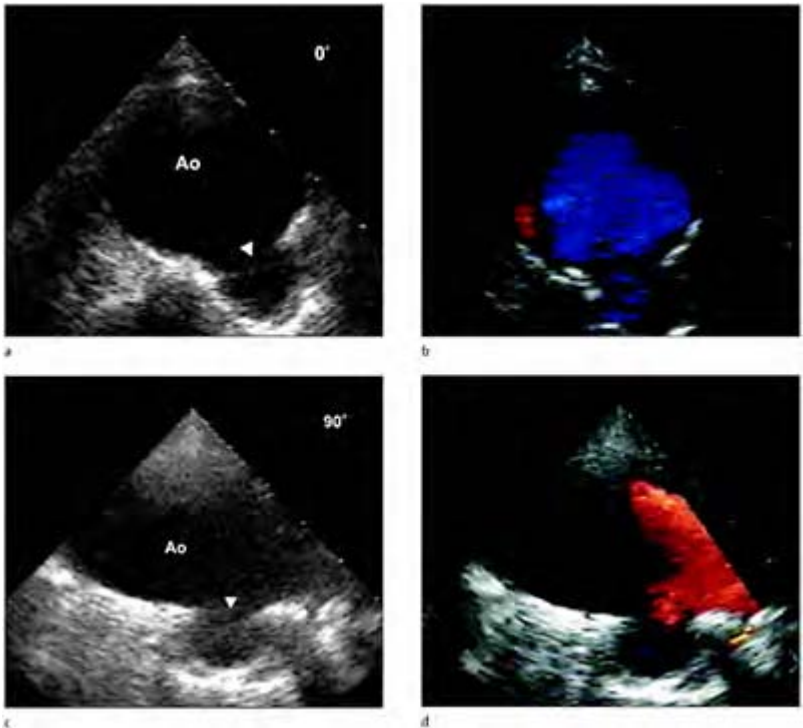
Case 5.50 Saccular aneurysm. Large saccular aneurysm of the descending thoracic aorta at approximately the upper mid-level at 28 cm from the incisors. Short axis view (a) and long axis (c) of the descending aorta demonstrating a wide neck saccular aneurysm, which fills with color flow Doppler (b, d).
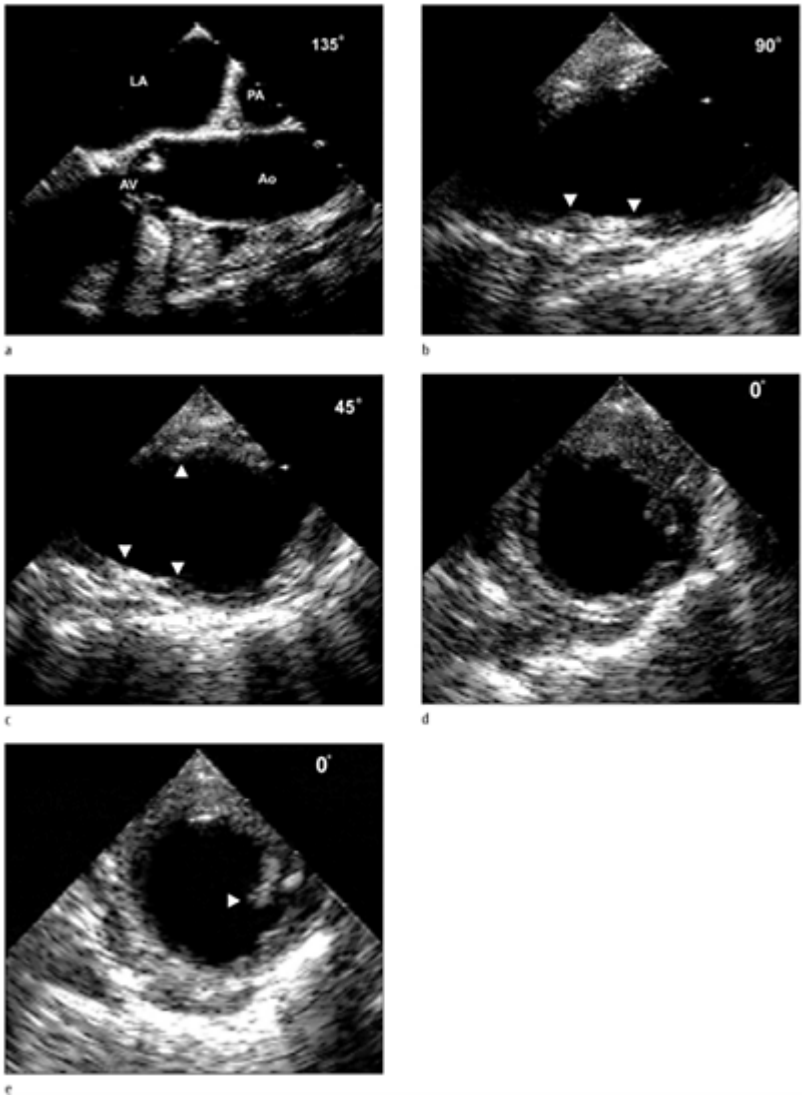
Case 5.51 Atherosclerotic disease. Severe calcific atherosclerotic disease of the entire aorta. Serial longitudinal images of the ascending aorta (a) and aortic arch (b, c), followed by horizontal images of the descending aorta (d–i).
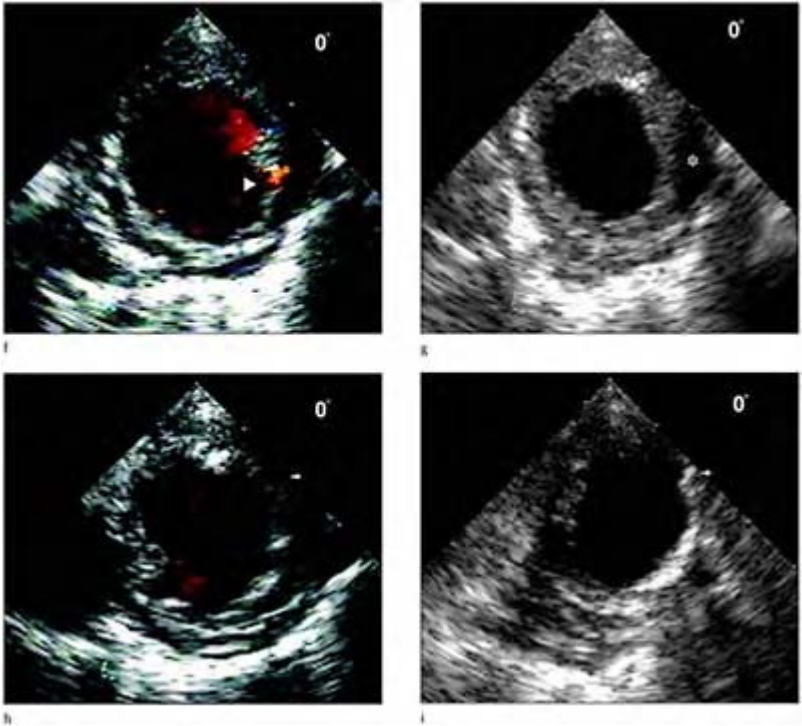
Note marked circumferential calcification in the aortic wall, with marked intimal thickening amid bright white lines of echogenicity, and shadowing artifact paralleling the aortic outline which is best appreciated in longitudinal planes.
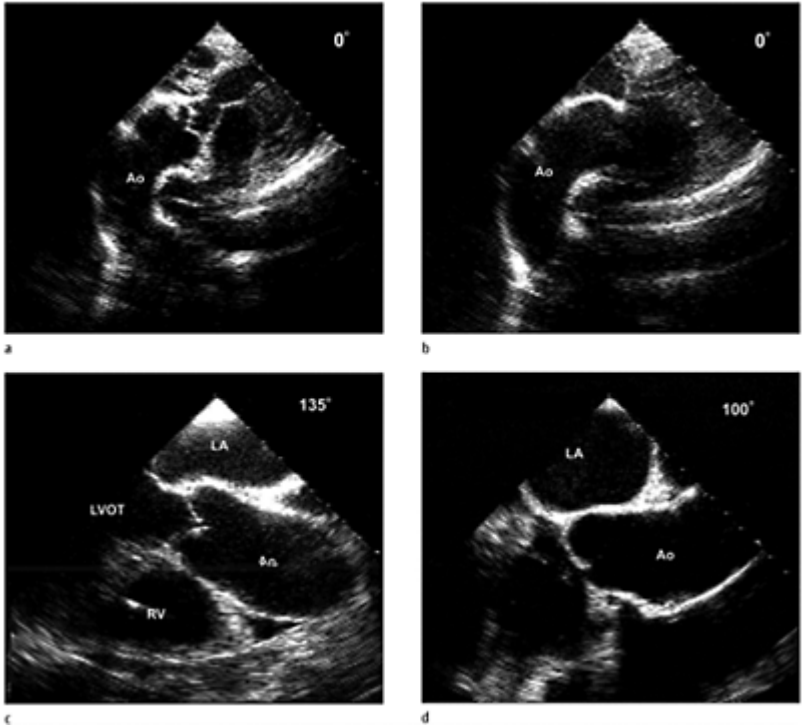
Case 5.52 Atherosclerotic disease. Severe calcification of the ascending aorta outlining the entire aorta in deep transgastric views 0° (a) and 35° (b). Longitudinal long-axis views of the aortic root (c) and ascending aorta (d). Severe circumferential calcification of the aorta may be denoted as a porcelain aorta. With a porcelain aorta, the aortic walls are lined with plates of calcium producing an eggshell appearance on diagnostic imaging and a firm hard sensation on palpation of the aorta during manipulation at surgery.
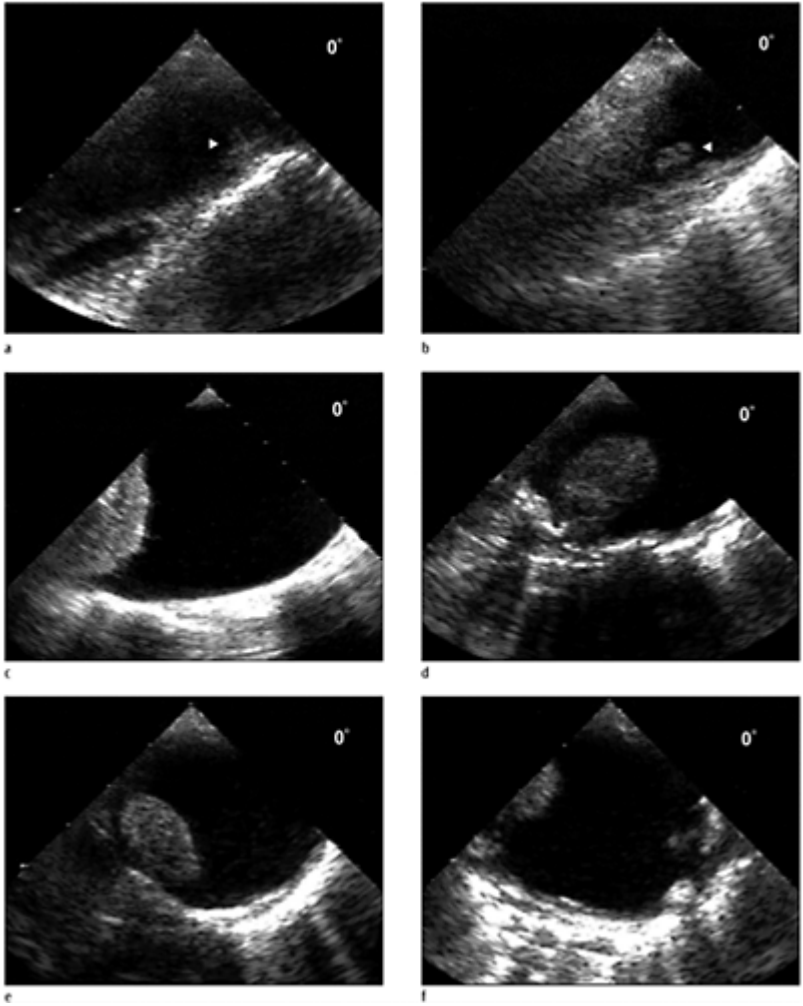
Case 5.53 Atherosclerotic disease. Discrete severe atherosclerotic disease of the distal ascending aorta and aortic arch. Intimal thickening with plaque is demonstrated in the distal ascending aorta (a) with severe narrowing of the aortic arch (b). Distal to the obstruction a large luminal filling thrombus is detected originating from an atheromatous ulcer in the distal aortic arch (c–f).
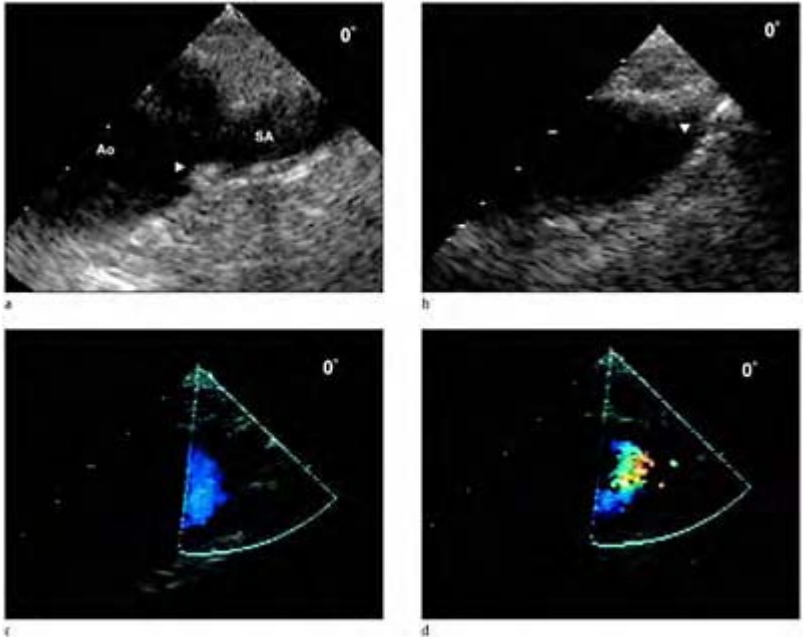
Case 5.54 Atherosclerotic disease. Atherosclerotic disease involving the aortic arch with mild plaque at the origin of the left subclavian (a) and severe narrowing of the origin of the left carotid artery takeoff (b). Color flow Doppler (c, d) failed to demonstrate flow to the left carotid, which was substantiated with arteriography.
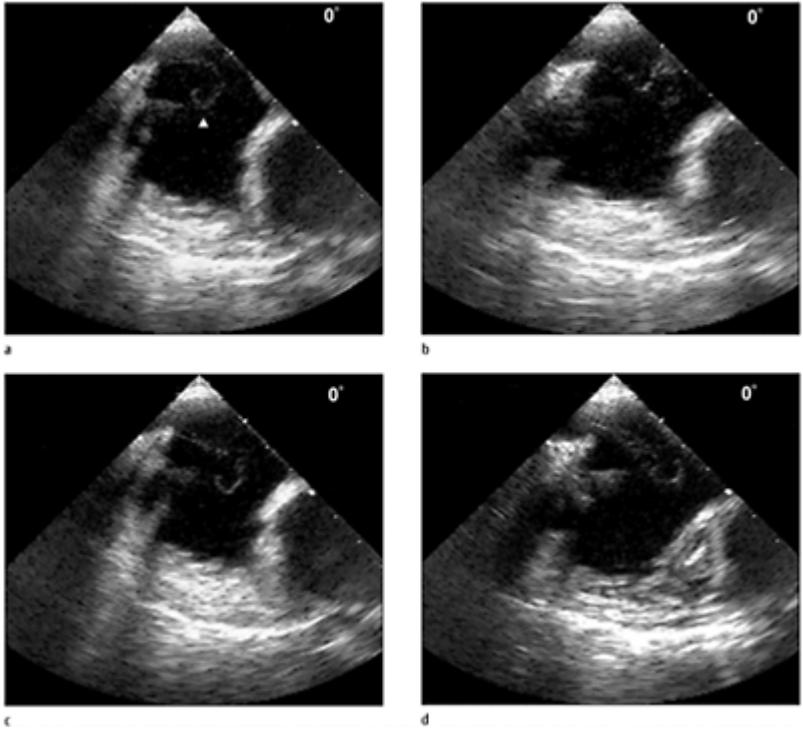
Case 5.55 Atherosclerotic disease. Severe atherosclerotic disease involving the descending thoracic aorta with debris noted as a thrombus with a large tail (a–d) moving with each aortic pulse, in sequential short-axis horizontal views.
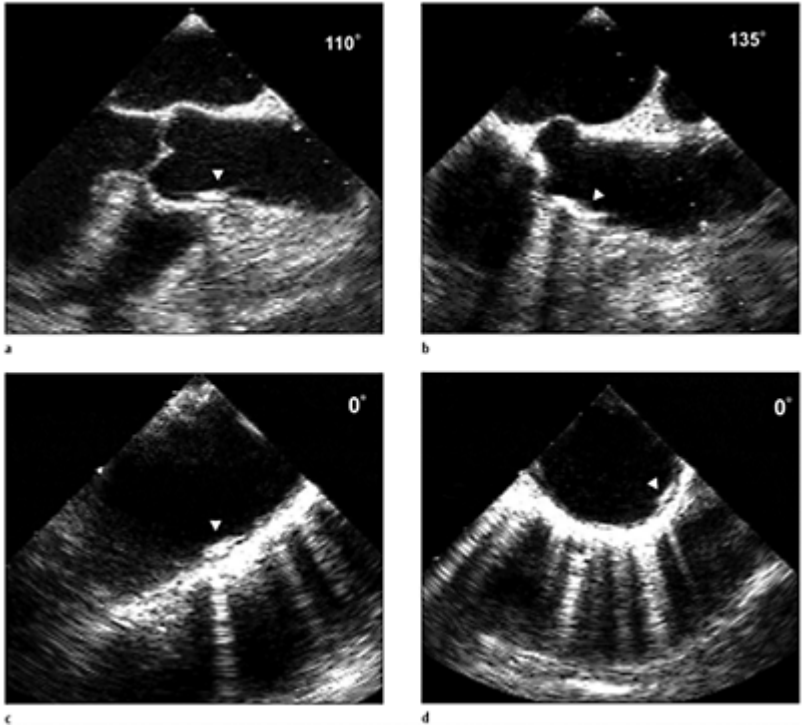
Case 5.56 Atherosclerotic disease. Severe atherosclerotic disease involving the ascending aorta (a–d). Plaque is noted near the origin of the right coronary artery (a) with discrete segmental involvement of multiple sights in the ascending (b, c) and descending aorta (d).
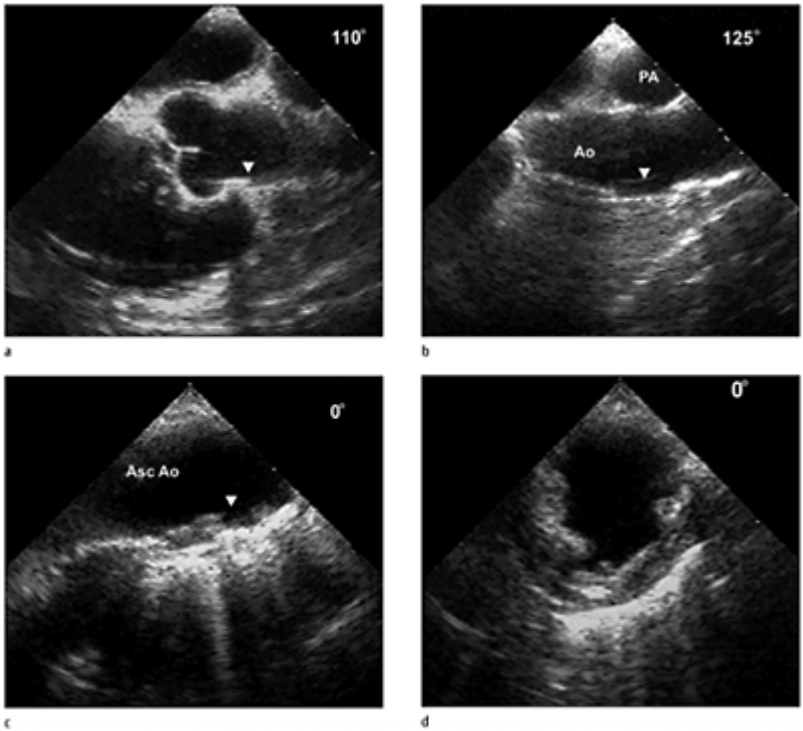
Case 5.57 Atherosclerotic disease. Atherosclerotic plaque at the origin of the right coronary artery (a) with mild disease of the ascending aorta (b). Severe intimal thickening and plaque is noted starting in the distal aortic arch (c) and descending thoracic aorta (d).
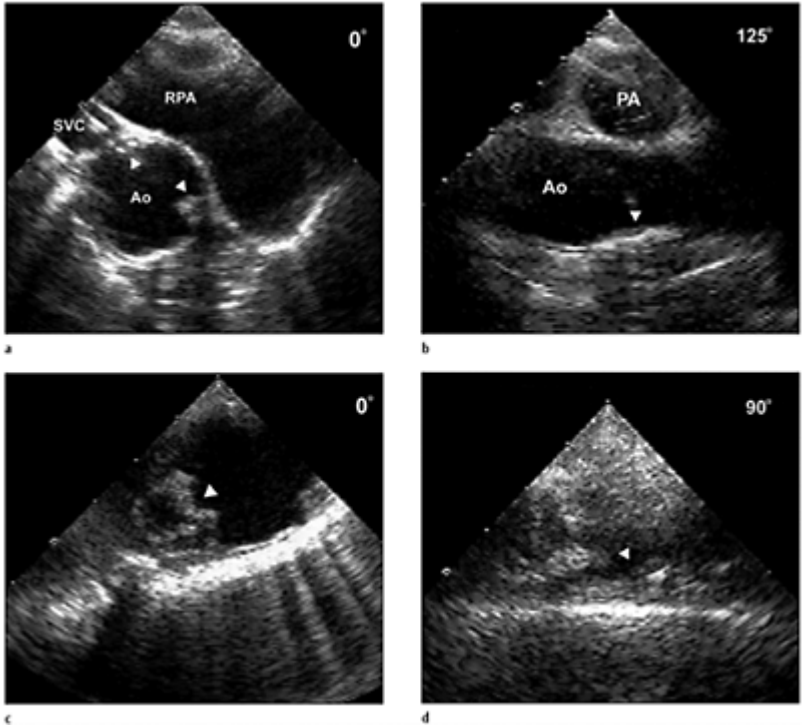
Case 5.58 Atherosclerotic disease. Marked ascending aortic atherosclerosis with discrete debris in the horizontal (a) and longitudinal (b) views. Severe atherosclerotic debris of the proximal descending aorta (c) with associated near total obstruction of the mid-descending thoracic aorta (d).
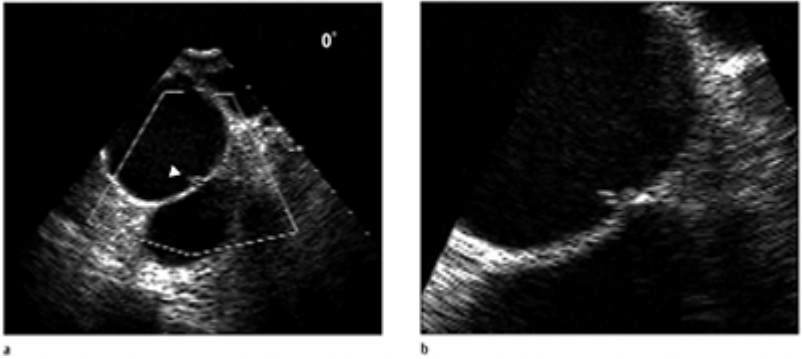
Case 5.59 Aortic transection. Traumatic aortic intimal tears appear as thin, mobile intraluminal projections emanating from the aortic wall close to the aortic isthmus. Short-axis proximal descending thoracic aorta (a) and in zoom mode (b) demonstrate an intimal aortic tear. Since intimal tears are small, the aortic contour and diameter usually remain normal and pseudoaneurysms usually do not occur.
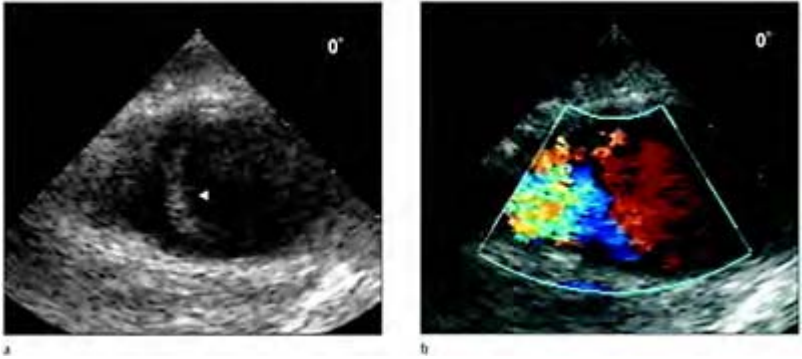
Case 5.60 Aortic transection. Traumatic aortic tear with associated subadventitial disruption. TEE demonstrates an abnormal thick intraluminal flap that produces a non-symmetrical aortic deformity. In longitudinal views the medial flap is nearly perpendicular to the aortic isthmus, which traverses vertically. Color flow Doppler demonstrates disruption of aortic blood flow in the vicinity of the aortic tear, which oscillates with each cardiac cycle and spontaneous contrast may be demonstrated between each layer of the aortic wall.
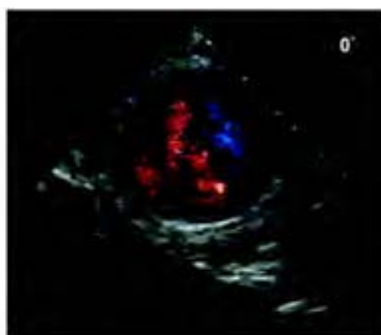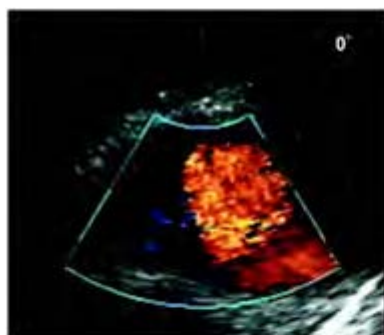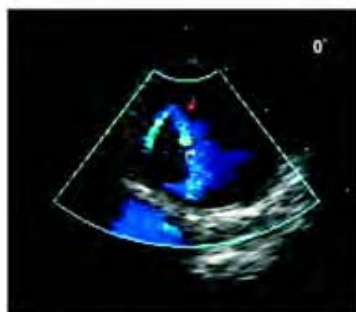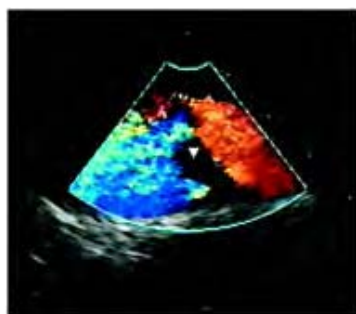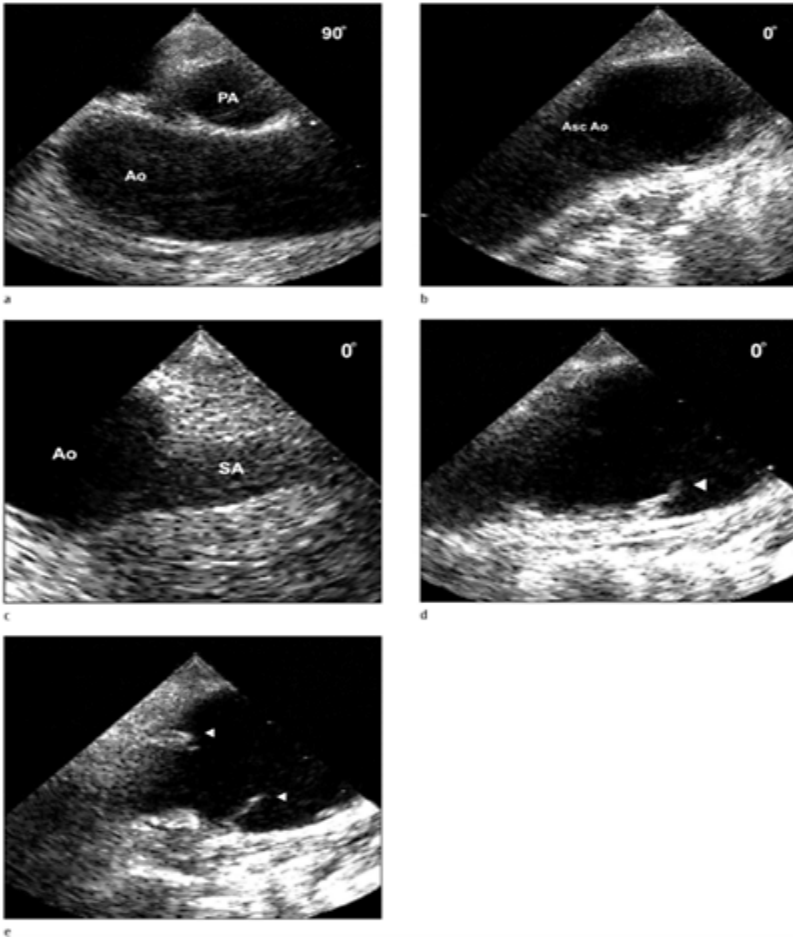
Case 5.61 Aortic transection. Traumatic aortic intimal tear with a small subadventitial disruption following an automobile accident. Views of the ascending aorta (a), arch (b) and left subclavian origin (c) are normal. A small intimal tear (d) is demonstrated on long axis view of the descending aorta just distal to the subclavian takeoff in the isthmus region. Short axis of the intimal tear (e) yields a small subadventitial disruption producing echogenicity within

the wall of the aorta with mild aortic deformity. A circumferential disruption (f–k) is demonstrated distal to the tear extending throughout the descending aorta.
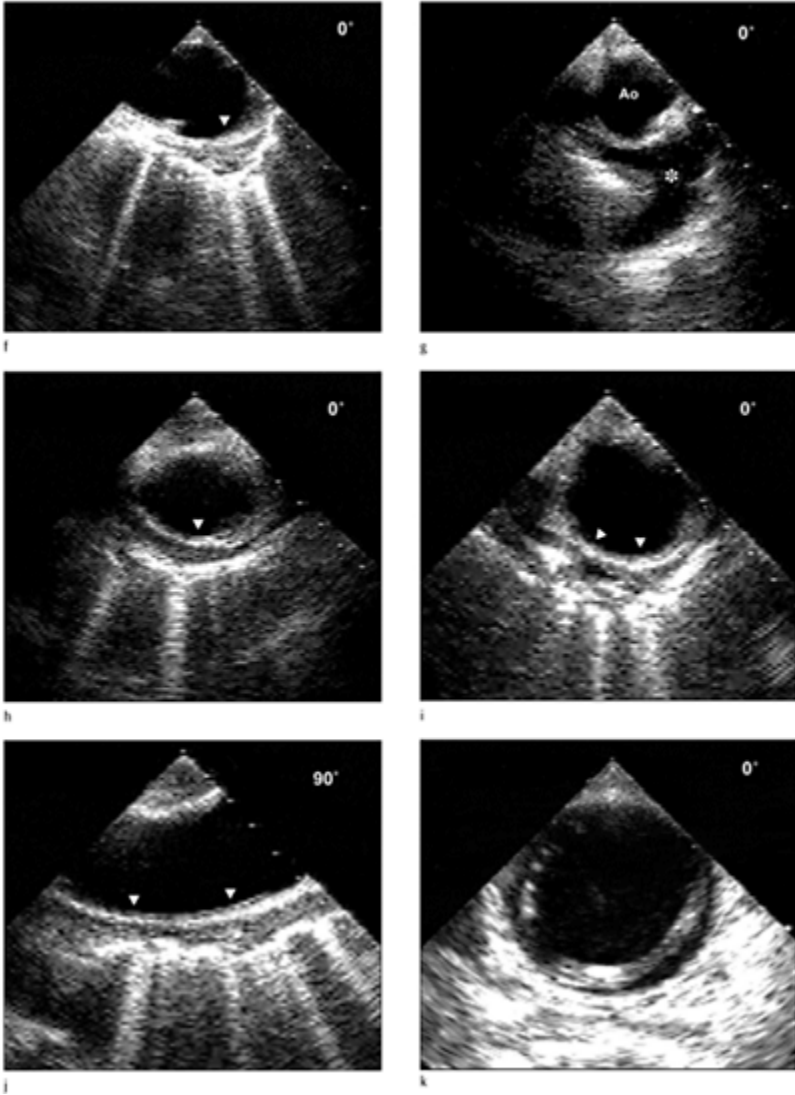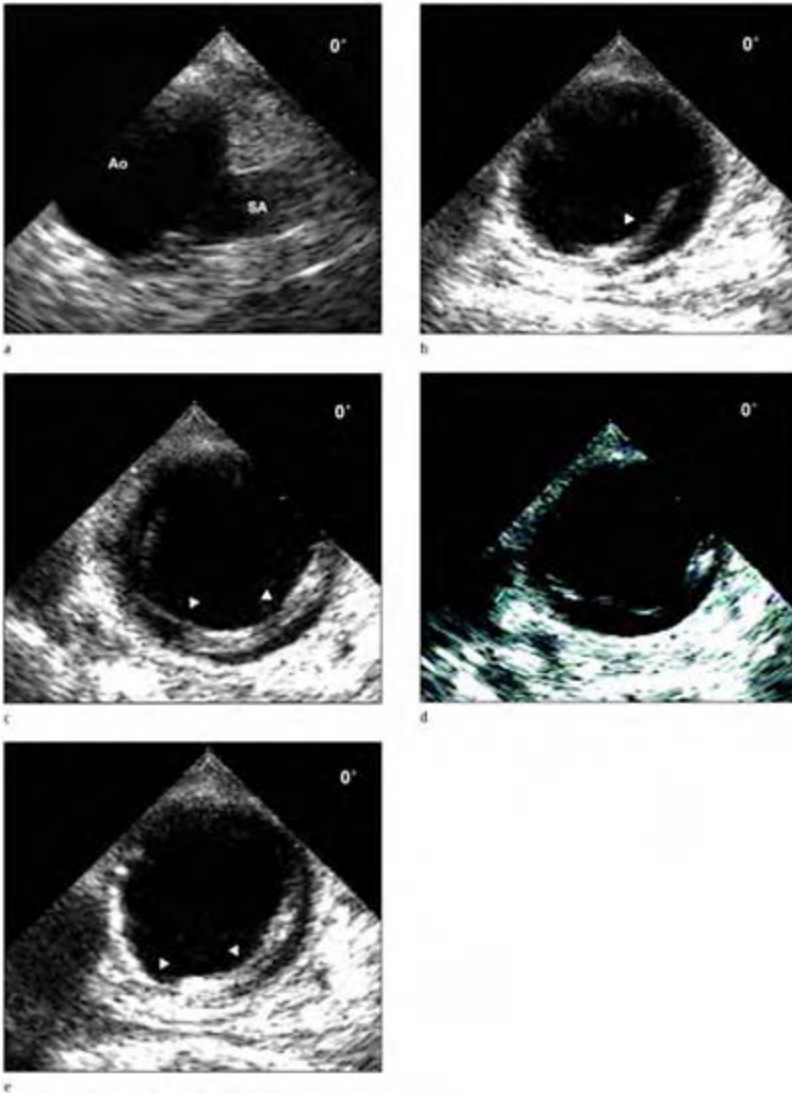
Case 5.62 Aortic transection. Complete
subadvential aortic disruption involves the
entire circumference of the aorta (a–e).
The aortic intima tear starting at the aortic
isthmus appears as a discontinuity of the
intimal-medial aortic layer, without
evidence of an intraluminal medial flap.
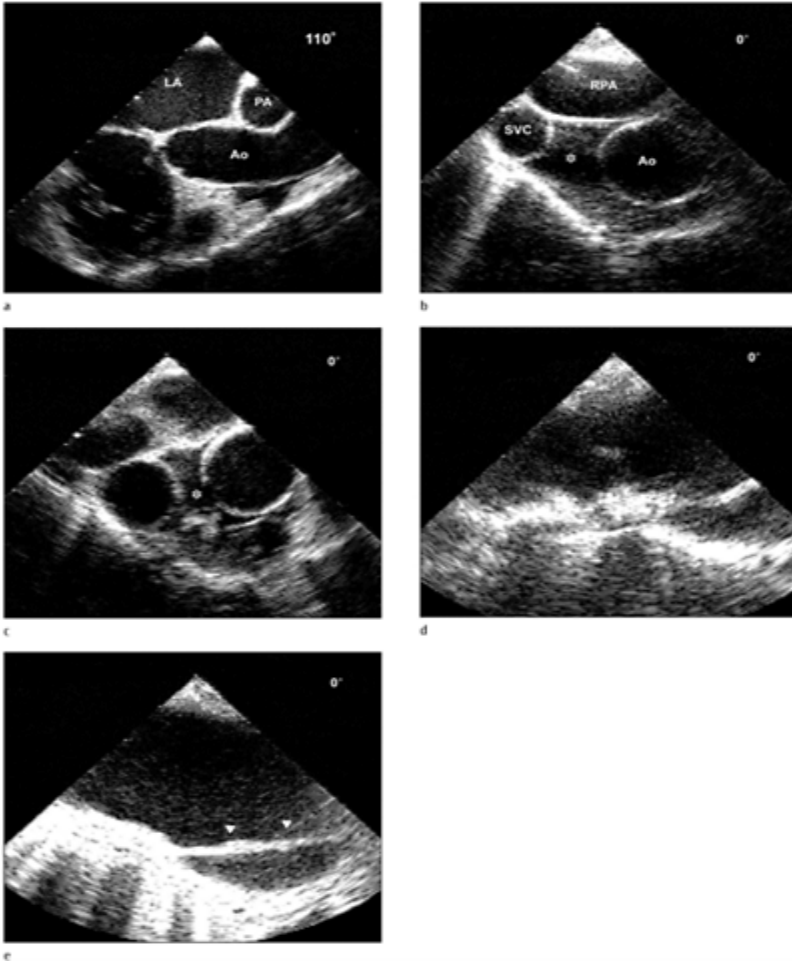
Case 5.63 Aortic transection. Mediastinal hematoma frequently occurs with aortic transection. An echo free space representing bloody fluid is demonstrated filling the transverse sinus (a–c) surrounding the aorta producing a large separation between the aorta and superior vena cava, which produces an obvious decrease in image quality. Other than the mediastinal fluid the proximal aortic anatomy appears normal. An aortic tear is demonstrated near the aortic isthmus (d)

associated with subadventitial disruption
in the proximal descending aorta (e),
which extends distally throughout the
entire descending thoracic aorta and
resembles a type III dissection.
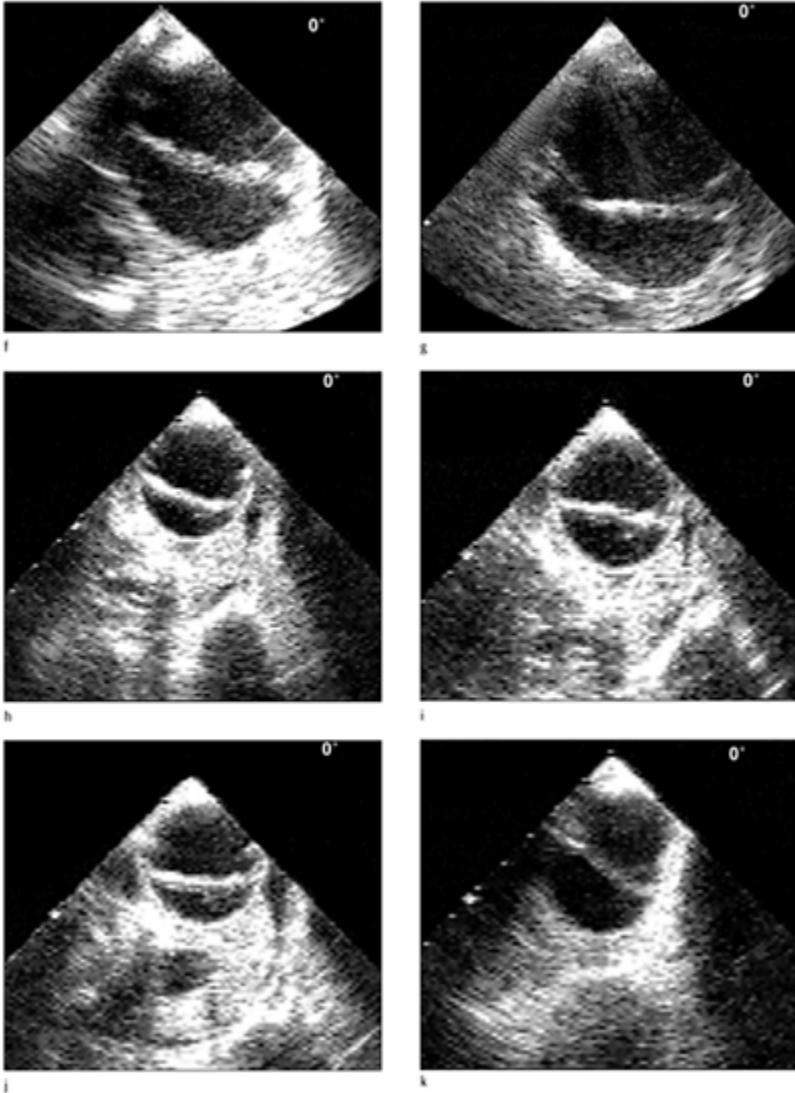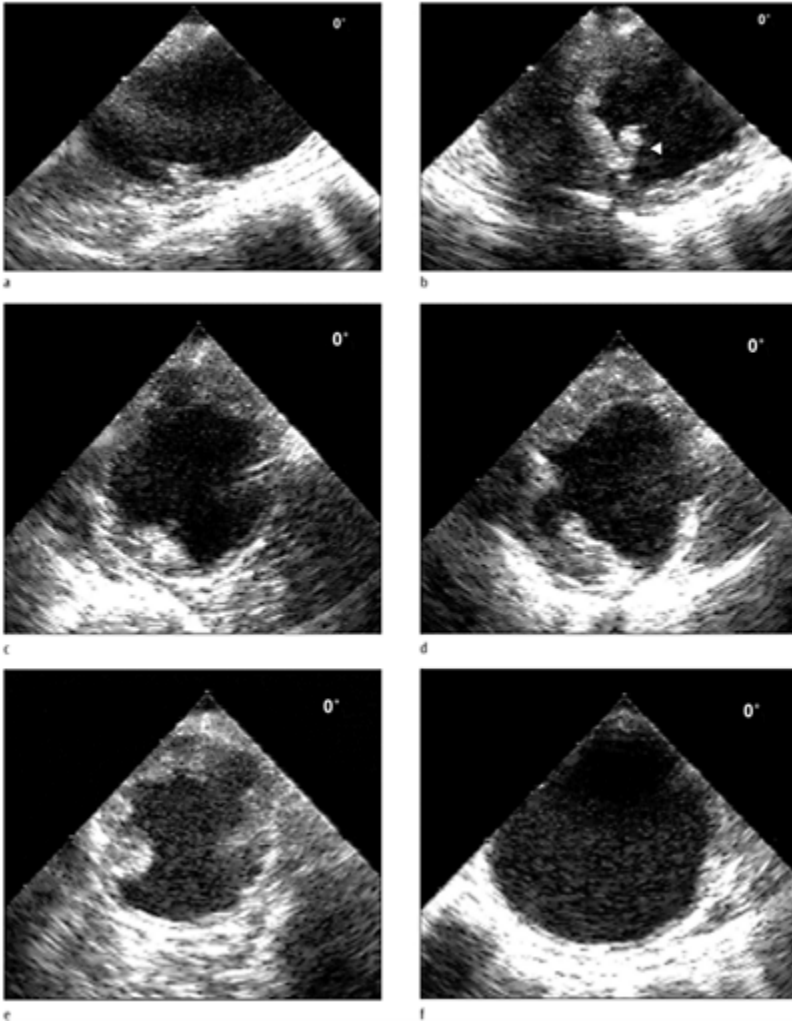
Case 5.64 Aortic transection. Traumatic
aortic intimal tear originating at the aortic
isthmus associated with subadventitial
aortic disruption producing a large
pseudoaneurysm in an aorta with
significant pre-existing atherosclerotic
disease of the descending thoracic aorta.
The pseudoaneurysm was visible by chest
X-ray as a hazy enlargement of the
contour of the aortic bulb.
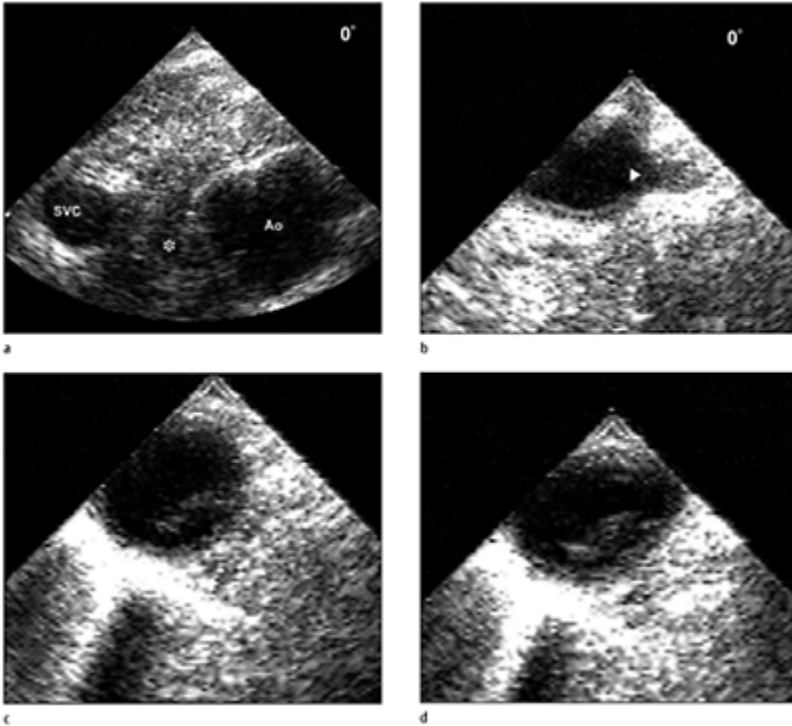
Case 5.65 Aortic transection. Large echogenic mediastinal hematoma in an aortic transection sustained 48 hours before multiplane TEE evaluation. A wide echogenic space representing thrombus (a) separates the ascending aorta and superior vena cava in short-axis imaging from the upper esophageal window, completely obscuring visualization of the right pulmonary artery. Hematoma in the region of the takeoff of the great vessels almost completely obscures the origin of the left subclavian artery (b). Horizontal views of the descending aorta demonstrate discontinuity of the intimal medial layer (c, d).
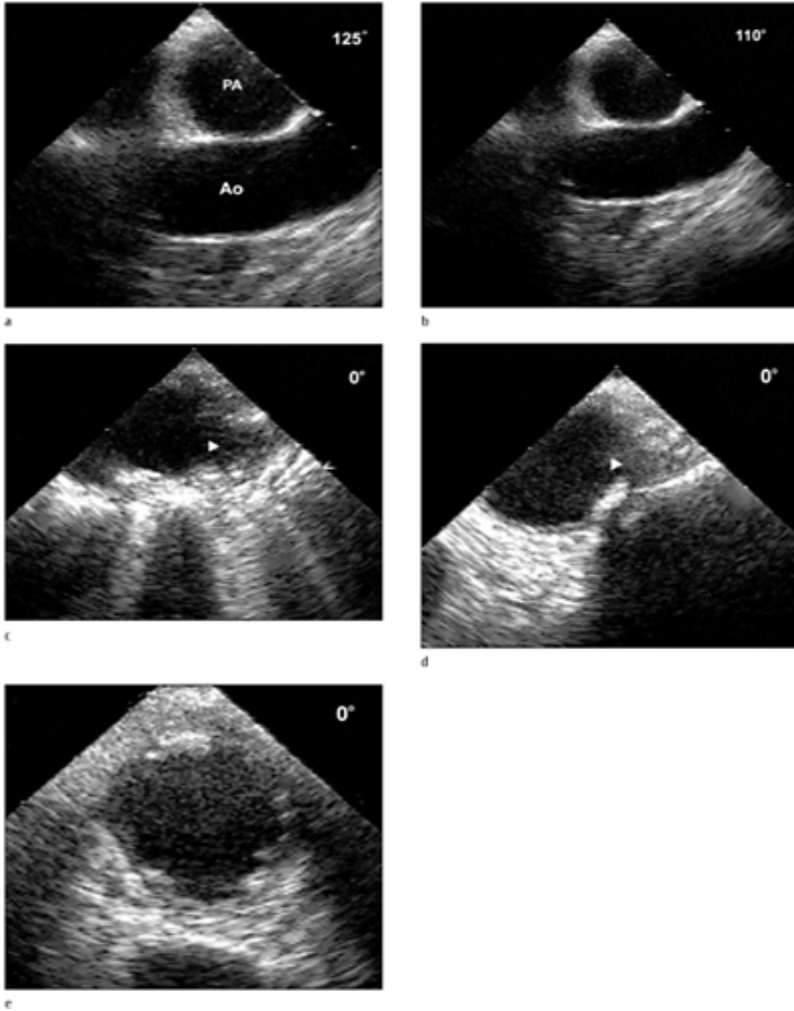
Case 5.66 Aortic transection. The most important ramification of a porcelain aorta is that the severely calcific aorta cannot be cannulated or cross-clamped without the risk of producing rupture, intimal laceration, dissection, or crushing of the aorta. Preoperative multiplane assessment of a porcelain aorta (a, b) with severe atherosclerotic plaque involving the distal aorta (c, f).
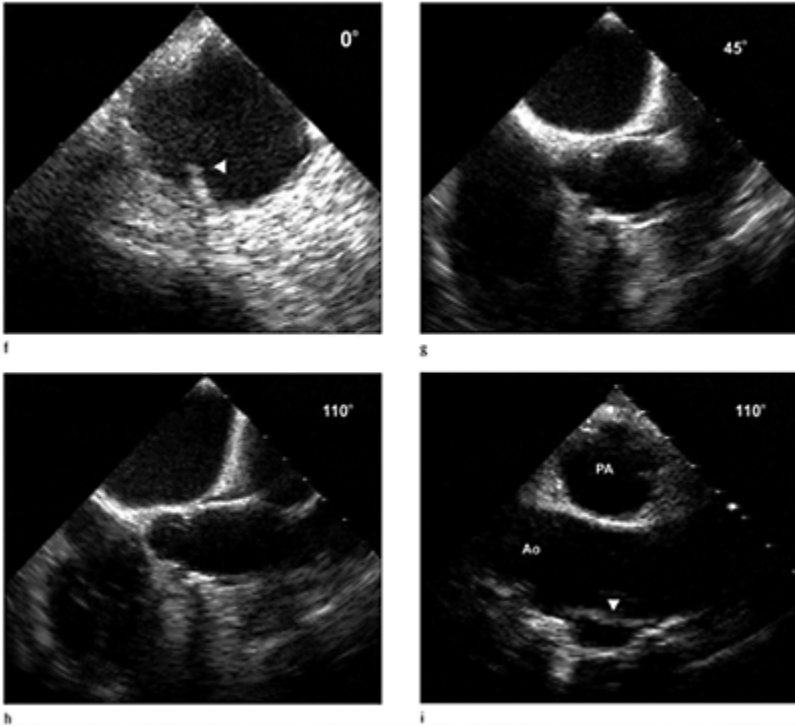
Immediately following removal of the aortic cross-clamp and weaning from cardiopulmonary bypass the aorta was noted to swell with a visible hematoma from the aortic cannulation site.
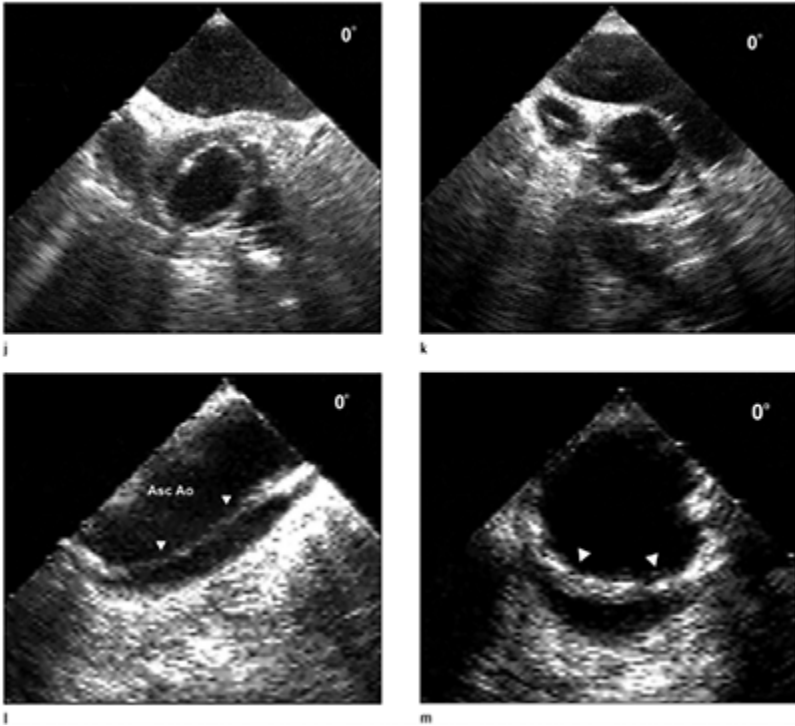
Multiplane TEE evaluation (g–m) of the aorta demonstrated a luminal defect at the site of the aortic cannulation (i) with a complete circumferential disruption of the intimal-medial layer (j–m) similar to the findings of an aortic transection.

References

1. Keen G. Closed injuries of the thoracic aorta. *Ann R Coll Surg Engl* 1972;51:137–56.
2. Laennec RTH. De l'Auscultations Médiate, ou Traité du Diagnostic des Maladies des Poumons et du Coeur, Fondé Principalement sur ce Nouveau Moyen d'Esploration. Paris: Brosson & Chaudé, 1819.
3. Shennan T. Dissecting aneurysms. Special report. London: Medical Research Council, 1934.
4. DeBakey ME, Cooley DA. Successful resection of aneurysms of the thoracic aorta and replacement by graft. *JAMA* 1953;152:673.
5. Passaro E, Pace WG. Traumatic rupture of the aorta. *Surgery* 1959;46:787–91.
6. Murray CA, Edwards JE. Spontaneous laceration of ascending aorta. *Circ* 1973;47:848–58.

7. Stanson AW, Kazmier FJ, Hollier LH, et al. Penetrating atherosclerotic ulcers of the thoracic aorta: natural history and clinico-pathologic correlations. *Ann Vasc Surg* 1986;1:15–23.

8. Picano E, Landini L, Distante A, et al. Fibrosis, lipids, and calcium in human atherosclerotic plaque: in-vitro differentiation from normal aortic walls by ultrasonic attenuation. *Circ Res* 1985;56:556–62.

9. Fossier AE. Size of the normal aorta. *Ann Clin Med* 1924;3:525.

10. Triulzi M, Gillam LD, Gentile F, et al. Normal adult cross-sectional echocardiographic values: linear dimensions and chamber areas. *Echocardiography* 1984;1:403.

11. Wright NL. Dissection study and measurement of the human aortic arch. *J Anat* 1969;104:377.

12. Reid K. The anatomy of the sinus of Valsalva. *Thorax* 1970;25:79.

13. Kunzelmann KS, Grande KJ, David TE, et al. Aortic root and valve relationships: impact on surgical repair. *J Thorac Cardiovasc Surg* 1994;107:162.

14. Maniet AR, Tardif, J-C, Esakof D, et al. Echocardiography– anatomic correlations. In: Roelandt JRTC, Pandian NG (eds): Multiplane transesophageal echocardiography. NY: Churchill Livingstone, 1996:27–68.

15. Bansal RC, Shakudo M, Shah PM, Shah PM. Biplane transesophageal echocardiography: technique, image orientation, and preliminary experience in 131 patients. *J Am Soc Echo* 1990;3:348–66.

16. Pandian NG, Hsu T-L, Schwartz SL, et al. Multiplane transesophageal echocardiography. *Echo* 1992;9:649–66.

17. DeBakey M, Noon G. Anuerysms of the thoracic aorta. *Mod Concepts Cardiovasc Dis* 1975;44:53–8.

18. Pressler V, McNamara JJ. Aneurysm of the thoracic aorta: review of 260 cases. *J Thorac Cardiovasc Surg* 1985;89:50–4.

19. Bickerstaff LK, Pairolero PC, Hollier LH, et al. Thoracic aortic aneurysms: a population-based study. *Surgery* 1982;92:1103–9.

20. Lilienfield DE, Gunderson PD, Spratfka JM, Vargas C. Epidemiology of aortic aneurysms. I. Mortality trends in the United States 1951 to 1981, . *Arteriosclerosis* 1987;7:637–43.

21. Waller BF, Clark MA, et al. Cardiac pathology in 2007consecutive forensic autopsies. *Clin Cardiol* 1992;15:760–5.

22. Crawford ES, Cohen ES. Aortic aneurysm: a multifocal disease. *Arch Surg* 1982;117:1393–400.

23. Svensson LG, Crawford ES, Hess KR, et al. Dissection of the aorta and dissecting aortic aneurysms: improving early and long-term surgical results. *Circ* 1990;82(5):IV 24–38.

24. Crawford ES, Hess KR, Cohen ES, et al. Ruptured aneurysm of the descending thoracic and thoracoabdominal aorta: analysis according to size and treatment. *Ann Surg* 1991;213:417–25.

25. Svensson LG, Sun J, Nadolony E, Kimmel WA. Prospective evaluation of minimal blood use for ascending aorta and aortic arch operations. *Ann Thorac Surg* 1995;59:1501–8.

26. Svensson LG, Crawford ES, Coselli JS, et al. Impact of cardiovascular operation on survival in the Marfan patient. *Circ* 1989;80(3):233–42.

27. Murdoch JL, Walker BA, Halpern BL, Kuzma JW, McKusick VA. Life expectancy and causes of death in the Marfan syndrome. *N Engl J Med* 1972;286:804.

28. Pyeritz RE, McKusick VA. The Marfan syndrome: diagnosis and management. *N Engl J Med* 1979;300:772–7.

29. Pyeritz RE. Marfan syndrome. *N Engl J Med* 1990;323:987–9.

30. Sun QB, Zhang KZ, Cheng TO, et al. Marfan syndrome in China: a collective review of 564 cases among 98 families. *Am Heart J* 1990;120:934–48.
31. McKusick VA. The cardiovascular aspects of Marfan syndrome: a heritable disorder of connective tissue. *Circ* 1955;2:321–41.
32. Beighton P, de Paepe A, Danks D, et al. International nosology of heritable disorders of connective tissue, Berlin, 1986. *Am J Med Genet* 1988;29:581–94.
33. Roberts WC, Honig HS. The spectrum of cardiovascular disease in the Marfan syndrome: a clinico-morphologic study of 18 necropsy patients and comparison to 151 previously reported necropsy patients. *Am Heart J* 1982;104:115–35.
34. Roman MJ, Rosen SE, Kramer-Fox R, Devereux RB. Prognostic significance of the pattern of aortic root dilatation in the Marfan syndrome. *J Am Coll Cardiol* 1989;14:422–8.
35. Svensson LG, Crawford ES. Aortic dissection and aortic aneurysm surgery: clinical observations, experimental investigations, and statistical analyses, part III. *Curr Probl Surg* 1993;30:1–163.
36. Spangler RD, Nora JJ, Lortscher RH, Wolfe RR, Okin JT. Echocardiography in Marfan syndrome. *Chest* 1976;69:443.
37. Pifarre R, Caralps JM, Sinha SN. Mitral valve replacement for regurgitation in an infant with Marfan syndrome. *J Thorac Cardiovasc Surg* 1974;67:233.
38. Chesler E, King RA, Edwards JE. The myxomatous mitral valve and sudden death. *Circ* 1983;67:632–9.
39. Pocock WA, Bosman CK, Chesler E, et al. Sudden death in primary mitral valve prolapse. *Am Heart J* 1984;107:378–82.
40. Nishimura RA, McGoon MD, Shub C, et al. Echocardiographically documented mitral valve prolapse: long term follow-up of 237 patients. *N Engl J Med* 1985;313:1305.
41. Farb A, Tang AL, Atkinson JB, et al. Comparison of cardiac findings in patients with mitral valve prolapse who die suddenly to those who have congestive heart failure from mitral regurgitation and to those with fatal noncardiac conditions. *Am J Cardiol* 1992;70:234–9.
42. Svensson LG, Crawford ES, Coselli JS, Safi HJ, Hess KR. Impact of cardiovascular operation on survival in the Marfan patient. *Circ* 1989;80(3):i233–42.
43. Shores J, Berger KR, Murphy EA, Pyeritz RE. Progression of aortic dilatation and the benefit of long-term B-adrenergic blockade in Marfan syndrome. *N Engl J Med* 1981;71:784–90.
44. Taherina AC. Cardiovascular anomalies in Marfan's syndrome: the role of echocardiography and beta-blockers. *South Med J* 1993;86:305–10.
45. Hwa J, Richards JG, Huang H, et al. The natural history of aortic dilatation in Marfan syndrome. *Med J Austral* 1993;158:558–62.
46. Larson E, Edwards W. Risk factors for aortic dissection: a necropsy study of 161 cases. *Am J Cardiol* 1984;53:849–55.
47. Abbot M. Coarctation of the aorta of the adult type, II: a statistical study and historical retrospect of 200 recorded cases, with autopsy, of stenosis or obliteration of the descending arch in subjects above the age of two years. *Am Heart J* 1928;3:392.
48. Gore I. Dissecting aneurysms of the aorta in persons under 40 years of age. *Arch Pathol* 1953;55:1–13.
49. Hahn R, Romas M, Mogtader A, Devereux R. Association of aortic dilatation with regurgitant, stenotic, and functionally normal bicuspid aortic valves. *J Am Coll Cardiol* 1992;19:283–8.
50. Roberts W. Aortic dissection: anatomy, consequences and causes. *Am Heart J* 1981;101:195–214.

51. Burks JM, Illes RW, Keating EC, Lubbe WJ. Ascending aortic aneurysm and dissection in young adults with bicuspid aortic valve: implications for echocardiographic surveillance. *Clin Cardiol* 1998;21:439–43.

52. Svensson LG, Crawford ES. Aortic dissection and aortic aneurysm surgery: clinical observations, experimental investigations, and statistical analyses: part II. *Curr Probl Surg* 1992;29: 915–1057.

53. Schnitker MA, Bayer CA. Dissecting aneurysm of the aorta in young individuals, particularly in association with pregnancy: with report of a case. *Ann Intern Med* 1944;20:486–511.

54. Pedowitz P, Perrel A. Aneurysms complicated by pregnancy; I: aneurysms of the aorta and its major branches. *Am J Obstet Gynecol* 1957;73:720–35.

55. Svensson LG, Crawford ES. Aortic dissection and aortic aneurysm surgery: clinical observations, experimental investigations, and statistical analyses, part III. *Curr Probl Surg* 1993;30:1–172.

56. Williams GM, Gott VL, Brawley RK, et al. Aortic disease associated with pregnancy. *J Vasc Surg* 1988;8:470–5.

57. Hirst AE, Johns VJ, Kime SW. Dissecting aneurysms of the aorta: a review of 505 cases. *Medicine* 1958;37:217.

58. Hirst AE, Gore I. The etiology and pathology of aortic dissection. In: Doroghazi RM, Slater EE (eds): Aortic dissection. New York, McGraw-Hill, 1983.

59. Hume M, Krosnick G. Dissecting aneurysm in pregnancy associated with aortic insufficiency: report of a case with successful surgical repair. *N Engl J Med* 1963;174:268.

60. Wolff J. Dissecting aortic aneurysms during pregnancy, parturition, and puerperium. *Ned T Verlosk (Dut)* 1961;61:23.

61. Pyeritz RE. Maternal and fetal complications of pregnancy in the Marfan syndrome. *Am J Med* 1981;71:784.

62. Mandel W, Evans EW, Walford RL. Dissecting aneurysm during pregnancy. *N Engl J Med* 1954;251:1059.

63. Konishi Y, Tatsuta N, Kumada K, et al. Dissecting aneurysm during pregnancy and the puerperium. *Jpn Circ J* 1980;44:726.

64. Wahlers T, Lass J, Alken A, Borst HG. Repair of acute type A dissection after cesarean section in the thirty-ninth week of pregnancy. *J Thorac Cardiovasc Surg* 1994;107:314.

65. Maruyama Y, Oguma F, Kosuge T, et al. Successful repair of an acute type A dissection during pregnancy. *Nippon Kyobur Geka Gakkai Zasshi* 1990;38:2296.

66. Ayzenberg O, Oettinger M, Kracoff OH, et al. Aortic dissecting aneurysm during pregnancy. *Harefuah* 1990;118:201.

67. Rossiter JP, Repke JT, Morales AJ, Murphy EA, Pyeritz RE. A prospective longitudinal evaluation of pregnancy in the Marfan syndrome. *Am J Obstet Gynecol* 1995;173:1599–606.

68. Becker RM. Intracardiac surgery in pregnant women. *Ann Thorac Surg* 1983;36:453.

69. Hayashi M, Terai T, Nishikawa K, et al. General anesthesia for cesarean section in a patient with Marfan syndrome associated with dissecting aortic aneurysm. *Masui* 1991;40:622.

70. DeBakey ME, Diethrich EB, Liddocoat JE, et al. Abnormalities of the sinuses of Valsalva: experience with 35 patients. *J Thorac Cardiovasc Surg* 1967;54:312.

71. DeBakey ME, Lawrie GM. Aneurysm of sinus of Valsalva with coronary atherosclerosis: successful surgical correction. *Ann Surg* 1979;189:303.

72. Morris GC Jr, Foster RP, Dunn RJ, Cooley DA. Traumatic aortic-ventricular fistula: report of two cases successfully repaired. *Am Surg* 1958;24:883.

73. Shumacker HB Jr. Aneurysms of the aortic sinuses of Valsalva due to bacterial endocarditis, with special reference to their operative management. *J Thorac Cardiovasc Surg* 1972;63:896.

74. Segal BL, Likoff W, Novack P. Rupture of a sinus of Valsalva aneurysm. *Am J Cardiol* 1963;12:544.

75. Spencer FC, Blake HA, Bahnson HT. Surgical repair of rupture aneurysm of sinus of Valsalva in two patients. *Ann Surg* 1960;152:963.

76. Shumacker HB Jr, Judson WE. Rupture of aneurysm of sinus of Valsalva into left ventricle and its operative repair. *J Thorac Cardiovasc Surg* 1963;45:650.

77. Trotter SE, Olsen EG. Marfan's disease and Erdheim's cystic medionecrosis: a study of their pathology. *Eur Heart J* 1991;12:83–7.

78. Wilson SK, Hutchins GM. Aortic dissecting aneurysms: causative factors in 204 subjects. *Arch Pathol Lab Med* 1982;106:175–80.

79. Roberts WC. Aortic dissection: anatomy, consequences, and causes. *Am Heart J* 1981;101:195–214.

80. Murray CA, Edwards JE. Spontaneous laceration of ascending aorta. *Circ* 1973;47:848.

81. Kilma T, Spjut HJ, Coelho A, et al. The morphology of ascending aortic aneurysms. *Hum Pathol* 1983;14:810.

82. Barsky SH, Rosen S. Aortic infarction following dissecting aortic aneurysm. *Circ* 1973;47:848.

83. Roberts CS, Roberts WC. Combined thoracic aortic dissection and abdominal aortic fusiform aneurysm. *Ann Thorac Surg* 1991;52:537.

84. Edwards JE. Manifestations of acquired and congenital diseases of the aorta. *Curr Probl Cardiol* 1979;3:1.

85. Levinson DC, Edmeades DT, Griffith GC. Dissecting aneurysm of the aorta: its clinical, electrocardiographic and laboratory features: a report of 58 autopsied cases. *Circ* 1950;1:360.

86. DeBakey ME, Henly WS, Cooley DA, et al. Surgical treatment of dissecting aneurysms of the aorta: analysis of 72 cases. *Circ* 1961;24:290.

87. DeBakey ME, Beall AC Jr, Cooley DA, et al. Dissecting aneurysms of the aorta. *Surg Clin North Am* 1966;46:1045.

88. Daily PO, Trueblood HW, Stinson EB, et al. Management of acute aortic dissections. *Ann Thorac Surg* 1970;10:237.

89. Cambria RP, Brewster DC, Gertler J, et al. Vascular complications associated with spontaneous aortic dissection. *J Vasc Surg* 1988;208:619.

90. Fradet G, Jamieson WR, Janusz MT, et al. Aortic dissection: a six year experience with 117 patients. *Am J Surg* 1988;155:697.

91. Miller DC, Stinson EB, Oyer PE, et al. Operative treatment of aortic dissections: experience with 125 patients over a 16-year period. *J Thorac Cardiovasc Surg* 1979;78:365.

92. Murphy DA, Craver JM, Jones EL, et al. Recognition and management of ascending aortic dissection complicating cardiac surgical operations. *J Thorac Cardiovasc Surg* 1983;85:247–56.

93. Ergin MA, Galla JD, Lansman S, Griepp RB. Acute dissections of the aorta: current surgical treatment. *Surg Clin North Am* 1985;65:721.

94. Crawford ES. The diagnosis and management of aortic dissection. *JAMA* 1990;264:2537.

95. Gore I, Seiwert VJ. Dissection aneurysm of the aorta. *Arch Pathol* 1952;53:121.

96. Roberts CS, Roberts WC. Aortic dissection with the entrance tear in transverse aorta: analysis of 12 autopsy patients. *Ann Thorac Surg* 1990;50:762.

97. Hufnagel CA, Conrad PW. Intimo-intimal intussusception in dissecting aneurysms. *Am J Surg* 1962;103:727.

98. DeBakey ME, Lawrie G. Intimal intussusception: unusual complication of dissecting aneurysm. *J Vasc Surg* 1984;1:566.

99. Miller DC, Mitchell RS, Oyer PE, et al. Independent determinants of operative mortality for patients with aortic dissections. *Circ* 1984;70:I153.

100. Davies MJ. Pathology of cardiac valves. London: Butterworths, 1980.

101. Cipriano PR, Griepp RB. Acute retrograde dissection of the ascending thoracic aorta. *Am J Cardiol* 1979;43:520.

102. Goldstein S, Mintz G, Lindsay J Jr. Aorta : comprehensive evalua-tion by echocardiography and transesophageal echocardiography. *J Am Soc Echocardiogr* 1993;6:634–59.

103. Ballal RS, Nanda NC, Gatewood R, et al. Usefulness of transesophageal echocardiography in assessment of aortic dissection. *Circ* 1991;84:1903–14.

104. Erbel R, Engberding R, Daniel W, et al. Echocardiography in diagnosis of aortic dissection. *Lancet* 1989;1:457–61.

105. Mohr-Kahaly S, Erbel R, Puth M, et al. Aortic intramural hematoma visualized by transesophageal echocardiography (abstr). *Circ* 1991;84: suppl 2:II-128.

106. Mohr-Kahaly S, Puth M, Erbel R, Meyer J. Intramural hematoma visualized by transesophageal echocardiography: an early sign of aortic dissection (abstr). *J Am Coll Cardiol* 1991;17(suppl A):20A.

107. Nienaber CA, Von Kodolitsch Y, Nicholas V, et al. The diagnosis of thoracic aortic dissection by noninvasive imaging procedures. *N Engl J Med* 1993;328:1–9.

108. Hashimoto S, Kumada T, Osakada G, et al. Assessment of transesophageal Doppler echocardiography in dissecting aortic aneurysm. *J Am Coll Cardiol* 1989;14:1253–62.

109. Mohr-Kahaly S, Erbel R, Rennollet H, et al. Ambulatory follow-up of aortic dissection by transesophageal two-dimensional and color-coded Doppler echocardiography. *Circulation* 1989;80:24–33.

110. Takamoto S, Omoto R. Visualization of thoracic dissecting aortic aneurysm by transesophageal Doppler color flow mapping. *Herz* 1987;12:187–93.

111. Ayala K, Chandrasedkaran K, Otto J, et al. Are the Doppler characteristics of the entry site of an intimal flap useful in the evaluation and follow up of aortic dissection? *J Am Coll Cardiol* 1992;19:279A.

112. Svensson LG, Labib S. Aortic dissection and aneurysm surgery. *Curr Opinion Cardiol* 1994;9:191–9.

113. Kyo S, Takamoto S, Omoto R, et al. Intraoperative echocardiography for diagnosis and treatment of aortic dissection. *Herz* 1992;17:377–89.

114. Svensson LG, Crawford ES. Aortic dissection: cardiovascular and vascular disease of the aorta. Philadelphia : W.B. Saunders Company, 1997:62.

115. Borst HG, Heinemann MK, Stone CD. Surgical treatment of aortic dissection. New York: Churchill Livingstone, 1996:24.

116. Nienaber CA, von Kodolitsch Y, Nicolas V, et al. Diagnosis of thoracic aortic dissection: magnetic resonance imaging versus transesophageal echocardiography. *Circ* 1992;85:434–47.

117. Krueger SK, Starke H, Forker AD, Eliot RS. Echocardiographic mimics of aortic root dissection. *Chest* 1975;67:441–4.

118. Hirschfeld DS, Rodriquez HJ, Schiller NB. Duplication of aortic wall seen by echocardiography. *Br Heart J* 1976;38:843–50.

119. Stever SW, Parameswaran R, Goldshlack P, Goldberg H. Unusual echocardiographic findings in aortic dissection. *Arch Intern Med* 1982;142:2221–3.

120. Kronzon I. Demopoulos l, Schrem SS, et al. Pitfalls in the diagnosis of thoracic aortic aneurysm by transesophageal echocardiography. *J Am Soc Echocardiogr* 1989;2:202–3.

121. Appelbe AF, Walker PG, Yeoh JK, et al. Clinical significance and origin of artifacts in transesophageal echocardiography of the thoracic aorta. *J Am Coll Cardiol* 1993;21:754–60.

122. Krukenberg E. Beiträge zur Frage des Aneurysma dissecans. *Beitr Pathol Anat Allg Pathol* 1920;67:329–51.

123. Wilson SK, Hutchins GM. Aortic dissecting aneurysms: causative factors in 204 subjects. *Arch Pathol Lab Med* 1982;106:175–80.

124. Gore I. Pathogenesis of dissecting aneurysm of the aorta. *Arch Pathol Lab Med* 1952;53:142–53.

125. Keren A, Kim CB, Hu BS, et al. Accuracy of biplane and multiplane transesophageal echocardiography in diagnosis of typical acute aortic dissection and intramural hematoma. *J Am Coll Cardiol* 1996;28:627–36.

126. Mohr-Kahaly S, Erbel R, Kearney P, Puth M, Meyer J. Aortic intramural hemorrhage visualized by transesophageal echocardiography: findings and prognostic implications. *J Am Coll Cardiol* 1994;23:658–64.

127. Yamada T, Takamiya M, Naito H, Kozuka T, Nakajima N. Diagnosis of aortic dissection without intimal rupture by x-ray computed tomography. *Nippon Acta Radiol* 1985;45:699–710.

128. Yamada T, Tada S, Harada J. Aortic dissection without intimal rupture: diagnosis with MR imaging and CT. *Radiology* 1988;168:347–52.

129. Wolff KA, Herold CJ, Tempany CM, Parravano JG, Zerhouni EA. Aortic dissection: atypical pattern seen at MR imaging. *Radiology* 1991;181:489–95.

130. Zotz RJ, Erbel R, Meyer J. Noncommunicating intramural hematoma: an indication of developing aortic dissection? *J Am Soc Echocardiogr* 1991;4:636–8.

131. Lui RC, Menkis AH, McKenzie FN. Aortic dissection without intimal rupture: diagnosis and management. *Ann Thorac Surg* 1992;53:886–8.

132. Nienaber CA, von Kodolitsch Y, Petersen B, et al. Intramural hemorrhage of the thoracic aorta: diagnostic and therapeutic implications. *Circ* 1995;92:1465–72.

133. Coady MA, Rizzo JA, Hammond GL, Pierce JG, Kopf GS, Elefteriades JA. Penetrating ulcer of the thoracic aorta: what is it? How do we recognize it? How do we manage it? *Journal of Vascular Surg* 1998;27(6):1006–15.

134. Willius FA, Cragg RW. A talk on dissecting aneurysm of the aorta. *Proc Staff Meet Mayo Clin* 1941;16:41–4.

135. Stanson AW, Kazmier FJ, Hollier LH, et al. Penetrating atherosclerotic ulcers of the thoracic aorta: natural history and clinicopathologic correlations. *Ann Vasc Surg* 1986;1:15–23.

136. Cooke JP, Kazmier FJ, Orszulak TA. The penetrating aortic ulcer: pathologic manifestations, diagnosis and management. *Mayo Clin Proc* 1988;63:718–25.

137. Kazerooni EA, Bree RL, Williams DM. Penetrating atherosclerotic ulcers of the descending thoracic aorta: evaluation with CT and distinction from aortic dissection. *Radiology* 1992;183:759–65.

138. Wann S, Jaff M, Dorros G, Sampson C. Intramural hematoma of the aorta caused by a penetrating atheromatous ulcer. *Clin Cardiol* 1996;19:438–9.

139. Hussain S, Glover JL, Bree R, Bendick PJ. Penetrating atherosclerotic ulcers of the thoracic aorta. *J Vasc Surg* 1989;9:710–17.

140. Yucel EK, Steinberg FL, Egglin TK, Geller SC, Waltman AC, Athanasoulis CA. Penetrating aortic ulcers: diagnosis with MR imaging. *Radiology* 1990;177:779–81.

141. Sommerville RL, Allen EV, Edwards JE. Bland and infected arteriosclerotic abdominal aortic aneurysms: a clinicopathologic study. *Medicine* 1959;38:207–21.

142. Osler W. The Gulstonian lectures on malignant endocarditis. *BMJ* 1885;1:467–70.

143. Chan FY, Crawford ES, Coselli JS, et al. In situ prosthetic graft replacement for mycotic aneurysm of the aorta. *Ann Thorac Surg* 1989;47:193–203.

144. Virmani R, McAllister HA Jr. Pathology of the aorta and major arteries. In: Lande A, Berkmen YM, McAllister HA (eds): Aortitis: clinical pathologic and radiographic aspects. New York: Raven Press, 1986:7.

145. Estes JE Jr. Abdominal aortic aneurysm: a study of 102 cases. *Circulation* 1950;2:258–64.

146. Shetty PC, Krasicky GA, Sharma RP, Vemuri BE, Burke MM. Mycotic aneurysms in intravenous drug abusers: the utility of intravenous digital subtraction angiography. *Radiology* 1985;155:319–21.

147. Lande A, Berkmen YM, McAllister HA Jr. Aortitis: clinical, pathologic and radiographic aspects. New York: Raven Press, 1986:1–70.

148. Castaneda-Zuniga WR, Noth PH, Zollikofer C, Velasquez G, Valdez-Davila O, Edwards E. Mycotic aneurysm of the aorta. *Cardiovasc Intervent Radiol* 1980;3:144–9.

149. Burger AJ, Messinco FC, Schulman P, Geller D. Mycotic aneurysm of the sinus of Valsalva due to *Eikeella corrodens* bacterial endocarditis. *Cardiology* 1984;71:220–8.

150. Reddy DJ, Shepard AD, Evans JR, et al. Management of infected aortoiliac aneurysms. *Arch Surg* 1991;126:873–8.

151. Kearney RA, Eisen HJ, Wolf JE. Nonvalvular infections of the cardiovascular system. *Ann Intern Med* 1994;121:219–30.

152. Johansen KJ, Devin J. Mycotic aortic aneurysms: a reappraisal. *Arch Surg* 1983;118:583–8.

153. Joffe II, Emmi RP, Oline J, et al. Mycotic aneurysm of the descending thoracic aorta: the role of transesophageal echocardiography. *J Am Soc Echocardiogr* 1996;9:663–7.

154. Harris KM, Malenka DJ, Plehn JF. Transesophageal echocardiographic evaluation of aortitis. *Clin Cardiol* 1997;20:813–15.

155. Kirsh MM, Behrendt DM, Orringer MB, Gago O. The treatment of acute traumatic rupture of the aorta. *Ann Surg* 1976;184:308–16.

156. Shorr RM, Critench M, Indeck M, et al. Blunt thoracic trauma: analysis of 515 patients. *Ann Surg* 1987;206:200–5.

157. Lundevall J. Mechanism of traumatic rupture of the aorta. *Acta Pathol Microbiol Scand* 1964;62:34–6.

158. Woodring JH. The normal mediastinum in blunt traumatic rupture of the thoracic aorta and brachiocephalic arteries. *J Emerg Med* 1990;8:467–76.

159. Svensson LG, Antunes MDJ, Kinsley RH. Traumatic rupture of the thoracic aorta: a report of 14 cases and a review of the literature. *S Afr J Med* 1985;67:853–7.

160. Parmley LF, Mattingly TW, Manion WC, Jahnke EJ. Nonpenetrating traumatic injury of the aorta. *Circulation* 1958;17:1086–101

161. Kearney PA, Smith DW, Johnson SB, Barker DE, Smith MD, Sapin PM. Use of transesophageal echocardiography in the evaluation of traumatic aortic injury. *J Trauma* 1993;34:696–701.

162. Smith MD, Cassidy JM, Souther S, et al. Transesophageal echocardiography in the diagnosis of traumatic rupture of the aorta. *N Engl J Med* 1995;332:356–62.

163. Sparks MB, Burchard KW, Marrin CAS, Bean CHG, Nugent WC, Plehn JF. Transesophageal echocardiography: preliminary results in patients with traumatic aortic rupture. *Arch Surg* 1991;126:711–14.

164. Brooks SW, Young JC, Cmolik B, et al. The use of transesophageal echocardiography in the evaluation of chest trauma. *J Trauma* 1992;32:761–5.

165. Moloney JF, Duffy CI, Plehn JF. Transesophageal echocardiographic findings in severe blunt chest trauma. *Circ* 1991;84(suppl II) :II-128.

166. Chirillo F, Totis O, Cavarzerani A, Bruni A, Cuzzato V. Assessment of severe blunt chest trauma by transesophageal echocardiography. *Eur Heart J* 1992;13:286.

167. Brooks SW, Cmolik Bl, Young JC, Townsend RN, Diamond DL. Transesophageal echocardiography examination of a patient with traumatic aortic transection from blunt chest trauma: a case report. *J Trauma* 1991;31:841–5.

168. Galvin IF, Black IW, Lee CL, Horton DA. Transesophageal echocardiography in acute aortic transection. *Ann Thorac Surg* 1991;51:310–11.

169. Locke TJ, Reeder GS, Khandheria BK, McGregor CGA. Diagnosis of traumatic aortic rupture by transesophageal echocardiography. *J Thorac Cardiovasc Surg* 1991;101:555–6.

170. De Belder A, Thomas M, Marrinan M. Traumatic rupture of the thoracic aorta diagnosed by transesophageal echocardiography. *Br Heart J* 1993;70:393–4.

171. Goarin JP, Le Bret F, Riou B, Jacquens Y, Viars P. Early diagnosis of traumatic aortic rupture by transesophageal echocardiography. *Chest* 1993;103:618–19.

172. Wolfenden H, Newman DC. Transesophageal echocardiography: an increasing role in the diagnosis of traumatic aortic rupture. *J Thorac Cardiovasc Surg* 1993;106:757–60.

173. Snow CC, Appelbe AF, Martin TD, Martin RP. Diagnosis of aortic transection by transesophageal echocardiography. *J Am Soc Echocardiogr* 1992;5:100–2.

174. Karalis DG, Victor MF, Davis GA, et al. The role of echocardiography in blunt chest trauma: a transthoracic and transesophageal echocardiographic study. *J Trauma* 1994;36:53–8.

175. Davis GA, Sauerisen S, Chandrasekaran K, Karalis DG, Ross JJ, Mintz GS. Subclinical traumatic aortic injury diagnosed by transesophageal echocardiography. *Am Heart J* 1992;123:534–6.

176. Shapiro MJ, Yanofsky SD, Trapp J, et al. Cardiovascular evaluation in blunt thoracic trauma using transesophageal echocardiography. *J Trauma* 1991;31:835–9.

177. Vignon P, Guéret P, Vedrinne JM, et al. Role of transesophageal echocardiography in the diagnosis and management of traumatic aortic disruption. *Circulation* 1995;92:2959–68.

178. Le Bret F, Ruel P, Rosier H, Goarin JP, Riou B, Viars P. Diagnosis of traumatic mediastinal hematoma with transesophageal echocardiography. *Chest* 1994;105:373–6.

179. Vaduganathan P, Ewton A, Nagueh SF, Weilbaecher DG, Safi HJ, Zoghbi WA. Pathologic correlates of aortic plaques, thrombi and mobile "aortic debris" imaged in vivo with transesophageal echocardiography. *J Am Coll Cardiol* 1997;30:357–63.

180. Tunick PA, Kronzon I. Protruding atherosclerotic plaque in the aortic arch of patients with systemic embolization: a new finding seen with transesophageal echocardiography. *Am Heart J* 1990;120:658–60.

181. Karalis DG, Chandrasekaran K, Victor MF, et al. Recognition and embolic potential of intraaortic atherosclerotic debris. *J Am Coll Cardiol* 1991;17:73–8.

182. Dávila-Román VG, Barzilai B, Wareing TH, Murphy SF, Schechtman KB, Kouchoukos NT. Atherosclerosis of the ascending aorta: prevalence and role as an independent predictor of cerebrovascular events in cardiac patients. *Stroke* 1994;25:2010–16.

183. Dávila-Román VG, Murphy SF, Nickerson NJ, Kouchoukos NT, Schechtman KB, Barzilai B. Atherosclerosis of the ascending aorta is an independent predictor of long-term neurologic events and mortality. *J Am Coll Cardiol* 1999;33:1308–16.

184. Ferrari E, Vidal R, Chevallier T, Baudouy M. Atherosclerosis of the thoracic aorta and aortic debris as a marker of poor prognosis: benefit of oral anticoagulants. *J Am Coll Cardiol* 1999;33:1317–22.
185. Fazio GP, Redberg RF, Winslow T, Schiller NB. Transesophageal echocardiography detected atherosclerotic aortic plaque is a marker for coronary artery disease. *J Am Coll Cardiol* 1993;21:144–50.
186. Simons AJ, Carlson R, Hare Cl, Obeid AI, Smolyan H. The use of transesophageal echocardiography in detecting aortic atherosclerosis in patients with embolic disease. *Am Heart J* 1992;123:224–6.
187. Loop FD, Lytle BW, Cosgrove DM, et al. Coronary artery bypass graft surgery in the elderly: indications and outcome. *Cleve Clin J Med* 1988;55:23–4.
188. Gardner TJ, Horneffer PJ, Manolio TA, et al. Stroke following coronary artery bypass grafting: a ten-year study. *Ann Thorac Surg* 1985;40:574–81.
189. Dávila-Romá VG, Phillips KJ, Daily BB, Dávila RM, Kouchoukos NT, Barzilai B. Intraoperative transesophageal echocardiography and epiaortic ultrasound for assessment of atherosclerosis of the thoracic aorta. *J Am Coll Cardiol* 1996;28:942–7.
190. Wareing TH, Dávilla-Román VG, Daily BB, Murphy SF, Barzilai B, Kouchoukos N. Strategy for the reduction of stroke incidence in cardiac surgical patients. *Ann Thorac Surg* 1993;55:1400–8.
191. Mendelsohn L, Steers JC, Pieniek MS, et al. Is there utility for transesophageal echocardiography during routine coronary artery surgery? *Circulation* 1976;94:I-455.
192. Svensson LG, Sun J, Cruz H, Shahian DM. Endarectomy for aortic valve stenosis and calcified porcelain aorta. *Ann Thorac Surg* 1996;61:149–52.
193. Coselli JS, Crawford ES. Aortic valve replacement in the patient with extensive calcification of the ascending aorta.*J Thorac Cardiovasc Surg* 1986;91(2):184–7.
194. Sakaguchi H, Kitamura S, Kawachi K, et al. Aortic valve replacement and coronary artery bypass grafting in a patient with a porcelain aorta due to aortitis syndrome. *J Jpn Ass Thorac Surg* 1993;41(6):1063–8.
195. Accola KD, Jones EL. Coronary revascularization in a patient with porcelain aorta and calcified great vessels. *Ann Thorac Surg* 1993;55(2):514–15.
196. Byrne JG, Aranki SF, Cohn LH. Aortic valve operations under deep hypothermic circulatory arrest for the porcelain aorta: "no-touch" technique. *Ann Thorac Surg* 1998;65:1313–15.
197. Shapira OM, Cruz HA, Shemin RJ. Endarterectomy of the ascending aorta: an alternative method in patients with extensively calcified (porcelain) aorta requiring aortic valve replacement. *J Card Surg* 1997;12:160–4.
198. Mizumoto T, Hiraiwa T, Kinoshita T, Fujii H. Left thoracotomy for coronary artery bypass grafting without cardiopulmonary bypass in a patient with porcelain aorta. *J Jpn Thorac Surg* 1997;45:161–4.
199. Henry WL, Gardin JM, Ware JH, et al. Echocardiographic measurements in normal subjects from infancy to old age. *Circulation* 1980;62:1054–61.

Index

Page numbers in italics refer to illustrations; numbers followed by 't' indicate tables